Polyether-based Lipids and Copolymers:

From Biomedical Applications to

Thermoresponsive Materials

Dissertation zur Erlangung des Grades
"Doktor der Naturwissenschaften" im Promotionsfach Chemie

am Fachbereich Chemie, Pharmazie und Geowissenschaften
der Johannes Gutenberg-Universität Mainz

Sophie Sabine Müller

geb. in Dresden

Mainz, 2014

In Dankbarkeit

Für meine Eltern

„Die Neugier steht immer an erster Stelle eines Problems, das gelöst werden will.“

Galileo Galilei

Danksagung (Acknowledgments)

Table of Contents

A. Appendix 279

Motivation and Objectives

During the past century, the oxyanionic ring-opening polymerization of epoxides has become a key technique for polymer synthesis. The resulting polyethers, particularly poly(ethylene glycol) (PEG), have enabled an immense variety of applications in pharmaceutics, cosmetics, and food production. The living polymerization technique allows for the precise control over the molecular weight, molecular weight distribution, architecture, and end group functionalization of these polymers. Furthermore, rapid progress in the synthesis of suitable epoxide monomers has provided a tool box for various functionalities that can be incorporated into the polyether backbone. Hydroxyl-, thiol-, allyl-, vinyl-, amine-, or acetal-groups, just to name a few, are accessible via orthogonal protection chemistry. By using a latent AB$_2$-type epoxide monomer, such as glycidol, in the ring-opening multibranching polymerization it is possible to achieve hyperbranched structures with a tailored number of hydroxyl groups. Hyperbranched polyglycerol (*hb*PG) exhibits high thermal stability, unique rheological behavior, excellent water-solubility, and biocompatibility, which render it an interesting material for pharmaceutical applications.

The combination of epoxide chemistry and functional initiators or end capping agents enlarges the tool box for functional polymers. Complexity of the molecular structures can be increased via the combination of epoxides such as ethylene oxide (EO), ethoxyethyl glycidyl ether (EEGE), and glycidol. Here, linear, linear-hyperbranched, or hyperbranched structures are achievable.

Introducing a hydrophobic initiator can give access to amphiphilic structures with highly interesting properties, e.g., in liposome research, as surfactants, or as surface active molecules. In particular, PEG-lipids have attracted increased attention due to their incorporation into phospholipid bilayers. It was found that the polymer sterically stabilizes these vesicles with favorable properties *in vivo.* The so-called "stealth" liposomes exhibit reduced aggregation and protein adsorption in biological media, as well as prolonged blood circulation times that render them suitable for anti-cancer therapy. However, the main drawback of PEG, besides its non-degradability, is the lack

of functional groups, especially for methoxyPEG (mPEG). However, functional groups are essential for the attachment of targeting groups or other derivatization reactions. As will be demonstrated in this thesis, the epoxide monomer tool box is ideal to overcome these disadvantages since polyfunctionality and various architectures can be tailored.

The aim of this thesis is the synthesis of tailor-made amphiphilic, complex polyether lipids with selected functional groups in the polymer backbone with a special focus on understanding the resulting liposomes and – for the first time - application *in vivo*. As a separate part of this work, novel thermoresponsive copolymers of glycidyl methyl ether, focusing on the use of the epoxide tool box for unprecedented copolymers, are presented.

The specific objectives of this thesis are described in the following.

i)   *Synthesis of Novel Functional Polymer Lipids as a "Functionalization Platform"*: The synthesis of novel polyether-based lipid analogues and the expansion of the epoxide tool box for this synthetic purpose is the main topic of the first part of this thesis. The creation of a "functionalization platform" for these types of lipids is an essential improvement, which is achieved by either postpolymerization reactions, e.g., introduction of alkyne groups or phosphonic acid groups for bone adhesion, or by using functional epoxides, like allyl glycidyl ether (AGE) for further derivatization with thiols.

ii) *Cleavable Polyether-Based Lipids*: pH-responsive polymer lipids are ideal components for liposomes in cancer therapy, since the tumor tissue exhibits a slightly acidic environment. Upon tumor accumulation, cleavage of the chains is promoted, leading to membrane-membrane fusion and cargo release. A challenging issue in the synthesis of acid-cleavable polyether-based lipids is the appropriate choice of epoxide monomers or functional initiators that withstand the reaction conditions and are stable under neutral pH. In this regard, a special emphasis of this thesis was placed on the exploration of polyether-based lipids with one or multiple cleavable acetal-groups.

iii.) *Interaction of Polymer Lipids with Phospholipid Monolayers*: The incorporation in membranes and interaction of the cholesterol-based polymers with phospholipid membranes is a key issue for the stability of lipid monolayers or bilayers. Hence,

the characterization of the physical behavior and the interaction of the synthetic polyether lipids and fluorescent labeled polymer lipids with phospholipids at the water-air interface was carried out in Langmuir-Blodgett films (in close collaboration with the groups of Prof. Jörg Kressler and Prof. Alfred Blume, Institute of Chemistry, Halle (Saale), Germany).

iv.) *Pre-In Vivo and In Vivo Studies:* The most important research objectives for the functionalized liposomes are (i) understanding their interaction with biological media and (ii) their organ distribution *in vivo*, which are highly relevant for their eventual use in biomedical applications. Therefore, the different polyether lipids and liposomes were evaluated in human blood serum by dynamic light scattering (DLS) in collaboration with the Institute of Physical Chemistry (Prof. Manfred Schmidt), Johannes Gutenberg University Mainz and the Max Planck Institute of Polymer Research (Dr. Kristin Mohr and Prof. Katharina Landfester). A special emphasis of these studies was the investigation of possible aggregation of the lipid assemblies with proteins in serum, which has been shown to compromise the efficiency of drug delivery systems.

Major steps towards applications *in vivo* are animal studies and biodistribution measurements. This step was carried out in collaboration with the research group of Prof. Rösch, Institute of Nuclear Chemistry, Johannes Gutenberg University Mainz and Prof. Miederer from the Nuclear Medicine Department. Systematic comparison of radiolabeled linear and linear-hyperbranched polymers, and the respective liposomes was performed with regard to their organ distribution via positron emission tomography (PET). To this end, we considered the application of the positron emitter fluorine-18 and labeling of the polymers as well as cholesterol itself as being advantageous for these studies to get first insights into the distribution of the liposomal assemblies during *in vivo* application.

iv.) *Challenging Copolymerization of EO and GME:* Expanding the abovementioned epoxide tool kit, the synthesis and characterization of copolymers that possessed tunable melting temperatures and thermoresponsive behavior depending on the monomer composition was developed. In this regard, the copolymerization of ethylene oxide (EO) and glycidyl methyl ether (GME) seemed to be facile, but unexpectedly, pronounced differences in reactivity made this approach

challenging. The traditional oxyanionic ring-opening polymerization was not suitable in this case. Therefore, a different approach was followed. The advantages of the employed "activated monomer polymerization" are the addition of an aluminum catalyst activating the epoxides and low reaction temperatures (-15 °C-20 °C), which translates to less hazardous reaction conditions compared to those used for the oxyanionic polymerization.

In the appendix of this thesis, various chapters summarize contributions to other areas of the polyether field that resulted from collaborations with colleagues of the research group of Prof. Frey or other collaboration partners.

Abstract

This thesis aims at the synthesis of tailor-made polyether-based lipids bearing selected functional groups, their incorporation into liposomes, and their characterization in contact with biological media, as well as novel polyether copolymers with thermoresponsive behavior. The work is motivated both by fundamental synthetic questions and potential applications of the resulting materials.

Chapter 1 gives an introduction to this thesis. A review on the synthetic strategies of polyether-based lipids with multivalent architectures and the current state-of-the-art in liposome research is given in **Chapter 1.1. Chapter 1.2** comprehensively reviews the synthetic strategies and biomedical applications of linear polyglycerol (*lin*PG) and gives an overview of the various functionalization reactions addressing either the termini or in-chain hydroxyl functions at the polymer backbone. The usage of *lin*PG as a valuable building block in block co-, or tercopolymers as well as a macroinitiator for the multibranching polymerization of glycidol is highlighted.

Chapter 2 focuses on the synthesis, functionalization, and characterization of cholesterol-based lipids obtained either by the usage of a functional epoxide tool box or postpolymerization reactions of the ready-made lipids. In **Chapter 2.1** a synthetic pathway for allyl-containing cholesterol-lipids with different architectures is developed. Using cholesterol as the initiator in the oxyanionic ring-opening polymerization of ethoxyethyl glycidyl ether (EEGE) and allyl glycidyl ether (AGE), *lin*PG with pendant hydroxyl and allyl groups is achievable. By combining various epoxides, complex architectures, such as block copolymers of PEG-*lin*PG with allyl groups grafted-from the polymer backbone or hyperbranched polyglycerol (*hb*PG) with allyl groups at the corona have been synthesized. The allyl groups were addressed in thiol-ene coupling reactions with thiols leading to functionalized lipids (postpolymerization functionalization). As an example, the hyperbranched structure with attached glutathione was successfully incorporated into liposomes, resulting in surface modified vesicles.

Although polyether lipids can stabilize liposomes, their non-degradability is a major issue, since membrane-membrane fusion and cargo release can be slowed down compared to non-stabilized vesicles. This aspect is tackled in **Chapter 2.2** which

describes the synthesis and characterization of acid-cleavable lipids with different architectures. The introduction of acetal moieties in hyperbranched polyether-based lipids was achieved via random or sequential copolymerization of the epoxide inimer 1-(glycidyloxy)ethyl ethylene glycol ether (GEGE) and glycidol (epoxide tool box) with amounts of GEGE between 8-49 mol%. In addition, hyperbranched polyethers with exactly one acetal unit were prepared using a functional cholesterol-initiator. Shedding of the liposomes was proven by using the linear analogue functionalized with an alkyne group and a fluorescent label, Atto 488 azide, via "click"-chemistry in collaboration with the group of Prof. Helm, Institute of Pharmacy and Biochemistry. Investigation of the acetal-cleavage under acidic pH (7.4-2.0) via fluorescence spectroscopy revealed a strong dependence on the pH.

In **Chapter 2.3** the synthetic concept of postpolymerization reactions of the pendant hydroxyl groups within the polymer backbone of *lin*PG is transferred to the introduction of phosphonic acid groups into cholesterol-*lin*PG polymers. (Bis-)phosphonates are ideal functional groups for the attachment onto $CaPO_4$-surfaces and therefore might be suitable in delivering vesicles to bone tissues for bone cancer treatment. The Michael-type addition of diethyl vinyl phosphonate to the hydroxyl groups of the polymer backbone and subsequent release of the phosphonic acid groups resulted in lipids with a tunable amount of functional moieties (29-76 mol%). Preliminary results of the incorporation into liposomes and the attachment onto $CaPO_4$-surfaces are described in this section.

The interaction of polymer lipids with phospholipid monolayers or bilayers is a crucial question which was addressed in **Chapter 3**. Two polyether-based linear-hyperbranched block copolymers with and without a covalently attached rhodamine fluorescence label (Rho) have been compared. Compression isotherms of co-spread phospholipids (DPPC or POPC) with the respective polymers were measured on the Langmuir trough, and the morphology development of the liquid-condensed (LC) domains was studied by epi-fluorescence microscopy. It was observed that the presence of the fluorescence label significantly influences the domain morphology, since the rhodamine labelled polymer showed higher line activity. Confocal laser scanning microscopy (CLSM) of giant unilamellar vesicles (GUVs) also confirmed the polymers' fast adsorption to and insertion into phospholipid membranes, which is crucial for potential applications.

Chapter 4 focuses on the comparison of linear and linear-hyperbranched cholesterol-lipids with respect to their applications in liposomes *in vivo*. In **Chapter 4.1** linear and linear-hyperbranched polymers are evaluated with respect to their steric stabilization properties of liposomes in human blood serum. Liposomes with different amounts of polymer (0-30 mol% respectively) were investigated in contact with biological media via dynamic light scattering (DLS). Slight aggregation of the PEGylated liposomes and a desired lack of aggregation of the liposomes with the branched polymer chains was detected by this sensitive method.

The application *in vivo* of the functionalized linear and linear-hyperbranched polymers as well as the respective sterically stabilized liposomes is discussed in detail in **Chapter 4.2.** The positron emitter fluorine-18 was attached to the polyether backbone via the copper-catalyzed azide-alkyne click reaction (CuAAC) and positron emission tomography (PET) was carried out *in vivo* for 1 h. *Ex vivo* biodistribution revealed different organ accumulation patterns of non-stabilized liposomes, in which cholesterol was labelled with ^{18}F, and the two differently stabilized stealth-type liposomes. Non-stabilized liposomes rapidly accumulated in liver and spleen, whereas the latter ones remained in the blood stream and other organs for a longer time.

Chapter 5 expands the scope of the epoxide tool box from lipids to novel polyether-based copolymers by the copolymerization of ethylene oxide (EO) and glycidyl methyl ether (GME). Although formally only one oxygen and a methylene group is added to each repeating unit of poly(ethylene glycol) (PEG), a material with different properties is obtained. Due to pronounced differences in reactivity of both monomers, not the oxyanionic ring-opening polymerization was used, but an "activated monomer process". The copolymers were amorphous or showed low melting temperatures, depending on the GME amount (30-100 mol%). Furthermore, temperature-dependent solubility in aqueous solution was observed, and the lower critical solution temperature (LCST) was tunable between 55 °C and 98 °C by varying the comonomer ratio. A major step compared to already literature-known polyethers synthesized by this technique, was the purification and removal of the initiator salt, which was found to influence the physical properties of the copolymers. A slightly tapered, but not block-like structure was revealed by differential scanning calorimetry (DSC) and triade sequence analysis (^{13}C NMR spectroscopy).

Graphical Abstract

1.1. Polyether-based Lipids Synthesized with an Epoxide Construction Kit: Multivalent Architectures for Functional Liposomes
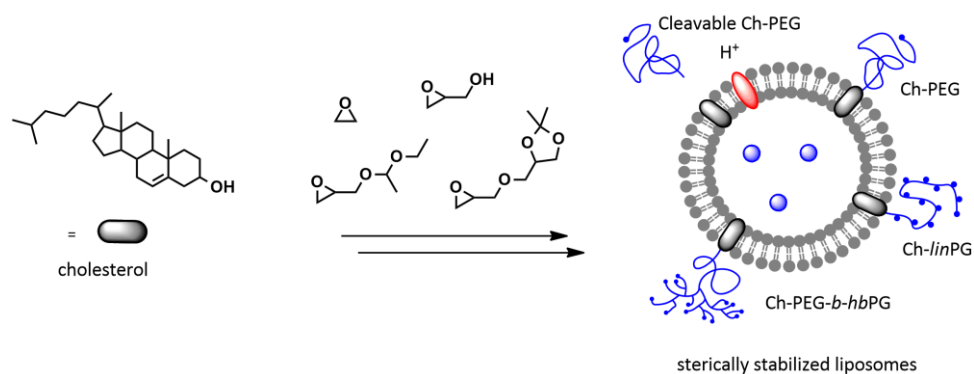
1.2. Beyond Poly(ethylene glycol): Linear Polyglycerol as a Multifunctional Polyether for Biomedical Applications
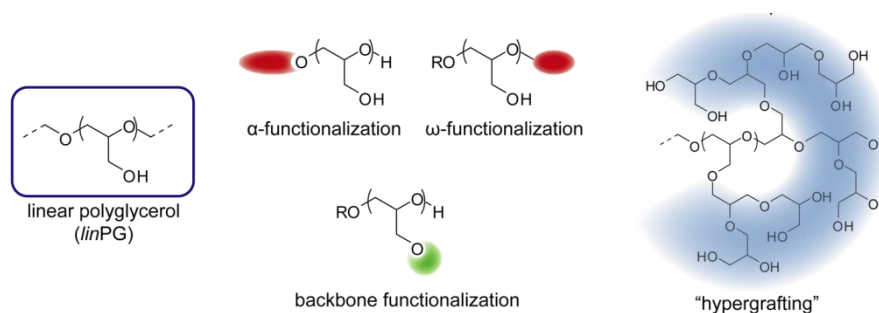
1.1. Allyl-Functionalized Cholesterol-Lipids: From Thiol-ene Coupling to Liposomes
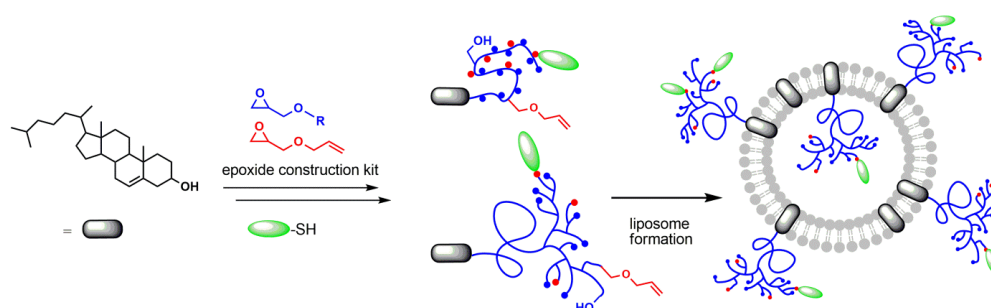
1.2. Tackling the Biodegradability of Hyperbranched Polyether-Lipids with In-Chain pH-Sensitive Linkages
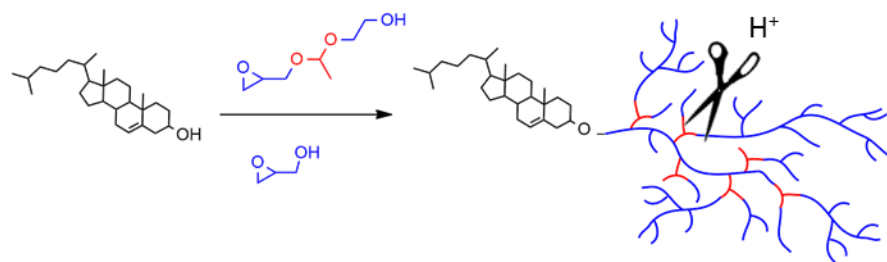
1.3. Phosphonoethylated Polyglycerol Amphiphiles: Liposomal Formulations for Bone Targeting
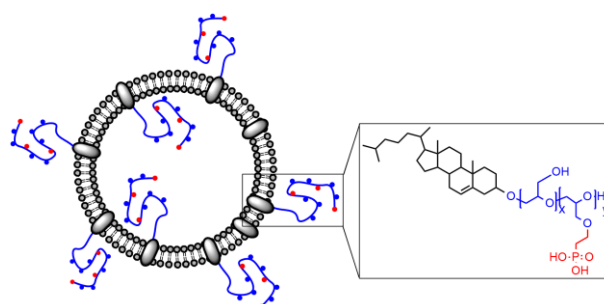
3. Unusual Triskelion Patterns and Dye-labeled GUVs: Consequences of the Interaction of Cholesterol Containing Linear-Hyperbranched Block Copolymers with Phospholipids
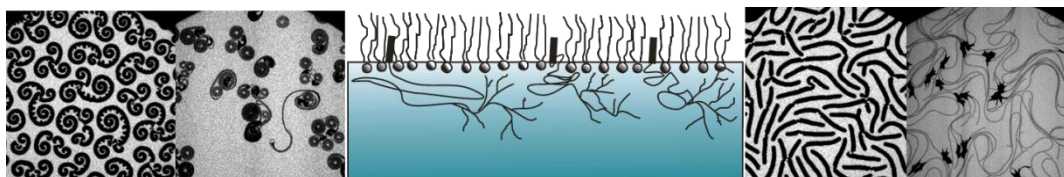
4.1. Evaluation of Multifunctional Liposomes in Human Blood Serum by Light Scattering
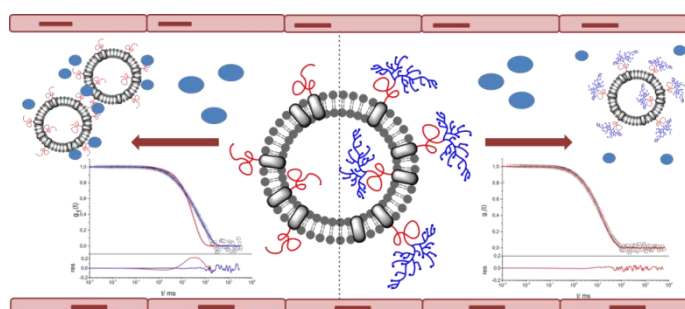
4.2. Characterization of Polyether-Lipids in Stealth Liposomes by ^{18}F-TEG-N$_3$ Click Radiolabeling and Positron Emission Tomography
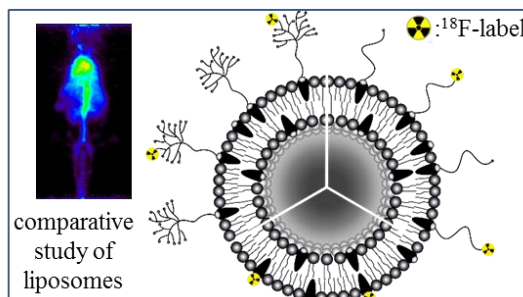
5. A Challenging Comonomer Pair: Copolymerization of Ethylene Oxide and Glycidyl Methyl Ether to Thermoresponsive Polyethers
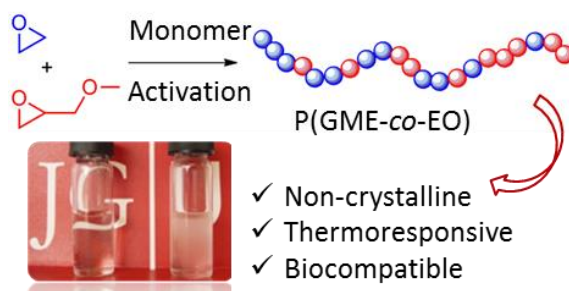
1 Introduction

1.1 Polyether-based Lipids Synthesized with an Epoxide Construction Kit: Multivalent Architectures for Functional Liposomes

*Sophie S. Müller[1,2], Carsten Dingels[1], Anna Maria Hofmann[1], and Holger Frey[1]*

[1]Institute of Organic Chemistry, Johannes Gutenberg University Mainz,

Duesbergweg 10-14, 55128 Mainz, Germany.

[2] Graduate School Materials Science in Mainz, Staudingerweg 9, 55128 Mainz

Abstract

Liposomes, vesicles consisting of phospholipids, are well known drug carriers, especially in anti-cancer treatment. Due to their improved pharmacokinetics, "stealth" liposomes, which are polymer coated vesicles, are being used in clinical applications with good results. One of the drawbacks of poly(ethylene glycol) (PEG) that is preferentially incorporated, is its lack of functional groups and its non-biodegradability. In this article new polyether-based lipids are presented that can be synthesized from an epoxide monomer library, resulting in tailored multivalent architectures. The cholesterol-based lipid-like structures offer further possibilities for functionalization, which is important for active targeting. Furthermore, a rather simple synthetic route has been developed, which leads to acid-cleavable cholesteryl-PEG, thus leading to possible controlled destabilization of the liposome formulation. This process is crucial for drug release *in vivo*.

Introduction

The formation of liposomes by self-assembly of phospholipids in water was discovered almost 40 years ago. Liposomes are colloidal vesicles consisting of a lipid bilayer with an aqueous medium interior.[1] Fundamental research on the preparation, stability, release profile, encapsulation efficiency and targeting of liposomes has led to clinical application. Especially for cancer therapies, the use of extremely toxic and aggressive drugs shows serious side effects. Effective delivery-systems, like liposomes, enabled an important step towards minimizing these undesired properties on healthy tissue. Advantages of these systems include a high local concentration of the anticancer drug, while protecting the body from a cytostatic drug before its release at the target site. A well known example is doxorubicin, an anthracycline, which has severe cardiotoxic effects in humans when applied directly. However, when encapsulated in lipid formulations it shows considerably increased circulation time compared to the free drug, and more importantly, lower concentration of the free drug and consequently lower cardiotoxicity. The respective product, known as Doxil™, was one of the first liposome formulations approved in the US.

Conventional liposomes (see Figure 1) as lipoidal carriers have been extensively studied as drug-delivery systems, motivated by the combination of reduced side effects on healthy tissue and passive targeting.[1,2] However, the main disadvantages of such systems are the rapid removal from the blood by macrophages (mononuclear phagocyte system, MPS) after opsonin binding and uptake into liver and spleen.[3] Additionally, their physical and chemical instability results in uncontrollable properties *in vivo*.[4,5] To overcome these drawbacks, so-called "stealth" liposomes with surfaces modified by mainly poly(ethylene glycol) (PEG), but also polysaccharides, were developed. The presence of PEG for example effects prolonged blood circulation time,[6,7] reduced MPS uptake,[8] reduced aggregation of PEGylated carriers and better (storage) stability of liposomal carriers.[9]
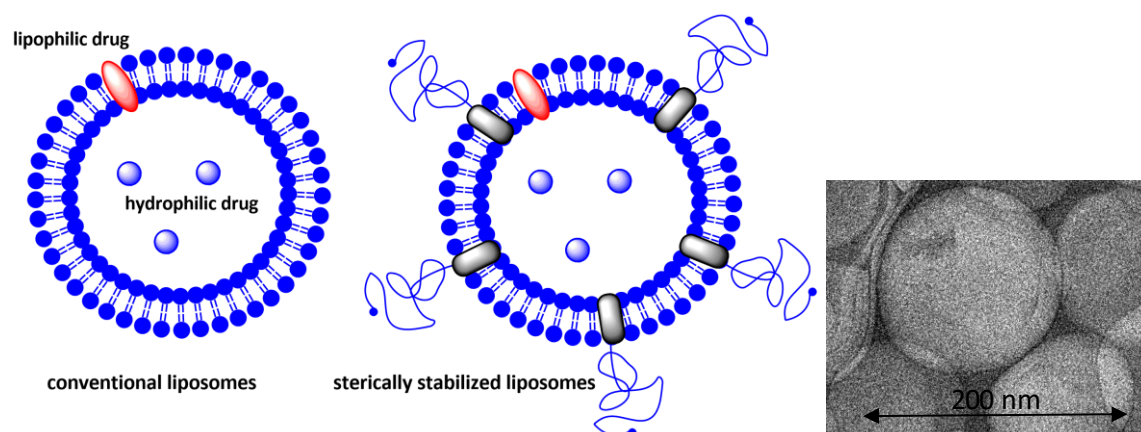
Figure 1: left: Schematic picture of conventional liposomes and sterically stabilized liposomes, right: TEM image of liposomes containing a lipid and cholesterol-PEG.

The present chapter will give a short overview of the recent developments in multifunctional "stealth" liposome preparations. This interdisciplinary area between synthetic polymer chemistry, advances in their characterization combined with new liposome preparation techniques leads to interesting new aspects in the area of "stealth" liposomes. Next to a short overview of polymeric amphiphiles currently used in "stealth" liposome preparations, the main focus will be on polyethers such as poly(ethylene glycol) (PEG) and alternative branched and hyperbranched structures recently developed in our group. Additionally, we will give a short summary of acid-cleavable polymers in the application of degradable liposomes.

Liposome stabilization: A polymer shell is necessary

In vivo studies of conventional liposomes have shown that they are rapidly opsonized by serum proteins, and therefore are taken up by cells of the mononuclear phagocyte system (MPS), such as Kupffer-cells or macrophages from the liver. This process is a key to control drug delivery, since the particles are not capable of performing their desired therapeutic task.[10] Although the exact mechanism is not clearly understood yet, it is known that the type and number of proteins that attach to the vesicle's surface can vary dramatically. Factors that influence the opsonization process include liposome size, composition, and charges. Harashima et al. demonstrated a correlation between

decreasing liposome size and decreasing opsonization. Furthermore, phagocytic cells remove liposomes in proportion to the amount of opsonization.[11] Negatively charged liposomes increase intracellular uptake into phagocytic cells and therefore accelerate their own clearance after administration.[12,13] Since the binding of proteins depends on a variety of physicochemical characteristics, the initial approaches to increase circulation time relied on changing these parameters. The simplest way to achieve this goal is to reduce the liposome size by sonication, extrusion or microfluidization.[1] A rather recent method for the preparation of small liposomes was presented by Massing et al.. They used a so-called dual asymmetric centrifuge (DAC) to produce a viscous vesicular phophoplipid gel (VPG), which can be diluted to a conventional liposome dispersion. The procedure is based on shear forces for efficient homogenization due to two rotating movements in this special centrifuge.[14] The authors also showed high entrapping efficiencies of siRNA under sterile conditions.[15]

Another route to improve circulation time is to graft a polymer shell onto the surface of the particles (see Figure 1). The attachment of e.g., poly(ethylene glycol) (PEG), can lead to a protective, hydrophilic polymer layer, which prevents opsonin adsorption via steric repulsion. Hence, opsonization is reduced, and the probability for the uptake by the MPS system is decreased. Research groups who studied the half-life times *in vivo* could show extended retention periods from 5 h up to 5 days.[16-19] Furthermore, it was proven that PEGylated liposomes showed improved biodistribution, which resulted in low amounts of "stealth" liposomes (10-15%) being taken up by the liver.[20]

Covalent attachment to lipids is clearly more stable than mere physical adsorption. Hence, "stealth" liposomes are prepared by polymer-modified lipids, which can be phospholipids or cholesterol, both natural membrane components. These polymer conjugates function as an anchor in the vesicle membrane. Selected biocompatible amphiphilic compounds used for this purpose are shown in Figure 2.
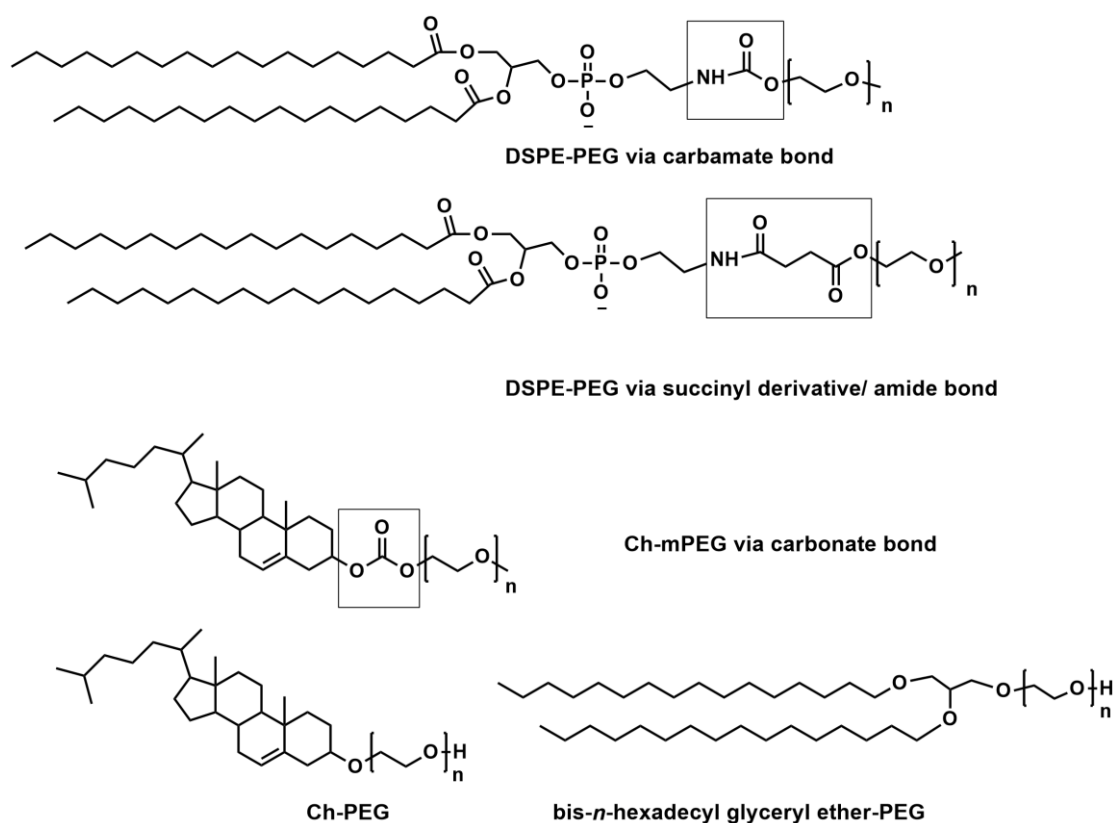
Figure 2: A selection of lipid-polymer conjugates for the incorporation into vesicle membranes to generate long-circulating "stealth" liposomes (DSPE= 1,2-Distearoyl-*sn*-glycero-3-phosphoethanolamine; Ch=cholesterol; PEG= poly(ethylene glycol); mPEG=methoxy poly(ethylene glycol)).

Several lipid-polymer conjugates consist of phospholipids, i.e. phosphatidyl ethanolamine (PE), which is coupled to methoxy poly(ethylene glycol) (mPEG) via carbamate or amide bond formation. Furthermore, cholesterol can be used as the hydrophobic anchor. Monomethoxy poly(ethylene glycol) can be coupled to cholesteryl chloroformate by a carbonate bond.[21] Our group also demonstrated an alternative method, which relies on aliphatic initiators, such as cholesterol or bis-*n*-hexadecyl glyceryl ether, for the ring-opening polymerization of ethylene oxide (EO). These syntheses are advantageous, since they do not require multiple reaction steps, coupling chemistry or laborious purification steps. Furthermore, the synthesized lipids contain a hydroxyl end group, which can be used for further functionalization.[22,23]

Clinical applications

Extensive studies on the biodistribution of liposomal formulations and improved pharmacokinetic behavior of "stealth" liposomes have been done in numerous clinical tests. The best known and commercially available liposomal anti-cancer treatment, doxorubicin, is sold under the name Doxil™. The following table (Table 1) shows a selection of conventional and PEGylated liposomes for clinical usage.

Table 1: Conventional and PEGylated liposomes in clinical usage: [9,21,24]

	Drug	Company	Product name	Indication
Conventional Liposomes	Doxorubicin	Elan	Myocet/ Evacet	Breast cancer
	Amphoterecin B	Astellas Pharma	Ambisome	Fungal infection
	Daunomycin	Gilead	DaunoXome	Kaposi's sarcoma
	Vincristine	Hana Biosciences	Marqibo	Non-Hodgkin's lymphoma
PEGylated Liposomes	Doxorubicin	Schering Plough	Doxil/ Caelyx	Kaposi's sarcoma, ovarian cancer
	Cisplatin	Regulon	Lipoplatin	Various cancer types
	Mitoxantone	Wyeth Lederle	Novantrone	Multiple sclerosis, prostate cancer, acute myeloid leukemia

Liposome stabilization: Alternatives to PEG

PEG attached to lipids in pharmaceutical formulations has been investigated intensely, and these system have shown the best performance in clinical studies to date. Nevertheless, alternatives are being studied, since there is the hope for improved performance in targeting, physicochemical properties, and biocompatibility. In a recent review by Schubert et al. the disadvantages of PEG, such as its non-biodegradability, the possible degradation under stress and potential toxic side-product, were highlighted. Furthermore, the authors mention the hypersensitivity found in some cases, indicated by an activation of the complement system by PEGylated liposomes. More studies on the mechanism and the influence of other factors are necessary. Additionally, it has to

be elucidated, whether other factors or the combination of several components lead to side effects.[25]

General requirements for an alternative to PEG are high water-solubility, i.e., hydrophilicity of the polymer, high biocompatibility, and flexibility of the respective chain.[9] Among non-biodegradable polymers poly(vinyl pyrrolidone) (PVP, commercially available) and poly(acryl amide) (PAA) have shown prolonged blood circulation times of coated liposomes *in vivo*.[26] Poly(2-oxazoline)s are studied intensely at present, since for this type of polymer similar behavior compared to PEG has been proven.[27] Figure 3 shows a selection of molecular structures of polymers currently considered for "stealth" liposome preparation.

poly(vinyl pyrrolidone)   poly(acryl amide)   poly(methyl oxazoline)   poly(ethylene glycol)
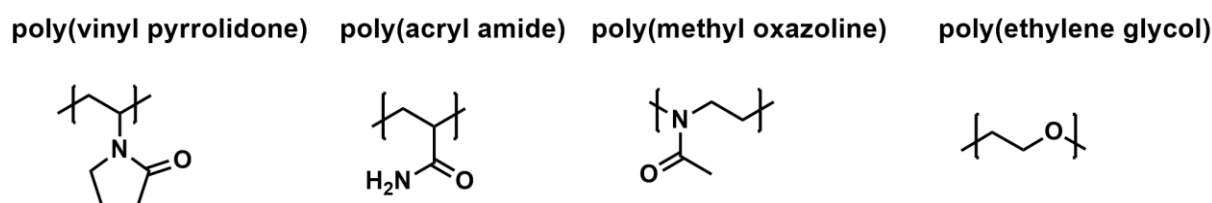
Figure 3: Molecular structures of polymers for "stealth" liposome preparation including poly(vinyl pyrrolidone), poly(acryl amide), poly(methyl oxazoline), and poly(ethylene glycol).

In general polyethers are interesting polymers in biomedical application. Not only linear poly(ethylene glycol), but also hyperbranched structures are promising with regard to their shielding behavior in drug delivery or liposome formulations. In fact, such systems have been used as hydrophilic shells, micelles or hydrogels.[28] Interestingly, surfaces covered with hyperbranched polyglycerol (*hb*PG) having a molecular weight around 1500-5000 g/mol showed slightly better protein repulsion than linear PEG. Presumably, the branched structure makes the polymer even more bulky, and more hydrophilic due to the high amount of hydroxyl groups, leading to a brush-like structure.[29, 30]

To date, there have been very few publications on "stealth" liposomes functionalized with polyglycerols. Maruyama et al. published the synthesis and investigation of dipalmitoylphosphatidyl polyglycerols (DPP-PG), which consisted of oligomeric linear polyglycerol (*l*PG) attached to the phospholipid via phospholipase D.[31] Effective shielding for diglycerol or tetraglycerol was observed upon using 8 mol% incorporation of the

polymer-conjugate, while octaglycerol only required 4 mol% for good performance with respect to circulation times. The best result was found for DPP-hexaglycerol, which prolonged the blood circulation time, when 6 mol% were incorporated. Interestingly, such PG oligomers displayed improved performance in relation to linear PEG. Usually, PEG chains with molecular weights between 1000-5000 g/mol are used for liposomal formulations, and around 5-8 mol% is necessary to generate a considerable "stealth" effect.

Polyether-based lipids: Multivalent architectures

Poly(ethylene glycol) (PEG) is the most widely studied polymer for the preparation of "stealth" liposomes, which is due to its outstanding properties as a shielding layer around the vesicular carriers. Its good biocompatibility, very low toxicity as well as immunogenicity, low cost and facile coupling chemistry to hydrophobic molecules render it attractive for biomedical applications. Furthermore, its flexibility and water solubility are crucial for *in vivo* applications.[32] However, as mentioned above, similar polyethers with different architectures exhibit the same or even better performance compared to PEG. In the following section we will highlight the recent work on polyether-based amphiphiles synthesized and characterized in our group.

Phospholipids are sensitive molecules that are not stable under the very basic conditions required for the polymerization of epoxides. In general, this polymerization is an anionic ring-opening polymerization (ROP) of ethylene oxide (EO). Since the labile phospholipids are excluded under these conditions, we looked for other biocompatible options, which led us to bisalkyl glyceryl ethers and cholesterol as suitable initiators for the polymerization. These two aliphatic molecules withstand the basic ring-opening conditions as well as acidic conditions used for the deprotection of other epoxide derivatives (see Figure 4). Using a combination of ethylene oxide (EO), ethoxyethyl glycidyl ether (EEGE), isopropylidene glycidyl glyceryl ether (IGG), and glycidol as an epoxide-based construction kit, a vast variety of linear and branched architectures becomes available. Among them are complex structures, such as linear-hyperbranched amphiphiles, which combine the advantageous properties of PEG and the

polyfunctionality of polyglycerol.[22, 33] This aspect is one of the most important improvements compared to conventional "stealth" liposomes: the additional hydroxyl groups increase water-solubility and provide the possibility for further functionalization, such as the attachment of markers (labeling), antibodies or targeting groups. Maximum biocompatibility is achieved by using cholesterol as the initiator and *hb*PG as a polymer with excellent biocompatibility.[28,34- 36]

Synthesis of multivalent architectures

The synthesis of multivalent lipids is described with cholesterol as an initiator, since the resulting polymer is expected to show very good biocompatibility. Cholesterol is a natural membrane component and also commercially available. In the lipid structures prepared, cholesterol can function as the membrane anchor.
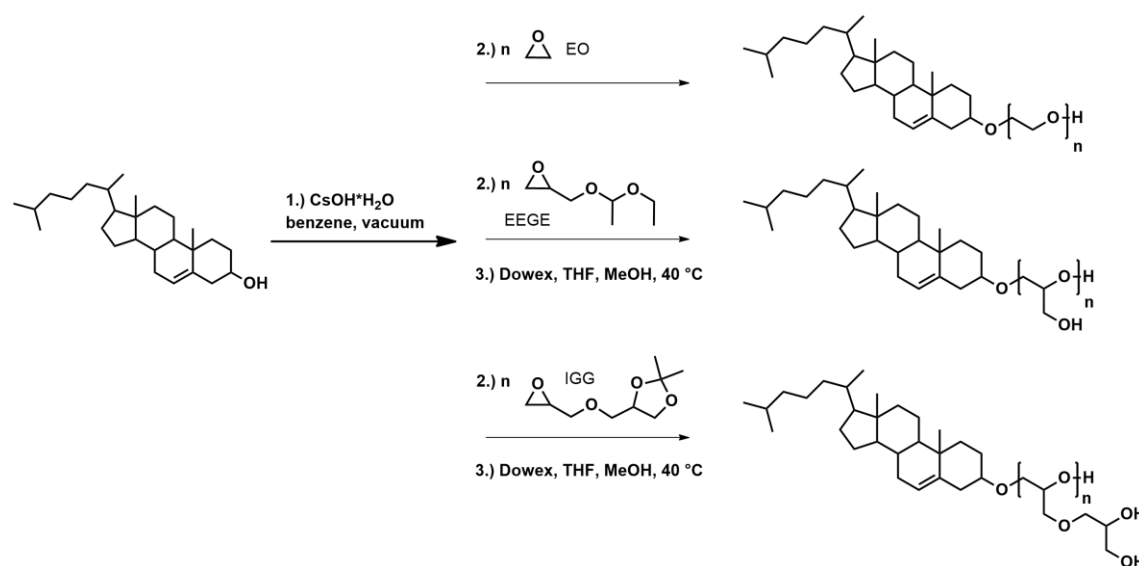
Figure 4: Reaction sequence for the synthesis of cholesterol initiated polyethers: Ch-PEG, Ch-*l*PG, Ch-*l*PGG.

The first step is the formation of the cholesterol alkoxides, which represent the initiator for the subsequent polymerization. The degree of deprotonation employed is 90% in the case of CsOH as the deprotonating agents. Due to the rapid proton exchange between cholesterol and the growing chain, almost 100% of the initiator molecules are incorporated into the resulting polyether amphiphile. To form the linear polymer,

ethylene oxide can be polymerized using the standard oxyanionic ring-opening polymerization technique.[37] In order to obtain linear polyglycerol, protected epoxide derivatives such as ethoxyethyl glycidyl ether (EEGE) or isopropylidene glycidyl glyceryl ether (IGG) can be used. Deprotection of the acetal groups leads to one (EEGE) or two (IGG) hydroxyl groups per monomer unit. Using this protocol, multifunctional, linear polyglycerol can be synthesized in a one-pot approach (Figure 4).

Using a two-step procedure, it is possible to tailor hyperbranched structures based on linear macroinitiators. Glycidol is polymerized by the ring-opening multibranching technique in a slow monomer addition step (Figure 5). The multihydroxy-precursor polymer is crucial for the "hypergrafting" of glycidol since excellent conditions and low polydispersities are required. Usually the degree of deprotonation is around 25%, which allows good control over the anion concentration and prevents homopolymerization of glycidol. For the slow monomer addition step a syringe pump is used, which adds the monomer in low concentration over a certain amount of time (around 18-24 h, depending on the batch size).
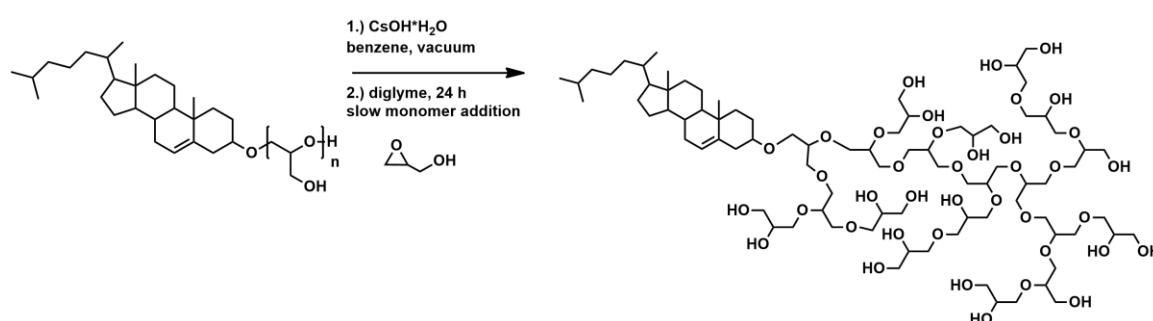
Figure 5: Reaction sequence for the synthesis of cholesterol initiated hyperbranched structures (Ch-*hb*PG).

Following the above mentioned reaction sequence, one can combine any epoxide derivative in the way of a molecular construction kit, permitting rapid access to polyfunctional lipids via ROP (see Figure 6). Random copolymerization allows for the synthesis of Ch-PEG-*co*-PGG or Ch-PEG-*co*-*l*PG using EO and IGG or EEGE, respectively. Additionally, linear hyperbranched structures are available via the ROP of ethylene oxide followed by EEGE or IGG, the deprotection step and subsequent slow monomer addition of glycidol onto the macroinitiator polymer. The resulting architectures show low to moderate polydispersities (PDI= 1.1-1.6) and can be characterized by size exclusion

chromatography (SEC), NMR spectroscopy or matrix assisted laser desorption/ionization time-of-flight mass spectrometry (MALDI-ToF MS). Furthermore, the critical micelle concentration (CMC) was determined to be in the range of 1.4-40.7 mg/L, depending on the molecular structure.[33]
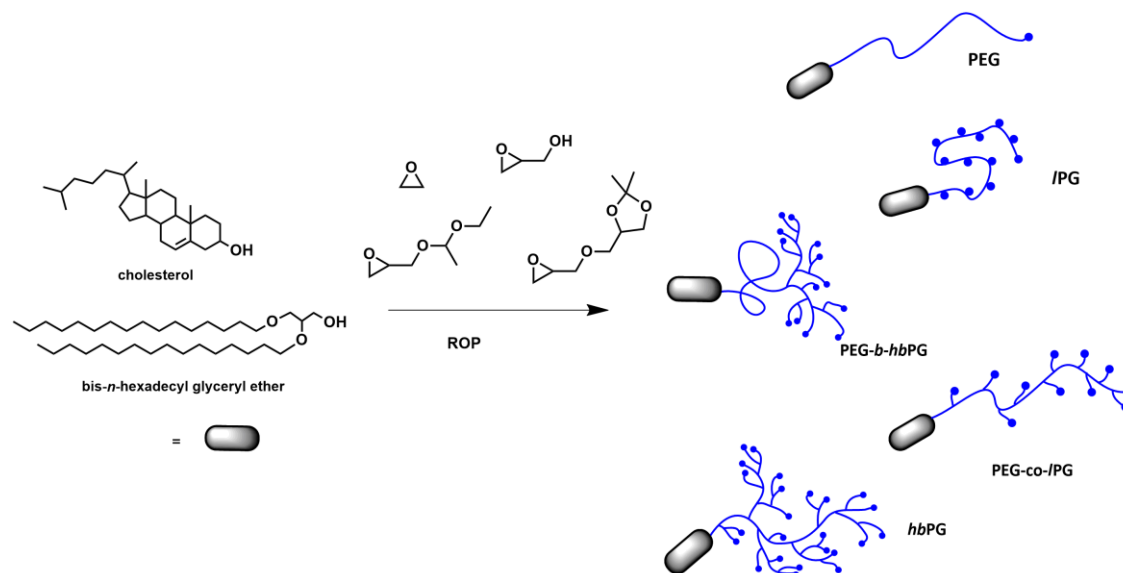
Figure 6: Possible lipid architectures available by using EO, EEGE, IGG, and glycidol for the ring-opening polymerization initiated by either cholesterol or bis-*n*-hexadecyl glyceryl ether.

In a recent work by Kressler et al. the linear poly(ethylene glycol)$_{30}$-*b*-*hb*PG$_{24}$ copolymer was investigated in mixed layers with 1,2-dipalmitoyl-*sn*-glycero-3-phosphocholine (DPPC). In adsorption measurements it was demonstrated that an intense affinity of the amphiphilic block copolymer to DPPC is given after the injection of the polymer into the water subphase. The surface pressure was determined to be 48.2 mN/m, showing the fast penetration of the hydrophobic cholesterol into the lipid monolayer, as well as good interaction with DPPC. Figure 7 shows the DPPC monolayer at the air-water interface with the amphiphilic polymer, which is attached to the lipid layer via its cholesterol moiety.[38]
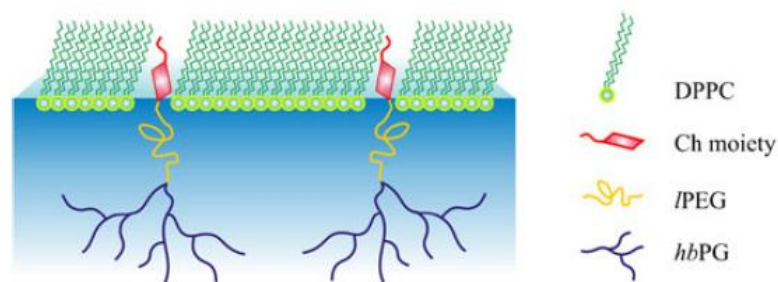
Figure 7: DPPC monolayer and adsorbed cholesterol moiety of Ch-PEG-*hb*PG to the air-water interface. (Reproduced with permission from reference 38. Copyright 2012 Springer Verlag.)

Several multifunctional polymers have been synthesized, showing generally good adsorption behavior at DPPC monolayers. In future works, the properties in liposomal formulations *in vivo* will be studied. These novel coatings combine the advantages of PEG as well as PG and might increase liposome stability. Furthermore, it is important to target the vesicles, which can be easily accomplished by the functionalization of peripheral hydroxyl groups. Model reactions, such as the attachment of the dye rhodamine B by click chemistry demonstrated the utility of the branched structure.[33] The performance in blood serum is currently under investigation, and further experiments *in vivo* will be carried out in the near future.

Liposome destabilization: pH-sensitive lipids with an acid-labile moiety

Acid-sensitive PEG amphiphiles, such as lipids, have attracted considerable attention in biomedical applications, since controlled destabilization of liposomes is necessary for the release of the drug incorporated in the vesicular transporter. Those "stealth" systems are usually stable at neutral pH, which translates to stability during the circulation in the body, whereas destabilization is needed for the fusion with membranes or the escape from endosomal vesicles.[39] The fusion and the release of the drug in slightly acidic tissue, such as tumor tissue or inflammatory tissues, can be realized with pH-sensitive PEG coated liposomes, where the protecting shell can be shed

at a pH around 6.5 for tumor tissues. One major advantage is that no external stimulus is required for triggering the drug release.

In this section we would like to focus on acid-sensitive PEG lipid analogs that have been used for liposome preparation. Furthermore, we present very recent work that has been carried out in our group, which is based on an acid-labile cholesterol derivative as the initiator for the ring-opening polymerization of ethylene oxide.

Different approaches have been developed to tune the pH-sensitivity of the polymer shell around nanoparticles or liposomes. Recently, Clawson et al. have published the synthesis and characterization of lipid-polymer hybrid nanoparticles with a PEG shell that sheds under acidic conditions. They used a lipid-(succinate)-mPEG as the amphiphilic polymer, which was synthesized via the coupling of 1,2-dipalmitoyl-*sn*-glycer-3-phospho(ethylene glycol) and methoxy poly(ethylene glycol), endfunctionalized with succinate prior to the coupling step.[40]

In 2003 an acid-labile poly(ethylene glycol) PEG-conjugated lipid, (*R*)-1,2-di-*O*-(1'*Z*,9'*Z*-octadecadienyl)-glyceryl-3-(ω-methoxy-poly(ethylene glycolate, MW5000) (BVEP), was synthesized and mixed with 1,2-dioleoyl-*sn*-glycero-3-phosphoethanolamine (DOPE) in liposomes to investigate destabilization and membrane-membrane fusion after acid-catalyzed hydrolysis of the vinyl ether linkages. The research group showed that PEG removal occurred after hydrolysis, but that it resulted in undesired payload leakage and liposome collapse as well.[41]

Using cholesterol as the lipophilic part, Boomer et al. presented a six-step synthesis for the preparation of cholesterol-vinyl ether-PEG conjugates (CVEP), which degraded under mildly lowered pH values. Cleavage resulted in PEG removal, leading to content release and thus an increased bioavailability of a potent drug.[42]

In our group a cholesterol derivative was used directly as the initiator for the ring-opening polymerization of ethylene oxide (EO).[43] The addition of the steroid (**1**) to 2-acetoxyethyl vinyl ether (AcVE, **2**) was carried out in dichloromethane, catalyzed by *p*-toluene sulfonic acid, leading to acetoxyethyl 1-(cholesteryloxy)ethyl ether (**3**). The advantages of AcVE are the following: The acetate group can be used as a protection group and is removed under basic conditions with little effort, leading to glycol 1-(cholesteryloxy)ethyl ether (**4**). Hence, the hydroxyl group, which is important for the oxyanionic polymerization, is liberated easily. This group is used as an alkoxide after

deprotonation and is structurally related to the growing chain end, which results in good initiation kinetics. Hence, it was possible to synthesize a scissile initiator for the polymerization of EO in three steps (Figure 8). The polymer (**5**) was characterized by NMR spectroscopy, SEC, and MALDI-ToF MS.
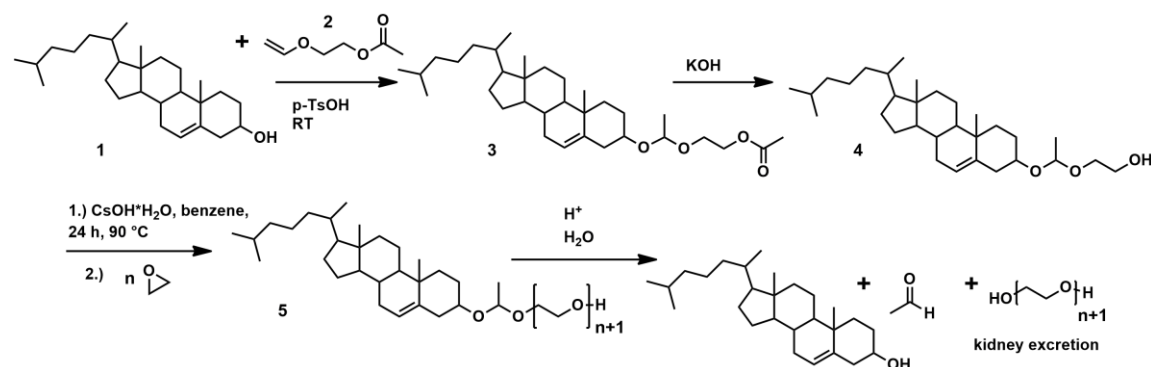
Figure 8: Synthesis of the pH-sensitive cholesterol derivative for the initiation of ethylene oxide.

The insertion of such a scissile hydrophobic unit leads to responsive materials that are cleaved under acidic condition leading to a loss of their amphiphilicity. This is a desired feature, when it comes to destabilizing the "stealth" liposomes.

Acid-sensitivity was demonstrated as a proof of principle in a UV-Vis spectrometer. An aqueous solution of the scissile lipid analog was acidified by adding hydrochloric acid. After a while the solutions turned turbid, as the released cholesterol precipitated and the transmission began to decrease. Almost all light was scattered in the end, due to cholesterol precipitation. As expected, cholesterol was released faster at higher reaction temperature (T=25 °C vs. T=37 °C), as indicated by the shorter initial phase and more negative slope of the trace. To confirm complete removal of the steroid, a similar experiment was performed with the scissile cholesteryl PEG, in which the precipitated cholesterol and the aqueous solution were separated and ^{1}H NMR spectra were recorded. A clean cholesterol spectrum was obtained, whereas the aqueous phase exhibited pure PEG diol. Hence, the cholesteryl initiator was released completely under these reaction conditions.

This system represents a novel approach towards cleavable amphiphiles, which are promising for "stealth" liposome preparation. One acid-sensitive moiety can be cleaved resulting in biocompatible cholesterol and PEG, respectively. The molecular weight of

the PEG polymer chain is typically around 2000-5000 g/mol, so the polymer is small enough to be excreted by the kidney and be eliminated from the body.

We believe this approach to be promising in shedding the protecting layer, and thus destabilizing liposomes at the site of action, where lower pH-values are present. Further studies are planned to synthesize acid-cleavable, hyperbranched lipids for multifunctional liposomes.

Conclusion

Many approaches have been made in the development of effective drug delivery systems, especially in the field of liposomes. The vesicles used as a transporter for hydrophilic or hydrophobic drugs suffered from several disadvantages such as low stability and low circulation times *in vivo*. One of the biggest steps towards long-circulating liposomes was the incorporation of a biocompatible, water-soluble polymer, such as poly(ethylene glycol) (PEG). The improved performance of the liposomal formulation resulted from the stabilizing polymer shell around the vesicle, which protects the drug carrier and additionally prevents opsonin adsorption. These unique properties lead to reduced blood clearance and hence prolonged blood circulation times. Additionally, the enhanced permeability and retention effect (EPR) helps to increase drug concentration at the site of action. It is no surprise that liposomal formulations, with or without a polymer shell, are used in clinical applications, especially in cancer treatment, due to their outstanding pharmacokinetics.

PEG coated liposomes, so-called "stealth" liposomes are applied in various treatments such as Kaposi's sarcoma, breast cancer or fungal infections. Nevertheless, new synthetic polymers offer various advantages that may further enhance the applicability of "stealth" liposomes. Among these are biodegradability and multifunctionality, which is important for the attachment of markers and targeting moieties. In this context we presented new polymeric amphiphiles based on poly(ethylene glycol) and polyglycerol (linear and hyperbranched) that represent a new class of multifunctional lipid analogs with various architectures. The multiple hydroxyl groups increase aqueous solubility of the polymer and offer the possibility for effective targeting through further

functionalization. In addition, the degradability of acid-sensitive Ch-PEG polymers was discussed, in contrast to chemically inert PEG, resulting in possible destabilization of the "stealth" liposome in the acidic tumor tissue or acidic endosomes. The desired destabilization is still one of the key tasks that remain problematic in liposome research. Regarding the advantages of the hyperbranched lipids, we believe that this class of lipids is promising with respect to drug delivery and "stealth" components. Investigations on the stealth effect *in vivo*, as well as monolayer studies, are currently examined.

References

1.	Sharma, A.; Sharma, U. S., *Int. J. Pharm.* **1997,** *154* (2), 123-140.
2.	Lian, T.; Ho, R. J. Y., *J. Pharm. Sci.* **2001,** *90* (6), 667-680.
3.	Lasic, D.; Papahadjopoulos, D., *Science* **1995,** *267* (5202), 1275-1276.
4.	Allen, T. M.; Chonn, A., *FEBS Lett.* **1987,** *223* (1), 42-46.
5.	Woodle, M. C.; Lasic, D. D., *Biochim. Biophys. Acta* **1992,** *1113* (2), 171-199.
6.	Woodle, M. C.; Matthay, K. K.; Newman, M. S.; Hidayat, J. E.; Collins, L. R.; Redemann, C.; Martin, F. J.; Papahadjopoulos, D., *Biochim. Biophys. Acta* **1992,** *1105* (2), 193-200.
7.	Torchilin, V. P.; Omelyanenko, V. G.; Papisov, M. I.; Bogdanov, A. A.; Trubetskoy, V. S.; Herron, J. N.; Gentry, C. A., *Biochim. Biophys. Acta, Biomembr.* **1994,** *1195* (1), 11-20.
8.	Blume, G.; Cevc, G., *Biochim. Biophys. Acta, Biomembr.* **1990,** *1029* (1), 91-97.
9.	Immordino, M. L.; Dosio, F.; Cattel, L., Int. J. Nanomed. **2006,** *1* (3), 297-315.
10.	Owens, D. E.; Peppas, N. A., *Int. J. Pharm.* **2006,** *307* (1), 93-102.
11.	Harashima, H.; Sakata, K.; Funato, K.; Kiwada, H., *Pharm. Res.* **1994,** *11* (3), 402-406.
12.	Lee, K. D.; Hong, K.; Papahadjopoulos, D., *Biochim. Biophys. Acta* **1992,** *1103* (2), 185-197.
13.	Gabizon, A.; Papahadjopoulos, D., *Biochim. Biophys. Acta* **1992,** *1103* (1), 94-100.
14.	Massing, U.; Cicko, S.; Ziroli, V., *J. Controlled Release* **2008,** *125* (1), 16-24.
15.	Hirsch, M.; Ziroli, V.; Helm, M.; Massing, U., *J. Controlled Release* **2009,** *135* (1), 80-88.
16.	Klibanov, A. L.; Maruyama, K.; Torchilin, V. P.; Huang, L., *FEBS Lett.* **1990,** *268* (1), 235-237.
17.	Senior, J.; Delgado, C.; Fisher, D.; Tilcock, C.; Gregoriadis, G., *Biochim. Biophys. Acta, Biomembr*. **1991,** *1062* (1), 77-82.
18.	Papahadjopoulos, D.; Allen, T. M.; Gabizon, A.; Mayhew, E.; Matthay, K.; Huang, S. K.; Lee, K. D.; Woodle, M. C.; Lasic, D. D.; Redemann, C.; Martin, F. J., *Proc. Natl. Acad. Sci. U. S. A.* **1991,** *88* (24), 11460-11464.
19.	Stathopoulos, G. P.; Boulikas, T.; Vougiouka, M.; Deliconstantinos, G.; Rigatos, S.; Darli, E.; Viliotou, V.; Stathopoulos, J. G., *Oncol. Rep.* **2005,** *13* (4), 589-595.
20.	Allen, T. M.; Hansen, C.; Martin, F.; Redemann, C.; Yau-Young, A., *Biochim. Biophys. Acta, Biomembr.* **1991,** *1066* (1), 29-36.
21.	Zhao, X. B.; Muthusamy, N.; Byrd, J. C.; Lee, R. J., *J. Pharm. Sci.* **2007,** *96* (9), 2424-2435.
22.	Hofmann, A. M.; Wurm, F.; Hühn, E.; Nawroth, T.; Langguth, P.; Frey, H., *Biomacromolecules* **2010,** *11* (3), 568-574.
23.	Reuter, S.; Hofmann, A. M.; Busse, K.; Frey, H.; Kressler, J., *Langmuir* **2010,** *27* (5), 1978-1989.
24.	Torchilin, V. P., *Nat. Rev. Drug Discov.* **2005,** *4* (2), 145-160.
25.	Knop, K.; Hoogenboom, R.; Fischer, D.; Schubert, U. S., Angew. Chem., Int. Ed. **2010,** *49* (36), 6288-6308.
26.	Torchilin, V. P.; Shtilman, M. I.; Trubetskoy, V. S.; Whiteman, K.; Milstein, A. M., *Biochim. Biophys. Acta, Biomembr.* **1994,** *1195* (1), 181-184.

27.   Zalipsky, S.; Hansen, C. B.; Oaks, J. M.; Allen, T. M., *J. Pharm. Sci.* **1996,** *85* (2), 133-137.

28.   Calderon, M.; Quadir, M. A.; Sharma, S. K.; Haag, R., *Adv. Mater.* **2010,** *22* (2), 190-218.

29.   Siegers, C.; Biesalski, M.; Haag, R., *Chemistry - A European Journal* **2004,** *10* (11), 2831-2838.

30.   Kainthan, R. K.; Zou, Y.; Chiao, M.; Kizhakkedathu, J. N., *Langmuir* **2008,** *24* (9), 4907-4916.

31.   Maruyama, K.; Okuizumi, S.; Ishida, O.; Yamauchi, H.; Kikuchi, H.; Iwatsuru, M., *Int. J. Pharm.* **1994,** *111* (1), 103-107.

32.   Roberts, M. J.; Bentley, M. D.; Harris, J. M., *Advanced Drug Delivery Reviews* **2002,** *54* (4), 459-476.

33.   Hofmann, A. M.; Wurm, F.; Frey, H., *Macromolecules* **2011,** *44* (12), 4648-4657.

34.   Wilms, D.; Wurm, F.; Nieberle, J.; Boehm, P.; Kemmer-Jonas, U.; Frey, H., *Macromolecules* **2009,** *42* (9), 3230-3236.

35.   Wilms, D.; Stiriba, S.-E.; Frey, H., *Acc. Chem. Res.* **2010,** *43* (1), 129-141.

36.   Kainthan, R. K.; Gnanamani, M.; Ganguli, M.; Ghosh, T.; Brooks, D. E.; Maiti, S.; Kizhakkedathu, J. N., *Biomaterials* **2006,** *27* (31), 5377-5390.

37.   Mangold, C.; Wurm, F.; Frey, H., *Polymer Chemistry* **2012,** *3* (7), 1714-1721.

38.   Peng, X.; Hofmann, A.; Reuter, S.; Frey, H.; Kressler, J., *Colloid. Polym. Sci.* **2012,** *290* (7), 579-588.

39.   Hong, R. L.; Huang, C. J.; Tseng, Y. L.; Pang, V. F.; Chen, S. T.; Liu, J. J.; Chang, F. H., *Clinical Cancer Research* **1999,** *5* (11), 3645-3652.

40.   Clawson, C.; Ton, L.; Aryal, S.; Fu, V.; Esener, S.; Zhang, L., *Langmuir* **2011**, *27* (17), 10556-10561.

41.   Boomer, J. A.; Inerowicz, H. D.; Zhang, Z. Y.; Bergstrand, N.; Edwards, K.; Kim, J. M.; Thompson, D. H., *Langmuir* **2003,** *19* (16), 6408-6415.

42.   Boomer, J. A.; Qualls, M. M.; Inerowicz, H. D.; Haynes, R. H.; Patri, V. S.; Kim, J.-M.; Thompson, D. H., *Bioconjugate Chem.* **2009,** *20* (1), 47-59.

43.   Dingels, C.; Müller, S.S.; Steinbach, T.; Tonhauser, C.; Frey, H., *Biomacromolecules*, **2013**, *14* (2), 448-459.

1.2 Beyond Poly(ethylene glycol): Linear Polyglycerol as a Multifunctional Polyether for Biomedical Applications
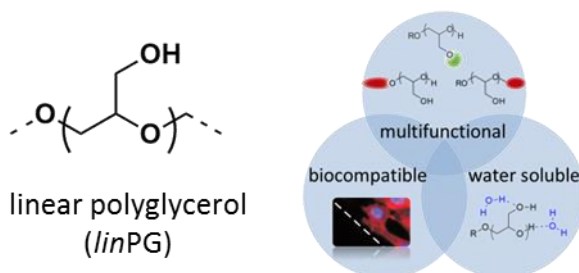
Anja Thomas,[†,§] Sophie S. Müller,[†,§] and Holger Frey*,[†]

[†]Institute of Organic Chemistry, Johannes Gutenberg-University Mainz, Duesbergweg 10-14, 55128 Mainz

[‡]Graduate School Materials Science in Mainz, Staudingerweg 9, 55128 Mainz

[§] both authors contributed equally

linear polyglycerol
(*lin*PG)

Abstract

Polyglycerols (sometimes also called "polyglycidols") represent a class of highly biocompatible and multihydroxy-functional polymers that may be considered as a multifunctional analogue of poly(ethylene glycol) (PEG). Various architectures based on a polyglycerol scaffold are feasible depending on the monomer employed. While polymerization of glycidol leads to hyperbranched polyglycerols, the precisely defined linear analogue is obtained by using suitably protected glycidol as a monomer, followed by removal of the protective group in a postpolymerization step. This review summarizes the properties and synthetic approaches toward linear polyglycerols (*lin*PG), which are at present mainly based on the application of ethoxyethyl glycidyl ether (EEGE) as an acetal-protected glycidol derivative. Particular emphasis is placed on the manifold functionalization strategies including, *e.g.*, the synthesis of end-functional *lin*PGs or multiheterofunctional modifications at the polyether backbone. Potential

applications like bioconjugation and utilization as a component in degradable biomaterials or for diagnostics, in which polyglycerol acts as a promising PEG substitute are discussed. In the last section, the important role of linear polyglycerol as a macroinitiator or as a highly hydrophilic segment in block co- or terpolymers is highlighted.

1. Introduction

Poly(ethylene glycol) (PEG) is employed in a vast range of areas, including detergents, cosmetics, paper coating, polyurethanes, textile modification, construction chemistry, and for an immense variety of pharmaceutical applications.[1] The reason for this exceptionally broad establishment in so many fields of application lies in the unique properties of PEG.[2-4] Different from most other synthetic polymers, PEG is soluble in both water and in a variety of organic solvents. PEG is highly biocompatible, nontoxic, shows hardly any immunogenicity and possesses antifouling properties. Once conjugated to a drug or protein (PEGylation),[5-7] PEG imparts a pronounced "stealth" effect and leads to an increase in the hydrodynamic radius of the respective hybrid structure, thereby drastically improving pharmacokinetics. However, some drawbacks need to be mentioned: (i) as a linear polyether, PEG only bears a maximum of two functional groups, which limits possibilities for derivatization, *e.g.*, for the attachment of targeting or imaging residues; (ii) oligo(ethylene glycol)s up to a molecular weight of 400 g·mol^{-1} have been found to be toxic due to enzyme-catalyzed oxidation processes; (iii) possible hypersensitivity reactions are controversially discussed for PEG conjugated drugs at present and (iv) there are some reports about the complement activation by different molecular weight PEGs as well as rapid clearance from the bloodstream after repetitive injection of PEGylated liposomes.[3]

In recent years, polyglycerols (also known as "polyglycidols") are increasingly recognized as a structurally similar, albeit multihydroxy-functional alternative to conventional PEG (Figure 1).
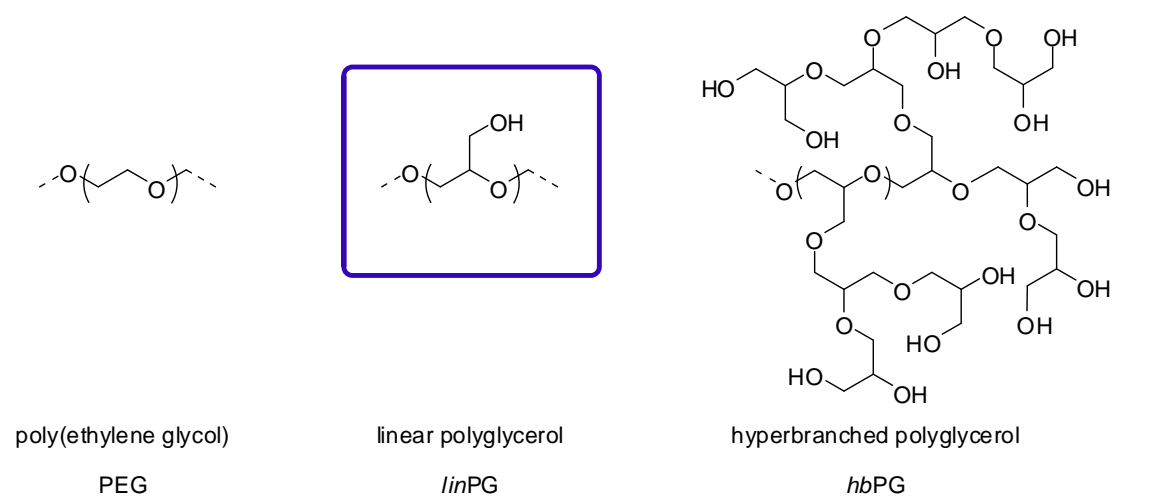
Figure 1. Chemical structures of poly(ethylene glycol) (PEG), linear polyglycerol (*lin*PG) and hyperbranched polyglycerol (*hb*PG). This review focuses on synthetic procedures, functionalization possibilities and potential applications of *lin*PG (middle).

It is a remarkable feature of the chemistry of glycidol and its protected derivatives that a plethora of different architectures ranging from linear to hyperbranched or even more complex structures are accessible, depending on the monomer and synthetic strategy applied. By using glycidol as a latent AB$_2$ monomer, hyperbranched polyglycerol scaffolds can be obtained *via* cationic or anionic polymerization. The synthetic pathways and properties of hyperbranched polyether polyols like polyglycerol (*hb*PG) have recently been reviewed in depth.[8-10] The branching reaction of glycidol during the polymerization process can be effectively prevented by protecting the hydroxyl function. This strategy gives access to versatile and precisely defined architectures from linear structures to comb-like or even more complex structural designs (Figure 2).

In contrast to *hb*PG, the application of protected glycidol monomers allows the incorporation of exactly one discrete end-functionality, while for *hb*PG the number of *in-chain* functional groups usually only averages the targeted value. In this context, some peculiar aspects concerning linear polyglycerol (*lin*PG) have recently been highlighted.[3, 4, 11, 12] In this review article, we aim at a comprehensive summary of the state of the art in this area.

Compared to PEG, the resulting water-soluble *lin*PG exhibits a similar or even slightly superior biocompatibility profile.[13-15] No significant effects on coagulation, complement

activation or cell viability have been observed to date. In fact, esters of oligoglycerols with a degree of polymerization up to 10 and considerable polydispersity both in molecular weight and structure were approved by the American Food and Drug Administration (FDA) as food and pharmaceutical additives and have been used for these purposes for several decades.[3, 16]

Antifouling properties of *lin*PGs employed for surface modification were intensively studied by Haag and co-workers and were found to be similar to PEG. The authors demonstrate that the adsorption of proteins, cells, or bacterial strains (compare Figure 3) significantly decreases with increasing degree of polymerization of *lin*PGs (DP_n = 10 or 16) or poly(glycidyl methyl ether) (P(GME)) (DP_n = 6, 10, or 16) as the fully methylated analogue attached to a model surface.[17-19] A minimum molecular weight of around 1000 g·mol^{-1} of the polyglycerol derivatives is described to provide efficient biorepellent properties.[18] Computational entropy estimations for PEG, *lin*PG, and P(GME) were suggested by the authors to give insight into the underlying protein repellent mechanism.[20] The studies revealed a slightly higher flexibility of PEG chains compared to *lin*PG or P(GME). Unfortunately, no significant conclusion could be drawn, as to whether an interfacial water layer or chain flexibility of the polymers attached determines the degree of protein resistance.
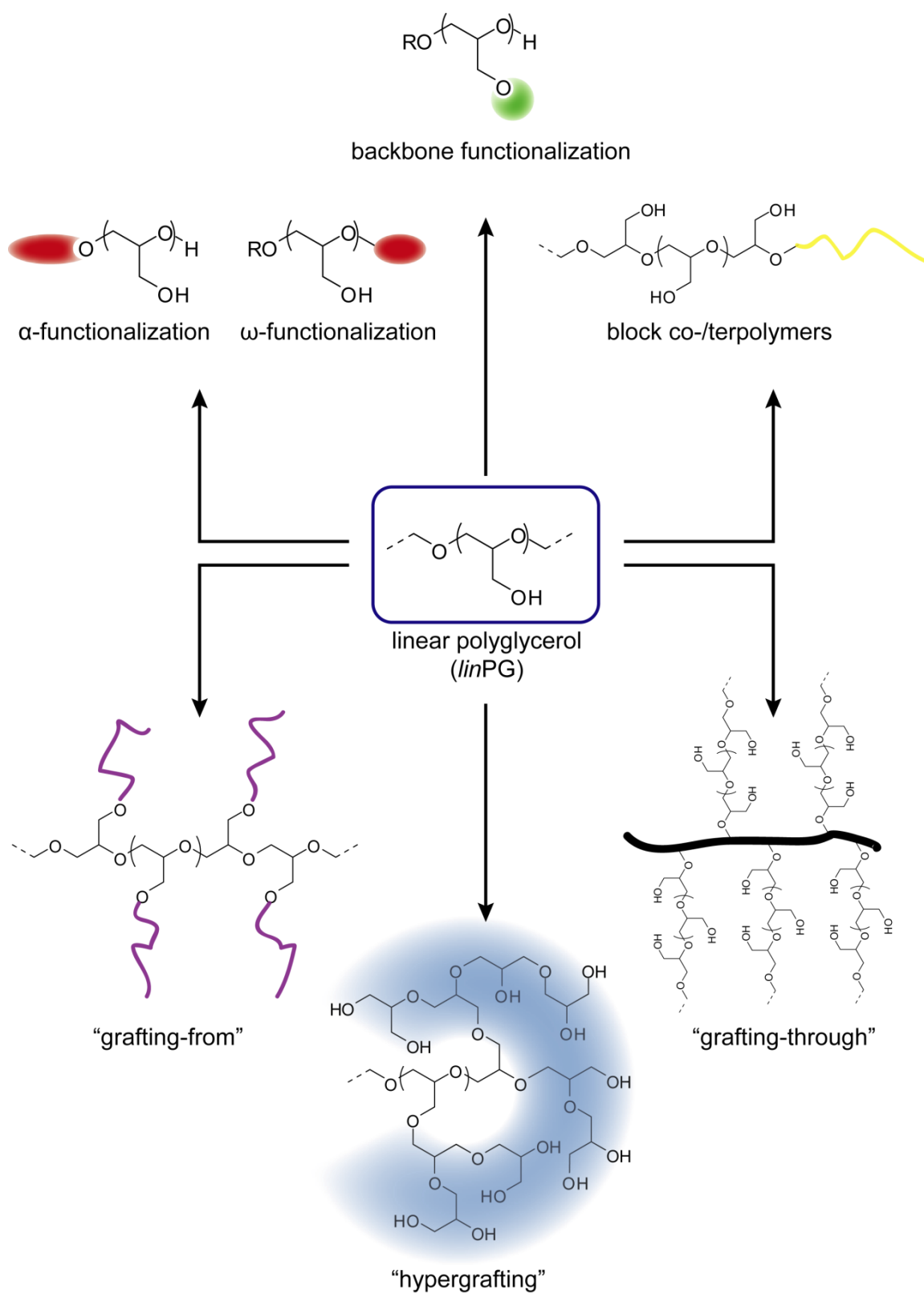
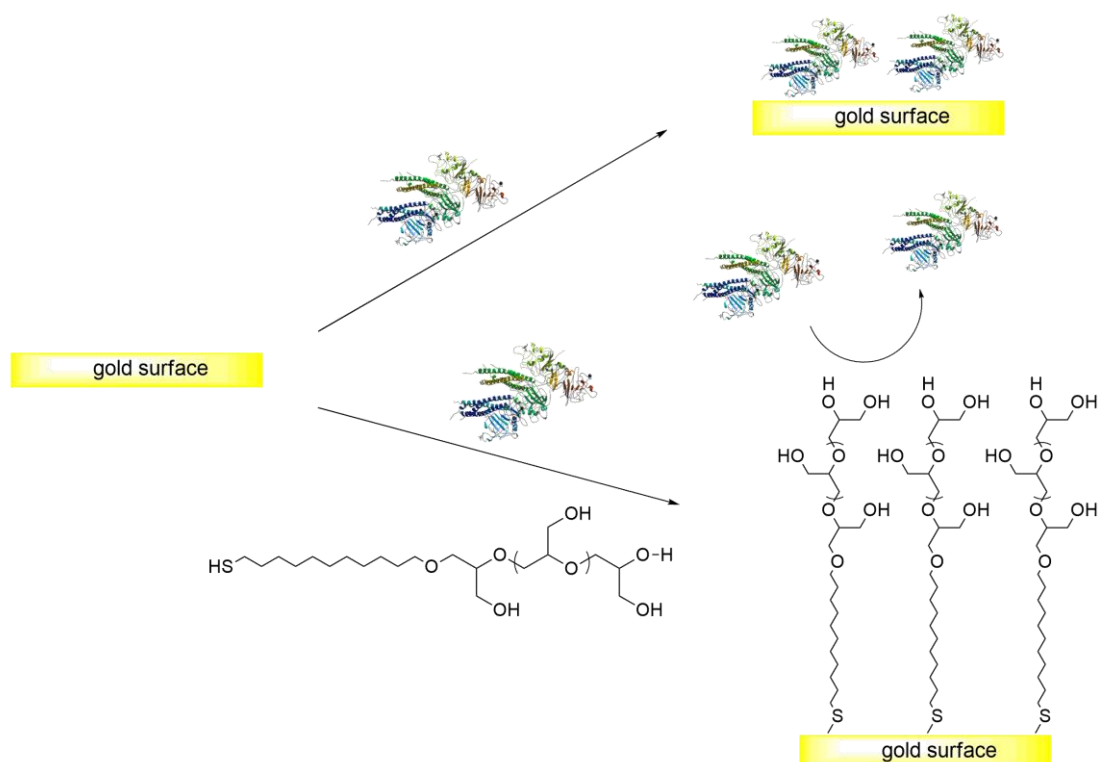*Figure 2.* Overview of the vast topological variety available based on *lin*PG building blocks.

Figure 3. Protein adhesion and antifouling properties of linear polyglycerol on a PG-model surface.

Although the chemical structures of PEG and *lin*PG are quite similar (Figure 1), the thermal properties of the linear polyethers differ drastically. PEG is a highly crystalline material with melting points up to about 63 °C for elevated molecular weights > 20.000 g·mol^{-1}.[1, 21] In contrast, the dense packing of the polyether chains is disturbed for *lin*PG due to the additional hydroxyl group per monomer unit, and the atactic nature of the polymer resulting in (highly) viscous and amorphous structures. It is interesting to note that studies on the synthesis of *lin*PGs with controlled stereochemistry and tacticity have only been sparsely reported in the literature,[22, 23] rendering this an almost neglected field at present. Glass transition temperatures (T_g) ranging from -8 °C to -27 °C for varying molecular weights have been mentioned occasionally,[23-26] however, it is surprising to note that no systematic investigation of the influence of molecular weight and initiator on the thermal properties of *lin*PG has been published to date. A slightly higher thermal and oxidative stability has been claimed for hyperbranched polyglycerols in comparison to PEG.[27] For *lin*PG, studies on the thermal degradation are rare, with the degradation of a single sample being reported to start at temperatures exceeding 250 °C.[25]

Although PEG is water-soluble in a broad temperature range, thermoresponsive behavior is observed at elevated temperatures, depending on molecular weight and concentration.[28] In the case of *lin*PGs, a lower critical solution temperature (LCST) can be induced by hydrophobic modification of the hydroxyl groups. Examples for this kind of derivatization are given in section 3.3.1.

2. Synthetic Strategies for *lin*PG

Ethylene oxide (EO) as the monomer of choice for the synthesis of PEG is industrially prepared on a large scale by epoxidation of ethene. Therefore, one major advantage of PEG is its commercial availability in a broad range of molecular weights that permits to tailor properties such as solubility and melting point for a specific application. For *lin*PGs, at present only the low molecular weight oligomers diglycerol and triglycerol can be purchased, however, usually containing cyclic or branched components. *Lin*PGs can be prepared from protected glycidol derivatives (glycidyl ethers) *via* oxyanionic ring-opening polymerization. The commonly applied glycidyl ethers are liquids, which renders the experimental procedure more facile compared to the use of the gaseous and highly toxic EO. The most commonly used monomers for the synthesis of *lin*PG are illustrated in Figure 4.

trimethylsilyl glycidyl ether	ethoxyethyl glycidyl ether	*tert*-butyl glycidyl ether	allyl glycidyl ether	isopropylidene glyceryl glycidyl ether
TMSGE	EEGE	*t*BGE	AGE	IGG
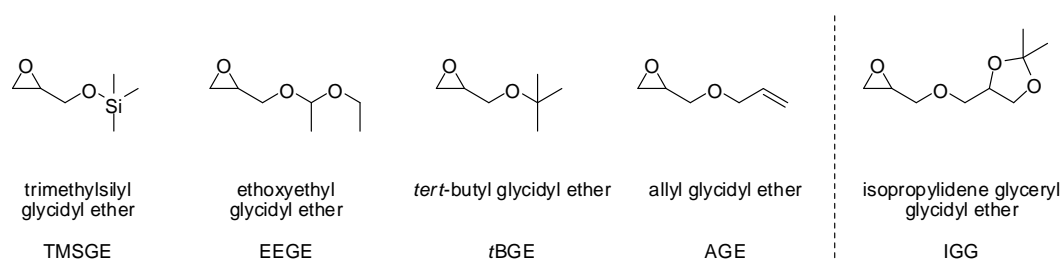
Figure 4. Typical monomers for the synthesis of linear polyglycerol (*lin*PG) structures.

While the monomers trimethylsilyl glycidyl ether (TMSGE), ethoxyethyl glycidyl ether (EEGE), *tert*-butyl glycidyl ether (*t*BGE), and allyl glycidyl ether (AGE) lead to linear polyglycerols after deprotection, isopropylidene glyceryl glycidyl ether (IGG)[30] (Figure 4, right) provides linear polyglycerols with additional pendant glycerols in each repeating unit, poly(glyceryl glycerol), offering additional options for functionalization.

Although *t*BGE and AGE are commercially available, EEGE is most frequently used for the preparation of linear PG due to the facile removal of the acetal protecting group under mild acidic conditions. EEGE can be prepared as described by Fitton *et al.*[29] by the reaction of glycidol and ethyl vinyl ether. IGG,[30] recently introduced by our group, gives access to interesting linear polyglycerol structures with pendant glycerol units providing vicinal 1,2-diols after removal of the acetonide protecting group. Typical polymerization procedures and general mechanisms for epoxide polymerization have recently been summarized in an excellent review by Carlotti *et al.*.[31] Therefore, only synthetic strategies applicable to the synthesis of *lin*PG will be discussed in this review.

First attempts to obtain *lin*PG were reported already in 1968, using mainly TMSGE or *t*BGE as monomers.[22, 23, 32-34] In particular, the polymerization of TMSGE has been studied to a large extent. While under base catalysis only low molecular weight oligomers were obtained due to the instability of the TMS protecting group, coordination polymerization led to higher molecular weight polymers. However, control of the molecular weight was not possible using coordination-type initiators. In groundbreaking work, Taton *et al.* reported the first successful anionic ring-opening polymerization of EEGE with molecular weights up to $\approx$ 30 000 g·mol^{-1} (M_w/M_n = 1.38 – 1.89 for CsOH as initiator).[35] Using potassium or cesium alkoxides as initiators for the polymerization of EEGE, Dworak *et al.* synthesized a series of well-defined *lin*PGs with narrow polydispersities (M_w/M_n < 1.20).[36, 37] Starting from the as-synthesized *lin*PG, they were also able to prepare advanced high molecular weight (M_n > 1 800 000 g·mol^{-1}) graft on graft structures by repeating sequential grafting cycles consisting of deprotonation, polymerization of EEGE and removal of protecting groups.[38] Expanding this work, Möller and co-workers described the synthesis of star-shaped *lin*PGs by using di(trimethylol propane) as a multifunctional initiator for the polymerization of EEGE.[39] These increasingly complex architectures will be further discussed in section 4.

To date, several low molecular weight initiators including potassium *tert*-butoxide (*t*-BuOK),[36, 37, 40, 41] potassium 3-phenyl propanolate (PPOK),[39, 41, 42] alkoxy ethanolates,[43, 44] potassium methoxide (MeOK)[43, 45] or BuLi/phosphazene base (Li$^+$/*t*-BuP$_4$)[41] have been successfully applied to polymerize EEGE in a controlled manner (Scheme 1).
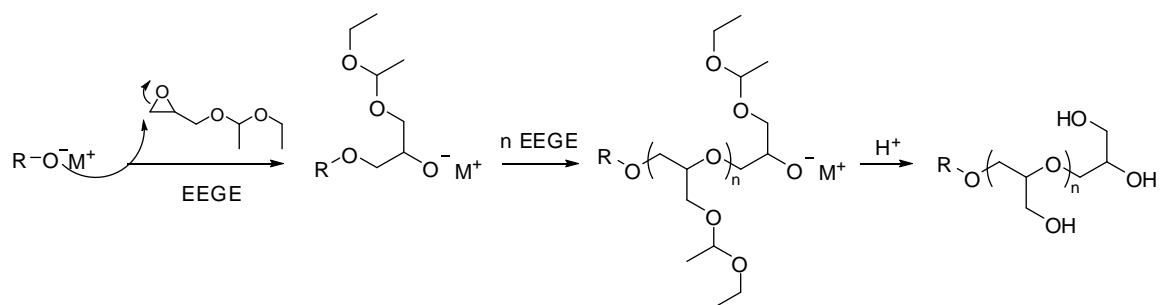
Scheme 1. Anionic ring-opening polymerization of EEGE followed by acidic deprotection of the acetal protecting group.

In an interesting work by Möller, Keul *et al*. homo- and random copolymers of EEGE, *t*BGE and AGE have been prepared by anionic ring-opening polymerization, and the authors studied selective removal of the protecting groups.[42] In this work, the authors developed an elegant synthetic strategy for the introduction of orthogonal protecting groups at the polyglycerol backbone. A schematic overview of the deprotection of the respective copolymers is given in Scheme 2. While exclusive deprotection of the acetal protecting group in P(EEGE-*co*-AGE) was successful, complete cleavage of protecting groups was observed for P(EEGE-*co*-*t*BGE) upon treatment with HCl. Deprotection of the *tert*-butyl protecting groups with trifluoroacetic acid (TFA) was selective for P(*t*BGE-*co*-AGE), but resulted also in *lin*PG for P(EEGE-*co*-*t*BGE) copolymers. During deprotection, a few hydroxyl groups were esterified by TFA. Allyl protecting groups were selectively cleaved by treatment with Pd/C and *para*-toluenesulfonic acid (*p*TSA); however, partial hydrolysis of the acetal moieties in P(EEGE-*co*-AGE) was observed.

Complete deprotection of both P(AGE), P(EEGE), and P(*t*BGE) homopolymers renders all of the protected glycidyl ethers suitable as precursor polymers for *lin*PG. Unexpectedly, in case of the homopolymers removal of the *tert*-butoxy group was not possible under the conditions used for the deprotection of P(EEGE). In a follow-up work, the same group described the selective deprotection of block copolymers of EEGE and *t*BGE, claiming a strong influence of the polymer microstructure on the stability of the protecting groups.[11,46]
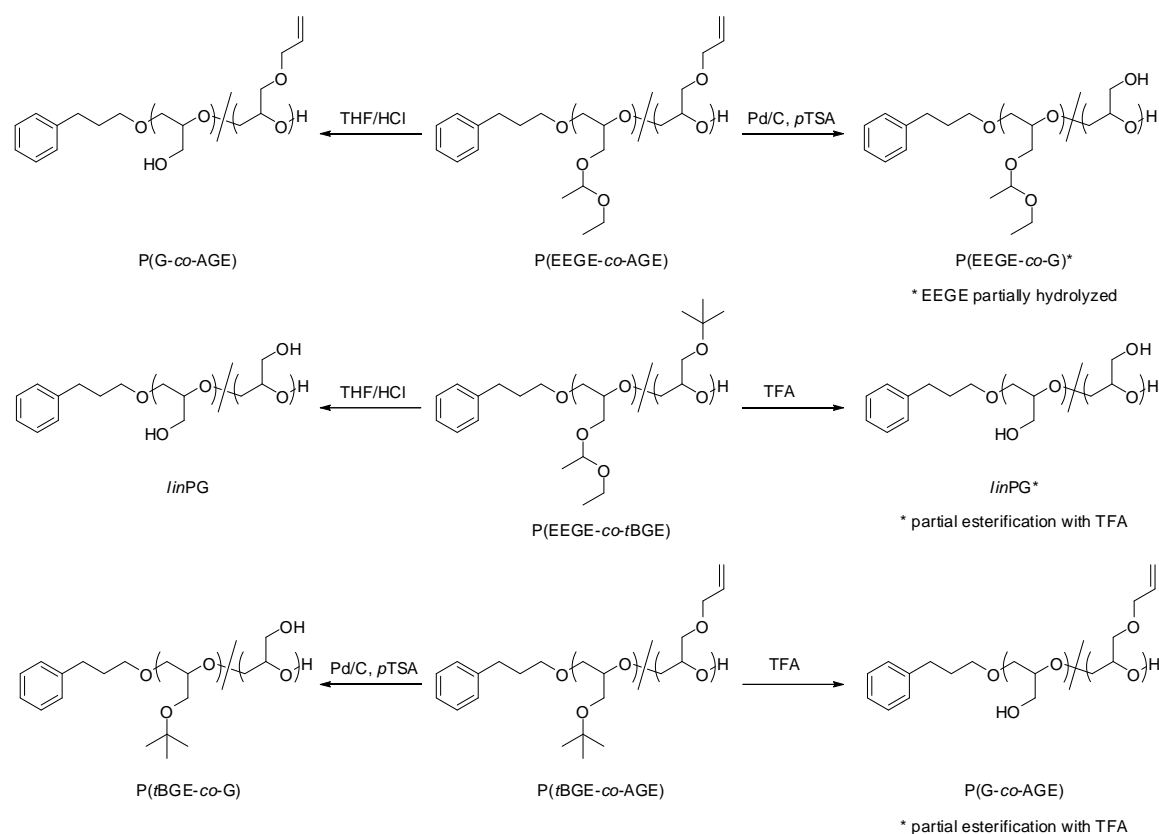
Scheme 2. Removal of orthogonal protecting groups in glycidyl ether copolymers,[42] leading to partially functionalized linear polyglycerols.

Despite the narrow molecular weight distribution obtained for the low to moderate molecular weight *lin*PGs, a limitation in molecular weight to ≈ 30 000 g·mol^{-1} for protected P(EEGE) was observed, which translates to a degree of polymerization (DP$_n$) of ≈ 200.[35, 41, 47] This limitation is explained by a chain transfer reaction between either the propagating chain or the initiator oxyanion and EEGE. During this chain transfer reaction (Scheme 3), a proton is abstracted from the methylene group adjacent to the oxirane ring, leading to the formation of an allyl alkoxide. This side reaction is also known in an analogous manner for other monosubstituted epoxides, *e.g.*, propylene oxide or phenyl glycidyl ether.[31]
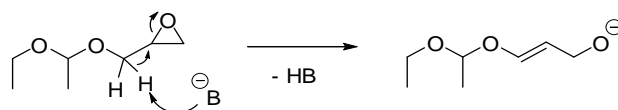
^{a}B = propagating polymer chain or initiator.

Scheme 3. Proton abstraction from an EEGE monomer by a strong base (B = propagating polymer chain or initiator) leading to chain transfer reactions.[41]

The influence of the reaction temperature, initiator and counterion on the EEGE polymerization has also been investigated by Keul, Möller, and co-workers.[41] The side reaction was described to become more pronounced for higher monomer to initiator ratios and for higher temperatures. A significant decrease of the transfer reaction was observed by lowering the temperature from 120 to 60 °C in polymerizations initiated with PPOK. However, for Li^+/t-BuP$_4$ as an initiating system, side reactions could not be prevented even in polymerizations performed at 20 °C. The high basicity of sec-BuLi and the phosphazene base itself are most likely responsible for this side reaction.[41] Consequently, it is generally assumed that in order to achieve high molecular weight polyethers, the active chain end has to exhibit high nucleophilicity to exert efficient ring-opening of the epoxide, but also low basicity to avoid proton abstraction and chain transfer.

As a first concept on the way to high molecular weight linPGs, the application of partially hydrolyzed diethylzinc (ZnEt$_2$/H$_2$O) as a catalyst was introduced. Scientists in the 1960s and 1980s already made use of this system to obtain the first high molecular weight linPGs by polymerization of TMSGE, as confirmed by high intrinsic viscosity.[22, 33] This was later adopted by Dworak and co-workers for the polymerization of EEGE. After deprotection, high molecular weight linPGs were obtained with M_n up to 1 000 000 g·mol^{-1}, however, accompanied by a loss of control over molecular weight and broader molecular weight distributions (M_w/M_n = 1.46 − 1.80),[48-50] owing to the little controlled catalytic process.

Utilization of a calcium amide-alkoxide catalyst in heptane resulted in P(EEGE)s with high molecular weights up to 180,000 g·mol^{-1}, however, polydispersities were even higher (M_w/M_n = 3.4-4.5) and only a maximum conversion of 52% was achieved.[51]

Important progress was achieved by Deffieux, Carlotti, and co-workers. Their strategy involves the activation of the monomer toward nucleophiles as well as a reduction of the basicity of the growing chain end by coordination of triisobutyl aluminum (i-Bu$_3$Al) (Scheme 4).[52-54] Both alkali metal alkoxides and ammonium salts (R$_4$N$^+$X$^-$) have been used as initiators. Ammonium salts lead to improved control of molecular weights and polydispersity. Within the range of ammonium salts, longer alkylene chains were found to increase monomer reactivity and polymerization rate.[55] Since especially a combination of i-Bu$_3$Al and ammonium salts was shown to significantly suppress the

transfer reaction of protons adjacent to the oxirane ring, this concept was also transferred to the polymerization of EEGE and tBGE to yield well-defined high molecular weight linPGs with impressive molecular weights up to 85 000 g·mol^{-1}.[56-58] For more details, see section 3.1.1.

X = Br or N$_3$
R = H, OtBu or OCHCH$_3$OC$_2$H$_5$
R' = butyl or octyl
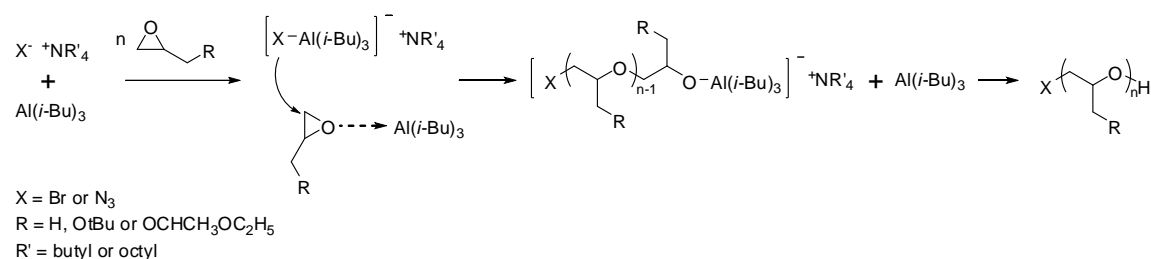
Scheme 4. Polymerization of oxiranes by X-Al(i-Bu)$_3$/NR$_4^+$ catalysts.

In contrast to the aforementioned chain growth mechanisms, low molecular weight linear oligoglycerols have been prepared as perfectly monodisperse oligomers by various multistep syntheses.[59, 60]

3. Heterofunctional linear polyglycerol

This section deals with versatile modification reactions leading to heterofunctional linPG. Polyglycerol bearing a variety of different functionalities can be obtained by a multitude of synthetic strategies comprising initiation by a functional molecule, end-capping with an appropriate reagent or postpolymerization modifications, transforming either the hydroxyl groups at the polymer backbone or the α- and/or ω-positions. In the ensuing paragraph, approaches leading to α- and/or ω-functional linPGs are discussed. As a special type of end-functional polymers, polyglycerol-based macromonomers are considered as precursors for highly functional graft copolymer structures and polymer brushes in the second paragraph. The third paragraph describes polymer modifications by reacting pendant hydroxyl groups at the backbone of linPG. Random copolymerization of functional glycidyl ethers with EO will not be part of this Review as such strategies have been highlighted recently by our group.[61,62]

3.1 End-functional *lin*PGs

End-functional polymers can either be prepared by using a suitable functional initiator or by efficient termination reactions.

3.1.1 Functional initiators for the synthesis of *lin*PG

The introduction of functionalities *via* specifically designed initiators presents an elegant synthetic pathway toward completely end-functionalized polymers. However, for the anionic ring-opening polymerization as the most common method for the preparation of *lin*PG, the applied initiator has to tolerate the harsh, basic conditions at elevated temperature without being subject to side reactions. A large number of heterotelechelic polyethers containing, *e.g.*, –OH, -NH$_2$, -COOH, -CHO or -SH moieties has been developed in the last decades. For PEG oligomers, various synthetic strategies have been highlighted by Thompson *et al.,*[63] and a general overview was given recently by Carlotti and co-workers.[31] We will focus on functional groups introduced in *lin*PG structures. The introduction of single amino groups in polymer chains has attracted enormous interest in the past, since amino groups are versatile functionalities for the attachment of biomolecules or conjugation chemistry in general. For a highly functional polymer like polyglycerol, the introduction of selectively reacting moieties is crucial to avoid side reactions during the conjugation step. In recent years, some approaches have been developed to attach one single amino group at the chain end of both linear and hyperbranched polyglycerol.[18,19,64] Most of them rely on the utilization of protected amine-containing initiators for the anionic ring-opening polymerization of glycidyl ethers. Protecting groups are usually cleaved by catalytic hydrogenation, thereby offering an orthogonal modification to the acid-labile acetal in EEGE. In an elegant work published by Klok *et al.*, amine-initiated polyglycerols of varying architectures were prepared *via* anionic ring-opening polymerization of EEGE. By using a methoxybenzyl-protected aminoethanol or serinol initiator, linear polyglycerols containing an end- or midchain amino functionality were obtained. After removal of both the methoxybenzyl and acetal protecting groups, the monoamino- and multihydroxy-functional polyglycerols were conjugated to various proteins (bovine serum albumin and lysozyme) *via* selective squaric acid coupling (see Figure 5).[64] This renders a "PGylation" with *lin*PG

feasible, in analogy to the widely employed PEGylation strategy that is currently used for a wide range of proteins to prolong circulatory time by reducing renal clearance. PGylation is a promising strategy with respect to therapeutic proteins and can permit to combine the well-known "stealth" effects of polyether chains with additional functional groups for targeting.

Similar to PEG, polyglycerol layers have been found to prevent undesired protein adsorption on surfaces. Haag and co-workers applied amino-functional *lin*PGs for the modification of several surfaces (gold and glass), thereby providing highly biorepellent coatings. The polymers were prepared utilizing an *N,N*-dibenzyl-protected aminopropanol initiator to synthesize well-defined α-amino *lin*PGs or P(GME)s *via* anionic ring-opening polymerization of EEGE or glycidyl methyl ether (GME). After subsequent palladium-catalyzed hydrogenation of the benzyl protecting groups, the monoamino-functional polyethers (M_n = 600–1500 g·mol^{-1}) were used as hydrophilic coatings for anhydride-functionalized gold surfaces.[18]
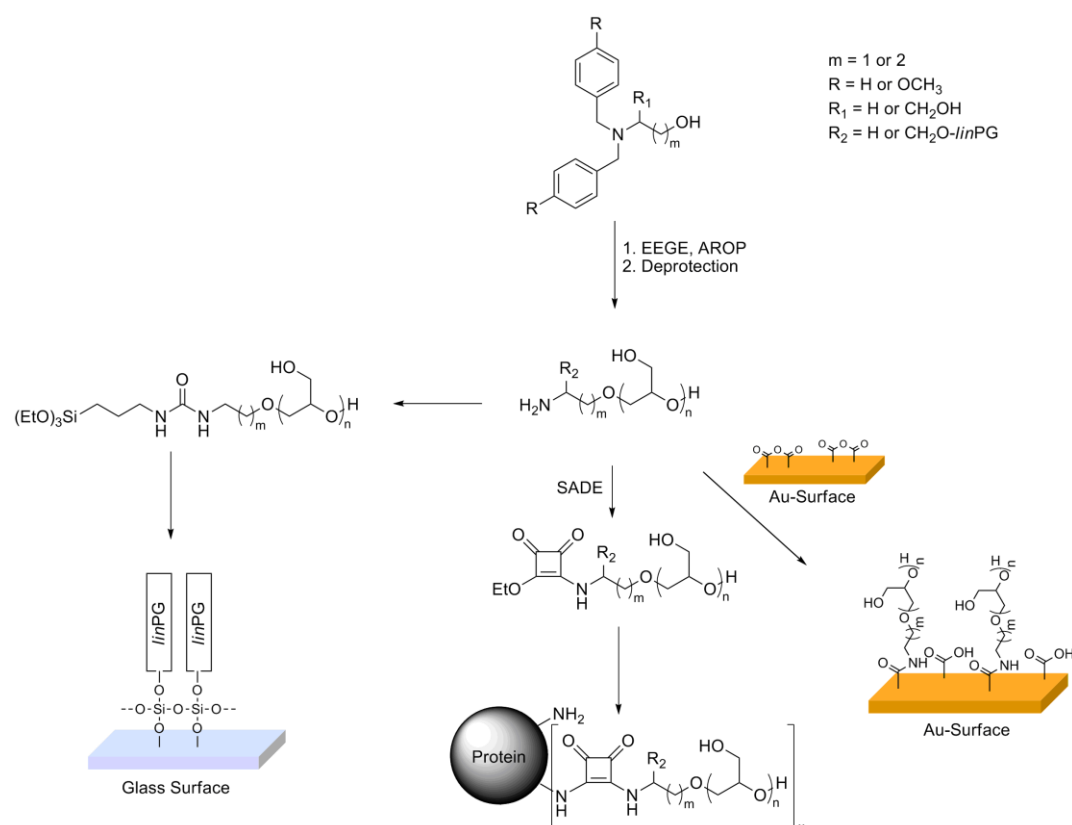

Figure 5. Summary of anionic ring-opening approaches targeting amino-functional linear polyglycerols for surface modification and bioconjugation developed by Haag et al. and Klok et al., respectively[18, 19, 64] (SADE = squaric acid diethyl ester). Adapted in part from ref 19. Copyright 2011 WILEY-VCH Verlag GmbH & Co. KGaA, Weinheim. With permission from John Wiley and Sons.

In a follow-up work, these amino-functional precursor polymers were reacted with 3-(triethoxysilyl)propyl isocyanate forming a stable urea bond. The triethoxysilyl moiety served as a strong anchoring unit for the covalent attachment to glass surfaces.[19] Pronounced biorepellent behavior similar or even superior to PEG was described for both gold and glass surfaces coated with these linear polyethers. An overview of amino-functional *lin*PGs synthesized *via* anionic ring-opening polymerization (AROP) and their use for surface modification and bioconjugation is given in Figure 5. In contrast to the above-mentioned straightforward approaches using an amine-functional initiator, amine-containing and truly monodisperse oligoglycerols (up to trimers) were also prepared *via* a multistep synthesis and their antifouling properties on gold surfaces were compared to different polyglycerol or P(GME) architectures.[17]

Besides amines, other functional groups have proven to be beneficial for the immobilization of polymers on various surfaces. Thiols show high affinity towards gold surfaces and have therefore been used as popular linkers in surface chemistry.[65] However, they have only very sparsely been reported for the end-functionalization of *lin*PGs. Weinhart *et al*. described the synthesis of thiol-functional *lin*PG by applying 11-benzylthio-undecanol as an initiator for the anionic ring-opening polymerization of EEGE or GME.[18] Deprotection of the thiol was carried out under careful exclusion of oxygen by using sodium in liquid ammonia/THF. The final thiol-functional PGs were deposited on gold surfaces to obtain biorepellent coatings (Figure 3).

Almost universal adhesion can be induced by the incorporation of catechol units into polymer structures.[66, 67] Catechols are a widespread constituent in naturally occurring molecules like neurotransmitters, polyphenols or amino acids. Especially, the nonessential amino acid L-DOPA has been found to be a major component in marine mussels and to be responsible for their intriguing adhesion properties.[66] Intense effort has been taken to make use of these properties in a variety of polymer architectures in biomimetic approaches.[67]
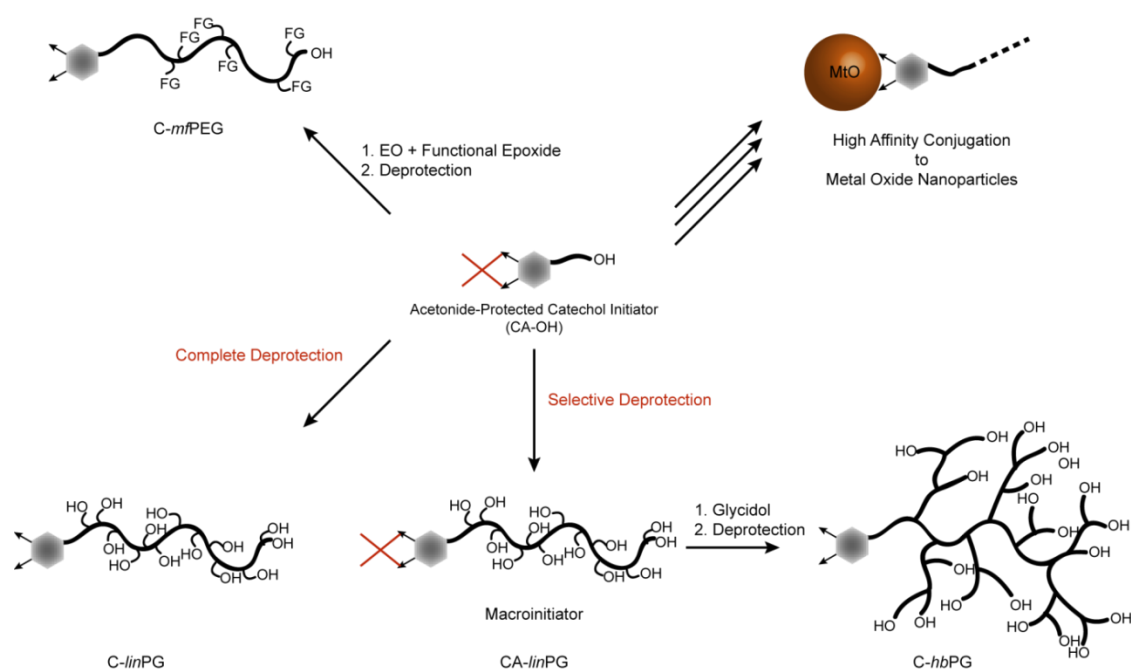
Figure 6. Overview of catechol initiated polyether structures including a selective deprotection step for EEGE under maintenance of the catechol acetonide protecting group. The catechol-bearing polyethers present suitable candidates for the hydrophilic coating of metal oxide nanoparticles.[68]

Very recently, our group developed a catechol-based initiator (Figure 7) allowing for the synthesis of a large variety of catechol-functional polyether structures by anionic ring-opening polymerization.[69] This initiator has also been used for the synthesis of well-defined linear and hyperbranched polyglycerols with a single catechol moiety (Figure 6).[68] Selective binding of the catechol moiety to manganese oxide (MnO) nanoparticles despite the presence of a large number of hydroxyl groups derived from the polyglycerol backbone has been demonstrated for both linear and hyperbranched catechol-initiated polyglycerols. Efficient dispersion of MnO nanoparticles in aqueous solution was observed for different types of hydrophilic polyethers, rendering them suitable as contrast agents for magnetic resonance imaging.[68, 69] Toxicity studies revealed high biocompatibility for all polyether-coated MnO nanoparticles up to a concentration of 50 µg·mL^{-1}.[70] The concept relies on the "*grafting-to*" strategy of prefabricated PG blocks and can be applied to a broad range of nanoparticles and surfaces to impart water solubility and also antibiofouling properties.
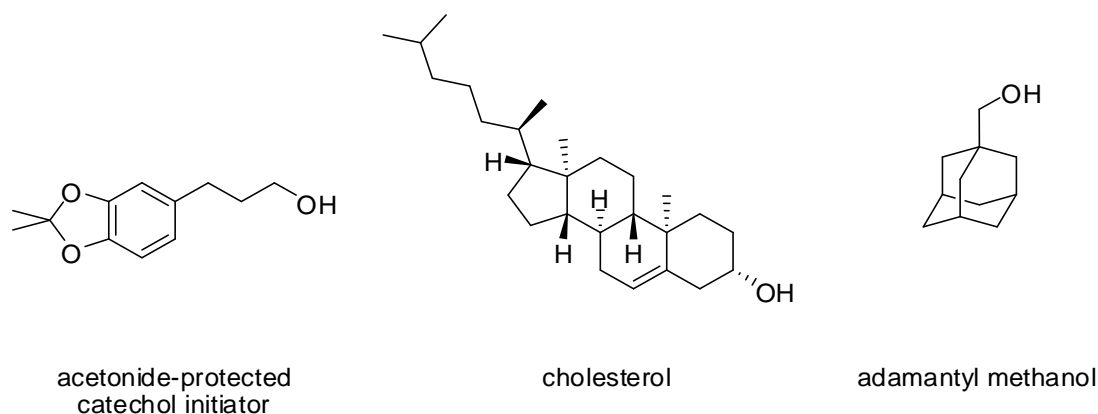
acetonide-protected
catechol initiator

cholesterol

adamantyl methanol

Figure 7. Nonconventional initiators used for the synthesis of *lin*PG.

Only few examples of functional initiators have been described that can be applied in oxyanionic ring-opening polymerizations without further protection steps. Among them, cholesterol as an essential structural component of the lipid bilayer in cell membranes is a valuable building block for the synthesis of amphiphilic architectures. Due to its inherent hydroxyl group, the readily available cholesterol can be used without further modification (Figure 7).[71] Anionic ring-opening approaches making use of cholesterol as an initiator have been studied intensively by our group. As a rather simple structure, cholesterol-initiated linear polyglycerol has been prepared by polymerizing EEGE and subsequent acidic cleavage of the acetal-protecting groups.[72] For a series of molecular weights, liquid crystalline order was observed in a broad temperature range up to 260 °C. Remarkably, the incorporation of a single cholesterol led to ordering of the usually amorphous *lin*PG chains with up to 26 glycerol units.[73] More complex linear-hyperbranched architectures using cholesterol as an initiator have also been realized *via* so-called "hypergrafting" strategies and will be discussed in section 3.3.3 together with potential applications.

Besides functional initiators that are capable of undergoing derivatization reactions, supramolecular, complex polymer structures assembled by host-guest interactions are of great interest. For this purpose, adamantyl methanol-initiated polyglycerols have been recently developed by our group (Figure 7).[74] Induced by the hydrophobic adamantyl residue, these slightly amphiphilic linear, hyperbranched, or linear-hyperbranched polyether polyols can form an inclusion complex with the hydrophobic cavity of cyclodextrin. Complex supramolecular graft copolymer structures comprising a

cyclodextrin-functional poly(methacrylate) backbone and supramolecularly linked polyglycerol side chains have been prepared and analyzed by isothermal titration calorimetry, demonstrating the effect of a PEG-spacer on the assembly.[74]

The synthetic strategy developed by Deffieux and co-workers including the monomer-activated anionic polymerization of EEGE or *t*BGE (see section 2) also leads to highly end-functional *lin*PGs. The employed tetraoctylammonium bromide and *i*-Bu₃Al initiator-catalyst system provides well-defined polyethers bearing a single bromine atom in their α-position.[57, 58] In another work, the authors showed that ammonium salts containing pseudo halogens can also efficiently be used as initiators in combination with *i*-Bu₃Al. α-Azido-functional polyethers including poly(alkylene oxide)s, poly(epichlorohydrin), and poly(EEGE) were prepared by using tetrabutylammonium azide/*i*-Bu₃Al as the catalyst in a one-step approach. A high degree of α-functionalization was indicated by matrix assisted laser desorption/ionization time-of-flight (MALDI-ToF) measurements,[56,58] and the azide functionalities were successfully reacted with alkyne-containing compounds in a copper-catalyzed azide-alkyne cycloaddition (CuAAC).

3.1.2 End-functional *lin*PGs *via* end-capping

Due to the living character of anionic polymerizations, oxyanionic ring-opening polymerization is a well-established method for the synthesis of well-defined end-functional polyethers *via* the end-capping technique.[166]

Möller *et al*. described the synthesis of vinylsulfonate-functional linear and star-shaped polyglycerols by reacting ω-hydroxy-functional protected polyglycerols with 2-chloroethylsulfonyl chloride. The attached vinyl sulfonate was found to react efficiently with various amines or alcohols, but not with thiols.[75, 76] In an approach by our group, *lin*PGs or poly(glyceryl glycerol) bearing one single alkyne moiety in the ω-position have been synthesized by end-capping living polymer chains with propargyl bromide.[44] Similar to the aforementioned azide-functional polyethers prepared by Carlotti and co-workers.[56, 58] the structures present promising precursors for complex architectures *via* click-reaction. Another approach by Kuckling *et al*. includes esterification of the ω-hydroxyl group by 2-halogenopropionyl halides, offering *lin*PG macroinitiators for the formation of block copolymers by atom transfer radical polymerization (ATRP).[47] End-capping reactions of polyglycerols have also been applied to introduce polymerizable

styrene or methacrylate residues. The synthesis of these macromonomers will be discussed in the next paragraph.

3.2 Macromonomers based on linear polyglycerol

Polyglycerol-based macromonomers have been prepared *via* strategies described in the following. Common preparation techniques for macromonomers include the "end-capping method" and the "initiator method". In the end-capping approach, an activated chain end is reacted with a polymerizable end-group, while in the "initiator method", the polymerization is initiated by the polymerizable unit of the macromonomer. In one of the pioneering works, Dworak and co-workers described end-capping of living P(EEGE) chains with *p*-chloromethylstyrene to obtain ω-vinylbenzyl-functional macromonomers.[36,37] The resulting acetal-protected macromonomers were copolymerized with styrene in a free radical polymerization and deprotected to afford polystyrene-*graft-lin*PG copolymers. However, a maximum conversion of only 65% of the macromonomer was observed. Higher conversions (up to 85%) were achieved when the deprotected macromonomers (ω-vinylbenzyl-polyglycerol) were used as "surfmers" (surfactant and monomer) in an emulsifier free emulsion polymerization with styrene to obtain hydrophobic styrene microspheres with a hydrophilic polyglycerol corona (Figure 8).
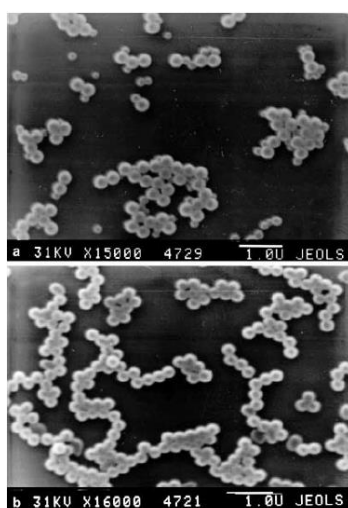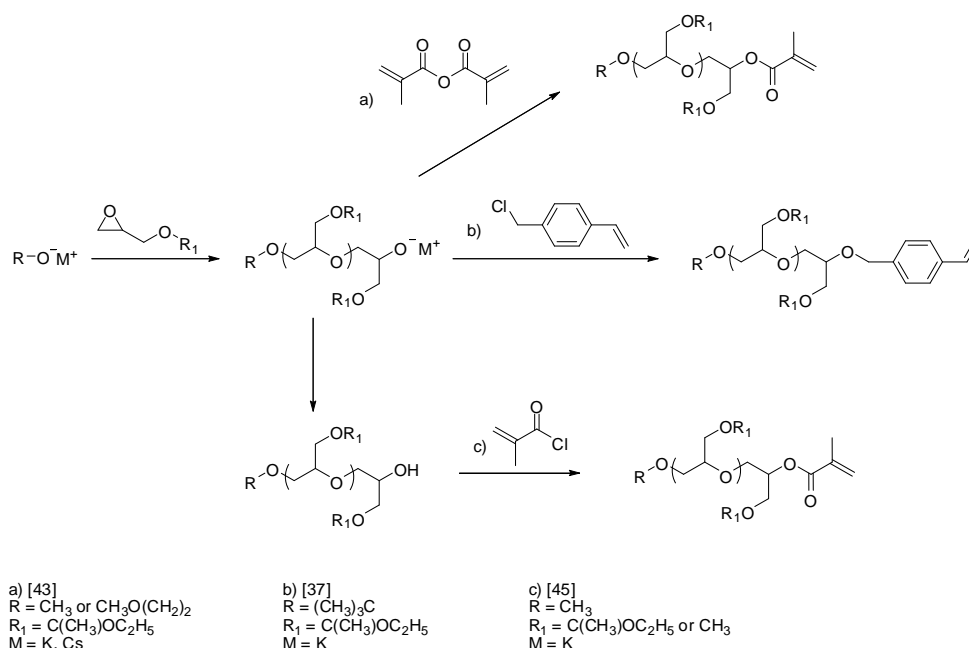

Figure 8. Scanning electron microscope microphotograph of poly(styrene/ω-vinylbenzyl-polyglycerol) microspheres.[77] Reproduced from ref 77. Copyright 2001 Springer-Verlag. With kind permission from Springer Science and Business Media.

These microspheres were later intensively investigated by Basinska and Slomkowski *et al*. Results on the composition and properties of the polyglycerol surface[77-83] as well as studies on protein adsorption[77,84] and potential biomedical applications[85-88] of the microspheres have been discussed at full length in a recent publication.[89] As a cleavable alternative to the ether-bound styrene functionality, the end-capping technique can also be applied to prepare polyglycerol-based macromonomers bearing one terminal methacrylate function covalently linked *via* an ester bond. This was accomplished both by our group and Haag *et al.*[43, 45] In our work, a straightforward one-pot approach is described.[43] EEGE was polymerized from alkoxide initiators (Figure 9) to obtain well-defined precursor oligomers. The living chain ends were directly end-capped by the sequential addition of excess triethylamine and methacrylic anhydride to the reaction mixture. Homopolymerization of the narrowly distributed macromonomers ($M_w/M_n < 1.30$) by ATRP and subsequent deprotection resulted in water-soluble and well-defined graft copolymers ($M_w/M_n < 1.31$) containing a methacrylate backbone and densely grafted oligoglycerol side chains. Due to steric crowding, the conversion in homopolymerization was limited to 65% but could be increased by the addition of different amounts of the sterically less demanding hydroxy ethyl methacrylate (HEMA) as a comonomer.

In various multistep protocols, Haag and co-workers synthesized a variety of oligoglycerol (meth-)acrylates, ranging from linear oligoglycerol methacrylate or oligo(GME) methacrylates to dendronized oligoglycerol acrylates.[45] Linear oligoglycerol methacrylates or oligo(GME) methacrylates were also prepared *via* anionic ring-opening polymerization of EEGE or GME. However, the precursor polymers were purified before, in a second reaction step, the terminal hydroxyl group was reacted with methacryloyl chloride. After deprotection, both linear and dendronized macromonomers were polymerized by ATRP from initiators attached to gold surfaces. Antifouling properties of the oligoglycerol brushes were determined and compared to brushes prepared of low molecular weight glycerol methacrylate. An overview of the end-capping approaches reported to date is given in Figure 9.

a) [43]
R = CH$_3$ or CH$_3$O(CH$_2$)$_2$
R$_1$ = C(CH$_3$)OC$_2$H$_5$
M = K, Cs

b) [37]
R = (CH$_3$)$_3$C
R$_1$ = C(CH$_3$)OC$_2$H$_5$
M = K

c) [45]
R = CH$_3$
R$_1$ = C(CH$_3$)OC$_2$H$_5$ or CH$_3$
M = K

Figure 9. Summary of the synthetic protocols developed for the preparation of macromonomers based on linear polyglycerol *via* the end-capping technique.[37, 43, 45]

The incorporation of a radically polymerizable group into the multihydroxy-functional polyglycerol structure also gives access to highly functional surface coatings. In a recent work by Carbonnier, Basinska, and Chehimi *et al.*, the aforementioned ω-vinylbenzyl-polyglycerol macromonomers were grafted from modified gold or stainless steel surfaces, leading to a strong increase in the wettability of the surfaces. Protein adsorption was investigated and found to be reduced for surfaces grafted with ω-vinylbenzyl-polyglycerol macromonomers compared to surfaces bearing only the initiator or for poly(hydroxyethyl methacrylate)-grafted surfaces.[90]

A different synthetic strategy was published by Keul and Möller *et al.*, who described the anionic ring-opening polymerization of EEGE and glycidol, respectively, initiated by vinylic initiators.[91] A variety of initiators including vinyl benzyl alcohol (VBA), *N*-(2-hydroxyethyl)-methacrylamide (HEMAm), *N*-(2-hydroxyethyl)-acrylamide (HEAAm), HEMA, and allyl glycol were deprotonated by the addition of potassium *tert*-butoxide, and the oxirane monomers were polymerized in the presence of hydroquinone as a radical stabilizer. As expected, for HEMA and HEAAm as initiators no controlled polymerization of epoxides was observed due to backbiting and the high reactivity of the acrylate double bond. Unexpectedly, no initiation by the hydroquinone stabilizer was

observed by the authors. The resulting macromonomers prepared with VBA and HEMAm were utilized in copolymerizations with low molecular weight comonomers. However, only rather low molecular weights for the resulting graft copolymers ranging from 1700 g·mol^{-1} to a maximum of 15 800 g·mol^{-1} were detected by SEC measurements. Similar to the works by Basinska, Slomkowski *et al.*, these VBA-initiated oligoglycerols (either branched (*b*) or linear (*lin*)) were also used as "surfmers" in the emulsion polymerization of styrene to form polystyrene particles with a hydrophilic polyglycerol periphery.[92] Amphiphilicity of the macromonomers was found to be a key parameter concerning polymerization rates. This is in analogy to other reports describing an improved and accelerated polymerization for PEG-based amphiphilic macromonomers due to micellar preorganization in water.[93-95] A similar micellar polymerization process was described for amphiphilic polyglycerol-based macromonomers by Kuckling and Dworak *et al.*[96, 97] The respective macromonomers were prepared *via* the end-capping technique using block copolymers of hydrophilic glycidol (acetal-protected precursor) and hydrophobic glycidyl phenyl ether.

A different, more general concept for the preparation of amphiphilic polyether polyol-based macromonomers *via* anionic ring-opening polymerization and click-chemistry was recently introduced by our group.[44, 98] In a copper-catalyzed azide-alkyne cycloaddition, well-defined, monoalkyne-functional *lin*PG and P(GG) hydrophilic precursors were reacted with azido alkyl methacrylates of variable spacer lengths. By varying both the block length of ω-alkyne-functional polyether polyols and the hydrophobic alkylene spacer, a set of macromonomers with tunable amphiphilicity was obtained. Polymerization of the amphiphilic macromonomers resulted in high molecular weight graft copolymers. For polyglycerol-based macromonomers conversion decreased for longer polyglycerol chains, whereas increasing the length of the alkylene spacer from propylene to more flexible hexylene or undecanoylene resulted in a significant increase to near quantitative conversion.[44, 98]

3.3 Backbone functionalization of linear polyglycerol

This section presents the synthetic routes for the functionalization of the multiple hydroxyl groups at the *lin*PG backbone. The pendant hydroxyl groups can either be

addressed in postpolymerization reactions using low molecular weight reactants or serve as a macroinitiator in "grafting-from" approaches aiming at different architectures, such as brush-like or grafted hyperbranched structures.

3.3.1 Hydrophobic and hydrophilic functionalized linear polyglycerol

The hydroxyl moieties of linear polyglycerol can be converted into various functional groups like ethers,[42, 73] esters,[99, 100] urethanes,[46, 101, 102] or carbonates[103] (see Figure 10), which are described in more detail below. Chau and co-workers presented a library of homofunctional and heterofunctional derivatives of linear polyether polyols including allyl, alkynyl, acyl and azide groups as orthogonal precursors for the attachment of, *e.g.*, drugs and biomolecules.[104]

The simplest method to functionalize *lin*PG and thereby tune the polarity is the methylation of the pendant hydroxyl groups of the polyether backbone. By using methyl iodide, for example, the interaction of the hydroxyl groups can be "switched off", which is useful for studying the importance of hydrophilic interactions on the thermal and rheological properties of *lin*PG.[73] A clearly more convenient strategy is the direct polymerization of GME (glycidyl methyl ether), where the hydroxyl group of glycidol is already methylated. GME is commercially available and can be used for anionic ring-opening polymerizations resulting in quantitatively methylated and thermoresponsive *lin*PG derivatives.[105-107] Furthermore, end-functionalized P(GME) (M_n between 600 and 1500 g·mol^{-1}) and its copolymer with ethyl glycidyl ether (EGE) can be used in surface modification reactions and as a potent protein repellent material.[18,108,109] Poly(ether imide) membranes functionalized with side chain-methylated oligoglycerols (O(GME)) showed good stability under oxidative conditions, which is also relevant in biomedical applications.[110-112]

Modification of the hydroxyl groups of *lin*PG can also be achieved through (partial) esterification with aliphatic acyl chlorides, *e.g.*, palmitoyl chloride. Such systems were investigated in comparison to their hyperbranched analogues as "nanocapsules" or "nanoreactors", but showed no or low encapsulation efficiency.[99, 113] In the respective publication, the fundamental difference between linear and hyperbranched polyglycerols derivatized with fatty acid esters has been established with respect to guest encapsulation, establishing the core-shell topology of the hyperbranched polymer.

Furthermore, acetic acid[36, 48] and acetic anhydride[100] were used as reactants for the hydrophobic modification of *lin*PG resulting in poly(glycerol-*co*-glycerol acetate)s with a varying degree of functionalization and LCST behavior (LCST = 4 to 100 °C). In another approach by Dworak and co-workers, LCST behavior was induced in *lin*PG by synthesizing ABA or BAB poly(ethylene glycol) (A)/poly(ethyl glycidyl carbamate) (B) amphiphilic block copolymers, in which the hydroxyl groups were modified with ethyl isocyanate.[101] For ABA copolymers, the cloud point was determined to be around 80 °C, and for BAB 46 °C was detected, whereas, remarkably, the AB diblock did not exhibit thermoresponsive behavior. Esterification with glutaric aldehyde,[114] poly(ethylene glycol)-*bis*-(carboxymethyl ether chloride)[115] or 3,3-dithiodipropionic acid[116] led to *lin*PG-based hydrogels with different swelling properties. Figure 10 gives an overview of the main chemical transformations of the polyglycerol backbone.

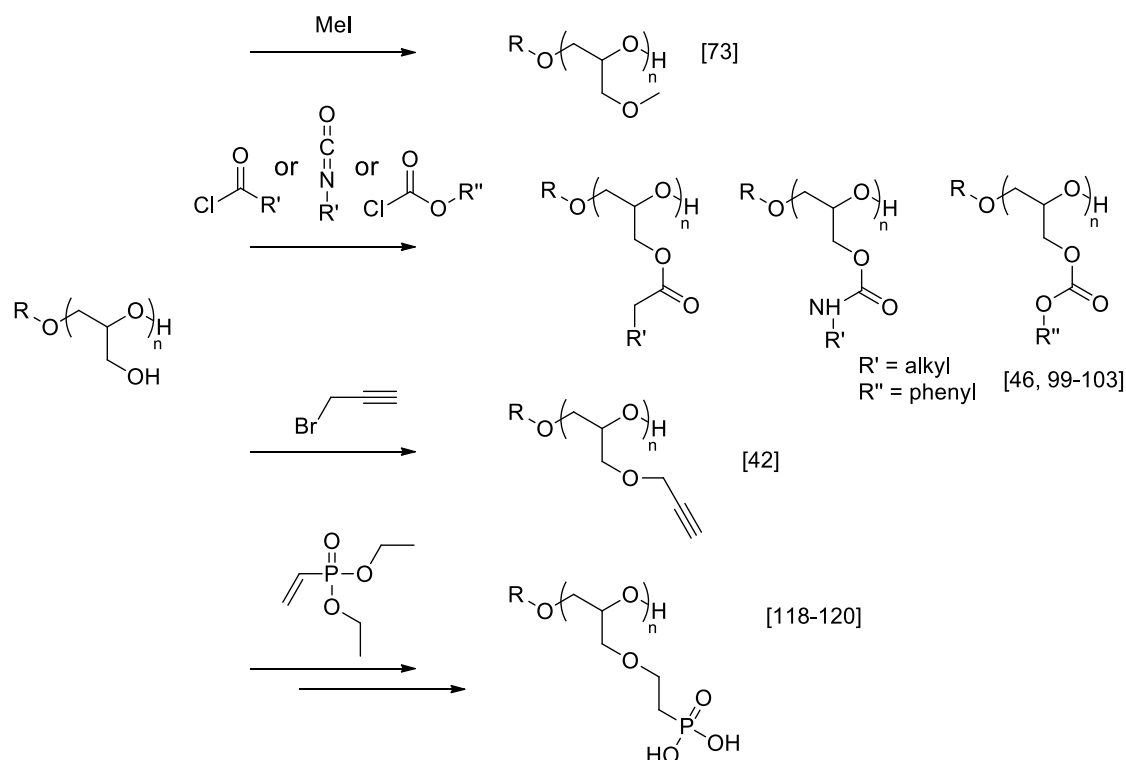*Figure 10.* Typical examples of backbone-modified linear polyglycerols.

CuAAC is widely used as an orthogonal method in postpolymerization modifications. Erberich, Keul and Möller were able to convert the partially protected linear polyglycerol backbone into an alkyne-functionalized polymer by using propargyl bromide. In a proof-of-principle concept they showed the cycloaddition of an azido-functional sugar moiety

to the glycidyl propargyl ether repeating units, aiming at heteromultifunctional polyethers.[42]

The introduction of functional groups, which are commonly hydrophilic, is interesting in biomedical applications, where the attachment of biomolecules is necessary or the attachment onto surfaces is desired. Penczek *et al.* successfully introduced both phosphonic and carboxylic acid groups along the polyglycerol backbone.[117] Phosphoethylated polyglycerols have been obtained by Michael addition of the hydroxyl groups of *lin*PG to diethyl vinylphosphonate. After hydrolysis, a tunable amount of phosphonic acid side groups is available for applications in biorelated fields.[118-120]

3.3.2 "Grafting-From" Strategies based on *lin*PG

Transformations of *lin*PG comprise small molecule chemistry addressing the hydroxyl groups as well as "grafting-from" approaches, in which *lin*PG is used as a macroinitiator. As an example, *lin*PG has been used as a suitable macroinitiator for the ring-opening grafting polymerization of cyclic esters. Various works have been published describing the synthesis of, *e.g.*, branched poly(lactide)s[121,122] or poly(glycerol-*graft*-ε-caprolactone)[39, 123, 124] with a combination of anionic and coordinative ring-opening polymerization. Chemoenzymatic approaches, *i.e.*, the combination of chemical and enzyme-catalyzed reactions, have led to densely or loosely grafted poly(ether-*graft*-polyester)s, respectively.[125-127] Heterografted polyether brushes *via* chemical and enzymatic reactions, mainly developed by Möller and co-workers, were highlighted in 2009.[11]

Interesting degradable polyether-*graft*-polyesters with pendant diethylphosphonatoethyl groups (DEPE) were prepared by enzymatic grafting of ε-caprolactone from *lin*PG. Via different reaction parameters, such as the ratio of lipase to monomer concentration, grafting densities could be varied from 31% to 81%.[119] The hydrolytically degradable materials contain only biocompatible (polyglycerol) and biodegradable (polyester/ phosphonate groups) segments. In a recent follow-up work, the group of Möller showed that poly((glycerol ethylphosphonatoethyl)-*co*-(glycerol-*graft*-ε-caprolactone)) copolymers can degrade within 7 d (*in vitro* study in phosphate-buffered solution at 55 °C), whereas poly((glycerol diethylphosphonatoethyl)-*co*-(glycerol-*graft*-ε-caprolactone)) was stable for prolonged periods of up to 63 d. The

reaction route is shown in Scheme 5. This demonstrates the significant influence of ethylphosphonate groups or diethylphosphonate groups on the degradation behavior of such biomaterials.[120]
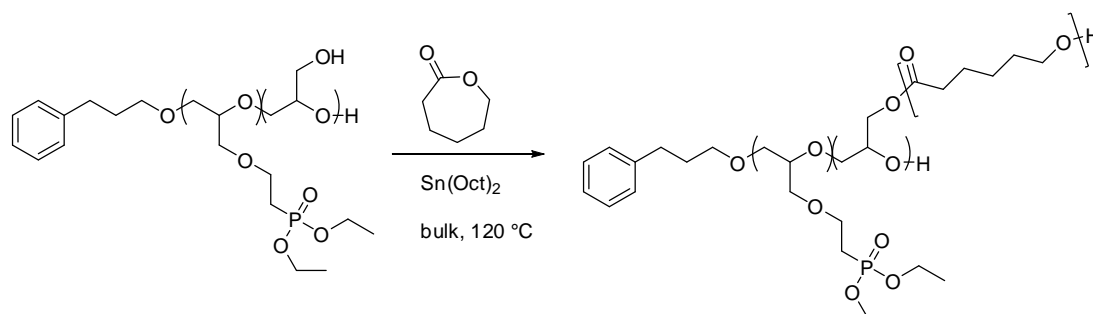
Scheme 5. Heterografted linear polyglycerol with poly(ε-caprolactone) as degradable side-arms.

Sequential grafting can also be used to synthesize remarkably high molecular weight (82 000 – 1 800 000 g·mol^{-1}) polyglycerol-*graft*-polyglycerol polymers. Due to the fast proton exchange between the alkoxide and hydroxyl groups, this multiple anionic "grafting-from" process yielded densely packed (grafting density ~ 70%-90%) arborescent-branched macromolecules.[38] In this context, "pom-pom like" structures based on polyethers have also been investigated.[128]

ABA type block-graft copolymers *via* a combination of CuAAC and atom transfer nitroxide radical coupling (ATNRC) reaction were also reported. Copolymerization of 4-glycidyloxy-2,2,6,6-tetramethylpiperidine-1-oxyl (GTEMPO) and EEGE provided a backbone with pendant TEMPO and hydroxyl groups. The hydroxyl groups were esterified with 2-bromoisobutyryl bromide, and ATRP was performed to generate graft copolymers.[129]
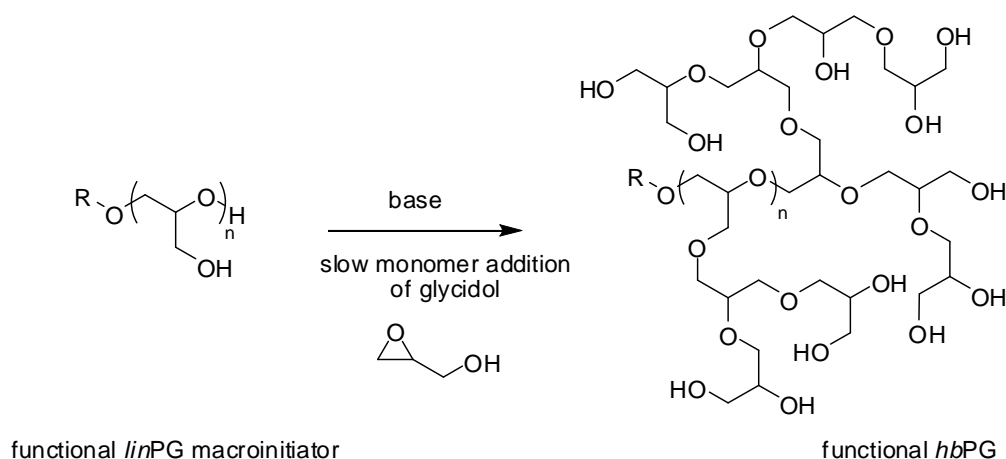
3.3.3 Linear polyglycerol as a macroinitiator for "hypergrafting" of glycidol

This section focuses on the use of linear polyglycerol segments as an excellent polyfunctional macroinitiator for the "hypergrafting" of glycidol, *i.e.*, the grafting of AB$_2$ or latent AB$_2$-type monomers onto a linear chain to form hyperbranched polyethers that can be analogous to dendronized polymers. The number of initiating hydroxyl groups is a critical issue for the control over molecular weight and the polydispersity (usually < 2) of the branched block. In simulation studies it could be shown that for the slow monomer

addition of an AB_n monomer, such as glycidol, the monomer/core functionality ratio is important. Furthermore, it was found that the polydispersity is in reciprocal relation to the number of functional groups (*f*, eq 1).[130]

$$\frac{M_w}{M_n} = 1 + \frac{1}{f} \qquad (1)$$

Equation 1 translates to decreasing polydispersity (M_w/M_n) with increasing core functionality *f*. Thus, rather monodisperse, multihydroxy-functional initiators are required for the controlled formation of hyperbranched polyglycerol. In addition, the probability for homopolymerization of glycidol is decreased in this case. This renders linear polyglycerol derivatives ideal candidates for the initiation of hyperbranched polyethers (Scheme 6) to generate a wide range of linear-hyperbranched polyglycerol hybrid structures.

functional *lin*PG macroinitiator   functional *hb*PG

Scheme 6. "Hypergrafting" process of glycidol onto a functional *lin*PG as the macroinitiator.[130b]

Our group introduced double-hydrophilic linear-hyperbranched block copolymers with PEG and polyglycerol segments.[24] To this end, a PEG-*lin*P(EEGE) block copolymer was deprotected under acidic conditions, providing PEG-*b*-*lin*PG copolymers with 13-40 hydroxyl groups. Partial deprotonation of the *lin*PG block and slow monomer addition of glycidol ("hypergrafting" process) afforded linear-hyperbranched PEG-*b*-*hb*PG copolymers. ABA-type block copolymers (*hb*PG-*b*-PEG-*b*-*hb*PG) were synthesized in a similar manner with low polydispersities (see section 4.2).[131] The obtained branched polyether structures have unique properties, *i.e.*, high terminal functionality and excellent biocompatibility.[8,9,13] Both architecture and multifunctionality can be tuned by

adjusting the degree of polymerization of polyglycerol, leading to polyether polyols with a predefined number of hydroxyl groups. The aforementioned advantages of the hyperbranched systems based on *lin*PG as a building block have been used for a variety of biomedical purposes. Non-covalent protein conjugation of linear-hyperbranched PEG-polyglycerols, *i.e.*, α, ωn-telechelics with one terminal amino group and multiple hydroxyl groups, have been investigated in the avidin-biotin system for supramolecular bioconjugation and in solubilizing carbon nanotubes.[132, 133] The double-hydrophilic linear-hyperbranched structure (PEG-*b-hb*PG) was also applied in a drug-delivery system based on micellar structures. In this case, doxorubicin was attached to the multiple hydroxyl groups *via* an acid-labile hydrazone bond, thereby rendering the polymer pH-sensitive. Increased drug loading efficiency, high biocompatibility, and water solubility of the polyether structures are proposed to be beneficial in anti-cancer treatment.[134]
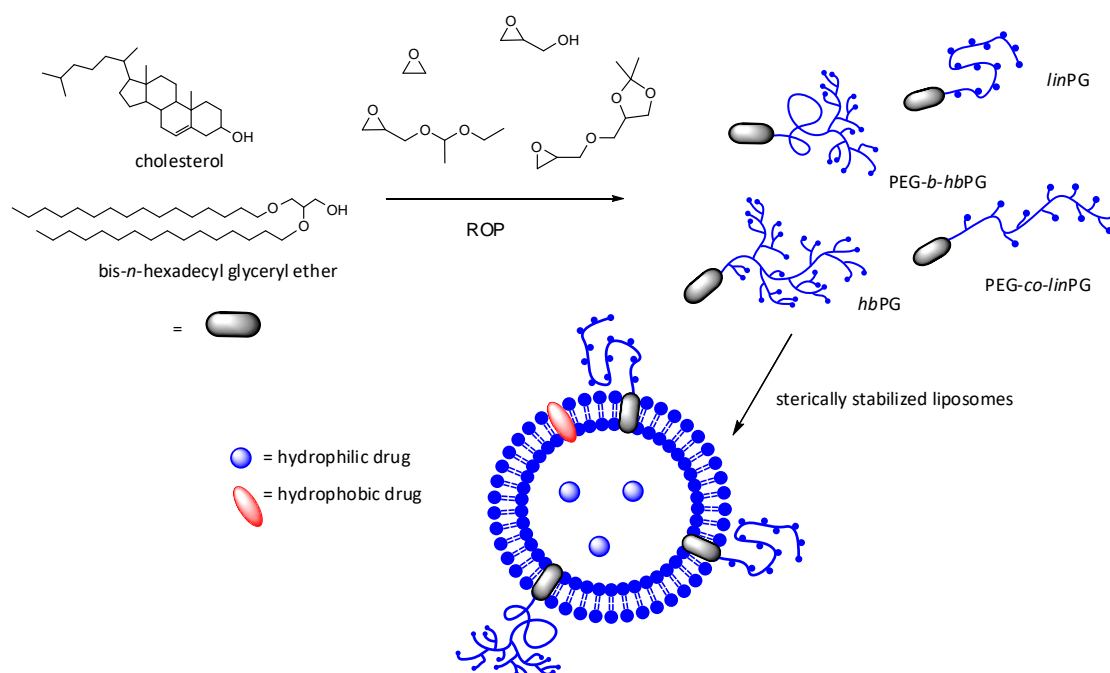
Figure 11. Epoxide construction kit for the synthesis of linear and branched polyether-lipids in novel sterically stabilized "stealth"-type liposomes.[72, 136, 137] Reproduced from refs 72 and 137. Copyright 2011 and 2013. American Chemical Society.

"Stealth" liposomes, polymer-coated vesicles commonly based on PEGylated lipids, are being exploited in clinical use with excellent results.[135] One of the drawbacks of methoxy poly(ethylene glycol) (mPEG) that is preferentially incorporated as a biorepellent shell, is its lack of functional groups. As mentioned in section 3.1.1, our group has used

cholesterol directly as an initiator for the oxyanionic polymerization of various epoxides including EO, EEGE, IGG, and glycidol (see Figure 11).[72, 136]

In contrast to cholesterol, phospholipids as initiators are not stable under the acidic and basic reaction conditions in the deprotection and "hypergrafting" step of glycidol. Cholesterol, as a natural membrane component, forms the hydrophobic segment in these polyether-based lipid mimetics. Cholesterol represents an excellent anchor in the phospholipid bilayer of the liposome.[138-141] The cholesterol-based multivalent structures, with tunable architectures and number of hydroxyl groups, offer further possibilities for derivatization, *e.g.*, *via* click-chemistry,[72, 141] which is important for active targeting. The concept of incorporating branched cholesterol-polyether polyols, was recently highlighted and remains promising to impart improved "stealth" properties in combination with functional groups to liposomes.[137a]

4. Block copolymers based on linear polyglycerol

Linear polyglycerol is an interesting component in block copolymers as a hydrophilic segment. Due to its multiple hydroxyl groups at the polyether backbone, it is highly water-soluble and therefore serves as an excellent, functional building block in amphiphilic block copolymers and nonionic polymer surfactants. In the following section the incorporation of *lin*PG into AB, ABA or even ABC block co- or terpolymers and other architectures will be highlighted.

4.1. Diblock copolymers containing linear polyglycerol

Möller and co-workers synthesized polystyrene-*b*-polyglycerol (PS-*b*-*lin*PG) block copolymers *via* carbanionic polymerization of styrene initiated with *sec*-butyl lithium and subsequent oxyanionic ring-opening polymerization of EEGE. To achieve sufficient reactivity of the propagating oxyanion, a phosphazene base (P$_4$-*t*-Bu) was added for the formation of the second block, resulting in block copolymers with polydispersities between 1.04 and 1.48 (M$_n$ = 18 000-102 000 g·mol^{-1}).[142, 143] P$_4$-*t*-Bu functions as a complexing agent for the cation (lithium) and thereby allows to "switch" directly from

carbanionic to oxyanionic living chains, without intermediate work-up of the first block. A phosphazene base system was also used in the low-temperature metal-free anionic ring-opening polymerization of EEGE and AGE, using 3-phenyl-1-propanol as the initiator. Using this method, well-defined EEGE/AGE diblock copolymers were obtained, which are versatile, functionalizable linear aliphatic polyethers.[144]

Another mild modification method was presented by Möller and co-workers for the synthesis of random and block copolymers with glycidol and glycidyl amines.[145] They used tetraoctylammonium bromide and i-Bu$_3$Al as a catalyst system for the copolymerization of EEGE and epichlorohydrin, which does not sustain the harsh conditions of a conventional base-initiated oxyanionic polymerization. In a three-step protocol, polyethers with hydroxymethyl and aminomethyl side chains were obtained after polymer modification, albeit with slightly increased polydispersities (M_w/M_n = 1.35 for random copolymers; M_w/M_n = 1.58 for block copolymers). Intermediate products, azide-functional polyethers, are useful for click-reactions for the functionalization of the copolymers.

The same group also prepared linear multifunctional polyethers *via* cationic ring-opening polymerization of a protected glycidyl ether (*t*BGE) with THF. Kinetic studies support the incorporation of both monomers into the polymer backbone. Deprotection resulted in linear poly(tetrahydrofuran-*co*-glycerol) with molecular weights up to 16 800 g·mol^{-1}and polydispersities < 1.8.[103]

Dendritic block copolymers are a complex class of polymers, and these architectures have also been achieved using polyglycerol building blocks in dendritic stars made from ethylene oxide and glycidol[146] or *t*BGE and glycidol.[147] Furthermore, P(EEGE)-*b*-hyperbranched polyglycerol-*co*-P(EEGE) was synthesized.[148] The preparation of all of these systems included EEGE as a hydrophobic comonomer, and the amphiphilic core-shell structures were investigated with respect to their encapsulation behavior.

4.2. Triblock copolymers containing linear polyglycerol

Pluronics™ are nonionic surfactants based on an amphiphilic ABA structure of linear triblock copolymers poly(ethylene glycol)-*b*-poly(propylene oxide)-*b*-poly(ethylene glycol) (PEG-*b*-PPO-*b*-PEG). They are produced on a large scale and are commercially

available with a variety of molecular weights. These highly established systems show interesting physical properties such as a LCST for short PEG-segments and good water-solubility with increasing molecular weight of the hydrophilic part. Applications range from cosmetic and pharmaceutical purposes to paper and textile modification.[149] As mentioned earlier, the PEG block can be replaced by linear polyglycerol to introduce numerous hydroxymethylene groups into the hydrophilic block. In a pioneering work, Tsvetanov and co-workers published a synthetic pathway toward polyglycerol-based Pluronics™ (linear glycerol/ propylene oxide- LGPs), which is shown in Scheme 7.[150] They used poly(propylene oxide) (PPO) as the macroinitiator for the anionic ring-opening polymerization of EEGE and subsequent acidic cleavage of the acetal protecting groups. Well-defined copolymers with varying amounts of linear polyglycerol (20-84 wt%) and a PPO block of 2000 g·mol^{-1} were prepared and characterized in solution. Their critical micelle concentration (CMC) was investigated, and a dependence on the *lin*PG content and temperature was found. The decrease of the CMC with decreasing length of the hydrophilic part was not as strong as for conventional Pluronic™ copolymers. In various follow-up works by the same group, detailed characterization and the influence of the PPO block length (1000 g·mol^{-1}) on the CMC were studied.[151-153] Additionally, P(EEGE)-*b*-PPO-*b*-P(EEGE) and PPO-*b*-P(EEGE)-*b*-PPO without the deprotected segments and their association behavior have been investigated.[154]
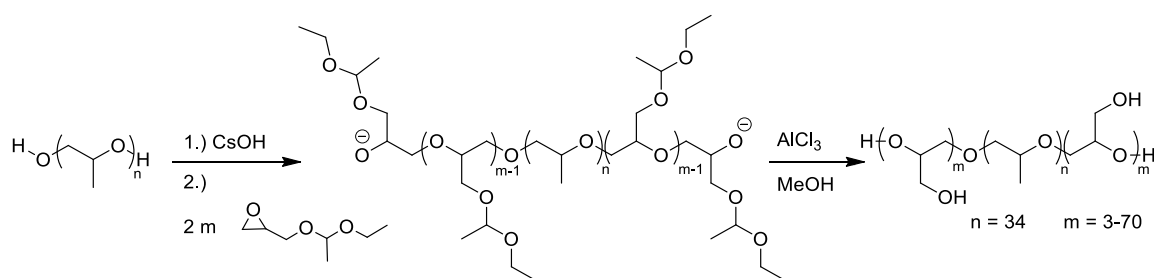
Scheme 7. Synthesis of "Pluronic-like" linear triblock copolymers *lin*PG-*b*-PPO-*b*-*lin*PG.[150]

These functional surfactants may also bear promise for the sensitization of multidrug resistant cancer cells in analogy to linear-hyperbranched surfactants based on a hyperbranched polyglycerol block.[154b] Interesting ABA triblock copolymers based on PEG and polyglycerol with an amphiphilic[101] or double-hydrophilic structure were prepared by Dworak *et al.*,[36,114] and by our group.[131] Subsequent to deprotonation of commercially available dihydroxy-functional PEGs and the anionic ring-opening

polymerization of EEGE, P(EEGE)-*b*-PEG-*b*-P(EEGE) was obtained, yielding *lin*PG-*b*-PEG-*b*-*lin*PG after removal of the acetal protecting group. Hyperbranched-linear-hyperbranched ABA-type polyethers were synthesized from a *lin*PG-*b*-PEG-*b*-*lin*PG polyfunctional macroinitiator with narrow molecular weight distributions (M_w/M_n = 1.19-1.45) and molecular weights between 6300 and 26,000 g·mol^{-1}.[131] Maximum biocompatibility is achieved by using merely polyethers as building blocks for these ABA architectures, and laborious coupling reactions between the blocks can be avoided. Surprisingly, studies of the thermal properties revealed that all samples were still crystalline to some extent, although the large hyperbranched block (high number of terminal functionalities, amorphous segment) was expected to impede crystallization of the PEG block. Dworak *et al.* reported the synthesis of polyglycerol-*b*-polystyrene-*b*-polyglycerol ABA structures under living reaction conditions with styrene and EEGE initiated with potassium naphthalenide.[36]

ABC triblock terpolymers consisting of polyglycerol-*b*-poly(ethylene glycol)-*b*-poly(D,L-lactide) were synthesized after deprotonation of 1-methoxy-2-ethanol, followed by the ring-opening polymerization of EEGE, EO and D,L-lactide. The formation of nonspherical micelles was observed.[155] PS-*b*-PEG-*b*-P(EEGE) triblock copolymers were obtained by combining carbanionic and oxyanionic polymerization techniques, capitalizing on a phosphazene base, allowing the one-pot synthesis of narrowly distributed (M_w/M_n = 1.02-1.10) terpolymers.[156]

4.3 Star polymers containing linear polyglycerol segments

Multifunctional low molecular weight initiators like trimethylolpropane,[157] di(trimethylolpropane),[39, 126, 157] pentaerythritol,[147, 158] dipentaerythritol,[75, 76, 147, 157, 159] and inositol[147] have efficiently been used for the synthesis of multiarm stars based on linear polyglycerol. The chemical composition and properties of the resulting stars can be easily modified by choosing glycidyl ethers that can be selectively deprotected. As an example, fully polyether-based amphiphilic star copolymers were prepared by Walach and co-workers *via* sequential polymerization of *t*BGE and EEGE from a multifunctional initiator followed by selective deprotection of the P(EEGE) block.[158] In a follow-up work,

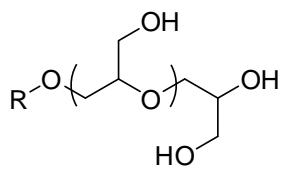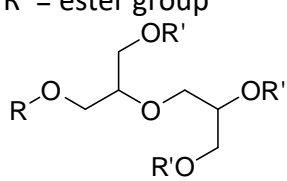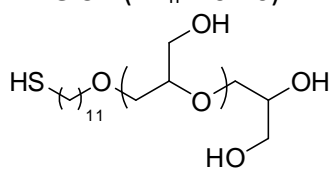"dendritic stars" were prepared by repeating the aforementioned reaction cycle (*t*BGE, EEGE, deprotection).[147]
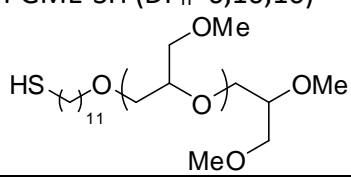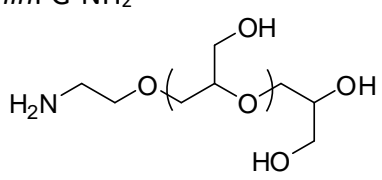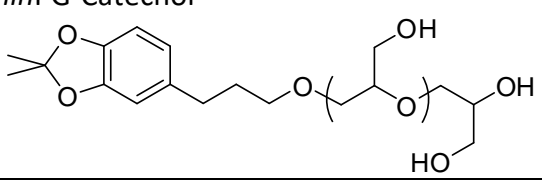
Multihydroxy-functional star-shaped polyglycerols serve as unusual macroinitiators for the synthesis of star block copolymers with a core-shell structure. The ring-opening polymerization of ε-caprolactone[39,126] and L-lactide from star-shaped PG-macroinitiators has been discussed in detail by Möller *et al.*.[160] Furthermore, they reported the use of multiarm P(EEGE)s blended with poly(ε-caprolactone) for the fabrication of hydrophilic, yet water-insoluble fibers showing decreased protein adsorption.[159] In another work, Keul et al. investigated 3-, 4-, and 6-arm *lin*PG-based stars modified with ATRP initiators with respect to their utility in the controlled radical polymerization of *tert*-butyl acrylate and methyl acrylate.[157]
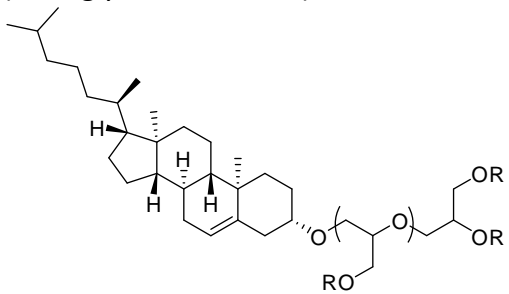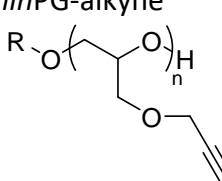
Various approaches have been described for the synthesis of heteroarm star polymers, bearing at least one *lin*PG arm.[161-165] As an example, Huang and co-workers prepared ABC-miktoarm star polymers by carbanionic polymerization of styrene, end-capping with EEGE and successive anionic ring-opening polymerization of EO and EEGE.[164]

5. Exploration of Biomedical and Pharmaceutical Applications

In comparison to the vast number of established applications of PEG, the development of actual applications of *lin*PG is still in its infancy. The excellent biocompatibility in combination with its biorepellent properties on surfaces have motivated various research groups to perform cell tests. In addition, conjugation with proteins ("PGylation") is likely to lead to further application-oriented concepts with respect to "functional bioconjugation" of therapeutic proteins. Table 1 summarizes all literature that is currently available on biomedical and pharmaceutical applications.

Table 1: Exploratory biomedical and pharmaceutical applications of *lin*PG.

Tested Polymer Structure	References	Exploratory test for biomedical and pharmaceutical applications
*lin*PG 	13-15	Hemocompatibility testing, red blood cell aggregation, blood viscosity measurements, cytotoxicity experiments, biocompatibility testing *In vivo* circulation/ biodistribution/ renal clearance
Esters of oligoglycerol (PG10-ester) R' = ester group 	3,16	FDA approved, pharma additives
Endfunctional *lin*PG		
*lin*PG-SH (DP$_n$=10-16) PGME-SH (DP$_n$=6,10,16) 	17,18,20 18, 20, 108	Surface modification/ SAM on gold Antifouling properties/ Biorepellent Resistant towards the adsorption of: fibrinogen, pepsin, albumin, and lysozyme protein and cell resistance
*lin*PG-NH$_2$ 	18,19 64 132	Surface modification gold/glass reduced non-specific protein adsorption of fibrinogen and BSA Bioconjugation →"PGylation" Noncovalent conjugation via avidin-biotin
*lin*PG-Catechol 	68 70	MnO Nanoparticle conjugation Biocompatibility studies

*lin*PG-Cholesterol derivatives (R=H; glycerol moieties)	72,136,137	"Stealth" liposome formation
Oligoglycerol brushes based on methacrylate	45	Antibiofouling properties
Copolymers containing *lin*PG		
PG-based microspheres	82,83,85, 86,87,88 79,84,89,90	Covalent attachment of antigens, proteins and marker (biosensors, diagnostic) → Determination of antibodies against Helicobacter pylori Protein adsorption studies
Backbone-functionalized *lin*PG		
Mono-heterobifunctional	104	Potential bioconjugation platform
*lin*PG-alkyne	42	Azido-functional sugar conjugation
Poly((glycerol ethylphosphonatoethyl)-*co*-(glycerol-graft-ε-caprolactone)	119 120	Enzymatic *grafting-from* *In vitro* degradation of ester side chains

6. Conclusion and Outlook

Although linear polyglycerol has been known for a long time, it appears that this material has been overlooked for a long time with respect to its high potential for biomedical and pharmaceutical application. Seminal reports by Fitton *et al.* and Taton *et al.* on the polymerization of EEGE, followed by facile removal of the protecting groups paved the way for the intense current interest. It should be emphasized that *lin*PG is

available by three simple synthetic steps only: (i) addition of vinyl ethyl ether to glycidol, (ii) subsequent anionic ring-opening polymerization and (iii) facile acidic deprotection in the same vessel within several minutes.

Only in the past decade, *lin*PG is increasingly considered as a promising biomedical material, mainly due to its high hydroxyl functionality, allowing an immense scope of further modifications and applications. This Review has presented both basic synthetic strategies toward linear and more complex architectures, versatile modification approaches as well as manifold block co- or terpolymer structures. Outstanding properties like high water solubility, excellent biocompatibility, and antifouling behavior have been explored, but clearly this field of research is by no means mature. Linear polyglycerol can be expected to show similar properties in biological systems as hyperbranched PG,[167, 168] but so far it has not been applied for biomedical purposes as much as PEG or *hb*PG. On the other hand, molecular encapsulation is different compared to *hb*PG[99] and rheological properties can be expected to vary as well. Nevertheless, the low intrinsic viscosity of *lin*PG makes it attractive in intraveneous applications.[13]

It is obvious that *lin*PG is not suitable to replace PEG for large-scale applications, such as for cosmetics and in established pharmaceutical fields; however, it may be considered as a promising highly functional building block in specialty applications. On the other hand, random copolymers comprising both PEG segments and a predefined amount of linear glycerol units can be obtained by random or block copolymerization of EO and EEGE, permitting one to obtain heteromultifunctional poly(ethylene glycol) copolymers with multiple hydroxyl groups. In this case, only a minor amount of EEGE is required. Via this approach, the high number of hydroxyl functionalities of *lin*PG can be "diluted" and thereby tailored for specific purposes, as is the case for the copolymerization of EO and EEGE, leading to structures that combine the properties of PEG with the functionality of PG.[169] A wide range of copolymerizations of EEGE with other glycidyl ethers has recently been studied to include other functional moieties in linear polyglycerols, *e.g.*, (1-adamantyl)methyl glycidyl ether[170] or for biocompatible nano- and microgels.[171] Recent publications have also shown strategies to overcome the non-degradability of *lin*PG by synthesizing poly(1,2-glycerol carbonate)s.[172,173] In summary, biomedical applications comprising drug delivery and controlled release, bioinert coatings, or tissue engineering

purposes as well as bioconjugation will benefit from the enormous versatility of *lin*PG as a highly functional biomaterial.

Acknowledgement

6. References

1. Dingels, C.; Schömer, M.; Frey, H., *Chem. Unserer Zeit* **2011,** *45* (5), 338-349.
2. Harris, J. M.; Zalipsky, S., *Poly(ethylene glycol) Chemistry and Biological Applications*. ACS Symposium Series: American Chemical Society Washington DC, **1997**; Vol. 680.
3. a.) Knop, K.; Hoogenboom, R.; Fischer, D.; Schubert, U. S., *Angew. Chem. Int. Ed.* **2010,** *49* (36), 6288-6308. b.) Barz, M.; Luxenhofer, R.; Zentel, R.; Vicent, M. J., *Polym. Chem.,* **2011**, *2*, 1900-1918. c.) Hamad, I.; Hunter, A. C.; Szebeni, J.; Moghimi, S. M., *Mol. Immunol.* **2008**, *46*, 225-232. d.) Ishida, T.; Kiwada, H., *Int. J. Pharm.*, **2008**, 354, 56-62.
4. Dimitrov, I.; Tsvetanov, C. B., *High-Molecular-Weight Poly(ethylene oxide).* In Polymer Science: A Comprehensive Reference, Elsevier: Amsterdam, **2012**; pp 551-569.
5. Otsuka, H.; Nagasaki, Y.; Kataoka, K., *Adv. Drug Delivery Rev.* **2003,** *55* (3), 403-419.
6. Harris, J. M.; Chess, R. B., *Nat. Rev. Drug Discovery* **2003,** *2* (3), 214-221.
7. Veronese, F. M.; Pasut, G., *Drug Discovery Today* **2005,** *10* (21), 1451-1458.
8. a) Wilms, D.; Stiriba, S.-E.; Frey, H., *Acc. Chem. Res.* **2010,** *43* (1), 129-141; b) Wilms, D.; Wurm, F.; Nieberle, J.; Böhm, P.; Kemmer-Jonas, U.; Frey, H. *Macromolecules* **2009**, 42, 3230–3236.
9. Calderon, M.; Quadir, M. A.; Sharma, S. K.; Haag, R., *Adv. Mater.* **2010,** *22* (2), 190-218.
10. Schömer, M.; Schüll, C.; Frey, H., *J. Polym. Sci., Part A: Polym. Chem.* **2013,** *51* (5), 995-1019.
11. Keul, H.; Möller, M., *J. Polym. Sci., Part A: Polym. Chem.* **2009,** *47* (13), 3209-3231.
12. Dworak, A.; Slomkowski, S.; Basinska, T.; Gosecka, M.; Walach, W.; Trzebicka, B., *Polimery* **2013,** *58* (9), 641-649.
13. Kainthan, R. K.; Janzen, J.; Levin, E.; Devine, D. V.; Brooks, D. E., *Biomacromolecules* **2006,** *7* (3), 703-709.
14. Klajnert, B.; Walach, W.; Bryszewska, M.; Dworak, A.; Shcharbin, D., *Cell Biol. Int.* **2006,** *30* (3), 248-252.
15. Imran ul-haq, M.; Lai, B. F. L.; Chapanian, R.; Kizhakkedathu, J. N., *Biomaterials* **2012,** *33* (35), 9135-9147.
16. O'Brien, R. D., *Fats and Oils: Formulating and Processing for Applications*. 2nd ed.; CRC Press LLC: Baco Raton, FL, **2004**.
17. Wyszogrodzka, M.; Haag, R., *Langmuir* **2009,** *25* (10), 5703-5712.
18. Weinhart, M.; Grunwald, I.; Wyszogrodzka, M.; Gaetjen, L.; Hartwig, A.; Haag, R., *Chem. Asian J.* **2010,** *5* (9), 1992-2000.
19. Weinhart, M.; Becherer, T.; Schnurbusch, N.; Schwibbert, K.; Kunte, H.-J.; Haag, R., *Adv. Eng. Mater.* **2011,** *13* (12), B501-B510.
20. Weber, M.; Bujotzek, A.; Andrae, K.; Weinhart, M.; Haag, R., *Mol. Sim.* **2011,** *37* (11), 899-906.
21. Staudinger, H.; Schweitzer, O., *Ber. Dtsch. Chem. Ges. A/B* **1929,** *62* (8), 2395-2405.

22. Haouet, A.; Sepulchre, M.; Spassky, N., *Eur. Polym. J.* **1983,** *19* (12), 1089-1098.
23. Price, C. C.; Vandenberg, E. J., *Coordination Polymerization*. Plenum Press, New York: **1983**; Vol. 19.
24. Wurm, F.; Nieberle, J.; Frey, H., *Macromolecules* **2008,** *41* (4), 1184-1188.
25. Atkinson, J. L.; Vyazovkin, S., *Macromol. Chem. Phys.* **2011,** *212* (19), 2103-2113.
26. Schömer, M.; Frey, H., *Macromolecules* **2012,** *45* (7), 3039-3046.
27. Siegers, C.; Biesalski, M.; Haag, R., *Chem. Eur. J.* **2004,** *10* (11), 2831-2838.
28. Kjellander, R.; Florin, E., *J. Chem. Soc., Faraday Trans. 1* **1981,** *77* (9), 2053-2077.
29. Fitton, A. O.; Hill, J.; Jane, D. E.; Millar, R., *Synthesis* **1987,** (12), 1140-1142.
30. Wurm, F.; Nieberle, J.; Frey, H., *Macromolecules* **2008,** *41* (6), 1909-1911.
31. Brocas, A.-L.; Mantzaridis, C.; Tunc, D.; Carlotti, S., *Prog. Polym. Sci.* **2013,** *38* (6), 845-873.
32. Vandenberg, E. J. High-molecular-weight hydroxyl-containing polyethers: glycidol polymers. US Patent US3446757A, **1969**.
33. Tsuruta, T.; Inoue, S.; Koenuma, H., *Makromol. Chem.* **1968,** *112* (1), 58-65.
34. Vandenberg, E. J., *J. Polym. Sci., Part A: Polym. Chem.* **1985,** *23* (4), 915-949.
35. Taton, D.; Leborgne, A.; Sepulchre, M.; Spassky, N., *Macromol. Chem. Phys.* **1994,** *195* (1), 139-148.
36. Dworak, A.; Panchev, I.; Trzebicka, B.; Walach, W., *Macromol. Symp.* **2000,** *153*, 233-242.
37. Dworak, A.; Panchev, I.; Trzebicka, B.; Walach, W., *Polym. Bull.* **1998,** *40* (4-5), 461-468.
38. Walach, W.; Kowalczuk, A.; Trzebicka, B.; Dworak, A., *Macromol. Rapid Commun.* **2001,** *22* (15), 1272-1277.
39. Hans, M.; Gasteier, P.; Keul, H.; Möller, M., *Macromolecules* **2006,** *39* (9), 3184-3193.
40. Schacht, C. S.; Schüll, C.; Frey, H.; de Loos, T. W.; Gross, J., *J. Chem. Eng. Data* **2011,** *56* (6), 2927-2931.
41. Hans, M.; Keul, H.; Möller, M., *Polymer* **2009,** *50* (5), 1103-1108.
42. Erberich, M.; Keul, H.; Möller, M., *Macromolecules* **2007,** *40* (9), 3070-3079.
43. Thomas, A.; Wolf, F. K.; Frey, H., *Macromol. Rapid Commun.* **2011,** *32* (23), 1910-1915.
44. Thomas, A.; Niederer, K.; Wurm, F.; Frey, H., *Polym. Chem.* **2014**, *5*, 899-909.
45. Gunkel, G.; Weinhart, M.; Becherer, T.; Haag, R.; Huck, W. T. S., *Biomacromolecules* **2011,** *12* (11), 4169-4172.
46. Backes, M.; Messager, L.; Mourran, A.; Keul, H.; Möller, M., *Macromolecules* **2010,** *43* (7), 3238-3248.
47. Mendrek, S.; Mendrek, A.; Adler, H.-J.; Walach, W.; Dworak, A.; Kuckling, D., *J. Polym. Sci., Part A: Polym. Chem.* **2008,** *46* (7), 2488-2499.
48. Dworak, A.; Trzebicka, B.; Wałach, W.; Utrata, A.; Tsvetanov, C., *Macromol. Symp.* **2004,** *210*, 419-426.
49. Jamróz-Piegza, M.; Utrata-Wesolek, A.; Trzebicka, B.; Dworak, A., *Eur. Polym. J.* **2006,** *42* (10), 2497-2506.
50. Rangelov, S.; Trzebicka, B.; Jamroz-Piegza, M.; Dworak, A., *J. Phys. Chem. B* **2007,** *111* (38), 11127-11133.
51. Dimitrov, P.; Hasan, E.; Rangelov, S.; Trzebicka, B.; Dworak, A.; Tsvetanov, C. B., *Polymer* **2002,** *43* (25), 7171-7178.

52. Deffieux, A.; Billouard, C.; Carlotti, S.; Desbois, P., *Polym. Prepr. (Am. Chem. Soc., Div. Polym. Chem.)* **2004,** *45* (2), 571-572.

53. Billouard, C.; Carlotti, S.; Desbois, P.; Deffieux, A., *Macromolecules* **2004,** *37* (11), 4038-4043.

54. Carlotti, S.; Billouard, C.; Gautriaud, E.; Desbois, P.; Deffieux, A., *Macromol. Symp.* **2005,** *226* (1), 61-68.

55. Labbé, A.; Carlotti, S.; Billouard, C.; Desbois, P.; Deffieux, A., *Macromolecules* **2007,** *40* (22), 7842-7847.

56. Gervais, M.; Labbé, A.; Carlotti, S.; Deffieux, A., *Macromolecules* **2009,** *42* (7), 2395-2400.

57. Gervais, M.; Brocas, A.-L.; Cendejas, G.; Deffieux, A.; Carlotti, S., *Macromolecules* **2010,** *43* (4), 1778-1784.

58. Gervais, M.; Brocas, A.-L.; Cendejas, G.; Deffieux, A.; Carlotti, S., *Macromol. Symp.* **2011,** *308* (1), 101-111.

59. Cassel, S.; Debaig, C.; Benvegnu, T.; Chaimbault, P.; Lafosse, M.; Plusquellec, D.; Rollin, P., *Eur. J. Org. Chem.* **2001,** *2001* (5), 875-896.

60. Debaig, C.; Benvegnu, T.; Plusquellec, D., *Oleagineux, Corps Gras, Lipides* **2002,** *9* (2-3), 155-162.

61. Obermeier, B.; Wurm, F.; Mangold, C.; Frey, H., *Angew. Chem. Int. Ed.* **2011,** *50* (35), 7988-7997.

62. Mangold, C.; Wurm, F.; Frey, H., *Polym. Chem.* **2012,** *3* (7), 1714-1721.

63. Thompson, M. S.; Vadala, T. P.; Vadala, M. L.; Lin, Y.; Riffle, J. S., *Polymer* **2008,** *49* (2), 345-373.

64. Wurm, F.; Dingels, C.; Frey, H.; Klok, H.-A., *Biomacromolecules* **2012,** *13* (4), 1161-1171.

65. Häkkinen, H., *Nat. Chem.* **2012,** *4* (6), 443-455.

66. Sedó, J.; Saiz-Poseu, J.; Busqué, F.; Ruiz-Molina, D., *Adv. Mater.* **2013,** *25* (5), 653-701.

67. Faure, E.; Falentin-Daudré, C.; Jérôme, C.; Lyskawa, J.; Fournier, D.; Woisel, P.; Detrembleur, C., *Prog. Polym. Sci.* **2013,** *38* (1), 236-270.

68. Thomas, A.; Bauer, H.; Schilmann, A.-M.; Fischer, K.; Tremel, W.; Frey, H., *Macromolecules,* submitted for publication.

69. Wilms, V. S.; Bauer, H.; Tonhauser, C.; Schilmann, A.-M.; Müller, M.-C.; Tremel, W.; Frey, H., *Biomacromolecules* **2013,** *14* (1), 193-199.

70. Bauer, H.; Thomas, A.; Herzberger, J.; Schilmann, A.-M.; Wichmann, K.; Heim, J.; Fischer, K.; Frey, H.; Tremel, W., **2013**, unpublished results.

71. Zhao, J.; Schlaad, H.; Weidner, S.; Antonietti, M., *Polym. Chem.* **2012,** *3* (7), 1763-1768.

72. Hofmann, A. M.; Wurm, F.; Frey, H., *Macromolecules* **2011,** *44* (12), 4648-4657.

73. Hofmann, A. M.; Wipf, R.; Stühn, B.; Frey, H., *Macromolecules* **2011,** *44* (17), 6767-6775.

74. Moers, C.; Nuhn, L.; Wissel, M.; Stangenberg, R.; Mondeshki, M.; Berger-Nicoletti, E.; Thomas, A.; Schäffel, D.; Koynov, K.; Klapper, M.; Zentel, R.; Frey, H., *Macromolecules*, **2013**, *46*, 9544-9553.

75. Haamann, D.; Keul, H.; Klee, D.; Möller, M., *Macromol. Symp.* **2010,** *296* (1), 1-4.

76. Haamann, D.; Keul, H.; Klee, D.; Möller, M., *Macromolecules* **2010,** *43* (15), 6295-6301.

77. Basinska, T.; Slomkowski, S.; Dworak, A.; Panchev, I.; Chehimi, M. M., *Colloid. Polym. Sci.* **2001,** *279* (9), 916-924.
78. Basinska, T., *e-Polym.* **2002,** *2* (1), 145-158.
79. Basinska, T.; Slomkowski, S.; Kazmierski, S.; Dworak, A.; Chehimi, M. M., *J. Polym. Sci., Part A: Polym. Chem.* **2004,** *42* (3), 615-623.
80. Basinska, T.; Slomkowski, S.; Kazmierski, S.; Chehimi, M. M., *Langmuir* **2008,** *24* (16), 8465-8472.
81. Griffete, N.; Dybkowska, M.; Glebocki, B.; Basinska, T.; Connan, C.; Maître, A.; Chehimi, M. M.; Slomkowski, S.; Mangeney, C., *Langmuir* **2010,** *26* (13), 11550-11557.
82. Gosecka, M.; Griffete, N.; Mangeney, C.; Chehimi, M. M.; Slomkowski, S.; Basinska, T., *Colloid Polym. Sci.* **2011,** *289* (13), 1511-1518.
83. Iovescu, A.; Gosecka, M.; Basinska, T.; Baran, A.; Stinga, G.; Slomkowski, S.; Anghel, D. F., *Dyes Pigm.* **2013,** *97* (2), 347-352.
84. Basinska, T., *J. Biomater. Sci. Polym. Ed.* **2001,** *12* (12), 1359-1371.
85. Basinska, T.; Krolik, S.; Slomkowski, S., *Macromol. Symp.* **2009,** *281* (1), 96-105.
86. Basinska, T.; Wisniewska, M.; Chmiela, M., *Macromol. Biosci.* **2005,** *5* (1), 70-77.
87. Slomkowski, S.; Basinska, T., *Macromol. Symp.* **2010,** *295* (1), 13-22.
88. Slomkowski, S.; Basinska, T.; Miksa, B., *Polym. Adv. Technol.* **2002,** *13* (10-12), 905-918.
89. Basinska, T.; Slomkowski, S., *Chem. Pap.* **2012,** *66* (5), 352-368.
90. Gam-Derouich, S.; Gosecka, M.; Lepinay, S.; Turmine, M.; Carbonnier, B.; Basinska, T.; Slomkowski, S.; Millot, M.-C.; Othmane, A.; Ben Hassen-Chehimi, D.; Chehimi, M. M., *Langmuir* **2011,** *27* (15), 9285-9294.
91. Pargen, S.; Omeis, J.; Jaunky, G.; Keul, H.; Möller, M., *Macromol. Chem. Phys.* **2011,** *212* (16), 1791-1801.
92. Pargen, S.; Willems, C.; Keul, H.; Pich, A.; Möller, M., *Macromolecules* **2012,** *45* (3), 1230-1240.
93. Ito, K.; Tanaka, K.; Tanaka, H.; Imai, G.; Kawaguchi, S.; Itsuno, S., *Macromolecules* **1991,** *24* (9), 2348-2354.
94. Ito, K.; Hashimura, K.; Itsuno, S.; Yamada, E., *Macromolecules* **1991,** *24* (14), 3977-3981.
95. Maniruzzaman, M.; Kawaguchi, S.; Ito, K., *Macromolecules* **2000,** *33* (5), 1583-1592.
96. Mendrek, A.; Mendrek, S.; Trzebicka, B.; Kuckling, D.; Walach, J.; Adler, H. J.; Dworak, A., *Macromol. Chem. Phys.* **2005,** *206* (20), 2018-2026.
97. Mendrek, A.; Mendrek, S.; Adler, H. J.; Dworak, A.; Kuckling, D., *Polymer* **2010,** *51* (2), 342-354.
98. Thomas, A.; Nuhn, L.; Johann, T.; Zentel, R.; Frey, H., unpublished results.
99. Stiriba, S. E.; Kautz, H.; Frey, H., *J. Am. Chem. Soc.* **2002,** *124* (33), 9698-9699.
100. Dworak, A.; Trzebicka, B.; Utrata, A.; Walach, W., *Polym. Bull.* **2003,** *50* (1-2), 47-54.
101. Dimitrov, P.; Utrata-Wesolek, A.; Rangelov, S.; Walach, W.; Trzebicka, B.; Dworak, A., *Polymer* **2006,** *47* (14), 4905-4915.
102. Ozdemir, F.; Keul, H.; Mourran, A.; Möller, M., *Macromol. Rapid Commun.* **2011,** *32* (13), 1007-1013.

103. Theiler, S.; Hoevetborn, T.; Keul, H.; Möller, M., *Macromol. Chem. Phys.* **2009,** *210* (8), 614-630.

104. Li, Z.; Chau, Y., *Bioconjugate Chem.* **2009,** *20* (4), 780-789.

105. Aoki, S.; Koide, A.; Imabayashi, S.-i.; Watanabe, M., *Chem. Lett.* **2002,** *31* (11), 1128-1129.

106. Labbé, A.; Carlotti, S.; Deffieux, A.; Hirao, A., *Macromol. Symp.* **2007,** *249-250* (1), 392-397.

107. Labbé, A.; Brocas, A.-L.; Ibarboure, E.; Ishizone, T.; Hirao, A.; Deffieux, A.; Carlotti, S., *Macromolecules*, **2011,** *44*, 6356-6364.

108. Weinhart, M.; Becherer, T.; Haag, R., *Chem. Commun.* **2011,** *47* (5), 1553-1555.

109. Höger, K.; Becherer, T.; Qiang, W.; Haag, R.; Frieß, W.; Küchler, S., *Eur. J. Pharm. Biopharm.* **2013,** *85*, 756-764.

110. Lange, M.; Braune, S.; Luetzow, K.; Richau, K.; Scharnagl, N.; Weinhart, M.; Neffe, A. T.; Jung, F.; Haag, R.; Lendlein, A., *Macromol. Rapid Commun.* **2012,** *33* (17), 1487-1492.

111. Braune, S.; von Ruesten-Lange, M.; Mrowietz, C.; Luetzow, K.; Roch, T.; Neffe, A. T.; Lendlein, A.; Jung, F., *Clin. Hemorheol. Microcirc.* **2013,** *54* (3), 235-248.

112. von Ruesten-Lange, M.; Luetzow, K.; Neffe, A. T.; Lendlein, A., *J. Appl. Biomater. Funct. Mater.* **2012,** *10* (3), 215-222.

113. Kumar, K. R.; Brooks, D. E., *Macromol. Rapid Commun.* **2005,** *26* (3), 155-159.

114. Dworak, A.; Baran, G.; Trzebicka, B.; Walach, W., *React. Funct. Polym.* **1999,** *42* (1), 31-36.

115. Utrata-Wesolek, A.; Trzebicka, B.; Dworak, A.; Ivanova, S.; Christova, D., *e-Polym.* **2007**, 019.

116. Groll, J.; Singh, S.; Albrecht, K.; Möller, M., *J. Polym. Sci. Part A: Polym. Chem.* **2009,** *47* (20), 5543-5549.

117. Penczek, S.; Pretula, J.; Kaluzynski, K., *J. Polym. Sci., Part A: Polym. Chem.* **2004,** *42* (3), 432-443.

118. Köhler, J.; Keul, H.; Möller, M., *Chem. Commun.* **2011,** *47* (28), 8148-8150.

119. Köhler, J.; Marquardt, F.; Keul, H.; Möller, M., *Macromolecules* **2013,** *46* (10), 3708-3718.

120. Köhler, J.; Marquardt, F.; Teske, M.; Keul, H.; Sternberg, K.; Möller, M., *Biomacromolecules* **2013,** *14* (11), 3985-3996.

121. Ouchi, T.; Ichimura, S.; Ohya, Y., *Polymer* **2006,** *47* (1), 429-434.

122. Geschwind, J.; Rathi, S.; Tonhauser, C.; Schömer, M.; Hsu, S. L.; Coughlin, E. B.; Frey, H., *Macromol. Chem. Phys.* **2013,** *214* (13), 1434-1444.

123. Hans, M.; Mourran, A.; Henke, A.; Keul, H.; Möller, M., *Macromolecules* **2009,** *42* (4), 1031-1036.

124. Turunen, M. P. K.; Laurila, T.; Kivilahti, J. K., *J. Appl. Polym. Sci.* **2006,** *101* (6), 3677-3688.

125. Hans, M.; Keul, H.; Heise, A.; Möller, M., *Macromolecules* **2007,** *40* (25), 8872-8880.

126. Hans, M.; Keul, H.; Möller, M., *Biomacromolecules* **2008,** *9* (10), 2954-2962.

127. Hans, M.; Xiao, Y.; Keul, H.; Heise, A.; Möller, M., *Macromol. Chem. Phys.* **2009,** *210* (9), 736-746.

128. Walach, W.; Trzebicka, B.; Justynska, J.; Dworak, A., *Polymer* **2004,** *45* (6), 1755-1762.

129. Jing, R.; Wang, G.; Huang, J., *J. Polym. Sci., Part A: Polym. Chem.* **2010,** *48* (23), 5430-5438.

130. a) Hanselmann, R.; Hölter, D.; Frey, H., *Macromolecules* **1998,** *31* (12), 3790-3801; b) C. Schüll, H. Rabbel, F. Schmid, H. Frey, *Macromolecules.* **2013**, *46*, 5823–5830.

131. Wurm, F.; Kemmer-Jonas, U.; Frey, H., *Polym. Int.* **2009,** *58* (9), 989-995.

132. Wurm, F.; Klos, J.; Raeder, H. J.; Frey, H., *J. Am. Chem. Soc.* **2009,** *131* (23), 7954-7955.

133. Wurm, F.; Hofmann, A. M.; Thomas, A.; Dingels, C.; Frey, H., *Macromol. Chem. Phys.* **2010,** *211* (8), 932-939.

134. Lee, S.; Saito, K.; Lee, H.-R.; Lee, M. J.; Shibasaki, Y.; Oishi, Y.; Kim, B.-S., *Biomacromolecules* **2012,** *13* (4), 1190-1196.

135. Sharma, A.; Sharma, U. S., *Int. J. Pharm.* **1997,** *154* (2), 123-140.

136. Hofmann, A. M.; Wurm, F.; Hühn, E.; Nawroth, T.; Langguth, P.; Frey, H., *Biomacromolecules* **2010,** *11* (3), 568-574.

137. a.) Müller, S. S.; Dingels, C.; Hofmann, A. M.; Frey, H., Polyether-Based Lipids Synthesized with an Epoxide Construction Kit: Multivalent Architectures for Functional Liposomes. In *Tailored Polymer Architectures for Pharmaceutical and Biomedical Applications*; American Chemical Society: Washington DC, **2013**; Vol. 1135, pp 11-25. b.) Müller, S. S.; Reddy, A.; Frey, H., **2014**, unpublished results.

138. Zhao, X. B.; Muthusamy, N.; Byrd, J. C.; Lee, R. J., *J. Pharm. Sci.* **2007,** *96* (9), 2424-2435.

139. Peng, X.; Hofmann, A. M.; Reuter, S.; Frey, H.; Kressler, J., *Colloid. Polym. Sci.* **2012,** *290* (7), 579-588.

140. Rao, Z.; Taguchi, T., *Colloids Surf. B: Biointerfaces* **2012,** *97* (0), 248-253.

141. Schöps, R.; Amado, E.; Müller, S. S.; Frey, H.; Kressler, J., *Faraday Discuss.* **2013,** *166,* 303-315.

142. Siebert, M.; Henke, A.; Eckert, T.; Richtering, W.; Keul, H.; Möller, M., *Langmuir* **2010,** *26* (22), 16791-16800.

143. Siebert, M.; Keul, H.; Möller, M., *Des. Monomers Polym.* **2010,** *13* (6), 547-563.

144. Kwon, W.; Rho, Y.; Kamoshida, K.; Kwon, K. H.; Jeong, Y. C.; Kim, J.; Misaka, H.; Shin, T. J.; Kim, J.; Kim, K.-W.; Jin, K. S.; Chang, T.; Kim, H.; Satoh, T.; Kakuchi, T.; Ree, M., *Adv. Funct. Mater.* **2012,** *22* (24), 5194-5208.

145. Meyer, J.; Keul, H.; Möller, M., *Macromolecules* **2011,** *44* (11), 4082-4091.

146. Dworak, A.; Walach, W., *Polymer* **2009,** *50* (15), 3440-3447.

147. Libera, M.; Walach, W.; Trzebicka, B.; Rangelov, S.; Dworak, A., *Polymer* **2011,** *52* (16), 3526-3536.

148. Oikawa, Y.; Lee, S.; Kim, D. H.; Kang, D. H.; Kim, B.-S.; Saito, K.; Sasaki, S.; Oishi, Y.; Shibasaki, Y., *Biomacromolecules* **2013,** *14* (7), 2171-2178.

149. Schmolka, I., *J. Am. Oil Chem. Soc.* **1977,** *54* (3), 110-116.

150. Halacheva, S.; Rangelov, S.; Tsvetanov, C., *Macromolecules* **2006,** *39* (20), 6845-6852.

151. Rangelov, S.; Almgren, M.; Halacheva, S.; Tsvetanov, C., *J. Phys. Chem. C* **2007,** *111* (35), 13185-13191.

152. Halacheva, S.; Rangelov, S.; Garamus, V. M., *Macromolecules* **2007,** *40* (22), 8015-8021.

153. Halacheva, S.; Rangelov, S.; Tsvetanov, C.; Garamus, V. M., *Macromolecules* **2010,** *43* (2), 772-781.

154. a) Dimitrov, P.; Rangelov, S.; Dworak, A.; Tsvetanov, C. B., *Macromolecules* **2004,** *37* (3), 1000-1008; b) Demina, T.; Grozdova, I.; Krylova, O.; Zhirnov, A.; Istratov, V.; Frey, H.; Kautz, H.; Melik-Nubarov N. *Biochemistry* **2005**, 44, 4042-4054.

155. Dimitrov, P.; Porjazoska, A.; Novakov, C. P.; Cvetkovska, M.; Tsvetanov, C. B., *Polymer* **2005,** *46* (18), 6820-6828.

156. Toy, A. A.; Reinicke, S.; Müller, A. H. E.; Schmalz, H., *Macromolecules* **2007,** *40* (15), 5241-5244.

157. Schmitz, C.; Keul, H.; Möller, M., *Eur. Polym. J.* **2009,** *45* (9), 2529-2539.

158. Libera, M.; Trzebicka, B.; Kowalczuk, A.; Walach, W.; Dworak, A., *Polymer* **2011,** *52* (2), 250-257.

159. Haamann, D.; Bispinghoff, M.; Hönders, D.; Suschek, C.; Möller, M.; Klee, D., *J. Appl. Polym. Sci.* **2012,** *125* (5), 3638-3647.

160. Keul, H.; Möller, M., *J. Polym. Sci., Part A: Polym. Chem.* **2009,** *47*, 3209-3231.

161. Wang, X.; Fu, P.; Liu, M.; Zhang, J.; Zhao, Q., *Adv. Mater. Res.* **2011,** *311-313*, 1161-1167.

162. Lapienis, G.; Penczek, S., *Biomacromolecules* **2005,** *6* (2), 752-762.

163. Lapienis, G., *Polymer* **2009,** *50* (1), 77-84.

164. Wang, G.; Huang, J., *Macromol. Rapid Commun.* **2007,** *28* (3), 298-304.

165. Dimitrov, P.; Rangelov, S.; Dworak, A.; Haraguchi, N.; Hirao, A.; Tsvetanov, C. B., *Macromol. Symp.* **2004,** *215* (1), 127-140.

166. Tonhauser, C.; Frey, H. *Macromol. Rapid Commun*. **2010**, *31*, 1938-1947.

167. Chapanian, R.; Constantinescu, I.; Brooks, D. E.; Scott, M. D.; Kizhakkedathu, J. N., *Biomaterials*, **2012**, *33*, 3047-3057.

168. Du, C.; Mendelson, A. A.; Guan, Q.; Chapanian, R.; Chafeeva, I.; da Roza, G.; Kizhakkedathu, J. N., *Biomaterials*, **2014**, *35*, 1378-1389.

169. Mangold, C.; Wurm, F.; Obermeier, B.; Frey, H. *Macromol. Rapid Commun.* **2010**, 31, 258-264.

170. Moers, C.; Wrazidlo, R.; Natalello, A.; Netz, I.; Mondeshki, M.; Frey, H., *Macromol. Rapid Commun.* **2014**, DOI: 10.1002/marc.201400017.

171. Schulte, B.; Walther, A.; Keul, H.; Möller, M. *Macromolecules* **2014**, *47* (5), 1633-1645.

172. Zhang, H.; Grinstaff, M. W., *J. Am. Chem. Soc.*, **2013**, *135* (18), 6806–6809.

173. Geschwind, J.; Frey, H., *Macromolecules*, **2013**, *46* (9), 3280–3287.

2 Functionalized and pH-Responsive Polymer Lipids

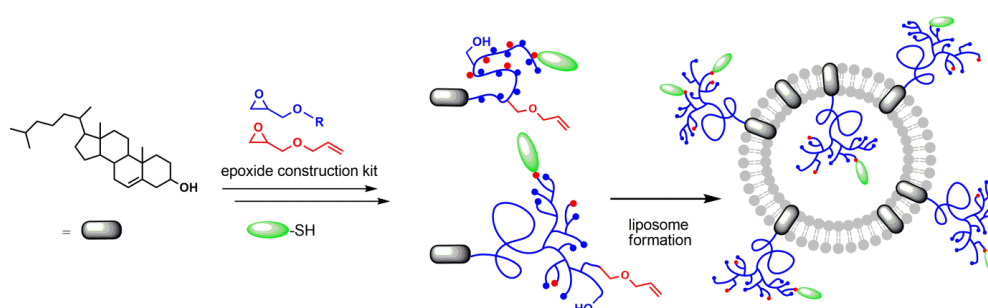## 2.1 Allyl-Functionalized Cholesterol-Lipids: From Thiol-ene Coupling to Liposomes

Sophie S. Müller,[1,2] Alissa Reddy,[1] and Holger Frey[1]

[1]Institute of Organic Chemistry, Johannes Gutenberg University Mainz, Duesbergweg 10-14, 55128 Mainz, Germany

[2]Graduate School Materials Science in Mainz, Staudingerweg 9, 55128 Mainz, Germany

Abstract

A variety of allyl-functional cholesterol-polyether lipids in the molecular weight range of 2000 to 5000 g mol^{-1} was synthesized via oxyanionic ring-opening polymerization of different epoxides. The initiator cholesterol was used as the hydrophobic segment and anchor in lipid bilayers. Random copolymers of ethoxyethyl glycidyl ether (EEGE) and allyl glycidyl ether (AGE) were prepared with AGE contents between 25-75mol% and polydispersity indices (M_w/M_n) below 1.25. Allyl groups were introduced into poly(ethylene glycol)-linear polyglycerol (PEG-*lin*PG) or hyperbranched polyglycerol (*hb*PG) lipids. ^{1}H NMR spectroscopy, differential scanning calorimetry (DSC), MALDI-ToF mass spectrometry, and surface tension measurements were employed for lipid characterization. The allyl groups were derivatized with thiols (benzyl mercaptan and glutathione, GSH) in thiol-ene coupling reactions. As an example, the hyperbranched polyether-lipid (Ch-*hb*PG$_{30}$-PAGE$_{10}$-GSH$_4$) was incorporated into liposomes formed by cholesterol and egg phosphatidylcholine (EPC) in order to investigate its potential in

drug delivery systems. Dynamic light scattering (DLS) and cryo-transmission electron microscopy (cryo-TEM) showed unilamellar vesicles of 150 nm. The results lay the foundation for active targeting, *e.g.*, in liposomes for anti-cancer treatment.

Introduction

Poly(ethylene glycol) (PEG) coated liposomes play an important role in drug delivery systems nowadays. These spherical vesicles are composed of phospholipid bilayers and (phospho)-lipids that carry biocompatible PEG chains. They can entrap both hydrophilic and hydrophobic drugs and deliver them to the site of action. PEGylated vesicles, so-called "stealth" liposomes, combine the advantages of passive targeting and the reduction of harmful side effects of anti-cancer drugs on healthy tissue.[1,2,3] The presence of a polymeric shell results in prolonged blood circulation times,[4,5,6] reduced mononuclear phagocyte system (MPS) uptake,[7] reduced aggregation in blood and improved stability of these liposomal carriers compared to conventional liposomes. The so-called "stealth effect" is ascribed to steric stabilization of the vesicle by the polymer corona.[8,9] Passive targeting can be achieved by the "enhanced permeability and retention" (EPR) effect, *i.e.*, the increased permeability of blood vessels in a tumor or inflamed tissue.[10,11] Doxil™, the most prominent commercially available liposomal drug carrier, with doxorubicin incorporated in PEGylated liposomes, is currently used against Kaposi's sarcoma and ovarian cancer.[8,12-14]
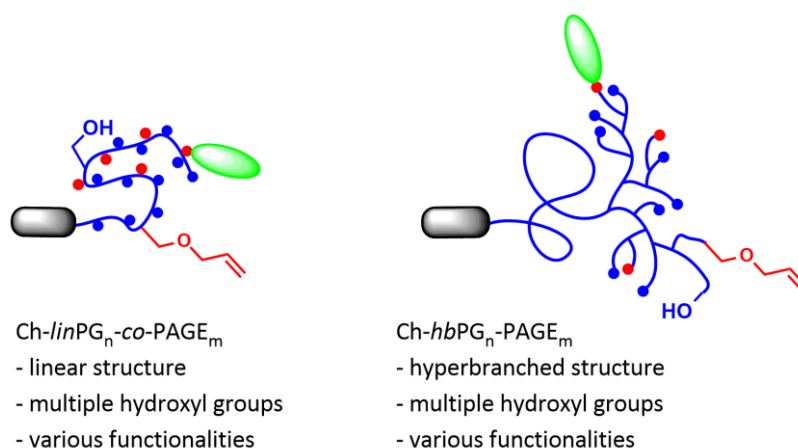
Besides improved pharmacokinetics and liposome stabilization, the strategy of PEGylation also implies several disadvantages. Methoxypoly(ethylene glycol) (mPEG) is often used in challenging coupling chemistry for the attachment to phospholipids.[13,15] The monofunctional polymer chain lacks additional groups for further functionalization, which can be necessary for active liposome targeting. Several efforts have been made to introduce additional functionalities along or at the end of the linear polymer backbone. To date, multiple hydroxyl groups have been introduced via ethoxyethyl glycidyl ether (EEGE). This acetal protected glycidyl monomer can be polymerized in the oxyanionic ring-opening polymerization (AROP) and carries one methylene hydroxyl group per monomer unit after the acidic deprotection step.[16-18] Using 1,2-(isopropylidene glyceryl)

glycidyl ether (IGG) two hydroxyl groups per monomer unit can be introduced.[19] Möller *et al.* published a useful synthesis for the preparation of linear polyglycerol (*lin*PG) with two orthogonal protecting groups. EEGE, allyl glycidyl ether (AGE), and *tert*-butyl glycidyl ether (*t*BGE) were combined in the AROP using potassium 3-phenyl-1-propanolate as initiator. Selective removal of only one protecting group led to various linear poly(glycerol ethers).[20] Recently, the random copolymerization of EEGE and AGE was demonstrated by in situ NMR-kinetics.[21] Our group has utilized epoxides for the synthesis of multifunctional lipids for liposome preparation in biomedical applications. By using the natural membrane component cholesterol directly as an initiator for the polymerization of EEGE or IGG, it is possible to obtain cholesterol-lipids with different architectures like *lin*PG or poly(glyceryl glycidyl ether) (PGG) with one or two hydroxyl groups per monomer unit, respectively. Complex structures such as hyperbranched polyglycerol (*hb*PG) lipids can be obtained when using glycidol in the slow monomer addition (SMA) technique.[22,23] Laborious coupling chemistry can be avoided and advantageous properties are expected with PEG as a flexible spacer and *hb*PG as a polymer with excellent biocompatibility.[24,25,26,27] Furthermore, the multifunctional polyethers bear numerous hydroxyl-groups for the subsequent attachment of markers or targeting moieties, resist the adsorption of proteins,[28,29] are highly water-soluble, and may show improved shielding compared to PEG due to the branched structure.

Furthermore, the aforementioned allyl groups, that can be converted into hydroxyl groups, were used for the functionalization of polyethers.[19,20] Random copolymers of AGE and ethylene oxide (EO) with molecular weights between 5000 and 13 600 g mol^{-1} were synthesized by our group in order to carry out thiol-ene coupling (TEC) with small (bio)-molecules. The well-defined hybrid materials with peptides conjugated to the PEG backbone provide a platform for bioconjugation.[30] Shortly after this work, Lee *et al.* published an investigation of high molecular weight (10 000-100 000 g mol^{-1}) poly(allyl glycidyl ether)s (PAGE) aiming at the correlation of the isomerization of allyl side chains and the reaction temperature. They found almost no isomerization in bulk or in solution with a temperature below 40 °C.[31] Furthermore, PAGE-PEG copolymers were used for ether-based polymer electrolytes.[32] Compared to the copper-catalyzed Huisgen 1,3-dipolar cycloaddition (click-reaction) the thiol-ene coupling requires several equivalents of the thiol compound. Nevertheless, it was proven to be an effective method to modify

various materials, such as inorganic polymers,[33] SBR rubbers[34] and has also been used for the synthesis of dendrimers.[35] Moreover, biologically important molecules like the anti-cancer drug doxorubicin were successfully attached to PEG-*co*-PAGE copolymers (~3wt%) via a pH-sensitive hydrazone bond in multiple steps by Ulbrich *et al.*.[36,37]

For biological applications the usage of copper is disfavoured due to its cytotoxicity. The ring-opening of strained heterocyclic electrophiles[38] and other metal-free click-reactions[39] can be used to overcome this issue but is often related to elaborated small molecule chemistry. Thiol-ene coupling, on the other hand, avoids metal catalysts but works via free radical addition (thermally or photochemically)[40,41] of thiols onto double bonds. High tolerance towards other functional groups, high regioselectivity, and high chemical stability of the resulting thioether are advantageous and make this synthetic route ideal for medical purposes.

Ch-*lin*PG$_n$-*co*-PAGE$_m$
- linear structure
- multiple hydroxyl groups
- various functionalities

Ch-*hb*PG$_n$-PAGE$_m$
- hyperbranched structure
- multiple hydroxyl groups
- various functionalities

Figure 1: Polyether-based lipids with multiple hydroxyl groups and allyl groups having a linear (left) or hyperbranched (right) architecture. Thiols can be coupled to the allyl groups (green ellipsis); Ch= cholesterol, *lin*= linear, *hb*= hyperbranched, PG= polyglycerol, PAGE= poly(allyl glycidyl ether).

In this work, we present a combination of multiple hydroxyl groups and allyl functionalities in polyether-based amphiphiles. Cholesterol was used as an initiator for the AROP of various epoxides for eventual anchoring in lipid bilayers. The lipids were synthesized with different architectures (linear, hyperbranched or a combination, see Figure 1). The allyl moieties were converted into thioethers via thiol-ene coupling reactions with benzyl mercaptan or glutathione (GSH). Using ^{1}H NMR spectroscopy, SEC, MALDI-ToF, and surface tension measurements, the polymer structures were characterized in detail. Cryo-TEM was employed to study the liposomes shape.

Experimental Section

Instrumentation

^{1}H NMR spectra were recorded using a Bruker AC 400 spectrometer operated at 400 MHz, employing CDCl$_3$, MeOD, or DMSO-d$_6$ as a solvent. All spectra were referenced internally to residual proton signals of the deuterated solvent. Size exclusion chromatography (SEC) measurements were carried out in dimethylformamide (DMF) with 0.25 g L^{-1} LiBr on PSS HEMA columns (300/100/40). For SEC measurements a UV (275 nm) and an RI detector were used. Calibration was carried out using poly(ethylene glycol) (PEG) standards provided by Polymer Standards Service (PSS). Aqueous MALS measurement were separated over a set of HEMA-Bio columns (40/100/1000) with 10 μm particles with a length of 300 mm and an internal diameter of 8 mm (MZ-Analysentechnik) providing an effective molecular weight range of 2000 to 3000,000 g mol^{-1} at a flow rate of 1.0 ml · min^{-1} (Agilent 1260 HPLC) in 100 mM phosphate, 50 mM sodium chloride, pH 6.5. Each sample injection was 100 μL. Elution profiles for mass analysis were detected using a UV detector (254 nm, Agilent 1260), a Wyatt miniDAWN TREOS MALS detector, a Wyatt ViscoStar II on-line differential viscometer and a differential refractometer (Agilent 1260). Using the elution-profile data, the weight-averaged molecular mass was calculated with Astra 6.1.1 software (Wyatt Technologies) using a dn/dc of 0.135 for the PEG polymer (American Polymer Standards Corporation). Differential scanning calorimetry (DSC) measurements were carried out using a Perkin-Elmer DSC 8500 in the temperature range of -100 to 20 °C, using heating and cooling rates of 20 °C min^{-1} (1st cycle) and 10 °C min^{-1} (2nd cycle), respectively. The values for the second cycle were used for analysis. The melting points of indium (T$_m$ = 156.6 °C) and Millipore water (T$_m$ = 0 °C) were used for calibration. Matrix-assisted laser desorption/ ionization time-of-flight mass spectrometry (MALDI-ToF MS) measurements were performed on a Shimadzu Axima CFR MALDI-ToF mass spectrometer equipped with a nitrogen laser delivering 3 ns laser pulses at 337 nm. Dithranol was used as a matrix. The samples were prepared by dissolving the polymer in methanol at a concentration of 10 g L^{-1}. A 10 μL aliquot of this solution, 10 μL of a 10 g L^{-1} solution of the matrix and 1 μL of a solution of silver trifluoracetate (AgTFA)

(0.1 M in methanol as a cationization agent) were added consecutively to a multistage target (dried-droplet method) and matrix/analyte films were created.

Critical micelle concentration (CMC) measurements

Surface tension measurements, to determine the critical micelle concentration (cmc) of the allyl-containing polyether lipids, were performed on a Dataphysics DCAT 11 EC tensiometer equipped with a TV 70 temperature control unit, a LDU 1/1 liquid dosing and refill unit, as well as a RG 11 Du Noüy ring. The Du Noüy ring was rinsed thoroughly with Millipore water and annealed in a butane flame prior to use. Surface tension data was processed with SCAT v3.3.2.93 software. The CMC presented is a mean value of two experiments. All solutions for surface tension measurements were stirred for 120 s at a stir rate of 50%. After a relaxation period of 360 s, three surface tension values were measured.

DLS measurement and cryo-TEM preparation

For light scattering, a Zetasizer Nano Series Nano ZS (Malvern instruments) was used with a constant scattering angle of 173° and a measuring temperature of 25 °C. The samples were diluted (1:1000) and measured three times in a disposable plastic cuvette. For cryo-TEM images, the grids (CF-2/2-3C-T50 Grids; Protochips) were washed in chloroform for an hour and rinsed five times with acetone. After drying, the grids were negatively glow discharged (30 s at 30 mA) and 3 µl of the liposome sample were placed on the grid. Cryo-samples were vitrified in liquid ethane using a Gatan Cryoplunge™3 (relative humidity: 92%; blotting time for double-sided blotting: 3 s; temperature: 18 °C) and imaged with an FEI Tecnai 12 (acceleration voltage: 120 kV) transmission electron microscope equipped with a TVIPS TemCam-F416 (TVIPS, Gauting, Germany).

Reagents

All reagents and solvents were purchased from Acros and used as received, unless otherwise mentioned. Anhydrous solvents were stored over molecular sieves and were purchased from Aldrich. Deuterated solvents were purchased from Deutero GmbH, and stored over molecular sieves. Cholesterol was purchased from Acros and stored at 8 °C. Ethoxyethyl glycidyl ether (EEGE) was synthesized as described in the literature[42], dried over CaH_2, and cryo-transferred prior to use. Allyl glycidyl ether (AGE) was purchased from Acros Organics, dried over CaH_2, and cryo-transferred prior to use. Glycidol was purified by distillation from CaH_2 directly prior to use. Azobisisobutyronitrile (AIBN,

Acros) was recrystallized from MeOH. Benzyl mercaptan was a product of Acros Organics and glutathione reduced was obtained from ABCR. Absolute ethanol was purchased from VWR international. Dulbeccos' phosphate buffered saline (DPBS solution) was purchased from Invitrogen/Gibco. Hydrogenated egg phosphatidylcholine (EPC-3) was a gift from Lipoid GmbH and stored at -20 °C. The extruder, the polycarbonate membranes and filters were purchased from Avanti Polar Lipids.

Polymer synthesis

Cholesterol *linear* Poly(glycerol) (Ch-*lin*PG$_{20}$)

Cholesterol (2 g, 5.2 mmol), CsOH monohydrate (0.782 mg, 4.7 mmol, 90% of deprotonation), and benzene were placed in a Schlenk flask. The mixture was stirred for about 30 min at room temperature (RT) to generate the cesium alkoxide. The salt was then dried under vacuum for 24 h at 90 °C. The salt was suspended in 50 mL anhydrous dioxane, the monomer EEGE was added (15.8 mL, 103 mmol) and the mixture was heated up to 90 °C for 24 h. A sample was removed for NMR and SEC analysis, the polymerization was stopped via addition of an excess of methanol and the acetal protecting groups of PEEGE were cleaved by the addition of an acidic ion-exchange resin (Dowex 50WX8) and 2 N HCl stirring at RT for 24 h. The solution was filtered, concentrated, and the crude product was precipitated in cold diethyl ether. The block copolymer was dried under vacuum.

Before deprotection: ^{1}H NMR (400 MHz, CDCl$_3$): δ (ppm) = 5.30 (C=C*H* cholesterol), 4.68 (C*H*O acetal group), 3.88-3.17 (polyether backbone; C*H*O cholesterol), 2.30-0.83 (C*H*$_2$, C*H* cholesterol), 0.65 (C*H*$_3$ cholesterol).

After deprotection: ^{1}H NMR (400 MHz, MeOD): δ (ppm) = 5.37 (C=CH cholesterol), 3.77-3.17 (polyether backbone; CHO cholesterol), 2.40-0.88 (CH$_2$, CH cholesterol), 0.72 (CH$_3$ cholesterol).

Ch-*lin*PG$_n$-*co*-PAGE$_m$ in bulk (Scheme 1)

Cholesterol (1 g, 2.6 mmol), CsOH monohydrate (0.391 mg, 2.3 mmol; degree of deprotonation 90%), and benzene were placed in a Schlenk flask. The mixture was stirred for about 30 min at RT to generate the cesium alkoxide. The salt was then dried under vacuum at 90 °C for 3-4 h. The monomers EEGE and AGE were added in different

molar ratios and the mixture was heated up to 65 °C for 48 h. A sample was removed for NMR and SEC analysis, the polymerization was stopped via an excess of methanol and the acetal protecting groups of the PEEGE block were removed by addition of an acidic ion-exchange resin (Dowex 50WX8) and 2 N HCl stirring at RT for 24 h. The solution was filtered, concentrated, and the crude product was precipitated in cold diethyl ether. The block copolymer was dried under vacuum. With higher amounts of AGE (75 mol%) precipitation in diethyl ether was difficult due to increasing solubility due to the allyl groups. Hence, the solution had to be centrifuged.

^{1}H NMR before deprotection: (400 MHz, CDCl$_3$): δ (ppm) = 5.87 (CH$_2$CH=CH$_2$, allyl), 5.33 (C=CH cholesterol), 5.27-5.13 (CH$_2$CH=CH_2, allyl), 4.68 (CHO, acetal group), 3.98 (CH_2CH=CH$_2$), 3.88-3.17 (polyether backbone; CHO cholesterol), 2.30-0.84 (CH$_2$, CH cholesterol), 0.66 (CH$_3$ cholesterol).

After deprotection: ^{1}H NMR (400 MHz, MeOD): δ (ppm) = 5.92 (m, CH$_2$CH=CH$_2$, allyl), 5.38 (C=CH cholesterol), 5.32-5.17 (dd, CH$_2$CH=CH_2, allyl), 4.02 (d, CH_2CH=CH$_2$), 3.88-3.16 (polyether backbone; CHO cholesterol), 2.37-0.88 (CH$_2$, CH cholesterol), 0.66 (CH$_3$ cholesterol).

Ch-PEG$_{26}$-*b-lin*PG$_7$ (Scheme 2)

Cholesterol (1 g, 2.6 mmol, 1 eq.), CsOH monohydrate (0.391 g, 2.3 mmol; degree of deprotonation 90%), and benzene were placed in a Schlenk flask. The mixture was stirred at RT for about 30 min to generate the cesium alkoxide. The formed salt was dried under vacuum at 90 °C for 24 h, anhydrous THF was added via cryo transfer, and ethylene oxide (3.9 mL, 77.6 mmol, 30 eq.) was cryo transferred first to a graduated ampule and then to the Schlenk flask containing the initiator solution. The mixture was allowed to warm up to RT, heated to 60 °C, and the polymerization was performed at 60 °C for 24 h under vacuum. Subsequently, a sample was removed for NMR and SEC analysis, EEGE (2.8 mL, 18.1 mmol, 7 eq.) was added via a syringe, and the reaction mixture was held at 60 °C for an additional 24 h. After removal of another sample for characterization, the polymerization was stopped via addition of an excess of methanol, and the acetal protecting groups of the PEEGE block were cleaved by addition of water and acidic ion-exchange resin (Dowex 50WX8) stirring at 40 °C for 12 h. The solution was

filtered, concentrated, and the crude product was precipitated in cold diethyl ether. The block copolymer was dried under vacuum.

Before deprotection: ^{1}H NMR (400 MHz, CDCl$_3$): δ (ppm) = 5.29 (C=CH cholesterol), 4.66 (CHO, acetal group), 3.86-3.11 (polyether backbone; CHO cholesterol), 2.34-0.81 (CH$_2$, CH cholesterol), 0.62 (CH$_3$ cholesterol).

After deprotection: ^{1}H NMR (400 MHz, DMSO-d$_6$): δ (ppm) = 5.31 (C=CH cholesterol), 4.37 (br, OH), 3.74-3.17 (polyether backbone; CHO cholesterol), 2.37-0.83 (CH$_2$, CH cholesterol), 0.65 (CH$_3$ cholesterol).

Ch-PEG$_{26}$-b-linPG$_7$-graft-PAGE$_4$ (Scheme 2)

The macroinitiator Ch-PEG$_{26}$-b-linPG$_7$ (0.4 g, 0.20 mmol), CsOH monohydrate (66 mg, 0.4 mmol, 25% of deprotonation of the total amount of hydroxyl groups), and benzene were placed in a Schlenk flask and stirred for 30 min. Then the mixture was dried under vacuum overnight at 90 °C. The polymer salt was dissolved in 2 mL anhydrous THF, AGE (0.16 mL, 1.4 mmol) was dissolved in 0.8 mL anhydrous THF and then slowly added at RT. The reaction was stirred for another 3 d. Termination was carried out via addition of an excess of methanol. The product was precipitated in cold diethyl ether and Ch-PEG$_{26}$-linPG$_7$-graft-PAGE$_4$ was dried under vacuum.

^{1}H NMR (400 MHz, MeOD): δ (ppm) = 5.92 (m, CH$_2$C*H*=CH$_2$, allyl), 5.36 (C=CH cholesterol), 5.30-5.14 (dd, CH$_2$CH=C*H$_2$*, allyl), 4.01 (d, C*H$_2$*CH=CH$_2$), 3.86-3.16 (polyether backbone; CHO cholesterol), 2.40-0.85 (CH$_2$, CH cholesterol), 0.71 (CH$_3$ cholesterol).

Ch-hbPG$_{30}$-graft-PAGE$_{10}$ (Scheme 3)

The synthesis of Ch-hbPG$_{30}$ was adapted from a literature protocol.[22,23] Subsequently, AGE was added *via* a syringe at RT in order to attach the allyl groups at the periphery of the lipid and the reaction mixture was stirred for another 12 h. Termination was carried out via addition of an excess of methanol. The product was precipitated in cold diethyl ether and the Ch-hbPG$_{30}$-graft-PAGE$_{10}$ was dried under vacuum.

Cholesterol-poly(isopropylidene glyceryl glycidyl ether) (Ch-PIGG$_5$). ^{1}H NMR (400 MHz, DMSO-d$_6$): δ (ppm) = 5.30 (C=CH cholesterol), 4.14 (CHO acetal), 3.96 (m, CH$_2$O acetal), 3.76-3.22 (polyether backbone; CHO cholesterol), 2.28-0.82 (CH$_2$, CH cholesterol), 1.31-1.26 (CH$_3$ acetal), 0.63 (CH$_3$ cholesterol).

Cholesterol-poly(glyceryl glycidyl ether) (Ch-PGG$_5$)

^{1}H NMR (400 MHz, DMSO-d$_6$): δ (ppm) = 5.30 (C=CH cholesterol), 4.27 (br, OH), 3.76-3.22 (polyether backbone; CHO cholesterol), 2.28-0.82 (CH$_2$, CH cholesterol), 0.63 (CH$_3$ cholesterol).

Ch-*hb*PG$_{30}$-*graft*-PAGE$_{10}$. ^{1}H NMR (400 MHz, MeOD): δ (ppm) = 5.94 (m, CH$_2$C*H*=CH$_2$, allyl), 5.38 (C=CH cholesterol), 5.32-5.16 (dd, CH$_2$CH=C*H*$_2$, allyl), 4.02 (d, C*H*$_2$CH=CH$_2$), 3.88-3.17 (hyperbranched polyether backbone; CHO cholesterol), 2.38-0.88 (CH$_2$, CH cholesterol), 0.73 (CH$_3$ cholesterol).

Thiol-ene coupling of benzyl mercaptan /glutathione reduced (Scheme 4)

Procedure described for Ch-linPG$_{29}$-co-PAGE$_9$ as an example. 0.5 g of Ch-*lin*PG$_{29}$-*co*-PAGE$_9$, 155 mg of AIBN (0.75 eq of allyl groups), and 10 eq. (of allyl groups) of the respective thiol were dissolved in 15 mL DMF (for benzyl mercaptan) or in 15-20 mL DMF/H$_2$O (for glutathione). After three freeze-pump-thaw cycles, the mixture was stirred at 75 °C for 48 h. For purification, the reaction mixtures were dialyzed (MWCO = 1000 g mol^{-1}) in water/MeOH (benzyl mercaptan) or water (glutathione) and dried under vacuum to give a yellowish, sticky polymer. Benzyl mercaptan attachment to Ch-*lin*PG$_{29}$-*co*-PAGE$_9$: ^{1}H NMR (400 MHz, MeOD): δ (ppm) = 7.31-7.22 (benzyl protons), 5.36 (C=CH cholesterol), 3.88-3.14 (polyether backbone; CHO cholesterol, SC*H*$_2$benzyl), 2.48 (br, SC*H*$_2$), 1.78 (br, SCH$_2$C*H*$_2$), 2.37-0.88 (CH$_2$, CH cholesterol), 0.71 (CH$_3$ cholesterol).

Liposome preparation

Liposomes consisting of the amphiphile Ch-*hb*PG$_{30}$-*graft*-PAGE$_{10}$-*graft*-GSH$_4$, cholesterol and egg phosphatidylcholine (EPC) were prepared by the thin film hydration method on a clean bench. A solution of EPC in ethanol, cholesterol in ethanol and the copolymer in a methanol/ethanol mixture (2:1) were blended at molar ratios of 55:40:5 mol%, respectively. The solvent was evaporated in a rotating evaporator to obtain a thin film of liposome components. The lipid film was hydrated with 1 mL of PBS buffer solution to obtain a final lipid concentration of 21 mg mL^{-1}, sonicated at 50 °C for 10 min to yield multilamellar vesicles (MLVs), and extruded through a 400 nm polycarbonate membrane 11 times, followed by the extrusion through a 100 nm membrane for 11 times to obtain

small unilamellar vesicles (SUVs). The suspension was stored at 4 °C in an Eppendorf tube.

Results and Discussion

Synthesis and Characterization of Ch-*lin*PG$_n$-*co*-PAGE$_m$

In recent publications, we presented the synthesis and characterization of multifunctional cholesterol-lipids based on hyperbranched (*hb*) or linear-hyperbranched polyethers (PEG-*b*-*hb*PG).[22,23,43] We introduced their successful application in liposomal formulations. In the present work, this concept is extended to allyl group-containing polyethers that are suitable for thiol-ene coupling reactions in order to enable the synthesis of functional liposomes for "active" targeting. In a rapid two-step protocol cholesterol-initiated linear polyglycerol-*co*-poly(allyl glycidyl ether) polymers (Ch-*lin*PG-*co*-PAGE) were synthesized in various monomer ratios (25 mol%, 50 mol%, 75 mol% of allyl groups compared to the total amount of monomer units). In the first step, cholesterol was directly used as the initiator for the ring-opening polymerization (ROP) of ethoxyethyl glycidyl ether (EEGE) and the commercially available allyl glycidyl ether (AGE). Deprotonation was achieved using CsOH, and the reaction was carried out for 48 h. It should be mentioned that the polymerization was not complete after 24 h, which was observed by residual epoxide resonances in the ^{1}H NMR spectrum. The polymerization was carried out in bulk, since previous studies showed isomerization of the allyl double bond using solvents and elevated temperature.[31] Since isomerization has to be prevented in order to carry out thiol-ene coupling in the functionalization step, it was convenient that both monomers are liquids, hence handling was facile. The solvent-free polymerization at 65 °C did not show any isomerized products, similar to the findings in literature.[31] The second step was the cleavage of the acetal groups to obtain *lin*PG units. This reaction was carried out with an acidic ion exchange resin and 2 N HCl in MeOH at RT for 24 h. Scheme 1 depicts the synthetic route for both steps including the oxyanionic copolymerization and the subsequent deprotection step to release the hydroxyl groups.
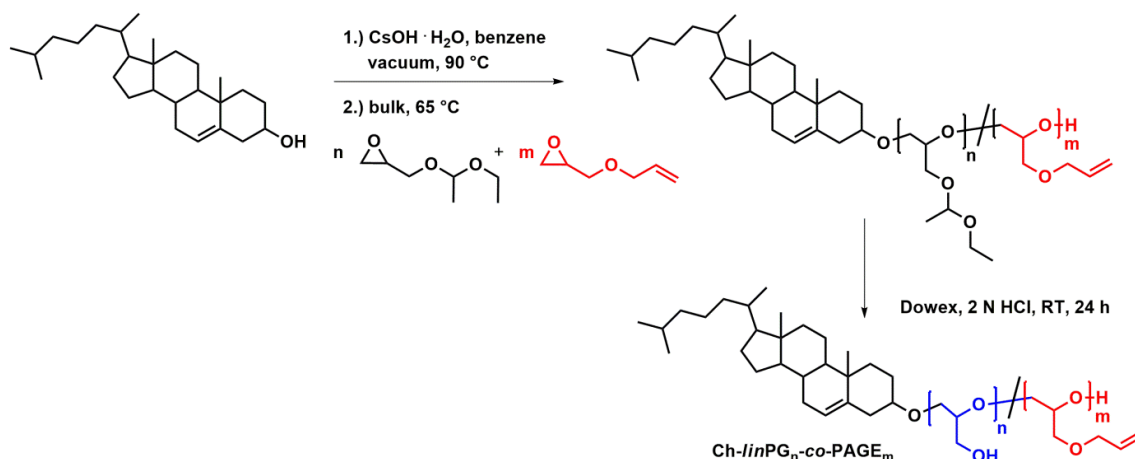
Scheme 1: Synthetic route for the oxyanionic ring-opening copolymerization of EEGE and AGE with cholesterol as an initiator, followed by acidic deprotection of the pendant hydroxyl groups under acidic conditions.

This approach resulted in a series of polymers with varying amounts of allyl groups (25-75 mol%) with relatively narrow polydispersity indices (M_w/M_n= 1.2-1.25) and controlled molecular weights between 3500 and 4500 g mol^{-1} (see Table 1). The targeted molecular weights were adjusted according to the molecular weights for PEG applied in "stealth" liposomes,[15] since polymeric steric hindrance and effective anchoring of the cholesterol unit are still assured.

Table 1: Compositions, molecular weights, polydispersity indices, glass transition temperatures (T_g), and critical micelle concentrations (CMC) for the synthesized allyl-functional cholesterol-lipids.

Composition (th)	Composition (NMR)	$M_n^{(th)}$ g mol^{-1}	$M_n^{(NMR)}$ g mol^{-1}	$M_n^{(SEC)}$ g mol^{-1}	M_w/M_n^a	T_g °C	CMC mg L^{-1}
Ch-*lin*PG$_{20}$	Ch-*lin*PG$_{21}$	1870	1940	1700	1.19	-50	14.4
Ch-*lin*PG$_{30}$-*co*-PAGE$_{10}$	Ch-*lin*PG$_{29}$-*co*-PAGE$_{9}$	3750	3560	2200	1.25	-51	18.8
Ch-*lin*PG$_{20}$-*co*-PAGE$_{20}$	Ch-*lin*PG$_{20}$-*co*-PAGE$_{19}$	4150	4030	2050	1.20	-57	4.0
Ch-*lin*PG$_{10}$-*co*-PAGE$_{30}$	Ch-*lin*PG$_{10}$-*co*-PAGE$_{29}$	4550	4430	2130	1.21	-64	n.s.
Ch-PEG$_{26}$-*lin*PG$_{7}$-PAGE$_{7}$	Ch-PEG$_{26}$-*lin*PG$_{7}$-PAGE$_{4}$	2850	2500	2000	1.12	n.a.	n.a.
Ch-*hb*PG$_{35}$-PAGE$_{13}$	Ch-*hb*PG$_{30}$-PAGE$_{10}$	4460	3750	1530	1.63	n.a.	40.4

n.s. This sample was not water soluble; n.a. Value not available
^{a}Determined by SEC (DMF, PEG standard)

The degree of polymerization was determined using ^{1}H NMR spectroscopy via integration of the methyl group of cholesterol (0.66 ppm, 3 H initiator). By integration of the acetal peaks of the protecting groups of EEGE (4.68 ppm, 3 H) and the double bond proton of AGE (5.87 ppm, 1 H), it was possible to calculate the degree of polymerization and composition. All values were in good agreement with expectation, showing that both epoxides were incorporated. Figure 2 depicts the ^{1}H NMR spectrum before and after the acidic deprotection step. Between 0.60 ppm and 2.40 ppm, the alkyl protons of the cholesterol initiator are observed, and the cholesterol double bond signal is observed at 5.32 ppm. The polyether backbone can be discerned between 3.0 ppm and 3.80 ppm, and the EEGE acetal group is observable at 4.68 ppm. Complete cleavage of the acetal groups can be proven by the disappearance of this resonance. The AGE double bonds generate a signal around 5.11 ppm (doublet), 5.22 ppm (doublet) and 5.87 ppm (multiplet). The methylene group next to the double bond appears at 3.98 ppm. Due to polymerization in bulk, no isomerization of the double bond was observed, which is favored for the coupling step of different thiols.
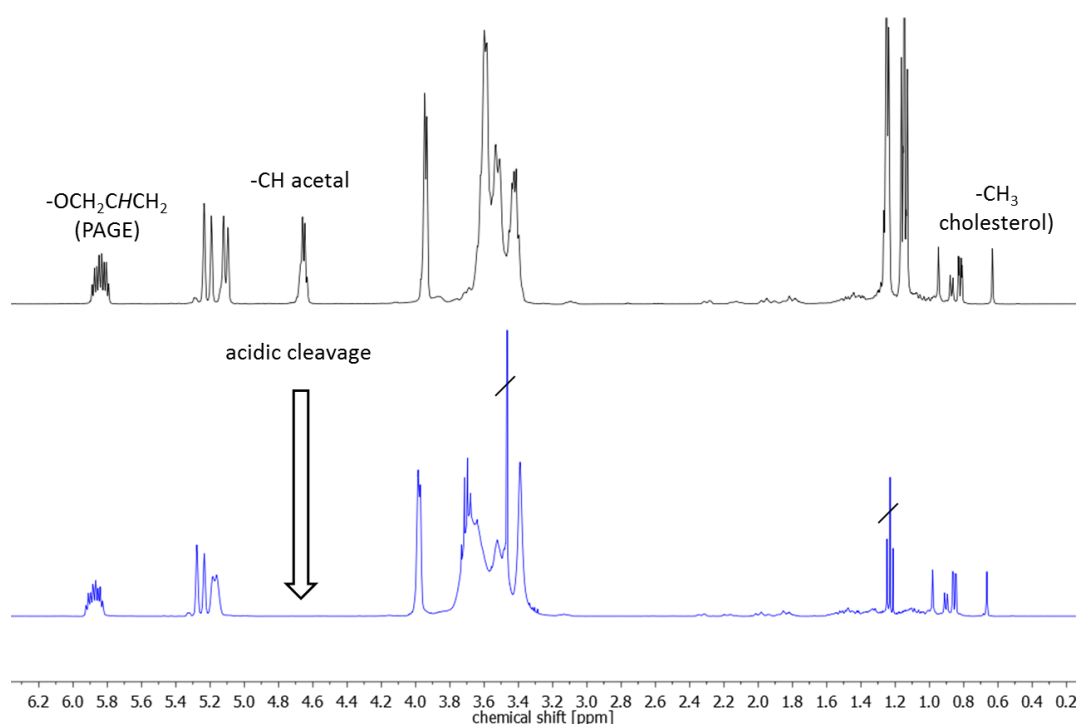
Figure 2: ^{1}H NMR spectrum in CDCl$_3$ (400 MHz) before (upper, black) and after the acidic deprotection step of Ch-*lin*PG$_{20}$-*co*-PAGE$_{19}$ (lower, blue) allowing the determination of the degree of polymerization for each monomer and showing the complete cleavage of the acetal groups.

Characterization via size exclusion chromatography (SEC) showed monomodal molecular weight distributions before and after acidic treatment. For the sample with 50 mol% EEGE units and 50 mol% AGE units, the SEC traces are exemplified in Figure 3. Ch-PEEGE$_{20}$-co-PAGE$_{19}$ (black) represents the polymer in DMF with acetal protecting groups and Ch-linPG$_{20}$-co-PAGE$_{19}$ (blue) represents the amphiphile with pendant hydroxyl and allyl groups. The shift to lower molecular weight indicates successful cleavage of the EEGE protecting groups. A comparison of the molecular weights calculated by ^{1}H NMR spectroscopy and the molecular weights determined by SEC (DMF, PEG standards) shows a general underestimation by SEC due to differences in the hydrodynamic radius of PEG and hydroxy-functional linPG (Table 1). Using MALDI-ToF MS the incorporation of both monomers, EEGE (deprotected 74 g mol^{-1}) and AGE (114 g mol^{-1}) in the polymer backbone could be verified (see Figure 4). The mass discrimination effect was observable, since the molecular weights are underestimated compared to the calculated molecular weights by ^{1}H NMR spectroscopy.
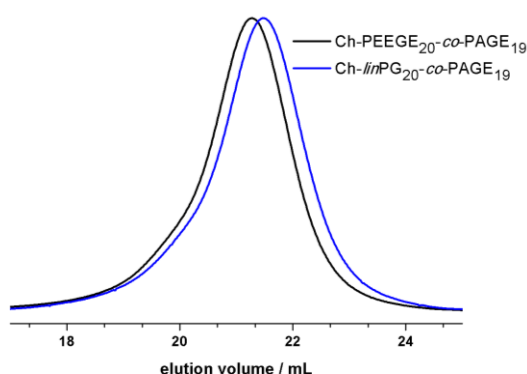

Figure 3: SEC elugram of Ch-PEEGE$_{20}$-co-PAGE$_{19}$ (black) and Ch-linPG$_{20}$-co-PAGE$_{19}$ (blue) in DMF.
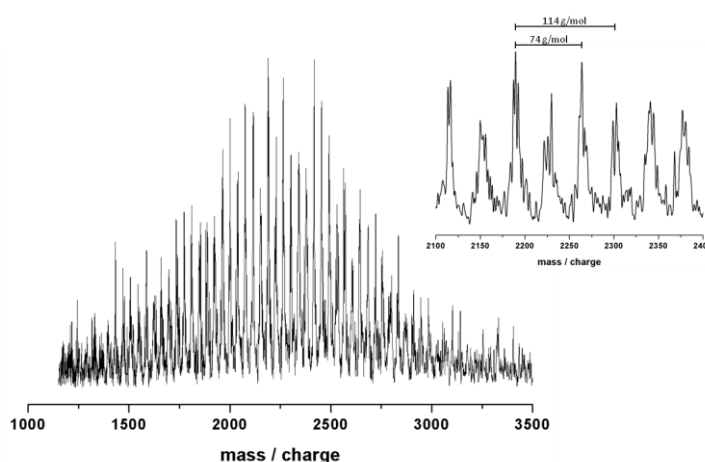

Figure 4: MALDI-ToF spectrum of Ch-linPG$_{10}$-co-PAGE$_{29}$ copolymer (Table 1, Sample 4) with Ag$^+$ as counter ion and dithranol as matrix.

Thermal analysis via differential scanning calorimetry (DSC) gave an additional hint for the successful incorporation of both monomers. For comparison, Ch-linPG$_{21}$ homopolymer was investigated and a glass transition temperature (T$_g$) of -50 °C was determined (compare Table 1). With increasing amount of allyl groups at the polyether backbone, the T$_g$ values decrease, which shows that with decreasing amount of hydroxyl groups the interaction via hydrogen bonds decreases concomitantly. This effect has already been observed for other copolymers of linPG.[44]

The amphiphilic character of the polymers was investigated by surface tension measurements and the determination of the critical micelle concentration (CMC). Table 1 summarizes the CMC values, showing a clear trend that correlates with the polarity of the compounds. Ch-linPG$_{21}$ with a CMC of 14.4 mg L^{-1} and Ch-linPG$_{29}$-co-PAGE$_9$ showing a CMC of 18.8 mg L^{-1} prove that the latter sample is slightly more hydrophilic due to additional hydroxyl groups at the backbone. The CMC of 4.0 mg L^{-1} for Ch-linPG$_{20}$-co-PAGE$_{19}$ clearly reflects the influence of the hydrophobic allyl groups. The hydrophobicity of the AGE repeating units also explains why Ch-linPG$_{10}$-co-PAGE$_{29}$ was not water soluble. The most interesting sample for the liposome formation purpose is Ch-linPG$_{29}$-co-PAGE$_9$, since it combines excellent water solubility with a high amount of allyl groups that can be functionalized in order to form modified lipids. The hyperbranched polymer Ch-hbPG$_{30}$-PAGE$_{10}$ shows the highest CMC value (40.4 mg L^{-1}), since it represents the most hydrophilic sample in Table 1.

Synthesis and characterization of Ch-PEG$_{26}$-linPG$_7$-$graft$-PAGE$_4$ and Ch-hbPG$_{30}$-$graft$-PAGE$_{10}$

Multifunctional poly(ethylene glycol)s (mfPEGs) combine the advantages of PEG, $i.e.$, the reduced aggregation and opsonization with the benefits of additional functional groups.[45] With these objectives in mind, block copolymerization of ethylene oxide (EO) (PEG spacer), EEGE, and AGE has also been carried out. The cholesterol-alkoxide was used as an initiator for the anionic ROP of EO, followed by the addition of EEGE. After acidic deprotection, the macroinitiator could be used for the addition of AGE. In order to prevent isomerization of the double bond, the reaction was stirred for three days at room temperature. This reaction route led to Ch-PEG$_{26}$-linPG$_7$-$graft$-PAGE$_4$ with a low polydispersity index of 1.2 and a molecular weight of 2500 g mol^{-1} (SEC= 2040 g mol^{-1}).

We aimed at a composition of 7 AGE groups per polymer, however, only 4 AGE groups were detected via ^{1}H NMR spectroscopy. Obviously, the more favorable bulk polymerization of AGE can lead to quantitative conversion, whereas at room temperature the reactivity of the system might not be high enough to reach complete conversion within three days.
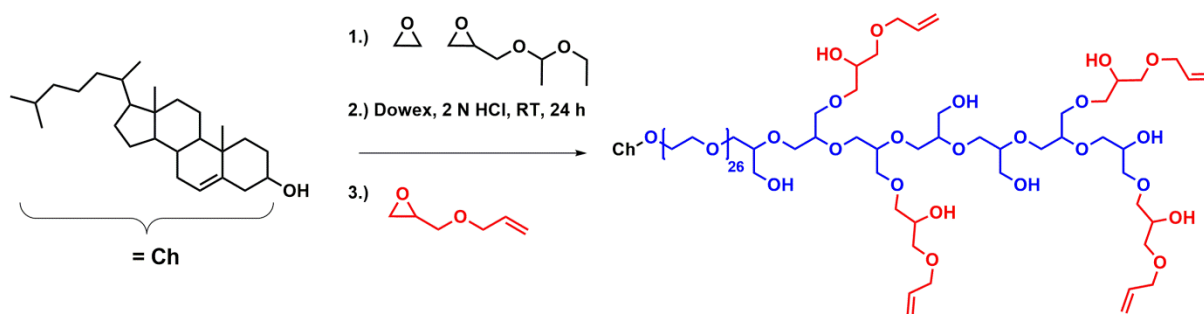

Scheme 2: Synthetic strategy for the linear, allyl-functional Ch-PEG$_{26}$-*lin*PG$_7$-*graft*-PAGE$_4$.

In order to increase the number of hydroxyl groups and to enhance steric hindrance of the polyether segment, allyl groups were also introduced into more bulky polymers. To this end, Ch-PGG$_5$ (polyglyceryl glycidyl ether) was used as a macroinitiator for the slow monomer addition of glycidol, followed by the addition of AGE. The macroinitiator was synthesized by using 1,2-isopropylidene glyceryl glycidyl ether (IGG) in diglyme with subsequent deprotection of the acetonide protecting groups under acidic conditions. The DP$_n$ of PIGG was determined by comparison of the methyl group signal of cholesterol at 0.63 ppm with the acetal signal of PIGG at 4.14 ppm before acidic treatment. Hence, the molecular weight was determined to be 1130 g mol^{-1} (5 repeating units). SEC revealed a molecular weight of 730 g mol^{-1} and a PDI of 1.52. For low degrees of polymerization, this relatively high PDI can be explained by statistic considerations.[46-48] The synthesis of a short macroinitiator with multiple hydroxyl groups (in this case 2 per monomer unit) is crucial for the subsequent hypergrafting process of glycidol, since with increasing number of initiating groups, the PDI can be lowered and homopolymerization of glycidol can be prevented.[49] The slow addition of glycidol was carried out as described in the literature[22] with an additional step for the subsequent oxyanionic ROP of AGE at room temperature. This straightforward one-pot route allows for the introduction of allyl groups in the periphery of hyperbranched polyether

structures, aiming at orthogonal, multifunctional amphiphiles (see Figure 1 and Scheme 3). Using this strategy, Ch-hbPG$_{30}$-PAGE$_{10}$ was synthesized with a molecular weight of 1530 g mol^{-1} (SEC) and a PDI of 1.63, which is reasonable for hyperbranched systems. Figure 5 shows the SEC elugram of the macroinitiator Ch-PGG$_5$ (dashed line) and Ch-hbPG$_{30}$-$graft$-PAGE$_{10}$ (solid line) with a clear shift to lower elution volume, which translates to higher molecular weights compared to the macroinitiator. Molecular weights of hyperbranched structures determined by SEC are commonly underestimated due to multiple hydroxyl groups and the globular structure (hydrodynamic radius) compared to the SEC standard PEG.
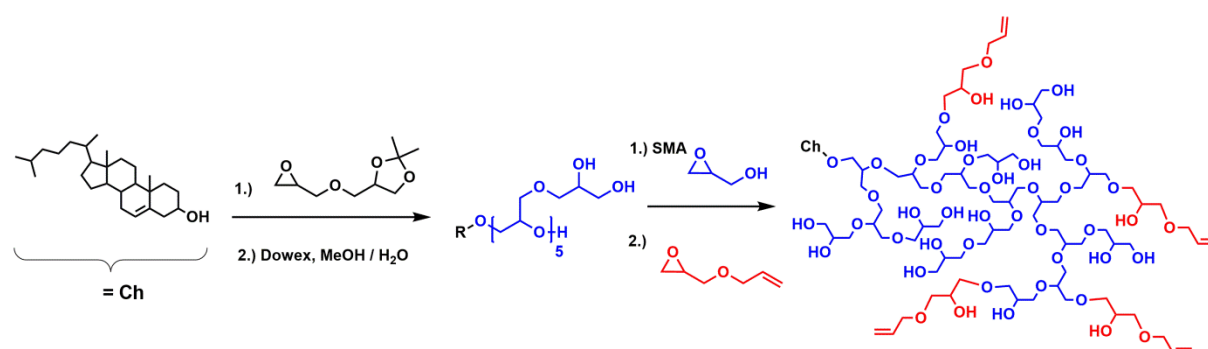
Scheme 3: Synthetic scheme for the preparation of the macroinitiator Ch-PGG$_5$ and hypergrafting of glycidol and AGE (consecutively) leading to Ch-hbPG$_{30}$-$graft$-PAGE$_{10}$ (SMA= slow monomer addition).
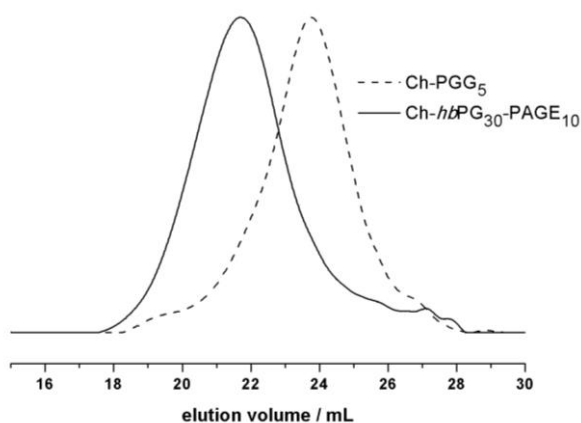

Figure 5: SEC elugram of Ch-PGG$_5$ (macroinitiator, dashed line) and Ch-hbPG$_{30}$-PAGE$_{10}$ (solid line).

Synthesis and characterization of thiol-functionalized cholesterol-lipids

The allyl groups at the polymer lipid backbone were used for further derivatization with two different thiols, i.e., benzyl mercaptan and glutathione reduced (GSH) (Scheme 4). Thiol coupling was chosen, since thiols are common functional groups in many biological molecules. In this proof-of-principle study, we demonstrate successful covalent

attachment of a small molecule, i.e, benzyl mercaptan with little steric hindrance and the biologically active tripeptide (GSH), which is sterically more demanding. Small molecules and peptides play a key role for targeted drug-delivery vehicles.

The thermally cleavable radical initiator azobisisobutyronitrile (AIBN) was used in thiol-ene coupling reactions, and the respective thiol was used in excess (10 eq.) in order to suppress cross-linking of the thiol groups.[30] Residual low molecular weight compounds and DMF were successfully removed by dialysis.
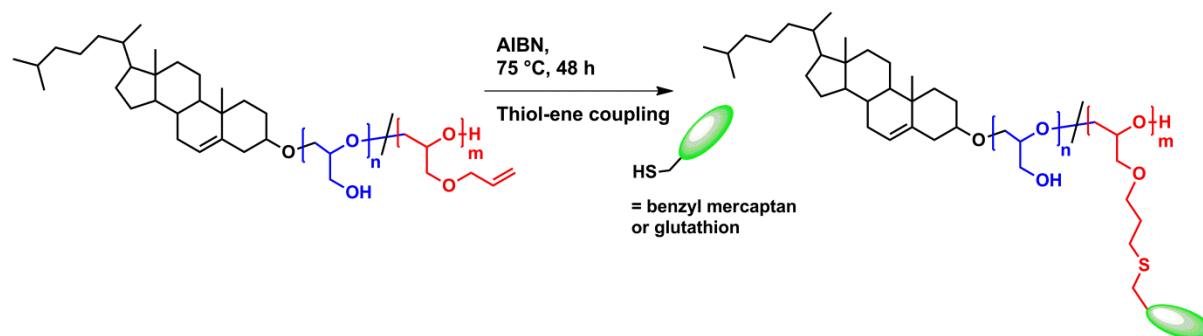
Scheme 4: Synthetic route for the functionalization of the pendant allyl groups of Ch-*lin*PG$_n$-*co*-PAGE$_m$ by thiol-ene coupling, using either benzyl mercaptan or glutathione (green ellipse).

Table 2: Composition, molecular weights, and polydispersity indices for the synthesized Ch-*lin*PG$_n$-*co*-PAGE$_m$ copolymers with pendant benzyl thioether or GSH moieties.

Composition [th]	Composition [NMR]	M$_n$ [NMR]	M$_n$ [th]	M$_n$ [SEC]	PDI [SEC]
		g mol^{-1}	g mol^{-1}	g mol^{-1}	
Ch-*lin*PG$_{29}$-*co*-PAGE$_9$-Benzyl$_9$	Ch-*lin*PG$_{29}$-*co*-PAGE$_9$-Benzyl$_9$	4680	4680	2760	1.30
Ch-*lin*PG$_{29}$-*co*-PAGE$_9$-GSH$_9$	Ch-*lin*PG$_{29}$-*co*-PAGE$_9$-GSH$_3$	6320	4480	-	-
Ch-PEG$_{26}$-*lin*PG$_7$-*graft*-PAGE$_7$-GSH$_4$	Ch-PEG$_{26}$-*lin*PG$_7$-*graft*-PAGE$_4$-GSH$_2$	3120	3400	5300 [a]	1.32 [a]
Ch-*hb*PG$_{30}$-*graft*-PAGE$_{10}$-Benzyl$_{10}$	Ch-*hb*PG$_{30}$-*graft*-PAGE$_{10}$-Benzyl$_{10}$	4990	4990	3200	1.29
Ch-*hb*PG$_{30}$-*graft*-PAGE$_{10}$-GSH$_{10}$	Ch-*hb*PG$_{30}$-*graft*-PAGE$_{10}$-GSH$_3$	6820	4670	5960 [a]	1.33 [a]

[a] Values obtained from aqueous SEC.

The functionalized amphiphiles were characterized by ^{1}H NMR spectroscopy and SEC in DMF and aqueous solution. Via ^{1}H NMR spectroscopy the conversion with benzyl mercaptan was calculated by the integration of the methyl group of cholesterol at 0.66 ppm ($-CH_3$) and the aromatic peaks around 7.30 ppm (Figure 6, Table 2). The AGE double bond proton at 5.87 ppm vanished completely in the case of benzyl mercaptan attachment, indicating quantitative conversion. SEC in DMF revealed a narrow molecular weight distribution (PDI=1.3; M_n=2760 g mol^{-1}). An additional UV-signal, due to the benzyl groups, superimposed with the RI-signal (Figure 7). Of the linear copolymers, only Ch-linPG$_{29}$-PAGE$_9$ was treated with benzyl mercaptan, since transformation of the other materials with higher content of allyl groups would lead to a higher degree of benzyl functionalization, resulting in more hydrophobic polymers with only limited aqueous solubility. Additionally, for drug-targeting, only a low degree of functionalization is necessary, because marker-receptor binding is highly specific and the polymer backbone needs to stay water soluble in order to maintain "stealth" behavior. For the hyperbranched cholesterol-amphiphile Ch-hbPG$_{30}$-PAGE$_{10}$, the thiol-ene coupling was carried out in the same way as for the linear analogues, leading to a UV-signal in SEC measurements and a PDI of 1.29. The lower PDI compared to the hyperbranched lipid without the benzyl groups can be explained by the dialysis purification step, in which low molecular weight fractions may have been separated from the main fraction.
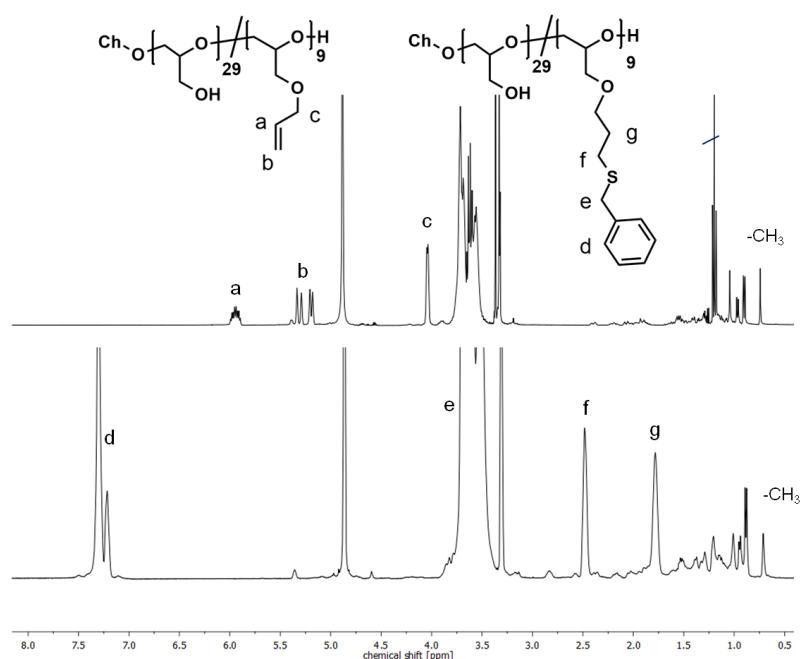

Figure 6: ^{1}H NMR spectrum in MeOD (400 MHz) before (upper) and after (lower) the thiol-ene coupling of benzyl mercaptan to Ch-linPG$_{29}$-PAGE$_9$.
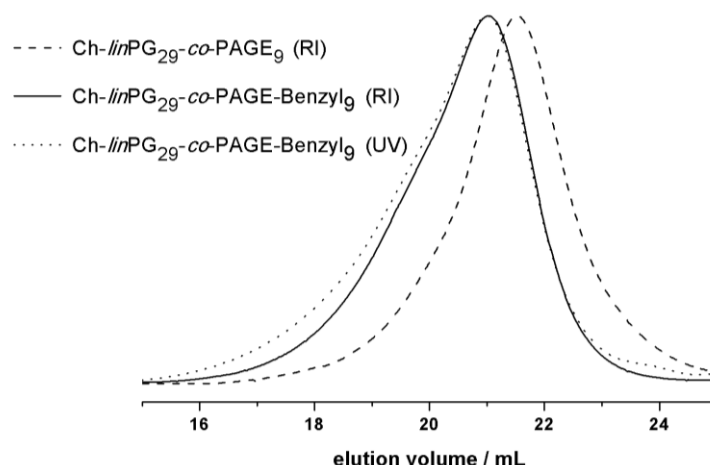
Figure 7: SEC elugrams of Ch-*lin*PG$_{29}$-*co*-PAGE$_9$ (RI-signal, dashed) and Ch-*lin*PG$_{29}$-*co*-PAGE-Benzyl$_9$ (RI-signal, straight; UV-signal, dotted) in DMF.

The conjugation of allyl-functionalized lipids with GSH turned out to be more challenging compared to low molecular weight benzyl mercaptan, since GSH is a sterically demanding tripeptide (307 g mol^{-1}). The coupling to Ch-*lin*PG$_{29}$-*co*-PAGE$_9$, Ch-PEG$_{26}$-*lin*PG$_7$-*graft*-PAGE$_4$, and Ch-*hb*PG$_{30}$-*graft*-PAGE$_{10}$ could not be driven to quantitative conversion, although 10 equiv. of GSH were used, which may be due to steric hindrance of the bulky tripeptide Nevertheless, ^{1}H NMR spectroscopy showed no resonances of remaining allyl groups. Unreacted allyl groups may have isomerized or crosslinked intramolecularly. SEC showed no high molecular weight traces, so intermolecular crosslinking can be excluded. In general, the interpretation of ^{1}H NMR spectra for those conjugates was challenging and integration of the GSH integrals may be imprecise, since the significant signals of GSH overlap with the polyether backbone and the cholesterol moiety. Therefore, the GSH amine group was taken into account for the calculation of the number of attached tripeptides (^{1}H NMR spectra see Supporting Information). It was estimated that at every 3rd allyl group one GSH unit was successfully attached, which in general should be sufficient for liposome targeting *in vivo*, since receptor-mediated targeting is very sensitive.[50] SEC characterization in DMF for Ch-*hb*PG$_{30}$-*graft*-PAGE$_{10}$-GSH was not successful, since reduced solubility in DMF and interactions with the column material occurred. However, the polymer-peptide conjugates were soluble in water and aqueous SEC exhibited narrow polymer molecular weight distributions below 1.35. (Table 2; aqueous SEC traces see Figure S1, Supporting Information).

Cryo-TEM und DLS

Liposome characterization

Liposomes consisting of Ch-*hb*PG$_{30}$-*graft*-PAGE$_{10}$-GSH$_4$, EPC, and cholesterol were prepared by the thin film hydration method and extrusion through a polycarbonate membrane. Dynamic light scattering (DLS) was performed to evaluate the size and polydispersity of the vesicles, which was calculated by the mean value of three measurements and was determined to be 0.054. The mean size was determined to be 153 nm, which is in good agreement with the membrane pores that were used (smallest: 100 nm). Cryo-transmission electron microscopy (cryo-TEM) was exploited to visualize the shape of the liposomes. The cryo-TEM image (Figure 8) shows that the lipid-polymer vesicles form unilamellar liposomes and demonstrates that nearly all vesicles are spherical. The estimated liposome sizes are in good agreement with the values obtained from DLS. The results indicate that GSH-modified cholesterol-based lipids incorporate into the lipid bilayer of vesicles and that a small tripeptide does not impede liposome formation. This is an important result as it is a prerequisite for the successful incorporation of targeting moieties via the strategy presented here, which is a key step for future development of this area.
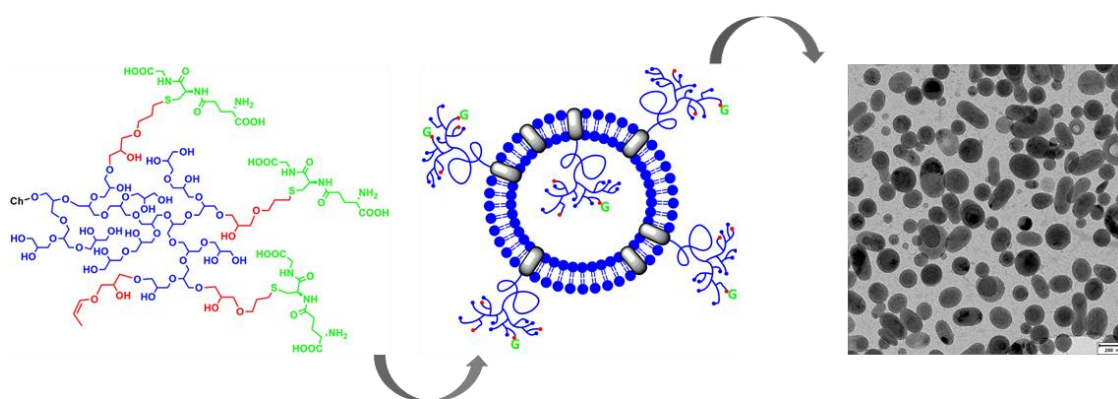

Figure 8. Cartoon and cryo-TEM image of liposomes consisting of Ch-*hb*PG$_{30}$-*graft*-PAGE$_{10}$-GSH$_4$, EPC, and cholesterol (5:55:40 mol%), scale bar 200 nm.

Conclusion

This study demonstrates the introduction of allyl groups into hydroxy-functional cholesterol-lipids via straightforward oxyanionic ring-opening polymerization of various epoxides such as allyl glycidyl ether (AGE). By selective combination of such epoxides the

following lipid architectures were achieved: i.) linear polyglycerol with pendant hydroxyl and allyl groups, ii.) block copolymers of PEG-linear polyglycerol with allyl groups grafted-from the polymer backbone, and iii.) hyperbranched polyglycerol with allyl groups at the corona. Via the solvent-free polymerization of AGE and EEGE, isomerization of the allyl double bond was avoided as proven by ^{1}H NMR spectroscopy. Maintaining the allyl double bonds is a crucial requirement for the subsequent thiol-ene coupling step for further functionalization. ^{1}H NMR spectroscopy and MALDI-ToF MS characterization gave evidence of the incorporation of cholesterol as initiator and the presence of AGE groups in the polymer. The double bonds were used in thiol-ene coupling reactions with benzyl mercaptan and glutathione (GSH), in which benzyl mercaptan resulted in full conversion, whereas GSH could not be attached quantitatively. Nevertheless, the AGE containing amphiphiles carry multiple functionalities and offer extraordinary possibilities for the attachment of, e.g., targeting moieties. As an example, the hyperbranched lipid Ch-*hb*PG$_{30}$-*graft*-PAGE$_{10}$-GSH$_4$ was successfully used in liposome formation. Ongoing studies concerning the *in vivo* distribution and the potential cross-linking behavior of the double bonds in the stabilizing polymeric shell of liposomes will be presented in the near future.

Acknowledgments

References

1. Gregoria.G; Wills, E. J.; Swain, C. P.; Tavill, A. S., *Lancet* **1974,** *1* (7870), 1313-1316.
2. Sharma, A.; Sharma, U. S., *Int. J. Pharm.* **1997,** *154* (2), 123-140.
3. Lian, T.; Ho, R. J. Y., *J. Pharm. Sci.* **2001,** *90* (6), 667-680.
4. Allen, T. M.; Hansen, C.; Martin, F.; Redemann, C.; Yau-Young, A., *Biochim. Biophys. Acta* **1991,** *1066* (1), 29-36.
5. Woodle, M. C.; Matthay, K. K.; Newman, M. S.; Hidayat, J. E.; Collins, L. R.; Redemann, C.; Martin, F. J.; Papahadjopoulos, D., *Biochim. Biophys. Acta* **1992,** *1105* (2), 193-200.
6. Torchilin, V. P.; Omelyanenko, V. G.; Papisov, M. I.; Bogdanov, A. A.; Trubetskoy, V. S.; Herron, J. N.; Gentry, C. A., *Biochim. Biophys. Acta* **1994,** *1195* (1), 11-20.
7. Blume, G.; Cevc, G., *Biochim. Biophys. Acta* **1990,** *1029* (1), 91-97.
8. Immordino, M. L.; Dosio, F.; Cattel, L., *Int. J. Nanomed.* **2006,** *1* (3), 297-315.
9. Needham, D.; McIntosh, T. J.; Lasic, D. D., *Biochim. Biophys. Acta* **1992,** *1108* (1), 40-48.
10. Maeda, H.; Wu, J.; Sawa, T.; Matsumura, Y.; Hori, K., *J. Controlled Release* **2000,** *65* (1-2), 271-284.
11. Duncan, R., *Nat Rev Drug Discov* **2003,** *2* (5), 347-360.
12. Cabanes, A.; Tzemach, D.; Goren, D.; Horowitz, A. T.; Gabizon, A., *Clin. Cancer Res.* **1998,** *4* (2), 499-505.
13. Torchilin, V. P., *Nat. Rev. Drug Discov.* **2005,** *4* (2), 145-160.
14. Lasic, D. D., *Nature* **1996,** *380* (6574), 561-562.
15. Woodle, M. C.; Lasic, D. D., *Biochim. Biophys. Acta* **1992,** *1113* (2), 171-199.
16. Dworak, A.; Baran, G. y.; Trzebicka, B.; Wallach, W., *React. Funct. Polym.* **1999,** *42* (1), 31-36.
17. Wurm, F.; Nieberle, J.; Frey, H., *Macromolecules* **2008,** *41* (4), 1184-1188.
18. Lee, S.; Saito, K.; Lee, H.-R.; Lee, M. J.; Shibasaki, Y.; Oishi, Y.; Kim, B.-S., *Biomacromolecules 13* (4), 1190-1196.
19. Wurm, F.; Nieberle, J.; Frey, H., *Macromolecules* **2008,** *41* (6), 1909-1911.
20. Erberich, M.; Keul, H.; Möller, M., *Macromolecules* **2007,** *40* (9), 3070-3079.
21. Schulte, B.; Walther, A.; Keul, H.; Möller, M., *Macromolecules* **2014,** *47* (5), 1633-1645.
22. Hofmann, A. M.; Wurm, F.; Hühn, E.; Nawroth, T.; Langguth, P.; Frey, H., *Biomacromolecules* **2010,** *11* (3), 568-574.
23. Hofmann, A. M.; Wurm, F.; Frey, H., *Macromolecules* **2011,** *44* (12), 4648-4657.
24. Wilms, D.; Wurm, F.; Nieberle, J.; Boehm, P.; Kemmer-Jonas, U.; Frey, H., *Macromolecules* **2009,** *42* (9), 3230-3236.
25. Wilms, D.; Stiriba, S.-E.; Frey, H., *Acc. Chem. Res.* **2010,** *43* (1), 129-141.
26. Kainthan, R. K.; Gnanamani, M.; Ganguli, M.; Ghosh, T.; Brooks, D. E.; Maiti, S.; Kizhakkedathu, J. N., *Biomaterials* **2006,** *27* (31), 5377-5390.
27. Calderon, M.; Quadir, M. A.; Sharma, S. K.; Haag, R., *Adv. Mater.* **2010,** *22* (2), 190-218.
28. Siegers, C.; Biesalski, M.; Haag, R., *Chemistry - A European Journal* **2004,** *10* (11), 2831-2838.

29.   Kainthan, R. K.; Zou, Y.; Chiao, M.; Kizhakkedathu, J. N., *Langmuir* **2008,** *24* (9), 4907-4916.

30.   Obermeier, B.; Frey, H., *Bioconjugate Chem.* **2011,** *22* (3), 436-444.

31.   Lee, B. F.; Kade, M. J.; Chute, J. A.; Gupta, N.; Campos, L. M.; Fredrickson, G. H.; Kramer, E. J.; Lynd, N. A.; Hawker, C. J., *J. Polym. Sci., Part A: Polym. Chem.* **2011,** *49* (20), 4498-4504.

32.   Barteau, K. P.; Wolffs, M.; Lynd, N. A.; Fredrickson, G. H.; Kramer, E. J.; Hawker, C. J., *Macromolecules 46* (22), 8988-8994.

33.   Herczynska, L.; Lestel, L.; Boileau, S.; Chojnowski, J.; Polowinski, S., *Eur. Polym. J.* **1999,** *35* (6), 1115-1122.

34.   Passaglia, E.; Donati, F., *Polymer* **2007,** *48* (1), 35-42.

35.   Killops, K. L.; Campos, L. M.; Hawker, C. J., *J. Am. Chem. Soc.* **2008,** *130* (15), 5062-5064.

36.   Hruby, M.; Konak, C.; Ulbrich, K., *J. Appl. Polym. Sci.* **2005,** *95* (2), 201-211.

37.   Hruby, M.; Konak, C.; Ulbrich, K., *J. Controlled Release* **2005,** *103* (1), 137-148.

38.   Jewett, J. C.; Bertozzi, C. R., *Chem. Soc. Rev.* **2010,** *39* (4), 1272-1279.

39.   Becer, C. R.; Hoogenboom, R.; Schubert, U. S., *Angew. Chem. Int. Ed.* **2009,** *48* (27), 4900-4908.

40.   Gress, A.; Völkel, A.; Schlaad, H., *Macromolecules* **2007,** *40* (22), 7928-7933.

41.   Campos, L. M.; Killops, K. L.; Sakai, R.; Paulusse, J. M. J.; Damiron, D.; Drockenmuller, E.; Messmore, B. W.; Hawker, C. J., *Macromolecules* **2008,** *41* (19), 7063-7070.

42.   Fitton, A. O.; Hill, J.; Jane, D. E.; Millar, R., *Synthesis* **1987,** (12), 1140-1142.

43.   Müller, S. S.; Dingels, C.; Hofmann, A. M.; Frey, H., Polyether-Based Lipids Synthesized with an Epoxide Construction Kit: Multivalent Architectures for Functional Liposomes. In *Tailored Polymer Architectures for Pharmaceutical and Biomedical Applications*, American Chemical Society: 2013; Vol. 1135, pp 11-25.

44.   Schömer, M.; Frey, H., *Macromolecules* **2012,** *45* (7), 3039-3046.

45.   Obermeier, B.; Wurm, F.; Mangold, C.; Frey, H., *Angew. Chem. Int. Ed.* **2011,** *50* (35), 7988-7997.

46.   Weibull, B.; Nycander, B., *Acta Chem. Scand.* **1954,** *8* (5), 847-858.

47.   Johnson, A. E.; Giessler, P. R.; Talley, L. D., *J. Am. Oil Chem. Soc.* **1990,** *67* (2), 123-131.

48.   Geissler, P. R.; Johnson, A. E., *J. Am. Oil Chem. Soc.* **1990,** *67* (8), 541-546.

49.   Hanselmann, R.; Hölter, D.; Frey, H., *Macromolecules* **1998,** *31* (12), 3790-3801.

50.   Mahon, E.; Salvati, A.; Bombelli, F. B.; Lynch, I.; Dawson, K. A., *J. Controlled Release* **2012,** *161,* 164-174.
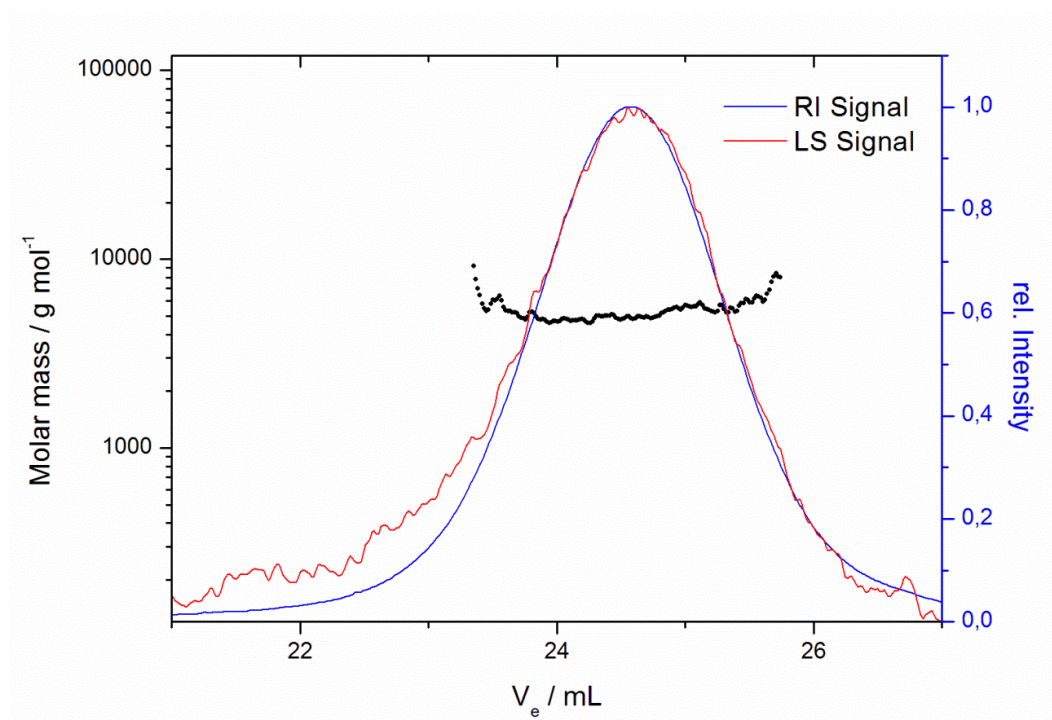
Supporting Information

Figure S1. Aqueous MALS measurement of Ch-*lin*PG$_{29}$-*co*-PAGE$_9$-GSH$_3$ with RI signal (blue), light scattering signal (red) and molar mass (black).
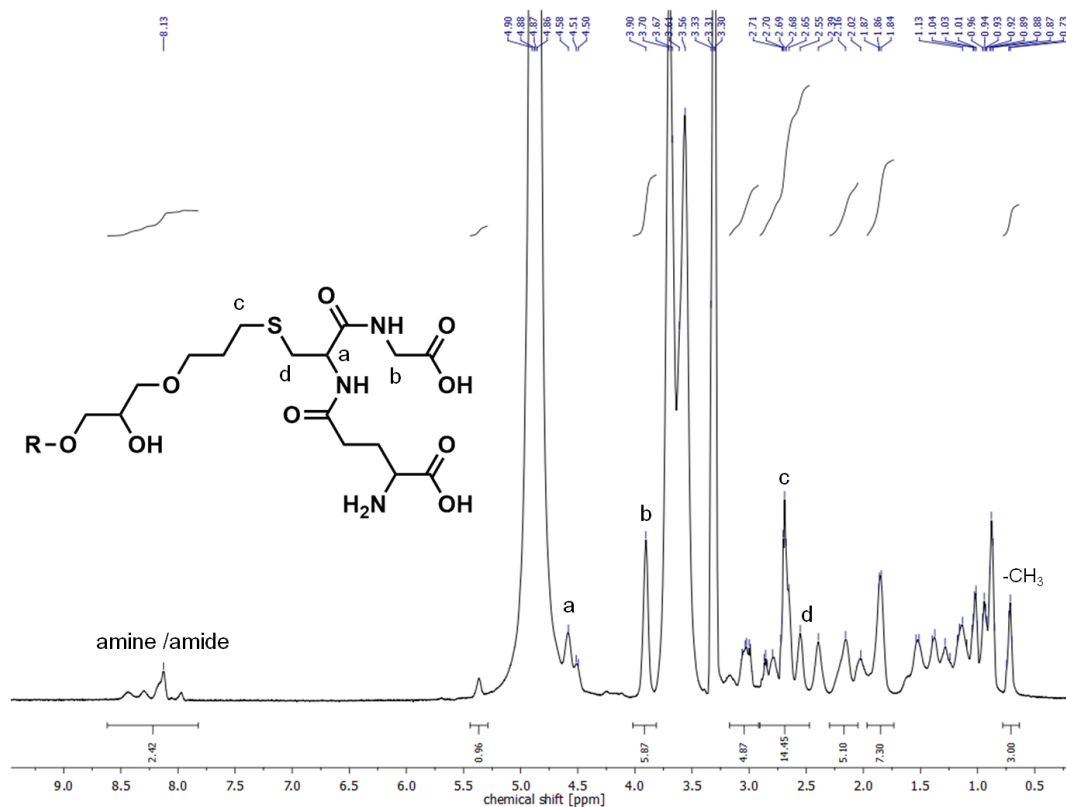

Figure S2. ^{1}H NMR spectrum of Ch-*lin*PG$_{29}$-*co*-PAGE$_9$-GSH$_3$ in MeOD (400 MHz).

Glutathione conjugated lipid Ch-linPG$_{29}$-co-PAGE$_9$-GSH$_3$

Due to micelle formation of the amphiphile, the cholesterol peaks are not visible, which makes the peak assignment more facile. The assignment was compared to the literature.[1]

^{1}H NMR (400 MHz, D$_2$O) δ = ppm, 4.51 (1H, C*H*CH$_2$S), 3.91 (2H, Gly-C*H$_2$*), 3.80-3.44 (backbone, Glu-C*H*, CH$_2$OC*H$_2$*CH$_2$CH$_2$), 3.32 (s, 3H, *H$_3$*CO), 3.05-2.76 (2H, CHC*H$_2$*S), 2.59 (2H, CHCH$_2$SC*H$_2$*), 2.49 (2H, Glu-C*H$_2$*CO), 2.12 (2H, Glu -CHC*H$_2$*), 1.81 (2H, OCH$_2$C*H$_2$*CH$_2$S), 1.20 (3H, *H$_3$*CCHS).
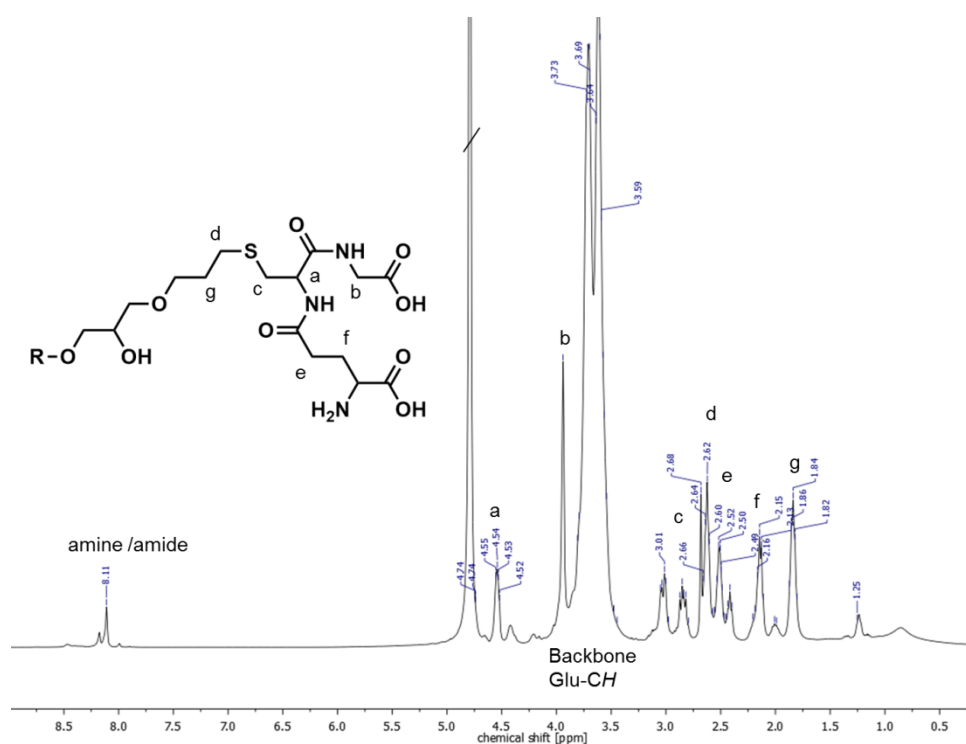
Figure S3. ^{1}H NMR spectrum of Ch-*lin*PG$_{29}$-co-PAGE$_9$-GSH$_3$ in D$_2$O (400 MHz).
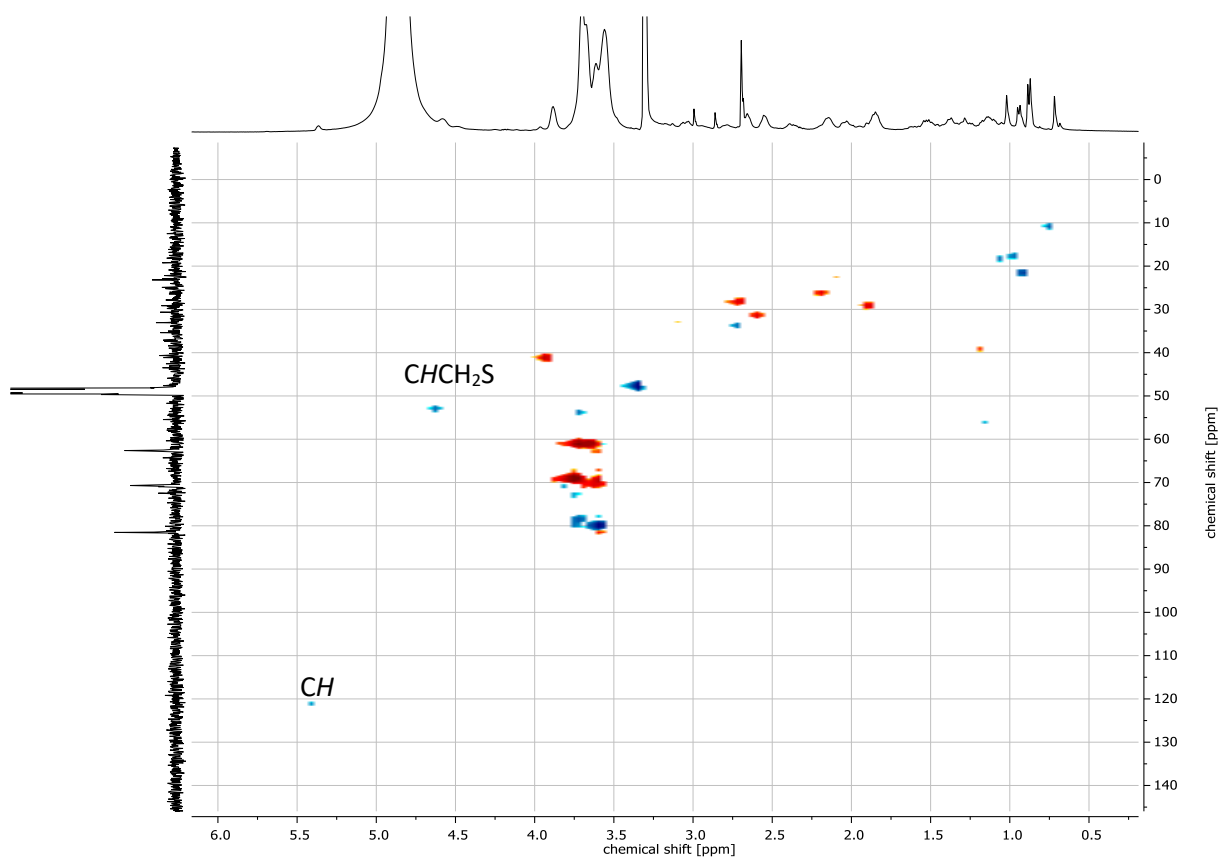
Figure S4. HSQC spectrum of Ch-*lin*PG$_{29}$-*co*-PAGE$_9$-GSH$_3$ in MeOD (400 MHz).
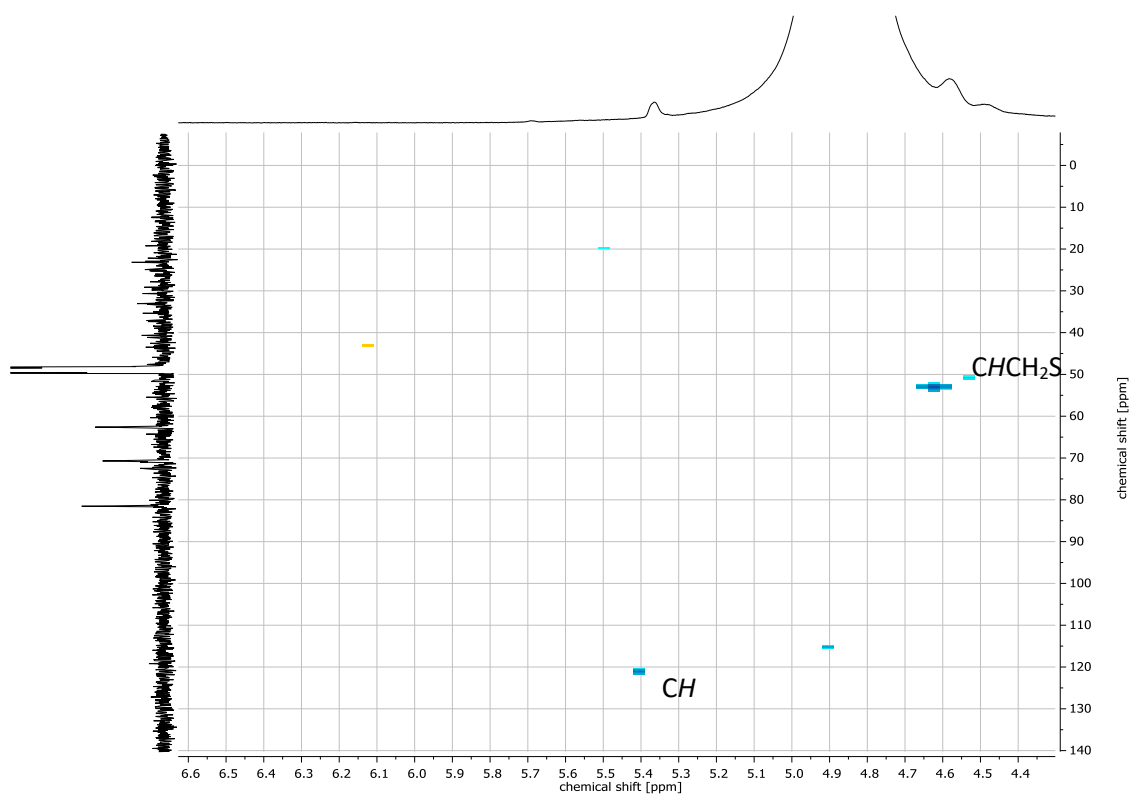
Figure S5. Zoom-In: HSQC spectrum of Ch-*lin*PG$_{29}$-*co*-PAGE$_9$-GSH$_3$ in MeOD (400 MHz).
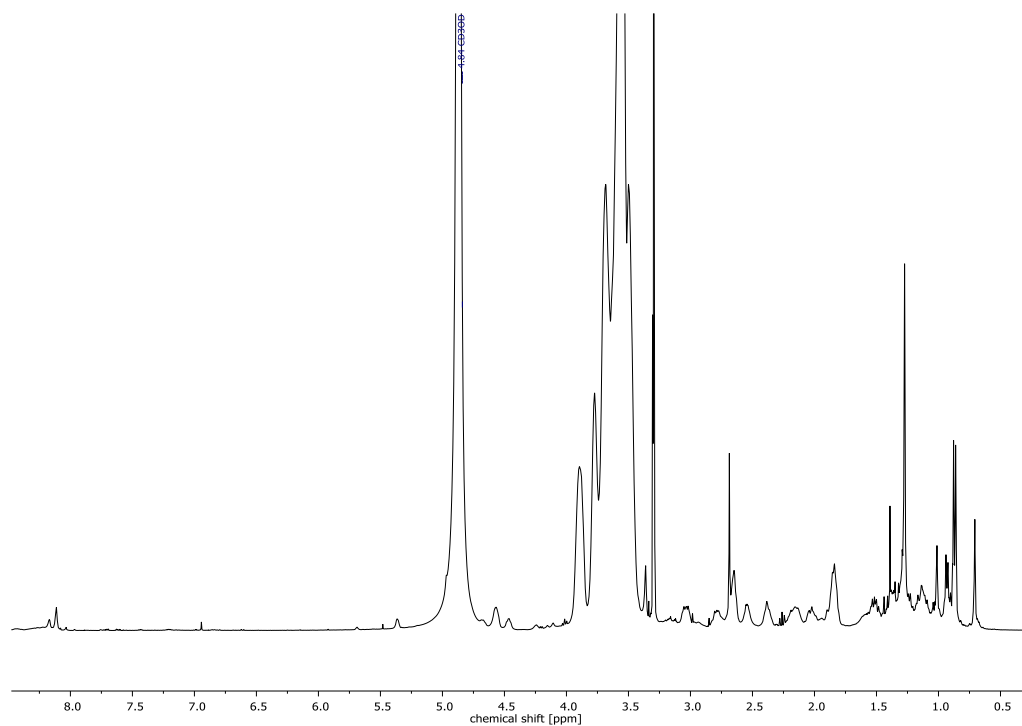
Figure S6. ^{1}H NMR spectrum of Ch-*hb*PG$_{30}$-*graft*-PAGE$_{10}$-GSH$_{3}$ in MeOD (400 MHz).

References

[1]   Obermeier, B., Frey, H. *Bioconjugate Chem*. **2011**, 22 (3), 436-444.

## 2.2 Tackling the Biodegradability of Hyperbranched Polyether-Lipids with In-Chain pH-Sensitive Linkages

Sophie S. Müller,[1,2] Thomas Fritz,[3] Florian Prochnow,[1] Marilena Gimnich,[1] Mark Helm[3] and Holger Frey[1,]*

[1]Institute of Organic Chemistry, Johannes Gutenberg University Mainz,

Duesbergweg 10-14, 55128 Mainz, Germany

[2]Graduate School Materials Science in Mainz, Staudingerweg 9, 55128 Mainz, Germany

[3]Institute of Pharmacy and Biochemistry, Johannes Gutenberg University Mainz,

Staudingerweg 5, 55128 Mainz, Germany
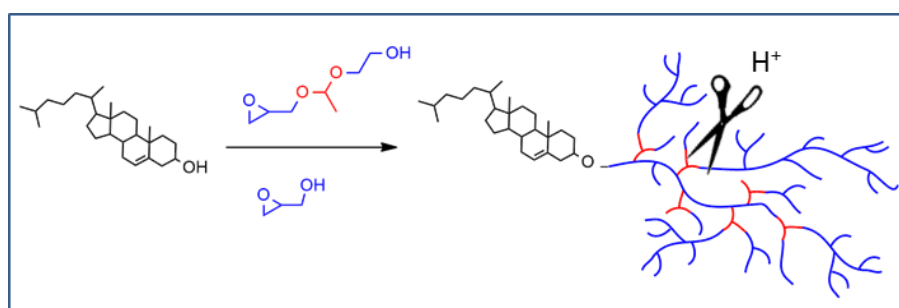
Abstract

The introduction of acid-degradable acetal moieties in hyperbranched polyether-based lipids was achieved *via* copolymerization of the epoxide inimer 1-(glycidyloxy)ethyl ethylene glycol ether (GEGE) and glycidol in the anionic ring-opening polymerization. Cholesterol-linear polyglycerol was used as the macroinitiator, resulting in branched polyethers with an adjustable amount of acid-cleavable units. Random copolymerization led to Ch-P(GEGE$_x$-*co*-G$_y$) copolymers, whereas sequential copolymerization led to Ch-P(GEGE$_x$-*b*-G$_y$) amphiphiles. The amount of GEGE was tuned between 8-49 mol% compared to the total amount of monomer units. In addition, hyperbranched polyethers with exactly one acetal unit were prepared using glycol-1-(cholesteryloxy)ethylether as

the initiator for the polymerization of allyl glycidyl ether (AGE) in bulk. Subsequent thiol-ene coupling of mercaptoethanol resulted in the hydroxyl functional macroinitiator used for the polymerization of glycidol. The novel polyether-based lipids were characterized in detail by ^{1}H NMR spectroscopy and size exclusion chromatography, revealing narrow to moderate molecular weight distributions. Degradation was achieved at pH 2. Shedding of the liposome was proven by using the linear analogue α-(1-(cholesteryloxy)ethoxy)-ω-hydro-PEG-CH_2-C≡CH with one cleavable group and a fluorescent label, Atto 488 azide. Investigation on the acetal-cleavage under acidic pH (7.4-2.0) *via* fluorescence spectroscopy was carried out.

Introduction

Drug delivery vehicles, such as liposomes, are well known carriers, especially in anti-cancer treatment.[1,2] Liposomes consist of amphiphilic phospholipids that form spherical vesicles in aqueous solution. Effective delivery systems enable an important step towards minimizing undesired properties of extremely toxic drugs, such as doxorubicin, on healthy tissue. Disadvantages like cardiotoxicity of doxorubicin and short circulation times can be avoided. The use of poly(ethylene glycol) (PEG) as a polymer shell at the liposome surface has become a popular approach to create long-circulating liposomes.[3,4] These systems are also called sterically stabilized or "stealth" liposomes, since the PEGylated liposomes obtain extraordinary properties due to the water-soluble and flexible polymer chains. The presence of PEG results in prolonged blood circulation times,[5,6] reduced mononuclear phagocyte system (MPS) uptake,[7] reduced aggregation of the carriers and increasing colloidal stability.[8] Nevertheless, the gold standard PEG possesses drawbacks that need to be overcome in advanced drug delivery systems. Having reached the target tissue and cells, the PEG shell can prevent the liposome from penetrating into cells or escaping from the endosome after endocytosis (PEG dilemma).[9,10] Currently established drug delivery systems that are based on such liposomes fail to release the drug actively and rely on passive diffusion or slow and non-specific liposome degradation. Ideally, PEGylated liposomes profit from the enhanced permeability and retention (EPR) effect,[11] and are stable under physiological pH (pH 7.4).

Preferentially, the polymer coating would be detached under local pathological conditions such as low pH, leading to destabilization and release of the cargo. The slightly acidic environment in endosomes, tumor tissues, or inflammatory tissue is one of the main differences to healthy tissue. Endocytic pathways lead to a drop from a neutral pH to pH 6 in late endosomes and pH 4 in lysosomes.[12,13] Cancer and inflammatory tissue also exhibit acidic pH around pH 6.5.[14] A perfectly tuned pH-sensitive nanoparticle would shed the polymer coating and thus enable membrane-membrane fusion and internalization. Fusion with the endosomal membrane is especially important for the release of a cargo into the cytoplasm.[15,16] This escape is crucial for acid-degradable cargo such as small interfering RNA (siRNA), proteins or acid-labile drugs.[17] The need for "stealth" liposomes that are stable under physiological conditions, but release their content at decreased pH at the site of action is proposed in an increasing number of publications in this field.

In the present work, we focus on pH-sensitive linkages between PEG and a hydrophobic anchor group which stabilizes the amphiphile in the phospholipid bilayer. Several examples have been reported for controlled release including acetals,[18,19] vinylethers,[20-22] (di-)ortho esters,[23-25] hydrazones,[26-28] and esters (e.g. succinates).[29,30]

The second drawback of PEG is its lack of functional groups. Methoxypoly(ethylene glycol) (mPEG), that is commonly used for the linkage to phospholipids or cholesterol, does not possess additional functional groups for derivatization. However, functional groups are important for the attachment of markers, antibodies or proteins for "active" tumor targeting.[31] Our group has introduced multifunctional polyether-based lipids synthesized from an epoxide "construction kit".[32-34] By using cholesterol directly as the initiator for the oxyanionic ring-opening polymerization (ROP) of various epoxides (ethylene oxide (EO), ethoxyethyl glycidyl ether (EEGE), isopropylidene glycidyl glyceryl ether (IGG), and glycidol), a variety of tailor-made architectures like linear, hyperbranched or linear-hyperbranched polyether amphiphiles can be obtained. The hyperbranched structures can be realized by using glycidol in the ring-opening multibranching technique via slow monomer addition (SMA) of the AB_2 monomer to a multihydroxy-precursor. With this method reproducible and narrowly distributed hyperbranched polyglycerol (hbPG) derivatives can be obtained.[35] Furthermore, the number of hydroxyl groups can be accurately tuned by the amount of glycidol utilized.

*Hb*PG has been extensively studied in drug delivery applications and as a biorepellent material due to its extraordinary biocompatibility,[36-38] multifunctionality and water-solubility.[39] Similar to the abovementioned PEG-lipids, its non-biodegradability can be an issue in special applications. To overcome this drawback, pH-sensitive polyether polyketals with tunable degradation in solution were synthesized by Kizhakkedathu and coworkers.[40-42] Hyperbranched acetal-containing polyethers were introduced by our group using the epoxide inimer 1-(glycidyloxy)ethyl ethylene glycol ether (GEGE) in a copolymerization reaction with glycidol.[43]

In the present study, we combine the benefits of multifunctional polyether-based lipids with the degradability of pH-sensitive acetal-containing polyglycerol. In all cases, cholesterol moieties were employed as the hydrophobic part of the amphiphilic structure, guaranteeing strong interaction with the phospholipid bilayer of liposomes. In the first strategy, we show the synthesis of hyperbranched acetal-containing polyglycerol by using GEGE and glycidol in a random copolymerization or a sequential polymerization (Figure 1a, Scheme 1). In the second approach, we expand the concept of glycol-1-(cholesteryloxy)ethylether recently presented by our group.[18] This initiator is used for the polymerization of AGE, subsequent thiol-ene coupling with 2-mercaptoethanol followed by the polymerization of glycidol. This pathway results in either linear multihydroxy-functional polyethers or hyperbranched polyethers having exactly one acetal group between the cholesterol anchor and the polymer chain (Figure 1b, Scheme 2). In the third case, the scope of α-(1-(cholesteryloxy)ethoxy)-ω-hydro-PEG is expanded by the functionalization with propargyl bromide followed by copper-catalyzed cycloaddition with Atto 488 azide. Acidic cleavage of the acetal group in functionalized liposomes was investigated *via* fluorescence spectroscopy. The shedding process could be monitored by fluorescence emission of the dye Atto 488 (Figure 1c, Figure 8).

With these different polymer systems comprising multiple or single acetal groups in hand, we introduce a platform of lipids that combine desired lipid pH-responsiveness with multifunctionality for drug delivery applications.
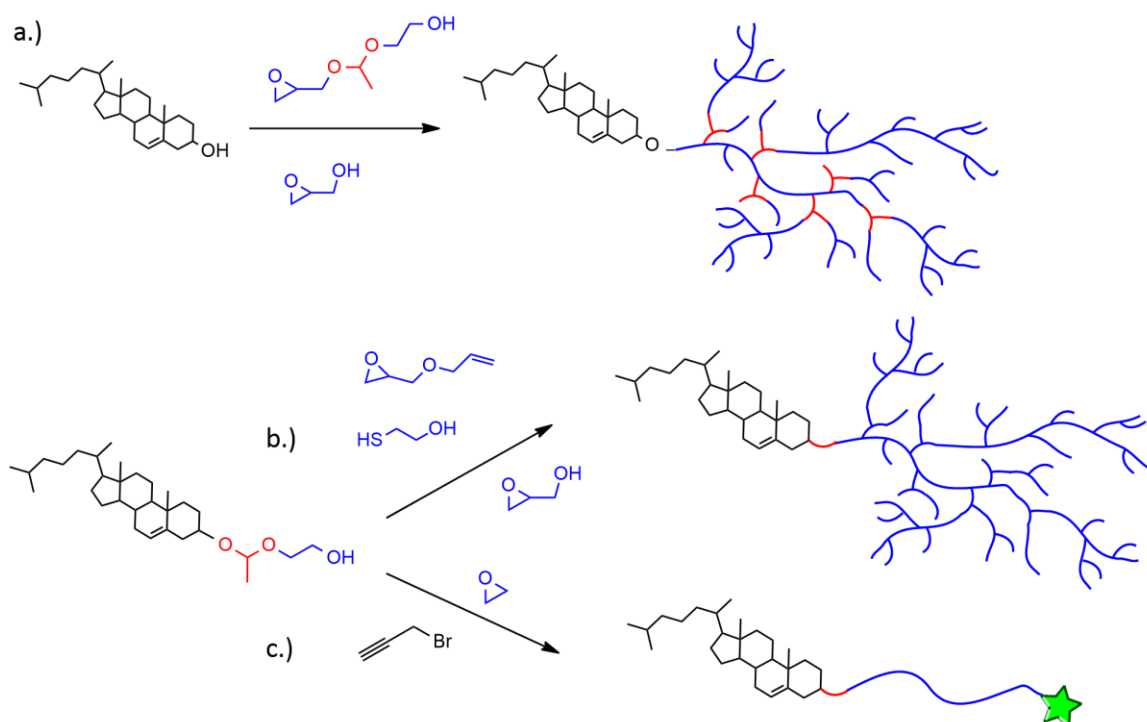
Figure 1: a.) Synthesis of hyperbranched polyglycerol lipids containing multiple acetal groups by using GEGE and glycidol in a random copolymerization or a sequential polymerization. b.) hyperbranched polyether lipids having exactly one acetal group starting from glycol-1-(cholesteryloxy)ethylether. c.) linear PEG lipids with one cleavable group functionalized with the fluorescence dye Atto 448.

Experimental

Methods

^{1}H NMR spectra (300 MHz and 400 MHz) were recorded using a Bruker AC300 or a Bruker AMX400, employing CD_2Cl_2, MeOD, or THF-d_8 as solvent. All spectra were referenced internally to residual proton signals of the deuterated solvent. Size exclusion chromatography (SEC) measurements were carried out in dimethylformamide (DMF) with 0.25 g L^{-1} LiBr on PSS HEMA columns (300/100/40). For SEC measurements UV (275 nm) and RI detectors were used. Calibration was carried out using poly(ethylene glycol) (PEG) standards provided by Polymer Standards Service (PSS). Matrix-assisted laser desorption/ionization time-of-flight mass spectrometry (MALDI-ToF MS) measurements were performed on a Shimadzu Axima CFR MALDI-ToF mass spectrometer equipped with a nitrogen laser delivering 3 ns laser pulses at 337 nm. Dithranol was used as a matrix. The sample was prepared by dissolving the polymer in methanol at a concentration of 10 g L^{-1}. A 10 µL aliquot of this solution was added to

10 μL of a 10 g L^{-1} solution of the matrix and 1 μL of a solution of potassium trifluoroacetate (KTFA) (0.1 M in methanol as a cationization agent). A 1 μL aliquot of the mixture was applied to a multistage target, methanol evaporated and a thin matrix/analyte film created.

Liposome Preparation

Liposomes bearing acetal-containing cholesterol-based amphiphiles were prepared as described previously.[44,45] Briefly, 32.5 μl of phosphate buffered saline (PBS) (137 mM NaCl, 2.7 mM KCl, 10 mM Na$_2$HPO$_4$, 2 mM KH$_2$PO$_4$, pH 7.4) was added to 17.5 mg of a dried lipid film consisting of cholesterol (Carl Roth), egg phosphatidyl choline (EPC, kindly provided by Lipoid) and α-(1-(cholesteryloxy)ethoxy)-ω-Hydro-PEG$_{46}$-CH$_2$C≡CH (40:55:5 molar ratio) and 250 mg ceramic beads (SiLiBeads ZY 0.6-0.8 mm, kindly provided by Sigmund Lindner, Warmensteinach, Germany). Non-cleavable liposomes were prepared with an equivalent cholesterol-PEG-CH$_2$C≡CH compound. After dual centrifugation in a Rotanta 400 centrifuge (customized with a prototype DC-rotor, Hettich, Tuttlingen, Germany) for 20 min at 2500 RPM and dilution with 100 μl PBS, 5 μl of the liposome suspension were exposed to click-modification with 50 μM Atto 488 azide (Atto-Tec, Siegen, Germany) in Milli-Q water (to a total volume of 40 μl), phosphate buffer (5.3 mM NaH$_2$PO$_4$, 94.7 mM Na$_2$HPO$_4$) pH 8, Tris(hydroxypropyltriazolylmethyl)amine (THPTA) (0.5 mM), CuSO$_4$ (0.1 mM) and sodium ascorbate (2.5 mM) and subsequent gel filtration through Sepharose 2B.

Liposome size was obtained *via* dynamic light scattering (DLS) on a Malvern Zetasizer Nano ZS, using disposable poly(styrene) cuvettes (Sarstedt, Germany). 1 μl of liposome stock suspension was diluted in 1 ml PBS. After equilibration to 25 °C, three measurements were performed, using the internal measurement optimization for both attenuator and measurement position. Refractive index (RI) and viscosity of the dispersant was set to 1.330 and 0.8872 cP, the RI of the particle to 1.59. The absorption of the particle was set to 0.01 and all measurements were performed at a scattering angle of 173°.

Cleavage of the polymeric liposome shell was observed via fluorescence spectroscopy on a FP-6500 spectrofluorimeter (Jasco, Tokyo, Japan) at 488 nm excitation wavelength and 523 nm emission wavelength during a time course measurement with a data interval of

1 min. 50 µl of purified liposomes were combined with 3 ml PBS in a 1 cm^3 quartz glass cuvette (Hellma Analytics, Müllheim, Germany) with a magnetic stirrer. After equilibration for 12 h at 37 °C, the pH of the suspension was adjusted by addition of 50 µl 2 M hydrochloric acid (HCl) (pH 2), 20 µl 2 M HCl (pH 3) or 15 µl 2 M HCl (pH 5.5). Fluorescence intensity was normalized to the intensity at the beginning of acidification.

Syntheses and Reagents

All reagents and solvents were purchased from Acros and used as received, unless otherwise mentioned. Anhydrous solvents were stored over molecular sieves and were purchased from Aldrich. Deuterated solvents were purchased from Deutero GmbH, and stored over molecular sieves. Cholesterol was purchased from Acros and stored at 8 °C. Ethoxyethyl glycidyl ether (EEGE) was synthesized as described in the literature[46], dried over CaH$_2$ and cryo-transferred prior to use. Glycidol and N-Methyl-2-pyrrolidon (NMP) were purified by distillation from CaH$_2$ directly prior to use. 1-(Glycidyloxy)ethyl ethylene glycol ether (GEGE) was synthesized according to the literature.[43] To release the hydroxyl group in the final reaction step, the benzyl protecting group was removed using catalytic hydrogenation (Pd(OH)$_2$/C, 10wt%). The product was purified by column chromatography in ethyl acetate. Glycol-1-(Cholesteryloxy)ethylether and α-(1-(cholesteryloxy)ethoxy)-ω-Hydro-PEG$_{46}$ were synthesized following reported procedures.[18] Propargyl bromide (0.8 M in toluene) was stored at 4 °C and used as received. Allyl glycidyl ether (AGE) was purchased from Acros Organics, dried over CaH$_2$ and cryo-transferred prior to use. Azobisisobutyronitrile (AIBN, Acros) was recrystallized from MeOH. 2-Mercaptoethanol (Acros) was stored at 5 °C and was used as received.

Etherification of α-(1-(cholesteryloxy)ethoxy)-ω-hydro-PEG$_{46}$ with propargyl bromide.
α-(1-(Cholesteryloxy)ethoxy)-ω-Hydro-PEG$_{46}$ (0.4 g, 0.16 mmol) was dissolved in anhydrous THF (7 mL), and sodium hydride (9.6 mg, 0.4 mmol) was slowly added under an argon stream at 0 °C. The reaction mixture was stirred for 30 min and after slow addition of propargyl bromide (0.17 mL, 0.6 mmol) allowed to warm up to room temperature. The reaction was stirred at room temperature for 24 h and was filtered. Removal of the solvent in vacuo and precipitation in cold diethyl ether resulted in the pure product. Yield: 90%.

^{1}H NMR (400 MHz, CD$_2$Cl$_2$): δ (ppm) = 5.34 (C=C*H* cholesterol), 4.79 (H$_3$C-C*H*O$_2$, acetal group), 4.18 (-OC*H*$_2$C≡CH), 3.80-3.40 (polyether backbone; C*H*O cholesterol), 2.49 (-C≡C*H*), 2.27-0.82 (C*H*$_2$, C*H* cholesterol), 0.68 (-C*H*$_3$ cholesterol).

Macroinitiator: Cholesterol initiated linear poly(glycerol) (Ch-*lin*PG$_{20}$; Ch-*lin*PG$_{13}$).

Cholesterol (2.0 g, 5.2 mmol), CsOH monohydrate (0.782 g, 4.7 mmol, 90% of deprotonation) and benzene (8 mL) were placed in a Schlenk flask. The mixture was stirred at 60 °C for about 30 min to generate the cesium alkoxide. The salt was then dried under vacuum at 90 °C for 24 h. The salt was suspended in 60 mL anhydrous dioxane, the monomer EEGE was added (5.5 mL, 36 mmol, 7 eq.) and the mixture was heated up to 80 °C for 24 h. A sample was removed for NMR and SEC analysis, the polymerization was stopped via addition of an excess of methanol and the acetal protecting groups of PEEGE were cleaved by the addition of an acidic ion-exchange resin (Dowex 50WX8) and 2 N HCl, stirring for 24 h at RT. The solution was filtered, concentrated, and the crude product was precipitated twice in cold diethyl ether. The block copolymer was dried under vacuum. Yield: ~80%.

No ^{1}H NMR spectrum was measured before the deprotection step, because residual cholesterol was detected in SEC diagrams, leading to incorrect integration of the resonances.

^{1}H NMR (300 MHz, MeOD-*d$_4$*): δ (ppm) = 5.37 (C=C*H* cholesterol), 3.80-3.40 (polyether backbone; C*H*O cholesterol), 2.40-0.82 (C*H*$_2$, C*H* cholesterol), 0.72 (-C*H*$_3$ cholesterol).

Ch-Poly(1-(glycidyloxy)ethyl ethylene glycol ether-*co*-glycerol) Ch-P(GEGE-*co*-G).

For random copolymerization of GEGE and glycidol Ch-*lin*PG$_{20}$ was used, and for sequential copolymerization (block copolymers) Ch-*lin*PG$_{13}$ was used as the macroinitiator. General procedure for the copolymerization of glycidol and GEGE: Ch-*lin*PG$_{13}$ (0.20 g, 0.15 mmol), CsOH monohydrate (10% of OH groups, 0.035 g, 0.21 mmol), and 1.2 mL of benzene were placed in a Schlenk flask and stirred for 30 min at 60 °C. All solvents were removed under reduced pressure, and the initiator salt was dried at 90 °C for at least 4 h under high vacuum. The initiator salt was dissolved in NMP and a mixture of glycidol in NMP and GEGE in NMP was slowly added under argon atmosphere using a syringe pump. For random copolymerization the monomers were mixed in NMP and

slowly added, whereas for block copolymers, GEGE in NMP was added before glycidol in NMP was added. The reaction was terminated by the addition of an excess of methanol. The mixture was concentrated and precipitated (2–4 times) into an excess of cold diethyl ether. Yield: 60-75%.

^{1}H NMR (300 MHz, MeOD-d_4): δ (ppm) = 5.38 (C=CH cholesterol), 4.79 (H$_3$C-CHO$_2$, GEGE acetal group), 3.80-3.40 (polyether backbone; CHO cholesterol), 2.36-0.87 (CH_2, CH cholesterol), 1.32 (H_3C-CHO$_2$, GEGE), 0.72 (-CH_3 cholesterol).

α-(1-(Cholesteryloxy)ethoxy)-ω-hydro-Poly(allyl glycidyl ether) in bulk.

Glycol-1-(Cholesteryloxy)ethylether (0.3 g, 0.63 mmol), CsOH monohydrate (0.095 g, 0.57 mmol; degree of deprotonation 90%), and benzene (8 mL) were placed in a Schlenk flask. The mixture was stirred for about 30 min at 60 °C to generate the cesium alkoxide. The salt was then dried under vacuum at 90 °C for 3 h. The monomer AGE was added (1.45 mL, 12.6 mmol, 20 eq.) and the mixture was heated up to 65 °C for 24 h. The polymerization was stopped using an excess of methanol. Yield: ~98%.

Ch-OCHCH$_3$O-PAGE$_{20}$: ^{1}H NMR (300 MHz, CD$_2$Cl$_2$): δ (ppm) = 5.93 (-CH$_2$CH=CH$_2$, allyl), 5.39 (C=CH cholesterol), 5.33-5.17 (-CH$_2$CH=CH_2, allyl), 4.82 (H$_3$C-CHO$_2$, acetal group), 4.01 (-CH_2CH=CH$_2$), 3.80-3.39 (polyether backbone; CHO cholesterol), 2.32-0.88 (CH_2, CH cholesterol), 1.30 (H_3C-CHO$_2$), 0.72 (-CH_3 cholesterol).

Thiol-ene coupling of Ch-OCHCH$_3$O-PAGE$_{20}$ with 2-mercaptoethanol.

Ch-OCHCH$_3$O-PAGE$_{20}$ (0.3 g, 0.1 mmol), 270 mg AIBN (0.75 eq. for each allyl group), and 2-mercaptoethanol (1.55 mL, 22 mmol, 10 eq. of allyl groups) were dissolved in 10 mL DMF. After three freeze-pump-thaw cycles, the mixture was stirred at 75 °C for 24 h. For purification, the reaction mixture was dialyzed against MeOH (MWCO = 1000 g mol^{-1}) for two days and dried under vacuum to give the polymer with a sticky appearance. Yield: 83%.

^{1}H NMR (400 MHz, THF-d_8): δ (ppm) = 5.34 (C=CH cholesterol), 4.81 (H$_3$C-CHO$_2$, acetal group), 4.00-3.30 (polyether backbone; CHO cholesterol), 2.72-2.40 (-CH_2SCH_2), 1.83 (-CH_2CH$_2$S), 2.37-0.87 (CH_2, CH cholesterol), 0.72 (- CH_3 cholesterol).

Hypergrafting of glycidol onto Ch-OCHCH₃O-thiol-coupling₂₀. The macroinitiator Ch-OCHCH₃O-thiol-coupling₂₀ (0.2 g, 0.05 mmol), CsOH monohydrate (20% of OH groups, 0.033 g, 0.19 mmol), and benzene were placed in a Schlenk flask and stirred for 30 min at 60 °C. All solvents were removed under reduced pressure and the initiator salt was dried at 90 °C for 24 h under vacuum. The initiator salt was dissolved in 0.5 mL NMP and glycidol in NMP (0.5 mL, 20 wt%) was slowly added under argon atmosphere using a syringe pump. The reaction was terminated by the addition of excess of methanol. The mixture was concentrated and precipitated into an excess of cold diethyl ether. Residual NMP could be removed by drying under vacuum and washing with CH_2Cl_2. Yield: 80%.

^{1}H NMR (400 MHz, DMSO-d_6): δ (ppm) = 5.32 (C=CH cholesterol), 5.11 (-OH) 4.81 (H_3C-CHO₂, acetal group), 3.90-3.20 (polyether backbone; CHO cholesterol), 2.65-2.52 (-CH_2SCH_2), 1.74 (-CH_2CH₂S), 2.40-0.84 (CH_2, CH cholesterol), 0.65 (-CH_3 cholesterol).

Results and Discussion

Synthesis of Amphiphilic Hyperbranched Lipids with Multiple Acid-Cleavable Moieties

Hyperbranched polyether-lipids with multiple pH-responsive acetal groups were prepared by oxyanionic ring-opening polymerization using cholesterol as the initiator. After deprotonation with cesium hydroxide, the alkoxide was used for the polymerization of ethoxyethyl glycidyl ether (EEGE) with subsequent acidic deprotection of the EEGE protecting group (Scheme 1).

Molecular weights for the macroinitiators were between 1300 and 1900 g mol⁻¹ (Table 1) according to ^{1}H NMR spectroscopy, with the usual underestimation by size exclusion chromatography (SEC). The linear polyglycerol repeating units were calculated by comparing the methyl group of cholesterol (0.72 ppm) and the polyether backbone resonances after acidic deprotection of the acetal protecting groups from the EEGE moieties. Molecular weights calculated by ^{1}H NMR spectroscopy for both macroinitiators were higher than the theoretical values. We aimed at seven glycerol units per macroinitiator, however, 20 and 13 units were obtained, respectively. Fast proton exchange results in the protonated form of cholesterol and deprotonated adducts of initiator and the first monomer unit.[47-49] This leads to different kinetics in the initiation

step and the propagation step, since the ethoxylated cholesterol exhibits higher reactivity than the cholesterol alkoxide. Hence, significant amounts of free initiator are found in the reaction mixture when oligomers are desired.[50] After acidic deprotection of the acetal groups, the polymer was precipitated multiple times in cold diethylether to remove excess cholesterol. This led to reduced yields and an enhanced concentration of longer polymer chains.
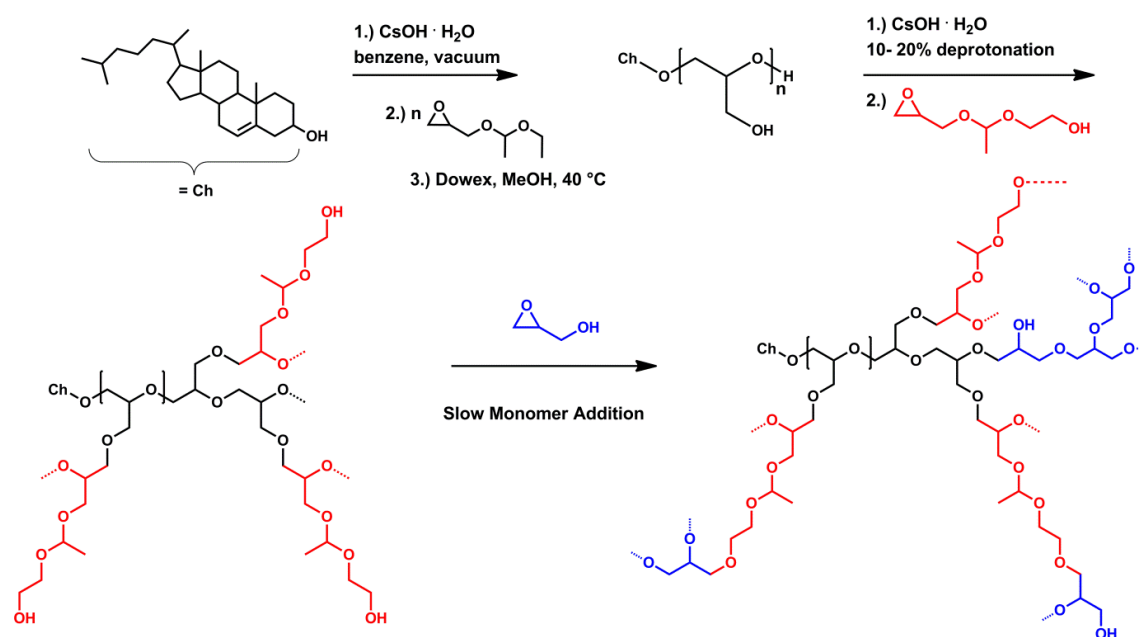
Scheme 1: Reaction scheme for the macroinitiator Ch-*lin*PG$_n$, followed by the slow monomer addition of GEGE and glycidol, which can be carried out simultaneously or sequentially as depicted here.

The resulting linear polyglycerol amphiphiles (Ch-*lin*PG$_{20}$; Ch-*lin*PG$_{13}$) function as the macroinitiator for the slow monomer addition of 1-(glycidyloxy)ethyl ethylene glycol ether (GEGE) and glycidol. Partial deprotonation and slow monomer addition permits good control over the alkoxide concentration resulting in equal growth of the polymer chain ends. This technique narrows the molecular weight distribution and prevents undesired homopolymerization of the cyclic inimers.[51] Deprotonation of the macroinitiator was adjusted to 10% (relative to the total amount of hydroxyl groups) in order to maintain solubility in N-methyl-2-pyrrolidon (NMP). Both monomers, i.e. GEGE and glycidol, can be copolymerized randomly or sequentially. The reaction route is shown in Scheme 1 (vide supra). The advantage of a sequential addition of the

monomers, in which GEGE is polymerized first, is that the cleavable acetal groups are located in the proximity of the cholesterol anchor group. Acidic cleavage would lead to scission near the phospholipid bilayer in the final liposomes, which could enhance shedding of the polymer and drug release.

This approach enabled the synthesis of a series of copolymers which carry multiple acetal groups distributed in the hyperbranched polymer or located near the cholesterol anchor. The random copolymers were prepared from a macroinitiator consisting of 20 linear glycerol units, whereas for the sequentially synthesized copolymers the macroinitiator Ch-linPG$_{13}$ was used. The molecular weights for the hyperbranched lipids were around 5000 g mol^{-1}, again with an underestimation in SEC due to differences in the hydrodynamic radius compared to the linear PEG polymer used for calibration. On the other hand, we assume a slight overestimation of the molecular weights in ^{1}H NMR spectroscopy, since residual solvent resonances can overlap with the polyether backbone signals. Polydispersity indices (PDI = M_w/M_n) below 1.15 were found for the two macroinitiators, whereas for the hyperbranched copolymers PDIs below 1.60 could be achieved. The last column of Table 1 summarizes the mol% of GEGE, which were successfully tuned between 8mol% and 49 mol% (in relation to the total amount of monomer units).

Table 1: Characterization data of the macroinitiators (Ch-linPG$_{20}$; Ch-linPG$_{13}$) and the pH-responsive copolymers (random: Ch-P(GEGE$_x$-co-G$_y$); block: Ch-P(GEGE$_x$-b-G$_y$).

Composition	M_n th g mol^{-1}	M_n ^{NMR} g mol^{-1}	M_n ^{SEC} g mol^{-1}	PDI ^{SEC}	GEGE mol%
Ch-linPG$_{20}$	904	1870	830	1.05	-
Ch-P(GEGE$_4$-co-G$_{48}$)	4160	4600	1600	1.57	8
Ch-P(GEGE$_{20}$-co-G$_{49}$)	5040	7200	2100	1.60	29
Ch-linPG$_{13}$	904	1350	980	1.14	-
Ch-P(GEGE$_{10}$-b-G$_{36}$)	4220	4700	2500	1.24	22
Ch-P(GEGE$_{18}$-b-G$_{36}$)	4660	6000	3000	1.29	33
Ch-P(GEGE$_{17}$-b-G$_{18}$)	4600	4500	2200	1.22	49

Figure 2 depicts SEC traces for a selection of copolymers that were synthesized from Ch-*lin*PG$_{13}$ (black solid line, Figure 2). All distributions were monomodal and molecular weights for the Ch-P(GEGE-*b*-G) copolymers were shifted to lower elution volumes compared to the macroinitiator. Because the determination of molecular weights via SEC leads to underestimated values, the absolute molecular weights were calculated from ^{1}H NMR integration of the resonances for the methyl group of cholesterol at 0.72 ppm with the polyether signals between 4.00–3.27 ppm (Figure 3). The number of GEGE units was calculated by comparing the integration of the resonances from the initiator (-CH$_3$; 0.72 ppm) with the acetal resonance at 4.79 ppm (arrow in Figure 3). The methyl group of the acetal moieties is observed at 1.32 ppm, but integration would be inaccurate due to an overlap with the cholesterol backbone. As an example, Figure 3 presents the ^{1}H NMR spectra of Ch-*lin*PG$_{13}$ (bottom) and Ch-P(GEGE$_{18}$-*b*-G$_{36}$) (top) in MeOD.
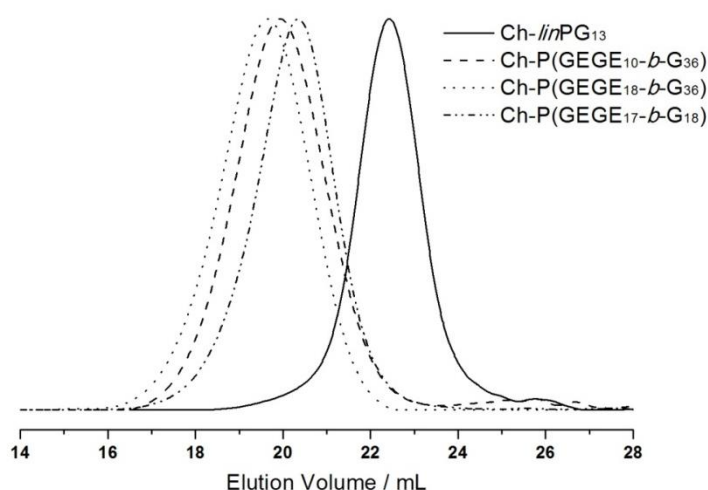

Figure 2: SEC traces (RI detection; DMF; PEG standard) for selected copolymer samples that were synthesized from Ch-*lin*PG$_{13}$ (black solid line).
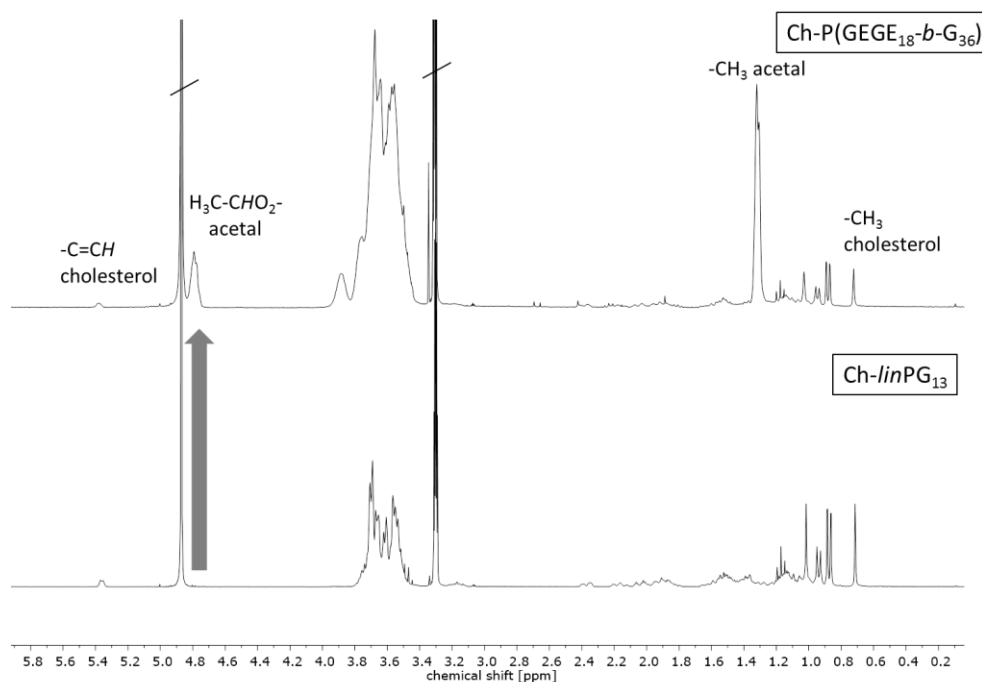
Figure 3: ^{1}H NMR spectra of Ch-*lin*PG$_{13}$ (bottom) and Ch-P(GEGE$_{18}$-*b*-G$_{36}$) (top) in MeOD.

Synthesis of Amphiphilic Hyperbranched Lipids with Exactly One Acid-Cleavable Moiety

In a recent publication, we presented the synthesis of glycol-1-(cholesteryloxy)-ethylether (Ch-acetal) as a pH-sensitive initiator for the anionic ring-opening polymerization of ethylene oxide.[18] This initiator can be synthesized in a three-step procedure starting from 1,2-ethanediol vinyl ether and acetic anhydride to form 2-acetoxyethyl vinyl ether.[52] This product can be reacted with commercially available cholesterol under acidic catalysis to produce the acetal group. After basic deprotection of the acetate protecting group, the hydroxy functional initiator glycol-1-(cholesteryloxy)ethylether is obtained, which can be used in the basic reaction conditions of the anionic polymerization of various epoxides. It was also proven that the pH-responsive lipid can be cleaved under acidic conditions.[18] Therefore, they are applicable in drug delivery systems, especially for tumor targeting, where the acidic pH of the tumor can be exploited in order to shed the polymer from the vesicle. Here, we expand the idea of exactly one acid-cleavable group in lipids from linear to hyperbranched polyethers. Decomposition products are cholesterol (natural membrane

component), biocompatible hyperbranched polyglycerol and acetaldehyde. Since usually the polymer has a molecular weight below 6000 g mol^{-1} excretion by the kidney is feasible after detachment from the hydrophobic anchor.

The abovementioned EEGE monomer contains an acetal protecting group, which is suitable for the oxyanionic ring-opening polymerization, but has to be cleaved under acidic conditions to obtain the linear polyglycerol as a macroinitiator for the hyperbranched structure. This synthetic route is not suitable in combination with the pH-sensitive initiator glycol-1-(cholesteryloxy)ethylether. Therefore, a different method had to be explored. The first monomer used for experiments with this objective was benzyl glycidyl ether. It is a commercially available glycidyl derivative and can be deprotected under catalytic hydrogenation. For the removal of the benzyl group H$_2$ pressure and a Pd-catalyst is usually applied. However, this approach did not lead to successful deprotection without cleavage of the acetal group, although different reaction conditions were tested (variation in temperature, pressure, Pd/C vs. Pd(OH)$_2$/C catalyst, solvent mixtures). Therefore, an altered synthetic route had to be introduced which is presented in Scheme 2.
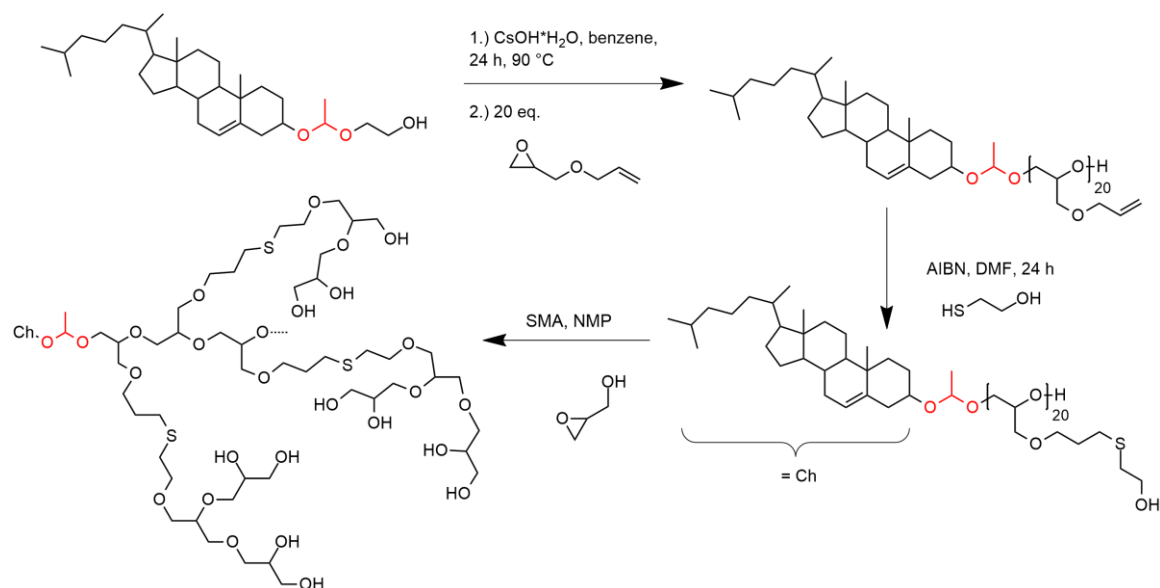

Scheme 2: Synthetic route for the synthesis of hyperbranched cholesterol-lipids with exactly one acetal group starting from glycol-1-(cholesteryloxy)ethylether (Ch-acetal); (SMA= slow monomer addition).

After deprotonation with cesium hydroxide, glycol-1-(cholesteryloxy)ethylether was used as an initiator for the oxyanionic ring-opening polymerization of allyl glycidyl ether

(AGE). This reaction was carried out in bulk to suppress isomerization of the allyl groups at elevated temperatures.[53,54] Table 2 summarizes the obtained characterization data for Ch-acetal-PAGE and supports quantitative polymerization of AGE. There is a good agreement between the theoretical amount of 20 AGE units and the repeating units calculated by ^{1}H NMR spectroscopy (20 AGE groups, see discussion below, Figure 4). The allyl groups were functionalized in a thiol-ene coupling reaction, using excess 2-mercaptoethanol and azobisisobutyronitrile (AIBN) as the radical initiator. The thiol-ene coupling was quantitative according to ^{1}H NMR spectroscopic characterization. This amphiphile already represents a novel multihydroxy-functional polyether with exactly one acetal group. Furthermore, it can be used as a macroinitiator for the hypergrafting process of glycidol in order to increase the amount of hydroxyl groups, as shown in Scheme 2. Molecular weights of the thiolether-containing hyperbranched polymer were around 6500 g mol^{-1} which is slightly higher than the commonly used molecular weights for "stealth" lipids (up to 5000 g mol^{-1}).[7] Table 2 summarizes all characterization data of the abovementioned copolymers. Column 4 illustrates that the molecular weights obtained from SEC (DMF, PEG standard) are lower than the theoretical molecular weights and the molecular weights calculated from ^{1}H NMR spectra. This trend is more pronounced for the hyperbranched structure due to the influence of the hyperbranched, globular polyglycerol on the hydrodynamic radius of the polymers compared to linear PEG. Polydispersity indices were below 1.2 (last column, Table 2). Figure 4 depicts the SEC traces for all three copolymer lipids, evidencing narrow polydispersity and monomodal distributions.

Table 2: Characterization data of the allyl containing polyether (Ch-acetal-PAGE$_{20}$), the thioether-functional lipid (Ch-acetal-thiol-coupling$_{20}$.; macroinitiator) and the hyperbranched lipid (Ch-acetal-*hb*PG$_{35}$) with one single cleavable group.

Composition	M_n th	M_n NMR	M_n SEC	PDI SEC
	g mol^{-1}	g mol^{-1}	g mol^{-1}	
Ch-acetal-PAGE$_{20}$	2750	2750	2050	1.09
Ch-acetal-thiol-coupling$_{20}$	4320	4320	3430	1.20
Ch-acetal-*hb*PG$_{35}$	6500	6900	5000	1.20
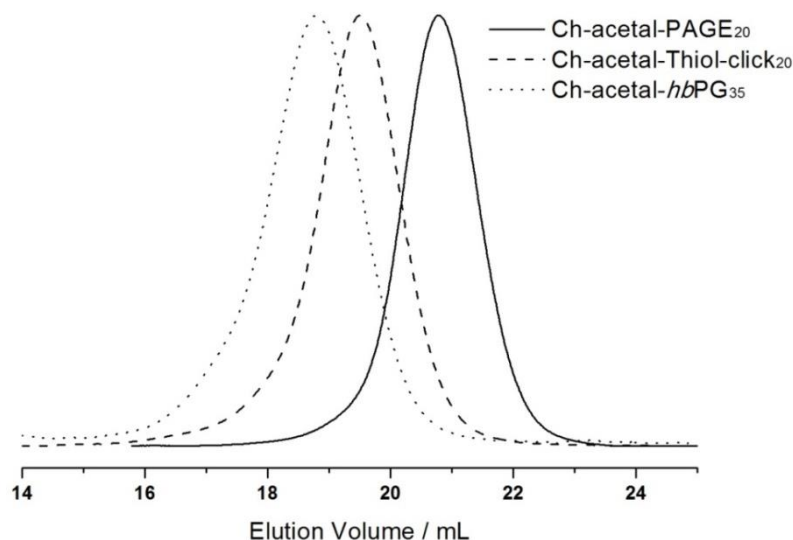
Figure 4: SEC traces (RI detection; DMF; PEG standard) for the copolymers with one single acetal group; allyl containing polyether Ch-acetal-PAGE$_{20}$ (black solid line), thiolether-containing lipid Ch-acetal-thiol-coupling$_{20}$ (dashed line), hyperbranched lipid Ch-acetal-*hb*PG$_{35}$ (dotted line).

Molecular weights, the degree of polymerization, and the degree of functionalization with 2-mercaptoethanol were calculated from ^{1}H NMR spectroscopy. The spectra are shown in Figure 5, in which the allyl functional polymer Ch-acetal-PAGE$_{20}$ (red, top) was measured in CD$_2$Cl$_2$, Ch-acetal-thiol-coupling$_{20}$ (green, middle) was measured in THF-d_8, and Ch-acetal-*hb*PG$_{35}$ (blue, bottom) was measured in DMSO-d_6. The degree of polymerization for the PAGE copolymer could be calculated by comparing the integration of the methyl group of cholesterol (0.72 ppm) with the resonance of the allyl proton at 5.93 ppm. Quantitative conversion was observed, and no isomerization of the allyl groups was found. Between 5.17 and 5.39 ppm an overlap of the allyl group and the cholesterol double bond resonances is noticeable. The acetal group was maintained and its signal can be detected at 4.82 ppm. The degree of functionalization for Ch-acetal-thiol-coupling$_{20}$ (green, middle) after the thiol-ene coupling was determined by comparing the cholesterol methyl group at 0.72 ppm with the resonances at 1.83 ppm and 2.62 ppm. These two resonances originate from the methylene groups adjacent to the sulfur (2.62 ppm) and the next but one methylene group. Here, the acetal group at 4.82 ppm and the cholesterol double bond at 5.34 ppm are still intact. After the hypergrafting of glycidol the spectrum for Ch-acetal-*hb*PG$_{35}$ was obtained in DMSO-d_6 (blue, bottom) which clearly shows that the resonances for the methylene groups near

the sulfur are still present. The grey frame highlights the acetal resonance, which remains at 4.82 ppm in every stadium of the reaction route. The resonances for the hydroxyl groups appear between 5.00 ppm and 5.20 ppm, whereas the cholesterol double bond shows a peak at 5.32 ppm. Integration of the resonances from the polyether backbone between 3.20 ppm and 3.80 ppm is used to calculate the number of glycidol groups by subtraction of the polyether signals from the precursor (macroinitiator). Residual CH_2Cl_2 originates from washing the polymer to remove traces of NMP.
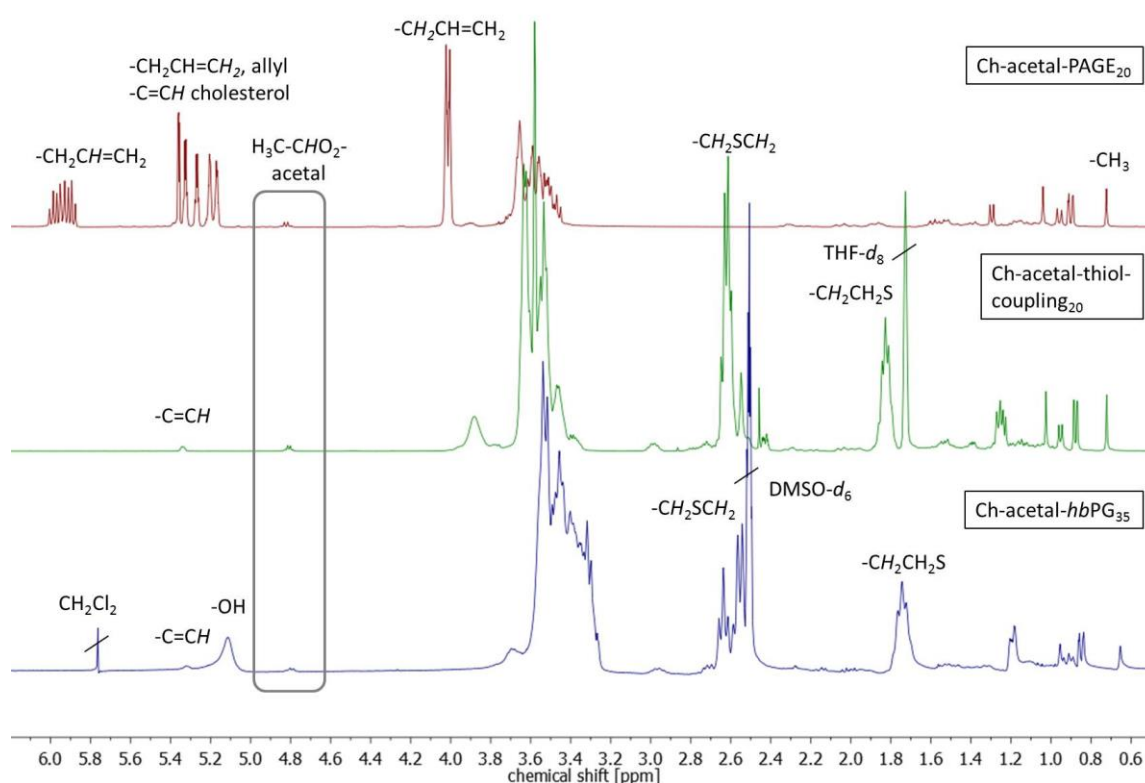
Figure 5: ^{1}H NMR spectra for the copolymers with one single acetal group; Top to bottom: red: Ch-acetal-PAGE_{20} in CD_2Cl_2; green: Ch-acetal-thiol-coupling_{20} in THF-d_8; blue: Ch-acetal-*hb*PG_{35} in DMSO-d_6.

Incorporation of the acetal containing cholesteryl initiator in every polymer chain is crucial for the amphiphilic character of the resulting lipid. The use of the lipophilic initiator permits anchoring of the polymers in the liposomal membranes. This was evidenced *via* matrix-assisted laser desorption/ionization time-of-flight mass spectrometry (MALDI-ToF MS) for Ch-acetal-PAGE_{20} and Ch-acetal-thiol-coupling_{20}, as shown in Figure 6. Figure 6a shows the distribution of Ch-acetal-PAGE_{20}, whereas Figure 6b depicts the distribution of Ch-acetal-thiol-coupling_{20}. In this spectrum, a very

small subdistribution was detected, which can be attributed to non-coupled, residual Ch-acetal-PAGE$_{20}$ (marked with an asterisk). An overlap of both spectra is shown in Figure 6c. The peak differences translate to exactly 114 g mol^{-1}, which represents the molecular weight of the allyl glycidyl ether repeating unit (Figure 6a). On the other hand, the molecular weight of 192 g mol^{-1}, which corresponds to the hydroxyl functional repeating units (C$_8$O$_3$SH$_{16}$), is detectable in the red spectrum from Figure 6b (Ch-acetal-thiol-coupling$_{20}$). In summary, the MALDI-ToF characterization confirms the structures of the novel lipids.
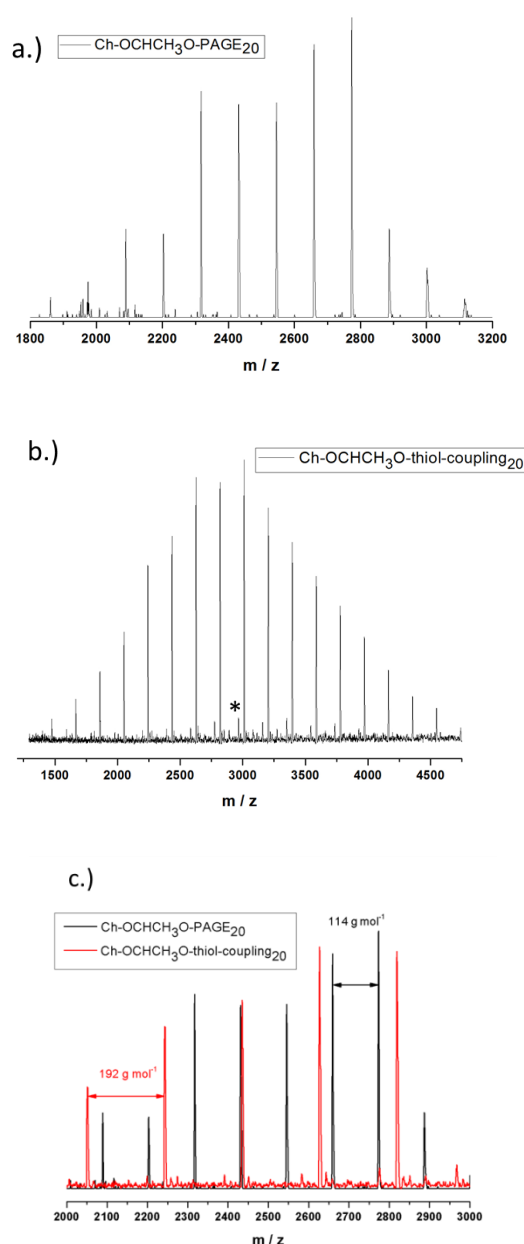

Figure 6: MALDI-ToF spectra for (a) Ch-acetal-PAGE$_{20}$ (b) Ch-acetal-thiol-coupling$_{20}$ (c) overlap of both spectra.

Degradation of Hyperbranched Lipid with Multiple pH-responsive Moieties

The acetal-containing polymer Ch-P(GEGE$_{17}$-b-G$_{18}$) was investigated using SEC measurements with respect to its acidic degradation at room temperature. For this purpose, the sample was dissolved in buffer solution (pH 2) and the sample was stirred for 24 h. Of course, pH 2 is not relevant for the degradation in tumor tissue, but for proof-of-concept studies, acidic hydrolysis can be demonstrated. Figure 7 depicts the SEC traces for the macroinitiator Ch-linPG$_{13}$ (dotted line), the acetal-containing polymer Ch-P(GEGE$_{17}$-b-G$_{18}$) (black line), and the degraded product of Ch-P(GEGE$_{17}$-b-G$_{18}$) (red line). As expected, the SEC trace for the degraded product shifts to higher elution volume, i.e., lower molecular weights. Furthermore, signals in the lower molecular weight range are observed which can be attributed to "polyether-arms" (fragments) that were cleaved under acidic conditions. The SEC trace for the cleaved polymer does not overlap with the macroinitiator (dotted line). This can be explained by the fact that during the addition of GEGE two different hydroxyl groups are formed. One forms at the end of the acid-labile acetal moiety, and a second one is covalently attached to the macroinitiator. As the likelihood for the addition of the following monomers (GEGE or glycidol) is the same for both hydroxyl groups, only half of the growing arms will be degradable afterwards. Hence, the formation of small fragments and a higher molecular weight mode compared to the macroinitiator, is detected.

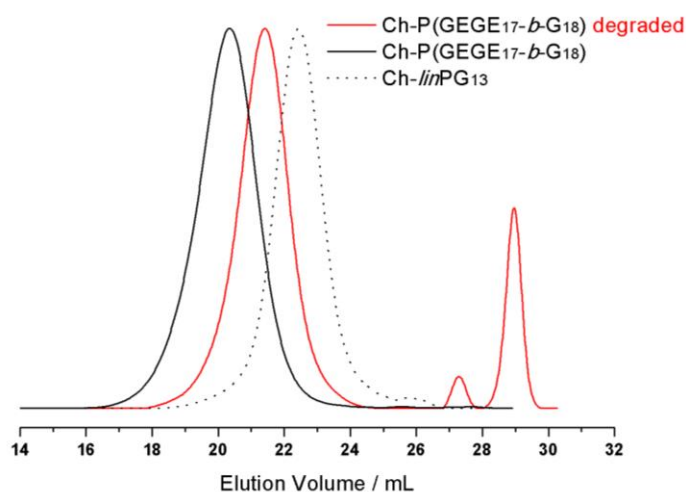*Figure 7*: SEC traces (RI detection; DMF; PEG standard) for the macroinitiator Ch-linPG$_{13}$ (dotted line), the acetal-containing polymer Ch-P(GEGE$_{17}$-b-G$_{18}$) (black line), and the degraded product of Ch-P(GEGE$_{17}$-b-G$_{18}$) (red line).

pH-cleavage of Ch-acetal-PEG-CH₂C≡CH and Shedding from the Liposome

As mentioned above, ideally, a polymer coating should be stable under physiological conditions (pH 7.4), but is cleaved at lower pH, thus enabling membrane-membrane fusion. As a proof-of-principle, we investigated alkyne-functionalized α-(1-(cholesteryloxy)ethoxy)-ω-hydro-PEG$_{46}$ (Ch-acetal-PEG$_{46}$-CH$_2$-C≡CH) in liposome formulations with respect to its shedding properties. To this end, a fluorescent dye (Atto 488 azide) was attached to the polymer after liposome preparation *via* click-chemistry and acetal cleavage was studied *via* fluorescent spectroscopy (schematic representation Figure 8). The crucial point is the protonation of the acetal groups that are located near the phospholipid membrane. As discussed below, it could be proven that acetal-cleavage takes place, although the PEG layer may impede proton diffusion.
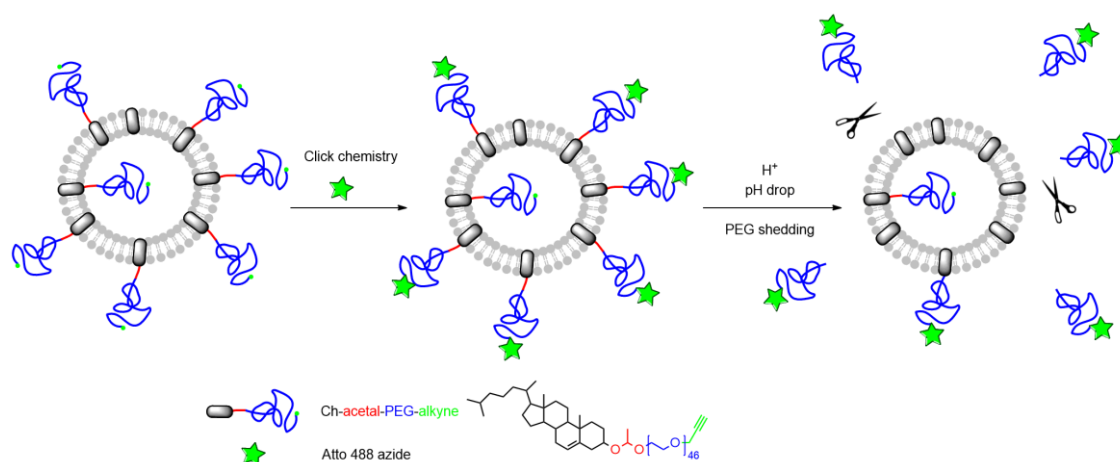
Figure 8: Schematic representation of the liposome functionalization and subsequent acidic cleavage of the PEG-coating.

Acetal-containing amphiphiles were incorporated into liposomes in a molar fraction of 5 mol%. Liposomes were prepared *via* dual centrifugation, resulting in z-average hydrodynamic radii (± standard deviation (SD) of 3 measurements) of 170 ± 2.8 nm ($\mu_2/\langle\Gamma\rangle^2 = 0.22$) and 154 ± 2.2 nm ($\mu_2/\langle\Gamma\rangle^2 = 0.10$) for amphiphiles with and without acetal groups, respectively. Low values for $\mu_2/\langle\Gamma\rangle^2$ indicated narrow size distributions as obtained from cumulant analysis of DLS data. After functionalization at the terminal alkyne group with Atto 488 azide, fluorescent liposomes enabled the observation of the acidic shedding. It turned out that after dilution in PBS and during ongoing equilibration the fluorescence emission decreased to a certain value. This observation is believed to

be due to changes in the microenvironment of the fluorophores, e.g., during the partial transition from vesicles to micelles. The cleavage process was then observed after acidification, leading to a strong increase of fluorescence emission intensity, as shown in Figure 9. This observation is believed to be due to changes in the microenvironment of the fluorophores, *e. g.* during the partial transition from vesicles to micelles. The cleavage process was then observed after acidification, leading to an increase of fluorescence emission intensity as shown in Figure 9.
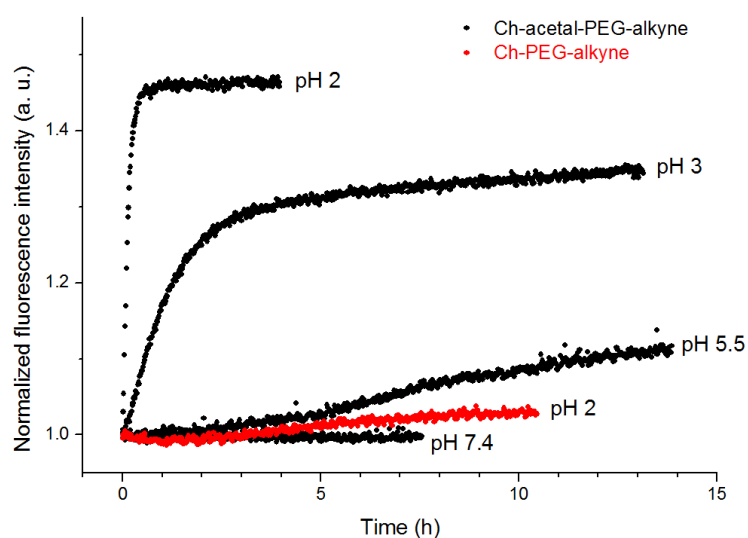
Figure 9: Fluorescence emission increases during acidic cleavage of acetal-containing amphiphiles (black). Amphiphiles without acetal groups (red) are stable at low pH.

As expected, a low pH value of 2 leads to a fast cleavage within several minutes and therefore high fluorescence emission, while the liposome system without cleavable amphiphiles shows no substantial increase (red data points). However, higher pH values provide degradation within hours (pH 3) or even days (pH 5.5). The increase in fluorescence intensity can be explained by both less thermal relaxation of fluorophores due to surface-related interactions and a potentially lower inner filter effect. While the complex microenvironment within liposomes leads to rather qualitative results, the kinetics of the cleavage are in good agreement with earlier measurements.[18] Although the cleavage at pH 5.5 is slow, it demonstrates a potential mechanism to shed the liposomal coating in lysosomal compartments. Therefore, the incorporation of acid-labile groups might enable both the elimination of polymeric moieties and the interaction between liposomal and cellular membranes.

Conclusion

In the present study we showed the incorporation of multiple cleavable groups by combining the epoxide inimer GEGE and glycidol in the oxyanionic ring-opening polymerization with cholesterol as the initiator. Random or block copolymers (Ch-P(GEGE$_x$-co-G$_y$) or (Ch-P(GEGE$_x$-b-G$_y$)) were synthesized with narrow molecular weight distributions and the degradation at pH 2 for a block copolymer was investigated by SEC. Furthermore, hyperbranched polyglycerol with a single acetal moiety was available using glycol-1-(cholesteryloxy)ethylether as the initiator for the polymerization of AGE, subsequent thiol-ene coupling of 2-mercaptoethanol and polymerization of glycidol. To the best of our knowledge, this represents the first synthesis of acetal-containing hyperbranched lipids for liposome preparations. The polymers obtained are promising with respect to the combination of the following properties: steric stabilization of liposomes, multifunctionality, acidic degradability, and biocompatibility. Degradability in liposome formulations was proven by using the linear analogue (1-(cholesteryloxy)ethoxy)-ω-hydro-PEG$_{46}$-CH$_2$C≡CH functionalized with a fluorescent label (Atto 488 azide) at pH between 7.4 and 2.0. A strong pH-dependence for the shedding process was observed. In the near future, liposome stability and shedding of the functionalized linear-hyperbranched lipids will be investigated. We believe that acid-labile lipids with a high number of functionalities and multiple cleavable groups mark a promising development step for polyether-based lipids for future biomedical applications.

Acknowledgments

References

(1)   Amselem, S.; Gabizon, A.; Barenholz, Y. *J. Pharm. Sci.* **1990,** *79* (12), 1045–1052.

(2)   Duncan, R.; Gaspar, R. *Mol. Pharmaceutics* **2011,** *8* (6), 2101–2141.

(3)   Woodle, M. C.; Lasic, D. D. *Biochim. Biophys. Acta* **1992,** *1113* (2), 171–199.

(4)   Sharma, A.; Sharma, U. S. *Int. J. Pharm.* **1997,** *154* (2), 123–140.

(5)   Woodle, M. C.; Matthay, K. K.; Newman, M. S.; Hidayat, J. E.; Collins, L. R.; Redemann, C.; Martin, F. J.; Papahadjopoulos, D. *Biochim. Biophys. Acta* **1992,** *1105* (2), 193–200.

(6)   Torchilin, V. P.; Omelyanenko, V. G.; Papisov, M. I.; Bogdanov, A. A.; Trubetskoy, V. S.; Herron, J. N.; Gentry, C. A. *Biochim. Biophys. Acta* **1994,** *1195* (1), 11–20.

(7)   Blume, G.; Cevc, G. *Biochim. Biophys. Acta* **1990,** *1029* (1), 91–97.

(8)   Immordino, M. L.; Dosio, F.; Cattel, L. *Int. J. Nanomed.* **2006,** *1* (3), 297–315.

(9)   Hong, R. L.; Huang, C. J.; Tseng, Y. L.; Pang, V. F.; Chen, S. T.; Liu, J. J.; Chang, F. H. *Clin. Cancer Res.* **1999,** *5* (11), 3645–3652.

(10)   Amoozgar, Z.; Yeo, Y. *WIREs Nanomed Nanobiotechnol* **2012,** *4* (2), 219–233.

(11)   Maeda, H.; Wu, J.; Sawa, T.; Matsumura, Y.; Hori, K. *J. Control. Release* **2000,** *65*, 271–284.

(12)   Mellman I., Fuchs R., and Helenius A. *Ann. Rev. Biochem.* **1986,** *55*, 663–700.

(13)   Andresen, T. L.; Jensen, S. S.; Jørgensen, K. *Prog. Lipid Res.* **2005,** *44* (1), 68–97.

(14)   Milito, A. de; Fais, S. *Future Oncol* **2005,** *1* (6), 779–786.

(15)   Asokan, A.; Cho, M. J. *J. Pharm. Sci.* **2002,** *91* (4), 903–913.

(16)   Yuba, E.; Kojima, C.; Harada, A.; Tana; Watarai, S.; Kono, K. *Biomaterials* **2010,** *31* (5), 943–951.

(17)   Remaut, K.; Lucas, B.; Braeckmans, K.; Demeester, J.; Smedt, S. C. de. *J. Control. Release* **2007,** *117* (2), 256–266.

(18)   Dingels, C.; Müller, S. S.; Steinbach, T.; Tonhauser, C.; Frey, H. *Biomacromolecules* **2013,** *14* (2), 448–459.

(19)   Gillies, E. R.; Goodwin, A. P.; Fréchet, Jean M. J. *Bioconjugate Chem.* **2004,** *15* (6), 1254–1263.

(20)   Shin, J.; Shum, P.; Thompson, D. H. *J. Control. Release* **2003,** *91*, 187–200.

(21)   Boomer, J. A.; Qualls, M. M.; Inerowicz, H. D.; Haynes, R. H.; Patri, V. S.; Kim, J.-M.; Thompson, D. H. *Bioconjugate Chem.* **2009,** *20* (1), 47–59.

(22)   Shin, J.; Shum, P.; Grey, J.; Fujiwara, S.-i.; Malhotra, G. S.; González-Bonet, A.; Hyun, S.-H.; Moase, E.; Allen, T. M.; Thompson, D. H. *Mol. Pharmaceutics* **2012,** *9* (11), 3266–3276.

(23)   Guo, X.; Szoka, F. C. *Bioconjugate Chem.* **2001,** *12* (2), 291–300.

(24)   Masson, C.; Garinot, M.; Mignet, N.; Wetzer, B.; Mailhe, P.; Scherman, D.; Bessodes, M. *J. Control. Release* **2004,** *99* (3), 423–434.

(25)   Xin Guo; J. Andrew MacKay; Francis C. Szoka Jr. *Biophys. J.* **2003**, 1784–1795.

(26)   Sawant, R. M.; Hurley, J. P.; Salmaso, S.; Kale, A.; Tolcheva, E.; Levchenko, T. S.; Torchilin, V. P. *Bioconjugate Chem.* **2006,** *17* (4), 943–949.

(27)   Kale, A. A.; Torchilin, V. P. *Bioconjugate Chem.* **2007,** *18* (2), 363–370.

(28)   Chen, D.; Jiang, X.; Huang, Y.; Zhang, C.; Ping, Q. *J. Bioact. Compat. Polym.* **2010,** *25* (5), 527–542.

(29)   Xu, H.; Deng, Y.; CHEN, D.; Hong, W.; Lu, Y.; Dong, X. *J. Control. Release* **2008,** *130* (3), 238–245.

(30) Clawson, C.; Ton, L.; Aryal, S.; Fu, V.; Esener, S.; Zhang, L. *Langmuir* **2011,** *27* (17), 10556–10561.

(31) Allen, T. M.; Moase, E. H. *Adv. Drug Deliv. Rev.* **1996,** *21* (2), 117–133.

(32) Hofmann, A. M.; Wurm, F.; Hühn, E.; Nawroth, T.; Langguth, P.; Frey, H. *Biomacromolecules* **2010,** *11* (3), 568–574.

(33) Hofmann, A. M.; Wurm, F.; Frey, H. *Macromolecules* **2011,** *44* (12), 4648–4657.

(34) Müller, S. S.; Dingels, C.; Hofmann, A. M.; Frey, H.Polyether-Based Lipids Synthesized with an Epoxide Construction Kit: Multivalent Architectures for Functional Liposomes. *Tailored Polymer Architectures for Pharmaceutical and Biomedical Applications*; ACS Symposium Series; American Chemical Society, 2013; pp 11–25.

(35) Wilms, D.; Stiriba, S.-E.; Frey, H. *Acc. Chem. Res.* **2010,** *43* (1), 129–141.

(36) Kainthan, R. K.; Janzen, J.; Levin, E.; Devine, D. V.; Brooks, D. E. *Biomacromolecules* **2006,** *7* (3), 703–709.

(37) Imran ul-haq, M.; Lai, B. F.; Chapanian, R.; Kizhakkedathu, J. N. *Biomaterials* **2012,** *33* (35), 9135–9147.

(38) Kainthan, R. K.; Hester, S. R.; Levin, E.; Devine, D. V.; Brooks, D. E. *Biomaterials* **2007,** *28* (31), 4581–4590.

(39) Siegers, C.; Biesalski, M.; Haag, R. *Chem. Eur. J.* **2004,** *10* (11), 2831–2838.

(40) Shenoi, R. A.; Lai, Benjamin F. L.; Kizhakkedathu, J. N. *Biomacromolecules* **2012,** *13* (10), 3018–3030.

(41) Shenoi, R. A.; Narayanannair, J. K.; Hamilton, J. L.; Lai, Benjamin F. L.; Horte, S.; Kainthan, R. K.; Varghese, J. P.; Rajeev, K. G.; Manoharan, M.; Kizhakkedathu, J. N. *J. Am. Chem. Soc.* **2012,** *134* (36), 14945–14957.

(42) Shenoi, R. A.; Lai, B. F.; Imran ul-haq, M.; Brooks, D. E.; Kizhakkedathu, J. N. *Biomaterials* **2013,** *34* (25), 6068–6081.

(43) Tonhauser, C.; Schüll, C.; Dingels, C.; Frey, H. *ACS Macro Lett.* **2013,** *1* (9), 1094–1097.

(44) Massing, U.; Cicko, S.; Ziroli, V. *J. Control. Release* **2008,** *125* (1), 16–24.

(45) Fritz, T.; Hirsch, M.; Richter, F. C.; Müller, S. S.; Hofmann, A. M.; Rusitzka, K. A. K.; Markl, J.; Massing, U.; Frey, H.; Helm, M. *Biomacromolecules* **2014**, *15*, 2440-2448.

(46) Fitton, A. O.; Hill, J.; Jane, D. E.; Millar, R. *Synthesis* **1987,** *12*, 1140–1142.

(47) Geissler, P.; Johnson, A. *J. Am. Oil Chem. Soc.* **1990,** *67*, 541–546.

(48) Johnson, A.; Geissler, P. *J. Am. Oil Chem. Soc.* **1990,** *67*, 123–131.

(49) Pollerberg, J. *Fette, Seifen, Anstrichm.* **1966,** *68*, 561–562.

(50) Santacesaria, E.; Di Serio, M.; Garaffa, R.; Addino, G. *Ind. Eng. Chem. Res.* **1992,** *31*, 2413–2418.

(51) Sunder, A.; Hanselmann, R.; Frey, H.; Mülhaupt, R. *Macromolecules* **1999,** *32* (13), 4240–4246.

(52) Greenland, B. W.; Liu, S.; Cavalli, G.; Alpay, E.; Steinke, J. H. *Polymer* **2010,** *51* (14), 2984–2992.

(53) Lee, B. F.; Kade, M. J.; Chute, J. A.; Gupta, N.; Campos, L. M.; Fredrickson, G. H.; Kramer, E. J.; Lynd, N. A.; Hawker, C. J. *Polym. Chem.* **2011,** *49* (20), 4498–4504.

(54) Alkan, A.; Natalello, A.; Wagner, M.; Frey, H.; Wurm, F. R. *Macromolecules* **2014,** *47* (7), 2242–2249.

2.3 Phosphonoethylated Polyglycerol Amphiphiles: Liposomal Formulations for Bone Targeting
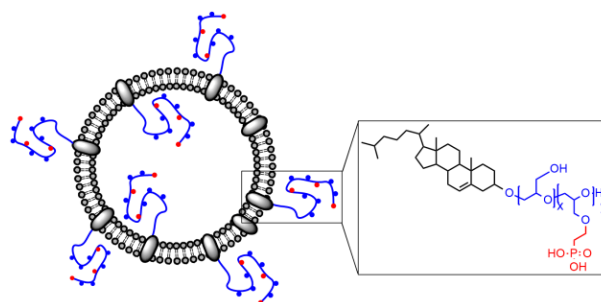
Sophie S. Müller,[1,2] Alissa Reddy,[1] Sandra Ritz,[3] Frederik R. Wurm,[3] and Holger Frey[1]

[1]Institute of Organic Chemistry, Johannes Gutenberg University Mainz,

Duesbergweg 10-14, 55128 Mainz, Germany

[2]Graduate School Materials Science in Mainz, Staudingerweg 9, 55128 Mainz, Germany

[3]Max Planck Institute for Polymer Research, Ackermannweg 10, 55128 Mainz, Germany

Abstract

Phosphonates exhibit strong interaction with inorganic calcium phosphate surfaces. Due to the strong interaction of phosphonates with bone surfaces, multifunctional lipid analogs with pendant phosphonate groups have been prepared We herein report on the straightforward synthesis of cholesterol-initiated linear polyglycerols which are functionalized with diethyl vinyl phosphonate (DEVP) via a Michael-type addition in molar ratios between 29-76 mol%. The phosphonoethylated polymers were successfully transformed to phosphonic acid-bearing lipids. The polymers were characterized by SEC, ^{1}H NMR, and ^{31}P NMR spectroscopy, permitting to monitor the different intermediate and final products of the synthetic protocol. This strategy allows for the preparation of liposomes containing different amounts of functional polymer (5 mol% and 15 mol%) as well as two different sizes (100 nm vs. 400 nm). The vesicles exhibit interaction with calcium phosphate surfaces, rendering them suitable for bone regeneration strategies, as confirmed by SEM and fluorescence microscopy. The novel liposomes with potential

"stealth" behavior are promising materials for systemic or local bone cancer treatment and may be loaded with suitable drugs.

Introduction

Drug delivery systems with targeting to bone tissue are important for the treatment of osteoporosis and osseous metastases. These diseases cause chronic pain and disability, and the number of people suffering is increasing dramatically. The most painful type of malignant diseases is bone cancer, which can also occur from spreading from other tumors to bone tissue via metastasis.[1,2] Surgical removal, radiation strategies, or chemotherapy are usually the treatments of first choice. Doxorubicin and paclitaxel are the main anti-tumor drugs applied. However, limitations in the design of bone-specific drug formulations are based on the low number of molecules with strong affinity to bone. Nowadays, bisphosphonates (BP) are promising candidates, since the two phosphonate groups, connected via a central carbon, exhibit high affinity to minerals.[3] Bisphosphonate-decorated liposomes employed for controlled release of anti-tumor drugs may be a useful tool to maintain appropriate drug levels to bone and help to reduce systemic side-effects of the drugs. In general, steric stabilization of liposomes *in vivo* can be increased by incorporating amphiphilic polymers, such as cholesterol- or phospholipid-based poly(ethylene glycol) (PEG). The hydrophobic part anchors the polymer in the phospholipid bilayer. Recently, various groups have explored the production of hydroxyapatite (HA)-specific phospholipids. Among these studies, Hengst *et al.* presented cholesteryl-trisoxyethylenebisphosphonic acid (CHOL-TOE-BP) as an amphiphile for targeted, sterically stabilized liposomes.[4] Alkyl-based amphiphiles bearing BP moieties also showed high affinity towards HA in a study by Anada *et al.*. Doxorubicin-loaded liposomes adsorbed at the HA-surface and significantly reduced the number of viable human osteosarcoma MG63 cells.[5] Lipids based on distearoylphosphoethanolamine-polyethylene glycol BP derivatives were investigated by Wang *et al.*.[6,7] Another approach was recently presented by Ikeuchi *et al.*, who used polyphosphoester ionomers with a cholesterol anchor group for liposome modification. The authors confirmed the enhanced affinity of vesicles to calcium by using

polyphosphoesters.[8] In general, phosphorus-containing polymers are attracting increasing interest due to their biodegradability, blood compatibility, strong affinity to bone tissue and for dental adhesion.[9,10,11,12]

As an example Penczek *et al.* synthesized ionic-nonionic block copolymers with the structure poly(ethylene glycol)-*block*-polyglycerol having both phosphonic and carboxylic acid functionalities.[13] Recently, Möller and coworkers presented the modification of linear polyglycerol (*lin*PG) with tunable amounts of phosphonate ester side groups. Employing basic conditions, the hydroxymethyl group was functionalized with diethyl vinyl phosphonate (DEVP) via a Michael-type addition. Hydrolysis with bromotrimethylsilane led to *lin*PG with phosphonic acid groups.[14,15,16] In a follow-up work, the authors reported on polyether-graft-polyester copolymers with pendant diethylphosphonatoethyl groups (DEPE).[17,18]

In the present article, we report on the straightforward synthesis of cholesterol-initiated linear polyglycerol with partial phosphonoethylation (29-76 mol% functionalization) using DEVP. Subsequent saponification of the diethylphosphonate groups with bromotrimethylsilane resulted in lipids bearing hydroxyl groups and phosphonate groups (Scheme 1). These lipid analogs were incorporated into liposomes, rendering them sterically stabilized and potentially with "stealth" properties due to the hydroxyl-functional polyether chain.[19,20,21] Subsequently, adsorption of the liposomes onto calcium phosphate cement via the phosphonic acid groups was investigated by SEM and fluorescence microscopy.
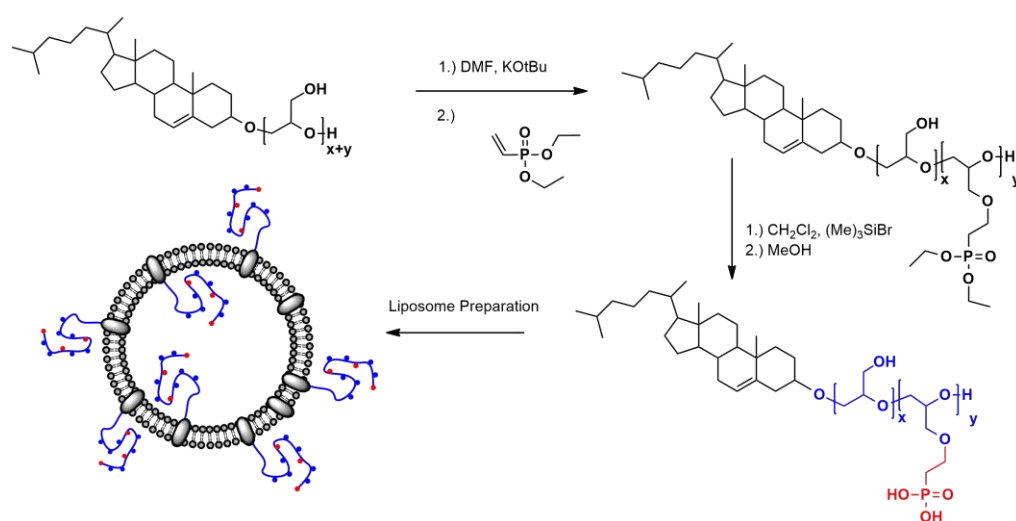
Scheme 1: Synthetic strategy for the synthesis of cholesterol-initiated linear polyglycerol with pendant phosphonate groups followed by liposome preparation.

Experimental

Methods

^{1}H NMR spectra and ^{31}P NMR spectra (300 MHz and 400 MHz) were recorded using a Bruker AC300 or a Bruker AMX400, employing CDCl$_3$ or MeOD as a solvent. All spectra were referenced internally to residual proton signals of the deuterated solvent. Size exclusion chromatography (SEC) measurements were carried out in dimethylformamide (DMF) with 0.25 g L^{-1} LiBr on PSS HEMA columns (300/100/40). For SEC measurements a UV (275 nm) and an RI detector were used. Calibration was carried out using poly(ethylene glycol) (PEG) standards provided by Polymer Standards Service (PSS).

Aqueous MALS measurement was separated over a set of HEMA-Bio columns (40/100/1000) with 10 µm particles with a length of 300 mm and an internal diameter of 8 mm (MZ-Analysentechnik) providing an effective molecular weight range of 2000 to 3 000 000 g mol^{-1} at a flow rate of 1.0 ml min^{-1} (Agilent 1260 HPLC) in 100 mM phosphate, 50 mM sodium chloride, pH 6.5. Each sample injection was 100 µL. Elution profiles for mass analysis were detected using a UV detector (254 nm, Agilent 1260), a Wyatt miniDAWN TREOS MALS detector, a Wyatt ViscoStar II on-line differential viscometer and a differential refractometer (Agilent 1260). Using the elution-profile data, the weight-averaged molecular mass was calculated with Astra 6.1.1 software (Wyatt Technologies) using a dn/dc of 0.135 for the PEG polymer (American Polymer Standards Corporation).

Differential scanning calorimetry (DSC) measurements were carried out using a Perkin-Elmer DSC 8500 in the temperature range of -100 to 50 °C, using heating and cooling rates of 20 °C min^{-1} (1st cycle) and 10 °C min^{-1} (2nd cycle), respectively. The values of the second heating cycle were used for analysis. The melting points of indium (T$_m$ = 156.6 °C) and Millipore water (T$_m$ = 0 °C) were used for calibration.

Reagents

All reagents and solvents were purchased from Acros and used as received, unless otherwise mentioned. Diethyl vinyl phosphonate (DEVP; > 97%), potassium *tert*-butoxide (1.0 M in THF), and bromotrimethylsilane (> 97%) were purchased from Sigma-

Aldrich and used as received. Cholesterol was purchased from Acros and stored at 8 °C. Lipid-EPC-3 (Hydrogenated egg phosphatidylcholine) was kindly provided by Lipoid. Phosphate buffered saline (PBS) was used from Gibco. Ethoxyethyl glycidyl ether (EEGE) was synthesized according to the literature.[22] The monomer was dried over CaH_2 and cryo-transferred prior to use. A micro-macro porous biphasic calcium phosphate cement (MBCP+), composed of 80% hydroxyapatite and 20% β-tricalcium phosphate, was donated from Biomatlante (Vigneux de Bretagne, France).

Synthesis

Synthesis of Ch-*lin*PG$_{21}$

Cholesterol (2.0 g, 5.2 mmol), CsOH monohydrate (0.781 g, 4.7 mmol, 90% of deprotonation), and benzene (6 mL) were placed in a Schlenk flask. The mixture was stirred at 60 °C for about 30 min to generate the cesium alkoxide. The salt was then dried under vacuum at 90 °C for 24 h. The salt was suspended in 50 mL anhydrous dioxane, the monomer EEGE was added (15.8 mL, 104 mmol, 20 eq.), and the mixture was heated to 80 °C for 24 h. A sample was removed for NMR and SEC analysis, the polymerization was stopped via addition of an excess of methanol, and the solvents were removed under reduced pressure. The acetal protecting groups of PEEGE were cleaved by the addition of methanol, an acidic ion-exchange resin (Dowex 50WX8), and 2 N HCl stirring at RT for 24 h. The solution was filtered, concentrated, and the crude product was precipitated twice in cold diethyl ether. The block copolymer was dried under vacuum. Yield: ~90%.

Before deprotection: ^{1}H NMR (300 MHz, CDCl$_3$): δ (ppm) = 5.30 (1H, C=CH cholesterol), 4.68 (1H, CHO, acetal group, PEEGE), 3.88-3.17 (polyether backbone; CHO cholesterol), 2.30-0.83 (CH$_2$, CH cholesterol), 0.65 (3H, CH$_3$ cholesterol).

After deprotection: ^{1}H NMR (300 MHz, MeOD-d_4): δ (ppm) = 5.37 (1H, C=CH cholesterol), 3.77-3.17 (polyether backbone, CHO cholesterol), 2.40-0.88 (CH$_2$, CH cholesterol), 0.72 (3H, CH$_3$ cholesterol).

Synthesis of linear cholesterol-poly(glycidol-diethylphosphonatoethyl-*co*-glycidol) lipid

Description for Ch-P(G^{DEPE}$_9$-*co*-G$_{12}$) as an example according to the literature: [16]

Ch-linPG$_{21}$ (0.521 g, 0.3 mmol) was dissolved in DMF (10 mL) in a Schlenk tube and potassium $tert$-butoxide (0.4 mL; 0.4 mmol, of a 1 M solution in THF) was slowly added within 2 h (until small amounts of coagulate formed). $Tert$-butanol was removed by applying reduced pressure. Diethyl vinyl phosphonate (DEVP) (0.45 mL, 2.95 mmol, 11 eq.) was added and the mixture was stirred for 6 d at room temperature under an argon atmosphere. The precipitate was removed by filtration and the product dried under vacuum. The polymer was redissolved in MeOH and precipitated in cold diethyl ether. Yield: 70-80%

^{1}H NMR (300 MHz, MeOD-d_4): δ (ppm) = 5.37 (1H, C=CH cholesterol), 4.18-4.04 (4H, POCH_2CH$_3$), 3.80-3.40 (polyether backbone; CHO cholesterol), 2.22-2.10 (2H, CH$_2$OCH$_2$CH_2P), 1.33 (6H, POCH$_2$CH_3), 2.40-0.86 (CH$_2$, CH cholesterol), 0.71 (3H, CH$_3$ cholesterol).

^{31}P NMR (MeOD-d_4): δ (ppm) = 30.1.

Synthesis of linear cholesterol-poly(glycidol-phosphonatoethyl-co-glycidol) lipid

Description for Ch-P(G$^{PE}_9$-co-G$_{12}$) as an example according to the literature: [16]

Ch-P(G$^{DEPE}_9$-co-G$_{12}$) (0.207 g, 0.06 mmol) was dissolved in anhydrous dichloromethane (6 mL) and cooled to 0 °C. Bromotrimethylsilane (0.288 mL, 2.18 mmol, 4 eq. of the silylating agent per diethylphosphonatoethyl group) was added slowly to the solution. The mixture was stirred for 24 h at room temperature. The solvent and other byproducts were removed under reduced pressure. MeOH (6 mL) was added and the solution was stirred for additional 24 h. The mixture was concentrated under reduced pressure and the crude polymer was precipitated in cold diethyl ether. Yield: 85-90%

^{1}H NMR (300 MHz, MeOD-d_4): δ (ppm) = 5.27 (1H, C=CH cholesterol), 3.85-3.35 (polyether backbone; CHO cholesterol), 2.10-1.90 (2H, CH$_2$OCH$_2$CH_2P), 2.30-0.77 (CH$_2$, CH cholesterol), 0.62 (3H, CH$_3$ cholesterol).

^{31}P NMR (MeOD-d_4): δ (ppm) = 25.8.

Liposome formation

Liposomes consisting of the amphiphile Ch-P(G$^{PE}_9$-co-G$_{12}$), cholesterol, and egg phosphatidylcholine (EPC) were prepared by the thin film hydration method on a clean bench. A solution of EPC in ethanol, cholesterol in ethanol and the copolymer were

blended at molar ratios of 55:40:5 mol% and 55:30:15 mol% in a small flask, respectively. The solvent was evaporated in a rotating evaporator to obtain a thin film of lipid components. The lipid film was rehydrated in 1 mL of PBS buffer solution to obtain a final lipid concentration of 21 mg mL^{-1}, sonicated for 20 min at 50 °C to yield multilamellar vesicles (MLVs), and extruded through a 400 nm polycarbonate membrane 11 times, followed by the extrusion through a 100 nm membrane for 11 times to obtain small unilamellar vesicles (SUVs). The liposomes with 15 mol% of Ch-P(G$^{PE}_9$-*co*-G$_{21}$) were only extruded through the 400 nm membrane 11 times, due to leaking of the extruding device.

Calcium phosphate attachment studies

The calcium phosphate particles (MBCP+, 80–200 mm, Biomatlante) were dispersed in ultrapure water (10 mg mL-^{1}, Millipore) and washed for 30 min under horizontal agitation (200 rpm) before use. Liposomes were diluted in buffer to application concentrations of 0.01% and 0.1% with deionized water in 1.5 mL Eppendorf centrifuge vials. The calcium phosphate granules were left in the liposome solution for 30 min immediately following deposition. After attachment the tube was washed with deionized water to remove the loose and weakly attached liposomes from the calcium-phosphate granules. The process of centrifuging, removing the liquid, replacing the liquid with fresh deionized water, and vortexing was repeated two additional times. After the three rinses were complete, the samples were centrifuged again and observed in the scanning electron microscope (SEM, Zeiss LEO Gemini 1530). Previous to the measurement a thin carbon coating layer was deposited using a vacuum coating system Balzer Union (BAE250).

Fluorescence measurements were carried out with BODIPY (boron-dipyrromethene, 4,4-difluoro-4-bora-3a,4a-diaza-s-indacene) as the dye and 200 ms exposure time.

Results and Discussion

In this report, we adapt a synthetic pathway presented by Köhler *et al.*[16] for hydroxyl groups at a polymer backbone to introduce pendant phosphonate groups into

cholesterol-based linear polyglycerol (Ch-*lin*PG). The amphiphilic polyether polyol was prepared by the oxyanionic ring-opening polymerization of ethoxyethyl glycidyl ether (EEGE) with cholesterol as the initiator and subsequent removal of the acetal protecting group under acidic conditions to release the multiple OH-groups. The polyalcohol Ch-*lin*PG$_{21}$ was obtained with $M_{n,SEC}$ = 1500 g mol^{-1} and a low molecular weight distribution (M_w/M_n = 1.25). Ch-*lin*PG$_{21}$ was reacted with potassium *tert*-butoxide and with diethyl vinyl phosphonate (DEVP) in a Michael-type addition (Scheme 1). The ratio of DEVP to hydroxyl groups was set to 0.29, 0.50, and 0.76, respectively. The *tert*-butanol formed during the reaction was removed under slightly reduced pressure, in order to shift the acid-base equilibrium towards deprotonation of the polyglycerol hydroxyl groups. The polymers cholesterol-poly(glycerol-diethylphosphonatoethyl-*co*-glycidol) (Ch-P(G$^{DEPE}_x$-*co*-G$_y$) were characterized by size exclusion chromatography (SEC) in DMF, ^{1}H NMR, and ^{31}P NMR spectroscopy. The molecular weights determined from SEC are typically underestimated compared to the theoretical molecular weights and those calculated from the ^{1}H NMR spectra (see Table 1). Molecular weight distributions between M_w/M_n=1.25-1.35 were obtained. This is attributed to the pronounced change in the hydrodynamic radius when hydroxyl groups and diethylphosphonate groups are introduced and compared to the SEC standards PEG. Figure 1 shows the monomodal distribution of the polyalcohol Ch-*lin*PG$_{21}$ and its functional derivative Ch-P(G$^{DEPE}_9$-*co*-G$_{12}$) as collected from SEC. There is a slight shift to higher elution volume translating to lower molecular weight, after the functionalization with DEVP indicating hydrogen bonding and a change in the hydrodynamic radius after phosphonoethylation.
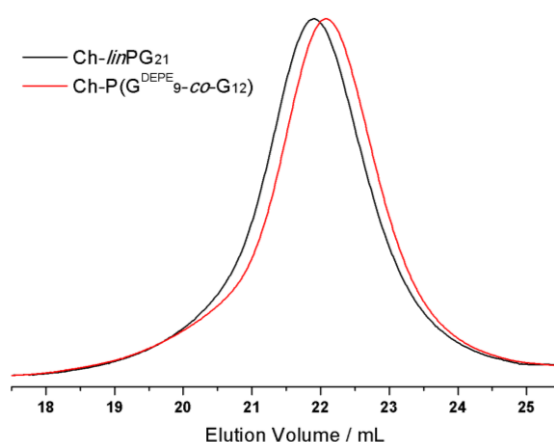

Figure 1: SEC elugrams (RI detection, DMF) of the polyol Ch-*lin*PG$_{21}$ (black) and its functional derivative Ch-P(G$^{DEPE}_9$-*co*-G$_{12}$) (red).

The ^{1}H NMR spectrum of Ch-P(G$^{DEPE}_9$-*co*-G$_{12}$) in Figure 2 shows, besides the typical resonances of Ch-*lin*PG, also a characteristic signal for the methylene group adjacent to phosphorus proving the successful phosphonoethylation. Figure 2 depicts the ^{1}H NMR spectra of Ch-*lin*PG$_{21}$, Ch-P(G$^{DEPE}_9$-*co*-G$_{12}$), and Ch-P(G$^{PE}_9$-*co*-G$_{12}$) in MeOD (bottom to top). For Ch-*lin*PG$_{21}$, between 0.70 ppm and 2.40 ppm only the resonances of cholesterol are detected. In the spectrum of Ch-P(G$^{DEPE}_9$-*co*-G$_{12}$) the methylene group adjacent to the phosphorus atom is detected as a multiplet between 2.10-1.90 ppm due to the coupling with the neighboring phosphorus (Figure 2, (a)). The resonances for the ethyl groups appear at 1.33 ppm (CH$_3$, triplet, (c)) and between 4.18-4.04 ppm for the methylene group (multiplet, (b)).

Saponification of the phosphonate groups to release the phosphonic acid groups was carried out with bromotrimethylsilane as the the silylating agent and methanol (methanolysis). The corresponding ^{1}H NMR spectrum of Ch-P(G$^{PE}_9$-*co*-G$_{12}$) is shown in Figure 2 (top). The efficient removal of the ethyl groups was proven by the absence of the typical diethyl phosphonate signals (1.33 ppm, 4.18-4.04 ppm). Furthermore, the resonance for the methylene group adjacent to phosphorus (Figure 2, (d), blue spectrum) is shifted to higher fields, due to a change in the chemical environment.

The degree of functionalization was determined by comparing the signal intensity of the cholesterol methyl group at 0.72 ppm with the methylene group next to the phosphorous in the spectrum of the Ch-P(G^{DEPE}-*co*-G) samples (resonance (a) Figure 2). The values for the series of samples were in good agreement with the feedstock of DEVP. All characterization data for the different polymers are summarized in Table 1. It has to be mentioned that in the spectra for the phosphonic acid-functionalized samples (Ch-P(G^{PE}-*co*-G)), integration of the signal of the methylene group next to the phosphorous yielded too high values for all samples in comparison to the signal at 0.72 ppm, which is presumably due to aggregation during the NMR measurement.
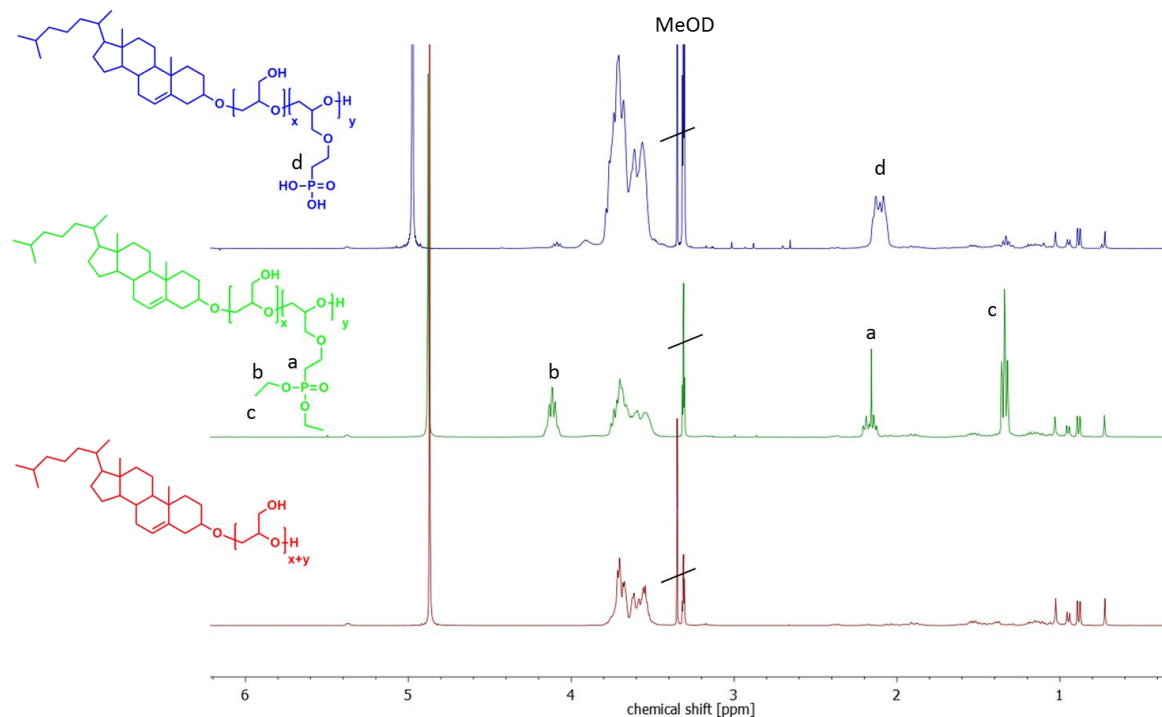
Figure 2: ^{1}H NMR spectra (400 MHz, CD$_3$OD) of Ch-*lin*PG$_{21}$ (red, bottom), Ch-P(G$^{DEPE}_9$-*co*-G$_{12}$) (green, middle), and Ch-P(G$^{PE}_9$-*co*-G$_{12}$) (blue, top).

Table 1: Characterization data of the different polymers: Ch-*lin*PG$_{21}$, Ch-P(G$^{DEPE}_x$-*co*-G$_y$), and Ch-P(G$^{PE}_x$-*co*-G$_y$).

Composition	M_n th g mol^{-1}	M_n ^{NMR} g mol^{-1}	M_n ^{SEC} g mol^{-1}	M_w/M_n SEC	*DEPE* mol% th / NMR	T_g °C
Ch-*lin*PG$_{21}$	1870	1940	1500	1.25	-	-50
Ch-P(G$^{DEPE}_6$-*co*-G$_{15}$)	2920	2920	1600	1.35	29/29	-36
Ch-P(G$^{DEPE}_9$-*co*-G$_{12}$)	3740	3410	1550	1.25	50/43	-40
Ch-P(G$^{DEPE}_{16}$-*co*-G$_5$)	4560	4560	1400	1.29	76/76	-43
Ch-P(G$^{PE}_6$-*co*-G$_{15}$)	2886	*n.a.*	*	*	-	*n.d.*
Ch-P(G$^{PE}_9$-*co*-G$_{12}$)	3706	*n.a.*	5100	1.30	-	-18
Ch-P(G$^{PE}_{16}$-*co*-G$_5$)	4526	*n.a.*	*	*	-	*n.d.*

n.a. not available, since the integration of the signal for OCH$_2$CH$_2$P was too high due to possible aggregation. *not soluble in DMF, no viable SEC trace was obtained. Ch-P(G$^{PE}_9$-*co*-G$_{12}$) was measured in aqueous solution. n.d. not determined.

Additionally, ^{31}P NMR spectroscopy was carried out to confirm the successful functionalization of the linear polyglycerol lipid with DEVP. It can clearly be seen that the sharp signal of DEVP at 18 ppm vanishes, and a broader signal at 30 ppm appears upon

functionalization resulting in Ch-P(G$^{DEPE}_9$-*co*-G$_{12}$). Saponification is evidenced by the spectrum of Ch-P(G$^{PE}_9$-*co*-G$_{12}$). Here, the signal for the DEPE group vanishes and a signal at 25.8 ppm appears which was assigned to the phosphonic acid groups. Figure 3 illustrates the ^{31}P NMR spectra for DEVP (red, bottom), Ch-P(G$^{DEPE}_9$-*co*-G$_{12}$) (green, middle), and Ch-P(G$^{PE}_9$-*co*-G$_{12}$) (blue, top).
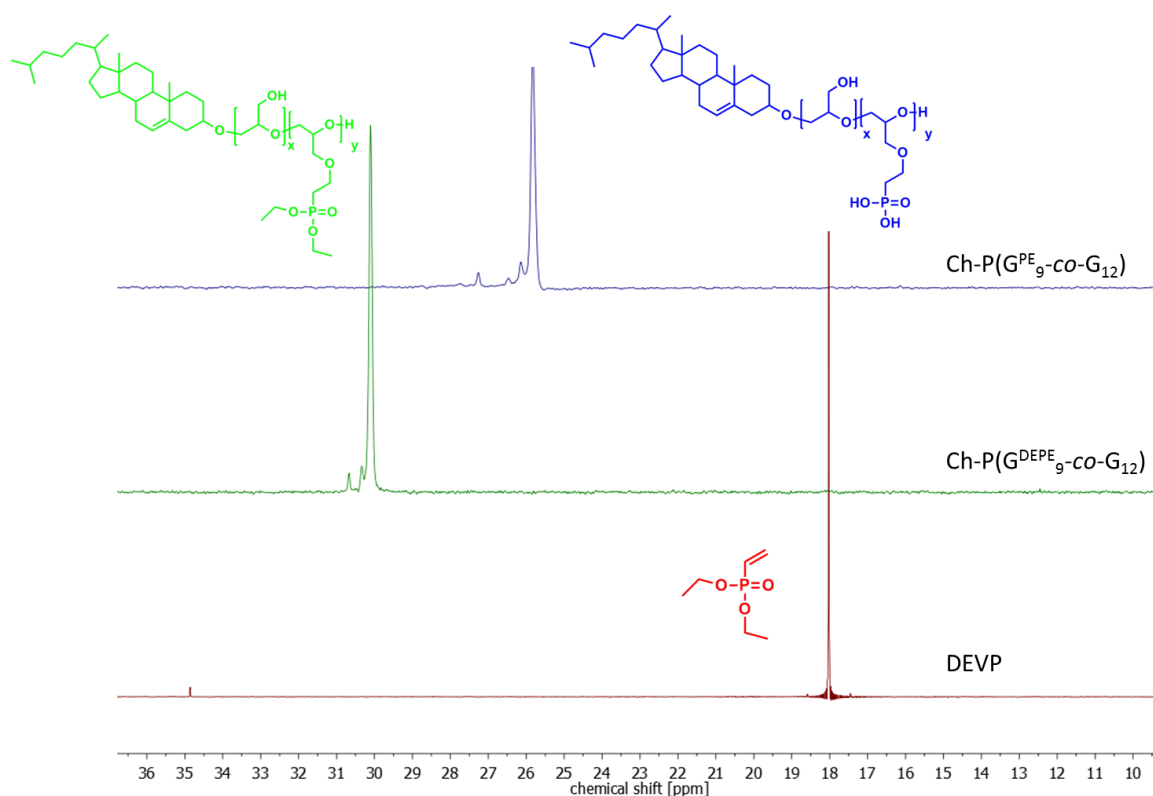
Figure 3: ^{31}P NMR spectra (400 MHz, CD$_3$OD) for DEVP (red, bottom), Ch-P(G$^{DEPE}_9$-*co*-G$_{12}$) (green, middle), and Ch-P(G$^{PE}_9$-*co*-G$_{12}$) (blue, top).

SEC measurements of Ch-P(G$^{PE}_x$-*co*-G$_y$) in DMF were not successful, since undefined SEC traces were obtained. Hence, Ch-P(G$^{PE}_9$-*co*-G$_{12}$) was measured in aqueous SEC. The result is depicted in Figure 4 with the blue trace representing the RI detector signal. The light scattering trace in red is in good agreement with the trace of the RI detector. Interestingly, the molecular weight was calculated to be 5100 g mol^{-1}, which is slightly higher than the theoretical value of 3700 g mol^{-1} (Table 1).
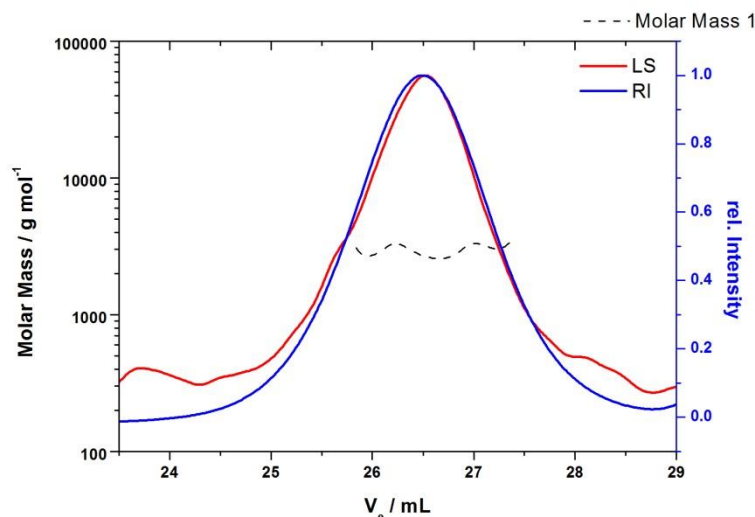
Figure 4: Aqueous MALS measurement for Ch-P(G^{PE}_9-*co*-G_{12}): RI signal in blue, light scattering in red, molar masses in black.

Thermal analysis

Thermal properties of the synthesized polymers were investigated via differential scanning calorimetry (DSC). The results are summarized in Table 1. All samples were amorphous, showing a glass transition (T_g). For the flexible Ch-*lin*PG$_{21}$ polyether a T_g of -50 °C was obtained. Upon phosphonoethylation the T_g increased to -43 °C for 16 DEPE groups, -40 °C for 9 DEPE groups, and -36 °C for 6 DEPE groups. The dependence on the degree of functionalization may be attributed to polymer substituents that interlace. A T_g of -18 °C was detected for the linear polyglycerol with phosphonic acid groups. This is expected, since strong hydrogen bonding between the residual hydroxyl groups and phosphonate groups occurs, which leads to an increase of T_g.

Synthesis and adsorption of functionalized liposomes on calcium phosphate cement studied by scanning electron microscopy (SEM) and fluorescence microscopy

The functionalized liposomes were synthesized by the thin film hydration method. Egg phosphatidyl choline (EPC-3), cholesterol, and Ch-P(G^{PE}_9-*co*-G_{12}) were blended in ratios of 55:40:5 mol% and 55:30:15 mol%. Liposomes with 5 mol% Ch-P(G^{PE}_9-*co*-G_{12}) were extruded through a 400 nm membrane and a 100 nm membrane. Liposomes with 15 mol% Ch-P(G^{PE}_9-*co*-G_{12}) were only extruded through a 400 nm membrane, which means that these vesicles are larger and contain more phosphonic acid anchor groups.

First of all, the attachment on calcium phosphate granules (MBCP+, 80–200 mm, Biomatlante) was investigated via scanning electron microscopy (SEM) for aqueous solutions containing either 0.01% liposomes or 0.1% liposomes. Figure 5 gives an overview of the obtained images. Figure 5a shows the negative control of the $CaPO_4$ granules without liposome solution treatment, whereas Figure 5b gives an overview of the granules. Figure 5c and 5d present the pictures after the incubation with a 0.01% and 0.1% solution of liposomes that were extruded through a 100 nm membrane (5 mol% Ch-P(G^{PE}_9-co-G_{12}), 0.01%/0.1%, 100 nm; smaller vesicles). For comparison, Figure 5e and 5f depict the results from larger liposomes containing more polymer (15 mol% Ch-P(G^{PE}_9-co-G_{12}), 0.01%/0.1%, 400 nm; larger vesicles). Since already the negative control exhibits small but few particles on the surface, which may be due to some remaining impurities, it is difficult to compare the pictures. For the granules treated with the smaller liposomes (100 nm, Figure 5c and d) there is no significant difference observable. Some small particles are found on the surface but they cannot solely be attributed to liposomes attached to the surface. For the larger particles (400 nm, Figure 5 e and f), the surface is not smooth anymore, but a liposome layer may be attached to the surface. This is possible, since the phospholipid membranes are flexible and can fuse and therefore may spread out as a sheet. In comparison, solid nanoparticles would be visible as spheres.[12]

Since the adsorption of functionalized liposomes onto the $CaPO_4$ surface could not clearly be proven by SEM, fluorescence microscopy was employed to visualize fluorescent liposomes. For this purpose a fluorescent marker (BODIPY) was incubated along with the liposomes. The $CaPO_4$ particles were treated with the liposome solution and were investigated via fluorescence microscopy. Figure 6a shows the negative control, in which the granules were incubated with the fluorescent dye, washed, and studied under the microscope. No intense fluorescence is visible, demonstrating that the dye does not adsorb onto the surface. Figure 6b depicts the small vesicles (5 mol% Ch-P(G^{PE}_9-co-G_{12}), 0.1% solution, 100 nm) on the surface and a stronger fluorescence is detectable. The fluorescence becomes more intense when studying larger liposomes (15 mol% Ch-P(G^{PE}_9-co-G_{12}), 0.01% solution, 400 nm Figure 6c and 15 mol% Ch-P(G^{PE}_9-co-G_{12}), 0.1% solution, 400 nm Figure 6d).
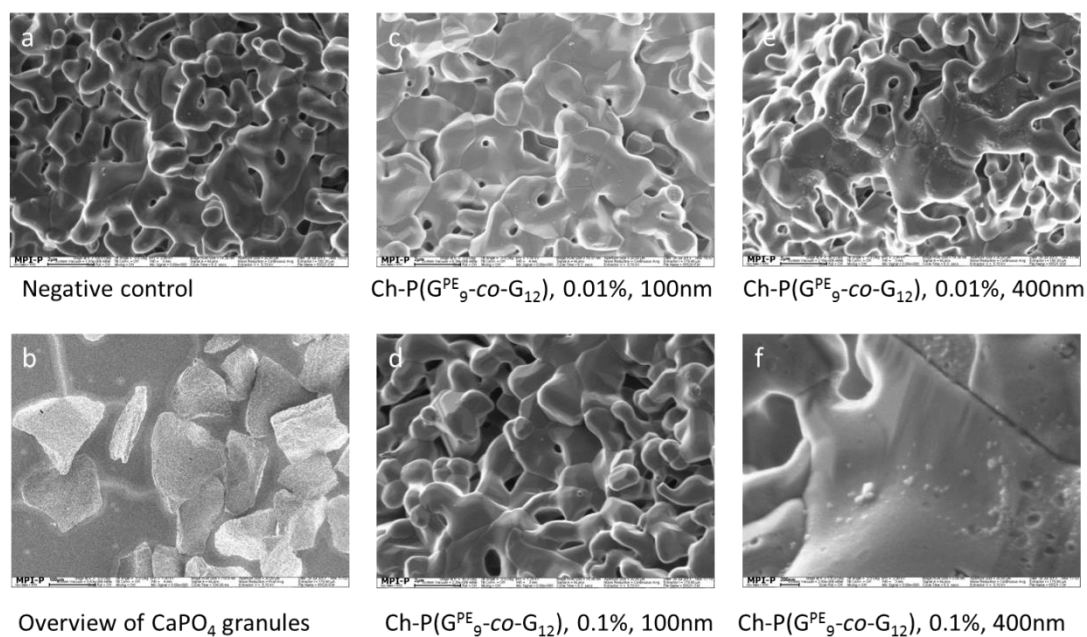
Figure 5: a) Negative control of the CaPO$_4$ granules' surface (scale bar 2 µm). b) overview of the CaPO$_4$ granules (scale bar 100 µm). c) 5 mol% Ch-P(G$^{PE}_9$-*co*-G$_{12}$), 0.01% solution, 100 nm (scale bar 2 µm). d) 5 mol% Ch-P(G$^{PE}_9$-*co*-G$_{12}$), 0.1% solution, 100 nm (scale bar 2 µm). e) 15 mol% Ch-P(G$^{PE}_9$-*co*-G$_{12}$), 0.01% solution, 400 nm (scale bar 2 µm). f) 15 mol% Ch-P(G$^{PE}_9$-*co*-G$_{12}$), 0.1% solution, 400 nm (scale bar 200 nm).

To sum up, the obtained results suggest adsorption of liposomes onto the CaPO$_4$ surface, but firm evidence cannot be given. Further investigations need to be conducted in order to prove the successful attachment and potential film formation.
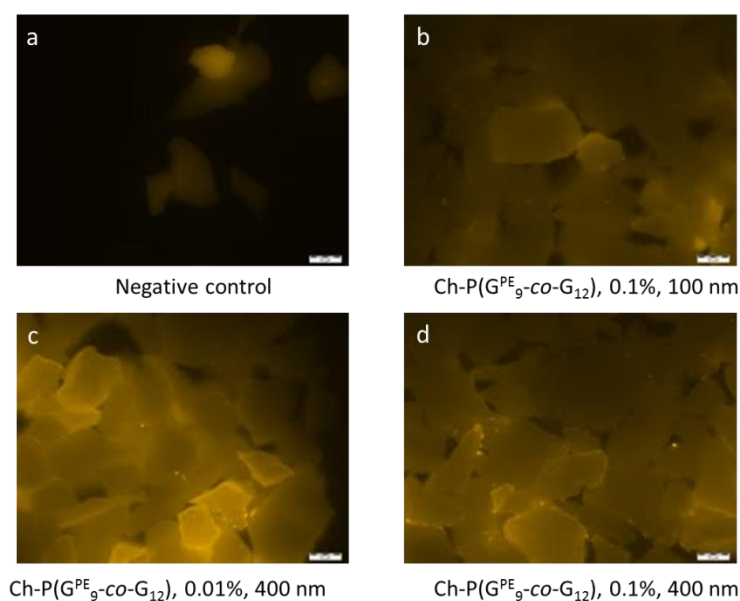
Figure 6: a) Negative control of the CaPO$_4$ granules' surface. b) 5 mol% Ch-P(G$^{PE}_9$-*co*-G$_{12}$), 0.01% solution, 100 nm. c) 15 mol% Ch-P(G$^{PE}_9$-*co*-G$_{12}$), 0.01% solution, 400 nm. d) 15 mol% Ch-P(G$^{PE}_9$-*co*-G$_{12}$), 0.1% solution, 400 nm. Scale bar 50 µm.

Conclusion

In this report we introduced novel polyether-based lipids bearing phosphonic acid groups for incorporation into liposomes. The amphiphiles were prepared by synthesizing linear polyglycerol using cholesterol as an initiator. Diethyl vinyl phosphonate was successfully conjugated via a Michael-type addition, followed by removal of the diethyl groups. The prepared liposomes exhibit potential inherent bone adhesion properties, which were investigated on $CaPO_4$ granules. However, adsorption could not be unequivocally proven. Since phospholipid membranes are flexible, adsorption as a layer is feasible, which makes detection difficult. Fluorescence microscopy supported these assumptions due to fluorescence being intense for larger liposomes (around 400 nm) with 15 mol% of Ch-P(G^{PE}_9-*co*-G_{12}). Therefore, the liposomes developed might be applied for drug encapsulation, e.g., for the drug paclitaxel, and in local treatment for bone cancer. Further studies are in progress to understand membrane fluidity and adsorption. The liposome size and potential "stealth" behavior will be investigated by dynamic light scattering (DLS in serum) and isothermal titration calorimetry (ITC) measurements. Furthermore, the usage of the Ch-P(G^{PE}_9-*co*-G_{12}) lipids as surfactants for the miniemulsion/solvent evaporation technique will be explored to obtain nanoparticles with a solid core, which would enhance detection in SEM.

Acknowledgements

References

(1)   Clines, G. A.; Guise, T. A. *Expert Rev Mol Med* **2008,** *10*, 1–16.

(2)   Buijs, J. T.; van der Pluijm, Gabri. *Cancer Letters* **2009,** *273* (2), 177–193.

(3)   Dominguez, L. J.; Bella, G.; Belvedere, M.; Barbagallo, M. *Biogerontology* **2011,** *12* (5), 397–408.

(4)   Hengst, V.; Oussoren, C.; Kissel, T.; Storm, G. *Int. J. Pharm.* **2007,** *331* (2), 224–227.

(5)   Anada, T.; Takeda, Y.; Honda, Y.; Sakurai, K.; Suzuki, O. *Bioorganic & Medicinal Chemistry Letters* **2009,** *19* (15), 4148–4150.

(6)   Wang, G.; Babadağli, M. E.; Uludağ, H. *Mol. Pharm.* **2011,** *8* (4), 1025–1034.

(7)   Wang, G.; Mostafa, N. Z.; Incani, V.; Kucharski, C.; Uludağ, H. *J. Biomed. Mater. Res.* **2012,** *100A* (3), 684–693.

(8)   Ikeuchi, R.; Iwasaki, Y. *Journal of Biomedical Materials Research Part A*, *101A* (2), 318–325.

(9)   Richards, M.; Dahiyat, B. I.; Arm, D. M.; Brown, P. R.; Leong, K. W. *J. Biomed. Mater. Res.* **1991,** *25* (9), 1151–1167.

(10)   Monge, S.; Canniccioni, B.; Graillot, A.; Robin, J.-J. *Biomacromolecules* **2011,** *12* (6), 1973–1982.

(11)   Marsico, F.; Wagner, M.; Landfester, K.; Wurm, F. R. *Macromolecules* **2012,** *45* (21), 8511–8518.

(12)   Alexandrino, E. M.; Ritz, S.; Marsico, F.; Baier, G.; Mailänder, V.; Landfester, K.; Wurm, F. R. *J. Mater. Chem. B* **2014,** *2* (10), 1298.

(13)   Penczek, S.; Pretula, J.; Kaluzynski, K. *J. Polym. Sci. A Polym. Chem.* **2004,** *42* (3), 432–443.

(14)   McKenna, C. E.; Higa, M. T.; Cheung, N. H.; McKenna, M.-C. *Tetrahedron Lett.* **1977,** *18* (2), 155–158.

(15)   Hu, N.; Johnson, L. M.; Pothayee, N.; Pothayee, N.; Lin, Y.; Davis, R. M.; Riffle, J. S. *Polymer* **2013,** *54* (13), 3188–3197.

(16)   Köhler, J.; Keul, H.; Möller, M. *Chem. Commun.* **2011,** *47* (28), 8148–8150.

(17)   Köhler, J.; Marquardt, F.; Keul, H.; Möller, M. *Macromolecules* **2013,** *46* (10), 3708–3718.

(18)   Köhler, J.; Marquardt, F.; Teske, M.; Keul, H.; Sternberg, K.; Möller, M. *Biomacromolecules* **2013,** *14* (11), 3985–3996.

(19)   Senior, J.; Delgado, C.; Fisher, D.; Tilcock, C.; Gregoriadis, G. *Biochimica et Biophysica Acta* **1991,** *1062* (1), 77–82.

(20)   Lasic, D. D.; Needham, D. *Chem. Rev.* **1995,** *95*, 2601–2628.

(21)   Amoozgar, Z.; Yeo, Y. *WIREs Nanomed Nanobiotechnol* **2012,** *4* (2), 219–233.

(22)   Fitton, A. O.; Hill, J.; Jane, D. E.; Millar, R. *Synthesis* **1987,** *12*, 1140–1142.

3 Interaction with Phospholipid Membranes

3.1 Unusual Triskelion Patterns and Dye-Labeled GUVs: Consequences of the Interaction of Cholesterol Containing Linear-Hyperbranched Block Copolymers with Phospholipids

Peggy Scholtysek[a], Sophie S. Müller[b,c], Regina Schöps[a], Holger Frey[b], Alfred Blume[a]*, and Jörg Kressler[a]*

[a] Institute of Chemistry, Martin Luther University Halle-Wittenberg, von-Danckelmann-Platz 4, D-06120 Halle (Saale), Germany

[b] Institute of Organic Chemistry, Johannes Gutenberg University Mainz, Duesbergweg 10-14, D-55128 Mainz, Germany

[c] Graduate School Materials Science in Mainz, Staudingerweg 9, D-55128 Mainz, Germany
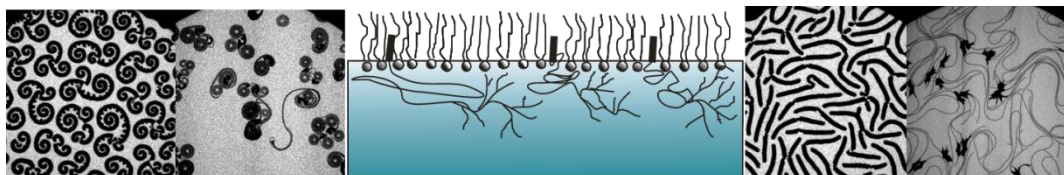
Abstract

Cholesterol (Ch) linked to a linear-hyperbranched block copolymer composed of poly(ethylene glycol) (PEG) and poly(glycerol) (hbPG) was investigated for its membrane anchoring properties. Two polyether-based linear-hyperbranched block copolymers with and without covalently attached rhodamine fluorescence label (Rho) were employed (Ch-PEG$_{30}$-b-hbPG$_{23}$ and Ch-PEG$_{30}$-b-hbPG$_{17}$-Rho). Compression isotherms of co-spread 1,2-dipalmitoyl-sn-glycero-3-phosphocholine (DPPC) or 1-palmitoyl-2-oleoyl-sn-glycero-3-phosphocholine (POPC) with the respective polymers were measured on the Langmuir trough, and the morphology development of the liquid-condensed (LC) domains was studied by epi-fluorescence microscopy. LC domains were strongly deformed due to the

localization of the polymers at the domain interface, thus indicating the line activity of both block copolymers. Simultaneously, it was observed that the presence of the fluorescence label significantly influences the domain morphology, the rhodamine labelled polymer showing higher line activity. Adsorption isotherms of the polymers to the water surface or to DPPC and 1,2-dioleoyl-sn-glycero-3-phosphocholine (DOPC) monolayers were collected, respectively. Again the rhodamine labelled polymer showed higher surface activity and a higher affinity for insertion into lipid monolayers. Calorimetric bulk investigations confirmed the results found with tensiometry. Confocal laser scanning microscopy (CLSM) of giant unilamellar vesicles (GUVs) also confirmed the polymers' fast adsorption to and insertion into phospholipid membranes.

Introduction

Biological membranes contain a complex mixture of different lipids, in the case of eukaryotic membranes mainly phospholipids, but also other components, such as proteins and cholesterol are present. Phospholipids consist of a hydrophilic headgroup, which is zwitterionic in the case of the phosphatidylcholines and a hydrophobic tail with two fatty acyl chains. Phospholipids self-organize into vesicular bilayer systems in aqueous suspensions mimicking simplified cell membranes. In these liposomes the fatty acid chains form a liquid crystalline lamellar phase in the hydrophobic membrane region, which is protected by the hydrophilic head groups from the outer and inner water phase of the vesicle. Phosphatidylcholines are of wide-spread occurrence in biological membranes and are commonly used as membrane models.[1-4]

Cholesterol, with 4 to 50 mol-%, is one of the most abundant molecules in biological membranes. It is a weakly amphiphilic molecule consisting of a hydrophobic sterol skeletal structure with a short branched alkyl chain and a hydrophilic hydroxyl group at the ring system. It appears in high amounts in eukaryotic cells and lipid rafts,[1,5] in human erythrocyte plasma membranes as well as in almost all mammalian membranes.[6] Mixed lipid/cholesterol membranes have therefore been the subject of intense scientific research. Cholesterol incorporation into lipid bilayers enhances the membrane rigidity and stability.[7,8] Besides its behavior in bilayer membranes[6,9,10] also lipid/cholesterol

monolayer systems have been studied in detail.[8,11-13] At the air/water interface phospholipid monolayers undergo changes from a gaseous to a liquid expanded (LE) phase at large molecular areas. In the case of long chain saturated lipids a phase transition into a liquid condensed (LC) state occurs upon further compression before the monolayer collapses at high surface pressure. In addition, the LE/LC transition has much in common with the gel to liquid-crystalline phase transition in bilayer systems. Earlier calorimetric studies of the cholesterol effect on the first order phase transitions of phospholipids have shown that with increasing concentration the temperature of the main LE/LC transition is gradually decreased and no phase transition is observed above a concentration of 50 mol% cholesterol, where in many cases cholesterol separates out of the membrane.[1,14,15] Cholesterol exhibits a so-called "condensing effect" on liquid-crystalline bilayers,[1,7,10] which can be understood as induction of an intermediate state of the lipid acyl chains between the ordered and the liquid crystalline. In this intermediate state the acyl chains are in an all-trans conformation but the molecules can rotate freely around their long axis. In lipid monolayers at the air/water interface this condensing effect on the liquid-expanded phase can be directly observed by a reduction of the mean molecular area.[1,12]

In this study, we employ cholesterol as an anchor for inserting a linear-hyperbranched block copolymer into lipid monolayers and bilayers. Cholesterol is linked via its hydroxyl group to a linear poly(ethylene glycol) (PEG) block and a hyperbranched poly(glycerol) (hbPG) block. Both polymer segments are hydrophilic in nature. The interaction of two block copolymers Ch-PEG$_{30}$-b-hbPG$_{23}$ and Ch-PEG$_{30}$-b-hbPG$_{17}$-Rho, where Rho stands for covalently attached rhodamine fluorescence label (see Scheme 1), with saturated and unsaturated phospholipids at the air/water interface and in lipid bilayers is investigated. 1,2-Dipalmitoyl-sn-glycero-3-phosphocholine (L-DPPC), 2,3-dipalmitoyl-sn-glycero-1-phosphocholine (D-DPPC), 1-palmitoyl-2-oleoyl-sn-glycero-3-phosphocholine (POPC), 1,2-dilauroyl-sn-glycero-3-phosphocholine (DLPC) and 1,2-dioleoyl-sn-glycero-3-phosphocholine (DOPC) are used as model lipids. The experiments are based on previous studies employing this type of linear-hyperbranched block copolymers.[16-18] Here, monolayer experiments are combined with epi-fluorescence microscopy and interactions of the fluorescent labelled block copolymer with phospholipid bilayers are

studied on giant unilamellar vesicles (GUVs) by confocal laser scanning microscopy (CLSM).
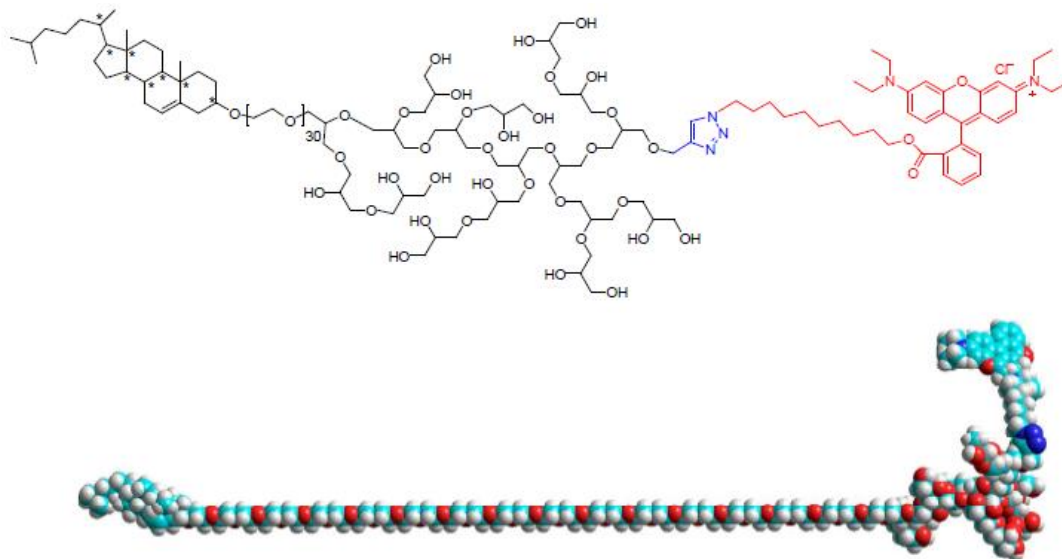
Scheme 1. Chemical structure of the rhodamine labelled Ch-PEG$_{30}$-*b-hb*PG$_{17}$-Rho and its CPK model with the PEG chain in an extended form

Experimental Section

Materials

All reagents and solvents for syntheses were purchased from Acros Organics (Geel, Belgium) and used as received, unless otherwise mentioned. Dry solvents were stored over molecular sieves. DMSO-d_6 was purchased from Deutero GmbH (Kastellaun, Germany). Ethoxyethylglycidyl ether (EEGE) was synthesized as described before[19] and dried over CaH$_2$ prior to use. Glycidol was purified by distillation from CaH$_2$ directly prior to use.

1,2-Dipalmitoyl-*sn*-glycero-3-phosphocholine (L-DPPC) and 2,3-dipalmitoyl-*sn*-glycero-1-phosphocholine (D-DPPC) were purchased from Sigma Aldrich (Schnelldorf, Germany) with purity > 99 %. 1-Palmitoyl-2-oleoyl-*sn*-glycero-3-phosphocholine (POPC), 1,2-dilauroyl-*sn*-glycero-3-phosphocholine (DLPC), 1,2-dioleoyl-*sn*-glycero-3-phosphocholine (DOPC) and 1-palmitoyl-2-oleoyl-*sn*-glycero-3-phosphoglycerol (POPG) were purchased from Genzyme Pharmaceuticals (Liestal, Switzerland) with purity > 99 %. The headgroup labelled fluorescence dye 1,2-dihexadecanoyl-*sn*-glycero-3-phosphoethanolamine-*N*-(lissaminerhodamine B sulfonyl) (Rhodamine-DHPE), the fatty acid labelled fluorescence

lipid 1-acyl-2-{12-[(7-nitro-2-1,3-benzoxadiazol-4-yl)amino]dodecanoyl}-sn-glycero-3-phosphocholine (NBD C_{12}-HPC) as well as the carbocyanine dye DiO were purchased from Invitrogen (Karlsruhe, Germany). 1,2-Distearoyl-sn-glycero-3-phosphoethanolamine-N-[biotinyl(polyethylene glycol)-2000] ammonium salt (DSPE-PEG-Biotin) with purity > 99 % was purchased from Avanti Polar Lipids (Alabama, USA). Streptavidin, bovine serum albumin (BSA) and biotinylated BSA were purchased from Sigma Aldrich (Schnelldorf, Germany) and used for glass coating in confocal microscopy experiments. Physico-chemical analyses and sample preparation were performed with ultrapure water from Millipore Quality (conductivity < 0.055 µS/cm, total organic carbon (TOC) < 5 ppm). Organic solvents for sample preparation were of HPLC-grade purity.

Synthesis of Ch-PEG$_{30}$-*b*-*hb*PG$_{23}$ and Ch-PEG$_{30}$-*b*-*hb*PG$_{17}$-Rho. The protocol was slightly modified from previous literature[20, 21] and therefore the detailed procedure is given here. Cholesterol (1.38 g, 3.6 mmol), CsOH monohydrate (0.539 g, 3.2 mmol; resulting in a degree of deprotonation of cholesterol of 90 %), and benzene were placed in a Schlenk flask. The mixture was stirred for about 30 min to generate the deprotonated species. The formed salt was dried under vacuum at 90 °C for 24 h, anhydrous tetrahydrofuran (THF) was added via cryo transfer, and ethylene oxide (5 mL, 100 mmol) was cryo transferred first to a graduated ampule and then to the Schlenk flask containing the initiator solution. The mixture was allowed to warm up to room temperature, heated to 60 °C, and the polymerization was performed for 12 h at 60 °C in vacuum. Subsequently, a sample was removed for NMR and SEC analyses, ethoxyethylglycidyl ether (EEGE) (3.8 mL, 25 mmol) was added via a syringe, and the reaction mixture was held at 60 °C for an additional 12 h. After removal of another sample for characterization, the polymerization was stopped via an excess of methanol and acetal protecting groups of the PEEGE block were removed by addition of water and acidic ion-exchange resin, stirring for 12 h at 40 °C. The solution was filtered, concentrated, and the crude product was precipitated in cold diethyl ether. The block copolymer was dried in vacuum. Yield~ 90%. Size exclusion chromatography (SEC): M_n= 1100 g mol^{-1}, PDI = 1.16.

For hypergrafting of the *hb*PG-block, the macroinitiator was placed in a Schlenk flask suspended in benzene, CsOH monohydrate was added to achieve 25 % of deprotonation of the total amount of hydroxyl groups and after 30 min the mixture was dried under

vacuum. The macroinitiator was dissolved in diethylene glycol dimethyl ether (diglyme) (25 wt%), heated to 90 °C and a 25 wt% solution of glycidol in diglyme was added slowly with a syringe pump over a period of 18 h. Termination was carried out via an excess of methanol and an acidic ion exchange resin. The crude product was filtrated, precipitated in cold diethyl ether and the Ch-PEG-*b*-*hb*PG block copolymer was dried in vacuum. Yield ~ 80%. SEC: M_n= 1170 g mol^{-1}, PDI= 1.27, NMR: M_n= 3430 g mol^{-1}.The rhodamine-B-11-azido-undecanyl ester was attached to the alkyne-functionalized polymer by click reaction (Reaction scheme see Supporting Information, Scheme S1; NMR for alkyne-functionalized polymer see Figure S2). The procedures were carried out as described elsewhere.[21, 25]

Polymer Characterization. ^{1}H NMR spectra were recorded using a Bruker AC 300 spectrometer operated at 300 MHz, employing DMSO-d_6 as solvent. SEC measurements were carried out in dimethylformamide (DMF) with 0.25 g L^{-1} LiBr. For SEC measurements a UV (275 nm) and an RI detector were used. Calibration was carried out using poly(ethylene glycol) standards provided by Polymer Standards Service (PSS).

Langmuir compression isotherms. The monolayer isotherms of mixed and pure DPPC and both polymers were determined using a Langmuir film balance (Riegler& Kirstein GmbH, Berlin, Germany; total area of 536 cm^2) with a compression ratio of 11.5. Pure and mixed samples were prepared from organic stock solutions to a total concentration of 1 mM in a solvent mixture of 9:1 (v:v) chloroform:methanol. The solvent was allowed to evaporate after spreading for at least 10 min. Continuous compression of the monolayers was performed with a constant compression rate of 2 Å^2 molecule^{-1} min^{-1} until the collapse of the respective monolayers was reached. To the isotherm of pure lipid and mixed lipid/polymer samples only one compression run was needed to cover the complete area range for all phases. For pure polymers the compression isotherms had to be combined from two measurements, respectively, due to their high area requirements. Measurements were performed at 20 °C.

Epi-fluorescence microscopy. The experimental setup for epi-fluorescence microscopy consists of an upright epi-fluorescence microscope Axio Scope A1 Vario (Carl Zeiss MicroImaging, Jena, Germany) with an HXP 120 C lamp and a Langmuir film balance (Riegler& Kirstein GmbH, Berlin, Germany; area of 264 cm^2). The film balance is mounted on an x-y-stage (Märzhäuser, Wetzlar, Germany; x-y-z-motion control by

Mac5000, Ludl Electronic Products, Hawthorne, USA). Pure lipid samples were prepared at a concentration of 1 mM in chloroform, mixed samples of lipid and polymer in different molar ratios 100:1 to 5:1 and pure polymer solutions were prepared to a total concentration of 1 mM each in a 9:1 (v:v) solvent mixture of chloroform:methanol. After spreading the samples, the solvent was allowed to evaporate for at least 10 min. Measurements were performed at 20 °C. As fluorescence dye the head group labelled lipid rhodamine-DHPE ($\lambda_{ex/em}$ = 557/571 nm) was added in an amount of only 0.01 mol%. The electron multiplier effect of the 3 CCD camera (ImageEM C9100-13, Hamamatsu, Herrsching, Germany) allows the use of these very low fluorescence label concentrations. The isotherms of the lipid-polymer mixtures are thus not influenced by the added fluorescence label. The Zeiss filter set 20 (green light) was used for fluorescence excitation of rhodamine-DHPE alone. Filter set 58 HE was used for co-localisation experiments with the rhodamin-labelled polymer Ch-PEG$_{30}$-*b*-*hb*PG$_{17}$-Rho co-spread with DPPC. The used objective was a long distance LD EC Epiplan-NEOFLUAR with 50 x magnification to observe the lipid domain formation at the air/water interface. Fluorescence images were taken during constant compression of the monolayers with a compression speed of 2 Å^2 molecule^{-1} min^{-1}. The images were collected with the Zeiss AxioVision software (Carl Zeiss MicroImaging, Jena, Germany).

Adsorption measurements at the air/water interface. Adsorption studies of the polymers were performed with a home-built circular film balance with fixed surface area of 28.3 cm^2 at a temperature of 20 °C. The subphase volume was 8.48 mL. Stirring for a homogeneous distribution of the specimen in the subphase was accomplished by a small stainless steel ball moving slowly in the field of a magnetic stirrer positioned underneath the trough. For surface activity tests aqueous solutions of the polymers with concentrations lower than the critical aggregation concentration (cac) were injected underneath the water surface to reach defined polymer concentrations from 500 nM up to 9 μM. For adsorption studies of the polymers to lipid monolayers, the lipid was first spread to different initial lateral surface pressures. Injections of the polymer solutions were then carried out 30 min after formation of the phospholipid monolayers. Measurements of the surface pressure were performed after the injection up to 20 h.

Differential scanning calorimetry (DSC). Calorimetric investigations were performed with a VP-DSC microcalorimeter (MicroCal Inc., Northhampton, USA). Pure or mixed

aqueous samples were prepared following the thin film preparation method[22] from higher concentrated stock solutions in organic solvents. After adding water to the lipid films to reach a total concentration of 2 mM the samples were vortexed a few times at about 67 °C and afterwards cooled to room temperature and filled into the sample cell of the DSC instrument. The reference cell was filled with ultrapure degassed water. Consecutive scans in a temperature range of 5-60 °C were performed to test for reproducibility. The water-water baseline wase subtracted from sample thermograms before analysis using the software ORIGIN (MicroCal Inc., Northhampton, USA). The thermograms presented in the figures are from the fourth upscan.

Confocal laser scanning microscopy (CLSM). GUVs were prepared from a thin dried film of 10 nmol phospholipid in 570 μL deionized water at 60 °C and 10 Hz frequency of an alternating electrical field (3 V) in a modified variant of electroformation,[23] using a chamber, built up of two ITO coated glass slides with a silicon ring seal in between, connected to a frequency generator. The phosphocholines (DLPC, POPC, DOPC) were mixed each with 2 mol% POPG to avoid GUV aggregation, 0.3 mol% DSPE-PEG-Biotin for GUV immobilization at a streptavidin coated glass surface and 0.1 mol% DiO ($\lambda_{ex./em.}$ = 487/501 nm) as fluorescent membrane dye.

A chamber of nearly 230 μL volume, formed by fixing a silicon ring (10 mm diameter, 3 mm high) onto a coverglass, passivated with BSA/biotinylated BSA in a molar ratio 10:1 and subsequently coated by streptavidin[24] was used for microscopic observation of the polymer adsorption. A 57 μL aliquot of freshly prepared GUV suspension (~1 nmol PC) was added to pure water in the chamber and GUVs were immobilized through the biotin containing phospholipid moiety onto the streptavidin coated cover glass surface. The actual amount of PC in the sample was controlled by comparing the overall intensity of the membrane dye emission against a prepared phospholipid/DiO standard. Appropriate volumes of a 10 μM aqueous polymer solution were added stepwise on top to obtain molar polymer/PC ratios of 1/100 to 50/100. For long-lasting observations the chamber was sealed by a second coverslip on top to avoid evaporation. All experiments were carried out at room temperature. A Leica TCS SP2 DM IRE2 confocal microscope was used with a HCX PL APO 63x 1.4 oil immersion objective (Leica Microsystems, Wetzlar, Germany) for two channel imaging. GUV membranes with DiO as membrane dye were visualized by excitation at 488 nm, detecting emission at 500-520 nm. The rhodamine

labelled polymer was excited at 543 nm by detection at 610-630 nm to avoid cross-talk. For quantitative analysis of the adsorption intensity the emission in the equatorial slice of the GUV membrane was used. Single scans were analyzed with Leica Quantify Software using the regions of interest (ROI), as described elsewhere[25] and illustrated in the supporting information (Figure S3). Data shown are in agreement with the observation of a single GUV over time or with addition of increasing polymer ratios. Each experiment was repeated several times to guarantee reproducibility.

Results and Discussion

Tensiometry and Epi-Fluorescence Microscopy. Because monolayers can be interpreted as half of a membrane[26] and represent an arrangement, which can be easily controlled in experiments, the properties of monolayers of phospholipid and cholesterol have been thoroughly investigated in the past. As we wanted to know how the newly synthesized polymers interact with lipid bilayers and monolayers, we determined first the monolayer isotherms of these polymers. The monolayer isotherms of Ch-PEG$_{30}$-*b*-*hb*PG$_{23}$ and Ch-PEG$_{30}$-*b*-*hb*PG$_{17}$-Rho were determined on the Langmuir trough in combination with epi-fluorescence microscopy to check for possible film heterogeneity (see Figure 1). As the polymers have much larger molecular areas due to their large headgroups (hydrophilic blocks) compared to lipids the isotherms had to be "stitched" together from two separate compression experiments. The two pieces of the isotherms are plotted separately into one diagram in order to demonstrate the reproducibility. Both polymer monolayers can be compressed to high lateral surface pressures of 38.3 mN m^{-1} for Ch-PEG$_{30}$-*b*-*hb*PG$_{23}$ and 33.1 mN m^{-1} for Ch-PEG$_{30}$-*b*-*hb*PG$_{17}$-Rho, respectively, before film collapse. The relatively high stability of the monolayer is due to the hydrophobic cholesterol unit anchoring the very hydrophilic polymers at the air/water interface. In both compression isotherms a weak pseudo plateau at a surface pressure of around 7.4 mN m^{-1} is observed which could indicate a squeeze-out of the hydrophilic PEG into the water subphase.[27,28] Further compression results in a transition at ~31 mN m^{-1} for Ch-PEG$_{30}$-*b*-*hb*PG$_{23}$ and 22-25 mN m^{-1} for Ch-PEG$_{30}$-*b*-*hb*PG$_{17}$-Rho. The kink found in the compression isotherm of the rhodamine labelled copolymer monolayer is reproducibly

found at lower surface pressure when Ch-PEG$_{30}$-*b-hb*PG$_{17}$-Rho is spread to smaller initial areas per polymer molecule. The transition reflected by the kink found for both polymers is not related to the pronounced transition from the gaseous state to the crystalline state found for pure cholesterol, because this occurs at much lower area per molecule (see insert of Figure 1).[16,29] Instead it is caused by a structural rearrangement of the hydrophilic headgroup consisting of the PEG spacer and the hyper-branched poly(glycerol) block. This rearrangement is well known from phospholipids with attached PEG chains. In DPPE-PEG2000 similar transitions are seen at surface pressures of 8 and 28 mN m^{-1}. The current interpretation of these transitions is the following. At high molecular area the PEG chain is located at the air-water interface and adopts the form of a pancake. Upon compression, a first transition into the so-called mushroom conformation occurs, where the PEG-chain is displaced from the air-water surface and extends into the subphase in mushroom-like conformation. At high pressure and lower molecular area the PEG-chain extends even more into the subphase forming the so-called brush conformation. The pressure and area at which these transitions occur depend on the number of EG units in the chain.[30-33] For the polymers with the cholesterol anchor a similar behavior is obviously present, however, modified by the presence of the hydrophilic poly(glycerol) group. As can be seen from the CPK model (see Scheme 1) of Ch-PEG$_{30}$-*b-hb*PG$_{23}$ the PEG chain is dominant in the area requirement at lower surface pressure while at higher pressure and areas below 100 Å^2 molecule^{-1}, when the PEG chain becomes more extended, the poly(glycerol) block will be the determining factor for the area at the air-water surface.
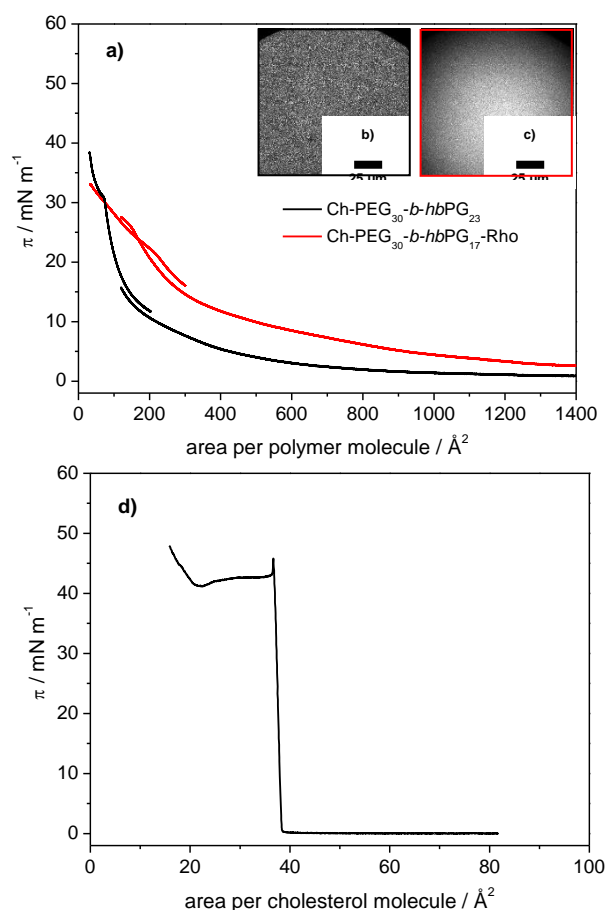
Figure 1. a) Compression isotherms of pure polymer monolayers; inset b) epi-fluorescence microscopy image of Ch-PEG$_{30}$-*b-hb*PG$_{23}$, 32.3 mN m^{-1}; inset c) epi-fluorescence microscopy image of Ch-PEG$_{30}$-*b-hb*PG$_{17}$-Rho, 32.2 mN m^{-1}; d) compression isotherm of pure cholesterol.

In order to investigate the influence of Ch-PEG$_{30}$-*b-hb*PG$_{23}$ and Ch-PEG$_{30}$-*b-hb*PG$_{17}$-Rho on the monolayer isotherms of different phosphatidylcholines, samples with molar mixing ratios from 100:1 to 5:1 phospholipid:polymer were co-spread to form mixed monolayers at the air/water interface and then compressed on the Langmuir trough (see Figure 2). The influence of both polymers on the observed isotherms is similar when mixed with L-DPPC or POPC. The lift-off of the mixed monolayer isotherms changes from a sharp rise at definite areas per lipid molecule, e.g. 85 Å^2 molecule^{-1} for L-DPPC, to a broader range for the increase of the surface pressure when mixed monolayer are compressed. As expected, the lift-off shifts to higher areas per lipid molecule the higher the amount of polymer in the mixture, for instance, to more than 400 Å^2 molecule^{-1} for the mixture of L-DPPC:Ch-PEG$_{30}$-*b-hb*PG$_{17}$-Rho = 5:1 (see Figure 2c). The plateau region

of the phase transition of L-DPPC is shifted to higher lateral pressures, e.g. from 5.2 mN m^{-1} for pure L-DPPC up to 10.8 mN m^{-1} for the mixture of L-DPPC:Ch-PEG$_{30}$-*b*-*hb*PG$_{17}$-Rho = 5:1 (see Figure 2c), due to the growing polymer influence which indicates a destabilization of the LC phase. At higher polymer content, the pancake-mushroom transition of the polymer coincides with the LE-LC transition of DPPC. This is particularly evident when mixtures with DPPC are compared with those containing POPC, in which the LE-LC transition is absent (see Figure 2a,b for Ch-PEG$_{30}$-*b*-*hb*PG$_{23}$ and Figure 2c,d for Ch-PEG$_{30}$-*b*-*hb*PG$_{17}$-Rho). Upon further compression the mushroom to brush transition of the polymer remains visible, particularly for the mixtures with Ch-PEG$_{30}$-*b*-*hb*PG$_{17}$-Rho it is quite pronounced and occurs of pressures around 30-32 mN m^{-1}. The molecular area shown in Figure 2 is calculated based on the phospholipid content. The shifts in molecular area are therefore mainly due to the presence of the polymer. At a surface pressure of 40 mN m^{-1} the molecular area of a 5:1 mixture of DPPC with Ch-PEG$_{30}$-*b*-*hb*PG$_{23}$ (16.6 mol%) is 59 Å^2 molecule^{-1} of DPPC. The molecular area of pure cholesterol at this pressure is 38 Å^2 compared to pure DPPC with a molecular area of 48 Å^2. The observed difference of 11 Å^2 molecule^{-1} of DPPC is thus larger than the calculated difference (7.6 Å^2 molecule^{-1} of DPPC) with the assumption that only the cholesterol anchor contributes to the molecular area. The conclusion is that at this pressure the polymer is still stably inserted into the monolayer as the available space for the polymer headgroup (5 x 48 Å^2 (DPPC) + 38 Å^2 (cholesterol) ≈ 278 Å^2 is still large enough for its accommodation below the lipid headgroups in the subphase. As can be seen from Figure 1, the mushroom-brush transition for Ch-PEG$_{30}$-*b*-*hb*PG$_{23}$ occurs below a molecular area of 100 Å^2 per polymer. The polymer headgroup in the mixture with DPPC can therefore adopt the mushroom conformation even at a surface pressure of 10 mN m^{-1}. Similar results are obtained for mixtures with Ch-PEG$_{30}$-*b*-*hb*PG$_{17}$-Rho, though in this case the mushroom-brush transition occurs at higher molecular area. This is then also evident in the isotherms of the mixtures where this occurs at a molecular area of ~100 Å^2 per lipid for the 5:1 mixture (see Figure 2c).

POPC is only in the LE state at room temperature. Therefore, the pseudo-plateau for the LE-LC transition is missing in the isotherms (Figure 1b,d) and only the transitions of the polymer remain visible, particularly the pancake to mushroom transition at lower

surface pressure. The mushroom to brush transition is somewhat obscured due to the lower stability of the monolayers containing POPC.

The collapse pressures of the mixed monolayers are hardly affected by the addition of the polymer and are in the range between 48 and 55 mN m^{-1} for mixtures with DPPC and between 42 and 44 mN m^{-1} for mixtures with POPC, which show again lower stability.

To obtain further information on morphological behavior of the co-spread PC/polymer monolayers in the LE-LC transition region, epi-fluorescence microscopy images for the mixtures of L-/D- and rac-DPPC with both polymers in the different mixing ratios were recorded at different surface pressures during constant compression of the film at low speed. The images shown in Figures 3 and 4 were obtained for the mixtures L- or rac-DPPC:Ch-PEG$_{30}$-b-hbPG$_{23/17}$(-Rho) = 10:1.
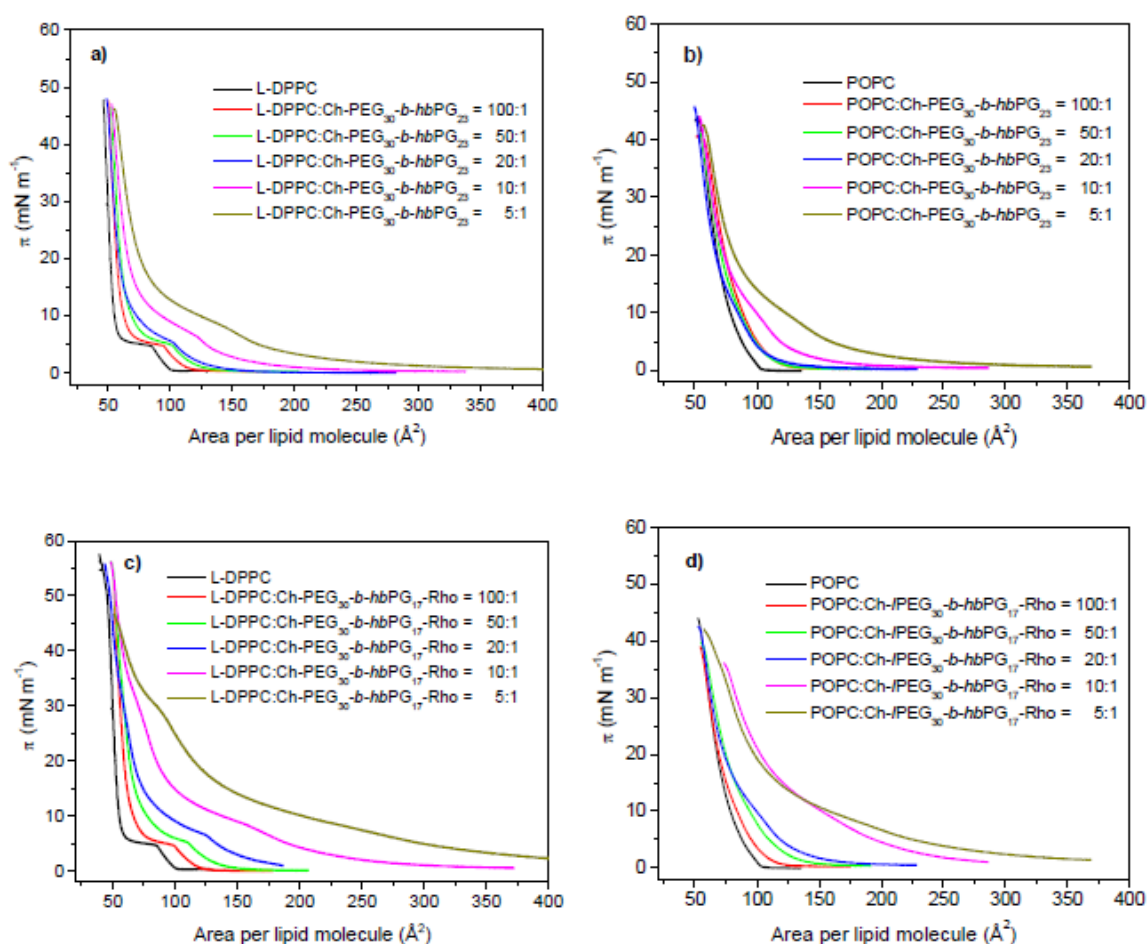
Figure 2. Compression isotherms of co-spread mixtures of the phospholipids L-DPPC and POPC in the mixture with the polymers Ch-PEG$_{30}$-b-hbPG$_{23}$ and Ch-PEG$_{30}$-b-hbPG$_{17}$-Rho in molar ratios of 100:1 to 5:1 phospholipid:polymer.
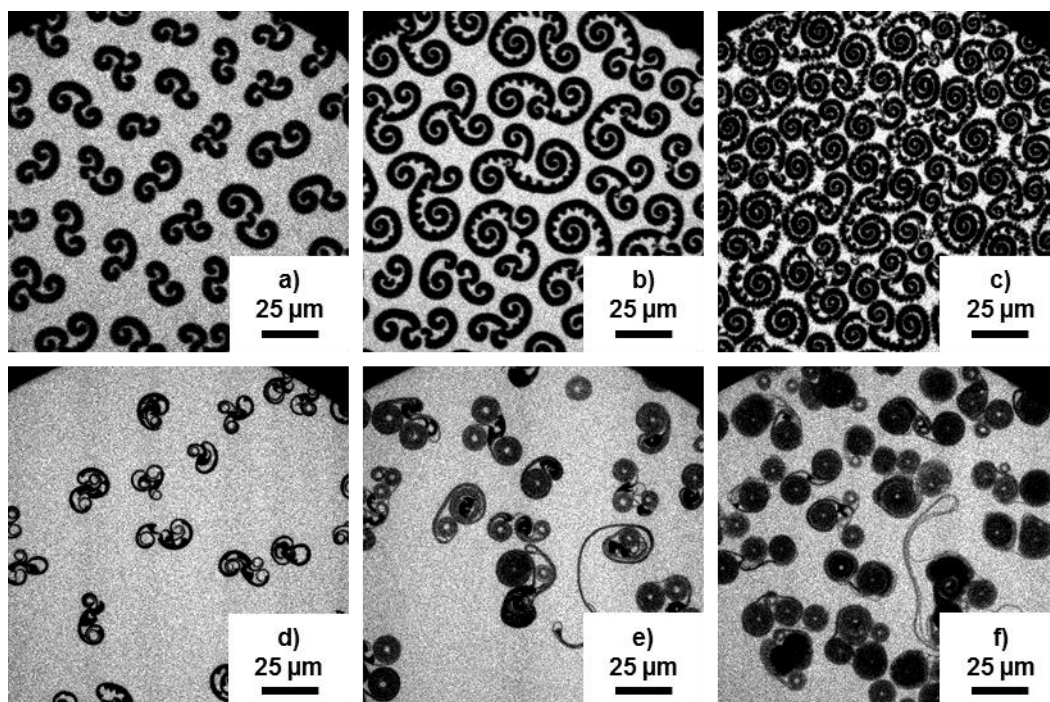
Figure 3. Epi-fluorescence microscopy of monolayer of a)-c) L-DPPC:Ch-PEG$_{30}$-*b-hb*PG$_{23}$ = 10:1 and d)-f) L-DPPC:Ch-PEG$_{30}$-*b-hb*PG$_{17}$-Rho = 10:1 at surface pressures of a) 9.8 mN m^{-1}; b) 14.0 mN m^{-1}; c) 23.9 mN m^{-1}; d) 10.3 mN m^{-1}; e) 11.8 mN m^{-1}; f) 14.2 mN m^{-1}.

The observed domain shapes are quite different for both polymers in the mixture with L- and rac-DPPC, respectively. For monolayers of mixtures of L-DPPC:Ch-PEG$_{30}$-*b-hb*PG$_{23}$ = 10:1, thinned domains which still exhibit the typical triskelion domain shape for pure L-DPPC can be found (Figure 3a). Domain thinning results from the insertion of the cholesterol anchor of the amphiphilic block copolymer into the monolayer and its concentration at the phase boundary of the LC lipid domains. The domain boundary of the LC-L-DPPC domain has a lower line tension than without polymer. This lower line tension allows that repulsive forces dominate leading to an elongation of the former compact triskelion domains.[34-36] Domain thinning has also been observed for mixtures of DPPC with pure cholesterol at a concentration of only 2 mol% cholesterol [37] Differences in domain shapes observed here from the domain shapes of L-DPPC with co-spread pure cholesterol obviously result from the influence of the hydrophilic hyperbranched poly(glycerol) and the linear poly(ethylene glycol) blocks. As can be seen in Figure 3b regular protuberances develop in the inside of the LC triskelions shaped domains which can be related to the macromolecular crowding at the interface.

Upon further compression of the L-DPPC:Ch-PEG$_{30}$-*b*-*hb*PG$_{23}$ monolayer growth of the LC domains occurs and the protuberances seem to be reduced (see Figure 3c). Protuberances only occur on the inside of the domain arms. Here, the line tension is lower than on the strongly curved outside. Zwitterionic lipids repel each other within the LC domains and in places where repulsion dominates the line tension, the excrescences develop. Totally different domain shapes result from the addition of the rhodamine labelled polymer Ch-PEG$_{30}$-*b*-*hb*PG$_{17}$-Rho to L-DPPC (see Figure 3d-f). A tremendous lowering of the line tension is observed, indicated by the formation of very narrow domain stripes. The domains appear as stripes which are frequently curled. The stripes do not coalesce upon further compression of the monolayer, hence the driving force for reducing the domain length between LE and LC domains is very low. From a chemical point of view, the only differences between the two polymers Ch-PEG$_{30}$-*b*-*hb*PG$_{23}$ and Ch-PEG$_{30}$-*b*-*hb*PG$_{17}$-Rho are the number of six glycerol units in the hyperbranched region and the additional covalently linked rhodamine label. These structural differences are both located within the hydrophilic region of the polymer, which is only located at the air-water interface at large molecular areas in the so-called pancake regime. At surface pressures between 10-14 mN m^{-1} the polymer is already in the mushroom conformation and should be extended into the subphase. As we observed these striking differences in the monolayer behavior of these two polymers we can conclude that for Ch-PEG$_{30}$-*b*-*hb*PG$_{17}$-Rho specific interactions between the hydrophilic headgroup of the polymer and the head groups of the phosphatidylcholine must exist. Most likely additional hydrogen-bonding and hydrophobic interactions are occurring. The fluorescent label is connected to the poly(glycerol) block via a hydrophobic spacer. The rhodamine moiety is composed of conjugated aromatic rings but also carries a positive charge. Therefore, this moiety is by itself amphipathic and may well be able to also insert into the interfacial region of the lipid headgroups. The observed larger molecular areas in mixtures of PCs with Ch-PEG$_{30}$-*b*-*hb*PG$_{17}$-Rho are support for this proposition as are the observed domain shapes indicating a much lower line tension between the domains caused by the additional interaction of the attached rhodamine dye with the lipid monolayer. For D-DPPC mixtures with the block copolymers very similar domain shapes are observed with the exception that the curling direction is opposite (images not shown).
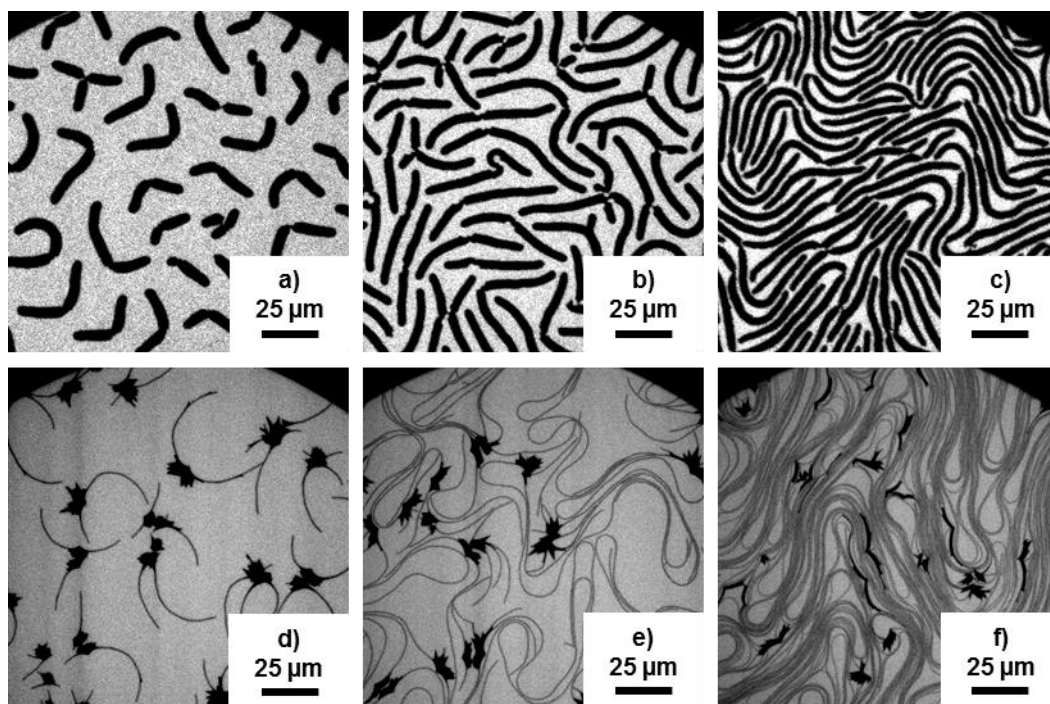
Figure 4. Epi-fluorescence microscopy of monolayers of a)-c) rac-DPPC:Ch-PEG$_{30}$-*b*-*hb*PG$_{23}$ = 10:1 and d)-f) rac-DPPC:Ch-PEG$_{30}$-*b*-*hb*PG$_{17}$-Rho = 10:1 at surface pressures of a) 9.4 mN m^{-1}; b) 11.8 mN m^{-1}; c) 17.7 mN m^{-1}; d) 10.3 mN m^{-1}; e) 10.8 mN m^{-1}; f) 12.9 mN m^{-1}.

The polymers with eight stereogenic centers within the cholesterol unit were investigated for their ability to influence the DPPC domain chirality at the air/water interface. Therefore, the polymers were mixed and co-spread with a racemic mixture of L- and D-DPPC. Epi-fluorescence images of the mixed monolayers in the LE-LC coexistence region are shown in Figure 4. Neither in mixtures of both polymers with L- or D-DPPC nor with racemic DPPC we observed a change in domain chirality. The preferred curling direction of L- and D-DPPC triskelions due to their own stereogenic center in the hydrophilic headgroup and the 30 ° tilt of the fatty acid chains[38] is unaltered by the incorporation of the cholesterol containing polymers. For racemic DPPC condensed domains without a preferred curling were observed. At higher lateral compression the LC domains appeared as bundles of parallel oriented stripes.

In monolayers of racemic DPPC the LC domains found for the mixture rac-DPPC:Ch-PEG$_{30}$-*b*-*hb*PG$_2$= 10:1 are again much thinner and thus affected by the cholesterol unit of the polymer and additionally by the hydrophilic blocks of poly(ethylene glycol) and hyperbranched poly(glycerol) (see Figure 4a-c). The observed domain thinning effects

again result from a lower line tension compared to the original phase boundary between the two co-existing DPPC phases.[34-37] As already observed before, the rhodamine labelled polymer Ch-PEG$_{30}$-*b*-*hb*PG$_{17}$-Rho has a totally different effect on the domain shapes compared to the polymer Ch-PEG$_{30}$-*b*-*hb*PG$_{23}$. The very thin striped domains start to grow from a star-like domain and run almost parallel over large distances. The stripe-like domains are very stable and do not coalesce upon compression of the film. This shows again that the rhodamine-labelled polymer is much more line active due to its fluorescent label with the hydrophobic moiety.

Time- and Concentration-Dependent Adsorption Measurements at the Air/Water Interface. In order to test the polymers for their surface activity concentration-dependent adsorption measurements of the polymers to the pure water surface were performed. After injection of different amounts of the polymer into the water subphase the increase in surface pressure was recorded over a time period of 20 h (see Figure 5a). Both polymers show a high surface activity. At the saturation concentration of ~9 µM for Ch-PEG$_{30}$-*b*-*hb*PG$_{23}$ the surface pressure was 28.6 mN m^{-1}. For Ch-PEG$_{30}$-*b*-*hb*PG$_{17}$-Rho the saturation concentration was somewhat lower with ~6 µM with a pressure of 27.3 mN m^{-1}. The results obtained with Ch-PEG$_{30}$-*b*-*hb*PG$_{23}$ are in agreement with previous results of experiments using only one defined concentration of 2 µM.[18] The surface activity of Ch-PEG$_{30}$-*b*-*hb*PG$_{17}$-Rho is thus slightly higher compared to its non-labelled analogue, again probably caused by the amphiphilic fluorescent label. This is particularly evident when the surface pressure at a concentration of only 500 nM is compared, where the two values are 12 mN m^{-1} for Ch-PEG$_{30}$-*b*-*hb*PG$_{23}$ and 19 mN m^{-1} for Ch-PEG$_{30}$-*b*-*hb*PG$_{17}$-Rho.
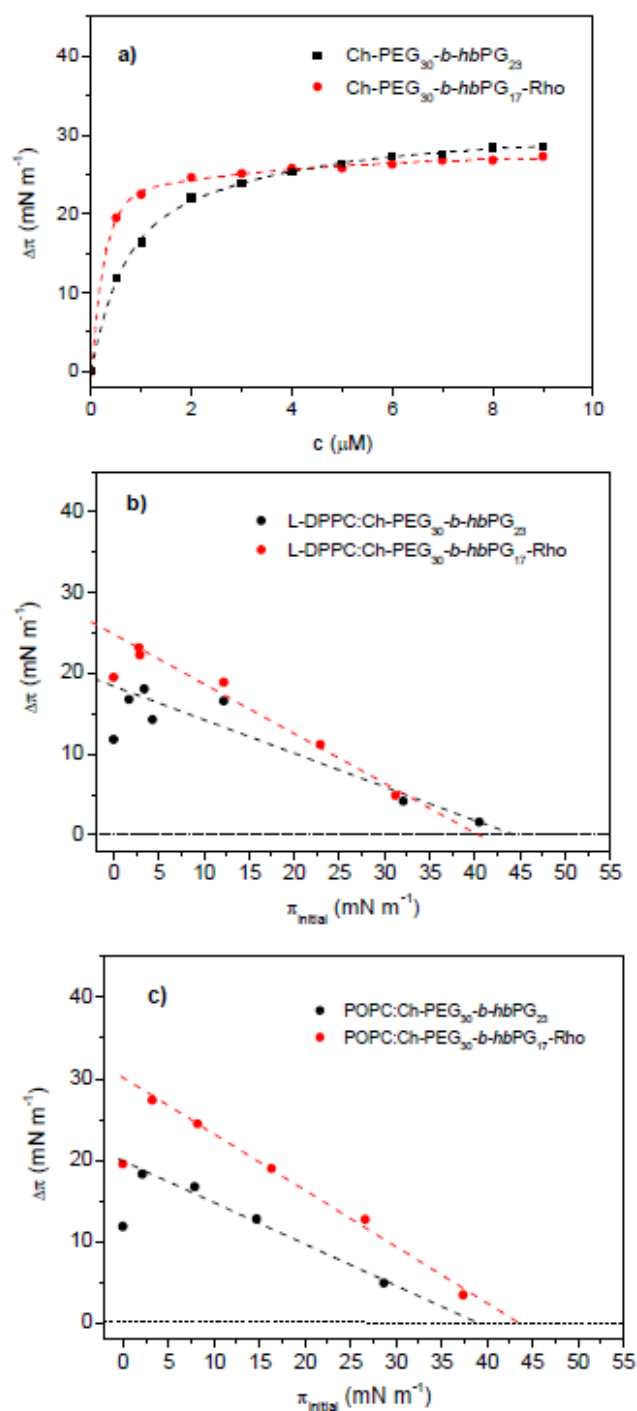
Figure 5. a) Surface pressure as a function of concentration for the adsorption of the polymers to the pure air-water surface. b) Change in surface pressure $\Delta\pi$ observed for the adsorption to monolayers of L-DPPC with different initial surface pressure π. c) Change in surface pressure $\Delta\pi$ observed for the adsorption to monolayers of L-POPC with different initial surface pressure π. Polymer concentration after injection was 500 nM in b) and c).

We then studied the adsorption of the polymers using lowest concentration of only 500 nM to preformed L-DPPC and POPC monolayers, which were spread to distinct surface pressures (see Figures 5b,c). The equilibrium surface pressure after injection of the polymers underneath the monolayer is reached after a significantly shorter time of only 2-3 h (not shown), i.e. the adsorption to the lipid monolayers occurs faster than to the air-water interface indicating an additional driving force due to the presence of the lipid monolayer at the surface. A plot of $\Delta\pi$ vs. π yields the maximal insertion pressure MIP of a compound when a linear fit of the data points is performed and extrapolated to $\Delta\pi = 0$. For this fit the first data points shown in Figures 5b,c, representing the surface pressure of a pure polymer film at the same concentration, have to be excluded. The maximal insertion pressure of Ch-PEG$_{30}$-b-hbPG$_{23}$ adsorption to L-DPPC is more than ~44 mN m^{-1} and for Ch-PEG$_{30}$-b-hbPG$_{17}$-Rho adsorption to L-DPPC it is ~40 mN m^{-1}. For the adsorption to POPC monolayers the respective values are 39 and 44 mN m^{-1}. The high MIP values show very clearly the high insertion capability of both polymers into biological membranes, considering that the so-called monolayer-bilayer equivalence pressure is 30-35 mN m^{-1}.[26] Thus both, the unlabelled and the rhodamine labelled polymer are capable of inserting into liquid expanded as well as into tightly packed liquid condensed PC monolayers although only a very low amount of aqueous polymer was injected. From Figures 5b and 5c it is furthermore obvious that surface pressures reached after the adsorption of the polymers to phospholipid monolayers are considerably higher than the maximum surface pressures reached from adsorption of the polymers alone to the air-water surface. This leads to the conclusion that strong attractive forces between PCs and the used polymers Ch-PEG$_{30}$-b-hbPG$_{23}$ and Ch-PEG$_{30}$-b-hbPG$_{17}$-Rho exist. The polymer adsorption behavior to phospholipid monolayers is different for both copolymers. Although they are both able to insert into even densely packed liquid condensed monolayers the adsorption data for the rhodamine labelled polymer exhibit higher surface pressure differences by adsorption than the unlabelled polymer. This difference is even more pronounced for adsorption to the liquid expanded POPC monolayer. This agrees with the higher surface activity of the labelled polymer and is again caused by the additional amphipathic rhodamine label attached to the hyperbranched poly(glycerol) block.

Differential Scanning Calorimetry. In order to test, whether the different results obtained for the interaction of the two polymers with monolayers at the air-water interface are also observable with bilayer systems of the same phospholipids, differential scanning calorimetry (DSC) measurements were performed. DSC is a suitable method to study the thermotropic behaviour of lipid bilayers. Changes in the width and temperature of the main phase transition of phospholipids from the gel to the liquid-crystalline lamellar phase are used as an indicator for the interaction of other molecules with the bilayer. For instance, the shift of the bilayer phase transition to lower temperature with concomitant broadening of the transition is usually interpreted as an indication for the insertion of hydrophobic parts of the interacting molecule into the hydrophobic region of the bilayer.

The main phase transition temperature of pure DPPC vesicles occurs at 41.6 °C. After addition of different polymer concentrations to L-DPPC leading to molar ratios lipid:polymer of 100:1 to 5:1 the change of the main phase transition peak was investigated. For both polymers in mixtures with L-DPPC similar effects were observed. Only one major transition peak is observed demonstrating that no phase separation into large domains with different composition occurs. The transition peaks in Figure 6a and 6b are shifted to lower transition temperatures with increasing amount of polymer. With higher mole fractions of cholesterol-linked block copolymer the pre-transition of pure DPPC bilayers, which marks the transition from the ordered L_β-phase to the P_β-ripple phase vanishes. Also the sharp narrow DPPC peak broadens and is almost absent for both 5:1 mixtures of L-DPPC with the polymers. The maximum in the shift is observed for the 5:1 mixture with a difference of 2.4 K for L-DPPC mixed with Ch-PEG$_{30}$-*b-hb*PG$_{23}$ (see Figure 6a) and of 2.2 K for L-DPPC mixed with Ch-PEG$_{30}$-*b-hb*PG$_{17}$-Rho (see Figure 6b). The temperature downshift can be interpreted as a consequence of the incorporation of the cholesterol anchor into the bilayer membrane of DPPC. A molar ratio of 5:1 corresponds to 16.6 mol% of cholesterol incorporated into the bilayer. When the DSC curves in Figure 6 are compared to those obtained with DPPC:cholesterol mixtures similarities are observable. For instance, for cholesterol contents between 10 and 20 mol% in DPPC:cholesterol mixtures, the DSC peaks consist of a relatively sharp peak overlapping with an underlying broad peak, the sharper peak being shifted to lower temperature compared to the main phase transition of pure DPPC.[1, 2, 5,15, 40] This

behavior is quite similar to the peaks observed for DPPC mixed with Ch-PEG$_{30}$-*b*-*hb*PG$_{23}$ shown in Figure 6a, indicating that the major effect comes solely from the incorporation of the cholesterol moiety into the lipid bilayer. This is different for the polymer with the rhodamine label. The DSC curves in Figure 6b for high polymer content do not show this superposition of the sharp component. While the cholesterol anchors the polymer to the lipid bilayer by being incorporated into the hydrophobic region, the rhodamine label has again an influence on the bilayer system by eliminating the sharp peak caused by the transition of residual pure DPPC. The stronger interaction of the hyperbranched poly(glycerol) block with the attached amphipathic rhodamine label with the lipid headgroup region apparently leads to a better mixing of the system.
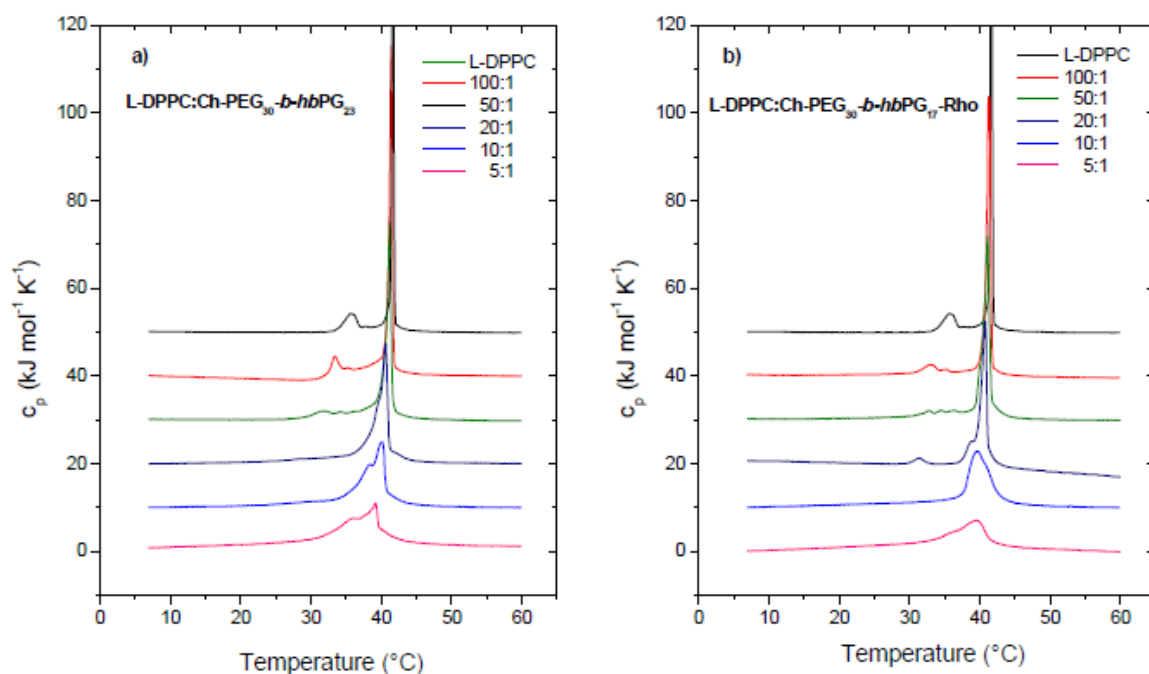
Figure 6. DSC thermograms of the upscans of pure DPPC and the binary mixtures of L-DPPC:Ch-PEG$_{30}$-*b*-*hb*PG$_{23}$ = x:1 (left) and L-DPPC:Ch-PEG$_{30}$-*b*-*hb*PG$_{17}$-Rho = x:1 (right).

Polymer interaction with phosphocholine giant unilamellar vesicles (GUVs). Using confocal imaging details of the interactions between the fluorescent labelled polymer in aqueous solution and GUVs of different phosphocholines can be studied. We find that the labelled block copolymer shows a high affinity to the different preformed GUVs of saturated 1,2-dilauroyl-*sn*-glycero-3-phosphocholine (DLPC), unsaturated 1,2-dioleoyl-*sn*-glycero-3-phosphocholine (DOPC) and asymmetric saturated/unsaturated 1-

palmitoyl-2-oleoyl-*sn*-glycero-3-phosphocholine (POPC) (see Figure 7 and 8). Fast polymer adsorption is already observed for the very small polymer/phospholipid ratio of 1/100, using a low polymer concentration of about 0.05 µM in the aqueous solution. Quantitative analysis of the membrane fluorescence intensity is an indicator of polymer adsorption (see Supp. Inf. Figure S3), i.e. it correlates with the polymer concentration (see Figure 7a) or it is a function of time (see Figure 7b). This clearly gives evidence for an interaction of the cholesterol anchor with the phospholipid membrane (see Scheme 2). In detail, the fluorescence intensity of the rhodamine label in the membrane is considerably higher for the GUVs composed of symmetrical phospholipids. Thus, polymer insertion into GUVs proceeds faster and easier for the higher ordered symmetrical phospholipid systems compared to asymmetrical POPC membranes. This is not obvious from monolayer experiments and it can be explained by the formation of a special interdigitated bilayer system by asymmetrical phospholipids. The insertion of a cholesterol anchor disturbs this kind of membrane mostly due to its hindrance of interdigitation.[15] Consequently, cholesterol is less attractive for POPC membranes compared to the DOPC- and DLPC-GUVs. As already known from adsorption investigations at phospholipid monolayers it confirms that the polymer insertion ability does not depend on the state of saturation of the fatty acid chains. The differences in the insertion behavior of the block copolymer can be explained by cholesterol solubility in the different hydrophobic regions of the bilayer systems.
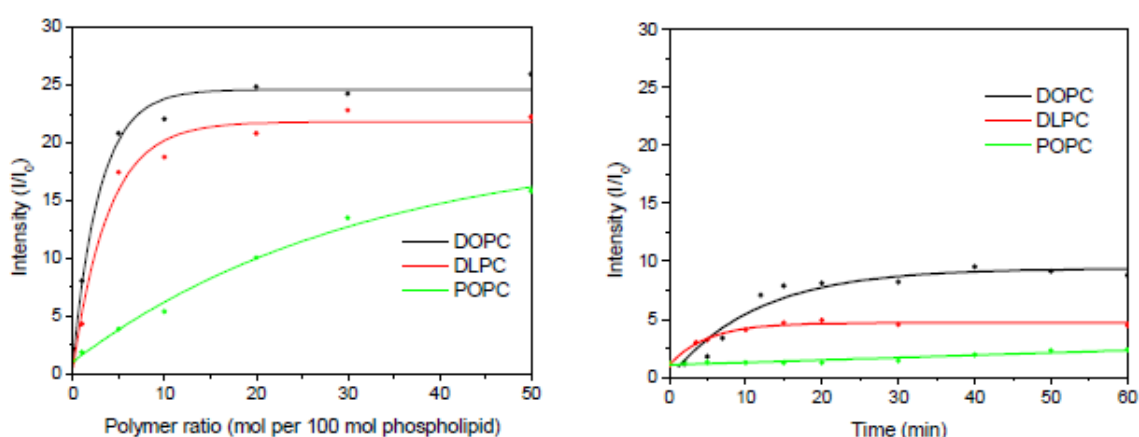
Figure 7. Adsorption intensity of Ch-PEG$_{30}$-*b*-*hb*PG$_{17}$-Rho at different single phase GUV membranes. a) adsorption of molar polymer ratios, data points taken at 30 min of incubation for the DLPC- and the DOPC-GUV, 1 h of incubation for the POPC-GUV; b) time-dependent adsorption from Ch-PEG$_{30}$-*b*-*hb*PG$_{17}$-Rho/phospholipid molar ratio of 1/100.

Confocal images of the GUV equatorial layers, shown in Figure 8, visualize the different insertion ability of the block copolymer into the membranes, decreasing in the order of DOPC>DLPC>POPC and they show the increasing rhodamine fluorescence intensity with increased ratio of polymer addition, analyzed in Figure 7a. Furthermore, the rhodamine fluorescence distribution proves a homogeneous arrangement of the polymer in the GUV membranes (see Figure 8 and 9). Up to a polymer/phospholipid ratio of 20-30/100 the vesicles remain stable for several days and no significant desorption processes are observed by changing the polymer solution to pure water (see Figure 9b).
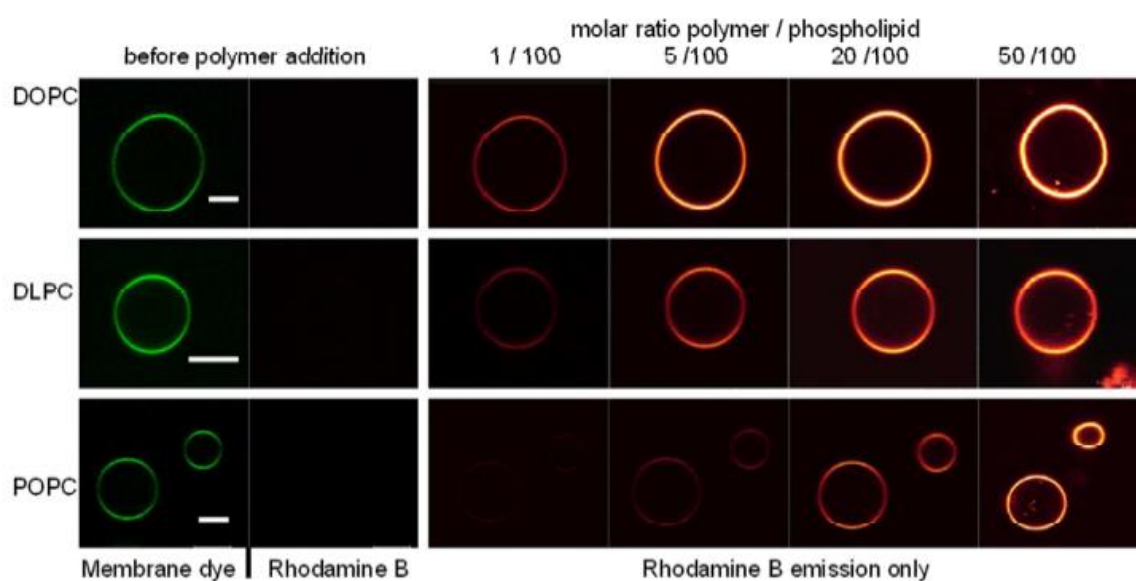
Figure 8. Confocal imaging of increasing polymer adsorption at DLPC, DOPC and POPC GUV membranes; green: membrane dye DiO; orange: rhodamine-labelled polymer Ch-PEG$_{30}$-*b*-*hb*PG$_{17}$-Rho. Scale bar is 5 µm, each.
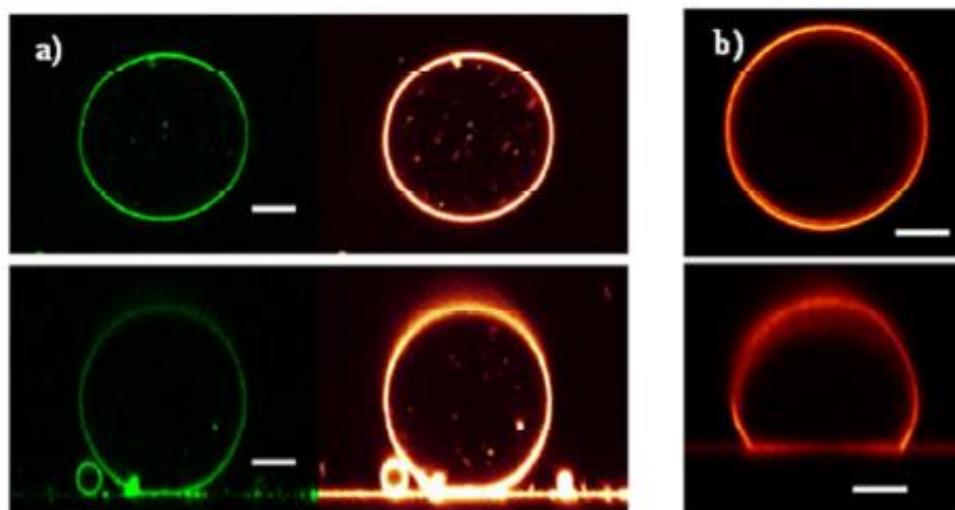
Figure 9. Confocal images of immobilized DLPC GUVs before and after incubation in aqueous polymer solution; on top: equatorial single scans, below: vertical single scans; green: membrane dye DiO; orange: rhodamine-labelled polymer Ch-PEG$_{30}$-*b-hb*PG$_{17}$-Rho; a) 24 h incubation with polymer/phospholipid ratio of 1:2; b) GUV after polymer adsorption (1:10 polymer ratio) transferred to pure water for 2 h. Scale bar is 5 μm.

Addition of higher polymer ratios affects the phospholipid membrane, the GUVs lose their stability and rigidity and membrane fluctuations occur. Small membrane pieces are released inside and outside the bilayer but also these GUVs can be stable for more than 24 h (see Figure 9a).

The occurrence of the polymer fluorescence inside the GUV might possibly indicate the ability of Ch-PEG$_{30}$-*b-hb*PG$_{17}$-Rho to generate membrane channels. Polymeric moieties might be able to cross the bilayer and it is very likely that cholesterol is the anchor which inserts into the outer as well as into the inner layer of the vesicular membrane. The more hydrophilic linear block as well as the hydrophilic hyperbranched block with the rhodamine label is exposed to water. Hence, the presented results match already published data on the interactions of cholesterol anchored poly(glycerols) with GUVs[25] as well as the more general knowledge about the membrane crossing properties of amphiphilic block copolymers depending on their molar mass and hydrophobic-hydrophilic balance. Copolymers are able to insert and to span phospholipid membranes as well as to form and close bilayer pores.[17,18, 41]

Conclusions

In the present work, we investigated the interactions of the phospholipids DPPC and POPC with the synthetic polyphiles Ch-PEG$_{30}$-*b-hb*PG$_{23}$ and Ch-PEG$_{30}$-*b-hb*PG$_{17}$-Rho consisting of a cholesterol unit covalently linked to a hydrophilic polyether-based block copolymer. Both polymers differ in six glycerol units within the hydrophilic hyperbranched part and a likewise covalently linked rhodamine fluorescence label. Tensiometry showed a high surface activity for both polymers which is caused by the hydrophobic cholesterol moiety anchoring the polymer to the air/water interface. The labelled polymer, however, shows a higher surface activity than the unlabelled analogue showing that the linker and the rhodamine label have apparently also ampathic character and therefore increase the surface activity.

Monolayer experiments of mixed lipid/polymer systems showed the miscibility of both polymers with the phospholipid monolayers in co-spread films as well as in adsorption experiments using preformed lipid monolayers. Co-spreading experiments combined with epi-fluorescence microscopy showed for both polymer mixtures with DPPC new and for both polymers very different liquid-condensed domain shapes. The polymers are inserted with the cholesterol moiety into the lipid monolayer and accumulate at the LC domain boundaries when the lipid film is compressed. Thus the line tension between the LE and LC domains is reduced, new "interfaces" can now more easily be formed. This leads to a thinning of the LC domains which can grow to very long stripes running parallel to each other and not coalescing at higher pressure due to domain repulsion. An influence of the stereogenic centers of the cholesterol unit on the chirality of the LC domains was not observed. The rhodamine labelled polymer was more effective in reducing the line tension. This is in line with its higher surface activity. Adsorption experiments confirmed the polymer insertion into phospholipid monolayers, even into LC layers of DPPC at high surface pressures. The observed MIP values were 40 mN m^{-1} or higher and thus well above the monolayer-bilayer equivalence pressure of 30-35 mN m^{-1}. Thus, the ability of the insertion of the polymers into model bilayer membranes was to be expected. This was indeed observed with lipid vesicle systems with added polymer. Increasing amounts of the block copolymer in the mixture with

DPPC lead to significant changes in the thermotropic behavior studied by DSC. The peak of the main transition of DPPC became much broader for lipid/polymer mixtures with molar ratios of 5:1. A comparison with the thermotropic behavior of DPPC/cholesterol mixtures lead to the conclusion that indeed the polymers have very similar effects on the transition behavior due to their cholesterol anchor. However, the rhodamine labelled polymer has different effects due to the interaction of the rhodamine label with the lipid headgroup region. Additional experiments were performed with GUVs using CLSM. The GUV experiments again proved the high affinity of the polymers for phospholipid membranes. The results obtained with GUVs are in good agreement with the adsorption measurements of the polymers to phospholipid monolayers. Quantitative analysis of the adsorption intensity of the rhodamine labelled polymer to different GUVs suggests again the interaction of the cholesterol anchor with the phospholipid bilayer.

Acknowledgments

References

(1)   Gennis, R.B. Biomembranes: Molecular structure and function, 2nd edition. Springer-Verlag: New York 2010.

(2)   Blume, A. Garidel, P. Lipid Model Membranes and Biomembr anes (Chapter 3) in: *From Macromolecules to Man,* R.B. Kemp, editor. Handbook of Thermal Analysis and Calorimetry Vol 4. Elsevier Press B.V.: Amsterdam 1999, 109 – 173.

(3)   Feigenson, G. W. Phase diagrams and lipid domains in multicomponent lipid bilayer mixtures. *Biochim Biophys Acta* **2009**, *1788*, 47-52.

(4)   Bhattacharya, S.; Biswas, J. Understanding membranes through the Molecular Design of Lipids. *Langmuir* **2010**, *26*, 4642-4654.

(5)   Silvius, J. R. Role of cholesterol in lipid raft formation: lessons from lipid model systems. *Biochim. Biophys. Acta* **2003**, *1610*, 174-183.

(6)   Chen, Z.; Rand, R. P. The Influence of Cholesterol on Phospholipid Membrane Curvature and Bending Elasticity. *Biophys. J.* **1997**, *73*, 267-276.

(7)   Quinn, P. J.; Wolf, C. The liquid-ordered phase in membranes. *Biochim Biophys Acta* **2009,** *1788*, 33-46.

(8)   Janout, V.; Turkyilmaz, S.; Wang, M.; Manaka, Y.; Regen, S. L. An Upside Down View of Cholesterol's Condensing Effect: Does Surface Occupancy Play a Role? *Langmuir* **2010**, *26*, 5316-5318.

(9)   Radhakrishnan, A.; McConnell, H. M. Chemical Activity of Cholesterol in Membranes. *Biochemistry* **2000**, *39*, 8119-8124.

(10)   Hung, W.-C.; Lee, W.-T.; Chen, F.-Y.; Huang, H. W. The Condensing Effect of Cholesterol in Lipid Bilayers. *Biophys. J.* **2007**, *92*, 3960-3967.

(11)   Demel, R. A.; Van Deenen, L. L. M.; Pethica, B. A. Monolayer interactions of Phospholipids and Cholesterol. *Biochim. Biophys. Acta* **1967**, *135*, 11-19.

(12)   Mozaffary, H. Cholesterol-phospholipid interaction: a monolayer study. *Thin Solid Films*, **1994**, *244*, 874-877.

(13)   Keller, S. K.; Radhakrishnan, McConnell, H. M. Saturated Phospholipids with High Melting Temperatures Form Complexes with Cholesterol in Monolayers. *J. Phys. Chem. B* **2000**, *104*, 7522-7527.

(14)   Blume, A. Thermotropic Behavior of Phosphatidylethanolamine-Cholesterol and Phosphatidylethanolamine-Phosphatidylcholine-Cholesterol   Mixtures. *Biochemistry* **1980**, *19*, 4908-4913.

(15)   Lee-Gau Chong, P.; Choate, D. Calorimetric studies of the effect of cholesterol on the phase transition of C(18):C(10) phosphatidylcholine. *Biophys. J.* **1989**, *55*, 551-556.

(16)   Reuter, S.; Hofmann, A. M.; Busse, K.; Frey, H.; Kressler, J. Langmuir and Langmuir-Blodgett Films of Multifunctional, Amphiphilic Polyethers with Cholesterol Moieties. *Langmuir* **2011**, *27*, 1978-1989.

(17)   Amado, E.; Kressler, J. Interactions of amphiphilic block copolymers with lipid model membranes. *Curr. Opin. Colloid Inter. Sci.* **2011**, *16*, 491-498.

(18)   Peng, X.; Hofmann, A. M.; Reuter, S.; Frey, H.; Kressler, J. Mixed layers of DPPC and a linear poly(ethylene glycol)-*b*-hyperbranched poly(glycerol) block copolymer having a cholesteryl end group. *Colloid Polym. Sci.* **2012**, *290*, 579-588.

(19)   Fitton, A. O.; Hill, J.; Jane, D. E.; Millar, R. Synthesis of Simple Oxetanes Carrying Reactive 2-Substituents. *Synthesis-Stuttgart* **1987**, *12*, 1140-1142.

(20)   Hofmann, A. M.; Wurm, F.; Hühn, E.; Nawroth, T.; Langguth, P.; Frey, H. Hyperbranched Polyglycerol-Based Lipids via Oxyanionic Polymerization: Toward Multifunctional Stealth Liposomes. *Biomacromolecules* **2010**, *11*, 568-574.

(21)   Hofmann, A. M.; Wurm, F.; Frey, H. Rapid Access to Polyfunctional Lipids with Complex Architecture via Oxyanionic Ring-Opening Polymerization. *Macromolecules* **2011**, *44*, 4648-4657.

(22)   Zhao, L.; Feng, S.-S. Effects of lipid chain length on molecular interactions between paclitaxel and phospholipid within model biomembranes. *J.Colloid Interface Sci.* **2004**, *274*, 55-68.

(23)   Angelova, M. I.; Dimitrov, D. S. Liposome electroformation. *Faraday Discuss. Chem. Soc.* **1986**, *81*, 303-311.

(24)   Lohse, B.; Bolinger, P. Y.; Stamou, D. Encapsulation Efficiency Measured on Single Small Unilamellar Vesicles. *J. Am. Chem. Soc.* **2008**, *130*, 14372-14373.

(25)   Schöps, R.; Amado, E.; Müller, S. S.; Frey, H.; Kressler, J. Block copolymers in giant unilamellar vesicles with proteins or with phospholipids. *Faraday Discuss. Chem. Soc.* **2013**,*166*, 303-315.

(26)   Blume, A. Comparative-Study of the Phase-Transitions of Phospholipid Bilayers and Monolayers. *Biochim.Biophys.Acta* **1979**, *557*, 32-44.

(27)   Winterhalter, M.; Bürner, H.; Marzinka, S.; Benz, R.; Kasianowicz, J. J. Interaction of Poly(ethylene-glycols) with Air-Water Interfaces and Lipid Monolayers: Investigations on Surface Pressure and Surface Potential. *Biophys. J.* **1995**, *69*, 1372-1381.

(28)   Kuhl, T. L.; Majewski, J.; Howes, P. B.; Kjaer, K.; von Nahmen, A.; Lee, K. Y. C.; Ocko, B.; Israelachvili, J. N.; Smith, G. S. Packing Stress Relaxation in Polymer-Lipid Monolayers at the Air-Water Interface: An X-ray Grazing-Incidence Diffraction and Reflectivity Study. *J. Am. Chem. Soc.* **1999**, *121*, 7682-7688.

(29)   Müller-Landau, F.; Cadenhead, D. A. Molecular packing in steroid-lecitin monolayer, Part I: Pure films of cholesterol, 3-doxyl-cholestane, 3-doxyl-17-hydroxyl-androstane, tetradecanoic acid and dipalmitoyl- phosphatidylcholine. *Chem. Phys. Lipids* **1979**, *25*, 299-314.

(30)   Baekmark, T.R., Elender, G., Lasic, D.D., Sackmann, E. Conformational Transitions of Mixed Monolayers of Phospholipids and Poly(ethy1ene oxide) Lipopolymers and Interaction Forces with Solid Surfaces. *Langmuir* **1995**,*11, 3975-3987*.

(31)   Tsukanova, V., Salesse, C. High-Pressure Transition of a Poly(ethylene glycol)-Grafted Phospholipid Monolayer at the Air/Water Interface. *Macromolecules* **2003**, *36*, 7227-7235.

(32)   Tsukanova, V., Salesse, C. On the Nature of Conformational Transition in Poly(ethylene glycol) Chains Grafted onto Phospholipid Monolayers. *J. Phys. Chem. B* **2004**, *108*, 10754-10764.

(33)   André Hädicke, A., Blume, A. Interactions of Pluronic block copolymers with lipid monolayers studied by epi-fluorescence microscopy and by adsorption experiments. *J. Coll. Interf. Sci.* **2013**, *407*, 327-338.

(34)   McConnell, H. M. Structures and transitions in lipid monolayers at the air-water interface. *Annu. Rev. Phys. Chem.* **1991**, *42*, 171-195.

(35)   Krüger, P.; Lösche, M. Molecular chirality and domain shapes in lipid monolayers on aqueous surfaces. *Phys. Rev. E* **2000**, *62*, 7031-7043.

(36)   Scholtysek, P.; Li, Z.; Kressler, J.; Blume, A. Interactions of DPPC with Semitelechelic Poly(glycerol methacrylate)s with Perfluoroalkyl End Groups. *Langmuir* **2012**, *28*, 15651-15662.

(37)   Weis, R. M.; McConnell, H. M. Cholesterol Stabilizes the Crystal-Liquid Interface in Phospholipid Monolayers. *J. Phys. Chem.* **1985**, *89*, 4435-4459.

(38)   Keller, D. J.; McConnell, H. M.; Moy, V. T. Theory of Superstructures in Lipid Monolayer Phase Transitions. *J. Phys. Chem.* **1986**, *90*, 2311-2315.

(39)   Weis, R. M. Fluorescence microscopy of phospholipid monolayer phase transitions. *Chem. Phys. Lipids* **1991**, *57*, 227-239.

(40)   Huang, T.-H.; Lee, C.W.B.; Das Gupta, S.K.; Blume, A.; Griffin, R.G. A ^{13}C and [2]H Nuclear Magnetic Resonance Study of Phosphatidylcholine/Cholesterol Interactions. Characterization of Liquid-Gel Phases. *Biochemistry* **1993**, *32*, 13277-13287.

(41)   Amado, E.; Blume, A.; Kressler, J. Novel non-ionic block copolymers tailored for interactions with phospholipids. *React. Funct.Polym.* **2009**, *69*, 450-456.

Supporting Information
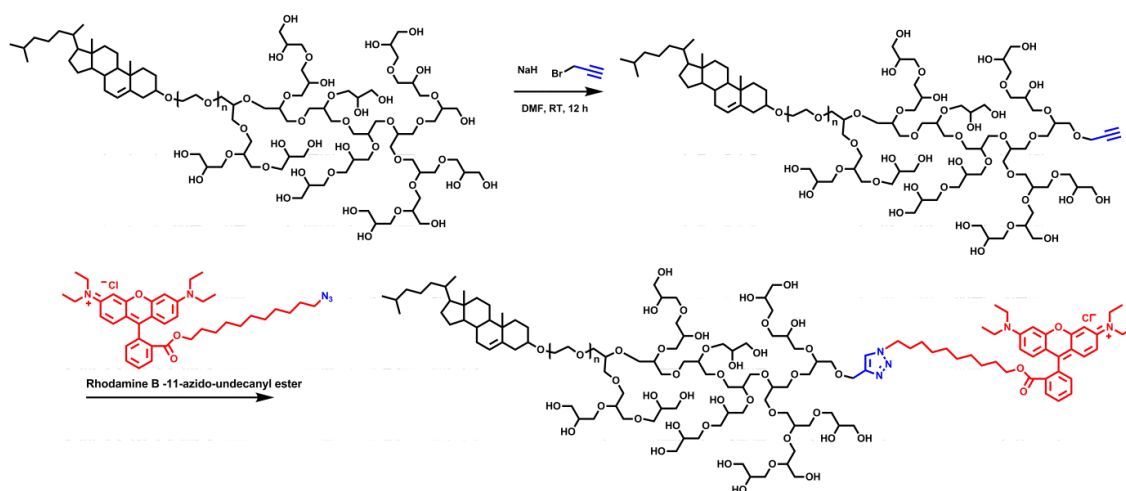
Scheme S1. Functionalization and derivatization reactions of the linear-hyperbranched polymer. Although one alkyne group per polymer chain is drawn here, there is a statistical distribution of alkyne groups within the sample. Polymer chains without or with more than one alkyne groups are possible.
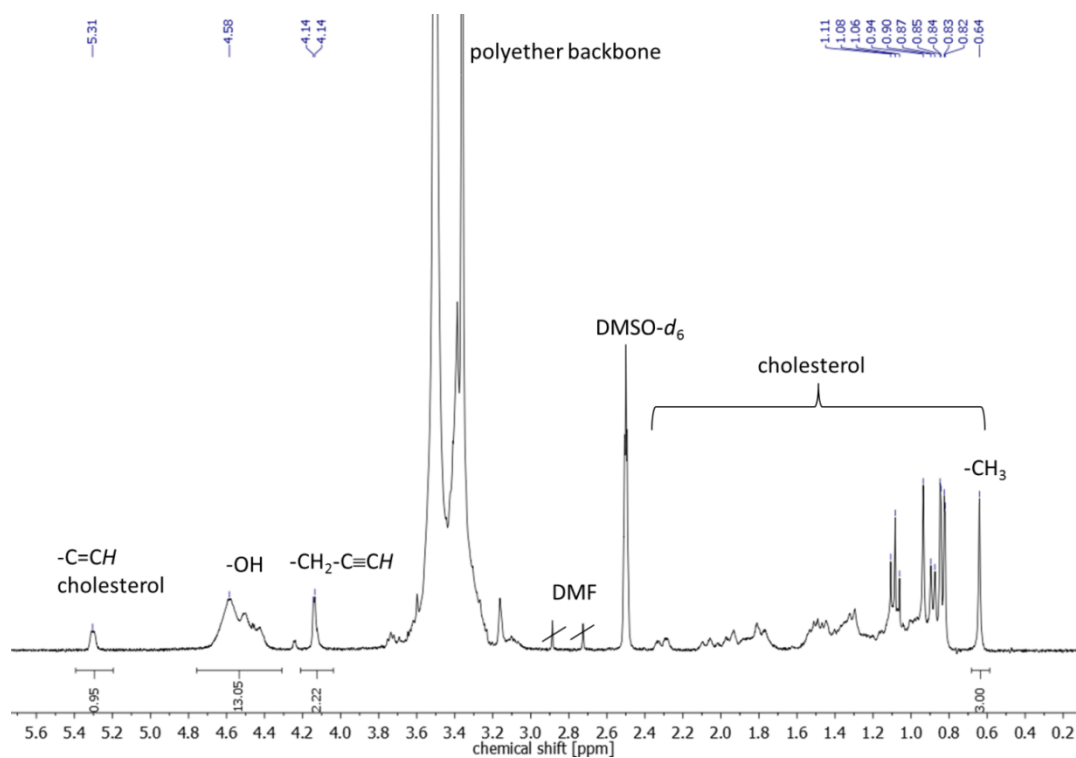
Figure S2. ^{1}H NMR spectrum of the alkyne-functionalized copolymer Ch-PEG$_{30}$-*hb*PG$_{17}$.

^{1}H NMR analysis:

Cholesterol-PEG-hbPG-OCH$_2$C≡CH: ^{1}H NMR (300 MHz, DMSO-d_6): δ (ppm) = 5.31 (C=CH cholesterol), 4.72-4.44 (br, OH, different signals due to hyperbranched PG), 4.24-4.13 (OCH$_2$-C≡CH), 3.60-3.16 (polyether backbone; CHO cholesterol), 2.29-0.82 (br, CH$_2$, CH cholesterol), 0.64 (br, -CH$_3$ cholesterol).

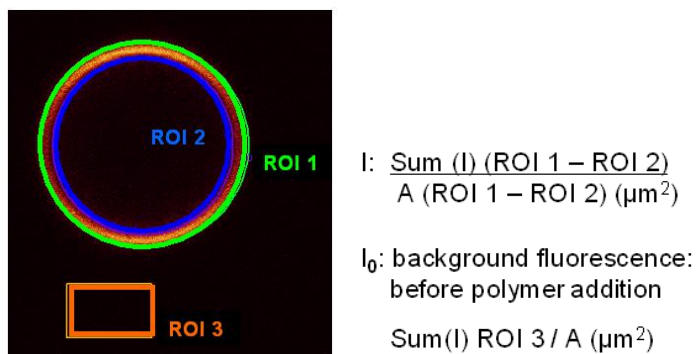*Figure S3.* Method of intensity determination of an equatorial GUV slice by use of ROI.

4 *Pre-In Vivo* and *In Vivo* Studies

4.1 Evaluation of Multifunctional Liposomes in Human Blood Serum by Light Scattering

Kristin Mohr,[1,2] Sophie S. Müller,[3,4]* Laura K. Müller,[2] Kristiane Rusitzka,[5] Sabine Gietzen,[1] Holger Frey,[3] and Manfred Schmidt[1,#]*

[1]Institute of Physical Chemistry, Johannes Gutenberg University Mainz, Welderweg 11, 55128 Mainz, Germany

[2]Max Planck Institute for Polymer Research (MPIP), Ackermannweg 10, 55128 Mainz, Germany

[3]Institute of Organic Chemistry, Johannes Gutenberg University Mainz, Duesbergweg 10-14, 55128 Mainz, Germany

[4]Graduate School Materials Science in Mainz, Staudingerweg 9, 55128 Mainz, Germany

[5]Institute of Zoology, Johannes Gutenberg University Mainz, Johannes-von-Müllerweg 6, 55118 Mainz, Germany

* Both authors contributed equally
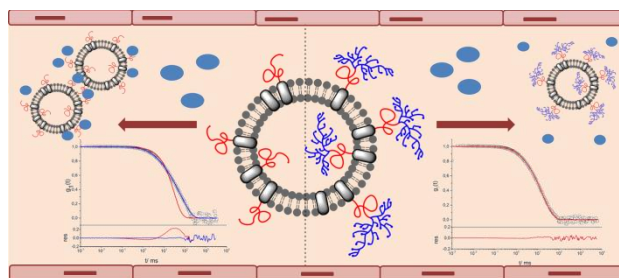
Abstract

To overcome the limited functionality of "stealth" lipids based on linear poly(ethylene glycol) (PEG) chains, hyperbranched polyether-based lipids that bear multiple hydroxyl groups for further chemical modification may be a suitable replacement for the "gold standard" PEG. This study focuses on the development and characterization of "stealth" liposomes modified with a novel hyperbranched polyglycerol lipid (Cholesterol-PEG$_{30}$-hbPG$_{23}$). An emphasis was placed on the stability of these liposomes in comparison to

those containing a linear PEG derivative (Cholesterol-PEG$_{44}$) directly in human blood serum, characterized *via* dynamic light scattering (DLS). Polymer lipid contents were varied between 0 mol% and 30 mol% resulting in liposomes with sizes between 150 nm and 80 nm in radius, depending on the composition. DLS analysis showed no aggregation inducing interactions between serum components and liposomes containing 10-30 mol% of the hyperbranched lipid. In contrast, liposomes functionalized with comparable amounts of linear PEG exhibited aggregate formation in the size range of 330 nm to 170 nm under similar conditions. In addition, cryo-TEM was employed for all liposome samples to prove the formation of unilamellar vesicles. These results demonstrate the outstanding potential of introducing hyperbranched polyglycerol into liposomes to stabilize the assemblies against aggregation while providing addition functionalization sites.

Introduction

Since the 1970s liposomes have played an important role for drug delivery systems, due to their capability to reduce harmful side effects of drugs on healthy tissue, while implementing passive targeting.[1,2,3] These spherical, vesicular structures are composed of lipid bilayers (usually phospholipid) that separates the hydrophilic interior compartment from the outside. Liposomes can entrap either hydrophilic drugs inside the vesicle or hydrophobic drugs inside the lipid bilayer, and deliver these materials to the desired site of action. Passive targeting can be achieved through the "enhanced permeability and retention" (EPR) effect, which describes the increased permeability of blood vessels in a tumor or inflamed tissue.[4,5] Prolonged plasma half-life leads to increasing time intervals, in which permeation of macromolecules or liposomes can occur.[6,7]

However, main disadvantages of conventional liposomes include their rapid removal from the blood by macrophages after opsonin binding by the mononuclear phagocyte system (MPS) as well as their physical and chemical instability.[8,9,10] Moreover, conventional liposomes exhibit low stability in plasma due to their interaction with low (LDL) and high density (HDL) lipoproteins.[11] To overcome these drawbacks, liposome

surfaces can be modified with synthetic polymers, like poly(ethylene glycol) (PEG), a highly biocompatible polyether. The presence of a polymer shell has been shown to lead to prolonged blood circulation times,[12-14] reduced MPS uptake,[15] reduced aggregation of PEGylated carriers, and better stability of these liposomal carriers. The resulting, so-called "stealth" effect is ascribed to steric stabilization of the vesicles by the polymer,[11,16] combined with the additional hydrophilicity of the PEG chains attached that can prevent the adsorption of blood components onto the liposome surface.[17] The "stealth" liposomes are already established in clinical use and anti-cancer treatment by the incorporation of cytostatic drugs, like doxorubicin, known as Doxil®/ Caelyx®.[11,18-20]

The MPS implies phagocytic cells that are responsible for the elimination of macromolecules and liposomes in the circulating blood stream.[21] This mechanism is believed to be promoted by serum proteins that adsorb at the surface of the particle, leading to phagocytosis by macrophages. Liposome charge and size, lipid composition, and liposomal surface coating all have a tremendous influence on particle-protein interactions, and can be used to tune the circulation times.[22-24]

Blood is an extremely diverse liquid system in the human body and is the first medium that comes into contact with drug-delivery materials upon intravenous injection. It is not the particles themselves that induce biological responses with foreign substances, but the protein layer that coats the particles.[25] The protein corona formed after exposure to the blood stream alters size and surface composition of nanoparticles or liposomes and with that, targeting properties, cellular uptake, and *in vivo* distribution are influenced.[26-29] Interaction with blood components or aggregation in serum influences the vesicle's fate *in vivo*.[28] Papahadjopoulos and coworker proposed that liposome stabilization results from surface concentration of highly hydrated groups. These moieties inhibit both electrostatic and hydrophobic interactions, which can occur between the vesicle's surface and several blood components.[30]

Improvement of methods that predict the *in vivo* pharmacokinetics of delivery systems, such as liposomes, without time-consuming and expensive animal tests is indispensable. Our group has established a method to detect aggregation of materials in undiluted human blood serum *via* dynamic light scattering (DLS), which is currently the closest analysis to resembling *in vivo* conditions. PEGylated poly-L-lysine, for example, was investigated with different degrees of PEGylation. Aggregates with a few hundreds of

nanometers could be detected with less than 10% PEGylation, while with over 20% functionalization, no aggregation was observed.[31] However, despite improved pharmacokinetics and vesicle stabilization that accompanies the incorporation of PEG into liposomes there are still several disadvantages to these systems. For instance, methoxypoly(ethylene glycol) (mPEG) has a single hydroxyl group that is used for the attachment to phospholipids, yet the lack of additional functionalities limits the possibilities for further modify the assembled liposomes for applications such as active targeting. In an effort to overcome this obstacle, our group has synthesized a variety of hyperbranched polyglycerol (*hb*PG)-based lipids by an oxyanionic ring-opening polymerization technique of glycidol or other functional epoxides.[32,33] Herein, we utilized cholesterol as the initiator to polymerize a diblock copolymer structure, where the first block was a linear PEG spacer linked to a multifunctional *hb*PG segment.[34-37] The *hb*PG block provides numerous hydroxyl groups that can be used for post-polymerization functionalization (*i. e.* with targeting or tracking species) or to promote aqueous solubility, improved liposome shielding, and resistance to protein adsorption.[38,39] Specifically, *hb*PG has been reported to exhibit similar or even better protein repulsion at surfaces than linear PEG with comparable molecular weight. This effect is believed to be related to the brush-like architecture and multiple hydroxyl groups of the hyperbranched polymer.[38,39,40] The linear-hyperbranched diblock copolymer structure used in this study combines the advantages of a flexible PEG chain with those of a multifunctional, presumably more densely packed *hb*PG (see Figure 1).
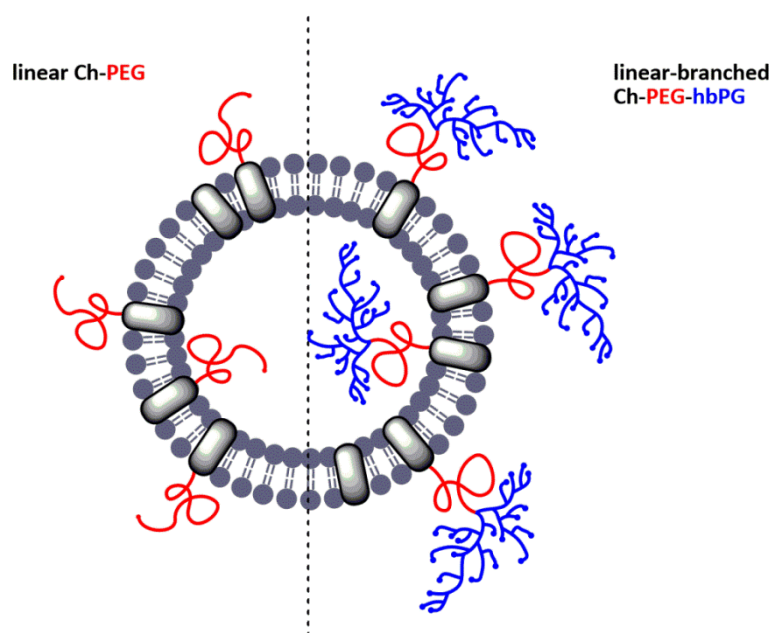
Figure 1: Cartoon of PEGylated liposomes left: coating with Ch-PEG chains (red); right: coating with Ch-PEG-*hb*PG (red and blue).

In the present work, liposomes based on cholesterol and egg phosphatidyl choline (EPC) with variable content (10-30 mol%) of either Ch-PEG$_{44}$ or linear-hyperbranched Ch-PEG$_{30}$-*hb*PG$_{23}$ were investigated with regard to their size in physiological buffer solution. Characterization of the liposomes in physiological buffer solutions was carried out in concentrated human blood serum with respect to their aggregation behavior with the serum proteome. Cryo-TEM was employed to prove the formation of vesicles.

Materials and Methods

Reagents

All reagents and solvents were purchased from Acros and used as received, unless otherwise mentioned. Dry solvents were stored over molecular sieves and were purchased from Fluka. Deuterated DMSO-d_6 was purchased from Deutero GmbH, and stored over molecular sieves. Ethanol (abs.) was purchased from VWR international. Phosphate buffered saline (PBS solution) was purchased from Invitrogen/Gibco. Cholesterol was purchased from Acros and stored at 8 °C. Hydrogenated egg phosphatidylcholine (EPC-3) was a gift from Lipoid GmbH and stored at -20 °C. The extruder, the polycarbonate membranes and filters were used from Avanti Polar Lipids.

Ethoxyethyl glycidyl ether (EEGE) was synthesized as described in the literature[41] and dried over CaH_2 prior to use. Glycidol was purified by distillation from CaH_2 directly prior to use.

Polymer synthesis

Ch-PEG$_{44}$: Cholesterol (0.800 g; 2.1 mmol), CsOH monohydrate (0.313 g; 1.9 mmol; degree of deprotonation 90%) and benzene were placed in a Schlenk flask. The mixture was stirred for about 30 min at RT to generate the cesium alkoxide. The salt was dried under vacuum at 90 °C for 24 h, anhydrous tetrahydrofuran (THF) was added *via* cryo transfer, and ethylene oxide was cryo transferred first to a graduated ampule and then to the Schlenk flask containing the initiator solution. The mixture was allowed to warm up to RT, heated to 60 °C, and the polymerization was performed at 60 °C in vacuum for 24 h. The reaction was quenched with methanol, stirred over acidic ion-exchange resin (Dowex 50WX8), the solvent was evaporated and the crude product was precipitated in cold diethyl ether. ($M_{n,NMR}$= 2300 g mol^{-1}, $M_{n,SEC}$= 1600 g mol^{-1}, PDI= 1.1).

Ch-PEG$_{30}$-*lin*PG; Macroinitiator for the hyperbranched block: The protocol was slightly modified from the previous literature.[32,33] Therefore the detailed procedure is given here.

Cholesterol (1.38 g; 3.6 mmol), CsOH monohydrate (0.539 g; 3.2 mmol; degree of deprotonation 90%), and benzene were placed in a Schlenk flask. The mixture was stirred for about 30 min at RT to generate the cesium alkoxide. The formed salt was dried under vacuum at 90 °C for 24 h, anhydrous THF was added *via* cryo transfer, and ethylene oxide (5 mL; 100 mmol) was cryo transferred first to a graduated ampule and then to the Schlenk flask containing the initiator solution. The mixture was allowed to warm up to RT, heated to 60 °C, and the polymerization was performed at 60 °C in vacuum for 24 h. Subsequently, a sample was removed for NMR and SEC analysis, ethoxyethyl glycidyl ether (EEGE) (3.8 mL; 25 mmol) was added *via* a syringe, and the reaction mixture was held at 60 °C for additional 12 h. After removal of another sample for characterization, the polymerization was stopped *via* an excess of methanol and acetal protecting groups of the PEEGE block were removed by addition of water and acidic ion-exchange resin (Dowex 50WX8), stirring for 12 h at 40 °C. The solution was

filtered, concentrated, and the crude product was precipitated in cold diethyl ether. The block copolymer was dried *in vacuo*.

Ch-PEG$_{30}$-*hb*PG$_{23}$; Hypergrafting of glycidol: The macroinitiator Ch-PEG$_{30}$-*lin*PG$_7$ (1.41 g; 0.6 mmol) was suspended in benzene and placed in a Schlenk flask, CsOH monohydrate (0.213 g; 1.3 mmol) was added to achieve 25% of deprotonation of the total amount of hydroxyl groups and after 30 min the mixture was dried under vacuum at 90 C. The macroinitiator was dissolved in diethylene glycol dimethyl ether (diglyme) (25 wt%), heated to 90 °C and a 25 wt% solution of glycidol (0.71 mL; 10.8 mmol) in diglyme was added slowly with a syringe pump over a period of 18 h. Termination was carried out *via* an excess of methanol and an acidic ion exchange resin. The crude product was filtrated, precipitated in cold diethyl ether and the Ch-PEG$_{30}$-*hb*PG$_{23}$ block copolymer was dried *in vacuo* ($M_{n,NMR}$= 3400 g mol^{-1}, $M_{n,SEC}$= 1400 g mol^{-1}, PDI= 1.16).

Liposome preparation

Liposomes consisting of either the amphiphilic Ch-PEG$_{44}$ or Ch-PEG$_{30}$-*hb*PG$_{23}$ block copolymer, cholesterol, and egg phosphatidylcholine (EPC) were prepared by the thin film hydration method on a clean bench. A solution of EPC in ethanol, cholesterol in ethanol and the copolymer in ethanol were blended at different molar ratios varying from 0 to 30 mol% (Table 1). The solvent was evaporated in a rotating evaporator to obtain a thin film of liposome components. The lipid film was hydrated with 1 mL of PBS buffer solution to obtain a final lipid concentration of 21 mg/mL, sonicated for 10 min at 50 °C to yield multilamellar vesicles (MLVs), and extruded through a 400 nm polycarbonate membrane 5 times, followed by the repeated extrusion through a 100 nm membrane (11 times) to obtain small unilamellar vesicles (SUVs). The suspension was stored at 4 °C in an Eppendorf tube.

Table 1: Different molar ratios used for the preparation of the novel sterically stabilized liposomes (Notation: L= Liposomes, 10, 15, 20, 30 = mol% of polymer, respectively).

	L0	**L10-*hb*PG**	L10-PEG	**L15-*hb*PG**	L15-PEG	**L20-*hb*PG**	L20-PEG	**L30-*hb*PG**	L30-PEG
Ch-PEG$_{44}$/mol%	0	**0**	10	**0**	15	**0**	20	**0**	30
Ch-PEG$_{30}$-*hb*PG$_{23}$/mol%	0	**10**	0	**15**	0	**20**	0	**30**	0
EPC/mol%	55	**55**	55	**55**	55	**55**	55	**55**	55
Cholesterol/mol%	45	**35**	35	**30**	30	**25**	25	**15**	15

Polymer Characterization

^{1}H NMR spectra were recorded using a Bruker AC 300 spectrometer operated at 300 MHz, employing DMSO-d_6 as solvent. Size exclusion chromatography (SEC) measurements were carried out in dimethylformamide (DMF) with 0.25 g L^{-1} LiBr. For SEC measurements a UV (275 nm) and an RI detector were used. Columns were MZ SDV 10000/500/50. Calibration was carried out using poly(ethylene glycol) standards provided by Polymer Standards Service (PSS).

Cryo-TEM preparation

The grids (CF-2/2-3C-T50 Grids; Protochips) were washed in chloroform for an hour and rinsed five times with acetone. After drying, the grids were negatively glow discharged (30 s at 30 mA) and 3 µl of the liposome sample were placed on the grid, respectively. Cryo-samples were vitrified in liquid ethane using a Gatan Cryoplunge™3 (relative humidty: 92%; blotting time for double-sided blotting: 3 s; temperature: 18 °C) and imaged with an FEI Tecnai 12 (acceleration voltage: 120 kV) transmission electron microscope equipped with a TVIPS TemCam-F416 (TVIPS, Gauting, Germany).

Preparation of blood serum

The human blood serum, prepared according to the standard guidelines, was obtained from the University Clinic of Mainz (Germany). Due to the high variation of protein composition of different patients a pool of serum obtained by the mixture of serum of several healthy donors was used for all measurements.[31]

Preparation of samples

All solutions for light scattering experiments were prepared in a dust free flow box. Cylindrical quartz cuvettes (20 mm diameter, Hellma, Müllheim) were cleaned by dust-free distilled acetone. Serum solutions were filtered through Millex GS filters, 220 nm pore size (Millipore). After testing several filters concentration losses of serum proteins by filtration with Millex GS filters were neglible.[31]

The liposomes were prepared in PBS buffer solution (GIBCO, Invitrogen) and filtered through an LCR450 nm filter in the light scattering cuvette. For the measurements of the liposomes in serum, serum and liposome solution dissolved in PBS buffer solution (GIBCO, Invitrogen) were given subsequently in the light scattering cuvette. Then, the cuvettes were incubated for 20 min on a shaker at room temperature prior to the measurement.

Light Scattering Apparatus

All light scattering experiments were carried out with an instrument consisting of a HeNe laser (632.8 nm, 25 mW output power), an ALV-CGS 8F SLS/DLS 5022F goniometer equipped with eight simultaneously working ALV 7004 correlators, and eight QEAPD Avalanche photodiode detectors.

Results and Discussion

Cholesterol as a natural membrane component has been widely used for the preparation of liposomes and as an anchor for polymeric lipids in lipid bilayers.[42,43,44,45] Recently, we were able to prove the strong interaction with linear-hyperbranched copolymer lipids and giant unilamellar vesicle (GUV) membranes, which shows the unique tendency of these polymer systems to incorporate into a phospholipid bilayer.[46] Cholesterol was used as the initiator for the oxyanionic polymerization of various epoxides leading to Ch-PEG$_{44}$ and Ch-PEG$_{30}$-hbPG$_{23}$ (see Figure 2), because standard phospholipids could not be used due to their instability to extreme reaction conditions during the reaction.[32,33,47-49]

This technique allows for the synthesis of well-defined amphiphilic polyether-lipids with molecular weights in the range of conventional PEG-lipids used in sterically stabilized

liposomes (2300 g mol^{-1} and 3400 g mol^{-1})[50,51] and low polydispersities (M_w/M_n: 1.1 and 1.16, respectively). The red PEG-part (left) represents the linear architecture of the Ch-PEG$_{44}$ amphiphile. The blue hydrophilic part (right) is the hyperbranched (*hb*) structure of the linear-*hb*PG lipid, which exhibits higher steric hindrance than its linear PEG analogue.
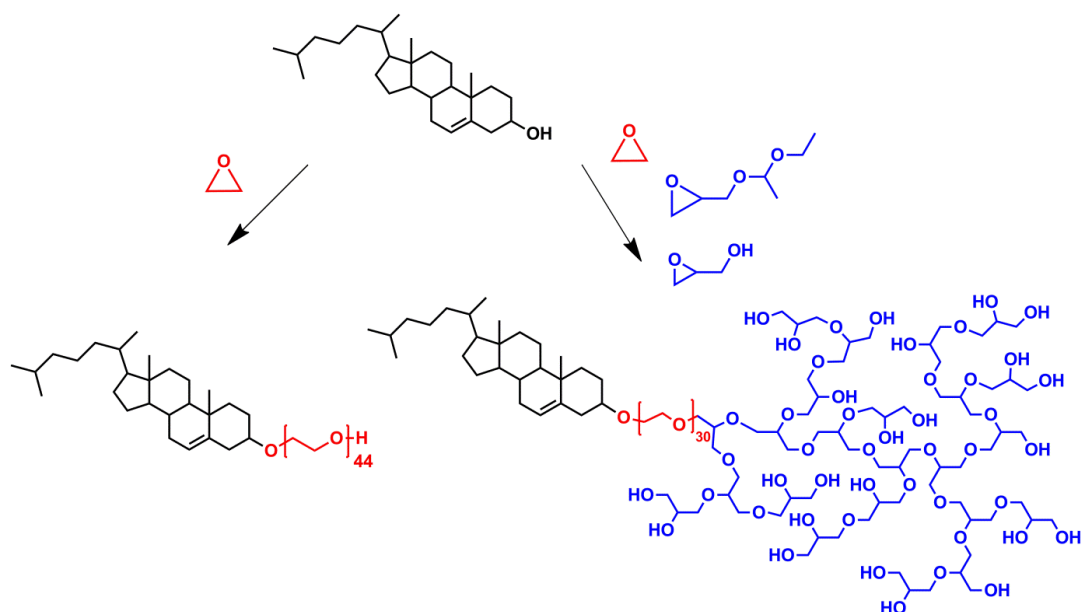

Figure 2: Molecular structures of the cholesteryl-amphiphiles (Ch-PEG$_{44}$ (left) and the Ch-PEG$_{30}$-*hb*PG$_{23}$ (right)).

Liposomes were prepared *via* the thin film hydration method and extrusion technology (400 and 100 nm membranes) with different polymer/lipid ratios (Table 1). For comparison between the linear PEG polymer and the linear-hyperbranched copolymer, liposomes were separately prepared with Ch-PEG$_{44}$ and Ch-PEG$_{30}$-*hb*PG$_{23}$ in different ratios (10-30 mol%), EPC, and cholesterol, and characterized by dynamic light scattering (DLS) in isotonic salt solution.

The resulting autocorrelation functions (ACFs) are described by a sum of two exponentials (eq. 1) for the polymers (linear and hyperbranched) and the respective liposomal formulations. Here the amplitudes are defined as a_i and the decay times as $t_i = 1/(q^2 D_i)$, while q is the absolute value of the scattering vector ($q = 4\pi \sin(\theta/2)/\lambda_o$) and D_i the Brownian diffusion coefficient of component i.

$$(1) \quad g_{1,np}(t) = a_{1,np} * \exp\left(-\frac{t}{\tau_{1,np}}\right) + a_{2,np} * \exp\left(-\frac{t}{\tau_{2,np}}\right)$$

The angular dependency of the hyperbranched polymer is shown in Figure 3, yielding a z-averaged hydrodynamic radius of $<1/R_h>_z^{-1}$ = 6.7 nm in PBS buffer (GIBCO, Invitrogen). For comparison, the linear Ch-PEG$_{44}$ displayed a hydrodynamic radius of $<1/R_h>_z^{-1}$ = 7.8 nm under identical conditions (data not shown). The radii are significantly larger than expected for the respective individual polymer chains, thus implying the polymers formed small micelles. This interpretation is confirmed by the fact that measurements were conducted at a concentration of 1 mg mL^{-1}, which is well above the critical micelle concentration (CMC) of Ch-hbPG systems (CMC = 1-9 mg L^{-1}).[33]
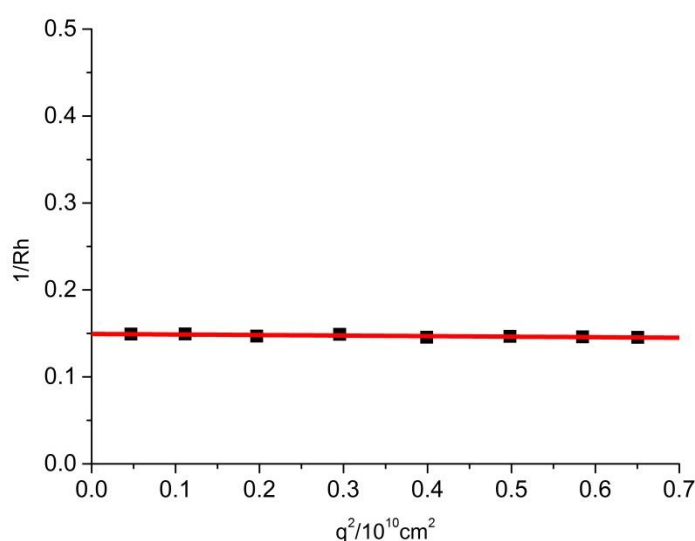

Figure 3: Angular dependency of the reciprocal hydrodynamic radius of the linear-hyperbranched polymer Ch-PEG$_{30}$-hbPG$_{23}$ (c = 1 mg mL^{-1}, PBS).

Table 2: Summary of the z-averaged hydrodynamic radii of all investigated liposomes with varying amount of polymer (0-30 mol%).

	L0	L10-*hb*PG	L10-PEG	L15-*hb*PG	L15-PEG	L20-*hb*PG	L20-PEG	L30-*hb*PG	L30-PEG
$<1/R_h>_z^{-1}$ /nm	115	97	144	81	120	96	112	102	92

The z-averaged hydrodynamic radii of all investigated liposomes with polymer contents between 0-30 mol% are summarized in Table 2. Conventional liposomes (L0) without a polymer shell showed a radius of $<1/R_h>_z^{-1}$ =115 nm. PEGylated liposomes with polymer contents between 10-30 mol% had radii between 144 nm (L10-PEG) and 92 nm (L30-

PEG), indicating that increasing the polymer content resulted in a slight decrease in the size of the structures. Liposomes containing Ch-PEG$_{30}$-hbPG$_{23}$ exhibited radii between 81 nm (L15-hbPG) and 102 nm (L30-hbPG), and a correlation between the radii and polymer content was not observed. However, the detected sizes of the liposomes are generally smaller than those with linear Ch-PEG$_{44}$, which may be attributed to a stronger effect on the liposome curvature by the bulky hyperbranched segments.

Cryo-TEM measurements of liposomes with the different polymers showed the existence of vesicular structures and the successful formation of primarily unilamellar assemblies. Figure 4 depicts the respective images for EPC/cholesterol liposomes with (15 mol% Ch-PEG$_{44}$ (B) or Ch-PEG$_{30}$-hbPG$_{23}$ (C)) or without polymer (A). The non-stabilized (conventional) liposomes formed both spherical and non-spherical vesicles, whereas sterically stabilized liposomes predominantly showed spherical vesicles with a narrower size distribution. Additionally, it was observed that the conventional liposomes tended to overlap, possibly aggregate, whereas those that were stabilized by polymers maintained spatial separation. Some vesicle preparations contained a small fraction of short rodlike structures, which could not be reproduced upon repeated preparation. Since for the goal of the present work, a small fraction of rods is not important, the formation of rodlike structures will be investigated in more detail in the near future.

Cholesterol Liposomes   15 mol% Ch-PEG$_{44}$ 15 mol% Ch-PEG$_{30}$-hbPG$_{23}$
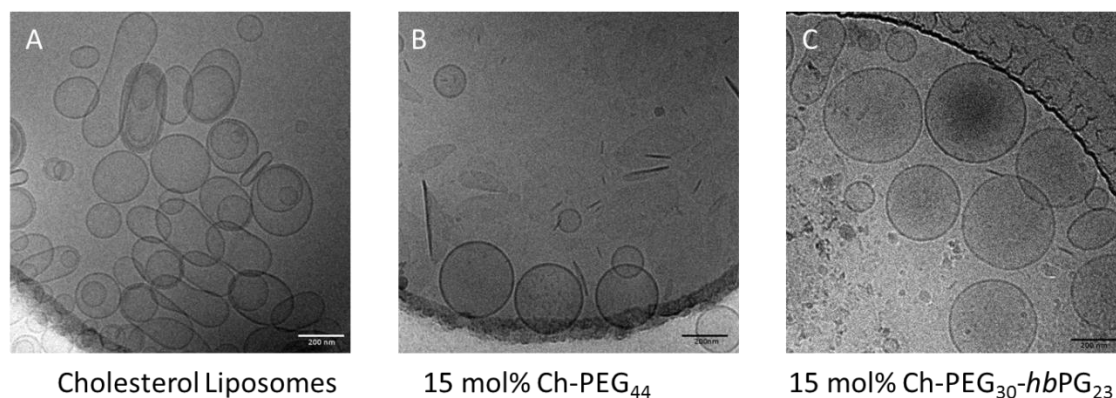
Figure 4: Cryo-TEM images of three different liposome samples. A) EPC and cholesterol (L0); B) EPC, cholesterol and 15 mol% of Ch-PEG$_{44}$ (L15-PEG); C) EPC, cholesterol and 15 mol% of Ch-PEG$_{30}$-hbPG$_{23}$ (L15-hbPG). Scale bar refers to 200 nm.

DLS of the Individual Polymer Chains and Functionalized Liposomes in Human Blood Serum

It is imperative to characterize the aggregation behavior of any potential drug carrier in human blood serum, so polymers (linear and hyperbranched) and functionalized liposomes were analyzed by DLS. In this case, the electric field autocorrelation functions of the complex mixture of proteins and other components in human serum is given by the sum of three exponentials (eq. 2):

(2) $\qquad g_{1,s}(t) = a_{1,s} * \exp\left(-\dfrac{t}{\tau_{1,s}}\right) + a_{2,s} * \exp\left(-\dfrac{t}{\tau_{2,s}}\right) + a_{3,s} * \exp(-\dfrac{t}{\tau_{3,s}})$

Through the use of the correlation functions of the serum components and fit functions (eq.1) for the individual polymers and liposomes it was possible to analyze the aggregation characteristics for mixtures of these materials in serum. If minimal aggregation takes place then ideally the resulting ACF of the serum/liposome or polymer mixtures should be fitted by the sum of the individual correlation functions. Since the known parameters of the different components are fixed, the only fit parameters are the intensity contributions of serum (f_s) and liposome or polymer (f_{np}) as seen in eq. 3.

(3) $\qquad\qquad g_{1,m}(t) = f_s g_{1,s}(t) + f_{np} g_{1,np}(t)$

However, if aggregation is observed due to interactions within the different mixtures eq. 3 must be modified, which is typically accounted for with an additional, longer ACF relaxation time related to the size of these aggregates (eq. 4). Here f_{agg} is the intensity contribution of the aggregates and their unknown relaxation times are given by $\tau_{1,agg}$, which leads to eq. 5.

(4) $\qquad\qquad g_{1,m}(t) = f_s g_{1,s}(t) + f_{np} g_{1,np}(t) + f_{agg} g_{1,agg}(t)$

(5) $\qquad\qquad g_{1,agg} = a_{1,agg} * \exp(-\dfrac{t}{\tau_{1,agg}})$

The relative intensity contribution (I) of the components can be described as shown in eq. 6 exemplarily for the aggregates. Thus, by adapting these equations we can define the relative intensity contribution of the components in the presence of aggregates by eq. 6.

(6) $\qquad\qquad I_{agg} = f_{agg}/(f_{agg}+f_S+f_{np})$

It should be noted that this method is especially sensitive for the detection of aggregates which are larger than the largest species in either the serum or pure liposome solution. It is only possible to detect additional sizes in the serum/polymer or liposome mixture if the intensity fractions (*i. e.* amplitudes) of the newly formed complexes surpass the detection limit for DLS. In detail, intensity fractions between 3% (for sizes outside the size range of the original components) and 20% (for sizes in the size range of the original components) of newly formed particles are necessary to be detected by the described fitting procedure.[52]

First, the aggregation behavior of the individual polymers (linear and hyperbranched) in human blood serum was studied, since there may be free polymer in the liposome samples post formation or liposome degradation may take place *in vivo*. As shown in Figure 5a the mixture of $Ch\text{-}PEG_{44}$ micelles and human serum does not meet the necessary requirements to simply use a combination of the ACFs of the single components, meaning that interactions between the polymer and serum components resulted in aggregation. DLS analysis showed the development of aggregates in the size range of $R_{h,Agg}$ $Ch\text{-}PEG_{44}$ = 151 nm.
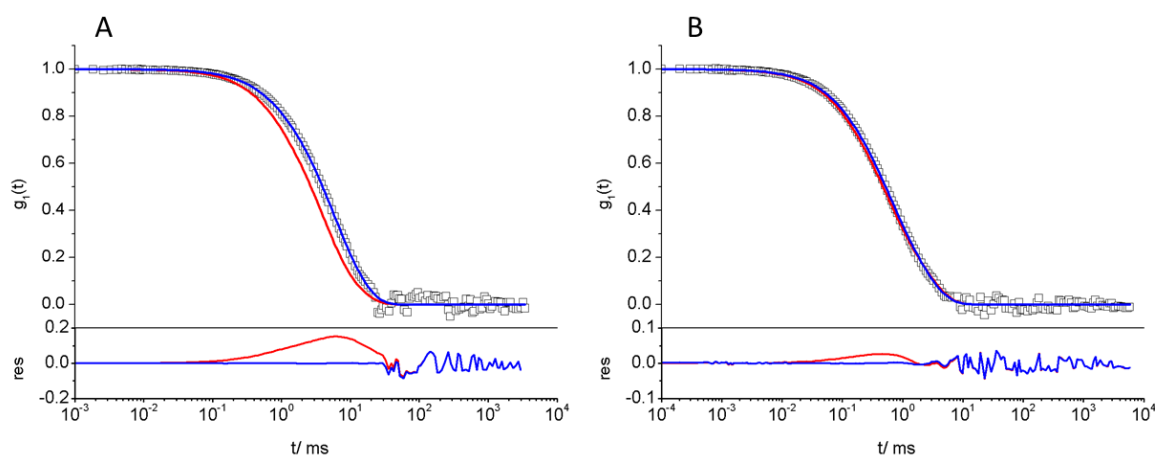
Figure 5: (A) ACF of $Ch\text{-}PEG_{44}$ micelles in serum red line, fit with eq. 3 and the resulting residue, blue line, fit with eq. 4 and the resulting residue □ data points of the ACF. Scattering angle 60°; (B) ACF of the hyperbranched polymer micelles in serum red line, fit with eq. 3 and the resulting residue, blue line, fit with eq. 4 and the resulting residue □ data points of the ACF. Scattering angle 60°.

Furthermore, the $Ch\text{-}PEG_{30}\text{-}hbPG_{23}$ micelle/serum mixture met the prerequisite conditions to be described by eq 4. In the $Ch\text{-}PEG_{30}\text{-}hbPG_{23}$ case there was a $R_{h,Agg,Ch\text{-}PEG30\text{-}hbPG23}$ = 60 nm with an intensity contribution from aggregates of $I_{Agg,PG}$ = 17%

observed, compared to $R_{h,Agg\ Ch\text{-}PEG44}$ = 151 nm with $I_{Agg,PEG}$ = 37% for the linear PEG example. The complete correlation function of the Ch-PEG$_{44}$ micelle serum mixture was clearly shifted to longer correlation times, indicating larger sizes, while the correlation function of the Ch-PEG$_{30}$-hbPG$_{23}$ micelle serum mixture showed no significant shift (see Figure 5b). These results indicate a much stronger aggregation of Ch-PEG$_{44}$ in comparison to Ch-PEG$_{30}$-hbPG$_{23}$, which might be explained by the high density of hydrophilic groups at the hyperbranched polymer that prevent the interaction between the cholesterol anchor and hydrophobic components of serum. Similar studies were carried out to compare mixtures of human serum with liposomes containing Ch-PEG$_{44}$ (10-30 mol%; L10-PEG, L15-PEG, L20-PEG, L30-PEG) versus Ch-PEG$_{30}$-hbPG$_{23}$ (10-30 mol%; L10-hbPG, L15-hbPG, L20-hbPG, L30-hbPG), and liposomes consisting of just EPC and cholesterol (L0) as a control. Since the investigation of the control sample did not result in consistent, reproducible aggregation values and cryo-TEM images depicted inhomogeneous vesicles, the data is not shown here. In any case, these conventional types of liposomes are known to reveal low colloidal stability and are usually not used in drug-delivery applications.

Table 3 summarizes the radii for the free polymers and sterically stabilized liposomes with either Ch-PEG$_{44}$ or Ch-PEG$_{30}$-hbPG$_{23}$ in human blood serum. There is aggregation for the PEGylated liposomes when they are introduced into human blood serum with an $R_{h,Agg}$ = 330 nm (10 mol% lipid), but the size of the aggregates decreased (170 nm) as the amount of Ch-PEG$_{44}$ (30 mol %) was increased. These values are much smaller than those for unmodified liposomes which formed macroscopic aggregates and demonstrated the stabilizing and shielding effects of the Ch-PEG$_{44}$ on the assemblies. Yet, liposomes stabilized with Ch-PEG$_{30}$-hbPG$_{23}$ showed an even better result when mixed with human blood serum, where the liposomes had no significant increase in their size in DLS. Figure 6 (Ch-PEG$_{44}$ liposomes) and Figure 7 (Ch-PEG$_{30}$-hbPG$_{23}$ liposomes) give an overview of the multicomponent analysis of the different investigated mixtures. It has to be noted that the aggregates detected are results of liposome protein bridging and cannot be explained by just a monolayer of proteins on the liposome surface. The total increase of the hydrodynamic radius with a thin protein corona would be too small to be detectable via DLS.

Table 3: Radii of liposomes containing different amounts of Ch-PEG$_{44}$/ Ch-PEG$_{30}$-*hb*PG$_{23}$ and radii of the pure polymers in buffer solution. Obtained radii of aggregates found in the mixture of the different formulations and human serum. Relative intensity contribution (I$_{Agg}$) of the aggregates in the mixture at a scattering angle of 64°.

Sample	$<1/R_h>_z^{-1}$ /nm	R_h/nm [a]	I$_{Agg}$/%[a]
Ch-PEG$_{44}$	7.8	151	37
L10-PEG	144	330	23
L15-PEG	120	206	22
L20-PEG	112	287	28
L30-PEG	92	170	15
Ch-PEG$_{30}$-*hb*PG$_{23}$	6.7	60	17
L10-*hb*PG	97	-	-
L15-*hb*PG	81	-	-
L20-*hb*PG	96	-	-
L30-*hb*PG	102	-	-

[a] scattering angle 64°.
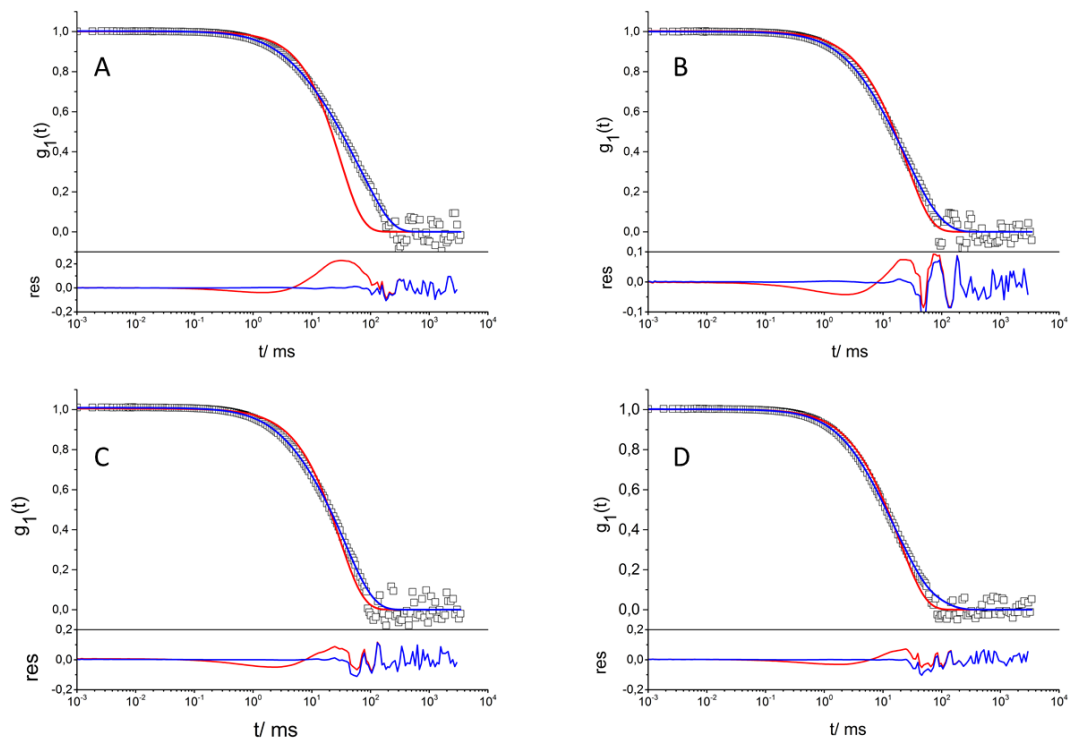
Figure 6: Liposomes containing Ch-PEG$_{44}$ in human serum: (A) L10-PEG, (B) L15-PEG, (C) L20-PEG, (D) L30-PEG in human serum, red line, fit with eq. 3 and the resulting residue. blue line fit with eq. 4 and resulting residue □ data points of the ACF. Scattering angle 30°.
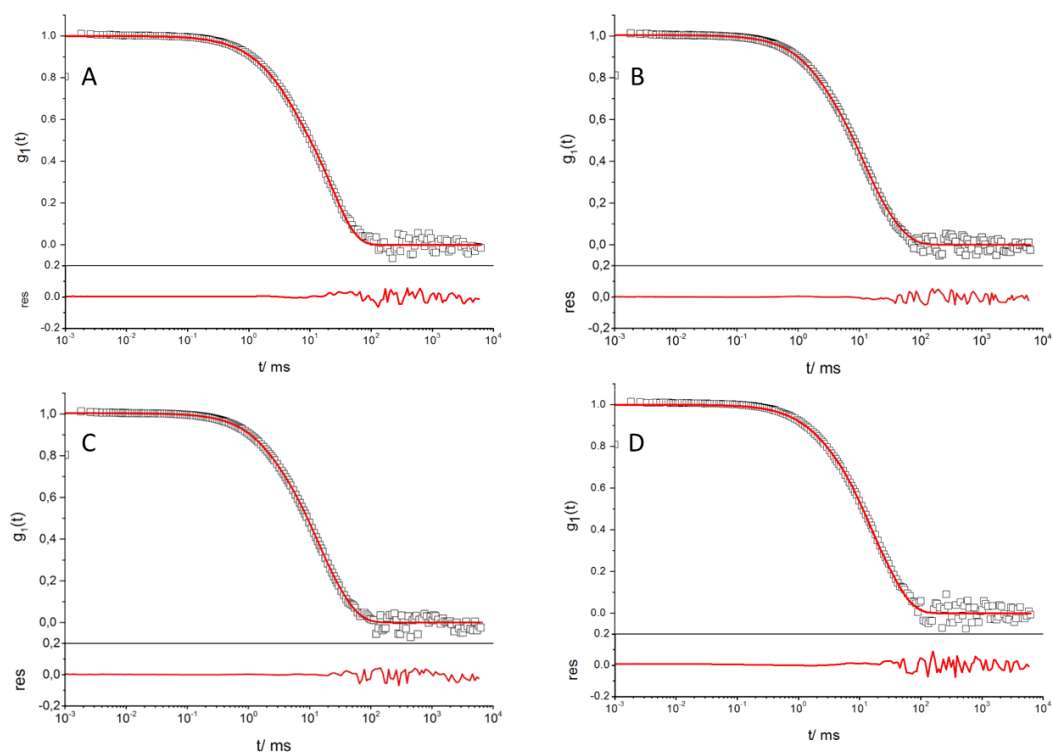
Figure 7: Liposomes containing Ch-PEG$_{30}$-*hb*PG$_{23}$ in human serum: (A) L10-*hb*PG, (B) L15-*hb*PG, (C) L20-*hb*PG, (D) L30-*hb*PG in human serum, red line, fit with eq. 3 and the resulting residue. □ data points of the ACF. Scattering angle 30°.

Conclusion

For the first time, the interaction between sterically stabilized liposomes and human blood serum was investigated via dynamic light scattering (DLS). This technique is a very sensitive method for the detection of aggregrates and provides an efficient tool to monitor their formation, when polymer drug-delivery systems come into contact with complex biological media. In this work, we investigated the behavior of two different kinds of sterically stabilized liposomes, containing either cholesterol-PEG$_{44}$ or linear-hyperbranched cholesterol-PEG$_{30}$-*hb*PG$_{23}$ with contents between 10-30 mol%, EPC, and cholesterol. The systems were compared concerning their aggregation profile in blood serum. Liposomes containing Ch-PEG$_{44}$ led to the formation of aggregates in the size range between 170 nm to 330 nm (R$_h$), depending on the polymer amount, while the Ch-PEG$_{30}$-*hb*PG$_{23}$ modified liposomes were stable against aggregation despite the polymer

content. Here, the adsorption of plasma proteins is assumed to be less likely due to the dense packing and multiple hydroxyl groups. Our results show the potential steric stabilizing effect of the novel, hyperbranched polyether lipids. Thus, based on the ability of hyperbranched polyethers to minimize interactions between lipososomes and human blood serum, we have demonstrated their relevance and potential advantages as drug delivery systems. Amphiphilic hyperbranched structures constitute a promising alternative to PEGylated "stealth" liposomes while showing favorable behavior in blood serum and introducing multiple functional groups on the vesicles' surfaces.

Acknowledgments

References

(1)   Gregoria, G.; Wills, E. J.; Swain, C. P.; Tavill, A. S. Drug-carrier potential of liposomes in cancer chemotherapy. *Lancet* **1974,** *1* (7870), 1313–1316.

(2)   Sharma, A.; Sharma, U. S. Liposomes in drug delivery: progress and limitations. *Int. J. Pharm.* **1997,** *154* (2), 123–140.

(3)   Lian, T.; Ho, R. J. Y. Trends and developments in liposome drug delivery systems. *J. Pharm. Sci.* **2001,** *90* (6), 667–680.

(4)   Maeda, H.; Wu, J.; Sawa, T.; Matsumura, Y.; Hori, K. Tumor vascular permeability and the EPR effect in macromolecular therapeutics: a review. *J. Control. Release* **2000,** *65*, 271–284.

(5)   Duncan, R. The dawning era of polymer therapeutics. *Nat Rev Drug Discov* **2003,** *2* (5), 347–360.

(6)   Maeda, H.; Seymour, L. W.; Miyamoto, Y. Conjugates of anticancer agents and polymers - Advantages of macromolecular therapeutics in vivo. *Bioconjugate Chem.* **1992,** *3* (5), 351–362.

(7)   Lammers, T.; Hennink, W. E.; Storm, G. Tumour-targeted nanomedicines: principles and practice. *British Journal of Cancer* **2008,** *99* (3), 392–397.

(8)   Allen, T. M.; Chonn, A. Large unilamellar liposomes with low uptake into the reticuloendothelial system. *FEBS Lett.* **1987,** *223* (1), 42–46.

(9)   Woodle, M. C.; Lasic, D. D. Sterically stabilized liposomes. *Biochim. Biophys. Acta* **1992,** *1113* (2), 171–199.

(10)   Lasic, D. D.; Papahadjopoulos, D. Liposomes revisited. *Science* **1995,** *267* (5202), 1275–1276.

(11)   Immordino, M. L.; Dosio, F.; Cattel, L. Stealth liposomes: review of the basic science, rationale, and clinical applications, existing and potential. *Int. J. Nanomed.* **2006,** *1* (3), 297–315.

(12)   Allen, T. M.; Hansen, C.; Martin, F.; Redemann, C.; Yau-Young, A. Liposomes containing synthetic lipid derivatives of poly(ethylene glycol) show prolonged circulation half-lives in vivo. *Biochim. Biophys. Acta* **1991,** *1066* (1), 29–36.

(13)   Woodle, M. C.; Matthay, K. K.; Newman, M. S.; Hidayat, J. E.; Collins, L. R.; Redemann, C.; Martin, F. J.; Papahadjopoulos, D. Versatility in lipid compositions showing prolonged circulation with sterically stabilized liposomes. *Biochim. Biophys. Acta* **1992,** *1105* (2), 193–200.

(14)   Torchilin, V. P.; Omelyanenko, V. G.; Papisov, M. I.; Bogdanov, A. A.; Trubetskoy, V. S.; Herron, J. N.; Gentry, C. A. Poly(ethylene glycol) on the liposome surface: On the mechanism of polymer-coated liposome longevity. *Biochim. Biophys. Acta* **1994,** *1195* (1), 11–20.

(15)   Blume, G.; Cevc, G. Liposomes for the sustained drug release in vivo. *Biochim. Biophys. Acta* **1990,** *1029* (1), 91–97.

(16)   Needham, D.; McIntosh, T. J.; Lasic, D. D. Repulsive interactions and mechanical stability of polymer-grafted lipid membranes. *Biochim. Biophys. Acta* **1992,** *1108* (1), 40–48.

(17)   Allen, T. M. The use of glycolipids and hydrophilic polymers in avoiding rapid uptake of liposomes by the mononuclear phagocyte system. *Adv. Drug Deliv. Rev.* **1994,** *13* (3), 285–309.

(18) Cabanes, A.; Tzemach, D.; Goren, D.; Horowitz, A. T.; Gabizon, A. Comparative study of the antitumor activity of free doxorubicin and polyethylene glycol-coated liposomal doxorubicin in a mouse lymphoma model. *Clin. Cancer Res.* **1998,** *4* (2), 499–505.

(19) Torchilin, V. P. Recent advances with liposomes as pharmaceutical carriers. *Nat. Rev. Drug Discov.* **2005,** *4* (2), 145–160.

(20) Lasic, D. D. Doxorubicin in sterically stabilized liposomes. *Nature* **1996,** *380* (6574), 561–562.

(21) Allen, T. M.; Murray, L.; Mackeigan, S.; Shah, M. Chronic liposome administration in mice- Effects on reticuloendothelial function and tissue distribution. *Journal of Pharmacology and Experimental Therapeutics* **1984,** *229* (1), 267–275.

(22) Chonn, A.; Semple, S. C.; Cullis, P. R. Association of blood proteins with large unilamellar liposomes in vivo- Relation to circulation lifetimes. *J. Biol. Chem.* **1992,** *267* (26), 18759–18765.

(23) Semple, S. C.; Chonn, A.; Cullis, P. R. Interactions of liposomes and lipid-based carrier systems with blood proteins: Relation to clearance behaviour in vivo. *Adv. Drug Deliv. Rev.* **1998,** *32,* 3–17.

(24) Aggarwal, P.; Hall, J. B.; McLeland, C. B.; Dobrovolskaia, M. A.; McNeil, S. E. Nanoparticle interaction with plasma proteins as it relates to particle biodistribution, biocompatibility and therapeutic efficacy. *Adv. Drug Deliv. Rev.* **2009,** *61* (6), 428–437.

(25) Liu, Z.; Jiao, Y.; Wang, T.; Zhang, Y.; Xue, W. Interactions between solubilized polymer molecules and blood components. *Journal of Controlled Release* **2012,** *160* (1), 14–24.

(26) Mahon, E.; Salvati, A.; Baldelli Bombelli, F.; Lynch, I.; Dawson, K. A. Designing the nanoparticle-biomolecule interface for "targeting and therapeutic delivery". *J. Control. Release* **2012,** *161* (2), 164–174.

(27) Salvati, A.; Pitek, A. S.; Monopoli, M. P.; Prapainop, K.; Bombelli, F. B.; Hristov, D. R.; Kelly, P. M.; Åberg, C.; Mahon, E.; Dawson, K. A. Transferrin-functionalized nanoparticles lose their targeting capabilities when a biomolecule corona adsorbs on the surface. *Nat Nanotechnol* **2013,** *8* (2), 137–143.

(28) Mohr, K.; Sommer, M.; Baier, G.; Schöttler, S.; Okwieka, P.; Tenzer, S.; Landfester, K.; Mailänder, V.; Schmidt, M.; Meyer, R. G. Aggregation Behavior of Polystyrene-Nanoparticles in Human Blood Serum and its Impact on the in vivo Distribution in Mice. *J. Nanomed. Nanotechnol.* **2014,** *05* (02).

(29) Pitek, A. S.; O'Connell, D.; Mahon, E.; Monopoli, M. P.; Baldelli Bombelli, F.; Dawson, K. A. Transferrin coated nanoparticles: study of the bionano interface in human plasma. *PLoS ONE* **2012,** *7* (7), e40685.

(30) Lasic, D. D.; Martin, F. J.; Gabizon, A.; Huang, S. K.; Papahadjopoulos, D. Sterically stabilized liposomes: A hypothesis on the molecular origin of the extended circulation times. *Biochim. Biophys. Acta* **1991,** *1070* (1), 187–192.

(31) Rausch, K.; Reuter, A.; Fischer, K.; Schmidt, M. Evaluation of Nanoparticle Aggregation in Human Blood Serum. *Biomacromolecules* **2010,** *11* (11), 2836–2839.

(32) Hofmann, A. M.; Wurm, F.; Hühn, E.; Nawroth, T.; Langguth, P.; Frey, H. Hyperbranched Polyglycerol-Based Lipids via Oxyanionic Polymerization: Toward Multifunctional Stealth Liposomes. *Biomacromolecules* **2010,** *11* (3), 568–574.

(33) Hofmann, A. M.; Wurm, F.; Frey, H. Rapid Access to Polyfunctional Lipids with Complex Architecture via Oxyanionic Ring-Opening Polymerization. *Macromolecules* **2011,** *44* (12), 4648–4657.

(34) Kainthan, R. K.; Gnanamani, M.; Ganguli, M.; Ghosh, T.; Brooks, D. E.; Maiti, S.; Kizhakkedathu, J. N. Blood compatibility of novel water soluble hyperbranched polyglycerol-based multivalent cationic polymers and their interaction with DNA. *Biomaterials* **2006,** *27* (31), 5377–5390.

(35) Wilms, D.; Wurm, F.; Nieberle, J.; Böhm, P.; Kemmer-Jonas, U.; Frey, H. Hyperbranched Polyglycerols with Elevated Molecular Weights: A Facile Two-Step Synthesis Protocol Based on Polyglycerol Macroinitiators. *Macromolecules* **2009,** *42* (9), 3230–3236.

(36) Wilms, D.; Stiriba, S.-E.; Frey, H. Hyperbranched Polyglycerols: From the Controlled Synthesis of Biocompatible Polyether Polyols to Multipurpose Applications. *Acc. Chem. Res.* **2010,** *43* (1), 129–141.

(37) Calderon, M.; Quadir, M. A.; Sharma, S. K.; Haag, R. Dendritic Polyglycerols for Biomedical Applications. *Adv. Mater.* **2010,** *22* (2), 190–218.

(38) Siegers, C.; Biesalski, M.; Haag, R. Self-Assembled Monolayers of Dendritic Polyglycerol Derivatives on Gold That Resist the Adsorption of Proteins. *Chem. Eur. J.* **2004,** *10* (11), 2831–2838.

(39) Kainthan, R. K.; Zou, Y.; Chiao, M.; Kizhakkedathu, J. N. Self-Assembled Monothiol-Terminated Hyperbranched Polyglycerols on a Gold Surface: A Comparative Study on the Structure, Morphology, and Protein Adsorption Characteristics with Linear Poly(ethylene glycol)s. *Langmuir* **2008,** *24* (9), 4907–4916.

(40) Knop, K.; Hoogenboom, R.; Fischer, D.; Schubert, U. S. Poly(ethylene glycol) in Drug Delivery: Pros and Cons as Well as Potential Alternatives. *Angew. Chem. Int. Ed.* **2010,** *49* (36), 6288–6308.

(41) Fitton, A. O.; Hill, J.; Jane, D. E.; Millar, R. Synthesis of simple oxetane carrying reactive 2-substituents. *Synthesis* **1987,** *12*, 1140–1142.

(42) Zhao, X. B.; Muthusamy, N.; Byrd, J. C.; Lee, R. J. Cholesterol as a bilayer anchor for PEGylation and targeting ligand in folate-receptor-targeted liposomes. *J. Pharm. Sci.* **2007,** *96* (9), 2424–2435.

(43) Peng, X.; Hofmann, A. M.; Reuter, S.; Frey, H.; Kressler, J. Mixed layers of DPPC and a linear poly(ethylene glycol)-b-hyperbranched poly(glycerol) block copolymer having a cholesteryl end group. *Colloid and Polymer Science* **2012,** *290* (7), 579–588.

(44) Rao, Z.; Taguchi, T. Spectroscopic studies on interactions between cholesterol-end capped polyethylene glycol and liposome. *Colloids and Surfaces B: Biointerfaces* **2012,** *97,* 248–253.

(45) Fritz, T.; Hirsch, M.; Richter, F. C.; Müller, S. S.; Hofmann, A. M.; Rusitzka, K. A.; Markl, J.; Massing, U.; Frey, H.; Helm, M. Click Modification of Multifunctional Liposomes Bearing Hyperbranched Polyether Chains. *Biomacromolecules* **2014,** *15*, 2440–2448.

(46) Schöps, R.; Amado, E.; Müller, S. S.; Frey, H.; Kressler, J. Block copolymers in giant unilamellar vesicles with proteins or with phospholipids. *Faraday Discussions* **2013,** 166, 303–315.

(47)   Müller, S. S.; Dingels, C.; Hofmann, A. M.; Frey, H. Polyether-Based Lipids Synthesized with an Epoxide Construction Kit: Multivalent Architectures for Functional Liposomes. *Tailored Polymer Architectures for Pharmaceutical and Biomedical Applications*; ACS Symposium Series; American Chemical Society, 2013; pp 11–25.

(48)   Wurm, F.; Nieberle, J.; Frey, H. Double-hydrophilic linear-hyperbranched block copolymers based on poly(ethylene oxide) and poly(glycerol). *Macromolecules* **2008,** *41* (4), 1184–1188.

(49)   Wurm, F.; Nieberle, J.; Frey, H. Synthesis and Characterization of Poly(glyceryl glycerol) Block Copolymers. *Macromolecules* **2008,** *41* (6), 1909–1911.

(50)   Owens, D. E.; Peppas, N. A. Opsonization, biodistribution, and pharmacokinetics of polymeric nanoparticles. *Int. J. Pharm.* **2006,** *307* (1), 93–102.

(51)   Shi, B.; Fang, C.; Pei, Y. Stealth PEG-PHDCA niosomes: Effects of chain length of PEG and particle size on niosomes surface properties, in vitro drug release, phagocytic uptake, in vivo pharmacokinetics and antitumor activity. *J. Pharm. Sci.* **2006,** *95* (9), 1873–1887.

(52)   Hemmelmann, M.; Mohr, K.; Fischer, K.; Zentel, R.; Schmidt, M. Interaction of pHPMA-pLMA copolymers with human blood serum and its components. *Mol. Pharm.* **2013,** *10*, 3769–3775.

4.2 Characterization of Polyether-Lipids in Stealth Liposomes by ^{18}F-TEG-N₃ Click Radiolabeling and Positron Emission Tomography

Achim T. Reibel,[1,§] Sophie S. Müller,[2,3,§] Stefanie Pektor,[4] Nicole Bausbacher,[4] Matthias Miederer,[4] Holger Frey,[2] and Frank Rösch[1]

[1] Institute of Nuclear Chemistry, Johannes Gutenberg University Mainz, Fritz-Strassmann-Weg 2, 55128 Mainz, Germany
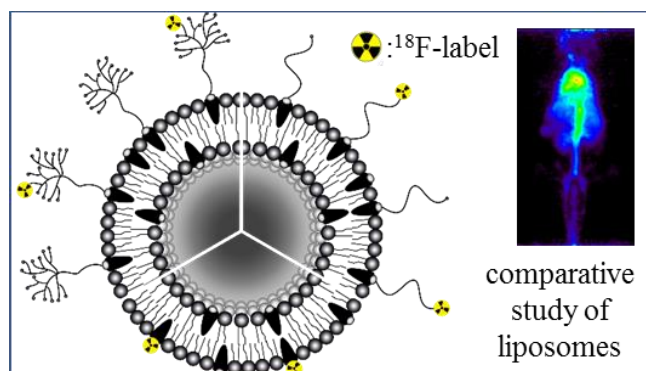
[2] Institute of Organic Chemistry, Johannes Gutenberg University Mainz, Duesbergweg 10-14, 55128 Mainz, Germany.

[3] Graduate School MAINZ, Staudingerweg 9, 55128 Mainz, Germany.

[4] Clinic for Nuclear Medicine, University Medical Center Mainz, Langenbeckstraße 1, 55101 Mainz, Germany

[§] both authors contributed equally

Abstract

"Stealth" liposomes play an important role in drug-delivery applications, due to long-circulation times and passive tumor accumulation. In this study, linear PEG and novel linear-hyperbranched polyglycerol (*hb*PG) cholesterol lipids were investigated in liposome formulations and systematically compared with regards to their

biodistribution. The polymers were functionalized with alkyne groups and rapidly labeled with [^{18}F]F-TEG-N$_3$ via click-chemistry. Organ uptake was followed by positron emission tomography (PET) for 1 h and *ex vivo* biodistribution for the polymers (polymer micelles) or the respective liposome formulations. For Ch-PEG$_{27}$-triazole-TEG-^{18}F 20 mol% polymer was incorporated and these liposomes revealed a diameter of 92 nm. Ch-PEG$_{30}$-*hb*PG$_{24}$-triazole-TEG-^{18}F was used in 5 mol% and 20 mol% in liposome formulations having diameters of 166 nm and 172 nm, respectively. For comparison, cholesterol was directly labeled with [^{18}F]F$^-$ and conventional liposomes with a diameter of 408 nm have also been studied. The results revealed fast uptake of the conventional liposomes by the liver, spleen, and lung. Polymer micelles were excreted from the blood stream via the kidney due to their hydrophilic character and low molecular weights. Most importantly, the novel sterically stabilized liposomes showed similar behavior to the PEG shielded vesicles considering spleen and liver uptake and retention in blood with the advantage of multifunctionality and a better blood to liver and blood to lung ratio.

Introduction

Liposomes are spherical vesicles that consist of a phospholipid bilayer. Such systems have been intensively investigated as drug delivery vehicles with good results.[1,2] Conventional liposomes suffer from fast removal of the mononuclear phagocyte system (MPS) via macrophages and uptake in liver and spleen which minimizes the *in vivo* circulation time. Key factors influencing the opsonization process, i.e., binding of an opsonin for marking a pathogen for ingestion and phagocytosis, include liposome size, composition and charges.[3] To overcome this drawback, poly(ethylene glycol) (PEG) is used as a stabilizing polymer coating.[4,5] PEG is covalently linked to cholesterol or phospholipids to ensure hydrophobic anchoring in the lipid bilayer. This protective, hydrophilic polymer layer prevents opsonin adsorption via steric repulsion.[6] Prolonged blood circulation times, reduced MPS uptake, reduced aggregation in serum, and better (storage) stability are the main advantages of the so-called "stealth" liposomes. Nevertheless, the "gold standard" PEG suffers from disadvantages such as its non-

biodegradability, possible degradation under stress and potentially toxic side-products, as well as hypersensitivity in some cases.[7] The main drawback of this polymer, however, is its lack of functional groups (especially when methoxyPEG is used). Promising alternatives are highly water-soluble polymers such as poly(vinyl pyrrolidone),[8] poly(acryl amide),[8] poly(2-oxazoline),[9] and hyperbranched polyglycerol (*hb*PG). In particular, it has been shown that *hb*PG reveals enhanced protein repulsion compared to PEG.[10,11] Additionally, the branched structure renders the polymer even more bulky and more hydrophilic due to the multiple hydroxyl groups. Recently, our group presented a synthetic approach for linear-hyperbranched polyether lipids. Using cholesterol directly as the initiator for the oxyanionic ring-opening polymerization (ROP) of various epoxides, different architectures and a tunable number of hydroxyl groups are achievable. A combination of ethylene oxide (EO), ethoxyethyl glycidyl ether (EEGE), isopropylidene glyceryl glycidyl ether (IGG), and glycidol make a vast variety of linear and branched architectures available.[12,13] Cholesterol-initiated linear-hyperbranched amphiphiles combine the advantageous properties of PEG and the polyfunctionality of polyglycerol with cholesterol as a natural membrane component.[14,15] The hydroxyl groups play an important role when it comes to functionalization with markers, antibodies for "active" targeting, or radiolabels, as shown in this article.

Liposomes labeled with radioisotopes (^{99m}Tc, ^{186}Re, ^{67}Ga, ^{111}In, ^{64}Cu, ^{18}F)[16-22] were previously investigated to study the biodistribution of various types of liposomes.[23] In general, single photon emission computed tomography (SPECT) and positron emission tomography (PET) can be used for *in vivo* visualization with the known advantages of PET like the possibility of quantification and better spatial and temporal resolution. Incorporation of ^{18}F into long-circulating liposomes was achieved by the encapsulation of 2-[^{18}F]-2-fluoro-2-deoxy-D-glucose (2-[^{18}F]FDG) during liposome formation.[24,25] Encapsulation efficiency was around 10%.[26,27] Direct ^{18}F labelling of 3-tosyl-1,2-dipalmitoyl glycerol by Ferrara and coworkers led to [^{18}F]fluorodipalmitin ([^{18}F]FDP), which was incorporated into the phospholipid bilayer.[28] The amphiphilic compound 1-[^{18}F]fluoro-3,6-dioxatetracosane was also used for *in vivo* trafficking of liposomes using PET as a noninvasive real-time imaging system.[29] In a recent work, Reiner and coworkers addressed limitations in creating targeted liposomes and the challenges for imaging,[30] where [^{18}F]FDP served as the radiolabeled lipid. The reaction between tetrazine in the

treated tumor tissue and *trans*-cyclooctene on the liposome surface was employed for bioorthogonal conjugation and *in vivo* click-chemistry. ^{18}F-Radiolabeled liposomes showed a significantly increased uptake in tetrazine-rich tumors. The synthesis of a ^{18}F-labeled cholesteryl ether lipid was recently presented by Jensen *et al.* who demonstrated another method for the visualization of radiolabeled liposomes.[31]

Although ^{18}F is a rather short-lived radionuclide ($t_{1/2}$ = 109.7 min) it combines ideal nuclear characteristics for PET imaging with not affecting the polymer structure, neither in size nor in charge.[32] This tool supports the study of initial biodistribution directly after application and excretion patterns and serves as a screening platform for potential drug delivery systems. It allows the general investigation of different liposome formulations and polymer structures regarding blood concentration, tumor, or MPS uptake.

In the present work, we focus on the investigation of multifunctional hyperbranched cholesterol-lipids in comparison with PEGylated liposomes and non-PEGylated (conventional) liposomes (Figure 1). The polyether-based lipids were functionalized with alkyne groups by the attachment of propargyl bromide to the hyperbranched polyglycerol block in a postpolymerization reaction.[13] In the case of the linear PEG analogue, propargyl bromide was used as the end-capping agent in the oxyanionic ROP of EO (Scheme 1). The copper-catalyzed azide-alkyne click reaction (CuAAC) was employed for the attachment of the radiolabeled synthon 1-azido-2(2-(2-[^{18}F]fluoroethoxy)ethoxy)ethane ([^{18}F]F-TEG-N$_3$). Compared to other investigations on sterically stabilized liposomes using PET, the main advantage of the chosen strategy is the labeling of the polymer structure itself that actually shields the liposome. Integration of the shielding polymer into the liposome membrane can be proven by this method which is not possible by using another probe. PET and *ex vivo* biodistribution studies allowed the investigation of both polymers and liposome formulations in mice.
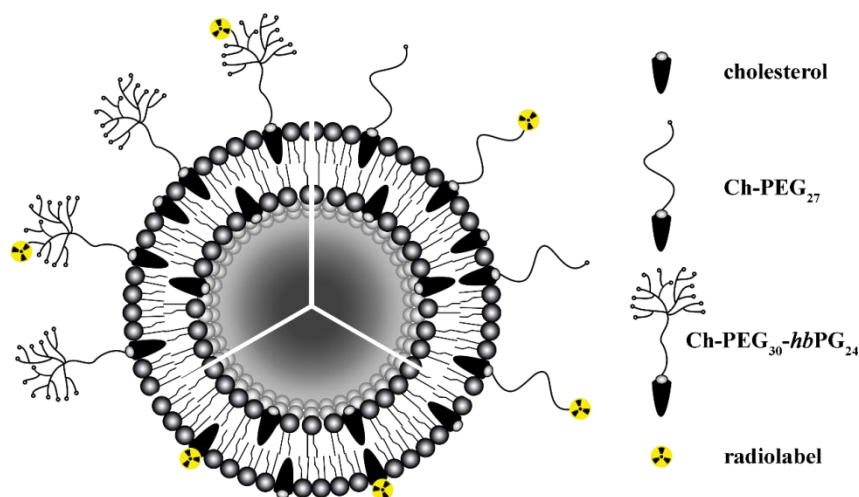
Figure 1: Schematic image of three different types of lipids incorporated in liposomes studied in this work: labeled cholesterol, linear poly(ethylene glycol) with a cholesterol anchor (Ch-PEG$_{27}$-CH$_2$-C≡CH) and linear-hyperbranched polyether-based lipids (Ch-PEG$_{30}$-*hb*PG$_{24}$-CH$_2$-C≡CH); all compounds were labeled with fluorine-18 for PET measurements.

Results and Discussion

Polymer synthesis and radioactive labeling with [^{18}F]fluorine via CuAAC-reaction

This work aims at a study of the *in vivo* behavior and biodistribution of liposomes, which are sterically stabilized by two fundamentally different polymer structures. Poly(ethylene glycol) (PEG) with a cholesterol anchor and linear-hyperbranched polyglycerol (PEG-*hb*PG) with a cholesterol anchor group have been investigated. Both polymers differ in the number of hydroxyl groups and the polymer architecture (linear vs. linear-hyperbranched, Figure 2). The polyether-based amphiphiles were synthesized according to the literature, using cholesterol as a hydrophobic initiator for the oxyanionic ring-opening polymerization of a combination of epoxides.[12-14] The molecular weights were chosen to be between 1500-3500 g mol^{-1} which is usually applied in sterically stabilized liposomes.[33] The renal threshold for PEG is known to be around $M_w < 40\,000$ g mol^{-1}, so fast excretion of the presented lipids from the body is assumed.[34] Polymers with higher M_w exhibit larger hydrodynamic volume and consequently may accumulate in the liver and spleen.

In order to attach the positron emitter fluorine-18 ($t_{1/2}$ = 109.7 min) to the polyether backbone, the polymers were functionalized with propargyl bromide. 1-azido-2(2-(2-

[^{18}F]fluoroethoxy)ethoxy)ethane ([^{18}F]F-TEG-N$_3$, (**8**)) was used as the synthon for click-chemistry which made both *ex vivo* organ distribution measurements as well as µPET imaging of the polymers possible. For the hyperbranched polymer Ch-PEG$_{30}$-*hb*PG$_{24}$-CH$_2$-C≡CH the general synthesis and functionalization was already published by our group.[13,35] The number of alkyne groups can be tailored by the amount of propargyl bromide used, albeit a statistical distribution at the polymer chain is inevitable. From ^{1}H NMR spectroscopy 1-2 alkyne groups per polymer chain were calculated. The linear analogue was prepared by the oxyanionic ring-opening polymerization of ethylene oxide (EO) using cholesterol as an initiator. Direct end-capping of the oxyanion with propargyl bromide led to the functionalized Ch-PEG$_{27}$-CH$_2$-C≡CH (**1**) polymer (Scheme 1).
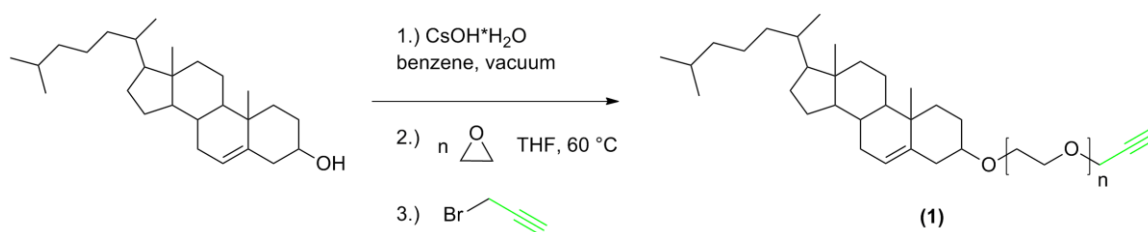

Scheme 1. Reaction scheme for the synthesis of Ch-PEG$_{27}$-CH$_2$-C≡CH (**1**) using cholesterol as an initiator for the ring-opening polymerization of ethylene oxide (EO).

Both polymers were characterized by ^{1}H NMR spectroscopy and size exclusion chromatography (SEC). Ch-PEG$_{27}$-CH$_2$-C≡CH (**1**) revealed a molecular weight of $M_{n,NMR}$ = 1600 g mol^{-1} and a narrow molecular weight distribution of M_w/M_n = 1.13 ($M_{n,SEC}$ = 1500 g mol^{-1}). The molecular weight of Ch-PEG$_{30}$-*hb*PG$_{24}$-CH$_2$-C≡CH (**2**) was $M_{n,NMR}$ = 3520 g mol^{-1} (calculated by ^{1}H NMR spectroscopy) and SEC revealed a distribution of M_w/M_n = 1.14 ($M_{n,SEC}$ = 1550 g mol^{-1}). The molecular weight determined by SEC is underestimated due to the globular polymer structure and therefore smaller hydrodynamic radius compared to the SEC standard PEG. The ^{1}H NMR spectrum for the linear polyether is given in Figure S1 (Supporting Information). Furthermore, MALDI-ToF mass spectrometry was employed to confirm the introduction of cholesterol and the alkyne group on every polymer chain, which is crucial for the functionalization with the radioactive compound in the subsequent click-reaction. The spectrum can be found in the Supporting Information (Figure S2).

The synthon [^{18}F]F-TEG-N$_3$ **(8)** was prepared in a slightly modified route, based on the approach recently presented by Rokka *et al.*.[36] The synthesis was carried out in a semi-automated, custom-built modular system. Starting from a tosylate precursor the nucleophilic fluorination reaction was carried out with a good radiochemical yield (RCY) of 86%. The preparation is explained in the Experimental Section, and the reaction scheme is given in Scheme S1 (Supporting Information). The main advantages of using fluorine-18 as a PET nuclide are its outstanding physical and nuclear properties, combined with high spatial resolution. Due to its size and lack of charge, no influence on the polymer conformation and hydrodynamic properties is assumed. Furthermore, the rather small molecule [^{18}F]F-TEG-N$_3$, having a polyether backbone, is believed to be ideal for the attachment onto polyether-based lipids.

The copper-catalyzed azide-alkyne cycloaddition reaction (CuAAC) between the alkyne-functionalized polymers and the radioactive azide-compound was carried out in (ethanolic) aqueous solution with RCY of > 95% for the linear and for the linear-hyperbranched lipid. The chemical structures and the overall strategy are presented in Figure 2. Cu(I) was prepared *in situ* through the reduction of copper(II)sulfate by sodium ascorbate. During optimization of the reactions, a strong variation of yields was observed, based on the ratio of catalyst to ascorbate and on the amount of copper itself. In addition, the solvent played an important role. Phosphate buffered saline was superior to water, whereas DMSO also gave very good yields. Because of the difficulties to remove DMSO (high boiling point) subsequent to the reaction in order to form a lipid film for the liposome preparation, the solvent system of choice was PBS and EtOH. Main advantages of the rapid attachment of fluorine-18 to the polymers compared to the commonly applied strategies are i.) fast click-reaction with high yields ii.) the novel shielding polymer itself is labeled instead of lipids such as [^{18}F]FDP iii.) incorporation of the polyether-based lipid into liposomes can be directly monitored and iv.) the behavior of the polymer itself can be investigated *in vivo* to study the excretion pathway.
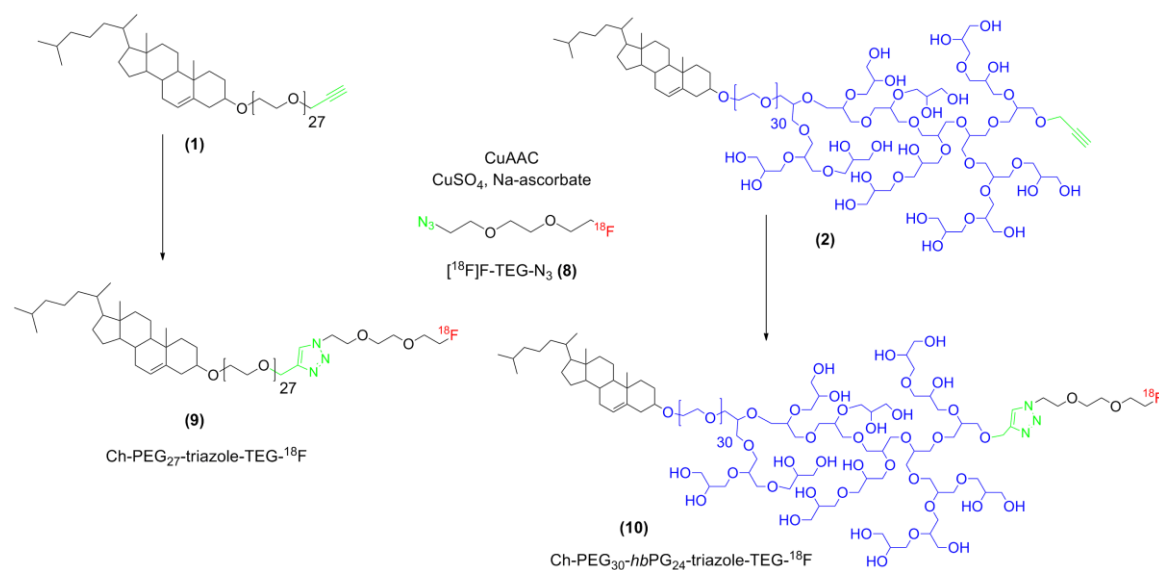
Figure 2: Reaction scheme for the radioactive labeling of Ch-PEG$_{27}$-CH$_2$-C≡CH **(1)** and Ch-PEG$_{30}$-*hb*PG$_{24}$-CH$_2$-C≡CH **(2)** lipids with [^{18}F]F-TEG-N$_3$ **(8)** using the copper-catalyzed azide-alkyne reaction (CuAAC), respectively.

Radioactive labeling of cholesterol

In addition to the radiolabeling of the polyether lipids with potential "stealth" behavior, labeling cholesterol with fluorine-18 was successfully carried out. Nozaki *et al.* and Fukushi *et al.* mentioned a labeled cholesterol compound in the 60s and 70s synthesized via AgF, but a detailed description was never given.[37,38] In the present case, the synthesis by direct labeling of the mesylated form of cholesterol was achieved. Starting from commercially available cholesterol (see Scheme 2), methanesulfonyl chloride was reacted with the hydroxyl group of cholesterol in order to introduce the leaving group in the first step. In the second step, the nucleophilic substitution was carried out using ^{18}F-fluoride and the tetrabutylammonium hydroxide (TBAH) system. 3-[^{18}F]fluoro-cholest-5-ene **(11)** was obtained with RCYs around 25%. While performing radiolabeling, characterization and purification, challenges in solubility were observed. The labeling reaction can be carried out in DMSO as well, but the purification via semi-preparative HPLC (*i*PrOH:MeCN as liquid phase) was not possible due to a breakthrough of the fluoro-cholestene. Diluting the reaction with sufficient amounts of water was also not possible. To avoid these points, labeling was performed in MeCN.
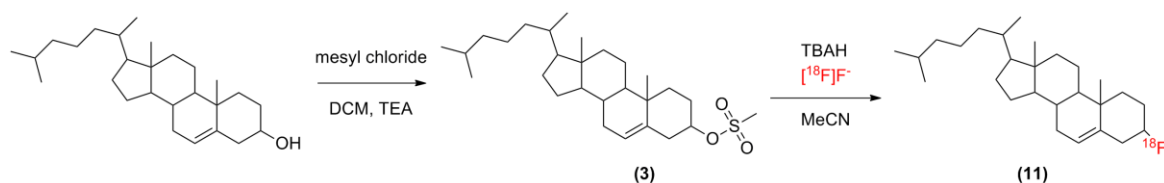
Scheme 2: Reaction scheme for the synthesis of 3-[18F]fluoro-cholest-5-ene **(11)** (abbreviated 18F-cholesten) starting from cholesterol.

Critical micelle concentration and liposome formation

In order to investigate potential polymer micelle formation in the blood stream, the linear polyether as well as the linear-hyperbranched polyether were characterized by surface tension measurements. Due to the amphiphilic character of the polymers, their critical micelle concentrations (CMC) were determined to be 7.9 mg L^{-1} for the linear and 11.0 mg L^{-1} for the branched structure. This is in line with expectation, since the latter polymer is more hydrophilic due to multiple hydroxyl groups and therefore should exhibit an increased CMC compared to the PEG polymer. For mice having a blood volume of about 1.6-2.4 mL, (20-30 g body weight)[39] this means that for a solution of free polymer in buffer with 1 mg mL^{-1}, micelle formation can be expected *in vivo*. The size of the micelles was studied with dynamic light scattering (DLS), and a hydrodynamic radius (R_h) of 6.9 nm for both polymers was found.

Liposomes consisting of Ch-PEG$_{27}$-triazole-TEG-18F, Ch-PEG$_{30}$-*hb*PG$_{24}$-triazole-TEG-18F, or 18F-cholestene, DOPC, and cholesterol were prepared by the thin film hydration method and extrusion through polycarbonate membranes (400 nm and 100 nm). DLS was performed to evaluate the size of the liposomes, because size influences the *in vivo* behavior of particles.[1] For liposomes that are stabilized by the linear polymer (20 mol%), R_h was determined to be 46 nm. For the linear-hyperbranched polymers stabilizing the liposomes, higher radii were found, i.e., $<1/R_h>_z^{-1}$ = 86 nm (5 mol%) and $<1/R_h>_z^{-1}$ = 83 nm (20 mol% polymer). These values are almost twice as high as for the PEGylated liposomes, although all suspensions were extruded through the 100 nm membrane in the same manner. Conventional liposomes containing 18F-cholestene exhibited even larger sizes ($<1/R_h>_z^{-1}$ = 204 nm) due to the lack of a stabilizing polymer. These results emphasize the importance of a stabilizing and shielding polymer anchored to the liposomes as drug-delivery vehicles.

Animal experiments

PET imaging

To investigate the dynamics of the initial biodistribution of the different compounds *in vivo*, μPET experiments were performed over 60 min. Figure 3 A, B, and C show coronal views of maximum intensity projections (MIPs) of early (0 – 3 min) and late (50 – 60 min) time frames of the linear polymer (Ch-PEG$_{27}$-triazole-TEG-^{18}F), the linear-hyperbranched polyether (Ch-PEG$_{30}$-*hb*PG$_{24}$-triazole-TEG-^{18}F) and of ^{18}F-cholestene, respectively. While the linear (A) and linear-hyperbranched (B) molecules, which are assumed to form micelles, are eliminated quickly via the renal excretion pathway, ^{18}F-cholestene (C) shows mainly uptake in the liver, as expected due to its hydrophobic character and the bile acid synthesis. Defluorination can be slightly seen in the late time frames by [^{18}F]F$^-$ uptake of the bones. The renal clearance of the linear-hyperbranched structure from the blood clearly exhibits slower kinetics than the linear structure.
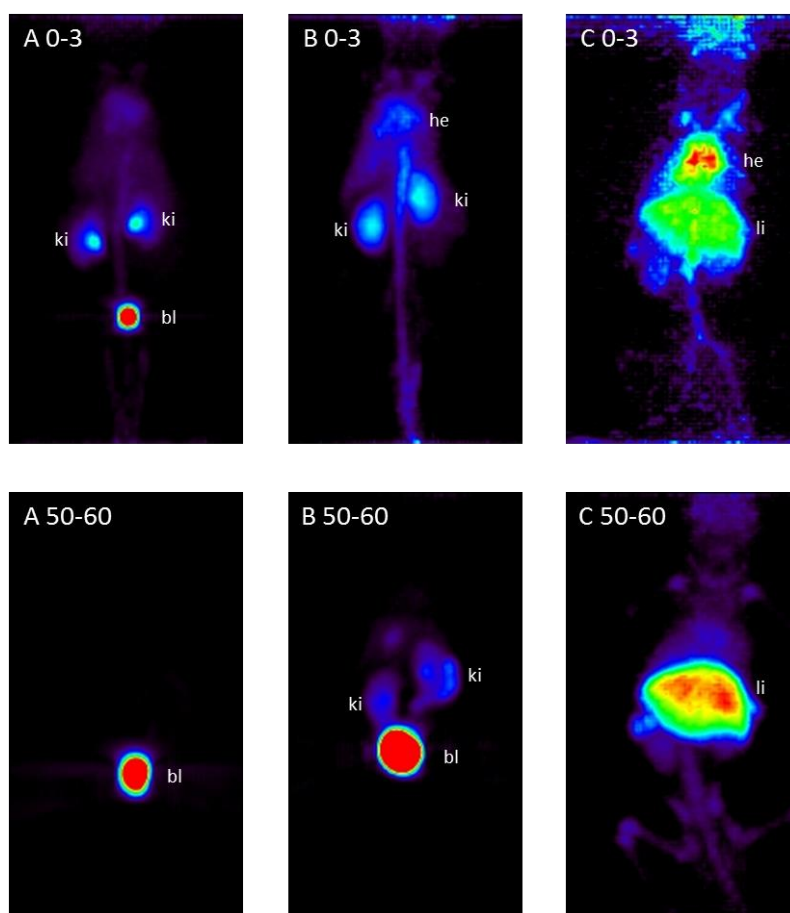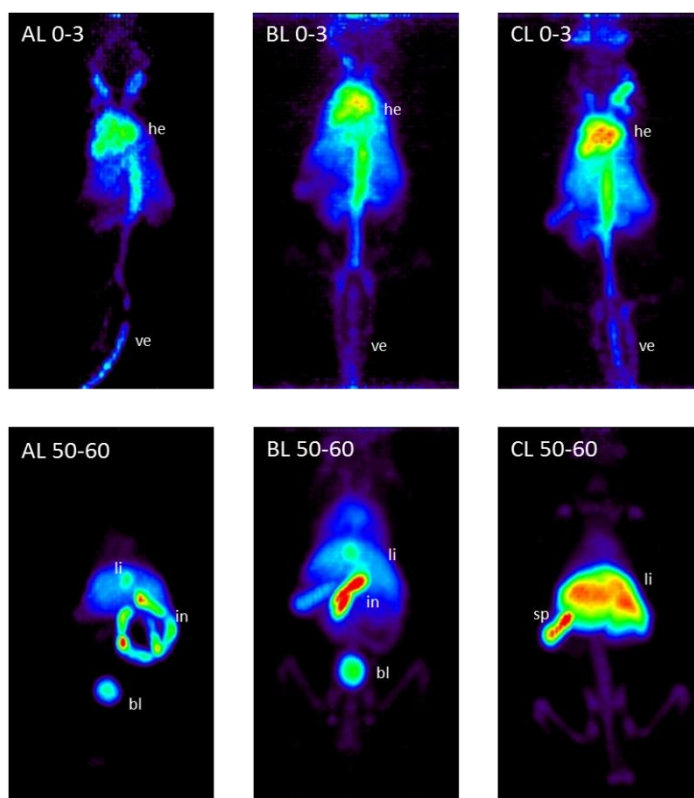

Figure 3: MIPs (coronal view) of whole body distribution for early (0-3 min) and late (50-60 min) time frames of Ch-PEG$_{27}$-triazole-TEG-^{18}F (A), Ch-PEG$_{30}$-*hb*PG$_{24}$-triazole-TEG-^{18}F (B), and ^{18}F-cholestene (C). ki: kidney, bl: bladder, he: heart, li: liver.

In comparison to these observations regarding the non-organized lipid molecules, Figure 4 depicts the liposomal formulations, abbreviated as AL, BL and CL, of the above mentioned compounds during the same time frames. Molar ratios of the liposomes containing Ch-PEG$_{27}$-triazole-TEG-^{18}F and Ch-PEG$_{30}$-hbPG$_{24}$-triazole-TEG-^{18}F (AL and BL) were DOPC:cholesterol:polymer (60:20:20). For ^{18}F-cholestene (CL) it was DOPC:cholesterol (60:40) plus the labeled cholesterol to keep the molar percentage of cholesterol and lipid constant. It is obvious, that the liposome biodistribution exhibits a different pattern compared to the polymer micelles. The renal clearance of the linear (AL) and linear-hyperbranched (BL) sterically stabilized liposomes is considerably lower than for the polymer micelles. Instead, uptake in the liver and intestines can be observed. However, the biodistribution of the liposomal ^{18}F-cholestene (CL) does not differ much from the single molecule. In the late time frame (CL 50-60), an increased uptake in the spleen can be observed, compared to the late time frame in Figure 4 (C 50-60).

Figure 4: MIPs (coronal view) of whole body distribution for early (0-3 min) and late (50-60 min) time frames of Ch-PEG$_{27}$-triazole-TEG-^{18}F Lipo 20mol% (AL), Ch-PEG$_{30}$-hbPG$_{24}$-triazole-TEG-^{18}F Lipo 20mol% (BL) and ^{18}F-cholestene Lipo (CL). he: heart, ve: vein, li: liver, in: intestine, sp: spleen.

Ex vivo biodistribution

To obtain a quantitative statement about the trafficking of the radiolabeled compounds an *ex vivo* biodistribution study was performed. Table 1 summarizes these results for the the radiolabeled compounds Ch-PEG$_{27}$-triazole-TEG-^{18}F **(9)**, Ch-PEG$_{30}$-*hb*PG$_{24}$-triazole-TEG-^{18}F **(10)**, and ^{18}F-cholestene (**11**) as well as the liposomal formulation of abovementioned cholesterol derivatives in male C57bl6J mice (24.8±1.9 g) 1 h post injection. The graphical summary of this data is shown in Figure 5.

Table 1: *Ex vivo* biodistribution data (n=3) of male C57bl6J mice 1 h p.i. (asterisk indicates n=2). Liposomal formulations are abbreviated with Lipo, (x mol%) is the molar percentage of the polymer added to the DOPC-cholesterol-mixture (60:40-x:x) before sonication and extrusion. Error values are given as standard error of the mean. For saving space the abbreviation "triazole-TEG" is not listed in the sample names. The values for all organs are summarized in the Supporting Information Table S1.

| %ID / g tissue (n=3)	lung	blood	liver	spleen	l kidney	r kidney	heart	urine	intestine (empty)
Ch-PEG$_{27}$-^{18}F	0.49±0.04	0.77±0.07	1.91±0.63	0.71±0.26	2.28±0.83	1.98±0.45	0.35±0.03	1070±141*	1.98±1.57
Ch-PEG$_{27}$-^{18}F Lipo (20mol%)	7.24±1.43	5.30±1.24	12.48±2.81	7.91±1.03	4.04±0.65	4.23±0.65	3.60±0.52	28.46±1.49*	1.10±0.35
Ch-PEG$_{30}$-*hb*PG$_{24}$-^{18}F	5.67±0.36	4.25±0.43	5.05±0.28	4.05±0.16	10.48±5.91	9.54±5.54	2.66±0.09	306±98	1.74±0.37
Ch-PEG$_{30}$-*hb*PG$_{24}$-^{18}F Lipo (5mol%)*	7.47±1.60	7.71±1.92	10.40±0.50	19.39±2.89	6.20±1.31	5.73±1.09	3.57±0.73	221±48	1.62±0.21
Ch-PEG$_{30}$-*hb*PG$_{24}$-^{18}F Lipo (20mol%)	15.50±0.80	15.56±2.05	16.92±1.69	25.60±5.38	8.48±0.54	8.71±0.56	6.91±1.05	26.46±12.40	5.94±0.87
^{18}F-cholestene*	27.62±7.59	5.21±0.45	40.37±3.99	29.60±4.39	5.81±1.02	6.04±0.82	3.72±0.39	1.82±0.96	1.44±0.54
^{18}F-cholestene Lipo	1.43±0.08	1.18±0.08	36.24±4.61	24.03±3.93*	0.47±0.00	0.50±0.01	1.30±0.66	5.12±2.04	0.29±0.04
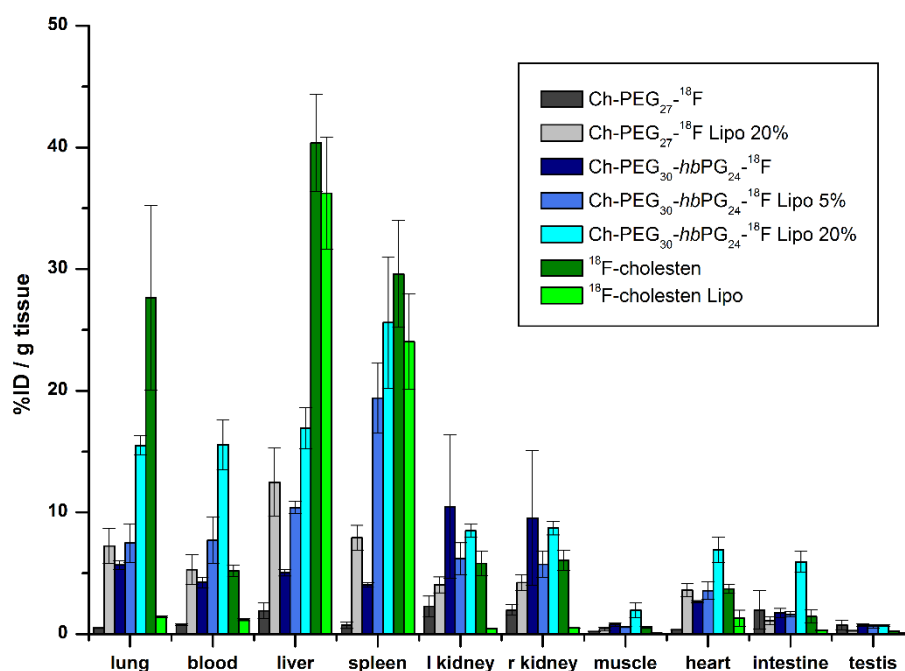
Figure 5: Graphical summary of *ex vivo* biodistribution data of Table 1. Data of urine is not shown to obtain a clear survey, but the values are given in Table 1.

Similar to the PET images, the linear and linear-hyperbranched polymer itself (micelles) showed fast renal clearance, which was confirmed by high amounts of radioactivity in the urine (> 300 %ID / g). Fast renal clearance of the polymers and no accumulation in organs is desired, as this represents the preferential elimination pathway subsequent to degradation of the liposomes. The linear-hyperbranched structure showed slightly increased retention in blood, lung, liver, spleen, and the kidneys, which can be attributed to differences in micelle surface properties of the branched polymer compared to linear PEG. Nevertheless, values for the kidneys were around 10 %ID / g which indicates fast renal clearance. ^{18}F-cholestene is mainly retained in liver, spleen, and lung (%ID / g > 27, Figure 5) and, as expected, shows almost no renal excretion, due to its hydrophobic character.
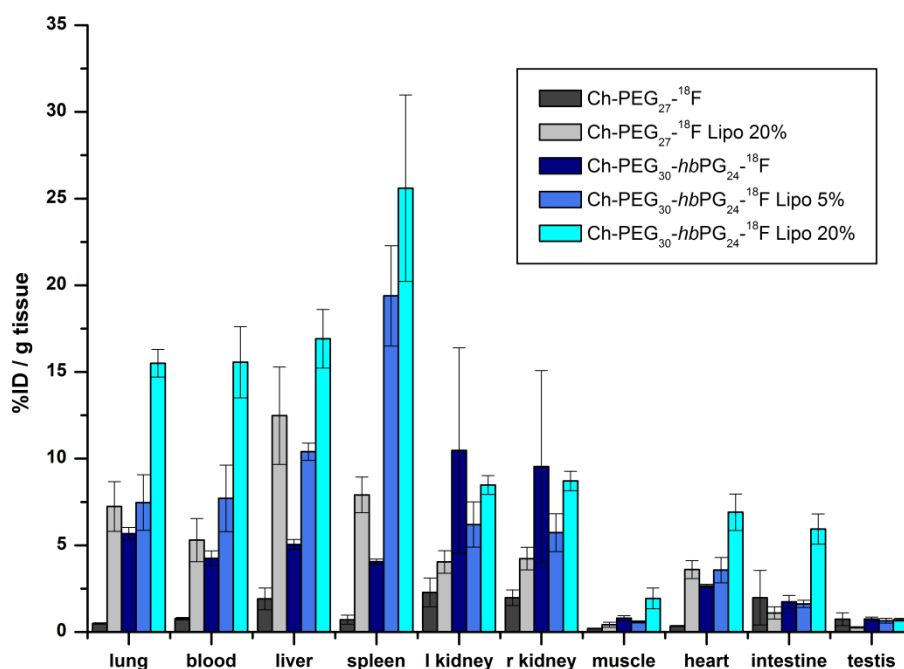
Figure 6: Graphical comparison of *ex vivo* biodistribution (1 h p.i.) between Ch-PEG$_{27}$-triazole-TEG-^{18}F (**9**) and Ch-PEG$_{30}$-*hb*PG$_{24}$-triazole-TEG-^{18}F (**10**) as polymer micelles and liposomal formulation. Data of urine is not shown.

The biodistribution patterns of the sterically stabilized liposomes with Ch-PEG$_{30}$-*hb*PG$_{24}$-triazole-TEG-^{18}F (5 and 20 mol%) or Ch-PEG$_{27}$-triazole-TEG-^{18}F Lipo (20 mol%) differ from the polymer micelles (Figure 6). For liposomes stabilized with PEG-lipids values of 28.46±1.49 %ID / g were found in the urine, which is much less than for PEG-lipid micelles with 1070±141 %ID / g. First, the different pattern hints indirectly at successful incorporation of the polymer into the liposomes and therefore advantageous biodistribution, which translates to longer retention times in the body. PEG-liposomes showed increased values in lung, liver, and spleen, but most importantly also in blood (5.30±1.24 %ID / g) and heart (3.60±0.52 %ID / g). For liposomes stabilized with the linear-hyperbranched-lipids values of 221±48 %ID / g (5 mol% polymer) and 26.46±12.40 %ID / g (20 mol% polymer) were found in the urine (Table 1). The first result points to insufficient incorporation of the bulky lipid into the liposomes for this concentration. Therefore, the amount of polymer was raised to 20 mol% (see also discussion below), maintaining the liposome size, since this was favorable for the organ distribution. Renal clearance was suppressed dramatically and retention in liver, lung, and spleen was observed. Simultaneously, retention in the blood stream

(15.56±2.50 %ID / g) and heart (6.91±1.05 %ID / g) after 1 h was measured, which is beneficial for prolonged blood circulation times. Compared to the linear-hyperbranched polyether micelles renal clearance is strongly suppressed, and retention in the organs is enhanced (compare Table 1).

As expected, non-stabilized liposomes accumulate strongly in the liver and the spleen (> 24 %ID / g, Table 1, Figure 5), which is attributed to fast removal from the blood stream by macrophages (MPS uptake) due to liposome size and possible aggregation with proteins. A comparison of the three types of liposomes is shown in Figure 7.
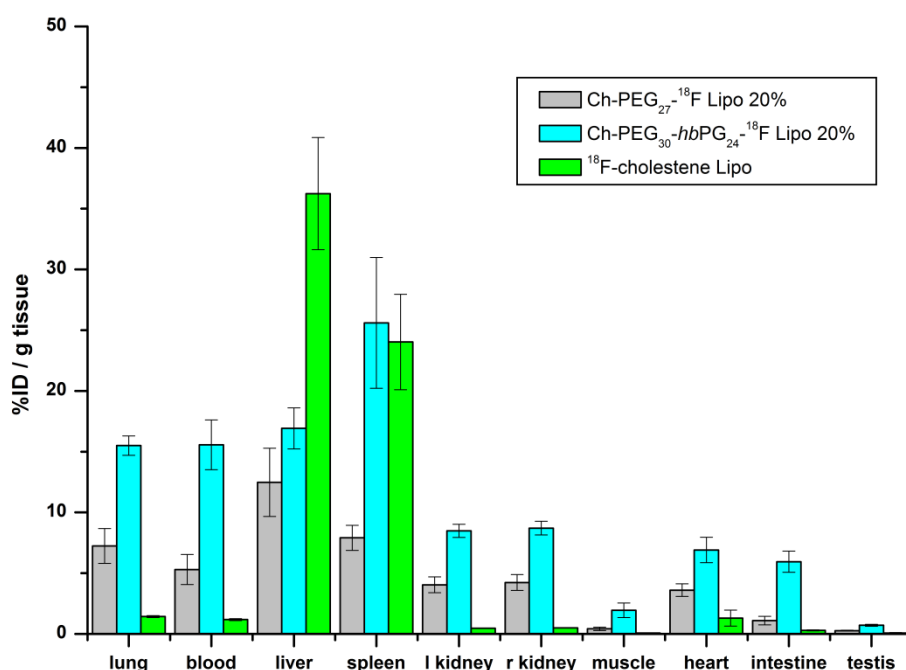

Figure 7: Graphical comparison of *ex vivo* biodistribution (1 h p.i.) between the liposomal formulations of Ch-PEG$_{27}$-triazole-TEG-[18]F (20 mol%), Ch-PEG$_{30}$-*hb*PG$_{24}$-triazole-TEG-[18]F (20 mol%) and non-stabilized liposomes labeled with ^{18}F-cholestene. Data of urine is not shown.

Approximate determination of polymer incorporation

The reason for increasing the amount of polymer lipid added to the lipid-cholesterol-mixture before sonication and extrusion was the rather rapid elimination in case of the 5 mol% linear-hyperbranched liposome formulation. To estimate the degree of integration of the shielding polymer lipid, the elution profile of the SEC after extrusion was recorded. The activity of each fraction was measured and decay-corrected. Furthermore, the remaining activity of the SEC column was determined. By dividing the

accumulated liposomal fractions by the total activity, a degree of integration was estimated. Because the linear-hyperbranched polymer was incorporated into the lipid bilayer only between 20-30 % according to our calculations, we scaled up the amount of polymer from 5 mol% to 20 mol%. The linear polymer and ^{18}F-cholestene were incorporated in higher quantities that are ~60 % and ~85 %, respectively, probably due to their less sterically demanding architecture. These findings once more emphasize the advantage of labeling the shielding polymer instead of incorporating a radioactive probe into the liposome membrane.

Comparison between linear and linear-hyperbranched stabilized liposomes

Comparing the 20 mol% liposomes of the linear with the linear-hyperbranched polymer lipids, the hyperbranched polyglycerol shielding exhibits higher uptake in lung, blood, liver, and spleen. However, Figure 8 depicts the ratios of blood to organ for these two formulations. It is clearly pointed out, that the liposomes with linear-hyperbranched shielding are superior considering blood to liver and blood to lung ratios. Furthermore, they show comparable ratios in blood to spleen to the linear shielded liposomes. The findings confirm that both polyether architectures are advantageous in drug delivery applications, with the hyperbranched structure introducing additional multifunctionality at the liposome surface.

Besides the type of shielding, the size of the liposomes has to be taken into consideration. It is believed that liposomes smaller than 100 nm are opsonized less quickly and to a lower extent compared to liposomes larger than 100 nm. Hence, the liposome uptake by the MPS increases with the size of the vesicles.[1] Unfortunately, even though they were all extruded through the same pore size, the size of the investigated liposomes differed. Showing a hydrodynamic radius of 46 nm, the linear shielded liposomes were the smallest structures, followed by the linear-hyperbranched liposomes shielded with $<1/R_h>_z^{-1}$ = 83 nm and 204 nm for the conventional liposomes. Comparing these sizes, the linear-hyperbranched shielded liposomes may even show more advantageous behavior *in vivo,* if the liposome sizes can be reduced below 100 nm in diameter.
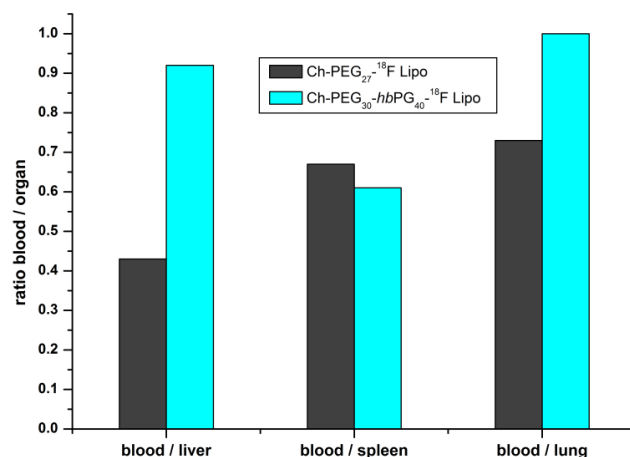
Figure 8: Blood to organ ratios of liposomal formulations (20 mol%) of Ch-PEG$_{27}$-triazole-TEG-^{18}F (grey) and Ch-PEG$_{30}$-*hb*PG$_{24}$-triazole-TEG-^{18}F (cyan).

Conclusion

The study presents a novel method for labeling and *in vivo* tracking conventional and sterically stabilized liposomes by ^{18}F-labeled cholesterol or polyether-based lipids. The labeled liposomes were injected into C57bl6J mice and tracked by non-invasive µPET for 1 h. The positron emitting isotope fluorine-18 enabled imaging with high spatial resolution. Furthermore, *ex vivo* biodistribution studies were carried out. The time frame used in this study is, of course, too short to prove an EPR-effect. Nevertheless, the technique is suitable to investigate initial body distribution of various liposomes. Special emphasis was placed on two different stabilizing polyether-based lipids with linear and linear-hyperbranched architectures, respectively. Radiolabeling of the polymers via copper-catalyzed click reaction instead of labeling the phospholipids, allowed not only the investigation of the fate of the liposomes, but also permitted to monitor the polymer micelles' fate *in vivo* and thus enabled an assessment of the impact of the liposome superstructure. In addition to these observations, a generally usable probe, ^{18}F-cholestene, for liposome labeling was provided. The architecture and therefore the number of functionalities, the polymer amount, and the liposome size play an important role in the biodistribution pattern. As it is known, conventional liposomes showed major

MPS uptake, which strongly confirms the need of a stabilizing polymer for these drug delivery systems. The "gold standard" PEG with a cholesterol anchor group exhibited satisfying results with moderate retention in lung, blood, liver, and spleen. Blood retention was the highest for linear-hyperbranched lipids incorporated into liposomes with 20 mol% via cholesterol. These first results demonstrate the advantageous properties of the novel polyether-based lipids which combine multifunctionality and steric stabilization of vesicles, hinting at "stealth" properties. By use of PET measurements, fast non-invasive screening and comparison of the body distribution of different polymer architectures is possible.

Acknowledgments

Experimental Section

Instrumentation

^{1}H NMR spectra (300 MHz and 400 MHz) were recorded using a Bruker AC300 or a Bruker AMX400, employing MeOD or CDCl$_3$ as solvent. ^{19}F NMR analysis was carried out with a Bruker DRX-400 at 400 MHz. All spectra are referenced internally to residual proton signals of the deuterated solvent. Size exclusion chromatography (SEC) measurements were carried out in dimethylformamide (DMF) with 0.25 g L^{-1} LiBr on PSS HEMA columns (300/100/40). For SEC measurements a UV (275 nm) and an RI detector were used. Calibration was carried out using poly(ethylene glycol) (PEG) standards provided by Polymer Standards Service (PSS). Surface tension measurements, to determine the critical micelle concentration (CMC) of the polyether lipids, were performed on a Dataphysics DCAT 11 EC tensiometer equipped with a TV 70

temperature control unit, a LDU 1/1 liquid dosing and refill unit, as well as a RG 11 Du Noüy ring. The Du Noüy ring was rinsed thoroughly with Millipore water and annealed in a butane flame prior to use. Surface tension data was processed with SCAT v3.3.2.93 software. The CMC presented is a mean value of two experiments. All solutions for surface tension measurements were stirred for 120 s at a stir rate of 50%. After a relaxation period of 360 s, three surface tension values were measured.

During radio-synthesis a Merck LaChrom HPLC system was used with Interface D-7000, Programmable Autosampler L-7250, Pump L7100 (2x), UV-Detector L-7400, Column Oven L-3000 with manual injection rheodyne and a Gabi Star (Raytest) for detecting activity. Radio-TLCs were analyzed by Packard Instant Imager. In *ex vivo* studies, fluorine-18 activities were measured using a Perkin-Elmer 2470 Wizard^2 γ-counter.

Solutions for light scattering experiments were prepared in a dust free flow box. Cylindrical quartz cuvettes (20 mm diameter, Hellma, Mühlheim) were cleaned by dust-free distilled acetone. All samples (Liposomes in PBS) were filtered through LCR450 nm filters (Millipore) into the cuvettes. All light scattering experiments were performed with an instrument consisting of a HeNe laser (632.8 nm, 25 mW output power), an ALV-CGS 8F SLS/DLS 5022F goniometer equipped with eight simultaneously working ALV 7004 correlators, and eight QEAPD Avalanche photodiode detectors. All correlation functions were typically measured from 30 to 150° in steps of 15°, 20° or 30° (DLS).

Liposome Formation

Liposomes consisting of the polymer lipid (Ch-PEG$_{27}$-triazole-TEG-^{18}F (**9**), Ch-PEG$_{30}$-*hb*PG$_{24}$-triazole-TEG-^{18}F (**10**), or ^{18}F-Cholesten (**11**)), cholesterol and 1,2-dioleoyl-sn-glycero-3-phosphatidylcholine (DOPC) were prepared by the thin film hydration method on a clean bench. A solution of DOPC in ethanol, cholesterol in ethanol and the radiolabeled copolymer/cholesten in ethanol were blended at molar ratios of 60:35:5mol% or 60:20:20mol%, respectively. The objective was to keep the molar ratios of lipid to cholesterol constant. Because of the cholesteryl anchored polymers, the total ratio of lipid to cholesterol was kept at 60:40 regardless of the amount of polymer added. The solvent was evaporated in a miniature rotating evaporator to obtain a thin film of liposome components. The lipid film was hydrated with 1 mL of PBS buffer solution to obtain the final lipid concentrations summarized in Table 2, sonicated for

10 min at 50 °C to yield multilamellar vesicles (MLVs), and extruded through a 400 nm polycarbonate membrane 11 times, followed by the extrusion through a 100 nm membrane for 11 times to obtain small unilamellar vesicles (SUVs) using a Mini-Extruder (Avanti Polar Lipids Inc.). Finally, the solution was purified via size exclusion chromatography (~0.5 g Sephadex G 75 packed in a 6 mL empty SPE tube with 20 µm PTFE frits at top and bottom) to separate the liposomes from not incorporated smaller molecules.

Table 2: Composition of different liposome formulations.

	molar ratios (DOPC:cholesterol:polymer)	DOPC / mg	polymer / mg	cholesterol / mg
Ch-PEG$_{27}$-^{18}F	60:20:20	13.13 (16.7µmol)	8.8 (5.5µmol)	2.15 (5.5µmol)
Ch-PEG$_{30}$-*hb*PG$_{24}$-^{18}F	60:35:5	2.62 (3.3µmol)	1.0 (0.28µmol)	0.75 (1.9µmol)
	60:20:20	2.62 (3.3µmol)	4.0 (1.12µmol)	0.43 (1.12µmol)
^{18}F-Cholesten	60:40:0	10.51 (13.4µmol)	-	3.45 (8.9µmol)

Animal studies

For *ex vivo* biodistribution and µPET studies male C57bl6J mice (Charles River Wiga, Sulzfeld, Germany) (body weight 20.8 g to 28.6 g) housed in the animal care facility of the Johannes Gutenberg-University of Mainz were used. All experiments had previously been approved by the regional animal ethics committee and were conducted in accordance with the German Law for Animal Protection and the UKCCCR Guidelines.[40]

***Ex vivo* biodistribution studies**

For *ex vivo* biodistribution studies, animals were injected with ^{18}F-labeled compounds in phosphate buffered saline solution (2.45-8.64 MBq) intravenously (i.v.) in a tail vein. After 60 min post injection (p.i.), the animals were sacrificed and different organs (lung, blood, liver, spleen, kidneys, skeletal muscle, heart, urine, small intestine, testes) were

excised. The samples were weighed and measured in a Perkin Elmer 2470 Wizard[2] γ-counter to calculate the percentage of injected dose per gram tissue (%ID/g).

In vivo **micro PET studies**

For *in vivo* µPET studies the mice were anaesthetized with isoflurane (2.5%) and the fluorinated compounds were injected into a tail vein. The µPET imaging was recorded on a Focus 120 small animal PET (Siemens/Concorde, Knoxville, USA). During PET measurements the mice were placed in a head first prone position. Dynamic PET studies were acquired in list mode. The injected activity of radiolabeled compounds was 4.74 ± 1.24 MBq (in 100 - 150 µL of phosphate buffered saline). The PET list mode data were histogrammed into 19 frames (3 x 20 s, 3 x 60 s, 3 x 120 s, 10 x 300 s) and reconstructed using FBP algorithm with dead time correction. Scatter correction was not applied.

Reagents

All reagents and solvents were purchased from Acros or Sigma-Aldrich and used as received, unless otherwise mentioned. Anhydrous solvents were stored over molecular sieves and were purchased from Sigma-Aldrich. Deuterated solvents were purchased from Deutero GmbH, and stored over molecular sieves. Cholesterol was purchased from Acros and stored at 8 °C. Ethoxyethyl glycidyl ether (EEGE) was synthesized as described in the literature,[41] dried over CaH_2 and cryo-transferred prior to use. Glycidol was purified by distillation from CaH_2 directly prior to use. Ethanol (abs.) was purchased from Merck. Phosphate buffered saline packs were purchased from Thermo Scientific. 1,2-dioleoyl-*sn*-glycero-3-phosphocholine (DOPC), the mini-extruder, the polycarbonate membranes, and filters were obtained from Avanti Polar Lipids.

^{18}F was delivered in ^{18}O-enriched water by the department of radiology, University Hospital Tübingen, Germany.

Polymer synthesis

Ch-PEG$_{27}$-CH$_2$-C≡CH **(1)**: Cholesterol (0.4 mg, 1.0 mmol), cesium hydroxide monohydrate (148 mg, 0.88 mmol), and benzene were placed in a Schlenk flask. The mixture was stirred at RT for about 30 min to generate the cesium alkoxide (degree of deprotonation 85%). The salt was dried under vacuum at 90 °C for 24 h, anhydrous THF was added via

cryo-transfer, and ethylene oxide (2.2 mL, 44 mmol) was cryo-transferred first to a graduated ampule and then to the Schlenk flask containing the initiator solution. The mixture was allowed to warm up to room temperature, heated to 60 °C, and the polymerization was performed for 12 h at this temperature under vacuum. The reaction was cooled, quenched with propargyl bromide (0.2 mL, 1.85 mmol) and stirred for additional 12 h. The solvent was evaporated and the crude product was precipitated into cold diethyl ether. Yield: ~70%

^{1}H NMR (400 MHz, CDCl$_3$): δ (ppm) = 5.32 (s, 1H), 4.20 (d, 2H), 3.80-3.40 (polyether backbone), 3.15 (s, 1H), 2.43 (t, 1H), 2.27-0.82 (CH_2, CH cholesterol), 0.66 (s, 3H).

Ch-PEG$_{30}$-hbPG$_{24}$-CH$_2$-C≡CH **(2)**: Compound **(2)** was prepared and functionalized with propargyl bromide according to the literature.[12,13]

Further Syntheses

Respective reaction schemes are given in the Supporting Information.

Methanesulfonic acid 3β-cholesteryl ester (3) (Scheme 2 and S1) was prepared according to Sun *et al.*.[42] To a solution of 1 g (2.6 mmol) cholesterol in 15 mL of anhydrous dichloromethane cooled to 0 °C, 0.55 mL (3.88 mmol) abs. triethylamine was added under stirring. 213 µL (2.72 mmol) methanesulfonyl chloride in 1 mL DCM was added slowly and 30 min after addition the solution was allowed to warm up to room temperature and stirred for another 16 h. After removing the solvent under reduced pressure, the resulting material was dissolved in 3 mL DCM, precipitated by the addition of 15 mL MeOH and **(3)** was collected by vacuum filtration. Subsequently, the solvent of the filtrate was removed under reduced pressure and the residual crude product was taken up by MeOH to obtain a second crop of **(3)** by filtration as a white solid (combined yield: 0.871 g, 72%).

^{1}H NMR (300 MHz, CDCl$_3$) ▯ 5.43 (m, 1H), 4.50 (m, 1H), 3.01 (s, 3H), 2.50 (m, 2H), 2.08-0.82 (m, 38H), 0.67 (s, 3H).

FD-MS: 464.4.

3-fluoro-cholest-5-ene (4) (Scheme S2) was prepared by slowly adding 264 µL (2 mmol) DAST (diethylaminosulfur trifluoride) in 5 mL anhydrous DCM to a stirred solution of 500 mg (1.29 mmol) cholesterol in 10 mL anhydrous DCM cooled to 5 °C under helium

atmosphere. After 40 min the ice bath was removed and the reaction was allowed to stir for another 60 min before it was quenched with 10 mL H_2O. After extracting the organic phase twice with water, DCM was dried over Na_2SO_4 and the solvent was removed under reduced pressure. To obtain (**4**) as a white solid (249 mg, 50%), the crude product was purified by column chromatography with hexane as mobile phase.

^{1}H NMR (400 MHz, CDCl$_3$) ⏃ 5.40 (m, 1H), 4.50-4.26 (dm, 1H), 2.44 (t, 2H), 2.06-0.80 (m, 38H), 0.68 (s, 3H).

^{19}F NMR (400 MHz, CDCl$_3$) ⏃ -168.91 (s).

FD-MS: 388.4.

2-(2-(2-Hydroxyethoxy)ethoxy)ethyl-4-*p*-toluenesulfonate (**5**) (Scheme S3) was prepared by adding 3.53 g (34.9 mmol, 2.1 eq) triethylamine to a solution of 5 g (33.3 mmol, 2 eq) triethylene glycol (TEG) in 30 mL of anhydrous THF under inert gas. While cooling to 0 °C, 3.16 g (16.65 mmol, 1 eq) *p*-toluenesulfonyl chloride dissolved in 10 mL THF was added slowly under stirring. After 16 h at ambient temperature, the suspension was vacuum filtrated and the solvent was removed under reduced pressure after drying over anhydrous Na_2SO_4. Purification via column chromatography (mobile phase EA:MeOH (4:1)) gave 3.51 g (11.53 mmol, 69% yield) (**5**).

^{1}H NMR (300 MHz, CDCl$_3$) δ 7.79 (m, 2H), 7.35 (m, 2H), 4.16 (m, 2H), 3.72-3.58 (m, 10H), 2.68 (s, 1H), 2.44 (s, 3H).

FD-MS: 609.5 [2M+1], 913.3 [3M+1].

2-(2-(2-Azidoethoxy)ethoxy)ethanol (6) (Scheme S3) was prepared by adding 1.87 g (28.83 mmol, 2.5 eq) sodium azide in small portions to a solution of 3.51 g (11.53 mmol, 1 eq) of the tosylate (**5**) in 30 mL anhydrous DMF. The solution was heated to 160 °C for 16 h. After cooling to RT and removing the solvent under reduced pressure, purification was carried out via column chromatography with ethylacetate:methanol (4:1) as mobile phase which gave 1.38 g (7.88 mmol, 68% yield) of (**6**).

^{1}H NMR (300 MHz, CDCl$_3$) ⏃ 3.72–3.58 (m, 10H), 3.36 (t, 2H), 2.68 (s, 1H).

FT-IR (cm^{-1}; liquid film): 3417 (-OH); 2871; 2108 (-N$_3$).

FD-MS: 198.5 [M+Na]$^+$

2-(2-(2-Azidoethoxy)ethoxy)ethyl-4-*p*-toluenesulfonate (7) (Scheme S3) was prepared by adding 2.38 g (23.5 mmol) triethylamine to a solution of 2.06 g (11.7 mmol) (**6**) in 10 mL DCM. After cooling the solution to 0 °C, tosyl chloride was added and the reaction

solution was stirred for 16 h. After adding 15 mL DCM, the organic phase was extracted with 15 mL HCl (3% in H_2O) and brine. After drying the organic phase over anhydrous Na_2SO_4, the solvent was removed under reduced pressure and after purification via column chromatography with ethylacetate:n-hexane (1:2.5) as mobile phase 2.89 g (8.78 mmol, 75% yield) (**7**) was obtained.

^{1}H NMR (300 MHz, $CDCl_3$) ⏃ 7.79 (m, 2H), 7.35 (m, 2H), 4.16 (m, 2H), 3.70 (m, 2H), 3.64 (m, 2H), 3.60 (s, 4H), 3.36 (t, 2H), 2.44 (s, 3H).

FT-IR (cm^{-1}; liquid film): 2871, 2109 (-N_3).

ESI-MS: 352.1 [M+Na]; 368.1 [M+K].

Radiosynthesis

Respective reaction schemes are given in the Supporting Information as mentioned below.

1-azido-2(2-(2-[^{18}F]fluoroethoxy)ethoxy)ethane ([^{18}F]F-TEG-N_3) (8) (Scheme S4) was prepared on a semi-automatic custom built modular system with RCY ~ 86% (TLC, EA:nHex (1:1), R_f : 0.8). In a first step, the [^{18}F]fluoride was trapped on a Waters QMA light Sep-Pak cartridge (preconditioned with 10 mL K_2CO_3 (1 M), 10 mL MilliQ H_2O and 20 mL air). To elute the activity into the reaction vessel 15 µmol K_2CO_3 and 40 µmol Kryptofix 222 in 1 mL acetonitrile (MeCN) were used. To remove residual water, the solvent was dried azeotropically by stepwise reducing the pressure and helium flow while the vessel was heated at 80 °C. After cooling to 40 °C and ventilation, 9.6 mg (29 µmol in 1 mL MeCN) of the tosylate precursor **(7)** were added to the reaction vessel and the nucleophilic fluorination reaction was performed at 90 °C for 10 min. After cooling again to 40 °C the reaction solution was quenched with 1 mL MeCN:H_2O (50:50), and the resulting 2 mL solution was automatically transferred to the sample loop of a semipreparative HPLC (Luna 10u Prep C18(2) 100A 250x10.00mm; 4 mL/min; MeCN:H_2O (50:50)). The separated fraction of **(8)** (R_f : 6 min) was collected in 35 mL of MilliQ H_2O and finally passed through a Merck Lichrolut EN cartridge (preconditioned with 10 mL MeCN, 10 mL MilliQ H_2O and 20 mL air) followed by drying in a stream of helium. To obtain **(8)**, the cartridge was eluted with 1.5 mL of diethyl ether into a reacti-vial with septum and stirring bar. Subsequent removal of the solvent under reduced pressure and

a stream of helium (850 mbar, 40 °C, He: 10 mL/min) within 8 min gave a synthon coated vial.

Ch-PEG$_{27}$- triazole-TEG-^{18}F (9) by CuAAC was carried out in a reacti-vial with stirring bar. A solution of 8.8 mg (5.5 µmol) **(1)** in 880 µL PBS was added directly to the synthon coated vial. After adding 320 µL PBS, 12.5 µL DMSO and 15 µL (15 µmol) CuSO$_4$ the reaction was started by adding 22.5 µL of sodium ascorbate (49.4 mg in 100 µL PBS) and heating the reaction vial at 70 °C for 15 min under stirring. Radiochemical yields (> 95%) of the triazole product were determined by TLC with EA:nHex (1:1) as mobile phase (R$_f$: 0, Synthon R$_f$: 0.8). After cooling down, the reaction solution was passed through 600 mg Chelex 100 in a 3 mL SPE tube (preconditioned with 0.8 mL HCl (1 M), 5 mL H$_2$O, 0.8 mL NaOH (1 M), 5 mL H$_2$O and 10 mL air) followed by 7 mL abs. EtOH to retain the copper from the reaction solvent. To confirm the absence of copper, an aliquot was taken and a few drops of sodium sulfide solution were added. The copper-free, but aqueous, ethanol containing solution was passed through a 6 mL SPE tube filled to 2/3 with anhydrous sodium sulfate (20 µm PTFE frits at top and bottom) and a 0.45 µm PTFE filter to remove the water. After flushing the self-assembled cartridge with 1 mL abs. EtOH and 10 mL air, the solvent was removed in a mini rotary evaporator to obtain the radiolabeled Ch-PEG$_{27}$-CH$_2$-triazole-TEG-^{18}F **(9)**.

Ch-PEG$_{30}$-*hb*PG$_{24}$-triazole-TEG-^{18}F (10) by CuAAC was carried out in a reacti-vial with a stirring bar. A solution of 1 mg (0.28 µmol) **(2)** in 100 µL PBS was added to the vial. After adding 500 µL PBS, 20 µL (20 µmol) CuSO$_4$ and [^{18}F]F-TEG-N$_3$ **(8)** taken up in 400 µL EtOH the reaction was started by adding 40 µL of sodium ascorbate (49.4 mg in 100 µL PBS) and heating the reaction vial to 70 °C for 15 min under stirring. Radiochemical yields (> 95%) of the triazole product were determined by TLC with EA:nHex (1:1) as mobile phase (R$_f$: 0, Synthon R$_f$: 0.8, (see Supporting Information). After cooling down, the reaction solution was passed through 600 mg Chelex 100 in a 3 mL SPE tube (preconditioned with 0.8 mL HCl (1 M), 5 mL H$_2$O, 0.8 mL NaOH (1 M), 5 mL H$_2$O and 10 mL air) followed by 7 mL abs. EtOH to remove the copper from the reaction solvent. To confirm the absence of copper, an aliquot was taken and a few drops of sodium sulfide solution were added.

The copper-free solution was passed through a 6 mL SPE tube filled to 2/3 with anhydrous sodium sulfate (20 µm PTFE frits at top and bottom) and a 0.45 µm PTFE filter

to remove the water. After flushing the self-assembled cartridge with 1 mL abs. EtOH and 10 mL air, the solvent was removed in a mini rotary evaporator to obtain the radiolabeled Ch-PEG$_{30}$-*hb*PG$_{24}$-triazole-TEG-^{18}F **(10)**.

3-[^{18}F]fluoro-cholest-5-ene (11) (Scheme 2 and Scheme S5) was prepared by direct fluorination of the mesylated cholesterol precursor **(3)** with RCY ~ 25%. [^{18}F]fluoride was trapped on a Waters QMA light Sep-Pak cartridge (preconditioned with 10 mL K$_2$CO$_3$ (1 M), 10 mL MilliQ H$_2$O and 20 mL air). After eluting the activity with 0.9 mL (52 µmol) TBAH in MeOH into a septum sealed reacti-vial the solution was dried under reduced pressure, and a stream of helium (260 mbar, 85 °C, 200 mL/min He). Residual water was removed azeotropically by adding 1 mL of MeCN (3x) under above mentioned conditions. Compound **(3)** (9.3 mg, 20 µmol) dissolved in 1 mL MeCN was added directly to the vial and heated for 20 min at 120 °C. During cool down in cold water for 5 min, the solution was quenched with 2-propanol (1 mL), followed by purification via semipreparative HPLC (Luna 10u Prep C18(2) 100A 250x10.00mm; 4 mL/min; *i*PrOH:MeCN (80:20)). The solvents of the separated fraction were removed within 10 min using a mini rotary evaporator (stepwise reducing pressure, starting with 200 mbar, 45 °C). Radiochemical yields of **(11)** were determined by RP-TLC (Merck TLC Silica gel 60 RP-18 F254s) with *i*PrOH:MeCN (4:1) as mobile phase (R$_f$: 0.4). Compound **(11)** was identified in HPLC and TLC via the reference compound **(4)**. For taking up **(11)** into an injectable phosphate buffered saline solution, (2-hydroxypropyl)-β-cyclodextrin (45 % (w/v) solution in water) was used as a solubilizer. For the liposome preparation no solubilizer was used.

References

(1)   Sharma, A.; Sharma, U. S. Liposomes in drug delivery: progress and limitations. *Int. J. Pharm.* **1997,** *154* (2), 123–140.

(2)   Torchilin, V. P. Recent advances with liposomes as pharmaceutical carriers. *Nat. Rev. Drug Discov.* **2005,** *4* (2), 145–160.

(3)   Harashima, H.; Sakata, K.; Funato, K.; Kiwada, H. Enhanced hepatic-uptake of liposomes through compliment activation depending on the size of liposomes. *Pharm. Res.* **1994,** *11* (3), 402–406.

(4)   Lasic, D. D.; Needham, D. The Stealth Liposome: A Prototypical Biomaterial. *Chem. Rev.* **1995,** *95*, 2601–2628.

(5)   Immordino, M. L.; Dosio, F.; Cattel, L. Stealth liposomes: review of the basic science, rationale, and clinical applications, existing and potential. *Int. J. Nanomed.* **2006,** *1* (3), 297–315.

(6)   Torchilin, V. P.; Omelyanenko, V. G.; Papisov, M. I.; Bogdanov, A. A.; Trubetskoy, V. S.; Herron, J. N.; Gentry, C. A. Poly(ethylene glycol) on the liposome surface: On the mechanism of polymer-coated liposome longevity. *Biochim. Biophys. Acta* **1994,** *1195* (1), 11–20.

(7)   Knop, K.; Hoogenboom, R.; Fischer, D.; Schubert, U. S. Poly(ethylene glycol) in Drug Delivery: Pros and Cons as Well as Potential Alternatives. *Angew. Chem. Int. Ed.* **2010,** *49* (36), 6288–6308.

(8)   Torchilin, V. P.; Shtilman, M. I.; Trubetskoy, V. S.; Whiteman, K.; Milstein, A. M. Amphiphilic vinyl-polymers effectively prolong liposome circulation time in-vivo. *Biochim. Biophys. Acta-Biomembr.* **1994,** *1195* (1), 181–184.

(9)   Zalipsky, S.; Hansen, C. B.; Oaks, J. M.; Allen, T. M. Evaluation of blood clearance rates and biodistribution of poly(2-oxazoline)-grafted liposomes. *J. Pharm. Sci.* **1996,** *85* (2), 133–137.

(10)   Siegers, C.; Biesalski, M.; Haag, R. Self-Assembled Monolayers of Dendritic Polyglycerol Derivatives on Gold That Resist the Adsorption of Proteins. *Chem. Eur. J.* **2004,** *10* (11), 2831–2838.

(11)   Kainthan, R. K.; Zou, Y.; Chiao, M.; Kizhakkedathu, J. N. Self-Assembled Monothiol-Terminated Hyperbranched Polyglycerols on a Gold Surface: A Comparative Study on the Structure, Morphology, and Protein Adsorption Characteristics with Linear Poly(ethylene glycol)s. *Langmuir* **2008,** *24* (9), 4907–4916.

(12)   Hofmann, A. M.; Wurm, F.; Hühn, E.; Nawroth, T.; Langguth, P.; Frey, H. Hyperbranched Polyglycerol-Based Lipids via Oxyanionic Polymerization: Toward Multifunctional Stealth Liposomes. *Biomacromolecules* **2010,** *11* (3), 568–574.

(13)   Hofmann, A. M.; Wurm, F.; Frey, H. Rapid Access to Polyfunctional Lipids with Complex Architecture via Oxyanionic Ring-Opening Polymerization. *Macromolecules* **2011,** *44* (12), 4648–4657.

(14)   Müller, S. S.; Dingels, C.; Hofmann, A. M.; Frey, H. Polyether-Based Lipids Synthesized with an Epoxide Construction Kit: Multivalent Architectures for Functional Liposomes. *Tailored Polymer Architectures for Pharmaceutical and Biomedical Applications*; ACS Symposium Series; American Chemical Society, 2013; pp 11–25.

(15)   He, Z.-Y.; Chu, B.-Y.; Wei, X.-W.; Li, J.; Edwards, C. K.; Song, X.-R.; He, G.; Xie, Y.-M.; Wei, Y.-Q.; Qian, Z.-Y. Recent development of poly(ethylene glycol)-cholesterol conjugates as drug delivery systems. *International Journal of Pharmaceutics* **2014,** *469* (1), 168–178.

(16)   Phillips, W. T.; Rudolph, A. S.; Goins, B.; Timmons, J. H.; Klipper, R.; Blumhardt, R. A simple method for producing a technetium-99m-labeled liposome which is stable In Vivo. *Nucl. Med. Biol.* **1992,** *19* (5), 539–547.

(17)   Bao, A.; Goins, B.; Klipper, R.; Negrete, G.; Phillips, W. T. Re-186-liposome labeling using Re-186-SNS/S complexes: In vitro stability, imaging, and biodistribution in rats. *J. Nucl. Med.* **2003,** *44*, 1992–1999.

(18)   Mauk, M. R.; Gamble, R. C. Preparation of lipid vesicles containing high levels of entrapped radioactive cations. *Anal. Biochem.* **1979,** *94* (2), 302–307.

(19)   Harrington, K. J.; Mohammadtaghi, S.; Uster, P. S.; Glass, D.; Peters, A. M.; Richard, G. V.; Stewart, J. S. W. Effective Targeting of Solid Tumors in Patients With Locally advanced cancers by radiolabled pegylated liposomes. *Clin. Cancer Res.* **2001,** *7* (243-254).

(20)   Gaspar, M. M.; Boerman, O. C.; Laverman, P.; Corvo, M. L.; Storm, G.; Cruz, Maria Eugénia Meirinhos. Enzymosomes with surface-exposed superoxide dismutase: in vivo behaviour and therapeutic activity in a model of adjuvant arthritis. *J. Control. Release* **2007,** *117* (2), 186–195.

(21)   Seo, J. W.; Zhang, H.; Kukis, D. L.; Meares, C. F.; Ferrara, K. W. A Novel Method to Label Preformed Liposomes with 64 Cu for Positron Emission Tomography (PET) Imaging. *Bioconjugate Chem.* **2008,** *19* (12), 2577–2584.

(22)   Oku, N.; Yamashita, M.; Katayama, Y.; Urakami, T.; Hatanaka, K.; Shimizu, K.; Asai, T.; Tsukada, H.; Akai, S.; Kanazawa, H. PET imaging of brain cancer with positron emitter-labeled liposomes. *Int. J. Pharm.* **2011,** *403* (1-2), 170–177.

(23)   Phillips, W. T.; Goins, B. A.; Bao, A. Radioactive liposomes. *Wiley Interdiscipl. Rev. Nanomed. Nanobiotechnol.* **2009,** No. 1, 69–83.

(24)   Hühn, E.; Buchholz, H.-G.; Shazly, G.; Maus, S.; Thews, O.; Bausbacher, N.; Rösch, F.; Schreckenberger, M.; Langguth, P. Predicting the in vivo release from a liposomal formulation by IVIVC and non-invasive positron emission tomography imaging. *Eur. J. Pharm. Sci.* **2010,** *41* (1), 71–77.

(25)   Efferth, T.; Langguth, P. Transport processes of radiopharmaceuticals and -modulators. *Radiat Oncol* **2011,** *6* (1), 59.

(26)   Oku, N.; Tokudome, Y.; Tsukada, H.; Kosugi, T.; Namba, Y.; Okada, S. In vivo trafficking of long-circulating liposomes in tumor-bearing mice determined by positron emission tomography. *Biopharm. Drug. Dispos.* **1996,** No. 17, 435–441.

(27)   Oku, N. Delivery of contrast agents for positron emission tomography imgaging by liposomes. *Adv. Drug Deliv. Rev.* **1999,** No. 37, 53–61.

(28)   Marik, J.; Tartis, M. S.; Zhang, H.; Fung, J. Y.; Kheirolomoom, A.; Sutcliffe, J. L.; Ferrara, K. W. Long-circulating liposomes radiolabeled with [F-18]fluorodipalmitin ([F-18]FDP). *Nuclear Medicine and Biology* **2007,** *34* (2), 165–171.

(29)   Urakami, T.; Akai, S.; Katayama, Y.; Harada, N.; Tsukada, H.; Oku, N. Novel Amphiphilic Probes for [18 F]-Radiolabeling Preformed Liposomes and Determination of Liposomal Trafficking by Positron Emission Tomography. *J. Med. Chem.* **2007,** *50* (26), 6454–6457.

(30)   Emmetiere, F.; Irwin, C.; Viola-Villegas, N. T.; Longo, V.; Cheal, S. M.; Zanzonico, P.; Pillarsetty, N.; Weber, W. A.; Lewis, J. S.; Reiner, T. 18 F-Labeled-Bioorthogonal Liposomes for In Vivo Targeting. *Bioconjugate Chem.* **2013,** *24* (11), 1784–1789.

(31)   Jensen, A. T. I.; Binderup, T.; Andresen, T. L.; Kjær, A.; Rasmussen, P. H. PET imaging of liposomes labeled with an [18 F]-fluorocholesteryl ether probe prepared by automated radiosynthesis. *Journal of Liposome Research* **2012,** *22* (4), 295–305.

(32)   Bauser, M.; Lehmann, L. Positronen-Emissions-Tomographie. *Chemie in unserer Zeit* **2012,** *46* (2), 80–99.

(33)   Woodle, M. C.; Lasic, D. D. Sterically stabilized liposomes. *Biochim. Biophys. Acta* **1992,** *1113* (2), 171–199.

(34)   Pasut, G.; Veronese, F. M. Polymer–drug conjugation, recent achievements and general strategies. *Prog. Polym. Sci.* **2007,** *32* (8-9), 933–961.

(35)   Fritz, T.; Hirsch, M.; Richter, F. C.; Müller, S. S.; Hofmann, A. M.; Rusitzka, K. A.; Markl, J.; Massing, U.; Frey, H.; Helm, M. Click Modification of Multifunctional Liposomes Bearing Hyperbranched Polyether Chains. *Biomacromolecules* **2014,** *15*, 2440–2448.

(36)   Rokka, J.; Snellman, A.; Zona, C.; La Ferla, B.; Nicotra, F.; Salmona, M.; Forloni, G.; Haaparanta-Solin, M.; Rinne, J. O.; Solin, O. Synthesis and evaluation of a 18F-curcumin derivate for β-amyloid plaque imaging. *Bioorganic & Medicinal Chemistry* **2014,** *22* (9), 2753–2762.

(37)   Nozaki, T.; Shimamura, A.; Karasawa, T. Preparation of 18F-labelled Compounds by the Bombardement of an Oxygen Stream. *IPCR Cyclotron Progr. Rep.* **1968**, 156–158.

(38)   Fukushi, K.; Irie, T.; Nozaki, T.; Ido, T.; Kasida, Y. Adrenal affinity and plasma lipoprotein binding of radio-halogeno derivatives of cholesterol. *J. Labelled Compd. Radiopharm.* **1979,** *16*, 49–51.

(39)   Barbee, R. W.; Perry, B. D.; Re, R. N.; Murgo, J. P. Microsphere and dilution techniques for the determination of blood flows and volumes in conscious mice **1992,** *Am. J. Physiol.* (263), R728–733.

(40)   Workman, P.; Aboagye, E. O.; Balkwill, F.; Balmain, A.; Bruder, G.; Chaplin, D. J.; Double, J. A.; Everitt, J.; Farningham, D A H; Glennie, M. J.; Kelland, L. R.; Robinson, V.; Stratford, I. J.; Tozer, G. M.; Watson, S.; Wedge, S. R.; Eccles, S. A. Guidelines for the welfare and use of animals in cancer research. *Br J Cancer* **2010,** *102* (11), 1555–1577.

(41)   Fitton, A. O.; Hill, J.; Jane, D. E.; Millar, R. Synthesis of simple oxetane carrying reactive 2-substituents. *Synthesis* **1987,** *12*, 1140–1142.

(42)   Sun, Q.; Cai, S.; Peterson, B. R. Practical Synthesis of 3β-Amino-5-cholestene and Related 3β-Halides Involving i -Steroid and Retro- i -Steroid Rearrangements. *Org. Lett.* **2009,** *11* (3), 567–570.

Supporting Information

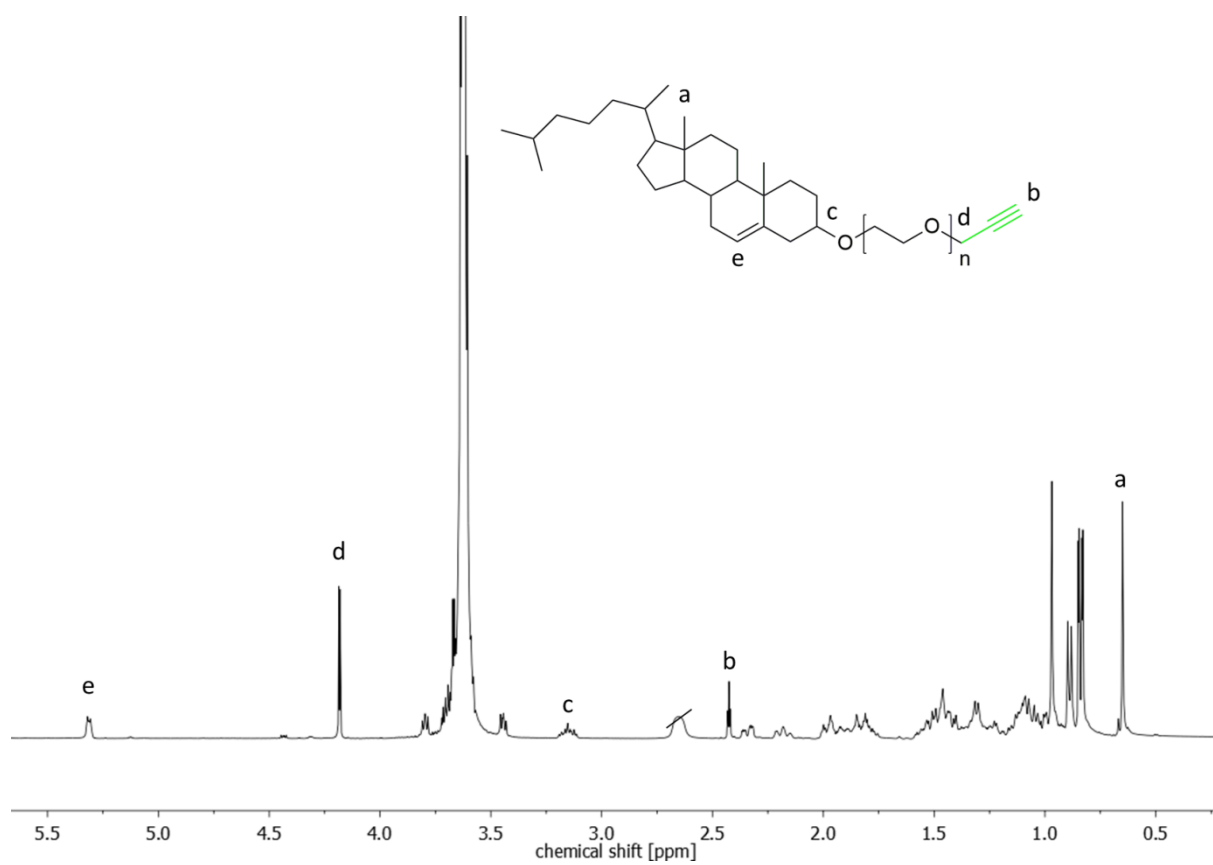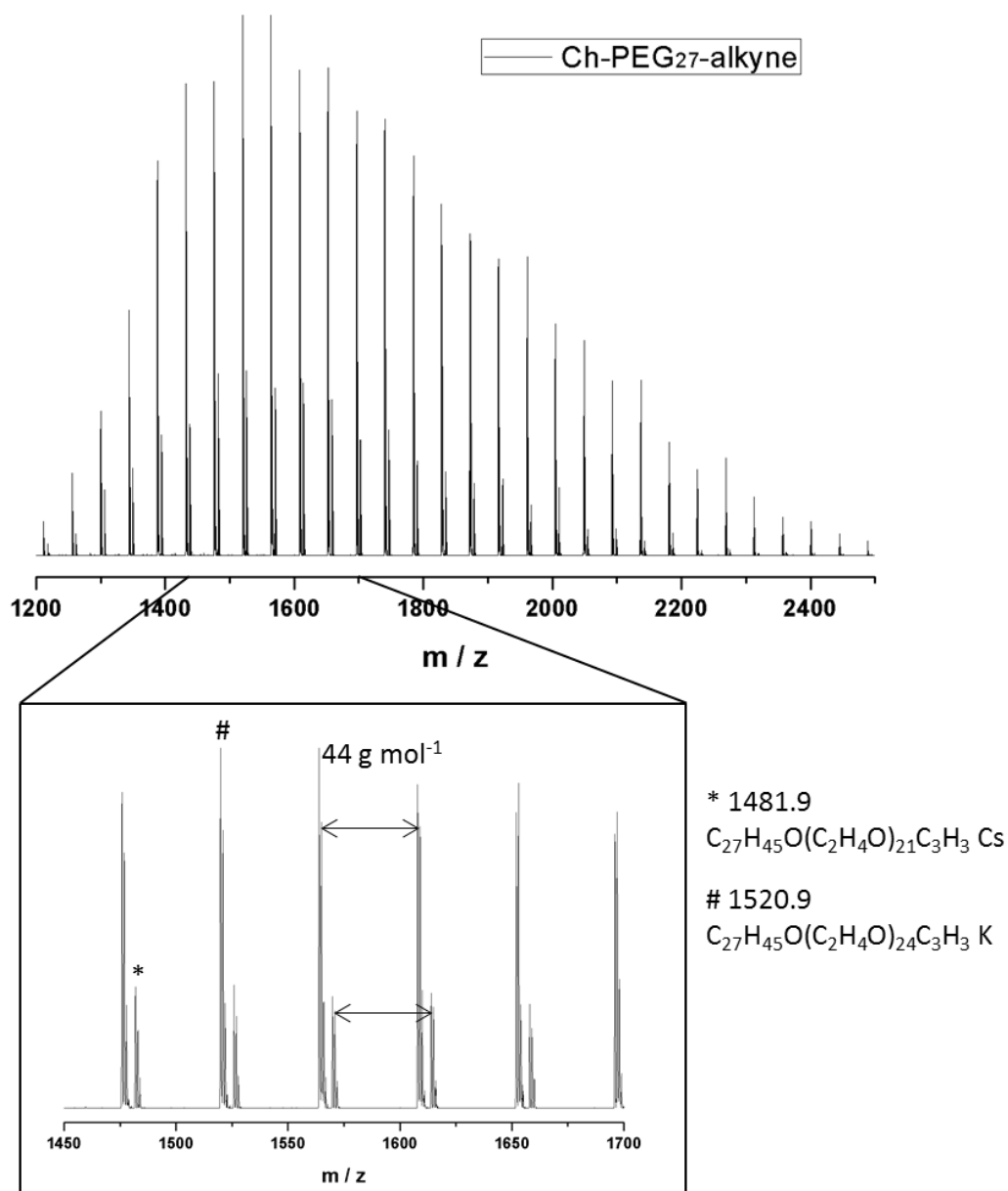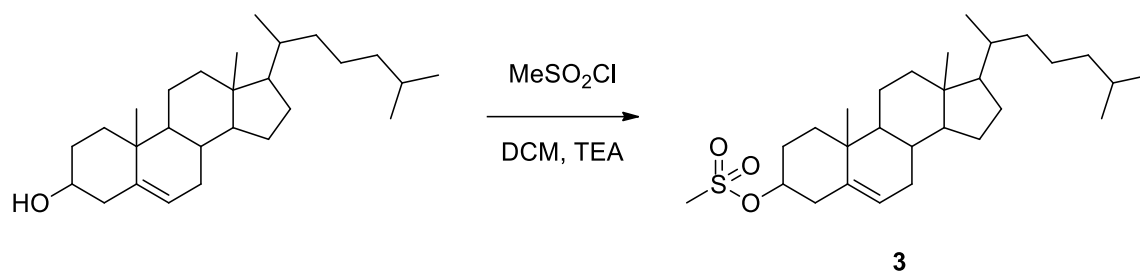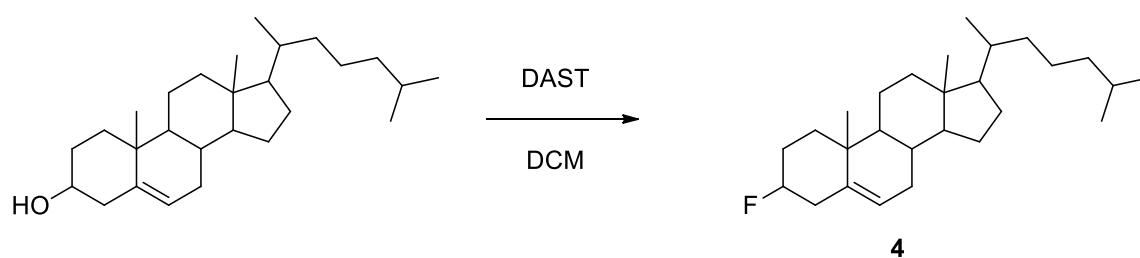*Figure S1*: ^{1}H NMR spectrum (400 MHz) of Ch-PEG$_{27}$-CH$_2$-C≡CH (**1**) in CDCl$_3$.

Figure S2: MALDI-ToF mass spectrum of Ch-PEG$_{27}$-CH$_2$-C≡CH (**1**) (Dithranol as matrix; potassium trifluoroacetate (KTFA) as cationization agent).
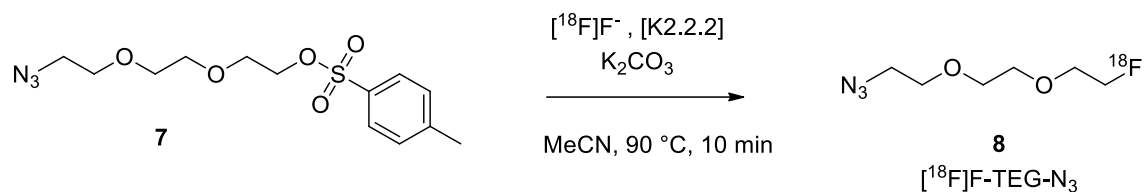
Scheme S1: Reaction scheme for the synthesis of methanesulfonic acid 3β-cholesteryl ester (**3**) starting from cholesterol.
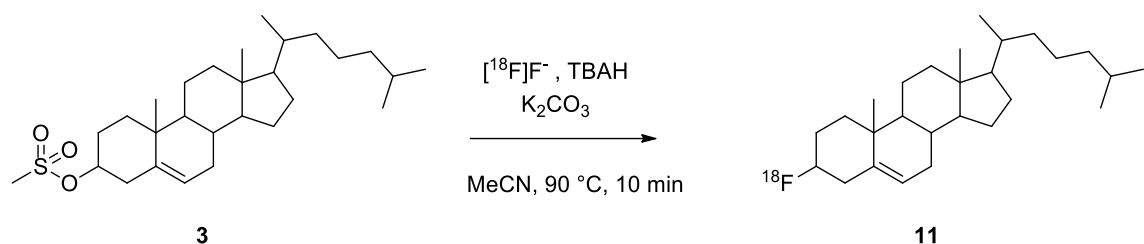

Scheme S2: Reaction scheme for the synthesis of 3-fluoro-cholest-5-ene (**4**) starting from cholesterol; DAST= diethylaminosulfur trifluoride.
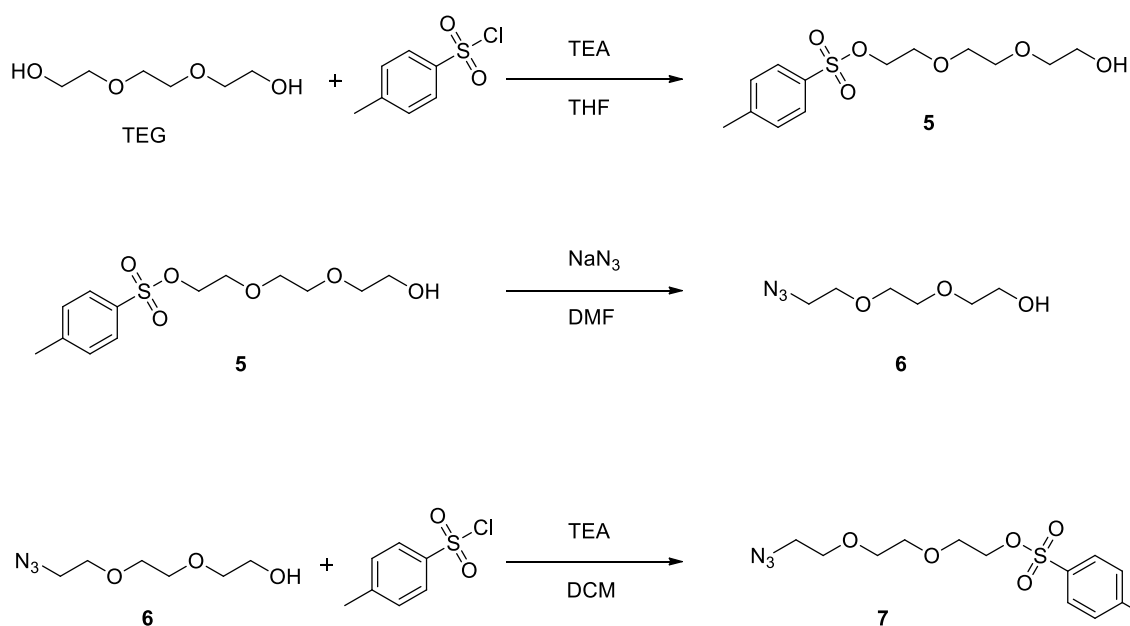

Scheme S3: Reaction scheme for the synthesis of 2-(2-(2-azidoethoxy)ethoxy)ethyl-4-p-toluenesulfonate (**7**) starting from triethylene glycol (TEG).

Scheme S4: Reaction scheme and reaction conditions for the radiosynthesis of 1-azido-2(2-(2-[^{18}F]fluoroethoxy)ethoxy)ethane ((**8**), [^{18}F]F-TEG-N$_3$) *via* the nucleophilic ^{18}F-fluorination using ^{18}F-fluoride-Kryptofix complex.

Scheme S5: Reaction scheme for the synthesis of 3-[^{18}F]fluoro-cholest-5-ene (**11**) starting from methanesulfonic acid 3β-cholesteryl ester (**3**); TBAH= Tetrabutylammoniumhydroxide.
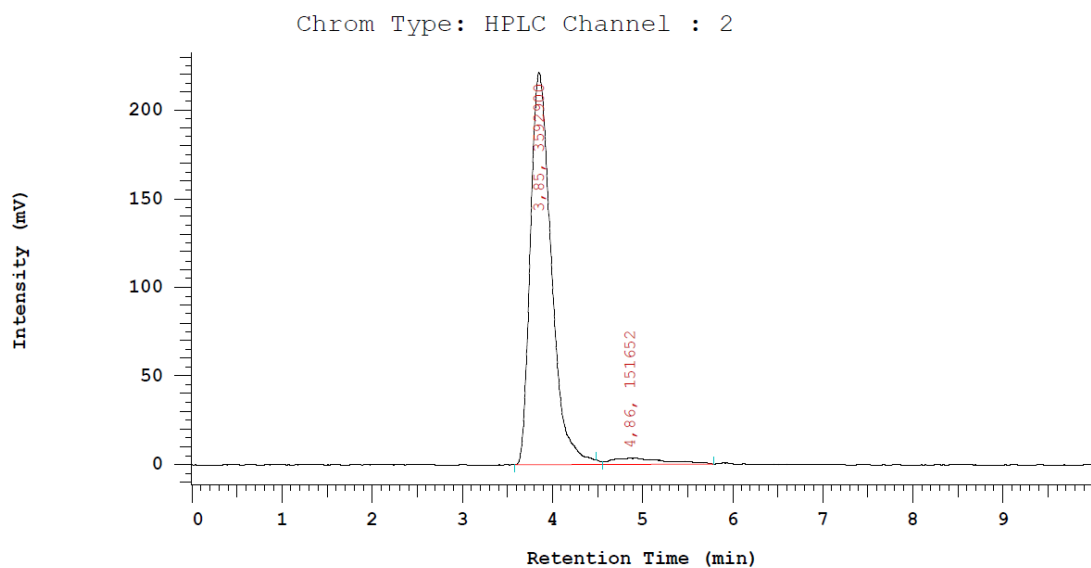
Figure S3: Chromatogram of [^{18}F]F-TEG-N$_3$: 2 Onyx Monolithic C18 in a row 75:25 (H$_2$O:MeCN), 2 mL flow.
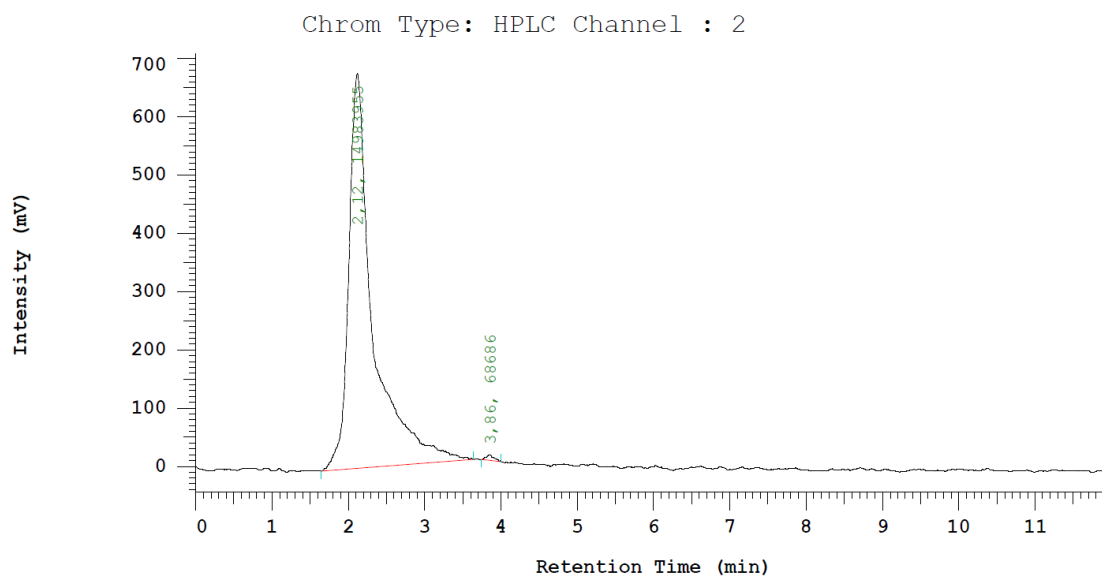
Figure S4: Chromatogram of reaction mixture (RCY>95%) Ch-PEG$_{30}$-*hb*PG$_{24}$-triazole-^{18}F: 2 Onyx Monolithic C18 in a row 75:25 (H$_2$O:MeCN), 2 mL flow.
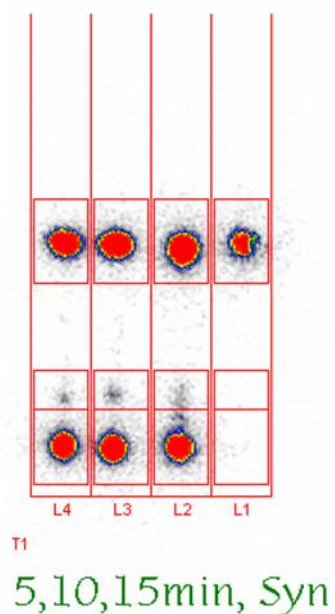
Figure S5: Radio-TLC of a CuAAC reaction (Ch-PEG$_{30}$-*hb*PG$_{24}$-triazole-TEG-^{18}F) after 5, 10, and 15 min plus [^{18}F]F-TEG-N$_3$ (Syn) with poor yields.
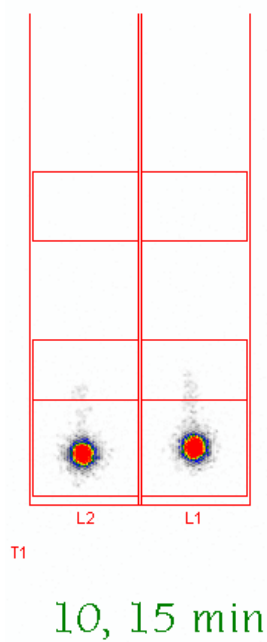
Figure S6: 5: Radio-TLC of a CuAAC reaction (Ch-PEG$_{30}$-*hb*PG$_{24}$-triazole-TEG-^{18}F) after 10 and 15 min with RCY > 95%.

5 Polyether-Based Copolymer as Thermoresponsive Materials

## 5.1 A Challenging Comonomer Pair: Copolymerization of Ethylene Oxide and Glycidyl Methyl Ether to Thermoresponsive Polyethers

Sophie S. Müller,[1,2] *Christian Moers,*[1,2] *and Holger Frey*[1,*]

[1]Institute of Organic Chemistry, Johannes Gutenberg University Mainz, Duesbergweg 10-14, 55128 Mainz, Germany

[2]Graduate School Materials Science in Mainz, Staudingerweg 9, 55128 Mainz, Germany
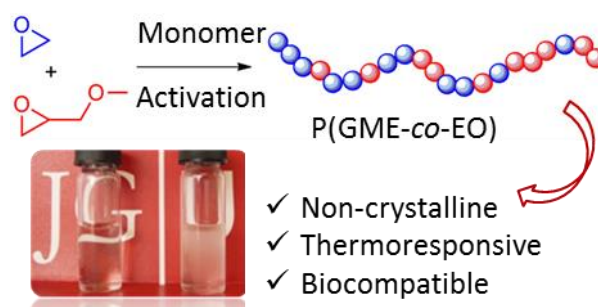
Abstract

Motivated by the oxygen-rich and fully amorphous structure of poly(glycidyl methyl ether) (PGME), a series of thermoresponsive poly(glycidyl methyl ether-*co*-ethylene oxide) copolymers P(GME-*co*-EO) with molecular weights in the range of 3000-20 000 g mol^{-1} was synthesized by the activated monomer polymerization technique. Tetraoctylammonium bromide (NOct$_4$Br) was employed as initiator in combination with triisobutylaluminum (*i*-Bu$_3$Al) as a catalyst under mild conditions. Polyethers with varying GME content between 31 mol% and 100 mol% were obtained. Triad sequence analysis using ^{13}C NMR spectroscopy proved that no pronounced block structure was obtained. Differential scanning calorimetry (DSC) revealed that samples exceeding 65 mol% content of GME are amorphous, whereas with lower GME content a low degree of crystallization was observed. Melting temperatures for these polyethers were in the

range of 9.8-37.5 °C. Furthermore, the copolymers' lower critical solution temperature (LCST) in aqueous solution was tuned between 55 °C for the PGME homopolymer up to 98 °C by varying the amount of GME. The approach permits to combine two highly biocompatible and water-soluble materials.

Introduction

Aliphatic polyethers are an important class of materials for a vast variety of applications, e.g., for pharmaceutical purposes and drug-delivery,[1] lithium-polymer batteries,[2] non-ionic surfactants,[3] and many others. They are commonly synthesized by the oxyanionic ring-opening polymerization (ROP) of epoxides using alkali metal alkoxides as initiators, but also via metal-free polymerization methods.[4] Poly(ethylene glycol) (PEG) is undoubtedly the most important polyether due to its outstanding property profile and remarkable solubility both in water and organic solvents. However, due to its high degree of crystallization, PEG is shows drawbacks for some applications, such as lithium-ion batteries.[5] To suppress crystallization, epoxide comonomers with pendant side groups can be introduced. Copolymerization of ethylene oxide (EO) and propylene oxide (PO) with a methyl side group is an established strategy to lower the melting temperature or completely prevent crystallization of PEG, as demonstrated by several industrial products, like polyether-amines with the trade name Jeffamines® (Huntsman corporation). Furthermore, random P(EO-co-PO) copolymers exhibit tunable thermoresponsive behavior in aqueous solution, which has only rarely been mentioned in literature.[6,7] Incorporating the hydrophobic monomer PO leads to lower critical solution temperatures (LCSTs) in aqueous solution in the range of 30-100 °C.[6,7,8] It has recently been demonstrated that multifunctional polyether copolymers consisting mainly of EO units generally show this interesting behavior in aqueous solution.[9]

One important drawback of the polymerization of alkene oxides, such as PO, is the high basicity of the initiating and propagating alkali metal alkoxide, combined with the harsh reaction conditions in conventional anionic ROP. Proton abstraction from the methyl

group of PO or the methylene group adjacent to the oxirane ring of a glycidyl ether results in an undesired transfer reaction to monomer, leading to the formation of an allyl alkoxide.[4,10] Therefore, the synthesis of polyethers under common oxyanionic conditions and high temperature usually is limited to moderate molecular weights (< 15 000 g mol^{-1} for PO).[11]

Deffieux, Carlotti et al. introduced an alternative strategy for the polymerization of various epoxides, leading to high molecular weight polymers with molecular weights up to 20 ,000 g mol^{-1} via a monomer activation process under mild reaction conditions.[12] The strategy relies on an anionic polymerization technique based on a trialkylaluminum catalyst (e.g., i-Bu$_3$Al) and a tetraalkylammonium salt as the initiator system (e.g., NOct$_4$Br).[13] The initiation by a rather weak nucleophile (e.g., bromide) is a key difference in comparison to the conventional anionic polymerization, which commonly requires much stronger nucleophiles leading to the abovementioned elimination side reactions. One main drawback on the other hand, is the removal of the remaining initiator salt (NOct$_4$OH), which is challenging due to its amphiphilic structure. In groundbreaking works, the monomer activation mechanism has been demonstrated for several systems, namely the (co)-polymerization of EO and PO,[14] glycidyl methacrylate (GMA) and glycidyl methyl ether (GME),[15] ethoxyethyl glycidyl ether,[16] epichlorohydrin,[17,18,19] and various hydrophobic epoxides[20] that are usually difficult to polymerize to high molecular weight products. Heterofunctional α-azido,ω-hydroxypolyethers using tetrabutylammonium azide as an initiator were obtained in one step.[21,22]

GME, the methylated form of glycidol, is an interesting, commercially available, and low cost glycidyl ether monomer. A direct strategy for the polymerization of GME is the anionic ROP, resulting in quantitatively methylated and thermoresponsive linear poly(glycerol).[23] In recent studies, the main focus for poly(glycidyl methyl ether) (PGME) was placed on application in protein repellent coatings,[24,25,26] as well as on its unique thermosensitive properties.[15,27,28] Aoki et $al.$ detected a LCST for the homopolymer at 57.7 °C, above which the polymer becomes insoluble in water.[29] However, only a few studies on the polymerization of GME have been reported to date, which might be due to the rather harsh polymerization conditions (reaction temperatures exceeding 110 °C and highly basic conditions) required to open the epoxide ring. Surprisingly, with the conventional anionic ring-opening method only molecular weights up to 3000 g mol^{-1}

have been reported for the polymerization of GME.[24,29] It is not yet understood why the GME monomer exhibits such low reactivity compared to other glycidyl ether derivatives. Obviously, the low reactivity is a challenge for copolymerization of GME with EO, since EO is a toxic gas (boiling point= 11 °C), and the elevated temperatures required would result in high pressures.[30]

Motivated by the structural simplicity of GME, its thermoresponsive behavior and biocompatibility, in the current work we developed a straightforward copolymerization protocol for the preparation of poly(glycidyl methyl ether-*co*-ethylene oxide) (P(GME-*co*-EO)) copolymers. To the best of our knowledge EO and GME have not been combined to date, despite the interesting biocompatibility of both homopolymers. The activated monomer procedure was used for the synthesis of the resulting thermosensitive polyethers. In this case the polymerization can be conveniently carried out at low temperatures (-15 °C-25 °C). The synthetic route is shown in Scheme 1. The resulting copolymers have been characterized with respect to their microstructure, thermal characteristics and cloud point in aqueous solution in dependence of the ratio of EO and GME units incorporated.
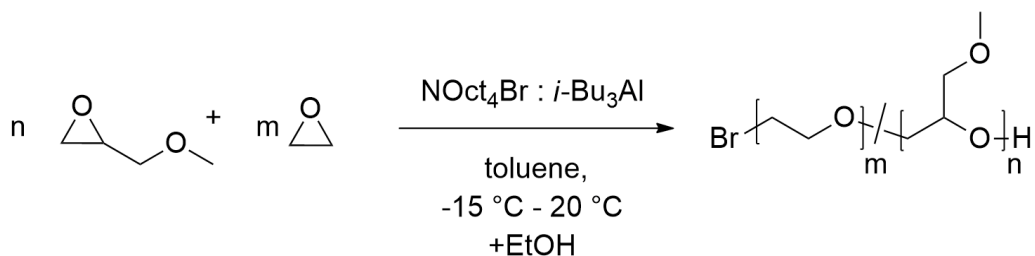
Scheme 1: Synthetic route for the copolymerization of glycidyl methyl ether (GME) and ethylene oxide (EO) using the monomer activation method.

Experimental Section

Instrumentation

^{1}H NMR spectra and inverse gated (IG) ^{13}C NMR spectra were recorded using a Bruker AC 400 spectrometer operated at 400 MHz or 100 MHz, respectively. All spectra are referenced internally to residual proton signals of the deuterated solvent. Size exclusion chromatography (SEC) measurements were carried out in dimethylformamide (DMF) with 0.25 g L^{-1} LiBr with Polymer Standards Service (PSS) HEMA columns (300/100/40).

For SEC measurements a UV (275 nm) and an RI detector were used. Calibration was achieved using poly(ethylene glycol) (PEG) standards provided by PSS. Differential scanning calorimetry (DSC) measurements were carried out using a Perkin-Elmer DSC 8500 in the temperature range of -100 to 100 °C, using heating and cooling rates of 20 °C min^{-1} (1st cycle) and 10 °C min^{-1} (2nd cycle), respectively. The values of the second heating cycle were used for analysis. The melting points of indium (T_m = 156.6 °C) and Millipore water (T_m = 0 °C) were used for calibration. UV/vis spectra were recorded at 20 °C using a Jasco V-630 photospectrometer containing a Jasco ETC-717 Peltier element. Cloud points were determined in deionized water at a concentration of 5 mg mL^{-1} and a heating rate of 1 °C min^{-1} with the same instrument. A light beam (λ = 500 nm) was radiated through a 1 cm quartz cell, and the relative intensity of transmitted light was measured in dependence of temperature, while recording data points every 0.1 °C. The transition from transparent to opaque solutions was taken as cloud point and defined as the temperature corresponding to 50% transmission. We will refer to the LCST of the copolymers in a general sense, although the term LCST in a stringent sense corresponds to the lowest cloud point temperature possible, which is observed only at a certain concentration of a polymer.

Reagents

Solvents and reagents were purchased from Acros Organics, Sigma Aldrich, or Fluka and used as received, unless otherwise stated. Deuterated solvents were purchased from Deutero GmbH, and stored over molecular sieves. Triisobutylaluminum (i-Bu$_3$Al, 1.1 M in toluene, Aldrich) was used without further purification. Tetraoctylammonium bromide (NOct$_4$Br, >99%, Aldrich) was azeotropically dried with toluene overnight at dynamic vacuum prior to use. Toluene was dried over sodium and was kept in a flask under vacuum until usage. Glycidyl methyl ether (GME, >85%, TCI) was distilled twice over CaH$_2$ at reduced pressure, stored in a fridge. GME was freshly dried over CaH$_2$ and cryo-transferred prior to use. Ethylene oxide (EO) was purchased from Fluka and was dried over CaH$_2$ in a graduated ampule before each reaction.

Polymer Synthesis

As an example, the procedure is described for P(GME$_{0.42}$-co-EO$_{0.58}$) (Sample 5, Table 1 theoretical 40 mol% GME: 60 mol% EO): The initiator NOct$_4$Br (0.3 g; 0.55 mmol) was weighed in a Schlenk flask, toluene was added and the mixture was dried overnight

under vacuum. Anhydrous toluene was added via cryo transfer, and the dried GME (1.6 mL; 17.6 mmol) was added via syringe. EO (1.3 mL; 26.3 mmol) was cryo transferred first to a graduated ampule with CaH_2 and then to the Schlenk flask containing the initiator-monomer solution. The mixture was cooled with an ice/salt mixture (-15 °C), so that EO was still liquid, and the i-Bu$_3$Al solution (0.75 mL; 0.8 mmol) was carefully added via syringe. The reaction was allowed to warm up to room temperature and stirred for about 21 h. Subsequently, 5 mL of ethanol were added to stop the reaction.

All polymerizations were carried out until quantitative conversion and produced samples with molecular weights between 3000 and 16 000 g mol^{-1} according to SEC. The materials were purified by column chromatography, since residual NOct$_4$OH can influence the copolymers´ properties, e.g., the crystallization peak of NOct$_4$OH is observed in DSC measurements, as described below. First, the initiator salt was eluted using diethylether: MeOH (10:3). Subsequently, the polymer was retrieved in a CHCl$_3$: MeOH flush (8:2). Higher molecular weight copolymers could be purified by dialysis in CH_2Cl_2, albeit with rather high reduction of the polymer yield. Dissolving the polymer in water and filtering is also suitable to remove a majority of residual NOct$_4$OH. Copolymers were obtained as colorless, viscous liquids. With increasing EO content, the products showed an increasingly crystalline appearance, as discussed in the section "Thermal Properties". Yields of the copolymers were generally in the range of 50-75% and depended on the purification procedure that was required to remove NOct$_4$Br. Full removal leads to strongly reduced yields.

Results and Discussion

As reported in literature, the monomer activated anionic polymerization initiated by NOct$_4$Br/i-Bu$_3$Al requires an excess of the aluminum compound with respect to the initiator NOct$_4$Br.[15,16,17] First, coordination of i-Bu$_3$Al to the initiator NOct$_4$Br takes place, forming a 1:1 "ate" complex. An excess of the aluminum compound can strongly activate the monomer, which is attacked by the nucleophilic "ate" complex. The nucleophilic bromide initiates the polymerization, while the monomers can insert and propagate. In

our case, EO and GME compete for the insertion process. The mechanism is depicted in Scheme 2 for GME and EO.
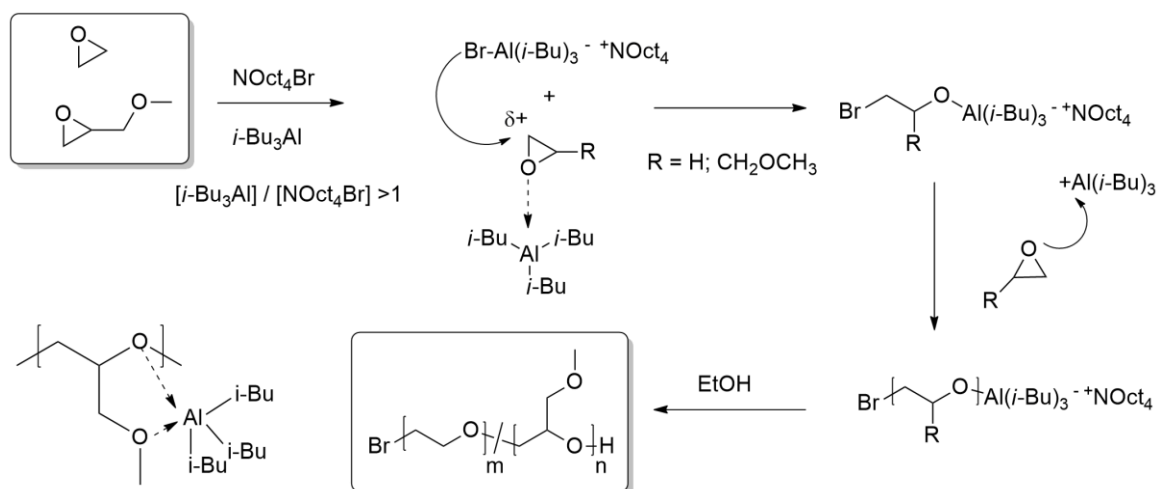
Scheme 2: Reaction mechanism with monomer activation, nucleophilic attack by bromide and subsequent monomer insertion step as well as the complexation of the aluminum compound by the oxygens of the PGME backbone.

Table 1 lists all experimental data, including molar masses and polydispersity indices (M_w/M_n= PDI) obtained by SEC (DMF, PEG standards). Molecular weights were varied between 3000 and 20 000 g mol^{-1}, and moderate PDIs between 1.21-1.70 were obtained. A slight broadening can be noticed for copolymers of molar masses exceeding 5000 g mol^{-1} and for high [i-Bu$_3$Al]/[NOct$_4$Br] ratios. A similar trend was already observed for the (homo)polymerization of PO[31] or EEGE[16], when using the trialkylaluminum/ tetraalkylammonium salt systems. The last column in Table 1 summarizes the catalyst vs. initiator ratios. Varying the composition turned out to be challenging, since for each comonomer composition different [i-Bu$_3$Al]/[NOct$_4$Br] ratios had to be used. In addition, for each molecular weight this ratio had to be adjusted, since the polymerization rate increases with increasing trialkylaluminum concentration, and a loss of polymerization control is observed. On the other hand, an insufficient concentration of trialkylaluminum compound may lead to incomplete conversion, as more i-Bu$_3$Al is required to trigger GME polymerization. Trialkylaluminum may be inactivated by complexation with the oxygens of PGME segments, as shown in Scheme 2. Higher PDIs at higher ratios [i-Bu$_3$Al]/[NOct$_4$Br] can be attributed to side-reactions associated with a temperature

increase in the reaction vessel and subsequent loss of control due to fast polymerization kinetics.[12]

All SEC traces are monomodal (compare selection in Figure 1) and translate to molecular weights slightly lower than targeted by the ratio of $NOct_4Br$ initiator/monomer. Since the polymerization is not based on a functional initiator, we were unable to use ^{1}H NMR spectroscopy to calculate exact molecular weights. However, ^{1}H NMR spectroscopy was used to calculate the incorporated GME/EO ratio from a comparison of the signal of the methyl group at 3.32 ppm to the polyether backbone signals between 3.40 ppm and 3.75 ppm (Figure 2).

Table 1. Copolymers of glycidyl methyl ether (GME) and ethylene oxide (EO) initiated with $NOct_4Br$ and *i*-Bu_3Al as the catalyst.

No.	Composition [a]	[GME]/ [EO] mol% [th]	M_n [th] [g mol^{-1}]	M_n [b] [g mol^{-1}]	M_w/M_n [b]	[*i*-Bu_3Al]/ [$NOct_4Br$]
1	PGME	100:0	10 000	5200	1.50	4
2	$P(GME_{0.78}$-*co*-$EO_{0.22})$	80:20	4760	4700	1.21	1.5
3	$P(GME_{0.68}$-*co*-$EO_{0.32})$	60:40	4900	3400	1.68	4
4	$P(GME_{0.67}$-*co*-$EO_{0.33})$	66:34	5400	4450	1.21	1.5
5	$P(GME_{0.42}$-*co*-$EO_{0.58})$	40:60	4933	3200	1.21	1.5
6	$P(GME_{0.31}$-*co*-$EO_{0.69})$	20:80	4750	4700	1.23	1.5
7	$P(GME_{0.61}$-*co*-$EO_{0.39})$	50:50	19 200	14 000	1.70	3
8	$P(GME_{0.55}$-*co*-$EO_{0.45})$	50:50	19 800	15 000	1.44	3
9	$P(GME_{0.75}$-*co*-$EO_{0.25})$	80:20	20 600	16 000	1.63	3

[a] Values calculated by ^{1}H NMR spectroscopy; [b] Determined by SEC (DMF, PEG standard).

The composition was calculated for all polymers, and the values are summarized in Table 1 ([GME]/[EO]). Additionally, the ratios can be calculated by comparing the resonances for both monomers in inverse gated (IG) ^{13}C NMR spectra (Figure 3). Here, the same results were obtained with a variation of about 5% that is due to integration errors. The percentages are given as numbers in subscripts in the polymer name (Table 1). The values are in rather good agreement with expectation. However, in some cases the values differ, possibly due to small differences in measuring liquid EO. A typical

problem of the activated monomer mechanism is the removal of the NOct$_4$OH initiator salt subsequent to the polymerization. Removing traces of NOct$_4$OH is challenging, since its amphiphilic structure renders separation from the polymer difficult. Precipitation of the polymer can be an option, if one finds a suitable solvent for NOct$_4$OH, in which the polymer product precipitates.[19] In our case, column chromatography was used for the low molecular weight copolymers in order to remove the salt. Dialysis in CH$_2$Cl$_2$ or filtration of an aqueous solution of the respective polymer, was more suitable and more convenient for the higher molecular weight copolymers. A representative ^{1}H NMR spectrum before and after removal of NOct$_4$OH by column chromatography is given in the Supporting Information (Figure S1).

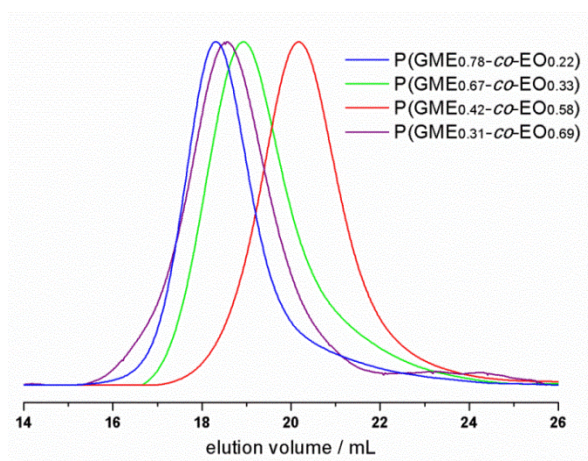*Figure 1*: SEC traces of selected copolymer samples; numbers in subscript indicate the ratio of GME and EO in mol%). P(GME$_x$-*co*-EO$_y$) copolymers in DMF (P(GME$_{0.78}$-*co*-EO$_{0.22}$); P(GME$_{0.67}$-*co*-EO$_{0.33}$); P(GME$_{0.42}$-*co*-EO$_{0.58}$); P(GME$_{0.31}$-*co*-EO$_{0.69}$).
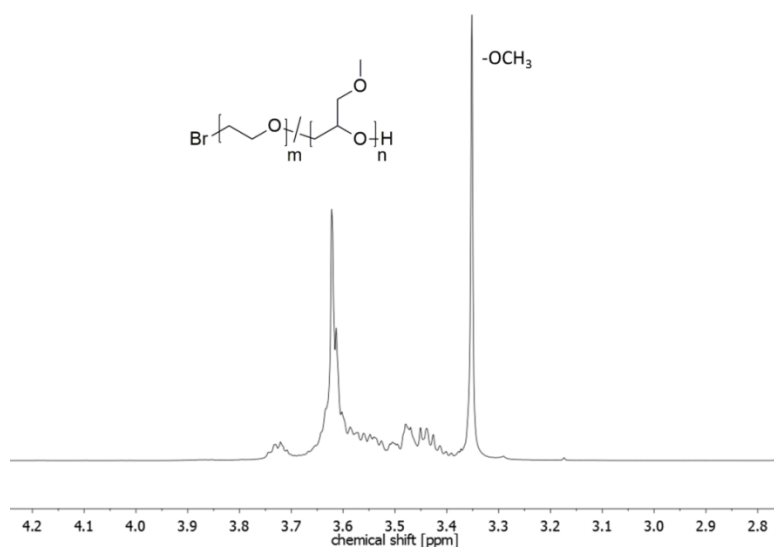
Figure 2: ^{1}H NMR spectrum of P(GME$_{0.67}$-EO$_{0.33}$) in CD$_2$Cl$_2$.

¹³C NMR Characterization (Triad Sequence Analysis)

Via copolymerization of GME and EO we targeted highly hydrophilic, non-crystalline and thermoresponsive linear polyethers. These properties do not only depend on the total GME/EO ratio incorporated into the polymer, but are also significantly influenced by the monomer distribution within in the polymer chain (block, gradient, random). The influence of adjacent units on the methylene and methine carbon shift on both monomer units allows for the determination of the polymers' microstructure. Triad sequence analysis is a well-established method that has also been used to analyze copolymers consisting of EO and PO,[14,32] ethoxyethyl glycidyl ether,[33] 1,2-isopropylidene glyceryl glycidyl ether,[34] allyl glycidyl ether (AGE) and *N,N*-dibenzylamino glycidol (DBAG)[35] or ethoxy vinyl glycidyl ether (EVGE).[36] This method clearly proved that copolymers of EO and glycidyl ether derivatives, like EVGE, resulted in random copolymers, when the oxyanionic polymerization method was employed. However, little is known about the comonomer incorporation in the case of monomer activation polymerization. Figure 3 displays the most important region of the IG ^{13}C NMR spectra of the low molecular weight P(GME-*co*-EO) copolymers. EO units are referred to as "E", while GME units are abbreviated with "G". Since both monomers possess two carbons (methylene and methine in the case of GME), they are referred to as "a" or "b". These carbon shifts are strongly influenced by the adjacent monomer units.

In the IG ^{13}C NMR spectra of five copolymers with different amount of GME (Figure 3), two main regions for characterization of the composition can be discerned. The carbon resonances of the polyether backbone appear between 69.6-73.6 ppm and from 78.5-79.4 ppm (Figure 3). Having the homopolymer of PGME in hand, all signals of the GME units can be assigned (methylene G_a and II, methine G_b, and the methyl group I, compare chemical structure Figure 3). By comparing the five spectra and based on reported literature values,[32] the methylene groups of the EO triad (E-E-E) can be clearly assigned. The spectra of the copolymers differ drastically from the PGME homopolymer. With increasing amount of incorporated EO, new resonances appear, which are marked in grey in Figure 3. These new resonances were assigned using literature values and based on simulated ^{13}C NMR spectra (ChemDraw Ultra 10.0).[32] With increasing amount of EO, the E-E-E triad signals at 71.0 ppm increase (Figure 3, top to bottom), while the triads for GME (G-G_a-G) at 73.1 ppm decrease.

Additionally, Figure 3 shows the chemical shift for the methine carbons of GME (G_b). Here, between 78.8 ppm and 79.4 ppm the G-G-G triad can be assigned based on the homopolymer spectrum. The splitting results from stereosequences/polymer tacticity.[20,37] With increasing amount of EO, these signals decrease and the more probable triad E-G-E appears at around 78.7 ppm. Interestingly, the signal for the methyl group of the GME unit also splits into two signals with increasing amount of EO. In Figure 3 (inset) only one peak is seen for the homopolymer at 59.4 ppm, whereas for the copolymers splitting of the resonance is observed. We attribute this to the interaction of the methyl group with the adjacent monomer units on both sides of the GME unit.

The more "complex" ^{13}C NMR spectra of the copolymers compared to the ^{13}C NMR spectrum of the homopolymer PGME demonstrate that a random or gradient distribution of EO and GME throughout the polyether backbone was obtained. Additionally, the interaction observed between the methyl group of GME and the adjacent monomer units clearly proves that no preferential block structure is formed during the polymerization. The thermal characterization discussed in the following section provides additional insight to distinguish between an ideally random or gradient type structure.
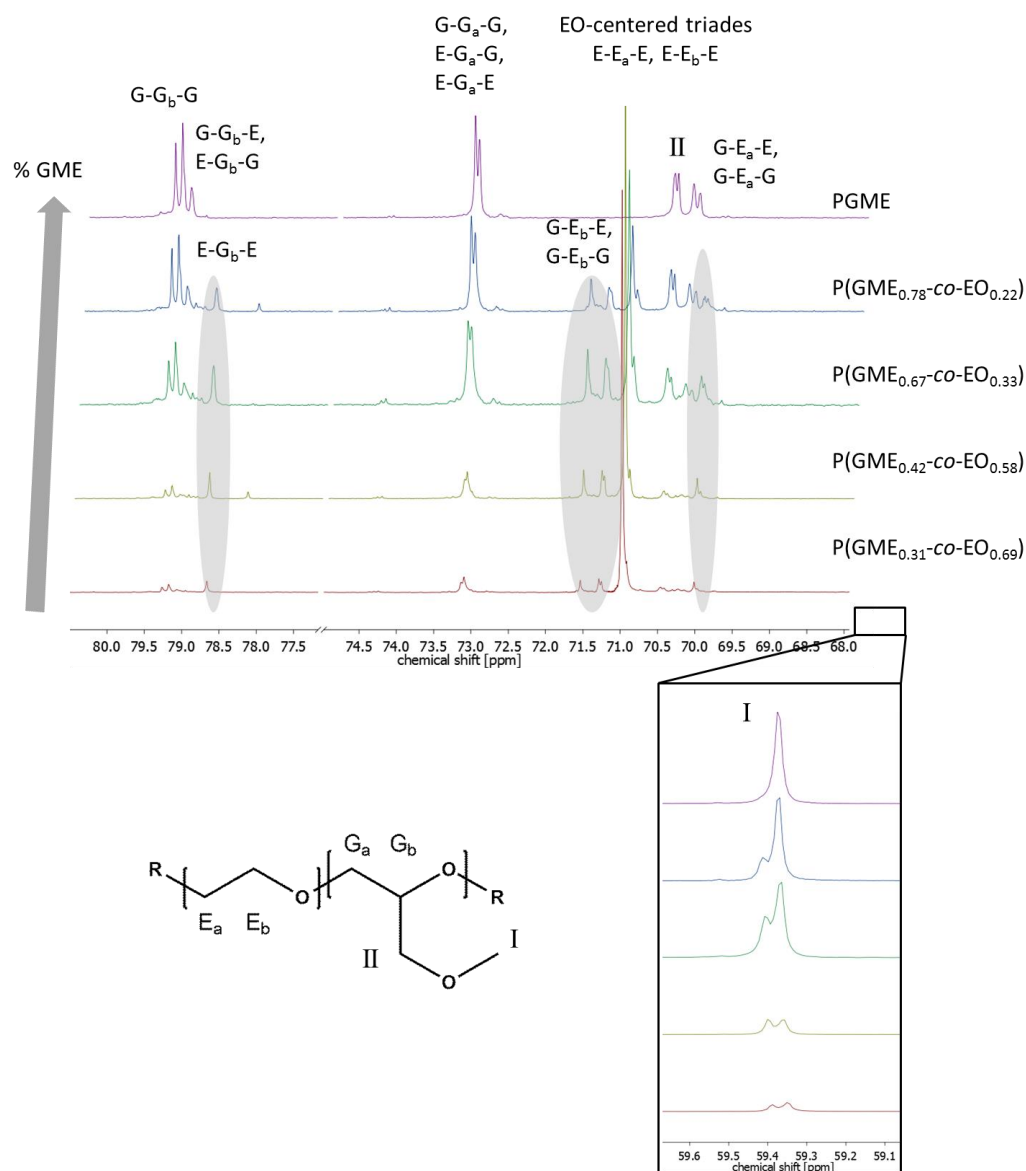
Figure 3: Inverse gated ^{13}C NMR spectra of $P(GME_x\text{-}co\text{-}EO_y)$ in CD_2Cl_2 with varying amounts of GME (31-100 mol% bottom to top; I, II, G_a and G_b belong to the GME units; E_a and E_b belong to the EO units).

Thermal Properties and Degree of Crystallization

The content of GME should permit to tailor the thermal properties of the copolymers. The effect of increasing incorporation of GME immediately became evident, since copolymers with GME content exceeding 42 mol% were transparent, viscous liquids, whereas elevating the EO content afforded increasingly crystalline samples.

Differential scanning calorimetry (DSC) was used to investigate the thermal properties of the copolymers. The melting temperature (T_m) of PEG is strongly dependent on its molecular weight.[38] For commercially available methoxy-poly(ethylene glycol) (mPEG-

350) one observes a broad melting endotherm around -4.0 °C, for mPEG-550 an increase of T_m to 12.5 °C is found, whereas mPEG-1100 exhibits a T_m at 37.5 °C. With increasing molecular weight the T_m steadily approaches its maximum of 66 °C.[38] On the other hand, due to its atactic nature the PGME homopolymer exhibits no melting. However, a low glass transition temperature (T_g -60 °C, sample 1, Table 2) is observed, which mirrors its amorphous character. For some samples that have not been repeatedly purified, a crystallization peak between 89-93 °C was observed, which cannot be ascribed to polyether structures, but is attributed to residual $NOct_4OH$ from the polymerization reaction.

DSC results demonstrate the impact of the GME units incorporated in the PEG backbone. Incorporation of GME repeat units in the polyether backbone disrupts the PEG segments, thereby reducing the melting temperature (e.g., to 9.8 °C for sample 7, Table 2), as well as the overall crystalline fraction of the polymers. As the amount of GME decreases, a T_m is detectable that increases up to about 37 °C at 31 mol% GME. The almost linear trend is depicted in Figure 4a, which also emphasizes that above 40 mol% GME content the copolymers exhibit melting temperatures below room temperature. The commercially available PEG-4400 exhibits a T_m at 59 °C. Surprisingly, the copolymer with 55 mol% GME and 45 mol% EO still showed a melting point at 16.6 °C, which was not expected for such high amounts of methyl side-chain containing GME units. Keeping in mind the melting point of mPEG-550 (approximately 13 EO repeating units) at 12.5 °C, these results lead us to the assumption that the polymer with 45 mol% EO units already contains significantly EO-enriched segments. In combination with the results of IG ^{13}C NMR characterization, we therefore propose a gradient-type structure of the copolymers. This hypothesis is further supported by the changes of the melting enthalpy, which is strongly reduced from 162 J g^{-1} for PEG-4400 to 11 J g^{-1} for P(GME$_{0.61}$-co-EO$_{0.39}$), reflecting the disturbance of the crystalline order by the comonomer GME. Nevertheless, the tapered structure does not appear to be very pronounced, since a linear correlation between the GME content and the melting enthalpy is observed (Figure 4b), which would not be expected for a strong comonomer gradient. From the values of the melting enthalpy the normalized crystalline fraction (χ_c) can be calculated according to Equation 1[39,40], dividing the melting enthalpy (ΔH_m) by the melting enthalpy for PEG with a hypothetic degree of crystallization of 100% (ΔH_m^∞) and normalizing this

value to the relative fraction of PEG (f_w^{PEG}), thereby taking the decrease of crystallizable PEG segments into account. The theoretical melting enthalpy for 100% crystalline PEG is 196.8 J g^{-1}.[41] For the commercially available PEG-4400 we determined a melting enthalpy of 162 J g^{-1}, which corresponds to a normalized degree of crystallization of 82.3%. With increasing amount of GME in the polyether backbone χ_c can be tuned between 48.6 J g^{-1} and 14.3 J g^{-1} (Table 2, last column) for GME contents between 31% and 61%. This may be important for specific applications and certain processing demands.

$$\chi_c = \frac{\Delta H_m}{\Delta H_m^\infty * f_w^{PEG}} \tag{1}$$

Table 2 lists the T_g values for all samples, however, no trend is observed for the copolymers. This is in line with expectation, since both polyether homopolymers exhibit a T_g around -60 °C. For PGME a T_g of -60 °C was detected, and for PEG-4400 a T_g at -57 °C was identified. The variation of the glass transition temperatures most likely originates from small changes in molecular weight and composition.

Table 2: Thermal properties of copolymers of glycidyl methyl ether (GME) and ethylene oxide (EO).

No.	Composition [a]	M_n (SEC) [g mol^{-1}]	T_g [°C]	T_m [°C]	ΔH^c [J g^{-1}]	Cloud Point T_c [°C]	X_c %
1	PGME	5200	-60.0	-	-	55	-
2	P(GME$_{0.78}$-*co*-EO$_{0.22}$)	4700	-65.3	-	-	64	-
9	P(GME$_{0.75}$-*co*-EO$_{0.25}$)	16 000	-64.6	-	-	58	-
4	P(GME$_{0.67}$-*co*-EO$_{0.33}$)	4450	-64.7	-	-	76	-
7	P(GME$_{0.61}$-*co*-EO$_{0.39}$)	14 000	-66.3	9.8	11	61	14.3
8	P(GME$_{0.55}$-*co*-EO$_{0.45}$)	15 000	-68.5	16.6	17	65	19.2
5	P(GME$_{0.42}$-*co*-EO$_{0.58}$)	3200	-65.0	16.4	39	98	34.2
6	P(GME$_{0.31}$-*co*-EO$_{0.69}$)	4700	-60.7	37.5	66	*n.d.*	48.6
10	PEG-4400	4300	-57.0[b]	58.8	162	*n.d.*[c]	82.3

[a] Values calculated by ^{1}H NMR spectroscopy; [b] The glass transition of PEG was not very pronounced; [c] PEG has a LCST higher than 100 °C.[42] X_c= Normalized degree of crystallization; *n.d.*: not detectable with this setup.
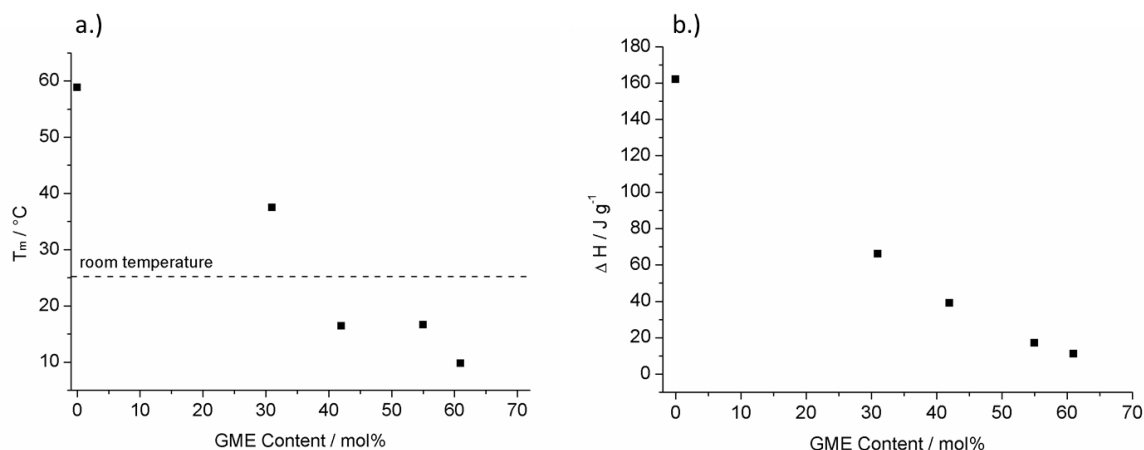
Figure 4: (a) Melting temperatures vs. GME content (mol%) and (b) Melting enthalpy vs. GME content (mol%) of a selection of polymers (PEG-4400; P(GME$_{0.31}$-*co*-EO$_{0.69}$); P(GME$_{0.42}$-*co*-EO$_{0.58}$); P(GME$_{0.55}$-*co*-EO$_{0.45}$); P(GME$_{0.61}$-*co*-EO$_{0.39}$).

Thermoresponsive Properties in Solution

Multifunctional PEGs with various side groups and tunable lower critical solution temperature (LCST) behavior between 9-82 °C have been investigated in our group in recent work.[9] These copolymers are interesting for biomedical applications, especially when the LCST is close to body temperature (~32 °C). Nevertheless, the synthesis of functional monomers that are suitable for the oxyanionc ring-opening polymerization can be cumbersome. In the present study, we were interested in GME as an extremely simple monomer structure, emphasizing the intriguing issue as to how the presence of the additional oxygen of GME influences the LCST in PEG copolymers, compared to the well-known and widely used P(EO-*co*-PO) copolymers.

Most of the P(GME-*co*-EO) copolymers exhibit temperature-dependent solubility in aqueous solution. The thermoresponsive behavior can be explained by the interplay of the hydrophilic PEG segments and the rather hydrophobic methyl groups of the GME units. Above the cloud point the polymer is immiscible in aqueous solution, forming a collapsed globule (polymer-polymer interaction), which can be detected by turbidimetry measurements using a temperature-controlled UV/vis spectrometer. Table 2 summarizes the cloud point temperatures (T$_c$) measured for different P(GME-*co*-EO) copolymers. Figure 5a depicts the laser light transmission with respect to temperature for P(GME-*co*-EO) copolymer solutions.
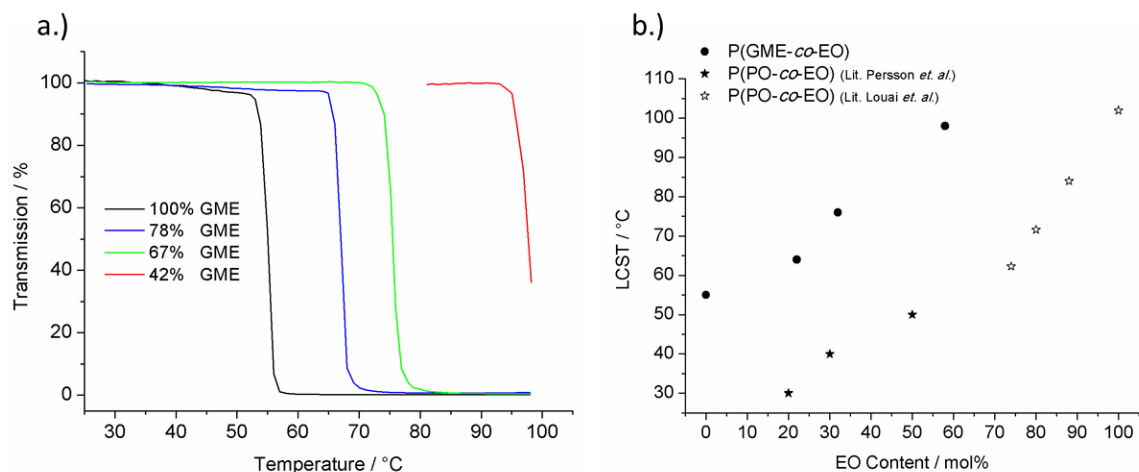
Figure 5: (a) Intensity of transmitted laser light vs. temperature for P(GME-*co*-EO) copolymers of various compositions at a concentration of 5 mg mL^{-1} in aqueous solution. (b) •: Effect of EO content on LCST of the P(GME-*co*-EO) copolymers. For comparison the LCST of P(PO-*co*-EO) copolymers are summarized; ★ data from literature [7]; ☆ data from literature. [6]

As can be seen from Table 2 and Figure 5, the thermoresponsive behavior shows a linear correlation with the composition of the copolymers. For the PGME homopolymer a T_c of 55 °C was detected, as reported in the literature. [27,29] By increasing the amount of the hydrophilic EO units the cloud point increases, as expected, up to a maximum of 98 °C. For PEG the thermoresponsive behavior at elevated temperatures depends on the concentration and molecular weight and has been reported to exceed 100 °C (values obtained under reduced pressure). [42,43] Figure 4b illustrates the linear relationship between the EO content and the LCST, enabling the controlled preparation of polymers with defined cloud points. Louai *et al*. and Persson *et al*. also reported a linear relationship between the EO content and the LCST for P(PO-*co*-EO) copolymers. The first group investigated star shaped random copolymers with molecular weights (M_w) around 30 000 g mol^{-1} and PO contents between 12-26%. The LCSTs increased in a linear fashion from 66-87 °C. [6] The second group determined LCSTs for copolymers (10%wt) with 50, 70, and 80% PO, which were found to be at 50, 40, and 30 °C, respectively. [7] For comparison, Figure 4b demonstrates that the LCST for both copolymer systems (P(GME-*co*-EO) and P(PO-*co*-EO)) is generally lowered by the incorporation of both GME and PO. However, in general, the LCST values for P(GME-*co*-EO)s are approximately 30 °C higher than for copolymers with PO units. This supports the idea that the hydrophilicity of the

GME unit is considerably higher than for the PO-units, leading to improved aqueous solubility. It is also known that an increase in molecular weight results in lowering the LCST, which is in line with the higher values for the 3000 g mol^{-1} samples compared to the 15 000 g mol^{-1} samples (Table 2).[6] This trend is reflected by the values in Table 2 when comparing P(GME$_{0.67}$-*co*-EO$_{0.33}$) (3000 g mol^{-1}) and P(GME$_{0.61}$-*co*-EO$_{0.39}$) (14 000 g mol^{-1}). The first sample shows a T$_c$ of 76 °C, whereas the latter with almost the same EO content, exhibits a T$_c$ of 61 °C. Figure S3 (Supporting Information) gives the intensity of transmitted laser light vs. temperature for the samples P(GME$_{0.75}$-EO$_{0.25}$), P(GME$_{0.61}$-EO$_{0.39}$), and P(GME$_{0.55}$-EO$_{0.45}$) in aqueous solution.

Reactivity of the comonomers

The copolymerization of GME and EO by the activated monomer mechanism represents a novel approach to combine glycidyl ethers and EO. Our group has observed that the copolymerization of these types of monomers usually results in ideally random copolymers, when oxyanionic ring-opening polymerization is applied.[34,36] The qualitative triad sequence analysis has demonstrated that no preferential block structure was obtained, as indicated by the inverse gated ^{13}C NMR spectra for the copolymers compared to the PGME homopolymer. DSC results suggest that there are some crystalline areas in the P(GME-*co*-EO) copolymers with rather high amounts of GME content (< 65 mol%). This result indicates that the microstructure is more of a gradient nature. We have also synthesized two copolymers using an low amount of *i*-Bu$_3$Al-catalyst ([NOct$_4$Br]/[*i*-Bu$_3$Al]= 1:2 for 20 000 g mol^{-1}; not shown in Table 1). Here, no full conversion was obtained, which was attributed to the insufficient concentration of activated monomer species, due to predominant complexation of *i*-Bu$_3$Al by the oxygens of the formed P(GME-*co*-EO) chains.[17] Instead of the targeted GME/EO ratio of 50/50 we observed an incorporation ratio of 28/72, while when aiming at GME/EO = 60/40 the final polymer contained a ratio of 40 mol% GME and 60 mol% EO. This outcome also points to faster incorporation of EO, resulting in a gradient structure. How can this be explained by the monomer activation mechanism? Rejsek *et al.* observed a similar trend for EO/PO copolymers synthesized via the activated monomer mechanism. They attributed this to larger steric hindrance of PPO-segments, keeping in mind that the monomer addition takes place with bulky aluminum complexes.[14] This could also be true

for the GME unit in a similar manner. In Scheme 2 the reaction mechanism has been presented, including the monomer activation by a slight excess of the Lewis acid trialkylaluminum (monomer-/i-Bu$_3$Al-complex). This coordination is different for an epoxide and a glycidyl ether derivative, as emphasized in Figure 5. In the case of EO, aluminum can only coordinate to the oxygen of the epoxide ring, thereby withdrawing electron density, which facilitates a nucleophilic attack. On the other hand, GME contains two oxygens that can coordinate to aluminum. In this case, electron density from the epoxide ring cannot be withdrawn as strongly as in the case of EO. Accordingly, the activation is weaker and hence the nucleophilic attack will be slower, which may also explain the "lower" reactivity of GME compared to EO.

Figure 5: Hypothetic complexation of i-Bu$_3$Al by the oxygen of EO (left) vs. the complexation of i-Bu$_3$Al by the oxygens of GME (right).

In summary, the copolymerization of GME and EO via the activated monomer mechanism results in a tapered structure, but the gradient is not very pronounced. This is supported by the linear relationship between the thermal properties and the GME content, which points to limited deviation from random incorporation.

Conclusion

To the best of our knowledge, this report describes the first copolymerization of ethylene oxide (EO) and glycidyl methyl ether (GME) to thermoresponsive polyether structures. Conventional oxyanionic copolymerization is not possible for this challenging comonomer pair. Using the activated epoxide monomer polymerization technique with a NOct$_4$Br/i-Bu$_3$Al ratio >1, the preparation of a series of P(GME-co-EO) copolymers with molecular weights between 3000 g mol^{-1} and 20 000 g mol^{-1} was achieved. Qualitative triad sequence analysis via inverse gated ^{13}C NMR spectroscopy proved that no preferential block structure is generated. Based on DSC measurements the presence of crystallizable polyether segments could be identified, even at rather high GME content,

which points to to EO-rich segments. Our hypothesis is that EO becomes incorporated slightly faster than GME, which is probably due to higher activation and thus faster insertion of EO.

Melting temperatures and morphology of the copolymers can be tuned depending on the GME vs. EO content, retaining the high hydrophilicity of PEG. Thermoresponsive behavior in aqueous solution also depends on the GME comonomer content, which is reflected by LCSTs between 55 °C and 98 °C. Thermoresponsive properties confirm that the gradient structure is not very pronounced, since a linear correlation between the lower critical solution temperature (LCST) and the GME content was found. When compared to the established P(PO-*co*-EO) copolymers, the materials generally show higher LCSTs, since GME is clearly more hydrophilic than PO.

The hydrophilic, thermoresponsive PEG copolymers are promising in applications for which crystallization of PEG is not desired, e.g., in lithium ion battery applications or for "smart window" devices. Based on the biocompatibility of both homopolymers, excellent biocompatibility is also expected for the copolymers of EO and GME. Therefore, the materials are of interest for biocompatible "smart" surfaces or surface coatings in biomedical applications and will also be tested for advanced PEGylation approaches in the near future.

Acknowledgments

References

(1) Knop, K.; Hoogenboom, R.; Fischer, D.; Schubert, U. S. *Angew. Chem. Int. Ed.* **2010,** *49* (36), 6288–6308.

(2) Barteau, K. P.; Wolffs, M.; Lynd, N. A.; Fredrickson, G. H.; Kramer, E. J.; Hawker, C. J. *Macromolecules* **2013,** *46* (22), 8988–8994.

(3) Schmolka, I. *J. Am. Oil Chem. Soc.* **1977,** *54* (3), 110–116.

(4) Brocas, A.-L.; Mantzaridis, C.; Tunc, D.; Carlotti, S. *Progress in Polymer Science* **2013,** *38* (6), 845–873.

(5) Berthier, C.; Gorecki, W.; Minier, M.; Armand, M. B.; Chabagno, J. M.; Rigaud, P. *Solid State Ionics* **1983,** *11* (1), 91–95.

(6) Louai, A.; Sarazin, D.; Pollet, G.; François, J.; Moreaux, F. *Polymer* **1991,** *32* (4), 703–712.

(7) Persson, J.; Kaul, A.; Tjerneld, F. *Journal of Chromatography B: Biomedical Sciences and Applications* **2000,** *743* (1-2), 115–126.

(8) Weber, C.; Hoogenboom, R.; Schubert, U. S. *Progress in Polymer Science* **2012,** *37* (5), 686–714.

(9) Mangold, C.; Obermeier, B.; Wurm, F.; Frey, H. *Macromol. Rapid Commun.* **2011,** *32* (23), 1930–1934.

(10) Hans, M.; Keul, H.; Moeller, M. *Polymer* **2009,** *50* (5), 1103–1108.

(11) Quirk, R. P.; Lizaarraga, G. M. *Macromol. Chem. Phys.* **2000,** No. 201, 1395–1404.

(12) Billouard, C.; Carlotti, S.; Desbois, P.; Deffieux, A. *Macromolecules* **2004,** *37* (11), 4038–4043.

(13) Carlotti, S.; Billouard, C.; Gautriaud, E.; Desbois, P.; Deffieux, A. *Macromol. Symp.* **2005,** *226* (1), 61–68.

(14) Rejsek, V.; Sauvanier, D.; Billouard, C.; Desbois, P.; Deffieux, A.; Carlotti, S. *Macromolecules* **2007,** *40* (18), 6510–6514.

(15) Labbé, A.; Brocas, A.-L.; Ibarboure, E.; Ishizone, T.; Hirao, A.; Deffieux, A.; Carlotti, S. *Macromolecules* **2011,** *44* (16), 6356–6364.

(16) Gervais, M.; Brocas, A.-L.; Cendejas, G.; Deffieux, A.; Carlotti, S. *Macromolecules* **2010,** *43* (4), 1778–1784.

(17) Carlotti, S.; Labbé, A.; Rejsek, V.; Doutaz, S.; Gervais, M.; Deffieux, A. *Macromolecules* **2008,** *41* (19), 7058–7062.

(18) Brocas, A.-L.; Cendejas, G.; Caillol, S.; Deffieux, A.; Carlotti, S. *J. Polym. Sci. A Polym. Chem.* **2011,** *49* (12), 2677–2684.

(19) Meyer, J.; Keul, H.; Möller, M.: Synthesis and Characterization. *Macromolecules* **2011,** *44* (11), 4082–4091.

(20) Gervais, M.; Brocas, A.-L.; Deffieux, A.; Ibarboure, E.; Carlotti, S. *Pure Appl. Chem.* **2012,** *84* (10).

(21) Gervais, M.; Labbé, A.; Carlotti, S.; Deffieux, A. *Macromolecules* **2009,** *42* (7), 2395–2400.

(22) Gervais, M.; Brocas, A.-L.; Cendejas, G.; Deffieux, A.; Carlotti, S. *Macromol. Symp.* **2011,** *308* (1), 101–111.

(23) Thomas, A.; Müller, S. S.; Frey, H. *Biomacromolecules* **2014,** *15* (6), 1935–1954.

(24) Weinhart, M.; Grunwald, I.; Wyszogrodzka, M.; Gaetjen, L.; Hartwig, A.; Haag, R. *Chemistry – An Asian Journal* **2010,** *5* (9), 1992–2000.

(25) Weinhart, M.; Becherer, T.; Haag, R. *Chem. Commun.* **2011,** *47* (5), 1553–1555.

(26) Höger, K.; Becherer, T.; Qiang, W.; Haag, R.; Friess, W.; Küchler, S. *Eur J Pharm Biopharm* **2013,** *85*, 756–764.

(27) Labbé, A.; Carlotti, S.; Deffieux, A.; Hirao, A. *Macromol. Symp.* **2007,** *249-250* (1), 392–397.

(28) Reinicke, S.; Schmelz, J.; Lapp, A.; Karg, M.; Hellweg, T.; Schmalz, H. *Soft Matter* **2009,** *5*, 2648–2657.

(29) Aoki, S.; Koide, A.; Imabayashi, S.-i.; Watanabe, M. *Chem. Lett.* **2002,** No. 11, 1128–1129.

(30) Dingels, C.; Schömer, M.; Frey, H. *Chem. Unserer Zeit* **2011,** *45* (5), 338–349.

(31) Labbé, A.; Carlotti, S.; Billouard, C.; Desbois, P.; Deffieux, A. *Macromolecules* **2007,** *40* (22), 7842–7847.

(32) Hamaide, T.; Goux, A.; Llauro, M.-F.; Spitz, R.; Guyot, A. *Angew. Makromol. Chemie* **1996,** *237* (1), 55–77.

(33) Mangold, C.; Wurm, F.; Obermeier, B.; Frey, H. *Macromol. Rapid Commun.* **2010,** *31* (3), 258–264.

(34) Mangold, C.; Wurm, F.; Obermeier, B.; Frey, H. *Macromolecules* **2010,** *43* (20), 8511–8518.

(35) Obermeier, B.; Wurm, F.; Frey, H. *Macromolecules* **2010,** *43* (5), 2244–2251.

(36) Mangold, C.; Dingels, C.; Obermeier, B.; Frey, H.; Wurm, F. *Macromolecules* **2011,** *44* (16), 6326–6334.

(37) Chisholm, M. H.; Navarro-Llobet, D. *Macromolecules* **2002,** *35* (6), 2389–2392.

(38) Mandelkern, L. *Chem. Rev.* **1956,** *56* (5), 903–958.

(39) Matyjaszewski, K.; Advincula, R.; Saldívar-Guerra, E.; Luna-Bárcenas, G.; González-Núñez, R.; Wanamaker, C. L.; Tolman, W. B.; Hillmyer, M. A. *Macromol. Symp.* **2009,** *283-284* (1), 130–138.

(40) Klein, R.; Schüll, C.; Berger-Nicoletti, E.; Haubs, M.; Kurz, K.; Frey, H. *Macromolecules* **2013,** *46* (22), 8845–8852.

(41) Pielichowski, K.; Flejtuch, K. *Polym. Adv. Technol.* **2002,** *13* (10-12), 690–696.

(42) Saeki, S.; Kuwahara, N.; Nakata, M.; Kaneko, M. *Polymer* **1976,** *17* (8), 685–689.

(43) Kjellander, R.; Florin, E. *J. Chem. Soc., Faraday Trans. 1* **1981,** *77* (9), 2053.

Supporting Information
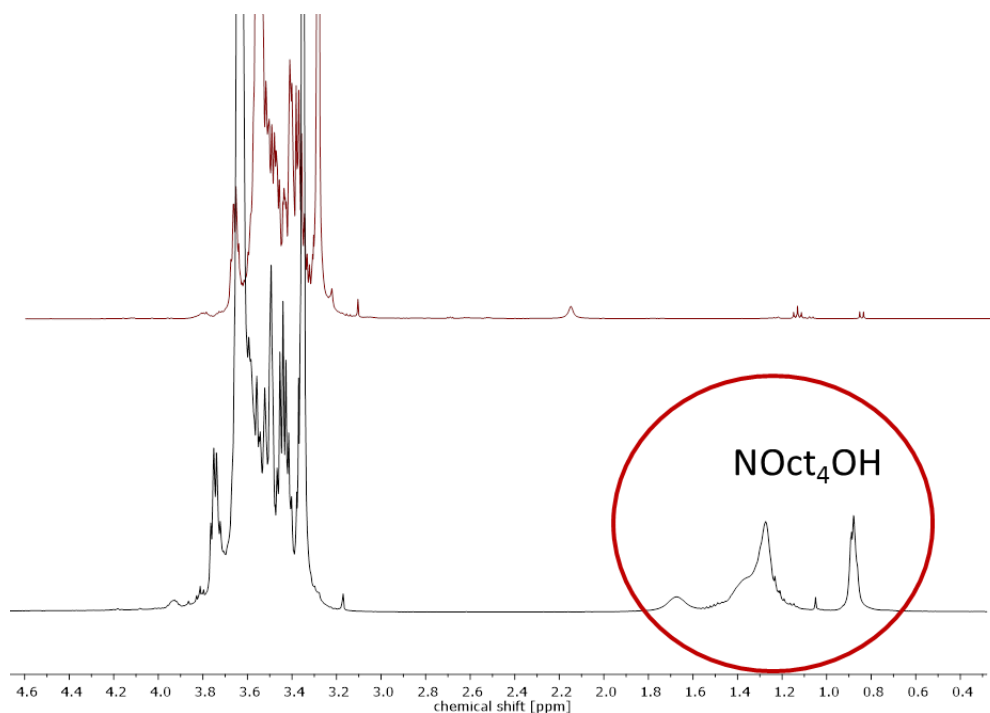
Figure S1: ^{1}H NMR spectrum of P(GME$_{0.67}$-EO$_{0.33}$) in CD$_2$Cl$_2$ before (bottom) and after (top) purification by column chromatography.
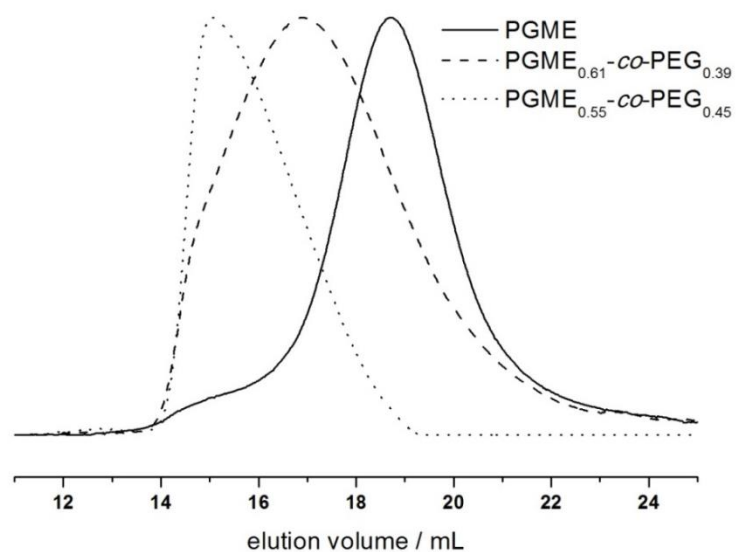
Figure S2: SEC traces for a selection of higher molecular weight P(GME-*co*-EO) copolymers in DMF (homopolymer PGME; P(GME$_{0.61}$-EO$_{0.39}$), P(GME$_{0.55}$-EO$_{0.45}$)).
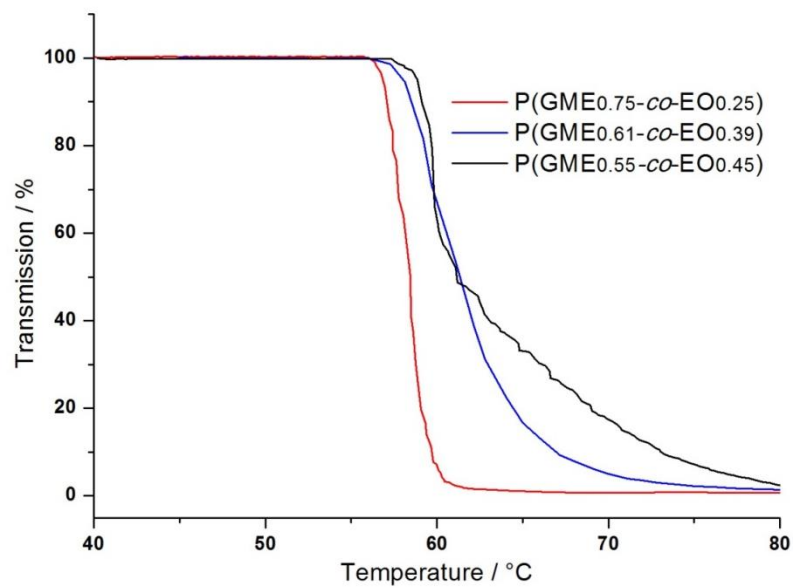
Figure S3: Intensity of transmitted laser light vs. temperature of P(GME$_{0.75}$-EO$_{0.25}$) (red); P(GME$_{0.61}$-EO$_{0.39}$) (blue); P(GME$_{0.55}$-EO$_{0.45}$) (black), at a concentration of 5 mg mL^{-1} in aqueous solution.

Outlook

Ongoing and Future Projects

Copper-Free Click Reaction on Norbornene-Functionalized Linear-Hyperbranched Polyethers Using a Tetrazine Fluorescent Label

(In collaboration with Matthias Worm (AK Frey), Thomas Fritz, Matthias Voigt, and Prof. Helm, Institute of Pharmacy and Biochemistry, Johannes Gutenberg University Mainz)

Methods for labelling polymers or biomolecules with fluorescent dyes have become an essential tool in biomedical applications. The conjugation of labels via copper-catalyzed alkyne-azide click reaction was presented in **Chapter 3** and **Chapter 4.2** as a versatile functionalization platform. The main drawback is the usage of transition metals and stabilizers which may limit the application *in vivo*, if residual copper remains in the product.[1] One option to circumvent these limitations is the strained-promoted alkyne-azide cycloaddition, but suitable alkyne derivatives usually have to be synthesized in a demanding manner.[2] An alternative route is the labeling strategy based on the inverse electron-demand Diels-Alder reaction.[3] A tetrazine (electron-deficient diene) can react with a norbornene (dienophile) wherein nitrogen is eliminated, rendering the reaction irreversible (Figure 1). The potential of this cycloaddition was shown in an efficient labelling route of DNA or RNA, respectively.[4,5] Advantages of this approach are the facile reaction procedure and mild reaction conditions (aqueous solution, room temperature, small excess of the tetrazine compound).
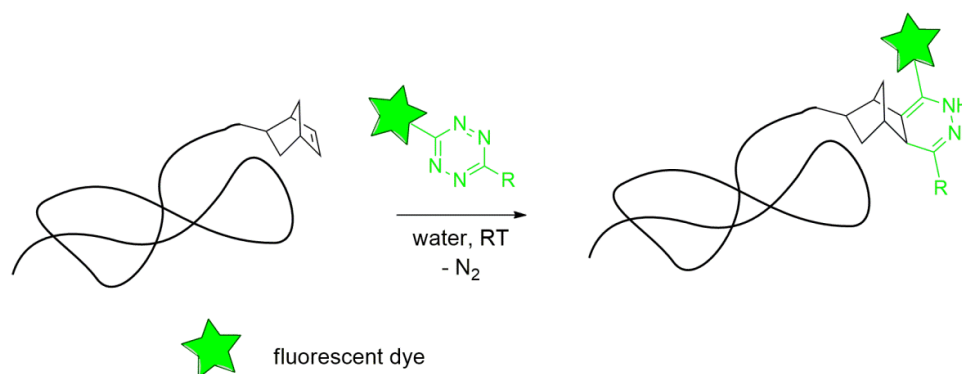
Figure 1: Diels-Alder reaction with inverse electron-demand on a norbornene-functionalized polymer.

In a recent project, linear-hyperbranched polyethers were functionalized with bicyclo[2.2.1]hept-5-ene-2,3-dicarboxylic anhydride (Figure 2) after deprotonation with cesium hydroxid. In the near future, the norbornene-functionalized polymers will be incorporated into liposomes by dual centrifugation (DC)[6,7] and subsequently labeled with a tetrazine-fluorescent dye (Atto 488 derivative) in a copper-free "click" reaction (Figure 2).
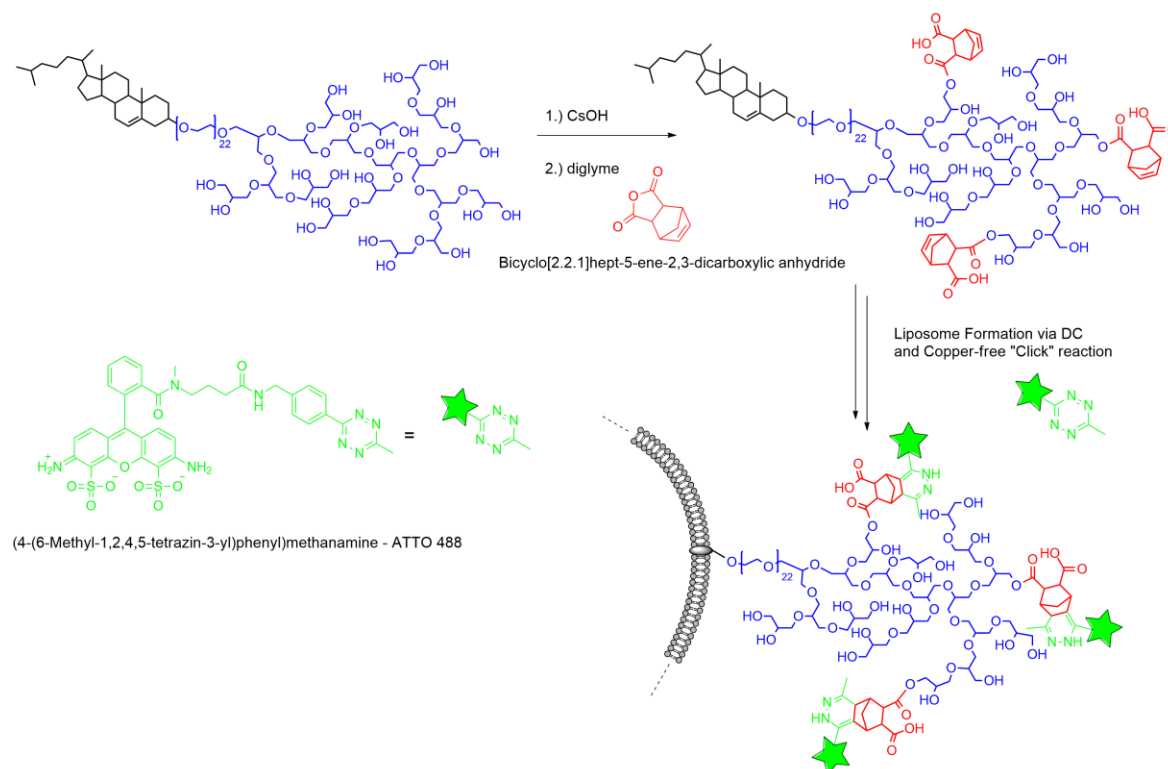
Figure 2: Reaction scheme for the copper-free "click" reaction of linear-hyperbranched polyethers functionalized with a norbornene derivative and a tetrazine-fluorescent label. As a hydrophobic anchor in the phospholipid bilayer of liposomes, cholesterol as well as bis-alkyl glyceryl ether will be investigated (Figure 3). Here, the main difference between

cholesterol and alkyl chains is based on their influence and stabilization of membranes, which can by systematically studied, e.g. in cells, when the lipids are labelled via a fluorescence marker.
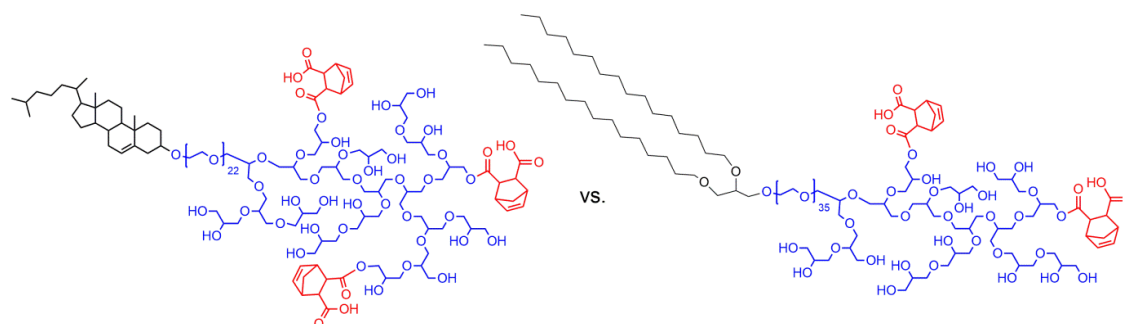
Figure 3: Norbornene-functionalized linear-hyperbranched polyether with cholesterol or 1,2-bis-*n*-hexadecyl glyceryl ether as the initiator and anchor in lipid membranes.

So far, the norbornene-functionalized, branched lipids have been characterized by ^{1}H NMR spectroscopy (Figure 4) and diffusion-ordered spectroscopy (DOSY) (Figure 5). In the ^{1}H NMR spectrum of Ch-PEG$_{22}$-*hb*PG$_{35}$-Nor$_6$ the signals of the cholesterol anchor are observed in the aliphatic region (0.72 ppm to 2.3 ppm) and the signals of the polyether backbone are seen between 3.4 ppm and 4.3 ppm. The resonance for the cholesterol double bond appears at 5.38 ppm and the double bonds of the norbornene moieties are detected between 6.14 ppm and 6.24 ppm (f/g, Figure 4). The residual resonances of the norbornene skeleton appear between 2.9 ppm and 3.20 ppm (b/c, d/e) but cannot clearly be distinguished. The signal of the bridge atom (a) is observed at 1.30 ppm overlapping with the signals of cholesterol. By integration of the cholesterol methyl group and the signals for the norbornene double bonds, the number of functional groups can be determined to be 6. DOSY proves the covalent attachment of the norbornene derivative to the polyether backbone. This is shown by the resonances of the norbornene double bonds at 6.30 ppm which exhibit the same diffusion coefficient of 2.93×10^{-6} m^2 s^{-1} as the polymer. The signal at 6.23 ppm with a diffusion coefficient of 1.88×10^{-5} m^2 s^{-1} may stem from free norbornene-derivatives but cannot clearly be assigned at the moment due to missing resonances of the remaining cyclic skeleton.
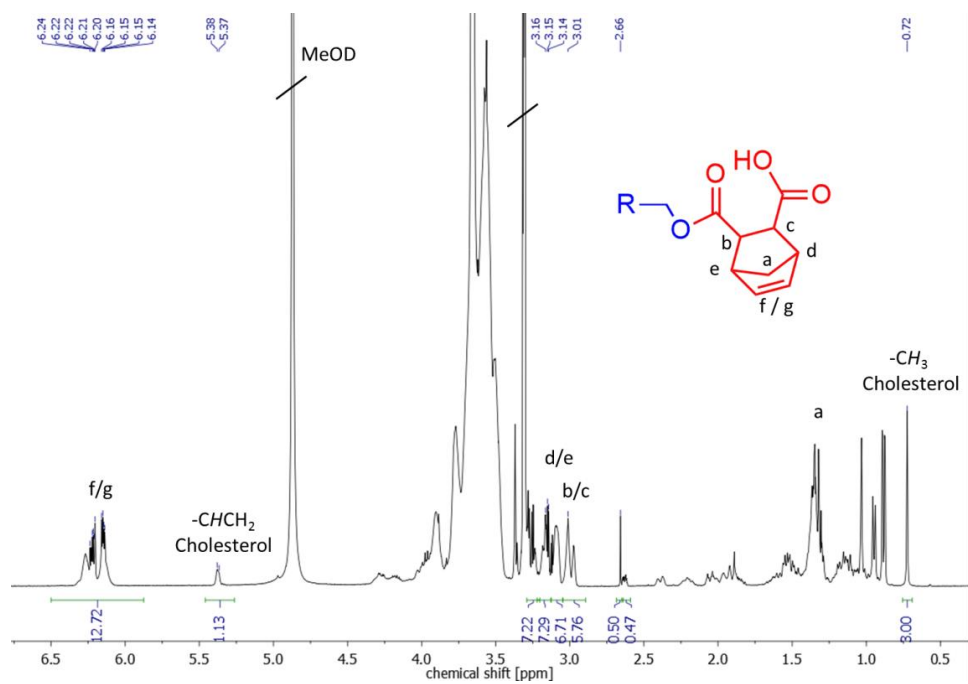
Figure 4: ^{1}H NMR spectrum of Ch-PEG$_{22}$-*hb*PG$_{35}$-Nor$_6$ in MeOD with peak assignments of the functional group.
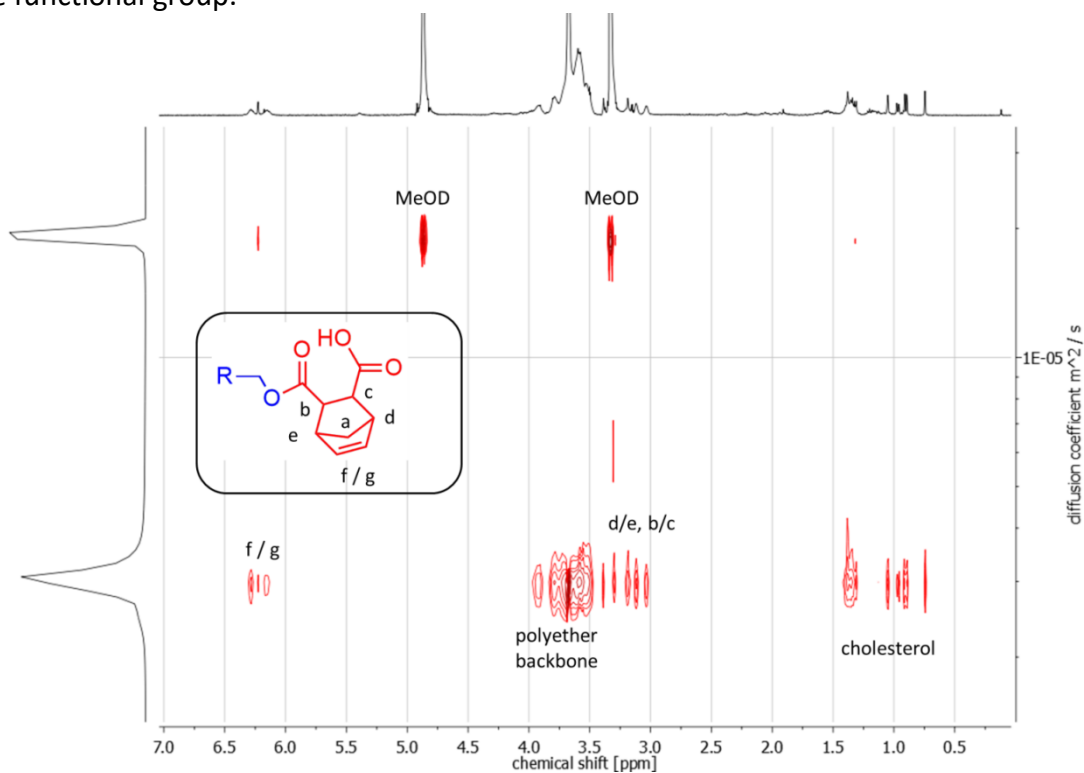
Figure 5: Diffusion-ordered spectroscopy (DOSY) of Ch-PEG$_{22}$-*hb*PG$_{35}$-Nor$_6$ in MeOD.

Novel linear-hyperbranched Polyether Amphiphiles with Phospholipids as the Hydrophobic Segment

Using cholesterol as the initiator for the oxyanionic ring-opening polymerization of epoxides is convenient, since cholesterol is commercially available and low priced. We could show that cholesterol anchors the polyether amphiphiles in the phospholipid membrane. Nevertheless, the attachment of a polymer can vary the native location of cholesterol in the membrane. Carrion *et al.* introduced a "spacer arm" which influenced and reinforced the flexibility of the PEG chain and the rigid cholesterol segment was believed to be inserted deeper into the bilayer of liposomes compared to lipids without a spacer.[8]

Phospholipids are an interesting alternative and they are often applied in "stealth" liposomes as, e.g., 1,2-distearoyl-*sn*-glycero-3-phosphoethanolamine-*N*-[methoxy-(polyethylene glycol)] (DSPE-mPEG) derivatives. However, the main disadvantages of these systems are their relatively high price and their lack of functional groups for further derivatization. In addition, phospholipids cannot be used as initiators for the epoxide construction kit, since they do not stand the basic reaction conditions and acidic conditions in the deprotection step of the PEEGE block. The attachment of phospholipids to linear-hyperbranched polyethers may be achieved *via* coupling chemistry. One option may be the coupling *via* squaric acid diethylester (SADE), which is usually used for reactions with amines.[9,10] Figure 6 presents the possible coupling between the amine group of DSPE and amine functionalized linear-hyperbranched polyethers mediated by squaric acid.
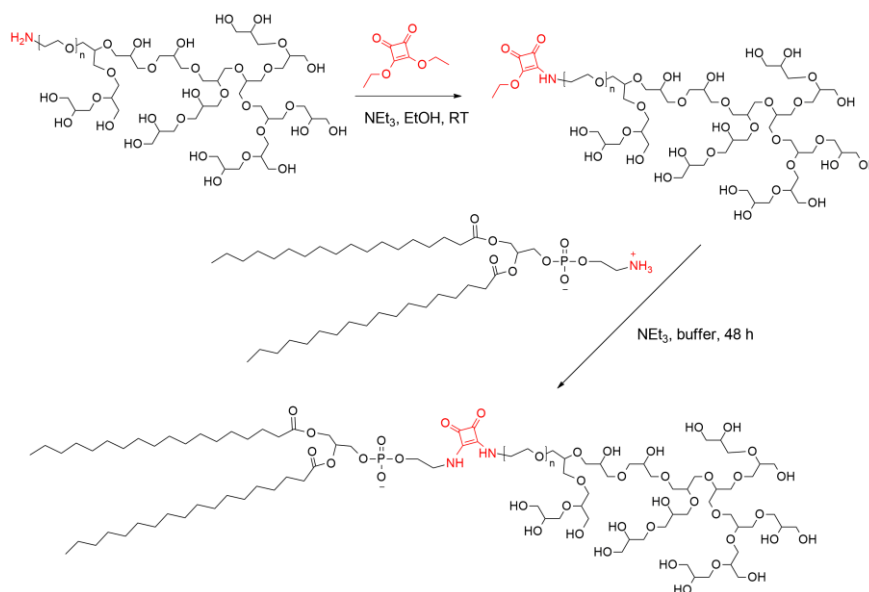
Figure 6: Possible coupling between the amine group of DSPE and amine functionalized linear-hyperbranched polyethers mediated by squaric acid.

In a proof-of-concept, the linear analogue PEG was investigated at the beginning. First results were obtained with mPEG-amine as shown in Figure 7 (SEC elugram, DMF) and in Figure 8 (^{1}H NMR spectrum). The mPEG-amine was functionalized with SADE and mPEG-SEA (mPEG-squaric ethylester amide) was obtained which exhibited a strong UV-signal in SEC measurements (red trace). Compared to mPEG (black trace) a shift to lower elution volume was observed (blue trace). The ^{1}H NMR spectrum of mPEG2000-SEA proved successful coupling of SADE to the polymer as depicted in Figure 8. The methoxy group is observed at 3.36 ppm (c) and the resonances of the PEG backbone is observed between 3.40 ppm and 3.90 ppm. The signal of the squaric ethylester amide moiety appears at 1.43 ppm (a) and 4.73 ppm (d) whereas the amine resonances can be seen at 6.66 ppm and 6.91 ppm. Furthermore, the peak integrations correspond well to the expected number of protons.
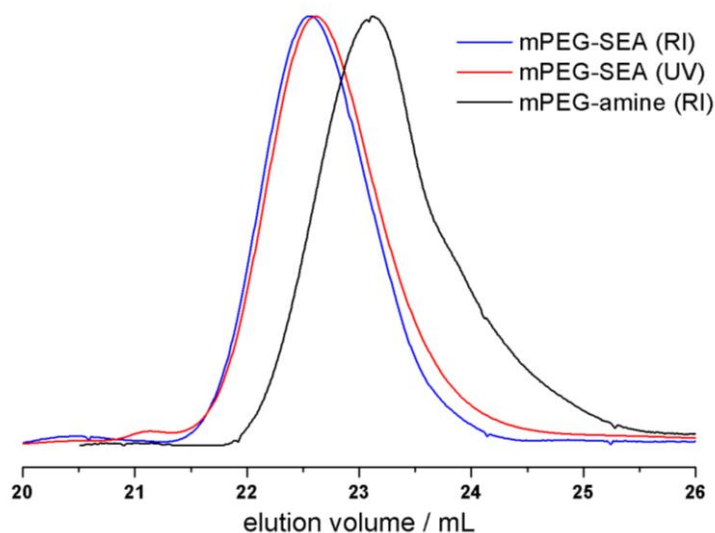
Figure 7: SEC elugram of mPEG2000-Amine (black); mPEG2000-SEA (blue, mPEG-squaric ethylester amide) → shift to higher molecular weights after successful reaction between mPEG2000-amine and SADE; UV-signal of mPEG2000-SEA (red) with good overlay of the RI signal.
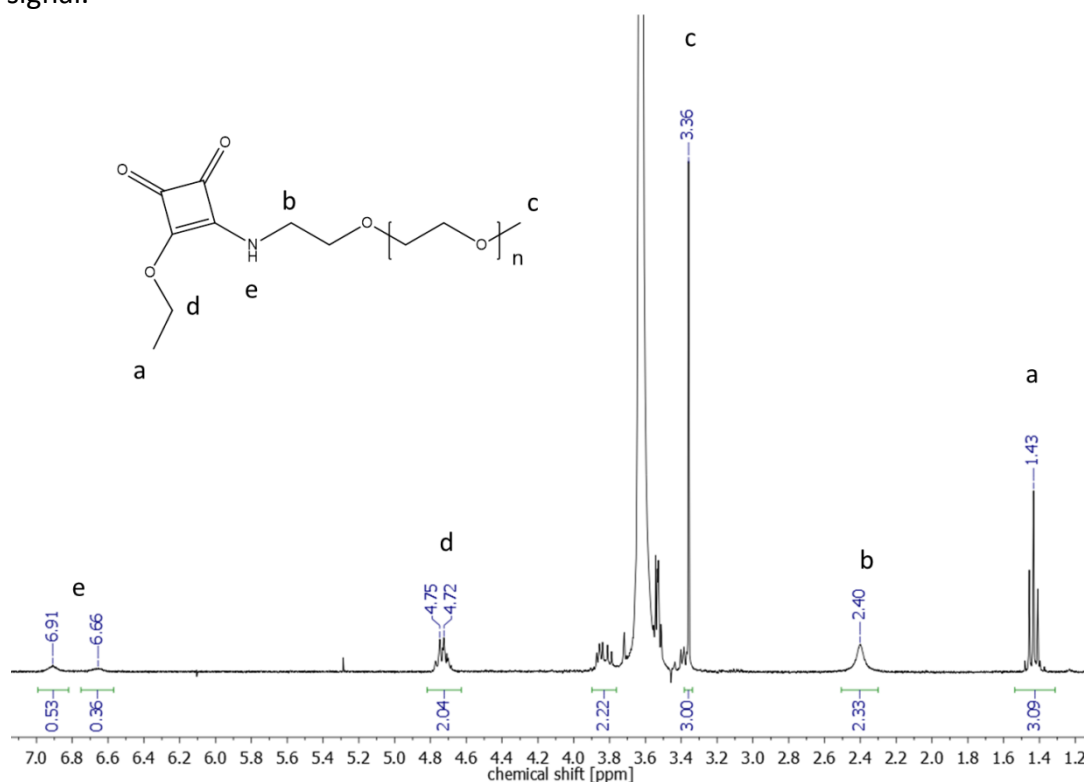
Figure 8: ^{1}H NMR spectrum of mPEG2000-SEA in CDCl$_3$; ^{1}H NMR (300 MHz, CDCl$_3$): ∂ (ppm) = 1.43 (t, 3 H, a), 2.40 (3 H, b), 3.33 (s, 3 H, c), 3.48-3.88 (polyether backbone), 4.74 (q, 2 H, d), 6.66 and 6.91 (br, 1 H, e).

The successful coupling between mPEG and SADE can also be detected by matrix assisted laser desorption/ionization time of flight mass spectrometry (MALDI-ToF MS). Figure 9 shows that the main distribution can be assigned to the functionalized PEG

chain with sodium as the counter ion, whereas the second distribution contains potassium as the counter ion (m/z = 1983.5 = mPEG$_{41}$-SEA + Na$^+$). Different characterization techniques can be exploit to prove the coupling of a polymer to SADE or the functionalized SADE-polymer to a second amine compound.
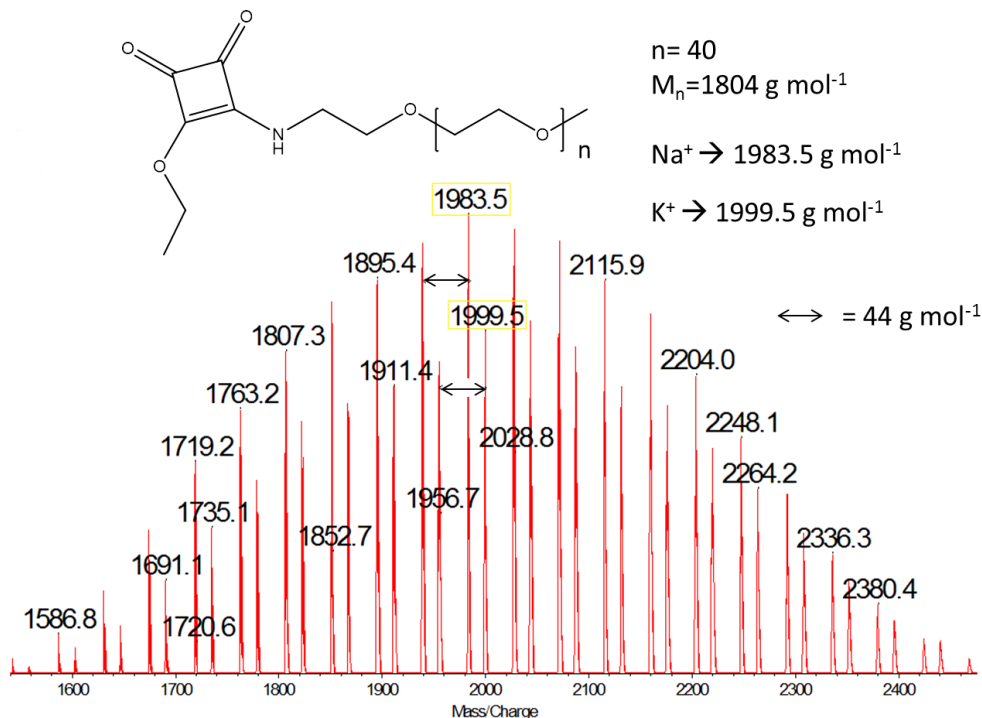
Figure 9: MALDI-ToF MS of mPEG2000-SEA with dithranol as the matrix and potassium trifluoroacetate as the cationization agent.

Preliminary experiments of the functionalization of linear-hyperbranched polyethers, containing an amine group, with SADE showed difficulties in the quantitative reaction between the amine group of the polymer and the squaric acid (data not shown). However, the main limitations are found in the last step in which the phospholipid DSPE was coupled to the derivatized polyether chain. This was evidenced by MALDI-ToF MS in which two distributions were found, one for mPEG2000-SEA, and one distribution for DSPE coupled to mPEG2000. Especially for the hyperbranched polymer, differences in solubility between the phospholipid and the polymer, steric hindrance, and lower reactivity of the DSPE amine are the main obstacles which have to be overcome. Nevertheless, optimization of the reaction conditions and a successful coupling between phospholipids and the complex polyether lipids, will expand the tool box for novel "stealth" lipids.

References

(1)   Gaetke, L. M.; Chow, C. K. *Toxicology* **2003,** *189* (1-2), 147–163.
(2)   Jewett, J. C.; Bertozzi, C. R. *Chem. Soc. Rev.* **2010,** *39* (4), 1272.
(3)   Devaraj, N. K.; Weissleder, R.; Hilderbrand, S. A. *Bioconjugate Chem.* **2008,** *19* (12), 2297–2299.
(4)   Schoch, J.; Wiessler, M.; Jäschke, A. *J. Am. Chem. Soc.* **2010,** *132* (26), 8846–8847.
(5)   Schoch, J.; Ameta, S.; Jäschke, A. *Chem. Commun.* **2011,** *47* (46), 12536.
(6)   Massing, U.; Cicko, S.; Ziroli, V. *J. Control. Release* **2008,** *125* (1), 16–24.
(7)   Fritz, T.; Hirsch, M.; Richter, F. C.; Müller, S. S.; Hofmann, A. M.; Rusitzka, K. A.; Markl, J.; Massing, U.; Frey, H.; Helm, M. *Biomacromolecules* **2014,** *15*, 2440–2448.
(8)   Carrion, C.; Domingo, J.; Madariaga, M. de. *Chemistry and Physics of Lipids* **2001,** *113* (1-2), 97–110.
(9)   Wurm, F.; Dingels, C.; Frey, H.; Klok, H.-A. *Biomacromolecules* **2012,** *13* (4), 1161–1171.
(10)   Wurm, F. R.; Klok, H.-A. *Chem. Soc. Rev.* **2013,** *42* (21), 8220.

Future Projects

The synthesis and characterization of complex polyether-based lipids, copolymers, and overall the initiated projects have motivated and inspired multiple other studies in related scientific areas. Due to the limited timeframe of this thesis and the broad, interdisciplinary fields, several projects could not be addressed, but should be examined in subsequent work.

Ketal groups. The introduction of pH-sensitive groups, such as acetals, is an ongoing topic. Acetal groups were shown to be cleaved under acidic conditions, but cleavage can take hours or up to days, depending on the pH and environment. Ketal groups exhibit faster degradation profiles (in a few hours) but on the other hand, the synthesis is challenging due to the sensitive chemical bond. Here, certain obstacles need to be overcome in order to successfully synthesize and incorporate these groups into the stabilizing shell of liposomes.

Folate attachment. First of all, the aspect of derivatization is crucial in order to obtain "active" targeting in the context of multifunctional liposome formulations. Folate-mediated endocytosis or folate-mediated tumor targeting *in vivo* remain an interesting question.

Crosslinking. In general, multihydroxyl PEG-PG-lipids with pendant allyl groups or double bonds are an exciting class of lipids, since they enable not only further functionalization, but also crosslinking of the stabilizing polymer shell. Successful incorporation has already been shown in preliminary results, but crosslinking after liposome formulation and the influence on the stability as well as on the *in vivo* properties remain to be investigated.

Amine groups. The platform of multifunctional PEG-PG lipids can be enlarged by introducing other functional groups, such as amines at the polymer corona. This can be carried out by using glycidol and *N,N*-diallyl glycidyl amine (DAGA) with subsequent isomerization of the allyl groups and acidic cleavage of the protecting groups to release the free amine groups. Such an approach opens up novel functionalization routes where selective amine chemistry can be employed. For example, the attachment of antibodies via amine moieties may be promising.

Cholesteryl- vs. Alkyl-anchor. Of course, not only variation in the polyether segments and additional functionalities can be carried out, but also variation in the hydrophobic anchor group is promising. It is known, that cholesterol has a totally different influence on the membrane stability and fluidity compared to linear alkyl chains. Furthermore, attaching a polymer chain to cholesterol influences its native location in the phospholipid bilayer. Hence, liposome stability may change drastically, which first of all may be studied in monolayers (Langmuir Blodgett trough) and CLSM measurements (when a fluorescent dye is attached). Furthermore, cell tests, membrane-membrane fusion, and endocytosis may be investigated in detail.

In vivo biodistribution. First results in *in vivo* and *ex vivo* biodistribution studies employing fluorine-18 labeled polyether lipids in liposome formulations are promising with regard to drug delivery applications. Here, totally new fields of investigations and questions emerge. First of all, liposome size plays a crucial role for biodistribution, therefore homogeneous sizes and small sizes (50 nm polycarbonate membranes) may be a point of interest. Of course, μPET measurements longer than 1 h are fundamental for clarification of the "stealth" effect of the hyperbranched lipids. Tumor-bearing mice

could give insight into tumor accumulation of the novel liposomes by "passive" or "active" targeting, e.g., if targeting molecules are attached to the liposome surface.

Solubilization of MnO NP. The cholesterol-or alkyl-initiated polyethers were also tested for their solubilizing properties of manganese oxide (MnO) nanoparticles in collaboration with Dr. Heiko Bauer (research group of Prof. Tremel, Mainz). Promising results were found for reversible, hydrophobic interactions between the alkyl segment and the hydrophobic oleic acid layer (capping agent) around the MnO particles, as depicted below. After treatment with the polymer, the particles became soluble in aqueous solution and were stable for at least four months. TEM pictures confirmed these results. This project is promising with regard to reversible solubilization of nanoparticles in different solvents. Here, again the steric hindrance of the hydrophobic segment (cholesterol vs. alkyl) plays an important role for the insertion into the oleic acid layer and needs to be investigated in more detail.

water soluble NP

A.Appendix

A.1 Synthesis of Oxetane-Functional Aliphatic Polyesters via Enzymatic Polycondensation
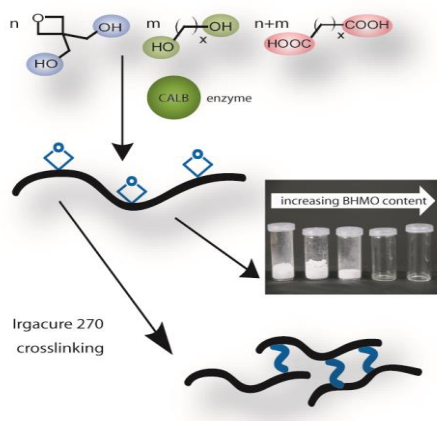
Sophie S. Müller,[1,2] and Holger Frey[1,]*

[1]Institute of Organic Chemistry, Johannes Gutenberg University Mainz, Duesbergweg 10-14, 55128 Mainz, Germany

[2]Graduate School Materials Science in Mainz, Staudingerweg 9, 55128 Mainz, Germany

Full Paper

Macromolecular
Journals

Synthesis of Oxetane-Functional Aliphatic Polyesters via Enzymatic Polycondensation

Sophie S. Müller, Holger Frey*

Synthesis, characterization, and thermal properties of a series of oxetane-functional aliphatic polyesters are investigated. The incorporation of the acid-sensitive 3,3-bis(hydroxymethyl)oxetane (BHMO) into polymers is achieved by using the enzyme CALB (*Candida antarctica Lipase B*) as a catalyst. This mild synthetic strategy provides well-defined, oxetane-functional polyesters. The enzymatic polycondensation allows for the synthesis of a series of aliphatic polyesters containing various ratios of the difunctional monomers sebacic acid, 1,8-octanediol, and BHMO with molecular weights between 5000–9800 g mol^{-1} and polydispersity indices ($\overline{M}_w/\overline{M}_n$) in the range of 1.25 and 1.92. Furthermore, crosslinking of BHMO and a polymer sample is carried out via opening of the pending oxetanes.
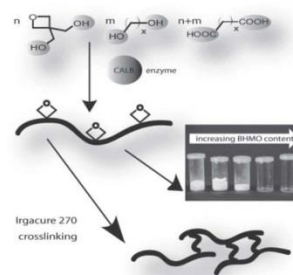
1. Introduction

Aliphatic polyesters play an important role in the field of biomedical materials and drug delivery systems.[1–3] The ester linkages render these synthetic polymers environmentally degradable and therefore useful for eco-friendly systems.[4] During the last 20 years, enzyme-catalyzed polymerizations have been studied extensively. Currently, immobilized Lipase B from *Candida antarctica* (CALB; Novozyme 435) is regarded as one of the most versatile catalysts for polycondensation reactions. The first *Aspergillus Niger* lipase-catalyzed AA-, BB-polycondensation was carried out by Okumura et al.[5] Kobayashi and co-workers[6] obtained rather high-molecular-weight polymers by carrying out the reaction under vacuum, increasing the degree of polymerization. Several reviews, mainly published by

Gross and Kobayashi, demonstrate the importance for the areas of medical and "green chemistry".[7–10] Additionally, extensive studies on the effect of substrates and solvents on the complex lipase-catalyzed polycondensation reaction have been carried out by Binns et al. and Gross and co-workers.[11–13] Furthermore, branched polymers have been synthesized, which shows the broad applicability of CALB in polymer synthesis.[14,15] The benefits of enzyme-catalyzed polymerizations are convincing: (1) Enzymes catalyze reactions under mild conditions, that is, rather low temperatures, low pressure, and moderate pH values, which makes them suitable for the reaction with acid sensitive monomers, (2) Enzymes can be employed in bulk, organic, or aqueous solutions and at water–oil interfaces, (3) Enzymes are recyclable, nontoxic and eco-friendly, which makes them interesting for the food and medical industry, where toxic catalysts are undesired, (4) The exclusion of water or air is not necessary, which makes handling facile.[16,17] In the context of the present work, it is relevant to mention that in contrast to a conventional step-growth polymerization (i.e., acidic catalysis), the polydispersity index (PDI) for enzyme-catalyzed reactions may even be lower than 2 (PDI ≤ 2) due to chain length or mass selectivity of CALB.[8,18]

S. S. Müller, Prof. H. Frey
Institute of Organic Chemistry, Johannes Gutenberg
University, Duesbergweg 10-14, D-55128 Mainz, Germany
E-mail: hfrey@uni-mainz.de
S. S. Müller
Graduate School MAINZ, Staudingerweg 9,
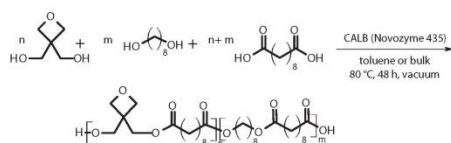D-55128 Mainz, Germany

wileyonlinelibrary.com

1783

Figure 1. Synthesis of oxetane-functional aliphatic polyesters.

Oxetane monomers belong to the category of strained, cyclic ethers.[19] Hydroxymethyl-substituted oxetanes have been exploited for the preparation of hyperbranched polyethers using the cationic ring-opening technique.[20–23] Furthermore, the copolymerization of oxetane and carbon dioxide via metal catalysts resulted in polycarbonate derivatives.[24–26] Crivello and Sasaki[27,28] employed oxetane units intensively for cationic photoinitiation and crosslinking of polymeric materials.

To the best of our knowledge, the incorporation of the difunctional oxetane monomer into aliphatic polyesters has not been reported to date. In this work, the scope and limitations of the enzymatic polycondensation of a cyclic diol monomer with orthogonal reactivity have been studied. Polyesters with varying ratios of 3,3-bis(hydroxymethyl)oxetane (BHMO), 1,8-octanediol, and sebacic acid have been synthesized via enzymatic polycondensation, aiming at the preservation of the heterocyclic element in the resulting polymer (Figure 1).

2. Experimental Section

2.1. Instrumentation

^{1}H NMR spectra were recorded using a Bruker AC 300 spectrometer operated at 300 MHz, employing CDCl$_3$ as solvent (referenced internally to solvent signals). ^{13}C NMR spectra were recorded at 75.5 MHz. FTIR spectra were recorded on a Nicolet iS 10 spectrometer equipped with a diamond ATR unit. Size-exclusion chromatography (SEC) measurements were carried out in tetrahydrofuran (THF). For SEC measurements, a UV (275 nm) and an RI detector were used. Calibration was carried out using poly(styrene) standards provided by Polymer Standards Service (PSS).

Matrix-assisted laser desorption/ionization time-of-flight mass spectrometer (MALDI–ToF MS) measurements were performed on a *Shimadzu* Axima CFR MALDI–ToF MS equipped with a nitrogen laser delivering 3 ns laser pulses at 337 nm. Dithranol was used as a matrix. The samples were prepared by dissolving the polymer in methanol at a concentration of 10 g L^{-1}. About 10 μL aliquot of this solution was added to 10 μL of a 10 g L^{-1} solution of the matrix and 1 μL of a solution of potassium trifluoroacetic acid (KTFA) (0.1 M in methanol as a cationization

agent). About 1 μL aliquot of the mixture was applied to a multistage target, methanol evaporated, and a thin matrix/analyte film created.

DSC measurements were carried out using a PerkinElmer DSC 7 with a PerkinElmer thermal analysis controller TAC7/DX in the temperature range of −100–150 °C, using heating and cooling rates of 40 °C min^{-1} (first cycle) and 10 °C min^{-1} (second cycle), respectively. The melting points of indium ($T_m = 156.6$ °C) and Millipore water ($T_m = 0$ °C) were used for calibration.

2.2. Reagents

Sebacic acid (Fluka), 1,8-octanediol (Sigma Aldrich), and trifluoroacetic anhydride (Acros Organics) were used as received. All solvents were purchased from Acros and used as received. Deuterated CDCl$_3$ and DMSO-d_6 were purchased from Deutero GmbH and stored over molecular sieves. Novozyme 435 (*Candida antarctica Lipase B* physically adsorbed on a macroporous support) was received from Novozymes and dried under vacuum at room temperature for 24 h prior to use. Irgacure 270 (a high-molecular-weight sulfonium hexafluoro phosphate) was donated from BASF (Germany). BHMO was prepared as described in the literature, using pentaerythritol and diethylcarbonate as starting compounds.[29] ^{1}H NMR (300 MHz, DMSO-d_6, δ): 4.54 (d, —CH$_2$OH), 4.27 (s, —CH$_2$O—), 4.75 (t, —CH$_2$OH).

2.3. General Procedure for Novozyme 435 catalyzed Copolymerization of BHMO, 1,8-Octanediol, and Sebacic Acid

Novozyme 435 was dried in vacuum prior to use. The monomers were weighed into a Schlenk tube and heated to 80 °C under an argon atmosphere. Novozyme 435 (10% by weight relative to total monomers) was transferred into the tube, and a small amount (1–2 mL) of toluene was added to stir the mixture. The tube was sealed with a rubber septum and maintained at 80 °C. After 2 h, the mixture was placed under reduced pressure (80 mbar). The reaction was stopped after 48 h by reducing the temperature and quenching with chloroform, stirred for 15 min, and the enzyme was removed by filtration. The mixture was concentrated, precipitated into an excess of methanol, and dried under vacuum. Polymer yields were generally between 60% and 80%, depending on the composition.

^{1}H NMR (300 MHz, CDCl$_3$, δ): 1.31 (s, —CH$_2$), 1.65 (q, —CH$_2$), 2.31 (m, —CH$_2$COO—), 4.04 (t, —CH$_2$OCO—), 4.30 (s, —CCH$_2$OCO— oxetane unit), 4.49 (s, —CH$_2$O— oxetane unit).

^{13}C NMR (75.5 MHz, CDCl$_3$, δ): 24.9–29.1 (CH$_2$-groups of aliphatic backbone), 34–34.3 (—CH$_2$COO—), 42.1 (quaternary carbon), 64.3 (—CH$_2$OCO—), 64.6 (—CCH$_2$OCO— oxetane unit), 75.5 (—CH$_2$O— oxetane unit), 173.6–174 (—COO—).

2.4. General Procedure for the End Functionalization of the Copolymers

The reaction was carried out in an NMR tube using 30 mg of the sample dissolved in 0.7 mL CDCl$_3$. A few drops of pyridine and

■ *Table 1.* Characterization data of oxetane-functional copolymers of BHMO, 1,8-octanediol, and sebacic acid.

No.	mol%[a] $n^{th.}$	mol%[a] $m^{th.}$	mol%[b] n^{NMR}	mol%[b] m^{NMR}	$\overline{M}_n$[c] [g mol^{-1}]	$\overline{M}_n^{NMR}$ [g mol^{-1}]	PDI[c]	conversion^{NMR} [%]
10	0	100	0	100	9800	3700	1.80	95
11	10	90	5	95	8100	3700	1.92	95
12	20	80	14	86	7800	2500	1.64	94
13	30	70	23	77	8000	4300	1.68	96
14	40	60	31	69	7200	2900	1.24	95
15	50	50	42	58	9200	3400	1.57	95
16	60	40	57	43	6700	1800	1.50	92
17	70	30	64	36	9300	1500	1.69	89
18	80	20	76	24	7500	3600	1.25	96
19	90	10	87	13	6300	2800	1.25	95
20	100	0	100	0	5000	2100	1.46	93
21*	50	50	–	–	2700	–	2.86	–

n = mole percentage of BHMO; m = mole percentage of 1,8-octanediol; [a]Theoretical values for the diol ratio used for the polymerization; [b]Diol ratios calculated by 1H NMR spectroscopy; [c]$\overline{M}_n$ and PDI determined via SEC-RI in THF with poly(styrene) standards. *DCC-mediated polymerization.

trifluoroacetic anhydride were added, the tube was shaken, and spectra were recorded to analyze the shift of the end group peaks.

2.5. Crosslinking of BHMO and Copolymer

322 mg of BHMO and 12.6 mg of the photoinitiator Irgacure 270 (0.66 mol%) were dissolved in 1.5 mL DMF in a petri dish and the solvent was evaporated again overnight to obtain a homogeneous mixture. The sample was irradiated under UV-light (254 nm, 12 W) for 3–4 h. After this period of time, an insoluble sample was obtained.

120 mg of sample **18** (Table 1) and 1.5 mg of Irgacure 270 were dissolved in CH$_2$Cl$_2$ and the solvent was evaporated. The sample was irradiated under UV-light (254 nm, 12 W) for 27 h. After this period of time, an insoluble, hard film was obtained, which was gel-like when trying to dissolve it in THF.

3. Results and Discussion

3.1. Synthesis and Characterization of Oxetane-Functional Aliphatic Polyesters

The synthesis of oxetane-functional aliphatic polyesters has been carried out using the enzymatic polycondensation technique since enzymatic formation of ester bonds is orthogonal to the cationic ring-opening chemistry of the oxetane moiety. To this end, different ratios (n and m parameters) of the sterically hindered and hydrophilic diol BHMO and 1,8-octanediol were used in combination

with the diacid sebacic acid. The polycondensation was catalyzed by Novozyme 435 (10% by weight relative to total monomers) (see Figure 1). All reactions were carried out under vacuum (80 mbar) to remove the byproduct water in order to increase molecular weights of the products. The copolymerization afforded polymers bearing either one of the two different alcohol end groups or the carboxylic end group of sebacic acid. Molecular weights were in the range of 5000–9800 g mol^{-1} as determined by SEC with a slight tendency to lower molecular weights with increasing content of BHMO, as shown in Table 1 and Figure 2. A possible reason for lower molecular weights
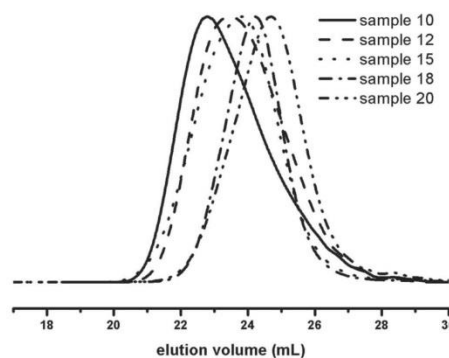
Figure 2. SEC traces (THF) of oxetane-functional aliphatic polyesters from selected samples (10, 12, 15, 18, 20).
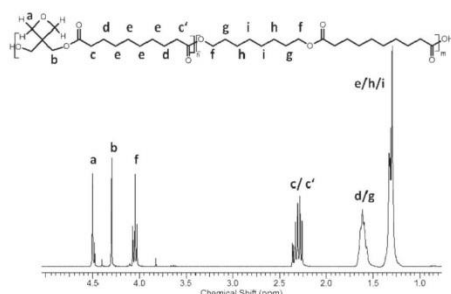
Figure 3. Representative ¹H NMR spectrum of sample **15** measured in CDCl₃.
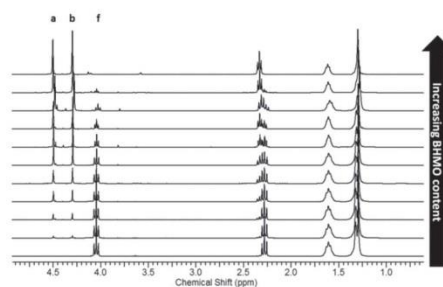
Figure 4. ¹H NMR spectra of oxetane-functional aliphatic polyesters (samples **10–20**) measured in CDCl₃.

with increasing amount of BHMO might be the steric bulk and the hydrophilicity of the monomer. We assume that, compared to the 1,8-octanediol monomer, entering the hydrophobic pocket of the enzyme's active center is more difficult for the BHMO molecule, which is likely to impede its attachment to the growing polymer chains. PDIs were in the range of 1.25 to 1.92 (see Table 1), which is unexpectedly low for polycondensations and may be related to the unusual mechanism that exhibits some features of chain growth.

Polymers with a percentage of BHMO ≥ 70% (samples **18–20**) were soluble in DMF due to their relatively high hydrophilicity, while all other samples (samples **10–17**) were also soluble in more hydrophobic solvents, such as THF, which was employed for SEC analysis.

The successful incorporation of BHMO into the aliphatic polymer chain was confirmed by ¹H NMR spectroscopy (Figure 3). The aliphatic backbone resonances appear in the region of 1.5–2.5 ppm (**d, e, g, h, i**), and the oxetane signals show up as singlets between 4.3–4.5 ppm (**a,b**). The methylene groups of 1,8-octanediol next to an ester bond are visible as a triplet at 4.05 ppm (**f**), whereas the methylene groups of sebacic acid next to an ester bond result in a multiplet at 2.29 ppm (**c/c′**). Using 2D NMR spectroscopy, this multiplet was found to consist of two triplets that are due to a different environment, depending on the adjacent diol attached (BHMO or 1,8-octanediol, **c/c′**; see Supporting Information). Figure 4 shows a comparison of the NMR spectra of all samples with increasing BHMO content.

Figure 5 shows the end-group functionalization and the corresponding ¹H NMR spectra of the polymers. End-group functionalization was achieved by converting carboxylic acid end groups to anhydrides by the reaction with trifluoroacetic anhydride. Due to this transformation, the signal of the methylene end group of sebacic

acid shifted from 2.2–2.4 ppm (**c″**) to 2.58 ppm (**c‴**). The methylene end groups next to the hydroxyl end groups (**a″, b″, f′**) shifted and disappeared under the backbone signal. The integrals of the signals of the methylene groups from sebacic acid in the polymer backbone (**c/c′** minus the end-group peak) were used as a reference since they appear in every repeat unit. Since there is no control over the type of end group, both spectra (integration of area of methylene peaks next to the hydroxyl end groups before functionalization and integration of area of methylene peaks from the carboxylic end groups after functionalization) are important for the determination of molecular weights by ¹H NMR spectroscopy (see Table 1).

The repetitive units x and y of the functional polyesters as well as the equations utilized for the determination of molecular weights are shown in Equation 1.[30] Molecular weights are given in Table 1.
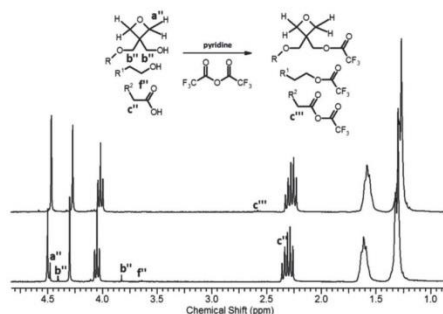

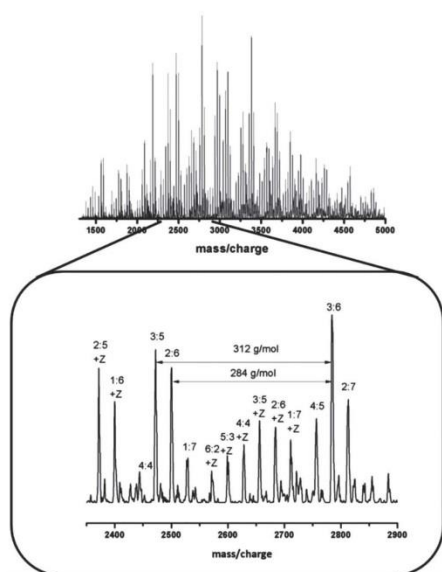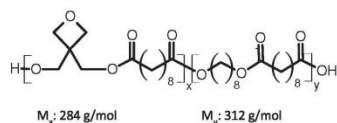*Figure 5.* ¹H NMR spectrum of sample 15 before (bottom) and after (top) end functionalization carried out in CDCl₃.

Figure 6. MALDI–ToF spectrum of a typical polymer sample with x:y ratios; zoom-in of the 2350–2900 g mol⁻¹ region. (Z = sebacic acid as end group), M_x = 284 g mol⁻¹, M_y = 312 g mol⁻¹.

M_x: 284 g/mol M_y: 312 g/mol

$$X_n = \frac{4}{\Sigma_{\text{endgroup}}}$$

$$\overline{M}_n = \frac{M_x}{2} * X_n * c_{\text{BHMO}} + \frac{M_y}{2} * X_n * c_{\text{oct}} \qquad (1)$$

Equation 1. Repetitive units x and y of the functional polyesters and the equations utilized for the determination of molecular weights.

Molecular weights observed by SEC are about 2–3 times higher than those observed by ¹H NMR spectroscopy. The overestimation is in part due to poly(styrene) being used as a standard for SEC analysis since the hydrodynamic radii of aliphatic polyesters and poly(styrene) are not comparable. One improvement to higher molecular weights for the future might be longer reaction times, higher temperature, and the application of higher vacuum. To further characterize the polymer structure, MALDI-ToF MS (Figure 6) were taken for representative samples. It is obvious that the samples exhibit various subdistributions due to the expected

range of combinations of the repetitive units x and y. The zoom-in displays the region of 2350–2900 g mol⁻¹ and shows selected combinations of x:y and the molecular weight differences of 312 g mol⁻¹ (M_x) and 284 g mol⁻¹ (M_y) that were observed for these units. Z symbolizes a sebacic acid molecule at the end of a polymer chain (184 g mol⁻¹).

3.2. Comparison of Enzymatic Polycondensation and DCC-Mediated Polycondensation

Since the monomer BHMO is an acid-sensitive oxetane derivative, enzymatic polycondensation reaction was chosen as a suitable method to polymerize this diol. The synthesis was also carried out using *N,N'*-dicyclohexylcarbodiimide (DCC) and the acyl transfer agent 4-(dimethylamino)pyridine (DMAP) as another option to couple BHMO with a diacid under mild conditions. Advantages of this route are the lower reaction time and the bonding of water by the coupling agent DCC, which forms the *N,N'*-dicyclohexylurea as a byproduct, making the application of vacuum unnecessary. However, a significant disadvantage of this reaction is the time-consuming purification because the byproduct is difficult to separate from the polymer. Filtration and threefold acidic solvent extraction was not sufficient to separate the polymer from *N,N'*-dicyclohexylurea. The SEC trace (see Supporting Information) shows a higher molecular weight distribution (PDI = 2.86) and a molecular weight of 2700 g mol⁻¹ for a polyester with a theoretical ratio of BHMO:1,8-octanediol:sebacic acid 1:1:2. The PDI is in the range of PDIs found for polycondensation reactions and underlines the difference to the enzymatic polycondensation. The SEC trace does not only show a broader molecular weight distribution and lower molecular weights compared to sample **15** (PDI = 1.57; 9200 g mol⁻¹), but also exhibits a high-molecular-weight shoulder that could not be explained.

In summary, both the DCC-mediated reaction and the enzymatic polycondensation are suitable for the copolymerization of two different diols and a diacid. However, the CALB-catalyzed reaction in vacuum resulted in higher molecular weights, lower PDIs, the purification steps were considerably more facile (filtration of the enzyme beads and precipitation), and pure materials were obtained.

3.3. SEC Monitoring of Polymer Formation

To study the polymer formation in the enzymatic polycondensation reaction, a sample was prepared with a ratio of BHMO:1,8-octanediol:sebacic acid 1:1:2. Samples for SEC and ¹H NMR analysis were taken before the addition of CALB, 10 min, 20 min, 1 h, 2 h, 6 h, 23 h, 30 h, and 48 h after the reaction had been started. The SEC traces in Figure 7 show selected data to illustrate the process. The formation of oligomers at the beginning of the reaction prior to the application of vacuum and the obtained
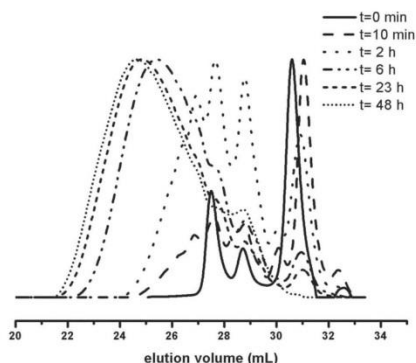
Figure 7. SEC traces (THF) for the condensation polymerization of BHMO:1,8-octanediol:sebacic acid (1:1:2; 10% wt CALB) at $t = 0$, = 10 min, $t = 1$ h, $t = 6$ h, $t = 23$ h, and $t = 48$ h.

high-molecular-weight products are visible after 6 h. This development is typical for a condensation reaction and was expected. However, rather low PDIs (≤ 2) could be achieved in this reaction, which is not typical for polycondensation. Gross and co-workers[18] have observed this phenomenon for the enzyme-catalyzed polymerization of 1,8-octanediol and adipic acid as a result of the chain growth occurring with a selectivity for the attachment of lower molecular weight oligomers. On the other hand, precipitation of the copolymers during work-up may also have contributed to the low PDIs observed.

^{1}H NMR spectra (CDCl$_3$:DMSO mixture 6:1) have been recorded after the reaction times given in Figure 8 to follow the reaction and to study details of the incorporation of the monomers into the polymer backbone. Looking at the BHMO:1,8-octanediol ratio at $t = 0$, it was shown that 61:39% of the monomers were present at the beginning of the reaction. At $t = 48$ h this ratio stayed at
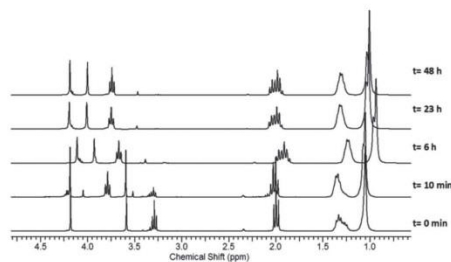
60:40, indicating that both monomers were incorporated into the polyester. From the NMR spectra, one can see that the triplet of the methylene group of the 1,8-octanediol at 3.29 ppm vanishes completely after 2 h, which indicates full incorporation of the diol at that time. Furthermore, the new triplet at 3.79 ppm confirmed this result. The signal for the BHMO monomer at 3.59 ppm and 4.12 ppm ($t = 0$) decreases and indicates increasing incorporation of this diol. The peaks at 4.0 and 4.20 ppm are caused by the BHMO monomer incorporated into the polyester backbone. However, the signal decrease for BHMO is slower than the one of 1,8-octanediol, indicating that the preferred diol for enzymatic polymerization in this case is the latter one. This result is in line with expectation since a more hydrophobic monomer is favored by the active center of the enzyme. Potential transesterification reactions should be mentioned in this context, which may lead to randomization of the repeat units.

3.4. Thermal Characterization of Oxetane-Functional Aliphatic Polyesters via DSC

Visual inspection of the samples shows that with increasing BHMO content the polymers change from a solid appearance to a wax, and finally to an oily consistency. Thermal properties of the different samples were investigated via differential scanning calorimetry (DSC) in a temperature range of –100–150 °C. Heating and cooling rates of 40 °C min^{-1} (first cycle) and 10 °C min^{-1} (second cycle) were applied. The second cycle was used for the determination of glass transition temperatures (T_g) and melting points. In some cases (samples **10–14**), only a melting temperature (T_m) was observed, whereas in samples **15-20** both T_m and T_g were detected (see Table 2 and Figure 9). Melting temperatures decreased with increasing BHMO content, which shows that this bulky unit impedes crystallization of these materials. As expected, the condensation product of sebacic acid and BHMO does not show a melting endotherm any more. It is important to note that, contrary to expectation, crystallization is not fully suppressed even in polymers with high BHMO content (e.g., sample **17**, 64% BHMO). This observation can be tentatively explained by the following phenomena: (1) oxetane units do not function as a major "defect" structure in those polymer systems; (2) completely random incorporation of the two diol units cannot be guaranteed, although transesterification aids to randomize the repeating units. The T_g values follow a slightly different trend compared to the melting temperatures. The highest T_g of –1.4 °C was observed for the sample with 42% of BHMO incorporated into the backbone. Surprisingly, the values drop to –59.2 °C and increase again with increasing BHMO content.

Figure 8. ^{1}H NMR spectra for the condensation reaction of BHMO, 1,8-octanediol, and sebacic acid at $t = 0$, 10 min, 6 h, 23 h, 48 h.

1788

Macromolecular
Journals

Macromol. Chem. Phys. **2012**, *213*, 1783–1790
© 2012 WILEY-VCH Verlag GmbH & Co. KGaA, Weinheim

Materials
Views
www.MaterialsViews.com

Table 2. Thermal properties of oxetane-functional copolymers of BHMO, 1,8-octanediol, and sebacic acid.

No.	mol%[a] n^{NMR}	mol%[a] m^{NMR}	$\overline{M}_n^{SEC}$ [g mol^{-1}]	$T_g^{b)}$ [°C]	$T_m^{b)}$ [°C]	ΔH [J g^{-1}]
10	0	100	9100	–	72.2	108.1
11	5	95	8100	–	67.4	93.3
12	14	86	7800	–	62.9	81.9
13	23	77	8000	–	57.2	75.9
14	31	69	7200	–	56.2	67.7
15	42	58	9200	−1.4	45.7	47.2
16	57	43	6700	−59.2	34.6	35.1
17	64	36	9300	−53.0	24.7	40.9
18	76	24	7500	−46.0	3.0	23.7
19	87	13	6300	−44.6	5.3	8.9
20	100	0	5000	−41.2	–	–

[a]Diol ratios calculated by ^{1}H NMR spectroscopy; [b]Values gained from the second heating cycle (10 °C min^{-1}).

3.5. Crosslinking of BHMO and Copolymer via Photoinitiated Cationic Ring-Opening Polymerization

The oxetane derivative BHMO and sample **18** were crosslinked separately using the photoinitiated cationic ring-opening technique. Irgacure 270 was used as the photoinitiator. After irradiation with UV-light (254 nm), the samples became insoluble in THF. IR spectra were recorded before and after the reaction to observe the characteristic oxetane band at 980 cm^{-1}.[27,31] Figure 10 shows the obtained results.

The top spectrum in Figure 10 shows that BHMO can be crosslinked cationically. Before irradiation, the spectrum shows a broad hydroxyl absorbance, while after crosslinking this absorbance decreased. The same applies for the oxetane vibration at 980 cm^{-1}. This band was taken as an indicator for successful ring-opening polymerization. In the bottom part of Figure 10, the spectrum
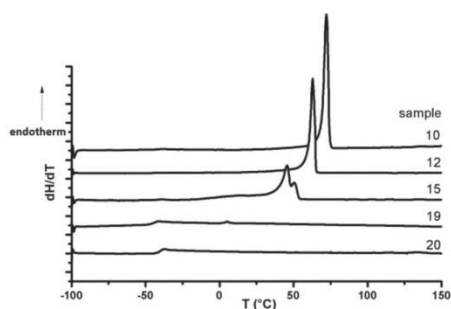

Figure 9. DSC measurements of selected samples (**10, 12, 15, 19, 20**), (10 °C min^{-1}).
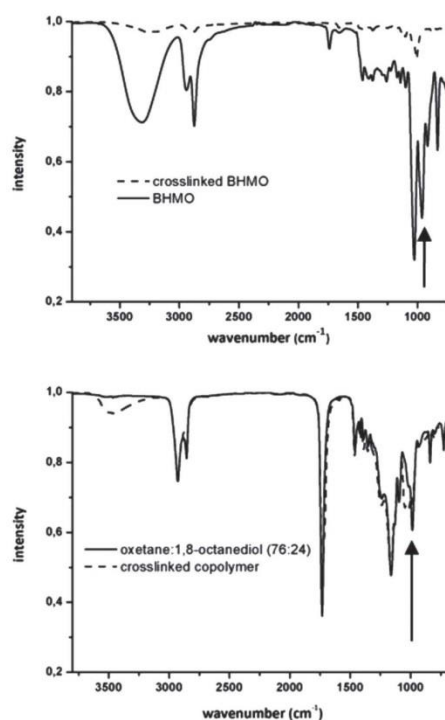
Figure 10. upper: BHMO before (solid) and after (dashed) crosslinking with Irgacure 270, lower: copolymer **18** before (solid) and after (dashed) crosslinking with Irgacure 270. The arrows show the oxetane peak around 980 cm^{-1}.

1789

for the crosslinked polymer is shown, in which the oxetane band decreased after irradiation with UV–Vis light. Low intensity absorbance of hydroxyl groups is visible, which indicates that the heterocyclic moiety has been ring-opened without subsequent connection to a neighboring cyclic ether group. Possible side reactions like transesterification reactions can neither be excluded nor controlled. At the same time typical bands between 1175 and 1020 cm^{-1} increase due to linear polyether formation. The reaction between the BHMO monomer and BHMO incorporated into the polymer strongly depends on other functional groups present, like ester groups,[27] which might explain the longer irradiation time for the polymer sample. Reduced chain mobility and thus reduced BHMO mobility might be a reason for incomplete conversion of the oxetane unit. The materials are promising with respect to application as photo-crosslinkable, potentially biodegradable polyesters.

4. Conclusion

We have synthesized oxetane-functional aliphatic polyesters, exploiting the enzymatic polycondensation catalyzed by CALB (*Candida antarctica Lipase B*). This orthogonal approach made it possible to employ the acid-sensitive monomer BHMO in a copolymerization with 1,8-octanediol and sebacic acid. Different diol ratios have been applied and the effect of BHMO in polyesters on their thermal behavior has been investigated. It was found that the cyclic ether derivative can be easily incorporated into the aliphatic backbone by CALB. By variation of the amount of BHMO, melting points (T_m) could be tuned, and interestingly it was shown that, although BHMO is a sterically demanding monomer, crystallization could only be suppressed with a BHMO percentage of ≥ 90%.

Incorporation of BHMO into aliphatic polyesters may broaden the field of application of oxetane monomers. The materials can be photo-crosslinked and therefore are promising in surface coating applications for biomedical purposes.

Supporting Information

Supporting Information is available from the Wiley Online Library or from the author.

[1] P. A. Gunatillake, R. Adhikari, *Eur. Cells Mater.* **2003**, *5*, 1.
[2] U. Edlund, A. C. Albertsson, *Adv. Drug Delivery Rev.* **2003**, *55*, 585.
[3] I. Taniguchi, W. A. Kuhlman, A. M. Mayes, L. G. Griffith, *Polym. Int.* **2006**, *55*, 1385.
[4] A.-C. Albertsson, I. K. Varma, *Adv. Polym. Sci.* **2002**, *157*, 2.
[5] S. Okumura, M. Iwai, Y. Tominaga, *Agricultural Biological Chem.* **1984**, *48*, 2805.
[6] H. Uyama, K. Inada, S. Kobayashi, *Chem. Lett.* **1998**, *12*, 1285.
[7] R. A. Gross, A. Kumar, B. Kalra, *Chem. Rev.* **2001**, *101*, 2097.
[8] H. Uyama, S. Kobayashi, in *Enzyme-Catalyzed Synthesis of Polymers*, Vol. 194, Springer, Berlin **2006**, p. 133.
[9] S. Kobayashi, *Macromol. Rapid Commun.* **2009**, *30*, 237.
[10] S. Kobayashi, *Proc. Jpn. Acad. Ser. B-Phys. Biol. Sci.* **2010**, *86*, 338.
[11] F. Binns, P. Harffey, S. M. Roberts, A. Taylor, *J. Polym. Sci., Part A: Polym. Chem.* **1998**, *36*, 2069.
[12] A. Mahapatro, B. Kalra, A. Kumar, R. A. Gross, *Biomacromolecules* **2003**, *4*, 544.
[13] A. Kumar, R. A. Gross, *Biomacromolecules* **2000**, *1*, 133.
[14] S. Skaria, M. Smet, H. Frey, *Macromol. Rapid Commun.* **2002**, *23*, 292.
[15] A. S. Kulshrestha, W. Gao, H. Fu, R. A. Gross, *Biomacromolecules* **2007**, *8*, 794.
[16] I. K. Varma, A. C. Albertsson, R. Rajkhowa, R. K. Srivastava, *Prog. Polym. Sci.* **2005**, *30*, 949.
[17] A. S. Kulshrestha, B. Sahoo, W. Gao, H. Y. Fu, R. A. Gross, *Macromolecules* **2005**, *38*, 3205.
[18] A. Mahapatro, A. Kumar, B. Kalra, R. A. Gross, *Macromolecules* **2003**, *37*, 35.
[19] J. A. Burkhard, G. Wuitschik, M. Rogers-Evans, K. Müller, E. M. Carreira, *Angew. Chem.* **2010**, *122*, 9236.
[20] E. J. Vandenberg, J. C. Mullis, R. S. Juvet, *J. Polym. Sci., Part A: Polym. Chem.* **1989**, *27*, 3083.
[21] M. Bednarek, *Polym. Int.* **2003**, *52*, 1595.
[22] M. Bednarek, P. Kubisa, S. Penczek, *Macromolecules* **2001**, *34*, 5112.
[23] Y. Chen, M. Bednarek, P. Kubisa, S. Penczek, *J. Polym. Sci., Part A: Polym. Chem.* **2002**, *40*, 1991.
[24] H. Koinuma, H. Hirai, *Die Makromol. Chem.* **1977**, *178*, 241.
[25] D. J. Darensbourg, A. I. Moncada, W. Choi, J. H. Reibenspies, *J. Am. Chem. Soc.* **2008**, *130*, 6523.
[26] D. J. Darensbourg, A. Horn Jr, A. I. Moncada, *Green Chem.* **2010**, *12*, 1376.
[27] J. V. Crivello, H. Sasaki, *J. Macromol. Sci., A: Pure Appl. Chem.* **1993**, *30*, 189.
[28] H. Sasaki, J. V. Crivello, *J. Macromol. Sci., Part A: Pure Appl. Chem.* **1992**, *29*, 915.
[29] D. B. Pattison, *J. Am. Chem. Soc.* **1957**, *79*, 3455.
[30] G. Odian, *Principles of Polymerization*, 4th Ed, John Wiley & Sons, Inc., Hoboken, USA **2004**.
[31] S. Jungermann, N. Riegel, D. Muller, K. Meerholz, O. Nuyken, *Macromolecules* **2006**, *39*, 8911.

A.2 Universal Concept for the Implementation of a Single Cleavable Unit at Tunable Position in Functional Poly(ethylene glycol)s

Carsten Dingels,[†] Sophie S. Müller,[†,‡] Tobias Steinbach,[†,‡] Christine Tonhauser,[†,‡] and Holger Frey[,†]*

[†]Institute of Organic Chemistry, Johannes Gutenberg University Mainz, Duesbergweg 10-14, 55128 Mainz, Germany

[‡]Graduate School Materials Science in Mainz, Staudingerweg 9, 55128 Mainz, Germany

Universal Concept for the Implementation of a Single Cleavable Unit at Tunable Position in Functional Poly(ethylene glycol)s

Carsten Dingels,[†] Sophie S. Müller,[†,‡] Tobias Steinbach,[†,‡] Christine Tonhauser,[†,‡] and Holger Frey*[,†]

[†]Department of Organic Chemistry, Johannes Gutenberg-Universität Mainz, Duesbergweg 10-14, D-55099 Mainz, Germany
[‡]Graduate School Materials Science in Mainz, Staudingerweg 9, D-55128 Mainz, Germany

S Supporting Information

ABSTRACT: Poly(ethylene glycol) (PEG) with acid-sensitive moieties gained attention particularly for various biomedical applications, such as the covalent attachment of PEG (PEGylation) to protein therapeutics, the synthesis of stealth liposomes, and polymeric carriers for low-molecular-weight drugs. Cleavable PEGs are favored over their inert analogues because of superior pharmacodynamic and/or pharmacokinetic properties of their formulations. However, synthetic routes to acetal-containing PEGs published up to date either require enormous efforts or result in ill-defined materials with a lack of control over the molecular weight. Herein, we describe a novel methodology to implement a single acetaldehyde acetal in well-defined (hetero)functional poly(ethylene glycol)s with total control over its position. To underline its general applicability, a diverse set of initiators for the anionic polymerization of ethylene oxide (cholesterol, dibenzylamino ethanol, and poly(ethylene glycol) monomethyl ether (mPEG)) was modified and used to synthesize the analogous labile PEGs. The polyether bearing the cleavable lipid had a degree of polymerization of 46, was amphiphilic and exhibited a critical micelle concentration of 4.20 mg·L^{-1}. From dibenzylamino ethanol, three heterofunctional PEGs with different molecular weights and labile amino termini were generated. The transformation of the amino functionality into the corresponding squaric acid ester amide demonstrated the accessibility of the cleavable functional group and activated the PEG for protein PEGylation, which was exemplarily shown by the attachment to bovine serum albumin (BSA). Furthermore, turning mPEG into a macroinitiator with a cleavable hydroxyl group granted access to a well-defined poly(ethylene glycol) derivative bearing a single cleavable moiety within its backbone. All the acetal-containing PEGs and PEG/protein conjugates were proven to degrade upon acidic treatment.
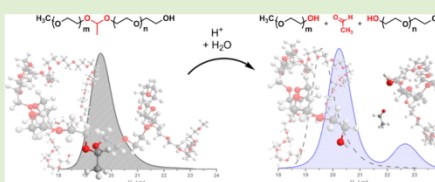
INTRODUCTION

Since the pioneering work of Davis and co-workers in the 1970s,[1,2] PEGylation, that is, the covalent attachment of poly(ethylene glycol) (PEG) to a substrate, has become one of the most important strategies to overcome the inherent disadvantages of protein therapeutics.[3−7] Pharmaceutically interesting proteins undergo proteolytic degradation as well as renal clearance and often are immunogenic or antigenic. Hence, they usually exhibit short body-residence times and a fast decrease from therapeutically effective concentrations to ineffective doses. The attachment of a water-soluble, synthetic polymer such as PEG to the protein leads to decreased renal filtration, decreased proteolytic degradation, and reduced immunogenicity of the conjugate in comparison to the unmodified protein. These effects result in prolonged body-residence times of the PEGylated proteins.

However, often decreased bioactivity of protein pharmaceuticals is observed when PEG chains are attached to their surface.[8] The attachment of PEG via a cleavable linker can be advantageous for some protein therapeutics.[9,10] PEGs with cleavable coupling units[11] or lipids[12−21] have also been investigated for other pharmaceutical applications where

reversible PEGylation of the desired substrate is favorable, such as the shielding of polyplexes and liposomes.

Besides a reduction in the PEG conjugates' bioactivity in most cases, PEGylation suffers from another disadvantage regardless of the substrate: Its application is limited to polyethers with average molecular weights below 40−60 kDa, because PEG is not biodegradable and otherwise will not be excreted, but accumulate in the liver.[22] However, the circulation times of PEGylated proteins improve by increasing the average molecular weight of the synthetic polymer.[23] In consequence, biodegradable poly(ethylene glycol)s carrying cleavable moieties in the backbone are of great interest. This statement is also true for pharmaceutical applications other than the PEGylation of proteins, polyplexes, or liposomes: Biocompatible and biodegradable polymers are well suited to carry low molecular weight drugs into tumor tissue making use of Ringsdorf's drug delivery concept[24] and the enhanced permeability and retention (EPR) effect.[25,26]
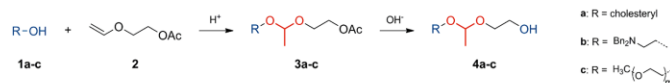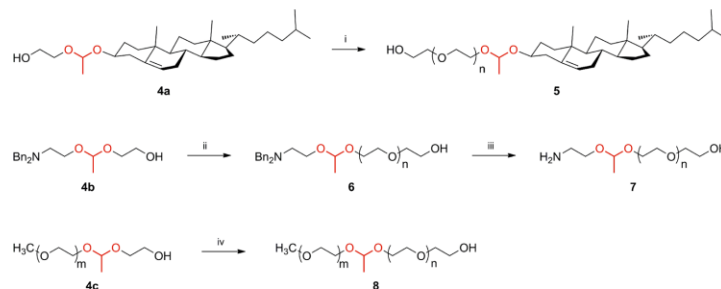
Scheme 1. Synthetic Route to AROP Initiators Containing a Single Acetal Moiety

Scheme 2. Synthesis of Scissile PEGs with Different Termini[a]

[a]Reagents and conditions: (i) 1. CsOH·H$_2$O, C$_6$H$_6$, 90 °C, vacuum. 2. Tetrahydrofuran (THF), nEO, 60 °C. 3. MeOH. (ii) 1. CsOH·H$_2$O, C$_6$H$_6$, 90 °C, vacuum. 2. THF/dimethylsulfoxide (DMSO), nEO. 3. MeOH. (iii) H$_2$, Pd(OH)$_2$/C, dioxane/water 1:1, 80 bar, 40 °C. (iv) 1. C$_6$H$_6$, 90 °C, vacuum. 2. KC$_{10}$H$_8$, THF/DMSO, nEO. 3. MeOH.

Various strategies have been employed to incorporate cleavable moieties into the backbone of PEG, such as *cis*-aconityl linkages[27] and acetals,[28−31] as well as esters and disulfides.[32] Unfortunately, neither of the aforementioned materials is well-defined because all of them were synthesized from telechelic PEGs via step-growth mechanisms. Nevertheless, promising results in terms of drug delivery and in vivo degradation were, for example, obtained by Tomlinson et al. who synthesized PEG-based polyacetals loaded with doxorubicin, a potent anticancer drug,[28] and demonstrated that acetaldehyde, which is formed by the degradation of acetaldehyde acetal-containing PEGs, is not cytotoxic.[29] Elisseeff and co-workers partially oxidized the ether bonds of PEG with Fenton's reagent to generate hemiacetals at the polyether backbone and demonstrated their degradability.[33] However, no degradation kinetics data was provided. Very recently, Lundberg et al. published a promising strategy to synthesize more defined degradable PEG derivatives via monomer-activated copolymerization of ethylene oxide and epichlorohydrin and subsequent elimination of hydrogen chloride.[34] The obtained vinyl ether-containing polymers exhibited polydispersity indices (PDI, M_w/M_n) below 1.4, but no concept for the attachment of therapeutics was presented.

Due to their stability in extremely basic media,[35] acetals and ketals tolerate the harsh conditions of the anionic ring-opening polymerization (AROP) of oxiranes and have been established as protecting groups for aldehyde and hydroxyl groups in AROP initiators[36−40] and monomers.[41,42] Further, these groups have been employed to generate degradable, water-soluble polyethers by epoxide AROP. Based on a ketal-containing branching unit Feng et al. demonstrated the synthesis of degradable dendrimer-like PEGs up to the seventh generation with a molecular weight of almost half a million g·mol^{-1}.[43] Although these polyethers are well-defined, the synthetic effort necessary for their production will probably hinder widespread applications. Hyperbranched poly(ethylene glycol)s with acetal groups at each branching point that can be synthesized by the copolymerization of ethylene oxide (EO) with the inimer glycidyloxyethyl ethylene glycol ether (GEGE) in a one-pot reaction were recently presented by our group.[44] In this context, the recent work of the group of Kizhakkedathu has to be mentioned, who used ketal-containing inimers for the oxyanionic polymerization[45] analogous to GEGE and multifunctional, ketal-containing initiators for the ring-opening multibranching polymerization of glycidol[46] to produce cleavable hyperbranched polyether polyols.

Acetal-functionalized PEGs are not solely interesting for biomedical applications. For instance, poly(ethylene glycol) bearing an acetaldehyde chloroethyl acetal terminus has been used to generate scissile PEG polystyrene block copolymers, which were investigated as precursors for porous films.[47]

Depending on the desired application of degradable PEG the cleavable moieties have to be located either in the backbone or at (one of) the functional terminus (termini). Herein, we present the implementation of a single, cleavable acetal moiety into conventional initiators for the anionic ring-opening polymerization of epoxides using a straightforward two-step protocol (Scheme 1), which gives access to both types of PEG, either cleavable in the backbone or at one of the terminal sites (Scheme 2). First, the original initiators, alcohols 1a−c, are added to 2-acetoxyethyl vinyl ether[48] (AcVE, 2) under acidic conditions to form the asymmetric acetaldehyde acetals 3a−c. Subsequently, the products are saponified to release the desired acetal-containing initiators 4a−c.

The developed methodology is in principle applicable to all acid stable AROP initiators and was proven for a diverse set of alcohols to underline its general usefulness: Cholesterol (1a) as an apolar initiator, dibenzylamino ethanol (1b), which carries an additional, orthogonally protected functional group, and poly(ethylene glycol) monomethyl ether (mPEG, 1c) as a macroinitiator. The scissile macroinitiator granted access to PEGs carrying a single acetal moiety in the backbone of the

polymer. The specific position of this acid labile group can be controlled by the molecular weight of the macroinitiator and the number of ethylene oxide (EO) units added.

■ EXPERIMENTAL SECTION

Materials. All reagents and solvents were purchased from Acros Organics, Fluka, or Sigma-Aldrich and were used without further purification unless stated otherwise. Ethylene glycol monovinyl ether was purchased from TCI Europe. Deuterated solvents were purchased from Deutero GmbH and stored over molecular sieves (except for deuterium oxide). 2-Acetoxyethyl vinyl ether[48] (**2**) and dibenzylamino ethanol[49] (**1b**) were prepared according to known protocols. Dry THF used for the anionic ring-opening polymerization of ethylene oxide was dried and stored over sodium. Care must be taken when handling the toxic, flammable, and gaseous ethylene oxide.

Methods. ^{1}H NMR spectra (400 MHz) were recorded on a Bruker ARX 400 with a 5 mm BBO probe. 2D and ^{13}C NMR spectra were recorded on a Bruker Avance-II 400 (400 MHz, 5 mm BBO probe, and B-ACS 60 auto sampler) if not stated otherwise. All spectra were recorded with 32 scans at 294 K using a relaxation delay of 1 s, unless stated otherwise and processed with MestReNova v6.1.1 software. Size-exclusion chromatography (SEC) measurements in DMF containing 0.25 g·L^{-1} of lithium bromide as additive were performed on an Agilent 1100 Series as an integrated instrument using PSS (Polymer Standards Service) HEMA column (106/105/104 g/mol), RI detector, and UV detector operating at 275 nm. Calibration was executed using poly(ethylene oxide) (PEO) standards from PSS. Matrix-assisted laser desorption/ionization time-of-flight mass spectrometry (MALDI-ToF MS) measurements of all polymers were recorded on a Shimadzu Axima CFR MALDI-ToF MS mass spectrometer, equipped with a nitrogen laser delivering 3 ns laser pulses at 337 nm. α-Cyano hydroxyl cinnamic acid (CHCA) or dithranol was used as a matrix and potassium triflouroacetate (KTFA) was added for ion formation. The analytes were dissolved in methanol at a concentration of 10 g·L^{-1}. An aliquot (10 μL) was added to 10 μL of a solution (10 g·L^{-1}) of the matrix and 1 μL of a solution of the cationization agent. A total of 1 μL of the mixture was applied on a multistage target and methanol evaporated, and a thin matrix/analyte film was formed.

Sodium dodecyl sulfate polyacrylamide gel electrophoresis (SDS-PAGE) was carried out with Tris-HCl gels (Biorad, 1.0 mm, 10 well, 8% resolving gel, 4% stacking gel). IR spectra were recorded on a Thermo Scientific Nicolet iS10 FT-IR spectrometer, equipped with a diamond ATR unit and were processed with OMNIC 8.1.210 software. Mass spectra were either measured on a Finnigan MAT 95 (field desorption, FD-MS) or a Waters/Micromass QToF Ultima 3 (electrospray ionization, ESI-MS). Surface tension measurements to determine the critical micelle concentrations (CMC) were performed on a Dataphysics DCAT 11 EC tensiometer equipped with a TV 70 temperature control unit, a LDU 1/1 liquid dosing and refill unit, as well as a RG 11 Du Noüy ring. Surface tension data was processed with SCAT v3.3.2.93 software. The CMC presented is a mean value of three experiments. All solutions for surface tension measurements were stirred for 120 s at a stir rate of 50%. After a relaxation period of 400 s, three surface tension values were measured. The mean values of the three measurements were plotted against the logarithm of the concentration. The slopes of the traces at high concentrations as well as in the low concentration range were determined by linear regression. The concentration at the fits' intersection was the CMC. The Du Noüy ring was rinsed thoroughly with water and annealed in a butane flame. Turbidimetry was performed in a Jasco V-630 UV–vis spectrometer at a wavelength of λ = 528 nm and was processed with the Time Course Measurement program of Spectra Manager v2.08 software.

Synthesis Procedures. *Acetoxyethyl 1-(Cholesteryloxy)ethyl Ether (3a).* Cholesterol (5.0 g, 13 mmol) and 2-acetoxyethyl vinyl ether (2.53 g, 19.4 mmol) were stirred for 45 min in dichloromethane with *p*-toluene sulfonic acid monohydrate (*p*TSA, 25 mg, 0.13 mmol). The solution was treated with triethylamine (250 μL) and washed with

1 N aqueous sodium hydroxide solution. After drying over sodium sulfate, the organic phase was evaporated to a small volume. Pure product (4.80 g, 9.29 mmol, 72%) was obtained by column chromatography (eluent: petrol ether/ethyl acetate 8:1) over silica. ^{1}H NMR (400 MHz, CDCl$_3$): δ [ppm] 5.32 (s, 1H, H-6), 4.85 (q, 1H, J_{AB} = 5.3 Hz, H$_3$C*CH*O$_2$), 4.26–4.12 (m, 2H, AcO-*CH$_2$*), 3.78–3.58 (m, 2H, AcO*CH$_2$*-*CH$_2$*), 3.65–3.36 (m, 1H, H-3α), 2.38–2.12 (m, 2H, H-4), 2.05 (s, 3H, H$_3$C—CO–), 2.03–1.94 (m, 1H, H-12α), 1.99–1.89 (m, 1H, H-7β), 1.87–1.79 (m, 2H, H-1β and H-2α), 1.87–1.74 (m, 1H, H-16β), 1.63–0.81 (m, 22H), 1.30 (d, 3H, J_{AB} = 5.3 Hz, H$_3$C-CHO$_2$), 0.99 (s, 3H, H$_3$-19), 0.90 (d, 3H, J_{AB} = 6.5 Hz, H$_3$-21), 0.84 (d, 3H, J_{AB} = 6.6 Hz, H$_3$-26), 0.83 (d, 3H, J_{AB} = 6.6 Hz, H$_3$-27), 0.65 (s, 3H, H$_3$-18). ^{13}C NMR (100.6 MHz, CDCl$_3$): δ [ppm] 170.1 (1C, MeCOO), 140.9 and 140.8 (1C, C-5), 121.9 and 121.8 (1C, C-6), 98.0 and 97.9 (1C, Me-CHO$_2$), 75.9 and 75.8 (1C, C-3), 63.9 (1C, AcO-*CH$_2$*), 61.6 (1C, AcOCH$_2$-*CH$_2$*-), 50.3 (1C, C-9), 42.4 (1C, C-13), 40.1 and 39.5 (1C, C-4), 39.8 (1C, C-12), 39.6 (1C, C-24), 37.5 and 37.3 (1C, C-1), 36.8 (1C, C-10), 36.3 (1C, C-22), 35.9 (1C, C-20), 32.0 (2C, C-7 and G-8), 29.5 and 28.7 (1C, C-2), 28.3 (1C, C-16), 28.1 (1C, C-25), 24.4 (1C, C-15), 23.9 (1C, C-23), 22.9 (1C, C-27), 22.7 (1C, C-26), 21.1 (2C, C-11 and CH$_3$-COO), 20.6 (1C, CH$_3$-CHO$_2$), 19.5 (1C, C-19), 18.8 (1C, C-21), 12.0 (1C, C-18). MS (ESI-MS, MeOH): *m/z* = 539.42 [M + Na]$^+$, 1055.86 [2M + Na]$^+$.

Acetoxyethyl 1-(2-Dibenzylamino ethoxy)ethyl Ether (3b). Dibenzylamino ethanol (5.0 g, 21 mmol) and 2-acetoxyethyl vinyl ether (5.0 g, 38 mmol) were stirred for 30 min in dichloromethane with trifluoroacetic acid (TFA, 7.1 g, 62 mmol). The solution was treated with triethylamine (1.5 mL) and washed with 1 N aqueous sodium hydroxide solution. After drying over sodium sulfate, the organic phase was evaporated to small volume. Pure product was obtained by column chromatography (eluent: petrol ether/ethyl acetate 6:1) over silica. Yield: 85%. ^{1}H NMR (400 MHz, CDCl$_3$): δ [ppm] 7.42 (d, 4H, J_{AB} = 7.2 Hz, 4 meta CH$_{Ar}$), 7.34 (t, 4H, J_{AB} = 7.4 Hz, 4 ortho CH$_{Ar}$), 7.26 (d, 2H, J_{AB} = 7.4 Hz, 2 para CH$_{Ar}$), 4.75 (q, 1H, J_{AB} = 5.4 Hz, H$_3$C-CHO$_2$), 4.21 (t, 2H, J_{AB} = 4.9 Hz, AcO-*CH$_2$*), 3.77–3.67 (m, 1H, NCH$_2$-*CH$_a$*), 3.76–3.67 (m, 1H, AcOCH$_2$-*CH$_a$*), 3.69 (s, 4H, 2 Ph-*CH$_2$*), 3.65–3.57 (m, 1H, AcOCH$_2$-*CH$_b$*), 3.61–3.52 (m, 1H, NCH$_2$-*CH$_b$*), 2.72 (t, 2H, J_{AB} = 6.3 Hz, N-*CH$_2$*-CH$_2$), 2.07 (s, 3H, H$_3$C—CO), 1.31 (d, 3H, J_{AB} = 5.4 Hz, H$_3$C-CHO$_2$). ^{13}C NMR (100.6 MHz, CDCl$_3$): δ [ppm] 171.0 (1C, Me-CO-O), 139.7 (2C, 2 quaternary C$_{Ar}$), 128.8 (4C, ortho CH$_{Ar}$), 128.2 (4C, meta CH$_{Ar}$), 126.9 (2C, para CH$_{Ar}$), 99.7 (1C, H$_3$C-CHO$_2$), 64.0 (1C, NCH$_2$-*CH$_2$*), 62.6 (1C, AcO-*CH$_2$*), 62.2 (1C, AcOCH$_2$-*CH$_2$*), 59.0 (2C, 2 Ph-*CH$_2$*), 52.9 (1C, N-*CH$_2$*-CH$_2$), 21.0 (1C, *H$_3$C*-CO), 19.5 (1C, *H$_3$C*-CHO$_2$).

1-(2-Acetoxyethoxy)ethoxy mPEG (3c). Poly(ethylene glycol) monomethyl ether (**1c**, 4.0 g, 2.0 mmol), 2-acetoxyethyl vinyl ether (1.3 g, 10 mmol), and *p*TSA (3.8 mg 0.2 mmol) were placed in a round-bottom flask, dissolved in dichloromethane (DCM, 20 mL), and stirred for 30 min. The reaction was quenched with triethylamine (0.2 mL) and washed with 1 N aqueous sodium hydroxide solution. The organic phase was dried over sodium sulfate and subsequently concentrated to small volume. Pure product was obtained by precipitation in cold diethyl ether. Yield: 87%. ^{1}H NMR (400 MHz, CDCl$_3$): δ [ppm] 4.77 (q, 1H, J_{AB} = 5.4 Hz, H$_3$C-CHO$_2$), 4.16 (t, 2H, J_{AB} = 4.8 Hz, AcO-*CH$_2$*), 3.86–3.36 (m, 180H, CH$_2$O), 3.33 (s, 3H, OCH$_3$), 2.03 (s, 3H, H$_3$C—CO), 1.28 (d, 3H, J_{AB} = 5.4 Hz, H$_3$C-CHO$_2$).

Glycol 1-(Cholesteryloxy)ethyl Ether (4a). Potassium hydroxide (1.00 g, 17.8 mmol) and acetoxyethyl 1-(cholesteryloxy)ethyl ether (**3a**, 1.00 g, 1.93 mmol) were stirred under reflux in a solution of ethanol (12 mL) and water (0.5 mL) for 3 h. After cooling, brine was added and the solution was extracted with DCM three times. After drying over sodium sulfate the organic phase was evaporated to small volume. Pure product (536 mg, 1.13 mmol, 59%) was obtained by column chromatography (eluent: petrol ether/ethyl acetate 2:1) over silica. ^{1}H NMR (400 MHz, CDCl$_3$): δ [ppm] 5.32 (s, 1H, H-6), 4.81 (q, 1H, J_{AB} = 5.3 Hz, H$_3$C-CHO$_2$), 3.75–3.64 (m, 2H, HO-*CH$_2$*), 3.71–3.53 (m, 2H, HOCH$_2$-*CH$_2$*), 3.94–3.34 (m, 1H, H-3α), 2.53 (t, 1H, J_{AB} = 5.8 Hz, OH), 2.35–2.12 (m, 2H, H-4), 2.04–1.94 (m, 1H,

H-12α), 1.99–1.90 (m, 1H, H-7β), 1.90–1.78 (m, 2H, H-1β and H-2α), 1.88–1.73 (m, 1H, H-16β), 1.63–0.80 (m, 22H), 1.32 (d, 3H, J_{AB} = 5.3 Hz, H_3C-CHO$_2$), 0.98 (s, 3H, H$_3$-19), 0.89 (d, 3H, J_{AB} = 6.5 Hz, H$_3$-21), 0.84 (d, 3H, J_{AB} = 6.6 Hz, H$_3$-26), 0.84 (d, 3H, J_{AB} = 6.6 Hz, H$_3$-27), 0.65 (s, 3H, H$_3$-18). ^{13}C NMR (100.6 MHz, CDCl$_3$): δ [ppm] 170.1 (1C, Me-CO—O), 140.9 and 140.8 (1C, C-5), 121.9 and 121.8 (1C, C-6), 98.0 and 97.9 (1C, Me-CHO$_2$), 79.5 and 75.8 (1C, C-3), 63.9 (1C, AcO-CH$_2$), 61.6 (1C, AcOCH$_2$-CH$_2$'), 50.3 (1C, C-9), 42.4 (1C, C-13), 40.1 and 39.5 (1C, C-4), 39.8 (1C, C-12), 39.6 (1C, C-24), 37.5 and 37.3 (1C, C-1), 36.8 (1C, C-10), 36.3 (1C, C-22), 35.9 (1C, C-20), 32.0 (2C, C-7 and G-8), 29.5 and 28.7 (1C, C-2), 28.3 (1C, C-16), 28.1 (1C, C-25), 24.4 (1C, C-15), 23.9 (1C, C-23), 22.9 (1C, C-27), 22.7 (1C, C-26), 21.1 (2C, C-11 and CH_3CO), 20.6 (1C, CH_3-CHO$_2$), 19.5 (1C, C-19), 18.8 (1C, C-18). MS (ESI-MS, MeOH): m/z = 497.42 [M + Na]$^+$, 971.81 [2M + Na]$^+$.

Glycol 1-(2-Dibenzylamino ethoxy)ethyl Ether (4b). Potassium hydroxide (3.2 g, 57 mmol) and acetoxyethyl 1-(2-dibenzylamino ethoxy)ethyl ether (**3b**, 6.0 g, 16 mmol) were stirred under reflux in a solution of ethanol (8.4 mL) and water (4.2 mL) for 3 h. After cooling, brine was added and the solution was extracted with DCM three times. After drying over sodium sulfate, the organic phase was evaporated to a small volume. Pure product was obtained by column chromatography (eluent: petrol ether/ethyl acetate 2:1) over silica. Yield: 58%. ^{1}H NMR (400 MHz, DMSO-d_6): δ [ppm] 7.41–7.27 (m, 8H, 4 *meta*-CH$_{Ar}$ and 4 *ortho*-CH$_{Ar}$), 7.22 (t, 2H, J_{AB} = 7.1 Hz, 2 *para*-CH$_{Ar}$), 4.63 (q, 1H, J_{AB} = 5.2 Hz, H_3C-CHO$_2$), 4.61 (t, 1H, J_{AB} = 4.7 Hz, HO-CH$_2$), 3.68–3.57 (m, 1H, NCH$_2$-CH$_a$), 3.60 (s, 4H, 2 Ph-CH$_2$), 3.53–3.43 (m, 1H, NCH$_2$-CH$_b$), 3.52–3.43 (m, 1H, HOCH$_2$-CH$_a$), 3.51 (m, 2H, HO-CH$_2$), 3.42–3.32 (m, 1H, HOCH$_2$-CH$_b$), 2.56 (t, 2H, J_{AB} = 6.2 Hz, N-CH$_2$-CH$_2$), 1.17 (d, 3H, J_{AB} = 5.3 Hz, H_3C-CHO$_2$). ^{13}C NMR (100.6 MHz, DMSO-d_6): δ [ppm] 139.5 (2C, 2 quaternary C$_{Ar}$), 128.5 (4C, *ortho*-CH$_{Ar}$), 128.2 (4C, *meta*-CH$_{Ar}$), 126.8 (2C, *para*-CH$_{Ar}$), 99.3 (1C, H$_3$C-CHO$_2$), 66.7 (1C, HOCH$_2$-CH$_2$), 63.1 (1C, NCH$_2$-CH$_2$), 60.4 (1C, HO-CH$_2$), 58.0 (2C, 2 Ph-CH$_2$), 52.4 (1C, N-CH$_2$-CH$_2$), 19.8 (1C, H$_3$C-CHO$_2$). MS (FD-MS, MeOH): m/z = 329.4 [M]$^+$, 569.6 [2M − Bn + 2H]$^+$, 659.7 [2M + H]$^+$, 691.7 [2M + MeOH + H]$^+$.

1-(2-Hydroxyethoxy)ethoxy mPEG (4c). Potassium hydroxide (1.2 g, 21 mmol) and **3c** (3.7 g, 1.9 mmol) were stirred under reflux in a solution of ethanol (3.0 mL) and water (1.5 mL) for 3 h. After cooling the solution was extracted with DCM three times and the combined organic phases were dried over sodium sulfate. DCM was evaporated and pure product was obtained by precipitation in cold diethyl ether. Yield: 67%. ^{1}H NMR (400 MHz, CDCl$_3$): δ [ppm] 4.77 (q, 1H, J_{AB} = 5.5 Hz, H$_3$C-CHO$_2$), 3.84–3.385 (m, 180H, (CH$_2$CH$_2$O)$_n$), 3.32 (s, 3H, OCH$_3$), 1.28 (d, 3H, J_{AB} = 5.2 Hz, H$_3$C-CHO$_2$).

α-(1-Cholesteryloxy)ethoxy) ω-Hydro PEG (5). Compound **4a** (427 mg, 0.900 mmol), cesium hydroxide monohydrate (134 mg, 0.798 mmol), and benzene were placed in a Schlenk flask. The mixture was stirred at RT for about 30 min to generate the cesium alkoxide (degree of deprotonation 89%). The salt was dried under vacuum at 90 °C for 24 h, dry THF was added via cryo-transfer, and ethylene oxide (2 mL, 51 mmol) was cryo-transferred first to a graduated ampule and then to the Schlenk flask containing the initiator solution. The mixture was allowed to warm up to room temperature, heated to 60 °C, and the polymerization was performed for 12 h at this temperature under vacuum. The reaction was quenched with methanol, the solvent was evaporated and the crude product was precipitated into cold diethyl ether. ^{1}H NMR (400 MHz, CDCl$_3$): δ [ppm] 5.31 (s, 1H, H-6), 4.83 (q, 1H, J_{AB} = 5.3 Hz, H$_3$C-CHO$_2$), 4.10–3.21 (m, 190H, CH$_2$O and H-3α), 2.35–2.12 (m, 2H, H-4), 2.04–1.89 (m, 2H, H-12α and 7β), 1.88–1.73 (m, 3H, H-1β, H-2α, and H-16β), 1.63–0.80 (m, 22H), 1.30 (d, 3H, J_{AB} = 5.3 Hz, H$_3$C-CHO$_2$), 0.98 (s, 3H, H$_3$-19), 0.89 (d, 3H, J_{AB} = 6.6 Hz, H$_3$-21), 0.85 (d, 3H, J_{AB} = 6.6 Hz, H$_3$-26), 0.84 (d, 3H, J_{AB} = 6.6 Hz, H$_3$-27), 0.65 (s, 3H, H$_3$-18).

α-(1-2-Dibenzylamino ethoxy)ethoxy) ω-Hydro PEG (6). Compound **6** was synthesized similar to protocols for *N,N*-dibenzylamino ethoxide-initiated anionic ring-opening polymerization of ethylene oxide known in the literature.[50,51] The following protocol is typical and

describes the example of **6** with a degree of polymerization (P_n) of 50 (**6$_{50}$**). Cesium hydroxide monohydrate (150 mg, 893 μmol) was added to a solution of **4b** (322.7 mg, 0.9796 mmol) dissolved in benzene (7 mL) in a dry Schlenk flask. The mixture was stirred for 30 min at 60 °C under slightly reduced pressure with closed stopcock. Moisture was removed by azeotropic distillation of benzene and subsequent drying at 80 °C under high vacuum for 3.5 h. After cooling to room temperature, dry THF (7 mL) was cryo-transferred into the Schlenk flask and dry DMSO (2 mL) was added via syringe. Subsequently, ethylene oxide (1.95 g, 44.3 mmol) was cryo-transferred via a graduated ampule to the initiator solution and the flask was closed tightly. The reaction mixture was stirred overnight at 40 °C and finally quenched by the addition of methanol (2 mL). The polymer was precipitated from methanol in cold diethyl ether twice and subsequently dried under reduced pressure. Yield: 2.07 g (91%). ^{1}H NMR (400 MHz, CDCl$_3$): δ [ppm] 7.32 (d, 4H, J_{AB} = 7.3 Hz, 4 ortho CH$_{Ar}$), 7.52 (t, 2H, J_{AB} = 7.4 Hz, 2 meta CH$_{Ar}$), 7.17 (t, 1H, J_{AB} = 7.2 Hz, para CH$_{Ar}$), 4.65 (q, 1H, J_{AB} = 5.3 Hz, H$_3$C-CHO$_2$), 3.97 (m, 208H, CH$_2$O), 2.62 (t, 2H, J_{AB} = 6.3 Hz, N-CH$_2$-CH$_2$), 1.23 (d, 3H, J_{AB} = 5.3 Hz, H$_3$C-CHO$_2$).

α-(1-(2-Amino ethoxy)ethoxy) ω-Hydro PEG (7). Hydrogenation of α-(1-(2-dibenzylamino ethoxy)ethoxy) ω-hydro PEG (**6**) was carried out similar to the protocol described for α-dibenzylamino ω-hydroxy-PEG.[51] The following protocol describes the synthesis of **7** with a degree of polymerization of 50 (**7$_{50}$**). Compound **6$_{50}$** (700 mg, 0.313 mmol) was dissolved in a water/dioxane 1:1 mixture and stirred with palladium(II)-hydroxide on activated charcoal (150 mg) under hydrogen (80 bar) for 3 days in a stainless steel reactor. After the solution had been filtered through Celite the filter cake was washed with methanol (2 L). The transparent solution was reduced to small volume and precipitated in cold diethyl ether. A second precipitation from DCM in cold diethyl ether yielded 457 mg (0.222 mmol, 71%) of **7$_{50}$**. ^{1}H NMR (400 MHz, DMSO-d_6): δ [ppm] 4.68 (q, 1H, J_{AB} = 5.2 Hz, H$_3$C-CHO$_2$), 4.59 (s, 1H, OH), 3.80–3.37 (m, 210H, CH$_2$O), 2.65 (t, 2H, J_{AB} = 5.8 Hz, H$_2$N-CH$_2$), 1.20 (d, 3H, J_{AB} = 5.2 Hz, H$_3$C-CHO$_2$).

α-(1-mPEG ethoxy) ω-Hydro PEG (8). Compound **4c** (1.00 g, 0.476 mmol) was dissolved in benzene (10 mL) in a dry Schlenk flask. The solution was stirred for 30 min at 90 °C under slightly reduced pressure with closed stopcock. Moisture was removed by azeotropic distillation of benzene and subsequent drying at 90 °C under high vacuum overnight. After cooling to room temperature dry THF (20 mL) was cryo-transferred into the Schlenk flask and potassium naphthalenide in THF (1 mL, c = 0.5 mol·L^{-1}, prepared under argon from potassium (235 mg, 6.0 mmol), naphthalene (770 mg, 6.0 mmol), and dry THF (12 mL) in a glovebox) was added via syringe. Subsequently, the generated hydrogen was evaporated including half the amount of THF and ethylene oxide (3.0 g, 68 mmol) was cryo-transferred via a graduated ampule to the macroinitiator solution. The reaction mixture was stirred for 3 h at 60 °C first and overnight at 40 °C. After the polymerization had been quenched by the addition of methanol (1.3 mL) the polymer was precipitated from methanol in cold diethyl ether twice and subsequently dried under reduced pressure. Yield: 3.64 g (91%). ^{1}H NMR (400 MHz, CDCl$_3$): δ [ppm] 4.75 (q, 1H, J_{AB} = 5.3 Hz, H$_3$C-CHO$_2$), 3.99–3.37 (m, 714H, CH$_2$O), 3.33 (s, 3H, OCH$_3$), 1.27 (d, 3H, J_{AB} = 5.4 Hz, H$_3$C-CHO$_2$).

α-(1-(2-Squaric acid ethyl ester amido)ethoxy)ethoxy) ω-Hydro PEG (10). Diethyl squarate (**9**, 60.7 mg, 357 μmol), **7$_{75}$** (100 mg, 29.2 μmol), and triethylamine (43 μL, 310 μmol) were stirred in a 1:1 water/ethanol solution (2 mL) for 4 h. After the ethanol had been removed by distillation, the solution was extracted with DCM four times. Subsequently, the organic phase was evaporated to small volume and precipitated in cold diethyl ether. The resulting polymer was precipitated several times from methanol in cold diethyl ether until no more diethyl squarate was detected by thin layer chromatography (TLC). ^{1}H NMR (400 MHz, CDCl$_3$): δ [ppm] 4.82–4.68 (m, 3H, H$_3$C-CH$_2$-O and H$_3$C-CHO$_2$), 3.99–3.37 (m, 311H, CH$_2$O and CH$_2$N), 1.50–1.38 (m, 3H, H$_3$C-CH$_2$O), 1.35–1.22 (m, 3H, H$_3$C-CHO$_2$).

■ RESULTS AND DISCUSSION

A.1. Addition of Conventional AROP Initiators to AcVE. The key step in the implementation of an acetaldehyde moiety between the hydroxyl group and the residue of established AROP initiators is the acid catalyzed addition of the alcohol to AcVE (Scheme 1). This vinyl ether was chosen for three reasons: First, upon the addition reaction the acetate can be saponified with little effort under basic conditions that every possible initiator for the AROP and the generated acetal will tolerate. Second, upon saponification a new hydroxyl group is generated, which is essential for the initiation of the anionic epoxide polymerization. And, finally, upon deprotonation the generated alkoxide is structurally related to the growing chain end, i.e., an alkyloxyethoxide, which is favorable for the initiation kinetics. The amount of acid necessary to promote the addition of the alcohol across the vinyl ether double bond varied depending on the nature of the alcohol (vide infra). Hence, the applied conventional initiators have to be more or less stable under acidic conditions. In contrast to the aforementioned and innovative, multifunctional, ketal-containing initiators used by Kizhakkedathu and co-workers,[46] our methodology yields asymmetric acetals from established initiators in a rapid two-step synthesis.

Cholesterol (**1a**) was chosen as a model compound to demonstrate the applicability of our acetal insertion protocol to apolar, monofunctional initiators for the oxyanionic ROP of epoxides. The addition of the steroid to AcVE was catalyzed by 1 mol % of *p*-toluene sulfonic acid. The conditions of the vinyl ether addition had to be adjusted for dibenzylamino ethanol (**1b**), because catalytic amounts of acid solely protonated the basic tertiary amine, but did not activate the vinyl ether double bond. The excess of trifluoroacetic acid which was necessary to provide a satisfactory reaction rate was determined by following the reaction kinetics via ^{1}H NMR spectroscopy. Figure S46 displays the reaction kinetics of the addition reaction in deuterated chloroform when 1.8 equiv of AcVE and 3 equiv of TFA were batched (for spectra see SI, Figure S47). An 85% conversion was achieved after **44 min**, whereas under identical conditions except for less acid fed to the reaction mixture (i.e., 2 equiv of TFA batched with respect to **1b**), 90% conversion was reached after 18 h (data not shown).

According to our protocol, a PEG macroinitiator opens up the synthesis of well-defined poly(ethylene glycol)s carrying a single acetal moiety in the backbone (Scheme 2). mPEG was chosen as the simplest precursor for this system, because it is chemically inert, except for the mandatory hydroxyl group. The necessary amount of acid was higher than in the analogous reaction with **1a**, reflecting the lower reactivity of the polymeric alcohol, but significantly lower than in the reaction with **1b**, because no basic residue was competing for protons with the double bond.

Complete conversion of the alcohols **1a–c** to the corresponding acetal acetates **3a–c** was confirmed by NMR spectra recorded in deuterated chloroform (Figure 1 and SI, Figures S1–S12). To assign all peaks in the ^{13}C and ^{1}H NMR spectra of the purified acetal acetates **3a** and **3b** 2D NMR experiments were carried out, that is, COSY (correlated spectroscopy), HSQC (heteronuclear single quantum coherence), and HMBC (heteronuclear multiple bond correlation) experiments (find 2D NMR spectra in the Supporting Information, Figures S3–S7 (**3a**) and S10–S12 (**3b**)). Additionally, the chemical shifts of the cholesteryl derivative
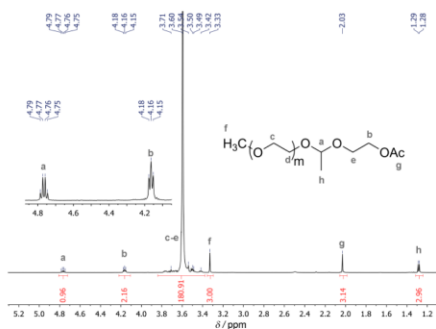
Figure 1. ^{1}H NMR spectrum (400 MHz) of **3c** in CDCl$_3$ at T = 294 K.

3a were compared to those of steroids known in the literature.[52,53] In the ^{1}H NMR spectra the conversion was determined from the ratio of the peaks assigned to the acetal methine protons (**3a**, 4.85 ppm; **3b**, 4.75 ppm; **3c**, 4.77 ppm) and protons of the former alcohol residues. These were the cholesteryl carbon–carbon double bond (H-6, 5.32 ppm), the aromatic protons (7.50–7.20 ppm), and the methoxy group of mPEG (3.33 ppm), respectively. Successful addition of the alcohols across the double bond of AcVE was further indicated by the carbonyl stretch vibrations of the acetates at 1741.2 cm^{-1} (**3a**), 1738.4 cm^{-1} (**3b**), and 1739.0 cm^{-1} (**3c**) in the IR spectra of the acetals (SI, Figures S32–S34). Full conversion of mPEG to 1-(2-acetoxyethoxy)ethoxy mPEG (**3c**) was also confirmed by MALDI-ToF MS. The mass spectrum (Figure 2A) revealed a single distribution of the desired polymeric species cationized either with sodium or potassium. Within the limits of the error the mass peaks satisfied the following equation with $M_{C^+} = M_{Na^+}$ = 23.0 g·mol^{-1} for sodium cationized molecules and $M_{C^+} = M_{K^+}$ = 39.1 g·mol^{-1} for those cationized with potassium.

$$M_{3c}(n) = M_{CH_3O} + M_{CH_3CO} + (2 + n) \cdot M_{EO} + M_{C^+}$$

$$= 74.1 \frac{g}{mol} + (2 + n) \cdot 44.05 \frac{g}{mol} + M_{C^+}$$

The SEC elugram of **3c** (Figure 3) shows a monomodal distribution and a slight increase in both the number-averaged molecular weight (M_n = 1700 g·mol^{-1} to M_n = 1900 g·mol^{-1}) and the polydispersity index (1.06–1.07) in comparison to the batched mPEG (**1c**). Data derived from SEC analysis can be regarded as trend only, because all samples were referenced to a PEG standard. The most important factor for the synthesis of **3c** is the reaction time, since slow transacetalization may take place. Upon longer exposure of the produced acetal to the acidic reaction conditions, the symmetric polymeric acetal, which is shown in Scheme 3, is formed. This side reaction can be followed by SEC as a second mode evolving at twice the molecular weight of the product (find elugrams in the Supporting Information, Figure S53). Therefore, quenching the reaction with triethylamine in time is important to yield quantitative conversion and avoid transacetalization reactions.

A.2. Saponification of Acetal Acetates. The acetal acetates **3a–c** were saponified to yield the scissile initiators **4a–c**, respectively, and the removal of the acetate was confirmed by NMR and IR spectroscopy. For the assignment
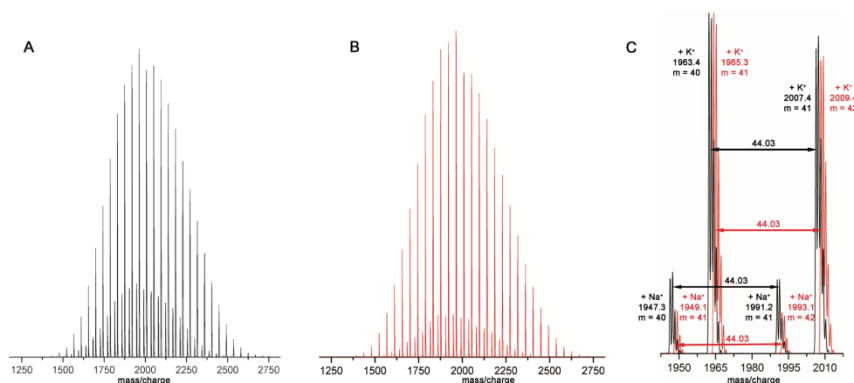
Figure 2. MALDI-ToF mass spectra of derivatized mPEGs. (A) Mass spectrum of **3c**. (B) Mass spectrum of **4c**. (C) Detail of overlay of mass spectra of **3c** (black) and **4c** (red). Masses given for averaged signals, mass differences calculated from monoisotopic peaks. All spectra were recorded in reflectron mode.
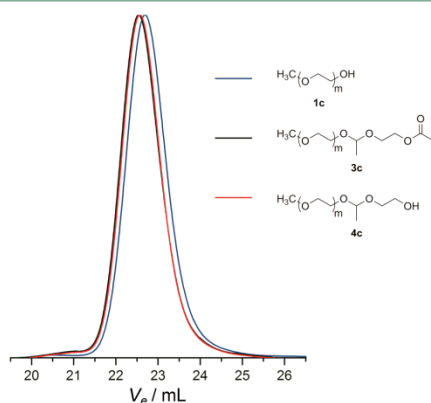
Figure 3. SEC elugrams of **3c** (black), **4c** (red), and the corresponding mPEG precursor (blue).

of all peaks in both ^{1}H and ^{13}C NMR spectra recorded of **4a** and **4b** additional 2D NMR experiments (COSY, HSQC, and HMBC) were carried out (Supporting Information). In the ^{1}H NMR spectra of all cleavable initiators (SI, Figures S13, S20, and S25) the characteristic acetyl peak at around 2.0 ppm of the corresponding precursors had disappeared. Further, the resonance of the methylene protons adjacent to the hydroxyl group exhibited a clear high-field shift compared to the corresponding signals of their analogous acetates. In the ^{13}C NMR spectra (SI, Figures S14 and S21), the carbonyl peaks had vanished completely as well as the bands of the carbonyl

stretches at around 1740 cm^{-1} in the IR spectra (SI, Figures S35−S37). Instead, all IR spectra exhibited broad hydroxyl bands at wavenumbers of about 3400 cm^{-1}.

The mPEG derivative **4c** was further characterized by MALDI-ToF MS and SEC. In the mass spectrum of **4c** (Figure 2B) the observed mass-averaged peaks satisfied the following equation.

$$M_{4c}(n) = M_{CH_3O} + M_H + (2 + n) \cdot M_{EO} + M_{C^+}$$
$$= 32.0 \frac{g}{mol} + (2 + n) \cdot 44.05 \frac{g}{mol} + M_{C^+}$$

The difference of the molecular masses of $M_{4c}(n + 1)$ and its precursor $M_{3c}(n)$ was calculated and found to be just 2 g·mol^{-1} (Figure 2C). Fortunately, the isotopic resolution obtained in the investigated measuring range allowed to clearly distinguish between the two series of polyether masses. The SEC trace of 1-(2-hydroxyethoxy)ethoxy mPEG was monomodal and shifted to a smaller hydrodynamic volume in comparison to the acetate derivative **3c** (Figure 3). Also, the PDI increased slightly to 1.08 upon saponification.

B.1. Use of Cleavable Initiators for EO Polymerization: PEG with Cleavable Cholesterol Initiator. Cholesteryl PEGs were subject to various studies for very different purposes: They are amphiphilic, can be utilized in the synthesis of stealth liposomes,[54−56] and exhibit liquid-crystalline behavior, if the degree of polymerization ($\bar{P}_n$) is low.[57,58] Insertion of a scissile unit between the polymer and the initiating unit will lead to pH-responsive materials, which lose their amphiphilic or mesogenic properties upon acidic treatment. PEGs attached to cholesterol via an acid labile linker are known already (vide supra), but the synthetic pathways presented are laborious or the overall yield limited.[13,14,19] According to our protocol, PEGs with a scissile terminal

Scheme 3. Possible Transacetalization During Synthesis of 3c
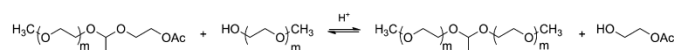
cholesterol unit can be synthesized rapidly in three steps. The resulting α-(1-(cholesteryloxy)ethoxy) ω-hydro PEG (**5**) was characterized by NMR spectroscopy, SEC, and MALDI-ToF MS. The mass spectrum of **5** (SI, Figure S39) displayed the distribution of the desired polydisperse compound cationized with potassium.

Successful initiation of the oxyanionic polymerization of EO with **4a** was also confirmed by the ^{1}H NMR spectrum of **5** (Figure 4) in which, besides the acetal peaks, the H-3 and H-6
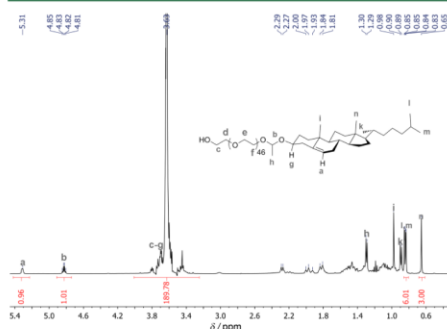
Figure 4. ^{1}H NMR spectrum (400 MHz) of **5** in CDCl$_3$ at T = 294 K. Peak assignment of cholesteryl moiety shown solely for characteristic protons for clarity.

resonances as well as the characteristic pattern of the cholesteryl methyl groups were clearly identified. The degree of polymerization and the number-averaged molecular weight were calculated from the area under the backbone peak (reduced by five protons arising from the initiator) related to the integral of a cholesteryl methyl resonance (H$_3$-18).

$$P_n = \frac{3}{4} \cdot \frac{I_{PEG} - 5}{I_{Me}} = 46$$

$$M_n = P_n \cdot M_{EO} + M_{4a}$$
$$= 46 \cdot 44 \frac{g}{mol} + 475 \frac{g}{mol}$$
$$\approx 2500 \frac{g}{mol}$$

These values are in very good agreement with the theoretically expected ones (P_n = 45, M_n = 2450 g·mol^{-1}), whereas the M_n derived from SEC analysis (see SEC elugram in the SI, Figure S44) was smaller (1690 g·mol^{-1}). The underestimation of M_n found by SEC results from the rather large apolar initiating moiety, which leads to a contraction of the polyether coil to reduce initiator/solvent interactions. Nevertheless, the SEC elugram corresponded to a well-defined polymer with a polydispersity index of 1.08. Because cholesteryl PEGs are known to be amphiphilic and form micelles in aqueous solutions, the critical micelle concentration of **5** was determined by measuring the surface tension of aqueous solutions of the scissile cholesteryl PEG with a ring tensiometer. Compound **5** has a CMC of 4.20 ± 0.39 mg·L^{-1}, which is in the order of CMCs expected for amphiphilic polyethers of similar molecular weights.[54,59]

The degradability of **5** was demonstrated by acidic hydrolysis of the acetal, followed by turbidimetry at pH 1. In Figure 5A, the relative transmission is plotted against the reaction time for two different temperatures (T = 25 and 37 °C). After an initial period, the solutions started to turn turbid, as the released cholesterol precipitated and the transmission began to decrease. Finally, so much cholesterol had precipitated that almost all light was scattered. As expected, cholesterol was released faster at higher reaction temperature as indicated by the shorter initial phase and the more negative slope of the trace.

Complete removal of the steroid was confirmed by ^{1}H NMR spectra recorded of both the precipitate as well as the residue of the aqueous phase of a similar experiment (Photographs of this experiment are shown in Figure 2B−D, find protocol in the SI).The former shows a clean cholesterol spectrum, despite of some water (SI, Figure S29), whereas the latter just exhibits pure PEG diol (SI, Figure S30).

B.2. Scissile Heterofunctional PEGs. Poly(ethylene glycol)s with cleavable terminal functionalities can be used to covalently bind PEG to different substrates such as other synthetic polymers, proteins, or low molecular weight drug molecules and subsequently release the substrate upon a suitable trigger. As mentioned before, such materials have been described in the past, but most of these approaches are based on the extensive modification of monofunctional mPEGs and do not allow any further modification of the polyether, such as the addition of a labeling or targeting moiety.

Three cleavable heterofunctional polymers 6_{P_n} were synthesized with varying degrees of polymerization and characterized by standard methods. The proton NMR spectrum (Figure 6) was referenced to the methyl group of the acetal and exhibits full incorporation of the initiator. The degree of polymerization and the number-averaged molecular weights were calculated from the integral values using the following equation, where I_{PEG} is the integral of the backbone peak.

$$P_n = \frac{3}{4} \cdot \frac{I_{PEG} - 10}{I_{Me}}$$

$$M_n = P_n \cdot M_{EO} + M_{4b} = P_n \cdot 44 \frac{g}{mol} + 329 \frac{g}{mol}$$

All molecular weights found were in good agreement with the calculated theoretical values as well as those determined by SEC (elugrams shown in Figure 7) and are summarized in Table 1. The SEC elugrams of all samples (Figure 7) revealed monomodal traces of well-defined polymers with PDIs lower than 1.08. Full incorporation of the initiator was further confirmed by the MALDI-ToF MS (Figure 8). All mass-averaged peaks satisfied the following equation.

$$M_6(n) = M_{4b} + n \cdot M_{EO} + M_{K^+}$$
$$= 329.4 \frac{g}{mol} + n \cdot 44.05 \frac{g}{mol} + 39.1 \frac{g}{mol}$$

In conclusion, we successfully applied **4b** as an initiator for the oxyanionic polymerization of ethylene oxide and confirmed its full incorporation into well-defined poly(ethylene glycol)s with adjustable molecular weights.

To obtain heterofunctional polyethers, all samples of **6** were hydrolyzed to the corresponding α-amino -ω-hydro PEGs 7_{50}, 7_{75}, and 7_{140}. Complete removal of the benzyl groups was verified by the absence of aromatic signals in the ^{1}H NMR spectrum (exemplary spectrum of 7_{50} shown in the Supporting
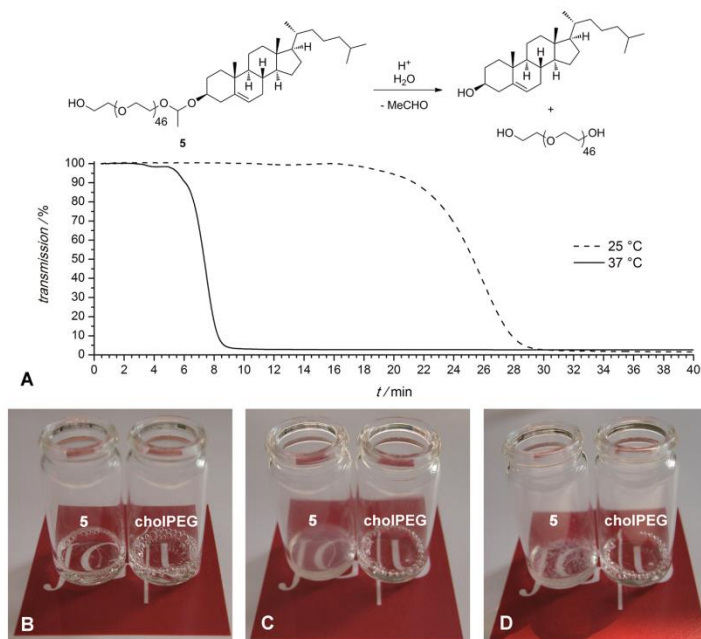
Figure 5. Acidic cleavage of scissile cholesteryl PEG **5**. (A) Cleavage followed by turbidimetry (λ = 528 nm) at pH 1 for two different temperatures (25 and 37 °C). (B−D) Photographs of **5**'s cleavage in comparison to regular cholesteryl PEG (cholPEG). (B) Aqueous polymer solutions. (C) Onset of cholesterol precipitation after addition of hydrochloric acid. (D) Precipitated cholesterol in case of scissile cholesteryl PEG **5**.
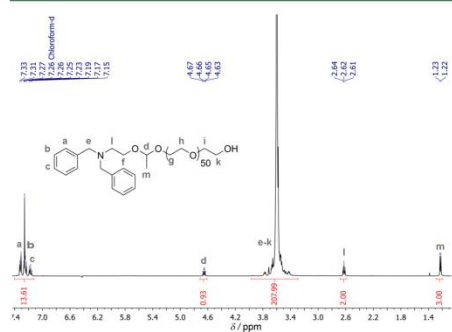
Figure 6. ^{1}H NMR spectrum (400 MHz) of 6_{50} recorded in CDCl$_3$.

Figure 7. SEC elugrams of **6** with various degrees of polymerization; RI detector signal.

Information, Figure S26). The residual initiator proton signals (quadruplet of methine at 4.68 ppm, triplet of methylene adjacent to the amino group at 2.65 ppm, and doublet of methyl group at 1.20 ppm) were still observed. The degrees of polymerization, determined by the following equation, were in good agreement with those of the corresponding precursors (Table 1). Hence, no cleavage of the acetal occurred during the hydrogenation step.

$$P_n = \frac{3}{4} \cdot \frac{I_{PEG} - 6}{I_{Me}}$$

The MALDI-ToF mass spectra of **7** (SI, Figures S40−S42) supported this result, as each of them revealed the distribution of mass peaks of the desired species.

As mentioned in a previous study, PEGs carrying a terminal amino group exhibit an apparent broadening of the molecular

Table 1. Characteristic Data of Scissile Heterofunctional PEGs 6, 7, and 10

polymer	$M_n{}^a$ (g·mol^{-1})	$M_n{}^b$ (g·mol^{-1})	$M_n{}^c$ (g·mol^{-1})	$M_w{}^c$ (g·mol^{-1})	$P_n{}^b$	PDI^c
6_{50}	2320	2510	2140	2320	50	1.08
6_{75}	3330	3630	3040	3260	75	1.07
6_{140}	5730	6490	5590	5900	140	1.06
7_{50}	2330	2400	d	d	51	d
7_{75}	3450	3470	d	d	75	d
7_{140}	6310	6500	d	d	144	d
10	3570	3610	3160	3360	76	1.06

^{a}Calculated. ^{b}Determined by ^{1}H NMR. ^{c}Determined by SEC, referenced to PEG standards. ^{d}Not determined, due to apparent broadening of molecular weight distribution in SEC analysis.
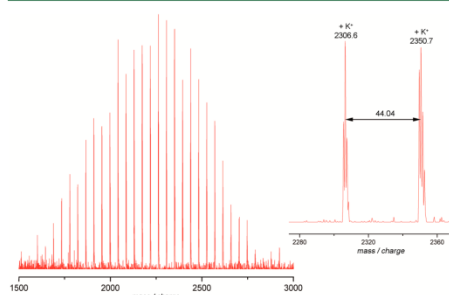
Figure 8. MALDI-ToF mass spectrum of 6_{50} and detail. Masses given for averaged signals, mass difference calculated from monoisotopic peaks. Spectrum was recorded in reflectron mode.

Figure 9. SEC elugrams of 6_{75} (red, RI detector), 7_{75} (dotted black, RI detector) and 10 (blue, UV detector). Note that amino PEGs often revealed a broadening of the mass distribution in the SEC analysis (on our system) leading to a apparent increase of the PDI.

weight distributions in SEC analysis with our system.[51] This effect was also observed for all samples of 7 (exemplary SEC elugram of 7_{50} shown in SI, Figure S45), which is why no reasonable molecular weight average and thus no PDI could be determined by SEC. However, upon derivatization of the amino group SEC revealed well-defined PEG with narrow molecular weight distribution (vide infra).

To confirm the accessibility of 7's cleavable terminal amino group for further derivatization reactions and activate the polyether for the bioconjugation with proteins, the recently established conversion of α-amino ω-hydroxyl PEGs into the corresponding squaric acid ester amides[51] was carried out. Compound 7_{75} was reacted with diethyl squarate to yield 10 (Scheme 4).

In Figure 9 the superimposed SEC traces of 10 and its precursors 6_{75} and 7_{75} are shown. The SEC elugrams of 10 and 6_{75} exhibited monomodal traces of well-defined polymers with corresponding molecular weight distributions. The PDI of 10 (1.06) was slightly lower than the PDI found for 6_{75} (1.07) which was attributed to a loss of a small low-molecular weight fraction of the polymer upon repetitive precipitation of 10 in

cold diethyl ether during the workup. Full conversion of the amino terminus to the squaric acid ester amide and complete retention of the acetal was verified by MALDI-ToF MS. The mass spectrum (SI, Figure S43) shows the expected distribution of potassium cationized polymer peaks. In the ^{1}H NMR spectrum of 10 (SI, Figure S28), the methyl protons showed an isolated signal around 1.28 ppm, whereas the corresponding methylene signal was superimposed by the acetal methine resonance at 4.76 ppm. The P_n determined from the NMR spectrum is in very good agreement with the values calculated for the amino PEG precursor. However, a small amount (<5 mol %) of acetaldehyde was detected in the proton NMR spectrum. Since the ethyl ester's methyl group integrated to the expected value, the MALDI-ToF MS detected a single distribution, and TLC of 10 showed a single UV-active compound, the detected partial acetal cleavage had occurred in the NMR tube.

A closer look was taken on the acidic cleavage of the acetals by following the hydrolysis of the α-(1-(2-dibenzylamino ethoxy)ethoxy) ω-hydro PEG 6_{75} at 37 °C in acidic D$_2$O solutions with various pD values (pD 2.4, 4.4, 4.9, and 5.4) with ^{1}H NMR spectroscopy. All integrals were referenced to the aromatic resonances of the benzyl groups and the integral of the acetal methyl signal was monitored to determine the residual acetal. The acidic acetal cleavage was also investigated for 10 at pD 4.9 in an experiment analogous to those described before. In Figure 10, the normalized integral values of the residual acetals of 6_{75} and 10 are plotted against time (find corresponding NMR spectra in the SI, Figures S48−S52). Because the solvent served as a reagent in the degradation and the samples were diluted (c_6 = 5.74 mM, c_{10} = 2.38 mM), it was assumed that acetal hydrolysis followed pseudo-first-order kinetics and, therefore, the experimental data was fitted with an exponential decay function:

Scheme 4. Synthetic Route to Scissile Squaric Acid Ester Amido PEGs
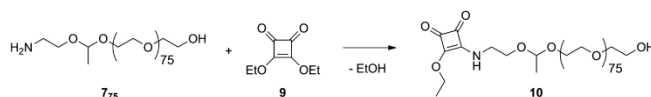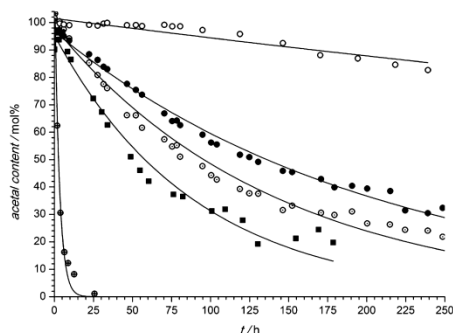
Figure 10. Acidic cleavage of scissile PEGs 6_{75} (circles) and 10 (squares) in deuterium oxide followed by ^{1}H NMR spectroscopy at various pD values at $T = 37$ °C: crossed circles, pD 2.4; dotted circles, pD 4.4; full circles/squares, pD 4.9; open circles, pD 5.4; solid lines, exponential fits.

$$I_{6_{75}}(\text{pD}, t) = e^{-k_{D_2O}t} \cdot I_{6_{75}}(\text{pD}, t = 0)$$

The cleavage rate constants in deuterium oxide k_{D_2O} and corresponding half-lives $t_{1/2}$ of all hydrolyses were calculated from the exponential fits and are listed in Table 2. Similar to the

Table 2. Acetal Cleavage Rate Constants and Half-Lives of Scissile PEGs in Acidic Deuterium Oxide

polymer	pD	k_{D_2O} (s^{-1})	$t_{1/2}$ (h)
6_{75}	2.4	1180 ± 100	2.12 ± 0.18
6_{75}	4.4	25.4 ± 0.7	98.2 ± 2.9
6_{75}	4.9	17.4 ± 0.3	143.1 ± 2.9
6_{75}	5.4	2.60 ± 0.23	961.4 ± 86.2
10	4.9	40.2 ± 1.9	62.1 ± 3.0

acidic degradation of recently presented poly(glycidyloxyethyl ethylene glycol ether) (PGEGE) copolymers,[44] a strong pH-dependence of the degradation kinetics was observed. At pD 2.4, half the amount of 6_{75} had been hydrolyzed after 2 h, whereas at pD 5.4 the polymer exhibited a half-life of over a month ($t_{1/2} = 40 ± 4$ d). Most interestingly, 10 degrades much faster than 6_{75} under the same conditions. The basic tertiary amino group adjacent to the acetal of 6_{75} is protonated and carries a positive charge in acidic media. Hence, the pre-equilibrium protonation of one of the acetal oxygens (due to the Coulomb forces most probably the one at the PEG side), which occurs prior to the cleavage of the acetal carbon−oxygen bond,[60] is hindered, and therefore, the hydrolysis rate of 6_{75} is comparably low. The corresponding nitrogen of 10 will not be protonated, because its electron lone pair is delocalized in the squaric acid amide bond, resulting in a faster acetal cleavage. Nevertheless, squaric acid amides are known to be protophilic[61] and 10 will be protonated at its squaric acid moiety to some extent. This explains why under comparable conditions the half-life of 10 is longer than that of $Bn_2NTrisP(G\text{-}co\text{-}GEGE)$, whose focal amino group is spatially separated from most of its acetaldehyde acetals.[44] Unfortunately, these values cannot be transferred directly to protic systems, as it has to be taken into account that the kinetic deuterium isotope effect for the

hydrolysis of (simple) noncyclic acetals in water is around $k_{D^+}/k_{H^+} = 2.6-2.7$.[60]

B.3. PEG with Scissile Backbone. Well-defined functional PEGs with a cleavable group in the backbone can be synthesized rapidly with our methodology using an AROP macroinitiator such as 1-(2-hydroxyethoxy)ethoxy mPEG ($4c$). The amount of EO batched in the polymerization was calculated to add a PEG block with a number-averaged molecular weight of 6.0 kg·mol^{-1}, allowing separation and distinction of this block from the macroinitiator precursor (2.0 kg·mol^{-1}) via SEC upon acidic cleavage of the acetal. For the interpretation of the ^{1}H NMR spectrum of the scissile mPEG 8 (SI, Figure S27) the peak integrals were again referenced to the signal of the methoxy group. Except for the larger backbone signal the spectrum was almost identical to that of the precursor. In agreement with the expected theoretical value the M_n was calculated from the ^{1}H NMR spectrum to be 7.9 kg·mol^{-1} using the following equation:

$$M_n = P_n \cdot M_{EO} + M_{CH_3OH} = \frac{3}{4} \cdot \frac{I_{PEG}}{I_{CH_3}} \cdot 44 \frac{\text{g}}{\text{mol}} + 32 \frac{\text{g}}{\text{mol}}$$

This value also corresponds well to the M_n determined from the SEC trace (7.5 kg·mol^{-1}, elugram shown in Figure 11).
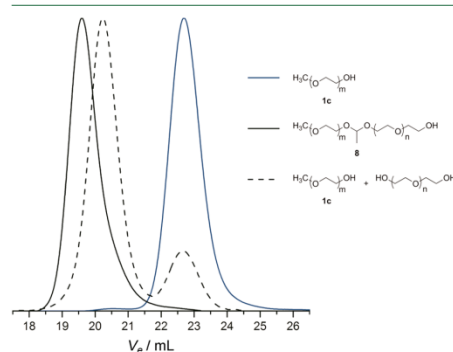
Figure 11. SEC elugrams of mPEG $1c$ (blue) and scissile mPEG 8 (black) before and after acetal cleavage; RI detector channel.

Note, that the trace was referenced to a PEG standard. Compared to the macroinitiator, the molecular weight distribution became broader and the polydispersity index increased to 1.09, still indicating a well-defined polyether. The cleavability of the in-chain acetal in acidic media was demonstrated by stirring the scissile mPEG 8 in aqueous 0.11 M p-toluene sulfonic acid for 3 h at room temperature. In Figure 11, the normalized SEC elugrams of 8 before and after degradation as well as its mPEG precursor $1c$ are shown. Note that the degraded sample exhibits a bimodal trace and the mode corresponding to a smaller hydrodynamic radius fits well to that of $1c$. The second mode is significantly shifted to a lower molecular weight in comparison to the SEC trace of 8 and was clearly assigned to the PEG block polymerized onto $4c$. Both modes of the degraded sample corresponded to narrowly distributed PEGs with number-averaged molecular weights of about 1.8 and 5.7 kg·mol^{-1}, respectively, which is in very good agreement with the expected values. Hence, we successfully

demonstrated the incorporation of a single acetal into the backbone of well-defined poly(ethylene glycol) monomethyl ether with full control over its position in the chain and the final cleavability of that moiety under acidic conditions.

C. Exploratory Results on Bioconjugation to BSA. A total of 13 equiv of **10** were coupled to BSA using a protocol for the squaric acid mediated PEGylation recently published by our group.[51] Successful covalent attachment of the acetal-containing squaric acid amido PEGs was evidenced by SDS-PAGE. In Figure 12 the Coomassie Blue-stained gel obtained
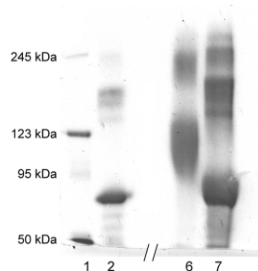
Figure 12. SDS-PAGE of PEGylated BSA: lane 1, MW marker; lane 2, BSA; lane 6, BSA PEGylated with **10**; lane 7, PEGylated BSA after acidic treatment.

from the electrophoresis is shown. Compared to BSA (lane 2), the BSA-PEG conjugate (lane 6) exhibits a clear shift toward higher molecular masses. Lane 2 further reveals the presence of a fraction of dimerized BSA, which also was PEGylated completely (high-molecular weight band in lane 6). The polydispersity of both the molecular weight of the synthetic polyether and the number of polymer chains attached to the protein result in the clear broadening of the protein−polymer conjugate band.

To demonstrate the cleavability of the acetals and the resulting release of BSA, the synthesized BSA-PEG conjugate was hydrolyzed in 1 N hydrochloric acid. SDS-PAGE of the product (Figure 12, lane 7) exhibits complete release of the protein, which migrated the same distance through the gel as the unmodified BSA. This is also true for the dimer. The slight broadening of the bands was attributed to the polydisperse number of squaramide linkers still attached to the protein. In conclusion, we successfully demonstrated that the incorporation of an acetal moiety into squaric acid amido PEGs does not decrease their applicability as PEGylation agents, but gives access to acid-sensitive protein−PEG conjugates. The detachment of the polyether from the conjugate under physiologically more relevant conditions is under current investigation.

CONCLUSION

We have developed the implementation of an acetaldehyde acetal into initiators for the anionic ring-opening polymerization of oxiranes, following a straightforward two-step protocol. Its general applicability to a variety of acid-stabile AROP initiators has been demonstrated by the conversion of a diverse set of chemically different alcohols: cholesterol, dibenzylamino ethanol, and poly(ethylene glycol) monomethyl ether. Upon polymerization of EO onto the obtained low

molecular weight initiators, polyethers with cleavable initiator moieties, but completely different properties were generated.

PEG carrying the cleavable cholesterol unit is an amphiphile with a CMC of 4.20 mg·L^{-1}, whereas the cleavable heterofunctional PEGs obtained from dibenzylamino ethanol could be subsequently derivatized and activated for the recently described squaric acid mediated PEGylation. The latter was proven in a first exploratory model reaction to BSA. In the case of the scissile macroinitiator, PEG carrying a single acetal moiety in the backbone of the polymer was synthesized. All PEGs were characterized by NMR spectroscopy, MALDI ToF mass spectrometry, and size-exclusion chromatography (SEC). The incorporation of a single acetal unit at the desired position was verified for each of the well-defined polyethers (PDIs ≤ 1.09). All of the obtained polymers and the PEGylated BSA were proven to be cleaved at the acetal moieties in acidic media.

In conclusion, we established a rapid methodology to incorporate a single acid labile moiety at a desired position in well-defined functional poly(ethylene glycol)s. These materials are highly interesting for the development of new pharmaceuticals as well as for materials science. Possible applications of the acid sensitive cholesteryl PEGs, for example, for the reversible stabilization of liposomes or acid sensors are subjects to ongoing studies. Also, the PEGylation of other proteins than BSA with the scissile polyethers, the pharmaceutical properties of the conjugates, especially the in vivo bioactivities, as well as their toxicities are under current investigation.

■ ASSOCIATED CONTENT

ⓢ Supporting Information
Further synthetic protocols, NMR spectra, IR spectra, SEC elugrams, and MALDI-ToF mass spectra, as well as procedures and spectra of reaction kinetics, followed by NMR spectroscopy. This material is available free of charge via the Internet at http://pubs.acs.org.

■ AUTHOR INFORMATION

Corresponding Author
*E-mail: hfrey@uni-mainz.de.
Notes
The authors declare no competing financial interest.

■ ACKNOWLEDGMENTS

■ REFERENCES

(1) Abuchowski, A.; van Es, T.; Palczuk, N. C.; Davis, F. F. *J. Biol. Chem.* **1977**, *252*, 3578−3581.
(2) Abuchowski, A.; McCoy, J. R.; Palczuk, N. C.; van Es, T.; Davis, F. F. *J. Biol. Chem.* **1977**, *252*, 3582−3586.
(3) Caliceti, P.; Veronese, F. M. *Adv. Drug Delivery Rev.* **2003**, *55*, 1261−1277.
(4) Harris, J. M.; Chess, R. B. *Nat. Rev. Drug Discovery* **2003**, *2*, 214−221.
(5) Veronese, F. M.; Pasut, G. *Drug Discovery Today* **2005**, *10*, 1451−1458.

Biomacromolecules

(6) Pasut, G.; Sergi, M.; Veronese, F. M. *Adv. Drug Delivery Rev.* **2008**, *60*, 69−78.

(7) Alconcel, S. N. S.; Baas, A. S.; Maynard, H. D. *Polym. Chem.* **2011**, *2*, 1442−1448.

(8) Zalipsky, S. *Adv. Drug Delivery Rev.* **1995**, *16*, 157−182.

(9) Roberts, M. J.; Milton Harris, J. *J. Pharm. Sci.* **1998**, *87*, 1440−1445.

(10) Filpula, D.; Zhao, H. *Adv. Drug Delivery Rev.* **2008**, *60*, 29−49.

(11) Knorr, V.; Allmendinger, L.; Walker, G. F.; Paintner, F. F.; Wagner, E. *Bioconjugate Chem.* **2007**, *18*, 1218−1225.

(12) Boomer, J. A.; Thompson, D. H. *Chem. Phys. Lipids* **1999**, *99*, 145−153.

(13) Guo, X.; Szoka, F. C. *Bioconjugate Chem.* **2001**, *12*, 291−300.

(14) Masson, C.; Garinot, M.; Mignet, N.; Wetzer, B.; Mailhe, P.; Scherman, D.; Bessodes, M. *J. Controlled Release* **2004**, *99*, 423−434.

(15) Hatakeyama, H.; Akita, H.; Kogure, K.; Oishi, M.; Nagasaki, Y.; Kihira, Y.; Ueno, M.; Kobayashi, H.; Kikuchi, H.; Harashima, H. *Gene Ther.* **2006**, *14*, 68−77.

(16) Sawant, R. M.; Hurley, J. P.; Salmaso, S.; Kale, A.; Tolcheva, E.; Levchenko, T. S.; Torchilin, V. P. *Bioconjugate Chem.* **2006**, *17*, 943−949.

(17) Xu, H.; Deng, Y.; Chen, D.; Hong, W.; Lu, Y.; Dong, X. *J. Controlled Release* **2008**, *130*, 238−245.

(18) Wong, J. B.; Grosse, S.; Tabor, A. B.; Hart, S. L.; Hailes, H. C. *Mol. BioSyst.* **2008**, *4*, 532−541.

(19) Boomer, J. A.; Qualls, M. M.; Inerowicz, H. D.; Haynes, R. H.; Patri, V. S.; Kim, J.-M.; Thompson, D. H. *Bioconjugate Chem.* **2008**, *20*, 47−59.

(20) Kuai, R.; Yuan, W.; Qin, Y.; Chen, H.; Tang, J.; Yuan, M.; Zhang, Z.; He, Q. *Mol. Pharmaceutics* **2010**, *7*, 1816−1826.

(21) Chen, D.; Jiang, X.; Huang, Y.; Zhang, C.; Ping, Q. *J. Bioact. Compat. Polym.* **2010**, *25*, 527−542.

(22) Pasut, G.; Veronese, F. M. *Prog. Polym. Sci.* **2007**, *32*, 933−961.

(23) Yamaoka, T.; Tabata, Y.; Ikada, Y. *J. Pharm. Sci.* **1994**, *83*, 601−606.

(24) Ringsdorf, H. *J. Polym. Sci., Polym. Symp.* **1975**, *51*, 135−153.

(25) Matsumura, Y.; Maeda, H. *Cancer Res.* **1986**, *46*, 6387−6392.

(26) Seymour, L. W. *Crit. Rev. Ther. Drug Carrier Syst.* **1992**, *9*, 135−342.

(27) DuBois Clochard, M.-C.; Rankin, S.; Brocchini, S. *Macromol. Rapid Commun.* **2000**, *21*, 853−859.

(28) Tomlinson, R.; Heller, J.; Brocchini, S.; Duncan, R. *Bioconjugate Chem.* **2003**, *14*, 1096−1106.

(29) Tomlinson, R.; Klee, M.; Garrett, S.; Heller, J.; Duncan, R.; Brocchini, S. *Macromolecules* **2002**, *35*, 473−480.

(30) Rickerby, J.; Prabhakar, R.; Ali, M.; Knowles, J.; Brocchini, S. *J. Mater. Chem.* **2005**, *15*, 1849−1856.

(31) Wang, Y.; Morinaga, H.; Sudo, A.; Endo, T. *J. Polym. Sci., Part A: Polym. Chem.* **2011**, *49*, 596−602.

(32) Braunová, A.; Pechar, M.; Laga, R.; Ulbrich, K. *Macromol. Chem. Phys.* **2007**, *208*, 2642−2653.

(33) Reid, B.; Tzeng, S.; Warren, A.; Kozielski, K.; Elisseeff, J. *Macromolecules* **2010**, *43*, 9588−9590.

(34) Lundberg, P.; Lee, B. F.; van den Berg, S. A.; Pressly, E. D.; Lee, A.; Hawker, C. J.; Lynd, N. A. *ACS Macro Lett.* **2012**, *1*, 1240−1243.

(35) Greene, T. W.; Wuts, P. G. M. *Protective Groups in Organic Synthesis*, 3rd ed.; Wiley: New York, 1999.

(36) Wagener, K. B.; Wanigatunga, S. *Macromolecules* **1987**, *20*, 1717−1720.

(37) Akiyama, Y.; Otsuka, H.; Nagasaki, Y.; Kato, M.; Kataoka, K. *Bioconjugate Chem.* **2000**, *11*, 947−950.

(38) Akiyama, Y.; Nagasaki, Y.; Kataoka, K. *Bioconjugate Chem.* **2004**, *15*, 424−427.

(39) Feng, X.; Taton, D.; Chaikof, E. L.; Gnanou, Y. *Biomacromolecules* **2007**, *8*, 2374−2378.

(40) Fan, X.; Huang, B.; Wang, G.; Huang, J. *Macromolecules* **2012**, *45*, 3779−3786.

(41) Taton, D.; Le Borgne, A.; Sepulchre, M.; Spassky, N. *Macromol. Chem. Phys.* **1994**, *195*, 139−148.

(42) Wurm, F.; Nieberle, J.; Frey, H. *Macromolecules* **2008**, *41*, 1909−1911.

(43) Feng, X.; Chaikof, E. L.; Absalon, C.; Drummond, C.; Taton, D.; Gnanou, Y. *Macromol. Rapid Commun.* **2011**, *32*, 1722−1728.

(44) Tonhauser, C.; Schüll, C.; Dingels, C.; Frey, H. *ACS Macro Lett.* **2012**, *1*, 1094−1097.

(45) Shenoi, R. A.; Narayanannair, J. K.; Hamilton, J. L.; Lai, B. F. L.; Horte, S.; Kainthan, R. K.; Varghese, J. P.; Rajeev, K. G.; Manoharan, M.; Kizhakkedathu, J. N. *J. Am. Chem. Soc.* **2012**, *134*, 14945−14957.

(46) Shenoi, R. A.; Lai, B. F. L.; Kizhakkedathu, J. N. *Biomacromolecules* **2012**, *13*, 3018−3030.

(47) Satoh, K.; Poelma, J. E.; Campos, L. M.; Stahl, B.; Hawker, C. J. *Polym. Chem.* **2012**, *3*, 1890−1898.

(48) Greenland, B. W.; Liu, S.; Cavalli, G.; Alpay, E.; Steinke, J. H. G. *Polymer* **2010**, *51*, 2984−2992.

(49) Dix, D.; Imming, P. *Arch. Pharm.* **1995**, *328*, 203−205.

(50) Wurm, F.; Hofmann, A. M.; Thomas, A.; Dingels, C.; Frey, H. *Macromol. Chem. Phys.* **2010**, *211*, 932−939.

(51) Dingels, C.; Wurm, F.; Wagner, M.; Klok, H.-A.; Frey, H. *Chem.—Eur. J.* **2012**, *18*, 16828.

(52) Blunt, J. W.; Stothers, J. B. *Org. Magn. Reson.* **1977**, *9*, 439−464.

(53) Muhr, P.; Likussar, W.; Schubert-Zsilavecz, M. *Magn. Reson. Chem.* **1996**, *34*, 137−142.

(54) Ishiwata, H.; Vertut-Doi, A.; Hirose, T.; Miyajima, K. *Chem. Pharm. Bull.* **1995**, *43*, 1005−1011.

(55) Vertut-Doi, A.; Ishiwata, H.; Miyajima, K. *Biochim. Biophys. Acta, Biomembr.* **1996**, *1278*, 19−28.

(56) Hofmann, A. M.; Wurm, F.; Hühn, E.; Nawroth, T.; Langguth, P.; Frey, H. *Biomacromolecules* **2010**, *11*, 568−574.

(57) López-Quintela, M. A.; Akahane, A.; Rodríguez, C.; Kunieda, H. *J. Colloid Interface Sci.* **2002**, *247*, 186−192.

(58) Xu, J.-T.; Xue, L.; Fan, Z.-Q.; Wu, Z.-H.; Kim, J. K. *Macromolecules* **2006**, *39*, 2981−2988.

(59) Hofmann, A. M.; Wurm, F.; Frey, H. *Macromolecules* **2011**, *44*, 4648−4657.

(60) Cordes, E. H. *Prog. Phys. Org. Chem.* **1967**, *4*, 1−44.

(61) Quinonero, D.; Frontera, A.; Ballester, P.; Deyá, P. M. *Tetrahedron Lett.* **2000**, *41*, 2001−2005.

A.3 Block Copolymers in Giant Unilamellar Vesicles with Proteins or with Phospholipids

Regina Schöps,[a] *Elkin Amado,*[a] *Sophie S. Müller,*[b] *Holger Frey,*[b] *and Jörg Kressler*[*,a]

[a]Department of Chemistry, Martin Luther University Halle-Wittenberg, D-06099 Halle (Saale), Germany.

[b]Institute for Organic Chemistry, Johannes Gutenberg University Mainz, Duesbergweg 10–14, D-55099 Mainz, Germany

Faraday Discussions

RSCPublishing

PAPER

Block copolymers in giant unilamellar vesicles with proteins or with phospholipids

Regina Schöps,[a] Elkin Amado,[a] Sophie S. Müller,[b] Holger Frey[b] and Jörg Kressler[*a]

Biocompatible, highly water-soluble, nonionic, amphiphilic block copolymers having different hydrophobic blocks and architectures, but similar molecular size and chemical nature of the hydrophilic blocks, were investigated to check for their ability to form hybrid giant unilamellar vesicles with proteins, and for their interactions with giant unilamellar phospholipid vesicles (GUV). PGM_{14}-b-PPO_{34}-b-PGM_{14} (PGM-PPO-PGM) consists of a poly(propylene oxide) middle block and outer poly(glycerol monomethacrylate) blocks. Ch-PEG_{32}-b-lPG_{18} (Ch-PEG-lPG) and Ch-PEG_{30}-b-$hbPG_{17}$ (Ch-PEG-hbPG) have a linear poly(ethylene glycol) block, linked to a cholesterol end group and to a linear (lPG) or hyperbranched (hbPG) polyglycerol block. Fluorescently-labelled polymers were synthesised to image and analyse the self-assembling and interaction processes using confocal laser scanning microscopy (CLSM). By implementing a novel strategy for polymersomes formation the copolymers were found to spontaneously form giant unilamellar vesicles with proteins in aqueous solution. Furthermore, the investigation of the interaction of the block copolymers with different phospholipid GUVs provided detailed information about the structure–behaviour relationship. Additionally, it was found that these neutral copolymers are able to cross artificial and natural phospholipid membranes.

Introduction

Biocompatible block copolymers composed of hydrophilic and hydrophobic blocks (amphiphilic) have attracted increasing interest in recent years due to their potential for biomedical applications such as tissue engineering, nanomedicine, and drug and gene delivery. Polymer interactions with phospholipids allow for the modification of liposomes, a popular drug and gene transport system, to achieve higher stability, permeability or *in vivo* circulation times.[1–3] Recently, the self-assembly of amphiphilic block copolymers is another focus of increasing

[a]Department of Chemistry, Martin Luther University Halle-Wittenberg, D-06099 Halle (Saale), Germany. E-mail: joerg.kressler@chemie.uni-halle.de

[b]Institute for Organic Chemistry, Johannes Gutenberg University Mainz, Duesbergweg 10–14, D-55099 Mainz, Germany

research activity.[4–7] In particular polymersomes, self-assembled spherical vesicles based on amphiphilic copolymers, which possess higher mechanical stability and better tunability of membrane properties[8] than liposomes and offer the possibility of surface functionalisation,[9] are promising systems for drug targeting and delivery,[10] for use as nanoreactors[11] or as synthetic membrane models in cell mimicking.[12–14] Despite the advances in this field, the preparation methods used for polymersomes are mainly those used for liposomes.[10,15] Thus, the range of suitable copolymers is limited to water-insoluble or slightly soluble copolymer families.[16–19]

Recently, we published a novel water-based method for the formation of giant unilamellar vesicles from a water-soluble nonionic triblock copolymer, consisting of two hydrophilic poly(glycerol monomethacrylate) outer blocks and a poly(propylene oxide) middle block, on a protein layer.[20] Here we apply this method to other biocompatible, nonionic, water-soluble block copolymers, differing in composition and architecture. They possess a cholesterol moiety as the hydrophobic unit and linear or hyperbranched poly(hydroxyl) polyether blocks as the hydrophilic units. It is found that the spontaneous formation of hybrid giant unilamellar vesicles through this method is a more general phenomenon than was previously established. The experimental results also support our previous hypotheses concerning the driving forces and mechanism.

Confocal laser scanning microscopy (CLSM) was used to explore the vesicle formation of fluorescently-labelled copolymers. It is an appropriate tool to image the morphology of giant vesicles and to study physicochemical events on such membranes.[21,22] Additional CLSM allowed an analysis of the interaction of the polymers under investigation with artificial GUVs and with natural membranes of living cells. Previous detailed studies of the molecular interactions between these block copolymers and phospholipids in Langmuir monolayers suggested their strong affinity.[23–26] In interactions with GUV phospholipid bilayers we observed clear differences assumed to arise from the different copolymer conformations in water. Moreover, it was found that the studied copolymers are able to cross artificial and natural phospholipid membranes.

Experimental section

Materials

The phospholipids 1,2-dipalmitoyl-*sn-glycero*-3-phosphocholine (DPPC), 1,2-dilauroyl-*sn-glycero*-3-phosphocholine (DLPC), 1,2-dioleoyl-*sn-glycero*-3-phosphocholine (DOPC), 1-palmitoyl-2-oleoyl-*sn-glycero*-3-phosphocholine (POPC) and 1-palmitoyl-2-oleoyl-*sn-glycero*-3-phosphoglycerol (POPG) were purchased from Genzyme Pharmaceuticals (Liestal, Switzerland) with a purity >99% and were used as received. DSPE-PEG-Biotin was delivered from Avanti Polar Lipids (Alabama, USA). Choline, streptavidin from *Streptomyces avidinii*, bovine serum albumin (BSA) and biotinylated BSA were purchased from Sigma Aldrich Chemie GmbH (Taufkirchen, Germany). The lipophilic carbocyanine dyes DiO and DiD and streptavidin Cy5 were purchased from Life Technologies, Invitrogen GmbH (Darmstadt, Germany). The fluorescent, rhodamine-labelled copolymers where synthesized by ourselves as described before.[20,27–29]

Formation of the giant unilamellar polymer protein vesicles

Chambers of nearly 230 μL volume, formed by fixing a silicon ring (10 mm diameter, 3 mm high) onto a cover glass were used for microscopic studies with an inverse microscope. The glass surface was passivated with BSA–biotinylated BSA in a molar ratio of 10 : 1 and subsequently coated by streptavidin. In a typical procedure[30] cover glasses were incubated for 10 min at room temperature with 100 μL of each protein solution (1: BSA 1 g L^{-1}; 2: streptavidin 0.025 g L^{-1}, with or without the fluorescent label) and gently rinsed between and after incubation (5 times with 200 μL of pure water). The chamber with a protein-coated glass surface was filled with pure water and an appropriate volume of a 1 mM aqueous solution of the fluorescently-labelled polymer was added to reach a 100 μM final polymer concentration. For microscopy the chamber was closed by a second cover glass. The experiments were carried out at room temperature.

Preparation of the giant unilamellar vesicles (GUVs)

GUVs were prepared from a thin dried film of 10 nmol phospholipid in 570 μL deionized water at 60 °C using 10 Hz frequency of an alternating electrical field (3V) in a modified variant of electroformation,[31] using a chamber built up of two ITO coated glass slides with a silicon ring seal in between, connected to a frequency generator. DSPE-PEG-Biotin 0.3 mol% was added to each single phosphocholine (PC) or lipid mixture for immobilisation and 0.1 mol% DiO or DiD were used as fluorescent membrane probes.

Polymer–GUV interaction experiments

A 57 μL aliquot of freshly prepared GUVs suspension (~1 nmol PC) was added. GUVs were immobilised using Biotin containing a phospholipid moiety onto the streptavidin-coated cover glass surface of the chamber, as described above. The actual amount of PC in the sample was controlled by comparing the overall intensity of the membrane dye emission against a standard. Appropriate volumes of a 10 μM aqueous polymer solution were added stepwise on top to obtain polymer/PC ratios of 1 mol% to 50 mol%. For long-lasting observations the chamber was sealed by a second coverslip on top to avoid evaporation. All experiments were carried out at room temperature.

Confocal imaging and quantitative intensity analysis

A Leica TCS SP2 DM IRE2 confocal microscope was used with a HCX PL APO 63× 1.4 oil immersion objective (Leica Microsystems, Wetzlar, Germany) for two channel imaging. GUV membranes with DiO as a membrane dye were visualised by excitation at 488 nm, detecting emission at 500–520 nm, and those with DiD were visualised by excitation at 633 nm, detected at 670–720 nm. The rhodamine-labelled polymer derivatives were excited at 543 nm and detected at 610–630 nm to avoid cross-talk. 3D images are processed from a z-stacking series with the Leica 3D software.

For quantitative analysis of the adsorption intensity the emission in the equatorial slice of the GUV membrane was used. Single scans were analysed using Leica Quantify Software by use of regions of interest (ROI), as illustrated in Fig. 4. The data shown result from the observation of a single GUV over time or from the addition of increasing polymer amounts. Each experiment was repeated several times with similar results.

Polymer interaction with living cells

Murine embryonic stem cells (C3H/10T1/2) were incubated at 37 °C (5% CO$_2$) with a low concentrated 2 μM solution of fluorescently-labelled Ch-PEG$_{30}$-hbPG$_{17}$ (see structure in Fig. 1c) in DMEM buffer for 0.5, 1, 2 and 4 h, then rinsed three times with PBS pH 7.4 and fixed with Mowiol 4–88 for microscopy.
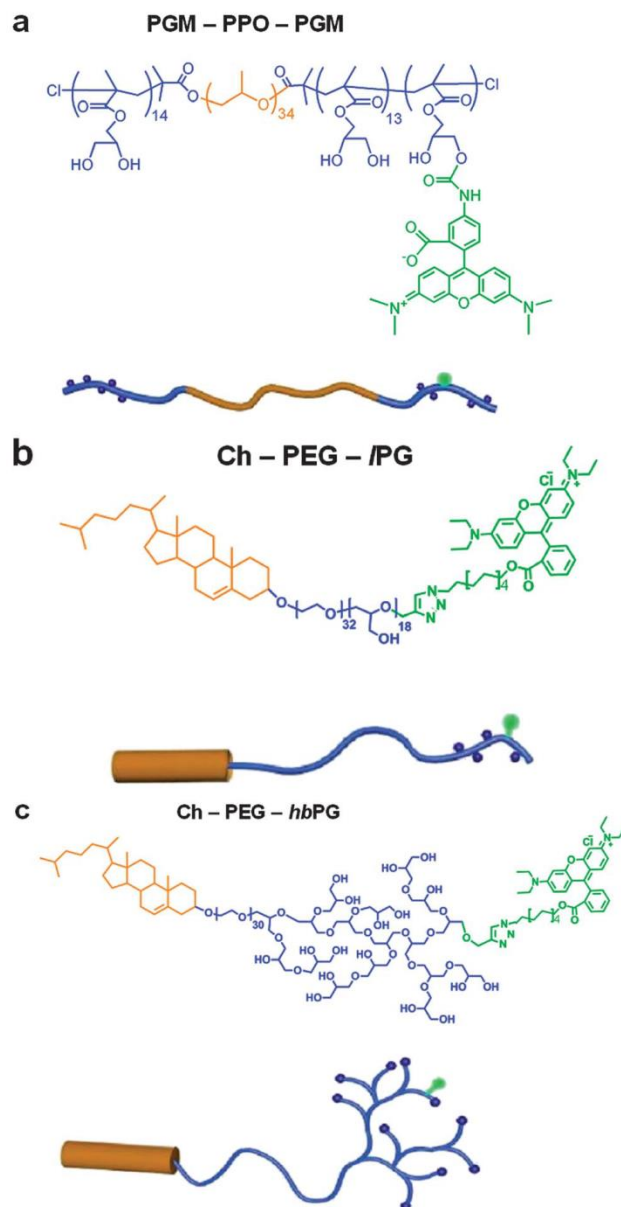
Fig. 1 Chemical structure and architecture of the fluorescently-labelled amphiphilic block copolymers: a) PGM-PPO-PGM, b) Ch-PEG-lPG, and c) Ch-PEG-hbPG.

Results and discussion

Polymer characterisation

Three amphiphilic block copolymers were studied for giant vesicle formation and interaction with phospholipid membranes. They are water-soluble, biocompatible[32,33] and suitable for further functionalisation at the hydroxyl groups of their hydrophilic blocks. The triblock copolymer PGM_{14}-b-PPO_{34}-b-PGM_{14} (PGM-PPO-PGM) consists of two hydrophilic poly(glycerol mono-methacrylate) (PGM) blocks with a weakly hydrophobic poly(propylene oxide) (PPO) middle block. Its critical micellar concentration (cmc) is about 52 µM (40 °C).[27] Ch-PEG_{32}-b-lPG_{18} (Ch-PEG-lPG) and Ch-PEG_{30}-b-$hbPG_{17}$ (Ch-PEG-hbPG) are hydrophilic diblock polyethers, consisting of a linear poly(ethylene glycol) (PEG) spacer, linked to a hydrophobic cholesterol end group (Ch), and a linear (lPG) or hyperbranched (hbPG) polyglycerol block. Their cmc is about 2.9 µM.[29] In most of the experiments performed the polymers were labelled with rhodamine derivatives as shown in Fig. 1. Labelling was done *via* click reactions,[20,28] followed by dialysis for purification. The absence of label impurities was checked using thin layer chromatography. Some slight effects of the label-derivatisation on the polymer properties might be assumed but they should not be relevant for the aspects studied.

Fig. 1 illustrates the similarity of all three copolymers in molecular size and in the poly(hydroxyl)-moieties chosen as hydrophilic blocks which are responsible for the high water-solubility. In contrast there are marked differences in structure and position of the hydrophobic blocks. Cholesterol, by itself a weak amphiphile and a component of natural membranes, is known for its strong interaction with phospholipids[34] and acts as an anchor in phospholipid layers.[26,29] The PPO-chain, as the weak hydrophobic middle block, is very flexible and can interact with phospholipid layers in different ways.[23,24] Furthermore, the different architectures of the hydrophilic blocks, linear or hyperbranched, are expected to show different spatial molecular conformations in dilute aqueous solutions. The flexible linear molecules of PGM-PPO-PGM and Ch-PEG-lPG are expected to have a coiled conformation, shielding the hydrophobic segment, whereas the hyperbranched Ch-PEG-hbPG adopts a more open structure with a more accessible hydrophobic moiety.

Formation of the giant unilamellar polymer–protein vesicles

Recently, we have published detailed studies on the formation of giant unilamellar vesicles of PGM-PPO-PGM by self-assembling in aqueous solution on a BSA–streptavidin layer.[20] Based on molecular modelling results, we assumed a hydrophilic interaction of the polymer hydrophilic block, specifically of the side chain hydroxyl groups of PGM, and the streptavidin surface as initial step leading to the formation of a polymer layer – and subsequently to vesiculation. Parts of the proteins are integrated into the membrane as shown in Fig. 2a. For this study we tested Ch-PEG-lPG and Ch-PEG-hbPG under the same experimental setting. These copolymers have quite different architectures but a similar chemistry of the hydrophilic side groups, supposed to be responsible for the initiation of the unusual self-assembly. We also found a
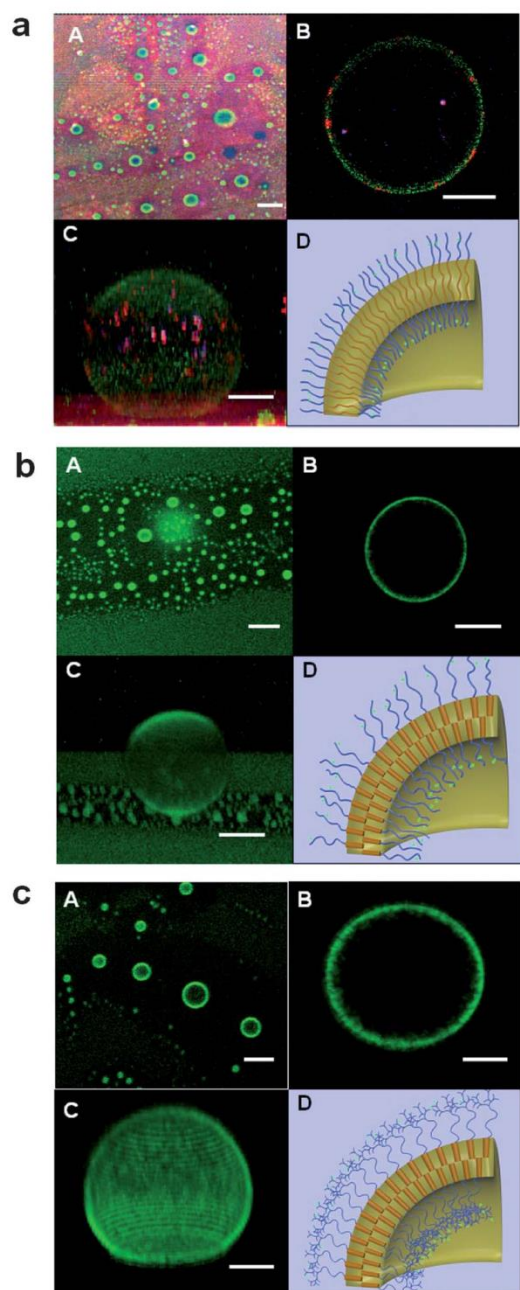
Fig. 2 Formation of giant unilamellar vesicles from aqueous solution of a) PGM-PPO-PGM, b) Ch-PEG-*l*PG and c) Ch-PEG-*hb*PG; (A) overview, (B) equatorial view, (C) 3D image, (D) schematic view of polymer organisation in a membrane segment: green: copolymer (rhodamine labelled), red: streptavidin (Cy5 labelled), blue: BSA (FITC labelled). Scale bars correspond to 5 μm.

fast, spontaneous formation of giant unilamellar polymer vesicles (Fig. 2 b and c).

Typically, spherical vesicles with diameters up to 25 μm were spontaneously formed without any mechanical or thermal stimulus. They were stable for days at room temperature and did not show changes in size or shape when the surrounding solution was replaced by pure water. In Fig. 2c (B, C) a ten day old vesicle in pure water is imaged. In contrast to PGM-PPO-PGM, assumed to form a membrane from a monolayer, Ch-PEG-*l*PG and Ch-PEG-*hb*PG are expected to form polymer bilayers because of their molecular structure. Accordingly, we find in the equatorial view of single vesicles (Fig. 2, images C) a sharp membrane contour for the PGM-PPO-PGM proteopolymersomes, but an apparently thicker membrane with a more diffused morphology for the polyglycerol copolymer vesicles, especially for the hyperbranched one. Since the experiments shown in Fig. 2b and c were initially carried out with non-labelled proteins, the exact localisation of the proteins cannot be assessed from them. However, in analogy to the previously studied PGM-PPO-PGM proteopolymersomes, it can be assumed that the giant vesicles of Ch-PEG-*l*PG and Ch-PEG-*hb*PG integrate proteins into their membranes. Experiments excluding a relevant influence of the fluorescent label on vesicle formation and proving the full biofunctionality of the membrane-integrated protein moieties were reported recently.[20] These results fully confirm our former hypothesis of a hydrophilic polymer–protein interaction as crucial step for vesicle formation from such highly water-soluble polymers at protein-coated supports.

Polymer interaction with phospholipid membranes

GUVs, popular membrane models, are a suitable tool to study membrane processes *via* optical microscopy. To analyse the interaction of the studied copolymers with phospholipid bilayers we incubated fluorescently-marked GUVs in aqueous solutions containing different ratios of the rhodamine-labelled copolymers. The polymer interaction was followed and imaged using confocal microscopy. Two channel imaging allowed the separate detection of the emissions from the polymer and the GUVs,

Fig. 3 presents confocal single scans of the equatorial layer of an observed DLPC GUV (DiO marked) with liquid crystalline membrane structure before and during or after incubation with the rhodamine-labelled polymers. Fig. 3a and b show the results of the adsorption/insertion of different ratios of the cholesterol anchor copolymers in very diluted unimeric polymer solutions of 0.05 μM (for 1 mol%) to 2.5 μM (for 50 mol%). With the same polymer concentrations no adsorption of PGM-PPO-PGM could be visualised. Only with a more than 10-fold higher polymer concentration (26 μM) was there a visible accumulation of the polymer emission at the GUV membrane, increasing with time (Fig. 3c).

Fig. 4 shows the results of a quantitative emission intensity analysis of images similar to those presented in Fig. 3. Both figures demonstrate a high adsorption affinity of all three polymers to the phospholipid membrane. Adsorption of the two cholesterol-anchored copolymers starts immediately after polymer addition and finishes at 20–30 min for the hyperbranched
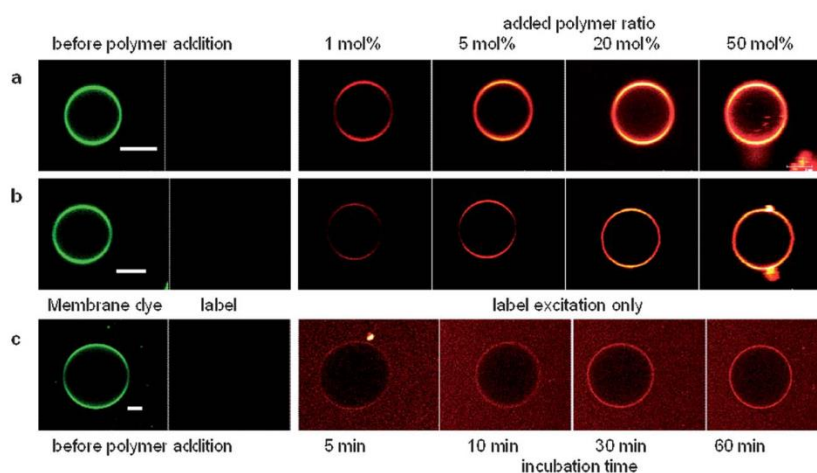
Fig. 3 Interaction of the copolymers (in glow-orange, rhodamine labelled) with DLPC GUVs (in green, DiO labelled) in water: a) Ch-PEG-*hb*PG, 30 min of polymer incubation; b) Ch-PEG-*l*PG, 1 h of polymer incubation; c) PGM-PPO-PGM, 26 μM, time lapse. Scale bars represent 5 μm.
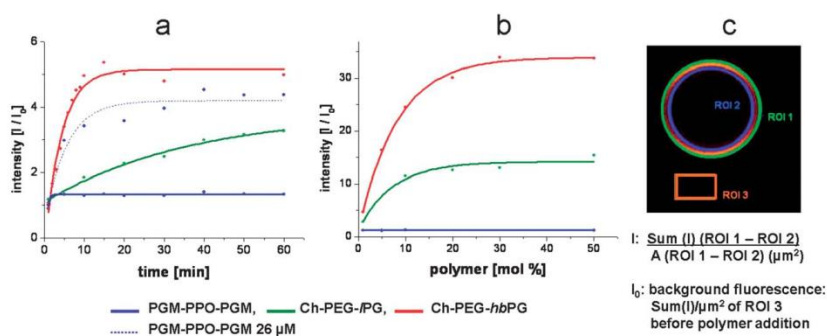
Fig. 4 Quantitative analysis of polymer emission intensity (*I*) at DLPC GUVs in water: a) time lapse of adsorption/insertion of 0.05 μM (1 mol%) polymer and for comparison from 26 μM PGM-PPO-PGM solution; b) adsorption of different percentages of polymer; Ch-PEG-*hb*PG after 30 min, Ch-PEG-*l*PG and PGM-PPO-PGM 1 h of polymer incubation; c) illustration of intensity determination by use of ROI.

Ch-PEG-*hb*PG, while it is still ongoing after 60 min for the linear Ch-PEG-*l*PG. The optimal loading capacity of the membrane seems to be reached at 20–30 mol%. Higher polymer ratios of approximately 50 mol% of the phospholipids' content in the sample affect the membrane structure and stability (Fig. 3a and b) in agreement with earlier calorimetric studies on the interaction of cholesterol with phospholipids, showing that concentrations beyond 50 mol% destroy the membrane structure.[35] GUVs with 10–20 mol% polymer loading remain stable for several days and the polymer adsorption/insertion is also irreversible in pure water.

Fig. 3 and 4 clearly show differences in the adsorption behaviour between the three polymers: The hyperbranched Ch-PEG-*hb*PG adsorbs quickly and strongly, the linear Ch-PEG-*l*PG more slowly, and PGM-PPO-PGM shows a visible

adsorption only at higher polymer concentrations. An explanation can be deduced from the differences in the polymers' architecture and resulting spatial molecular conformations in an aqueous environment.

Assuming interactions between the membrane and the polymers as illustrated in Scheme 1, the exposed cholesterol unit of most Ch-PEG-*hb*PG molecules is free for direct insertion into the phospholipid membrane and the kinetics of the interaction depends mainly on the diffusion of the polymer from the aqueous bulk phase. The coiled conformation of the linear copolymers, PEG-*l*PG and PGM-PPO-PGM, that shields the hydrophobic units, limits hydrophobic interactions. Additional constraints for PGM-PPO-PGM arise from the position of the hydrophobic middle block.

To prove the hypothesized insertion of the polymers into phospholipid bilayers according to Scheme 1 we also studied the interaction of the hyperbranched copolymer with GUVs of unsaturated phospholids (DOPC, POPC), which indicated a hindrance of insertion by unsymmetrical fatty acid tails and a correlation with cholesterol-solubility in different hydrophobic regions of bilayer systems.[36] Phase-separated GUVs with phospholipid domains of different fluidity allow the study of further aspects of polymer–phospholipid interactions. Fig. 5 shows horizontal layers of cholesterol-containing phase-separated GUVs, formed from a ternary lipid mixture (DPPC : DOPC : cholesterol, 2 : 2 : 1), after 24 h of incubation in aqueous polymer solutions of an optimal concentration. The membrane dye (DiD, red) prefers the liquid-disordered (l_d) phase,[37,38] the DPPC and cholesterol rich liquid-ordered (l_o) domains appear dark. The cholesterol-anchored copolymer (Fig. 5a) is exclusively inserted in the l_d phase, explained by its better solubility in the cholesterol-poor lipid phase. PGM-PPO-PGM interacts unspecifically with the whole membrane area (Fig. 5b).

Membranes of cholesterol-free binary phospholipid mixtures (DPPC : DOPC, 1 : 1) show phase separation in highly-ordered gel phase domains rich in DPPC with a higher phase transition temperature, and l_d domains. In Fig. 6 the interaction of Ch-PEG-*hb*PG with this kind of GUV is demonstrated. The membrane dye (DiO, green) prefers the l_d phase,[39] but in contrast the polymer is inserted particularly in the dark patch domains (gel phase) without changing domain size or shape.
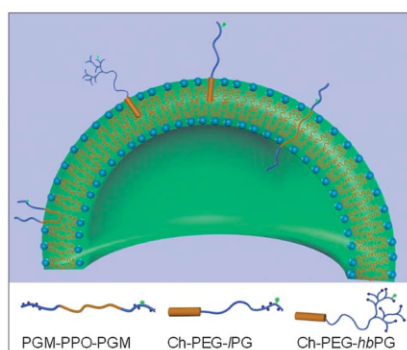
Scheme 1   Insertion of Ch-PEG-*hb*PG, Ch-PEG-*l*PG and PGM-PPO-PGM into phospholipid membranes.
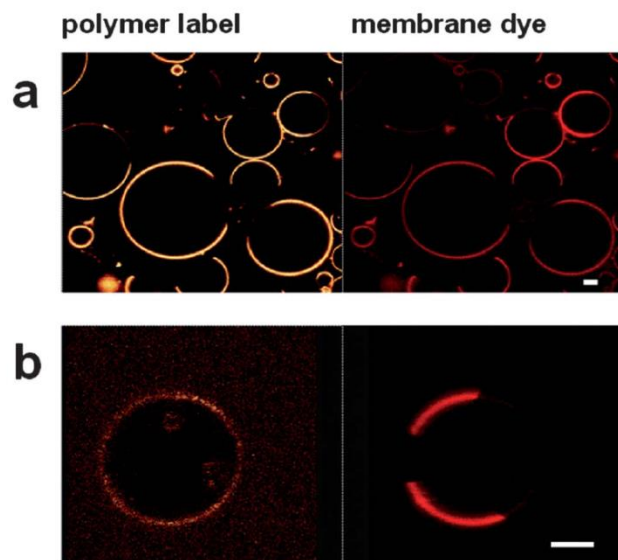
Fig. 5 Interaction of a) Ch-PEG-*hb*PG (10 mol%) and b) PGM-PPO-PGM (150 μM) (both in glow-orange, rhodamine labelled) with liquid phase separated GUVs (in red, DiD labelled); scale bars correspond to 5 μm.
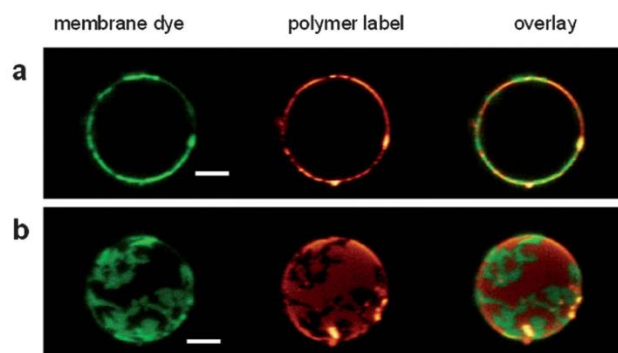
Fig. 6 Interaction of Ch-PEG-*hb*PG (in glow-orange, rhodamine labelled) with gel–l$_d$ phase separated GUV (in green, DiO labelled); scale bars correspond to 5 μm. a) Equatorial layer, b) half projection from a z-stacking series.

By observation of the polymer interactions with GUVs including smaller vesicles inside, we noticed the surprising polymer label emission at the inner vesicles membrane, indicating a membrane crossing ability of the polymers. Fig. 7 clearly demonstrates this effect for the hyperbranched cholesterol-anchored copolymers at GUVs from different phospholipids. Similar results were obtained for the linear Ch-PEG-*l*PG. In Fig. 5b the same behaviour can be observed for PGM-PPO-PGM.

The ability to transport across membranes has already been reported for other amphiphilic block copolymers,[1] but to our knowledge vesicle membrane crossing
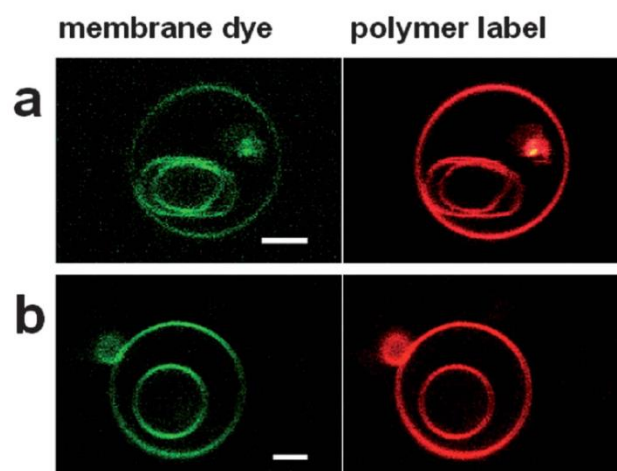
Fig. 7 Ch-PEG-*hb*PG labelled emission (in glow-orange) at membranes (in green, DiO labelled) of inner vesicles from a) DLPC GUV, and b) POPC GUV; scale bars correspond to 5 μm.
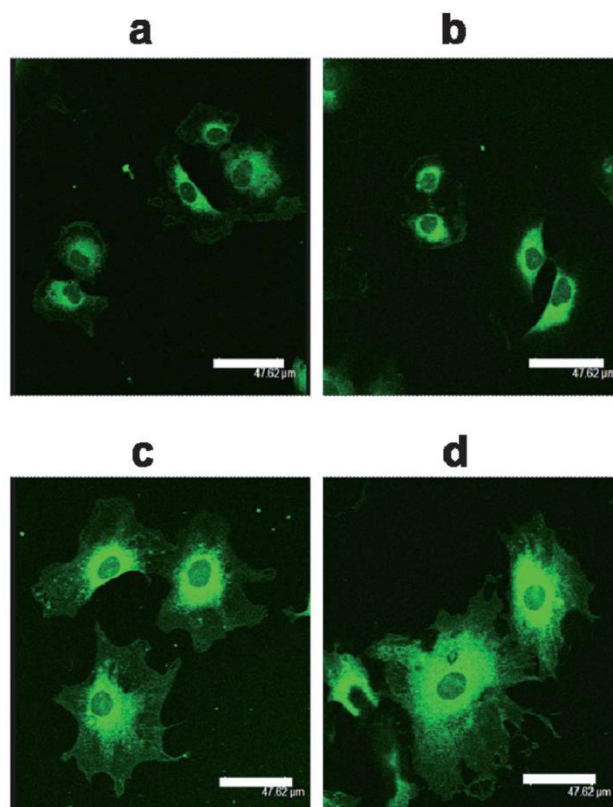
Fig. 8 Interaction of Ch-PEG-*hb*PG (in green, rhodamine labelled) with living cells at different incubation times: a) 0.5 h, b) 1 h, c) 2 h, d) 4 h. Scale bars correspond to 50 μm.

by a bulky polymer has not yet been observed by imaging. The mechanism involved requires further investigation. Pore formation as well as endocytosis-like processes, recently imaged for the uptake of nanoparticles into GUVs,[40] are under discussion.

Since phospholipid bilayers are widely used as simplified models of cell membranes it is interesting to test if permeation also takes place with natural membranes. For this purpose murine embryonic stem cells were incubated with Ch-PEG-*hb*PG solutions for different lengths of time. Fig. 8 shows an accumulation of the copolymer inside the living cells increasing over time. It is localised mainly inside the cytoplasm or at cell organelle membranes in the nucleus-surrounding region. The cells are still alive after 4 h of incubation, suggesting that the polymer might be non-cytotoxic for the cell line used. These results confirm the cell membrane permeation ability of the copolymers.

Conclusions

A novel strategy for the formation of stable giant vesicles from highly water-soluble nonionic amphiphilic biocompatible copolymers with proteins initially developed for linear copolymers was extended to a different family of amphiphilic polymers, involving a rather different molecular architecture including a hyperbranched hydrophilic block. Our earlier theses about the driving forces and mechanism of the unknown self-assembling process, based on molecular modelling studies, are confirmed by the presented results. Vesicle formation in an aqueous solution starts spontaneously from a polymer layer, formed through hydrophilic interactions between the polymer side groups bearing hydroxyl moieties and a streptavidin-coated surface. The molecular composition and architecture of the amphiphilic copolymers affect the membrane structure without hindering vesiculation. The method yields biocompatible proteopolymersomes incorporating proteins in their vesicle membrane, which offers multiple possibilities for applications in biomedical research.

In the second part of this study, the interaction of the block copolymers with model membranes and living cells was studied using confocal imaging. The high affinity of these polymers to phospholipid layers was proved and new insights regarding the influence of the polymer conformation in water on the interaction were gained. Polymer interactions with phospholipid vesicles have been under investigation for many years and studied by several methods but a direct observation and imaging of polymer interaction with pre-formed membranes has, to our knowledge, not been reported. Additionally, it was found that all three copolymers are able to cross model membranes. Experiments with living cells indicate their ability to also permeate natural membranes and confirms their biocompatibility. In conclusion, these results offer new possibilities for the studied polymers to be used for biomedical applications.

Acknowledgements

References

1 E. Amado and J. Kressler, *Curr. Opin. Colloid Interface Sci.*, 2011, **16**, 491–498.
2 W. H. Binder, *Angew. Chem., Int. Ed.*, 2008, **47**, 3092–3095.
3 M. Schulz, A. Olubummo and W. H. Binder, *Soft Matter*, 2012, **8**, 4849–4864.
4 Ch. Wang, Z. Wang and X. Zhang, *Acc. Chem. Res.*, 2012, **45**, 608–618.
5 K. Kita-Tokarczyk, M. Junginger, S. Belegrinou and A. Taubert, *Adv. Polym. Sci.*, 2011, **242**, 151–201.
6 Z. Liu and N. Zhang, *Curr. Pharm. Des.*, 2012, **18**, 3442–3451.
7 J.-K. Oh, *Soft Matter*, 2011, 7, 5096–5108.
8 J.-F. Le Meins, O. Sandre and S. Lecommandoux, *Eur. Phys. J. E*, 2011, **34**, 1–17.
9 S. Egli, H. Schlaad, N. Bruns and W. Meier, *Polymers*, 2011, **3**, 252–280.
10 J. S. Lee and J. Feijen, *J. Controlled Release*, 2012, **161**, 473–483.
11 K. Renggli, P. Baumann, K. Langowska, O. Onaca, N. Bruns and W. Meier, *Adv. Funct. Mater.*, 2011, **21**, 1241–1259.
12 M. Marguet, C. Bonduelle and S. Lecommandoux, *Chem. Soc. Rev.*, 2013, **42**, 512–529.
13 M. Marguet, O. Sandre and S. Lecommandoux, *Langmuir*, 2012, **28**, 2035–2043.
14 F. Meng and Z. Zhong, *J. Phys. Chem. Lett.*, 2011, **2**, 1533–1539.
15 J. F. Liao, C. Wang, Y. J. Wang, F. Luo and Z. Y. Qian, *Curr. Pharm. Des.*, 2012, **18**, 3432–3441.
16 L. Zhang and A. Eisenberg, *Science*, 1995, **268**, 1728–1731.
17 K. T. Kim, J. Zhu, S. A. Meeuwissen, J. Cornelissen, D. J. Pochan, R. Nolte and J. van Hest, *J. Am. Chem. Soc.*, 2010, **132**, 12522–12524.
18 H.-J. Choi and C. D. Montemagno, *Nano Lett.*, 2005, **5**, 2538–2542.
19 R. Rodríguez-García, M. Mell, I. López-Montero, J. Netzel, T. Hellweg and F. Monroy, *Soft Matter*, 2011, **7**, 1532–1542.
20 E. Amado, R. Schöps, W. Brand and J. Kressler, *ACS Macro Lett.*, 2012, **1**, 1016–1019.
21 E. E. Ambroggio, L. A. Bagatolli in *IUL Biotechnology Series*, ed. M. A. R. B. Castanho, International University Line Press, 2010, vol. 9, pp. 169–192.
22 S. Bibi, R. Kaur, M. Hendriksen-Lacey, S. E. Mc Neil, J. Wilkhu, E. Lattmann, D. Christensen, A. R. Mohammed and Y. Perrie, *Int. J. Pharm.*, 2011, **417**, 138–150.
23 E. Amado, A. Kerth, A. Blume and J. Kressler, *Langmuir*, 2008, **24**, 10041–10053.
24 E. Amado, A. Kerth, A. Blume and J. Kressler, *Soft Matter*, 2009, **5**, 669–675.
25 S. Reuter, A. Hofmann, K. Busse, H. Frey and J. Kressler, *Langmuir*, 2011, **27**, 1978–1989.
26 X. Peng, A. M. Hofmann, S. Reuter, H. Frey and J. Kressler, *Colloid Polym. Sci.*, 2012, **290**, 579–588.
27 E. Amado, C. Augsten, K. Mäder, A. Blume and J. Kressler, *Macromolecules*, 2006, **39**, 9486–9496.
28 A. M. Hofmann, F. Wurm, E. Hühn, T. Nawroth, P. Langguth and H. Frey, *Biomacromolecules*, 2010, **11**, 568–574.
29 A. M. Hofmann, F. Wurm and H. Frey, *Macromolecules*, 2011, **44**, 4648–4657.
30 B. Lohse, P.-Y. Bolinger and D. Stamou, *J. Am. Chem. Soc.*, 2008, **130**, 14372–14373.
31 M. I. Angelova and D. S. Dimitrov, *Faraday Discuss. Chem. Soc.*, 1986, **81**, 303–3011.
32 C. Wang, B. Yu, B. Knudsen, J. Harmon, F. Moussy and Y. Moussy, *Biomacromolecules*, 2008, **9**, 561–567.
33 D. Wilms, S.-E. Stiriba and H. Frey, *Acc. Chem. Res.*, 2010, **43**, 129–141.
34 R. A. Demel, L. L. M. Van Deenen and B. A. Pethica, *Biochim. Biophys. Acta, Biomembr.*, 1967, **135**, 11–19.
35 E. Kannenberg, A. Blume, R. N. McElhaney and K. Poralla, *Biochim. Biophys. Acta, Biomembr.*, 1983, **733**, 111–116.
36 P. Scholtysek, S. Müller, A. Meister, R. Schöps, H. Frey, J. Kressler, A. Blume, unpublished work in preparation.
37 T. Baumgart, G. Hunt, E. R. Farkas, W. W. Webb and G. W. Feigenson, *Biochim. Biophys. Acta, Biomembr.*, 2007, **1768**, 2182–2194.
38 J. Juhasz, J. H. Davis and F. J. Sharom, *Biochem. J.*, 2010, **430**, 415–423.
39 J. Juhasz, J. H. Davis and F. J. Sharom, *Biochim. Biophys. Acta, Biomembr.*, 2012, **1818**, 19–26.
40 K. Tahara, S. Tadokoro, Y. Kawashima and N. Hirashima, *Langmuir*, 2012, **28**, 7114–7118.

A.4 Click Modification of Multifunctional Liposomes Bearing Hyperbranched Polyether Chains

Thomas Fritz,[†] Markus Hirsch,[†] Felix C. Richter,[†] Sophie S. Müller,[‡,§] Anna M. Hofmann,[‡] Kristiane A. K. Rusitzka,[‖] Jürgen Markl,[‖] Ulrich Massing,[⊥] Holger Frey,[‡] and Mark Helm,[†]*

[†]Institute of Pharmacy and Biochemistry, Johannes Gutenberg-University Mainz, Staudingerweg 5, 55122 Mainz, Germany

[‡]Institute of Organic Chemistry, Johannes Gutenberg-University Mainz, Duesbergweg 10-14, 55122 Mainz, Germany

[§]Graduate School MAINZ, Staudingerweg 9, 55128 Mainz, Germany

[‖]Institute of Zoology, Johannes Gutenberg-University Mainz, J.-J. Becher-Weg 7, 55122 Mainz, Germany

[⊥]Department of Clinical Research, Tumor Biology Center, 79106 Freiburg, Germany

Click Modification of Multifunctional Liposomes Bearing Hyperbranched Polyether Chains

Thomas Fritz,[†] Markus Hirsch,[†] Felix C. Richter,[†] Sophie S. Müller,[‡,§] Anna M. Hofmann,[‡] Kristiane A. K. Rusitzka, [∥] Jürgen Markl, [∥] Ulrich Massing,[⊥] Holger Frey,[‡] and Mark Helm*,[†]

[†]Institute of Pharmacy and Biochemistry, Johannes Gutenberg-University Mainz, Staudingerweg 5, 55122 Mainz, Germany
[‡]Institute of Organic Chemistry, Johannes Gutenberg-University Mainz, Duesbergweg 10-14, 55122 Mainz, Germany
[§]Graduate School MAINZ, Staudingerweg 9, 55128 Mainz, Germany
[∥]Institute of Zoology, Johannes Gutenberg-University Mainz, J.-J. Becher-Weg 7, 55122 Mainz, Germany
[⊥]Department of Clinical Research, Tumor Biology Center, 79106 Freiburg, Germany

Ⓢ Supporting Information

ABSTRACT: Aiming at controlled modification of liposomal surface structures, we describe a postpreparational approach for surface derivatization of a new type of multifunctional, sterically stabilized liposomes. Application of dual centrifugation (DC) resulted in high encapsulation efficiencies above 50% at very small batch sizes with a total volume of 150 μL, which were conductive to fast and efficient optimization of variegated surface modification reactions. Cholesterol-polymer amphiphiles, including complex hyperbranched polyether structures bearing 1−4 terminal alkynes, were used in DC formulations to provide steric stabilization. The alkyne moieties were explored as anchors for the conjugation of small molecules to the liposomal surface via click chemistry, binding 350−450 fluorophores per liposome as examples for surface active molecules. Using Förster resonance energy transfer (FRET) spectroscopy, the conjugation reaction as well as the uptake of FRET-labeled liposomes by RBE4 cells was monitored, and the distribution of the fluorescent lipids among cellular structures and membranes could be studied. Thus, the combination of clickable hyperbranched amphiphiles and dual centrifugation provides access to well-defined liposomal formulations with a variety of surface moieties.
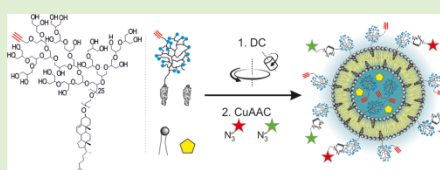
■ INTRODUCTION

Surface decoration of nanoscale objects, including liposomes, has become of increasing importance ever since Ehrlich publicized his vision of the "Magic Bullet". Intense efforts have been made to direct delivery of pharmaceutical compounds to specific target tissue. In the field of tumor targeting, the two dominating concepts for nanoscale drug carriers[1] are the enhanced permeability and retention (EPR) effect[2−5] on one hand, and directed targeting via specific ligand−receptor interaction on the other hand. Currently, directed targeting is almost exclusively carried out via antibody-drug conjugates in the clinic,[6−9] but intense research has developed numerous targeting strategies based on macromolecular and small molecule ligands alike.[10−13]

Important requirements for nanoscale drug delivery systems include protection of the payload from degradation in the systemic circulation, and the ability to incorporate ligands for active targeting. Correspondingly, substantial research effort has gone into the development of flexible and specific conjugation methods for potential targeting vectors like antibodies, peptides, aptamers, or small molecules that act as receptor ligands.[14]

Among the different strategies that have emerged for the decoration of nanoscale particles with targeting moieties, the time point of modification, i.e., incorporation of the targeting moieties, is a crucial aspect. Modification has been conducted before, during,[15,16] or after synthesis of the nanocarrier,[17,18] where the targeting moieties are subsequently conjugated onto the surface of nanocarriers. Another method is postinsertion, which implies the insertion of amphiphilic targeting moieties into existing membrane structures of preformed lipid particles.[19] Postinsertion of targeting vectors is typical for the preparation of liposomes, which are defined as nanoscale spherical vesicles consisting of a lipid bilayer membrane surrounding an aqueous core.[20] Depending on its biophysical properties, a payload can be entrapped both within the hydrophilic core or within the lipophilic membrane,[21] and besides direct entrapment during preparation, membrane gradients can facilitate active loading.[22,23] Liposomes typically contain naturally occurring lipid building blocks of cell membranes like cholesterol or phosphatidylcholine, and
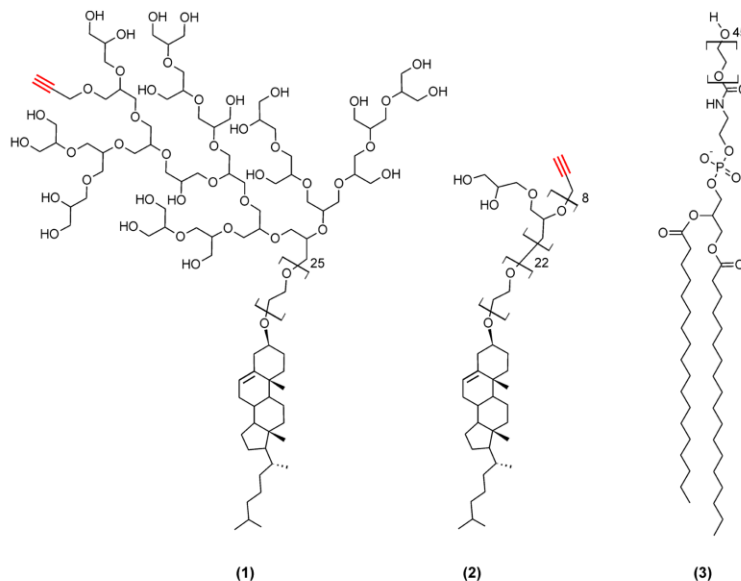
Figure 1. Representative structures of polymer–lipid conjugates used in this study. Structures include Chol-PEG$_{25}$-hbPG$_{21}$ (1), Chol-PEG$_{22}$-PGG$_8$ (2), and, as a reference, the commercially available DSPE-mPEG2000 (3).

therefore generally possess high biocompatibility and biodegradability. By selecting specific membrane compositions, the characteristics of liposomal formulations can be tailored.[24,25] Liposomes containing fluorescent amphiphiles allow for the detailed study of both their intra- and extracellular fate.[26,27]

Liposomal formulations suitable for in vivo applications typically require compatibility with biological systems and pharmaceutical suitability, comprising diameters below 300 nm, narrow size distributions with polydispersity indices (PDI) below 0.5,[28] high encapsulation efficiencies, and reasonable shelf lives. Common strategies for the preparation of liposomes include lipid film rehydration[20] followed by membrane extrusion[29] or ultrasonication,[30] micro injection/solvent removal[31,32] techniques, and high pressure homogenization (HPH).[33,34]

An established concept to overcome fast clearance of liposomes from the bloodstream due to rapid uptake by the reticuloendothelial system (RES)[35] is to shield the surface with polymeric structures providing steric hindrance and decreasing protein adsorption.[36–41] The most widespread structures used for so-called "sterically stabilized" or "stealth" liposomes and related nanoscale objects are derived from poly(ethylene glycol) (PEG). However, recently hyperbranched polyglycerol (hbPG) was shown to exhibit advantageous characteristics regarding biocompatibility and water solubility, while providing a larger number of functional end groups for potential derivatization.[42–46]

For studies investigating the suitability of new lipid compounds in liposomal formulations, the supposedly most important limiting factor is the requirement for substantial amounts of these experimental compounds, which are typically available only on a small scale. Therefore, testing different lipid compositions, e.g., in a quest to achieve optimal surface decoration of liposomes with targeting moieties, is extremely straining when material-intensive methods such as extrusion, sonication, or HPH are used.

We have recently published the synthesis of cholesterol-anchored, hyperbranched polyglycerol-based lipids, which easily integrate into vesicular structures and are amenable to derivatization post formulation.[46–48] These findings have prompted us to investigate their integration into properly formulated, well-characterized liposomes for potential pharmaceutical applications. Faced with the necessity of performing multiple optimization series with limited amounts of experimental amphiphiles, we have turned to a recently developed formulation technique termed dual centrifugation (DC), which overcomes major disadvantages of the above-mentioned techniques for liposome preparation.[49] Previous reports on DC have turned out promising results, such as high entrapping efficiencies of hydrophilic compounds like siRNA in small scales and sterile conditions.[50] Here, we report on proof-of-concept studies of the postpreparational surface decoration of new types of alkyne-containing, PEG-, linear poly(glycidyl glycerol) (PGG)-, and hbPG-stabilized liposomes (PGGL and hbPGL, respectively), and the synergistic effects of using DC for the formulation of liposomes with valuable lipids on a very small scale. (Structures used in this study are listed in Figure 1.) The surface functionalization with a pair of corresponding fluorescent dyes allowed observation of Förster resonance energy transfer (FRET) on the liposomal membrane. In a first line of evaluation, we have studied the fate of the newly

Biomacromolecules

Table 1. Lipid Compositions Used for Liposome Preparation

ID	χ_{Chol}	χ_{EPC}	$\chi_{Polymer}$	structure (polymer amphiphile)	M_w [g/mol]	PDI
CL	0.45	0.55	0			
PGGL	0.40	0.55	0.05	Cholesterol–PEG$_{22}$–PGG$_8$–(–CH$_2$–C≡CH)$_4$	2780	1.08
*hb*PGL	0.40	0.55	0.05	Cholesterol–PEG$_{25}$–*hb*PG$_{21}$–(–CH$_2$–C≡CH)	3100	1.11
SSL	0.45	0.50	0.05	DSPE–PEG$_{45}$–O–CH$_3$		n. d.

Abbreviations: Conventional liposomes (CL), PGG-coated liposomes (PGGL), *hb*PG-coated liposomes (*hb*PGL), and PEG-sterically stabilized liposomes (SSL); PDI: M_w/M_n; χ: molar fraction of specific compound.

developed labeled lipid compounds during cellular uptake and distribution.

MATERIALS AND METHODS

Materials. All chemicals were purchased from Sigma-Aldrich (St. Louis, MO, United States), unless specified otherwise. Cholesterol, egg phosphatidylcholine (EPC) and DSPE-mPEG2000 were kindly provided by Lipoid GmbH (Ludwigshafen, Germany). Atto 488 azide was purchased from Atto-Tec (Siegen, Germany). Alexa Fluor 594 azide was purchased from Life Technologies (Darmstadt, Germany).

Synthesis of Cholesterol-Based Lipids. Cholesterol–PEG$_{22}$–PGG$_8$–(–CH$_2$–C≡CH)$_4$ (Chol-PGG, M_n = 2780 g/mol, PDI = 1.08) and Cholesterol–PEG$_{25}$–*hb*PG$_{21}$–(–CH$_2$–C≡CH) (Chol-*hb*PG, M_n = 3100 g/mol, PDI = 1.11) were synthesized via cholesterol-initiated oxyanionic ring-opening polymerization and subsequent derivatization with propargyl bromide as reported previously.[46,47] Average molecular weights M_n and the degree of functionalization were assessed by integration of ^{1}H NMR spectra measured in deuterated dimethyl sulfoxide (DMSO-d_6), using a Bruker AC 300 spectrometer operated at 300 MHz. NMR spectra are listed in Supporting Information Figures S1 and S2, and FT-IR characterization is shown in Figure S3. Polydispersity indices (PDI) were determined by size exclusion chromatography (SEC) in dimethylformamide (DMF, 50 °C, 1 mL/min, containing 0.25 g/L of lithium chloride as an additive), using an Agilent 1100 Series SEC setup with a PSS HEMA column ($10^6/10^5/10^4$ g/mol) and a UV (254 nm) and RI detector. Calibration was achieved using PEG standards provided by Polymer Standards Service.

Preparation of Liposomes via DC. Stock solutions of available lipids in ethanol were prepared and combined to the final lipid compositions as listed in Table 1. Total amounts of lipid were adjusted to yield 17.5 mg of total lipid content for a 50 mg batch. Lipids were combined in 0.65 mL screw-cap reaction tubes (Carl Roth, Karlsruhe, Germany) and dried in a vacuum centrifuge (Eppendorf, Hamburg, Germany) at 40 °C for 6 h in a first step and then in a lyophilization unit (Alpha 2–4 LD, Christ, Osterode am Harz, Germany) for at least 72 h. Dried lipid compositions were stored at −20 °C until usage.

For liposome preparation, 32.5 μL of phosphate buffered saline (PBS) (137 mM NaCl, 2.7 mM KCl, 10 mM N$_2$HPO$_4$, 2 mM KH$_2$PO$_4$, pH 7.4) or a solution of designated cargo in PBS and 250 mg of ceramic beads (SiLibeads ZY 0.6–0.8 mm, kindly provided by Sigmund Lindner, Warmensteinach, Germany) were added to the dry lipid film and incubated for 8 min at room temperature. After DC in a Rotanta 400 centrifuge (customized with a prototype DC-rotor, Hettich, Tuttlingen, Germany) for 20 min at 2500 rpm, the obtained vesicular phospholipid gel (VPG) was diluted with 100 μL of PBS, resulting in approximately 150 μL of highly concentrated liposome suspension. These stock solutions were subjected to two additional 2 min centrifugation runs at 2500 rpm for a thorough dispersion, reversing the orientation of the vials between both runs. Stock suspensions were stored at 4 °C until usage.

Postpreparational Functionalization. The click reaction was carried out in 1.5 mL reaction tubes (Carl Roth, Karlsruhe, Germany) at 25 °C in a total volume of 40 μL, including 5 μL of liposome stock suspension. Reactants were added in this order with the final concentrations in brackets: Milli-Q water (to a total volume of 40 μL), phosphate buffer (5.3 mM NaH$_2$PO$_4$, 94.7 mM Na$_2$HPO$_4$) pH 8,

tris(hydroxypropyltriazolylmethyl)amine (THPTA) (0.5 mM), CuSO$_4$ (0.1 mM), and sodium ascorbate (2.5 mM).[51] Azides or a mixture of azides was added to these mixtures to achieve final concentrations of 25–200 μM. After thorough mixing, the reaction was incubated for 2 h at room temperature. For removal of free dye, mixtures were subjected to gravity flow gel permeation chromatography (GPC) on custom-made Sephadex G-100 GPC columns.

Degree of Functionalization. The number of fluorophores per liposome was obtained from fluorescence intensities of purified liposome fractions and therefore the concentrations of fluorophores C_{FL} and a liposome concentration C_{Lipo}, which was estimated from the encapsulation efficiency and the hydrodynamic radius according to the method of Pidgeon et al.[52] Briefly, the number of liposomes was estimated from their sizes and the encapsulated volume. For subsequent calculations, liposomes were assumed to be unilamellar with a lamellar thickness of 5 nm, an assumption that is supported to a certain extend by Supporting Figure S4. Spectrometric changes due to successful conjugation were neglected. The number of fluorophores N per liposome is obtained from $N = C_{FL}/C_{Lipo}$ (for details on the calculation, see the Supporting Information, page S6).

Fluorescence spectra were recorded using 15 or 45 μL quartz glass cuvettes (Hellma Analytics, Müllheim, Germany) in a FP-6500 spectrofluorimeter (Jasco, Tokyo, Japan). Besides the general measurement parameters (excitation and emission bandwidth 3 nm, data pitch 1 nm, scanning speed 1000 nm/min, response 0.5 s, PMT voltage depending on concentration but constant within each experiment, spectral correction active), fluorophores were detected with these specific parameters: Atto 488 (Excitation wavelength: 490 nm, emission range 500–750 nm, emission maximum at 523 nm for quantification), Alexa 594 (Exc. wl.: 590 nm, em. r.: 600–750 nm, em. max.: 617 nm), Calcein (Exc. wl.: 490 nm, em. r.: 500–650 nm, em. max.: 516 nm). Emission due to FRET was measured via excitation of the donor dye Atto 488 and exc. wl.: 590 nm, em. r.: 600–750 nm, em. max.: 617 nm.

FRET Depletion. Donor bleed through (BT(D)) and acceptor cross excitation (CE(A)) were determined with monolabeled samples, which were prepared identically to bilabeled samples. Fluorescence intensities of both donor and acceptor fluorophores were measured as described above. In the following, D and A represent emission intensities measured at the wavelength of maximum emission for the donor and the acceptor, respectively. The indices D and A indicate the specific excitation wavelength for acceptor and donor fluorophore, respectively. BT(D) and CE(A) can be described by BT(D) = A_D/D_D and CE(A) = A_D/A_A. As an example, BT(D) therefore describes the emission intensity of the donor fluorophore at the emission maximum of the acceptor fluorophore, relative to donor emission intensity at its emission maximum. For correction, the fluorescence intensity in the FRET channel (acceptor emission measured at donor excitation: A_D) of the samples was decreased by relative amounts of the emission intensity: $A_{D,corrected} = A_D − A_A \times CE(A) − D_D \times BT(D)$. In addition, corresponding emission intensities of blank samples were subtracted to eliminate background signals. All measurements were carried out in both PBS and PBS containing 0.5% Triton-X 100 (Sigma-Aldrich), determining the influence of the detergent on the spectral properties of the dyes. Typical fluorescence spectra which illustrate the FRET effect, as well as the decrease of acceptor emission after disintegration are enclosed in Supporting Figure S6.

Agarose Gel Electrophoresis. Agarose gel electrophoresis was performed with a mass fraction of 0.2% agarose gel (Invitrogen,

Karlsruhe, Germany) in TRIS-borate-EDTA-buffer (TBE) (Carl Roth). Electrophoresis was run at 100 V for 2–3 h, and gels were imaged on a Typhoon 9400 multimode imager (GE Healthcare, Wendlingen, Germany) with the following settings: Atto 488: Exc. 488 nm, em. 520 nm BP40; Alexa 594: Exc. 532 nm, em. 610 nm BP30.

Dynamic Light Scattering. (DLS) experiments were performed on a Malvern Zetasizer Nano ZS using disposable polystyrene cuvettes (Sarstedt, Germany), filled with 1 mL of freshly filtered PBS. Either 1 μL of unpurified liposome suspensions or 10 μL of purified sample was added, which resulted in count rates of 300 ± 50 kcounts per second, as recommended by the supplier. Generally, after equilibration to 25 °C, three measurements were performed, with the instrument optimizing the number of runs for each measurement. Z-averaged hydrodynamic radii and polydispersity indices were obtained from cumulant analysis. The refractive index (RI) and viscosity of the dispersant (preset: water) was set to 1.330 and 0.8872 cP, respectively, the RI of the particle was set to 1.59. The absorption of the particle was set to 0.01, both attenuator and measurement position were controlled by the instrument, and all measurements were performed at a scattering angle of 173°.

Encapsulation Efficiency. For measurement of the encapsulation efficiency, a 50 mM solution of calcein was encapsulated in the respective liposomes. After GPC purification of a specific volume of liposome suspension V_{crude}, the diluted total volume V_{pure} of the purified liposome suspension was gravimetrically determined. Spectrofluorimetric measurement of the calcein concentration in the purified sample, c_{pure}, and in the same volume V_{crude} of crude liposome suspension, c_{crude}, enables calculation of the encapsulation efficiency $EE = (c_{pure} \times V_{pure}) \times (c_{crude} \times V_{crude})^{-1}$.

Cell Culture. For uptake studies, rat brain endothelial (RBE4)[53] cells were grown in 45% v/v Dulbecco's Modified Eagle's Medium (DMEM), 45% v/v Ham's F-10, 10% v/v fetal bovine serum (FBS), and 100 μg/mL penicillin streptomycin and 1 ng/mL basic fibroblastic growth factor (all Invitrogen, Karlsruhe, Germany). All used buffers were either autoclaved, sterile filtered or already sterile when supplied and were prewarmed to 37 °C. Cultured cells were incubated at 37 °C in high humidity and with 5% CO_2. Cells were grown in 75 cm^2 standard cell culture flasks (Sarstedt, Nürmbrech, Germany) to a confluence of 80–90% and seeded 2–3 times per week at a density of 40 000 cells/cm^2. For live cell imaging, 20 000 cells/well were seeded in 8-well μ-slides (Ibidi, Munich, Germany) in 250 μL growth medium. For incubation experiments, fresh growth medium was supplemented with liposome suspensions and incubated for the indicated time span. Before imaging, cells were rinsed with DPBS (Invitrogen) and supplied with fresh medium.

Confocal Laser Scanning Microscopy. CLSM was performed on a Leica TCS SP-5 confocal fluorescence microscope, equipped with 405 nm, 488 nm, 561 and 635 nm laser lines on which a 63×/1.4 oil objective was used. Standard settings for all experiments were 1024 × 1024 pixels, 8 bit resolution, laser intensity of 25% for 488 and 561 nm lasers and 50% for 405 nm laser in image acquisition software, 488 nm laser intensity at 20% in laser settings, a scan speed of 600 Hz, and a numerical aperture of one airy unit. Channels for fluorophores: Atto 488: Excitation at 488 nm, PMT2, PMT voltage 576 V, detection bandwidth 500–550 nm; Alexa 594: Excitation at 561 nm, PMT3, PMT voltage 693 V, detection bandwidth 600–650 nm; FRET: Excitation at 488 nm, PMT3, PMT voltage 693 V, detection bandwidth 600–650 nm; transmission: Excitation at 488 nm, PMT1, PMT voltage 411 V. Microscopy of living cell samples was performed within 30 min after removal from incubation unit. Optical inspection indicated immaculate viability of cells over the whole observation time.

■ RESULTS AND DISCUSSION

Polyglycerol Amphiphiles. Complex hyperbranched polyether structures as multifunctional building blocks, linked to cholesterol moieties,[46,47] offer highly attractive perspectives for the formulation of sterically stabilized liposomes for drug delivery. Figure 1 shows chemical structures of two polyglycerol amphiphiles **1** and **2** and a comparable methoxy poly(ethylene glycol) (mPEG) phospholipid conjugate **3** used in this study. Compounds **1** and **2** carry terminal alkyne groups at the apex of the hydrophilic part of the molecules, which offer the possibility for postpreparational modification of the resulting liposomes by "click" chemistry.[54] The availability of terminal hydroxyl groups scales directly with the molecular weight of the amphiphiles, allowing for more than one alkyne group per polymer chain and therefore overcoming a typical drawback of comparable PEG structures. While only one alkyne group is shown in each structure, the average number of alkyne groups between one (compound **1**) and four (compound **2**) was achieved via stoichiometric control (compare Supporting Figures S1–3). Since both compounds were prepared with narrow size distributions as indicated by PDIs (M_w/M_n) below 1.12, they qualify in general for pharmaceutical applications, which typically require well-defined systems. Hyperbranched poly-(glycerol)-based amphiphiles provide a large number of terminal hydroxyl groups for derivatization, at least equals comparable PEG structures in biocompatibility,[55] and can be tailored to meet specific demands.

Liposome Preparation and Characterization. We have explored the use of alkynylated PGG- and *hb*PG-cholesterol compounds in formulations of small liposomes, which can be rapidly produced by DC.[49] For comparison, the alkyne-derivatized containing PG-cholesterol compounds **1** and **2** were analyzed along with conventional liposomes (CL) and liposomes containing linear DSPE-PEG conjugate **3**, the latter being a compound often used in sterically stabilized liposomes (SSL) of the "stealth" type.[19,56] Based on previous experience,[49] we used a composition that was derived from classical liposomes, which typically consist exclusively of cholesterol and egg phosphatidyl choline (EPC) in a ratio of 45:55. From this model composition, a cholesterol fraction of 5 mol % was substituted with the lipid–polymer amphiphiles, as was previously described to provide suitable steric stabilization and a prolonged circulation time in the bloodstream.[56] Some characteristics of the compounds and corresponding liposomal preparations are given in Table 1. Because inhomogeneity was reported to occur for certain lipid compositions and preparation techniques,[56] we verified by ^{1}H NMR (Supporting Figure S7) that the molar lipid fractions χ are stable throughout the purification process, and concluded that the deployed lipids are homogeneously integrated in the liposomes.

In order to consume minimal amounts of test compounds while maintaining high entrapping efficiency, we developed a combination of small scale (~20 mg of lipid mixture) and high lipid content formulation (vesicular phospholipid gel, VPG). In suitable reaction tubes, lipid films were prepared first by evaporation of the ethanol in which the lipids were dissolved. These lipid films were supplemented with buffered aqueous cargo solution in a ratio of only ~2:3 (w/w). After addition of ceramic beads, the content was in-vial homogenized by DC, as detailed in the Materials and Methods section. From the resulting highly viscous VPG, liposomal preparations were obtained after dispersion in a suitable volume of aqueous buffer, typically in a 1:2 ratio.

As characterized by DLS and shown in Figure 2, the preparations exhibited z-average diameters in the range of 110–160 nm and can therefore be classified as small liposomes. Narrow size distributions were found, as indicated by PDIs (derived from cumulant analysis) of 0.1–0.2 (size distributions are listed in Supporting Figure S8), showing the potential of DC to prepare nanoscale vesicles with low polydispersity. Sizes
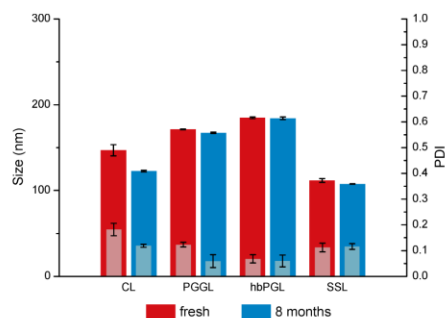
Figure 2. Stability of liposomal stock dispersions: Comparison of liposome z-average diameters directly after preparation (red) and after 8 months of storage at 4 °C (blue), both stored as stocks of diluted vesicular phospholipid gel. PDI values are given in gray bars; error bars indicate the standard deviation of three measurements.

and size distributions are in good agreement with the few examples of DC-liposomes reported before[49,50,57] and with cryo transmission electron micrographs prepared from liposome stock suspensions (Supporting Figure S4). Both of the alkyne-bearing liposomal preparations exhibit slightly higher diameters than CL and SSL preparations, presumably due to a higher steric demand of the polyglycerol chains on the inner lipid bilayer surface. To assess the long-term stability, the liposomal formulations were reevaluated by DLS after storage of highly concentrated stocks at 4 °C for 8 months. Importantly, the comparison of size distribution and PDI, as given in Figure 2, revealed no significant alterations upon extended storage.

Typical entrapping efficiencies (EE) in the range of 50% were determined from the amount of encapsulated calcein, a widely used fluorescent dye to measure encapsulation.[58] Table S9 shows details of EE for the four liposomal formulations CL, PGGL, hbPGL, and SSL. The higher EE of both polyglycerol-based liposomes might be an indication, that the interstitial space between liposomes, whose aqueous volume contains the nonentrapped cargo, is blocked by flexible portions of the hyperbranched surface structures.

DC is a rather novel preparation technique for liposomes, and while applications are still rare in the literature, previous reports and our own data provide consistent evidence that DC reliably produces liposomes of well-defined size with a shelf life of several months.[43] In summary, based on a number of parameters including the amount of starting material, size distribution, encapsulation efficiency, and shelf life, DC-formulation offers a competitive alternative to conventional formulation techniques. The advantages of DC are of paramount importance, especially in the case of testing novel polymeric amphiphiles, when only small amounts are available for the liposome preparation. Some of the preparations described above were successfully scaled down to a lipid mass in the single digit milligram scale. Furthermore, the small volumes of the aqueous phase permit working with highly concentrated solutions of expensive payload. In combination with the low interstitial volume in the resulting VPG, high encapsulation efficiencies are promoted, even when membrane permeating cargo equilibrates between volumes inside and outside the liposomes.[59]

Functionalization of Liposomes. Functionalization of terminal alkyne groups on the surface of liposomes was carried out via the copper(I)-catalyzed azide alkyne Huisgen-like cycloaddition (CuAAC) with aliquots of the preparations described above. Typically, an aliquot of 5 μL of a liposome preparation, representing about 1/20 of each of the preparations, was functionalized with azide-derivatives of the commercially available fluorophores Atto 488, Alexa 594, or a combination of both (structures are provided in Figure S10). After purification of liposomes via GPC, successful covalent conjugation was verified by fluorescence spectrometry measurements of fractions, resulting in a chromatogram as shown exemplarily in Figure 3A. Fluorescence intensity chromato-
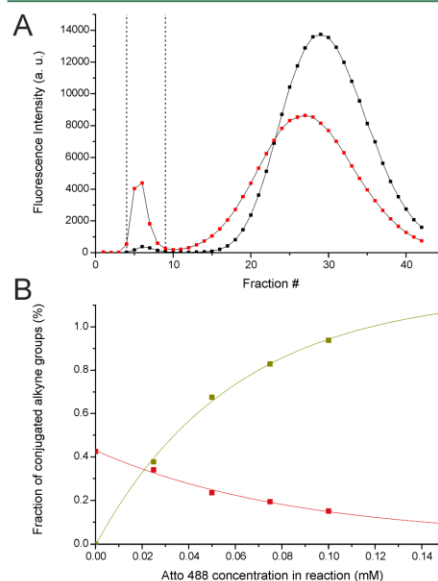
Figure 3. (A) Gel permeation chromatogram of liposome formulation hbPGL, both CuAAC-derivatized with Atto 488 azide (red) and a negative control without Cu^{II} and sodium ascorbate (black). Liposomes are contained in the exclusion limits (fractions 4−9, dotted lines, residual free dye after fraction 15). (B) Saturation of liposomal surface alkyne moieties with CuAAC conjugated azide dyes.

grams show peaks in the range of the void volume, indicating the presence of successfully labeled liposomes, and peaks at higher retention times accounting for residual free dye. A potential unspecific adsorption on the liposomal surface was excluded by a control experiment, in which copper ions and sodium ascorbate were omitted. The absence of a fluorescent peak in the void volume clearly shows that association of the dye with liposomes is contingent upon click conjugation in the presence of copper ions. This negative control was non-fluorescent only for the aforementioned, relatively hydrophilic dye azides, whereas in reactions with more lipophilic derivatives such as, e.g., Atto 590 and Atto 647N, fluorescence was also detected in the GPC void volume, presumably because the

more lipophilic molecules inserted into the lipophilic part of the liposome membranes or formed high molecular weight aggregates (data not shown). In a titration experiment designed to optimize the concentration of valuable dye reagent, conducted with increasing concentrations of Atto 488 azide (green dye), liposome labeling began to saturate around 0.1 mM. To assess remaining unreacted alkyne moieties at the liposomal surface, the resulting liposomes were submitted to a second round of click labeling with Alexa 594 azide (red dye) and a supplement of sodium ascorbate. The amount of thus immobilized red dye decreased correspondingly with increasing green dye coverage (Figure 3B). In a first reaction step, 5 μL of PGGL stock suspension were subjected to click reaction with Atto 488 azide in concentrations indicated on the x-axis, while free alkyne moieties were probed in a second step with a constant Alexa 594 azide concentration of 0.05 mM. Derived from fluorescence intensities, the fractions of theoretically available alkyne moieties that are conjugated to Atto 488 and Alexa 594 are indicated in green and red, respectively. The latter approaches saturation at about 1.2% of theoretically available alkyne moieties, as extrapolated from a monoexponential fit of the data points shown in Figure 3B. Since fluorescence values are virtually saturated at a dye concentration of about 0.5−1 mM, it appears that steric shielding and consequently restricted availability of alkyne groups is a limiting factor for maximum dye coverage rather than the number of incorporated alkyne moieties. In addition, alkyne moieties are present in excess, a fact that has been characterized as detrimental to Cu-THPTA catalysis.[51] The alkyne excess can be expected to be locally enhanced on liposomal surfaces, further compounding a decrease in reactivity.

We furthermore established an electrophoresis method as a fast reaction control to verify covalent conjugation of dye azide to the cholesterol−polymer compounds. Dye conjugates clearly separated from unreacted free dye after brief electrophoresis in a 0.2% agarose gel (Supporting Figure S11). This method is adequate for monitoring the reaction progress of liposomal click derivatization as well as the efficient separation of liposomes from unreacted dye by GPC.

In order to estimate the number of fluorophores per liposome, the liposome concentration was approximated from the EE and the hydrodynamic radii by the method of Pidgeon et al.[52] Liposomes were approximated to be unilamellar, which is supported to a certain extend by cryo transmission electron micrographs (Supporting Figure S4), although a small fraction of liposomes proved to be multilamellar. Taking into account the fluorescence of liposome fractions, the number of fluorophores per liposome was determined to match approximately 350−450 fluorophore molecules per liposome, depending on the specific formulation and the azide used. Repeated characterization by DLS (Figure 4) of both liposome formulations bearing alkyne residues before and after derivatization did not show any substantial variations in liposome size and polydispersity, confirming that the click reaction postformulation did not significantly alter these specific properties.

Our proof-of-principle is one of very few examples of postpreparational click functionalization of liposomes,[60−62] although the concept is certainly highly attractive given the ever growing number of available azide compounds for CuAAC. Reliable characterization and reaction control are major obstacles and currently represent a rate limiting step in the development of this concept. We have used fluorescence as
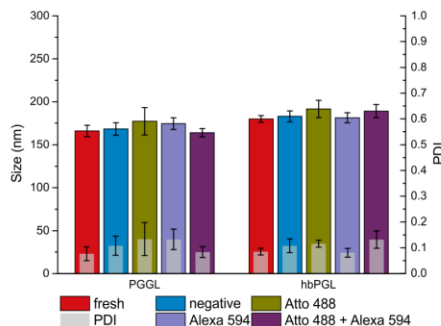
Figure 4. Influence of surface functionalization on z-average diameters and PDI (light gray) of freshly prepared liposomes PGGL and hbPGL (red) and after click reaction with Atto 488 azide (green), Alexa 594 azide (light purple), Atto 488 azide and Alexa 594 azide (dark purple), as well as the negative control without copper (blue). Error bars indicate standard deviations of three technical replicates and three measurements in the DLS experiment.

a highly sensitive detection method with short turnaround time for verification of the attachment of the azide moiety by CuAAC. While analytical characterization via NMR or vibrational spectroscopy could provide structural information, both are not applicable to single digit microgram amounts of fluorophore. Fluorescence spectroscopy outmatches both methods in sensitivity and is therefore an adequate analytical tool for DC. With the applicability of fluorescence-based analysis now outlined, we find it likely that future surface decorations will employ trifunctional molecules containing a fluorophore in addition to the azide and a targeting structure for selective cellular uptake.

On-Liposome FRET. The described postpreparational functionalization is a first approach toward the simultaneous conjugation of two types of fluorophores on the polymer layer. To confirm the coexistence of both fluorophores on liposomes, we made use of FRET, which is widely applied for probing spatial proximity of a so-called förster pair of communicating fluorophores in a distance range around 5 nm.[63,64] In addition to confirming colocalization, a FRET signal can also be exploited to monitor the integrity of nanoscale objects, since its structural disintegration can be monitored as a breakdown of the FRET intensity. To this end, liposomes were labeled with both fluorophores (Ccompare Figure 3). The resulting preparation exhibited fluorescence emission in the range of the specific emission maximum of Atto 488 upon selective excitation at 488 nm. Similarly, characteristic Alexa 594 emission was observed upon excitation at 590 nm. In addition, a substantial emission of Alexa 594 was measured upon excitation of Atto 488. As the two dyes are both immobilized in the spatially restricted common surface of liposomes, we assumed this additional fluorescence to be the result of FRET, and conducted control experiments for verification. This included in particular control measurements of aliquots of the same material, in which the liposomes had been destroyed to abrogate the spatial proximity of the two communicating fluorophores. A disintegration of the liposomal structures by addition of the detergent Triton-X (Figure 5) or of isopropanol (data not shown) resulted in a depletion of the FRET-caused
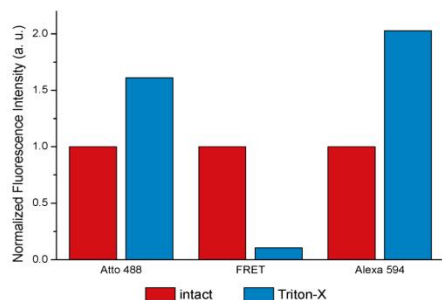
Figure 5. FRET-loss: Relative fluorescence intensities of liposomes PGGL labeled with both donor (Atto488) and acceptor dye (Alexa 594), measured in PBS (red) and PBS-Triton-X 0.5% (blue). In each channel (Atto 488, FRET and Alexa 594), emission intensities were normalized to the emission intensity measured in PBS, assuming liposomes to be intact. Both emission intensities were corrected against donor bleed through and acceptor cross excitation estimated from single-labeled liposomes.

fluorescence. While the disintegration in a solution of Triton-X leads to a boost of the emission intensities in both acceptor and donor channel, the intensity of a FRET-caused emission decreases substantially (compare Supporting Figure S6), strongly suggesting an increased spatial distance of the involved fluorophores. Further control measurements (see the Materials and Methods section) accounted for the effects of detergent or solvent on the spectral properties of both dyes. The statistical distance between two alkyne-bearing polymer structures was gauged from the average liposome surface (obtained from the liposome hydrodynamic radius) and the headgroup areas of cholesterol and EPC[65] and thus estimated to be in the range of 4 nm. Considering that typical Förster radii of structurally and spectrally related dyes are in the order of ∼50 Å (e.g., 54 Å for Alexa 488/Alexa 594[63]), approximately 8 alkyne-polymer lipids were to be expected in sufficient proximity. Taking into account an average number of 400 fluorophores per liposome, our observation of a FRET between dyes is consistent with their covalent immobilization on a common liposomal surface. This approach allowed for monitoring the success of the CuAAC reaction as well as the disintegration of the liposomes in the cuvette, and might be further optimized toward a tool to measure the integrity in vitro.

Cell Uptake Experiments. In order to assess the mode of interaction of the novel liposomal structures with cells, cell culture experiments with liposomal formulations carrying surface-clicked dyes were performed. RBE4 cells (rat brain endothelial cells)[53] were incubated with liposomes function-
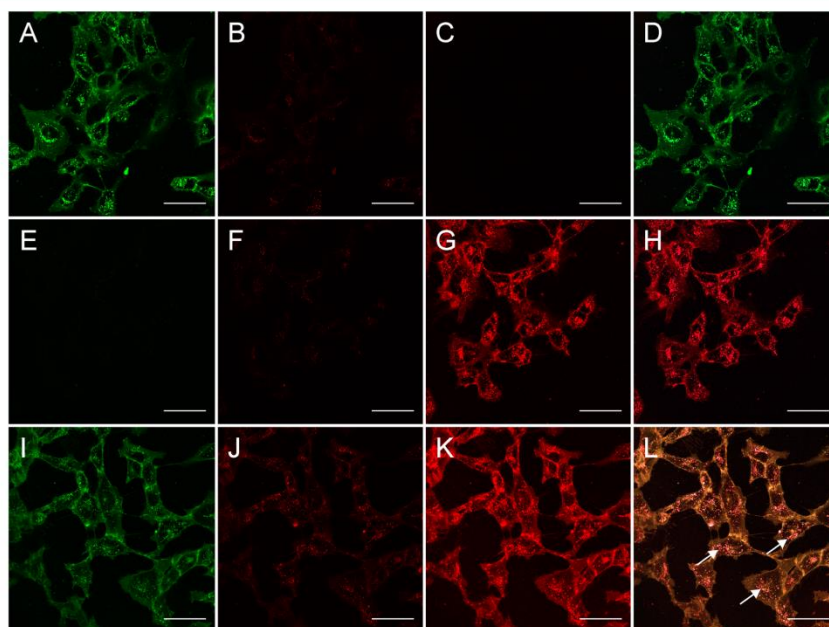
Figure 6. RBE4 cell incubation. Fluorescence micrographs of RBE4 cells, incubated with functionalized derivatives of liposome PGGL for 4 h. Columns [A,E,I], [B,F,J], [C,G,K] and [D,H,L] show channels for detection of the donor dye (Atto 488), FRET, acceptor dye (Alexa 594) and a merge of both donor and acceptor emission, respectively. Rows 1–3: RBE4 cells incubated with donor- (A–D), acceptor- (E–H) and both donor- and acceptor- (I–L) functionalized liposomes. Scale bars: 50 μm.

alized with either Atto 488, Alexa 594, or both fluorophores, and subjected to confocal laser scanning microscopy (CLSM). After 4 h, cells exhibited a substantial membrane fluorescence as well as a high fluorescence intensity of intracellular vesicles (Figure 6, white arrows). Substantial emission can be observed in the FRET channel [J] of the double-labeled liposome, although intensities are not corrected against acceptor cross excitation or donor bleed through. Red emission intensity upon excitation of the green dye was significantly higher in FRET samples than in either donor-only samples or acceptor-only samples, confirming that the red emission arose from FRET rather than from donor bleed through (Figure 6B) and acceptor cross excitation (Figure 6F). Furthermore, this was supported by data analysis of the FRET-caused emission as described by Hachet-Haas et al. (data not shown).[66]

Given the high intensity of the membrane fluorescence, which persisted after washing the cells with PBS, we investigated the time-scale of lipid uptake and intracellular distribution. Intense membrane fluorescence was observed already after 30 min incubation (Figure S12), followed by fluorescence of endocytic compartments and their membranes (Figure S13). The intracellular vesicles, which apparently formed during constitutional or induced endocytosis after membrane staining, were shown to exhibit membrane fluorescence without an intravesicular fluorescence. Further investigations revealed fast green membrane staining by Atto 488, while encapsulated cargo did no longer colocalize with the labeled amphiphile (Figure S14 and Movie S15). These observations support earlier reports,[48] but rather than a conventional endocytic uptake, the chronology of these observations implies a membrane integration process, which is known to be an additional mode of interaction.[67] Interestingly, the observed membrane staining suggests that a considerable fraction of lipid-polymer conjugate is introduced into the membrane. This is not expected *per se* for polymer-stabilized liposomal formulations, since cholesterol-based steric stabilization is described to lead to a certain inertness of the vesicles.[68] These results warrant further investigations of suitable lipophilic anchors and the role of lipophilic spacers between the cholesterol and the polymer chains, but they also show an interesting experimental approach to stain cell membranes and endosomal structures based on the newly developed hyperbranched compounds.[69]

CONCLUSIONS

Novel types of sterically stabilized liposomes featuring polyether-based multifunctional hyperbranched and clickable surface structures have been prepared by DC. We demonstrate liposome preparation via DC with very low lipid amounts on the 20 mg scale with very high concentrations of about 500 mg/mL, while the payload is dissolved in volumes as small as ~30 µL. Encapsulation efficiencies in the range of 50% were obtained for the investigated lipid compositions, which are competitive values for the entrapment of a highly hydrophilic cargo. The prepared alkyne-bearing polymer-coated liposomes were functionalized in a postpreparational approach via CuAAC. The use of Atto 488 and Alexa 594 in a simultaneous derivatization allowed to demonstrate the occurrence of FRET on the liposomal surface. This dual labeling also facilitated studying cellular uptake and intracellular distribution of the new compounds employed here. *hb*PG and related compounds were shown to readily fuse with cellular membranes, allowing the imaging of both cellular and endosomal membranes.

The work presented here is clearly an initial exploration concerning the application of DC to new polymeric amphiphiles, but demonstrates the substantial benefits allowing to test rationally designed polymer architectures in microscales. Tailored polyether lipids are promising candidates for a versatile strategy toward multifunctional liposomes, bearing a variety of targeting ligands to exploit synergistic effects.

ASSOCIATED CONTENT

⑤ Supporting Information

Further NMR and FT-IR characterization, cryo-transmission electron micrographs, calculation details, fluorescence spectra, DLS data, encapsulation efficiency data, fluorophore structures, agarose gel images, CLSM micrographs and live cell movies are presented. This material is available free of charge via the Internet at http://pubs.acs.org.

AUTHOR INFORMATION

Corresponding Author

*Mailing address: Institute of Pharmacy and Biochemistry, Johannes Gutenberg-University Mainz, Mainz, Germany, Staudingerweg 5, D-55128 Mainz, Germany. Phone +49-6131-3925731; fax +49-6131-3920373; e-mail: mhelm@uni-mainz.de.

Notes

The authors declare no competing financial interest.

REFERENCES

(1) Zhang, L.; Gu, F. X.; Chan, J. M.; Wang, A. Z.; Langer, R. S.; Farokhzad, O. C. *Clin. Pharmacol. Ther.* **2008**, *83*, 761–9.
(2) Maeda, H.; Seymour, L. W.; Miyamoto, Y. *Bioconjugate Chem.* **1992**, *3*, 351–62.
(3) Maeda, H.; Matsumura, Y. *Crit. Rev. Ther. Drug Carrier Syst.* **1989**, *6*, 193–210.
(4) Matsumura, Y.; Maeda, H. *Cancer Res.* **1986**, *46*, 6387–92.
(5) Yuan, F.; Dellian, M.; Fukumura, D.; Leunig, M.; Berk, D. A.; Torchilin, V. P.; Jain, R. K. *Cancer Res.* **1995**, *55*, 3752–6.
(6) Alley, S. C.; Okeley, N. M.; Senter, P. D. *Curr. Opin. Chem. Biol.* **2010**, *14*, 529–37.
(7) Lewis Phillips, G. D.; Li, G.; Dugger, D. L.; Crocker, L. M.; Parsons, K. L.; Mai, E.; Blättler, W. a; Lambert, J. M.; Chari, R. V. J.; Lutz, R. J.; Wong, W. L. T.; Jacobson, F. S.; Koeppen, H.; Schwall, R. H.; Kenkare-Mitra, S. R.; Spencer, S. D.; Sliwkowski, M. X. *Cancer Res.* **2008**, *68*, 9280–90.
(8) Lambert, J. M. *Curr. Opin. Pharmacol.* **2005**, *5*, 543–9.
(9) Casi, G.; Neri, D. *J. Controlled Release* **2012**, *161*, 422–8.
(10) Yamazaki, N.; Kojima, S.; Bovin, N. V.; André, S.; Gabius, S.; Gabius, H.-J. *Adv. Drug Delivery Rev.* **2000**, *43*, 225–244.
(11) Stein, M. *J. Exp. Med.* **1992**, *176*, 287–292.

Biomacromolecules

(12) Low, P. S.; Henne, W. A.; Doorneweerd, D. D. *Acc. Chem. Res.* **2008**, *41*, 120−9.

(13) Ng, E. W. M.; Shima, D. T.; Calias, P.; Cunningham, E. T.; Guyer, D. R.; Adamis, A. P. *Nat. Rev. Drug Discovery* **2006**, *5*, 123−32.

(14) Moses, J. E.; Moorhouse, A. D. *Chem. Soc. Rev.* **2007**, *36*, 1249−62.

(15) Lee, R. J.; Low, P. S. *Biochim. Biophys. Acta, Biomembr.* **1995**, *1233*, 134−144.

(16) Blessing, T.; Kursa, M.; Holzhauser, R.; Kircheis, R.; Wagner, E. *Bioconjugate Chem.* **2001**, *12*, 529−37.

(17) Allen, T. M.; Brandeis, E.; Hansen, C. B.; Kao, G. Y.; Zalipsky, S. *Biochim. Biophys. Acta, Biomembr.* **1995**, *1237*, 99−108.

(18) Meng, F.; Engbers, G. H. M.; Feijen, J. *J. Controlled Release* **2005**, *101*, 187−98.

(19) Uster, P. S.; Allen, T. M.; Daniel, B. E.; Mendez, C. J.; Newman, M. S.; Zhu, G. Z. *FEBS Lett.* **1996**, *386*, 243−6.

(20) Bangham, A. D.; Standish, M. M.; Watkins, J. C. *J. Mol. Biol.* **1965**, *13*, 238−IN27.

(21) Kulkarni, S. B.; Betageri, G. V.; Singh, M. *J. Microencapsul.* **1995**, *12*, 229−46.

(22) Madden, T. D.; Harrigan, P. R.; Tai, L. C.; Bally, M. B.; Mayer, L. D.; Redelmeier, T. E.; Loughrey, H. C.; Tilcock, C. P.; Reinish, L. W.; Cullis, P. R. *Chem. Phys. Lipids* **1990**, *53*, 37−46.

(23) Haran, G.; Cohen, R.; Bar, L. K.; Barenholz, Y. *Biochim. Biophys. Acta* **1993**, *1151*, 201−15.

(24) Schroit, A. J.; Fidler, I. J. *Cancer Res.* **1982**, *42*, 161−7.

(25) Kirjavainen, M.; Urtti, A.; Jääskeläinen, I.; Marjukka Suhonen, T.; Paronen, P.; Valjakka-Koskela, R.; Kiesvaara, J.; Mönkkönen, J. *Biochim. Biophys. Acta - Lipids Lipid Metab.* **1996**, *1304*, 179−189.

(26) Kleusch, C.; Hersch, N.; Hoffmann, B.; Merkel, R.; Csiszár, A. *Molecules* **2012**, *17*, 1055−73.

(27) Maier, O.; Oberle, V.; Hoekstra, D. *Chem. Phys. Lipids* **2002**, *116*, 3−18.

(28) Massing, U.; Fuxius, S. *Drug Resist. Updates* **2000**, *3*, 171−177.

(29) Olson, F.; Hunt, C. a; Szoka, F. C.; Vail, W. J.; Papahadjopoulos, D. *Biochim. Biophys. Acta* **1979**, *557*, 9−23.

(30) Saunders, L.; Perrin, J.; Gammack, D. *J. Pharm. Pharmacol.* **1962**, *14*, 567−572.

(31) Kim, S.; Turker, M. S.; Chi, E. Y.; Sela, S.; Martin, G. M. *Biochim. Biophys. Acta, Biomembr.* **1983**, *728*, 339−348.

(32) Pons, M.; Foradada, M.; Estelrich, J. *Int. J. Pharm.* **1993**, *95*, 51−56.

(33) Talsma, H.; Özer, A. Y.; van Bloois, L.; Crommelin, D. J. A. *Drug Dev. Ind. Pharm.* **1989**, *15*, 197−207.

(34) Brandl, M.; Bachmann, D.; Drechsler, M.; Bauer, K. H. *Drug Dev. Ind. Pharm.* **1990**, *16*, 2167−2191.

(35) Poste, G.; Bucana, C.; Raz, A.; Bugelski, P.; Kirsh, R.; Fidler, I. J. *Cancer Res.* **1982**, *42*, 1412−22.

(36) Papahadjopoulos, D.; Allen, T. M.; Gabizon, A.; Mayhew, E.; Matthay, K.; Huang, S. K.; Lee, K. D.; Woodle, M. C.; Lasic, D. D.; Redemann, C. *Proc. Natl. Acad. Sci. U. S. A.* **1991**, *88*, 11460−4.

(37) Torchilin, V. P.; Levchenko, T. S.; Whiteman, K. R.; Yaroslavov, A. A.; Tsatsakis, A. M.; Rizos, A. K.; Michailova, E. V.; Shtilman, M. I. *Biomaterials* **2001**, *22*, 3035−44.

(38) Torchilin, V. P.; Shtilman, M. I.; Trubetskoy, V. S.; Whiteman, K.; Milstein, A. M. *Biochim. Biophys. Acta* **1994**, *1195*, 181−4.

(39) Maruyama, K.; Okuizumi, S.; Ishida, O.; Yamauchi, H.; Kikuchi, H.; Iwatsuru, M. *Int. J. Pharm.* **1994**, *111*, 103−107.

(40) Romberg, B.; Oussoren, C.; Snel, C. J.; Hennink, W. E.; Storm, G. *Pharm. Res.* **2007**, *24*, 2394−401.

(41) Allen, T. M.; Chonn, A. *FEBS Lett.* **1987**, *223*, 42−6.

(42) Wilms, D.; Stiriba, S.-E.; Frey, H. *Acc. Chem. Res.* **2010**, *43*, 129−41.

(43) Lee, C. C.; MacKay, J. A.; Fréchet, J. M. J.; Szoka, F. C. *Nat. Biotechnol.* **2005**, *23*, 1517−26.

(44) Müller, S. S.; Dingels, C.; Hofmann, A. M.; Frey, H. *Tailored Polymer Architectures for Pharmaceutical and Biomedical Applications*; Scholz, C.; Kressler, J., Eds.; ACS Symposium Series; American Chemical Society: Washington, DC, 2013; Vol. *1135*, pp 11−25.

(45) Wurm, F.; Nieberle, J.; Frey, H. *Macromolecules* **2008**, *41*, 1184−1188.

(46) Hofmann, A. M.; Wurm, F.; Frey, H. *Macromolecules* **2011**, *44*, 4648−4657.

(47) Hofmann, A. M.; Wurm, F.; Hühn, E.; Nawroth, T.; Langguth, P.; Frey, H. *Biomacromolecules* **2010**, *11*, 568−74.

(48) Schöps, R.; Amado, E.; Müller, S. S.; Frey, H.; Kressler, J. *Faraday Discuss.* **2013**, *166*, 303−315.

(49) Massing, U.; Cicko, S.; Ziroli, V. *J. Controlled Release* **2008**, *125*, 16−24.

(50) Hirsch, M.; Ziroli, V.; Helm, M.; Massing, U. *J. Controlled Release* **2009**, *135*, 80−8.

(51) Hong, V.; Presolski, S. I.; Ma, C.; Finn, M. G. *Angew. Chem., Int. Ed. Engl.* **2009**, *48*, 9879−83.

(52) Pidgeon, C.; Hunt, C. a *J. Pharm. Sci.* **1981**, *70*, 173−6.

(53) Roux, F.; Durieu-Trautmann, O.; Chaverot, N.; Claire, M.; Mailly, P.; Bourre, J. M.; Strosberg, A. D.; Couraud, P. O. *J. Cell. Physiol.* **1994**, *159*, 101−13.

(54) Kolb, H. C.; Finn, M. G.; Sharpless, K. B. *Angew. Chem., Int. Ed. Engl.* **2001**, *40*, 2004−2021.

(55) Kainthan, R. K.; Janzen, J.; Levin, E.; Devine, D. V.; Brooks, D. E. *Biomacromolecules* **2006**, *7*, 703−9.

(56) Allen, T. M.; Hansen, C.; Martin, F.; Redemann, C.; Yau-Young, A. *Biochim. Biophys. Acta, Biomembr.* **1991**, *1066*, 29−36.

(57) Adrian, J. E.; Wolf, A.; Steinbach, A.; Rössler, J.; Süss, R. *Pharm. Res.* **2011**, *28*, 2261−72.

(58) Jousma, H.; Talsma, H.; Spies, F.; Joosten, J. G. H.; Junginger, H. E.; Crommelin, D. J. a. *Int. J. Pharm.* **1987**, *35*, 263−274.

(59) Moog, R.; Burger, a. M.; Brandl, M.; Schüler, J.; Schubert, R.; Unger, C.; Fiebig, H. H.; Massing, U. *Cancer Chemother. Pharmacol.* **2002**, *49*, 356−66.

(60) Cavalli, S.; Tipton, A. R.; Overhand, M.; Kros, A. *Chem. Commun. (Camb).* **2006**, 3193−5.

(61) Said Hassane, F.; Frisch, B.; Schuber, F. *Bioconjugate Chem.* **2006**, *17*, 849−54.

(62) Tarallo, R.; Accardo, A.; Falanga, A.; Guarnieri, D.; Vitiello, G.; Netti, P.; D'Errico, G.; Morelli, G.; Galdiero, S. *Chemistry* **2011**, *17*, 12659−68.

(63) Schuler, B.; Lipman, E. A.; Eaton, W. A. *Nature* **2002**, *419*, 743−7.

(64) Järve, A.; Müller, J.; Kim, I.-H.; Rohr, K.; MacLean, C.; Fricker, G.; Massing, U.; Eberle, F.; Dalpke, A.; Fischer, R.; Trendelenburg, M. F.; Helm, M. *Nucleic Acids Res.* **2007**, *35*, e124.

(65) Zidovska, A.; Evans, H. M.; Ahmad, A.; Ewert, K. K.; Safinya, C. R. *J. Phys. Chem. B* **2009**, *113*, 5208−16.

(66) Hachet-Haas, M.; Converset, N.; Marchal, O.; Matthes, H.; Gioria, S.; Galzi, J.-L.; Lecat, S. *Microsc. Res. Technol.* **2006**, *69*, 941−56.

(67) Lakkaraju, A.; Rahman, Y. Y.-E.; Dubinsky, J. J. M. *J. Biol. Chem.* **2002**, *277*, 15085−92.

(68) Beugin, S.; Edwards, K.; Karlsson, G.; Ollivon, M.; Lesieur, S. *Biophys. J.* **1998**, *74*, 3198−210.

(69) Carrion, C.; Domingo, J. C.; de Madariaga, M. A. *Chem. Phys. Lipids* **2001**, *113*, 97−110.

A.5 Cytotoxycity and Chemosensitizing Activity of Amphiphilic Poly(glycerol)-Poly(alkylene oxide) Block Copolymers

Tatiana V. Demina,[†] *Olga A. Budkina,*[†] *Gennadii A. Badun,*[†] *Nickolay S. Melik-Nubarov,*[†] *Holger Frey,*[‡] *Sophie S. Müller,*[‡] *Jörg Nieberle,*[‡] *and Irina D. Grozdova*[*,†]

[†]Chemistry Department, Lomonosov Moscow State University, Vorobiovy Gory, Moscow 119991, Russia

[‡]Institute of Organic Chemistry, Johannes Gutenberg-University, Duesbergweg 10-14, 55128 Mainz, Germany

Cytotoxicity and Chemosensitizing Activity of Amphiphilic Poly(glycerol)−Poly(alkylene oxide) Block Copolymers

Tatiana V. Demina,[‡] Olga A. Budkina,[†] Gennadii A. Badun,[†] Nickolay S. Melik-Nubarov,[†] Holger Frey,[‡] Sophie S. Müller,[‡] Jörg Nieberle,[‡] and Irina D. Grozdova*[,†]

[†]Chemistry Department, Lomonosov Moscow State University, Vorobiovy Gory, Moscow 119991, Russia

[‡]Institute of Organic Chemistry, Johannes Gutenberg-University, Duesbergweg 10-14, 55128 Mainz, Germany

ABSTRACT: All polymeric chemosensitizers proposed thus far have a linear poly(ethylene glycol) (PEG) hydrophilic block. To testify whether precisely this chemical structure and architecture of the hydrophilic block is a prerequisite for chemosensitization, we tested a series of novel block copolymers containing a hyperbranched polyglycerol segment as a hydrophilic block (PPO-NG copolymers) on multi-drug-resistant (MDR) tumor cells in culture. PPO-NG copolymers inhibited MDR of three cell lines, indicating that the linear PEG can be substituted for a hyperbranched polyglycerol block without loss of the polymers' chemosensitizing activity. The extent of MDR reversal increased with the polymers affinity toward the cells and the expression level of P-glycoprotein. In contrast with Pluronic L61, which increases viability of tumor cells in the absence of drugs, PPO-NG chemosensitizers are completely devoid of this property undesired in cancer therapy, making them promising candidates for application as novel MDR reversal agents.
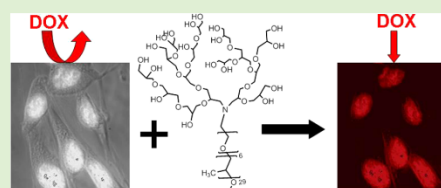
■ INTRODUCTION

Multi-drug resistance (MDR) of tumor cells to structurally and functionally unrelated cytotoxic agents is one of the major current obstacles of cancer chemotherapy. Different mechanisms of MDR elucidated to date include alterations in cell cycle, failure of apoptotic mechanisms, repair of damaged cellular targets, and reduced drug accumulation.[1] The latter is often associated with the overexpression of the MDR1-encoding 170 kDa integral membrane protein, P-glycoprotein (P-gp), a member of a large ATP-binding cassette family.[2,3] P-gp acts as an energy-dependent efflux pump for a broad spectrum of natural products and synthetic chemotherapeutic agents.[4,5] The main function of P-gp is cell protection from injuring effects of xenobiotics, including many anticancer drugs. Overexpression of P-gp in cancer cells is often the main cause of cell resistance to a wide range of drugs and as a consequence the undesired inefficiency of chemotherapy.

To overcome the resistance mediated by P-gp, numerous efforts have been aimed at suppressing its expression in tumor cells, for instance, by use of hammerhead ribozymes and interfering microRNAs targeted against the MDR1 gene.[6−8] Alternative strategies target an increase in intracellular drug accumulation by inhibition of P-gp activity with resistance reversing agents (chemosensitizers).[9] P-gp activity can be reduced by amphiphilic nonionic polyethoxylated surfactants such as Tween-80, Cremophor EL (polyethoxylated castor oil),[10] and Solutol HS15.[11] Special attention in this area was paid to uncharged nonionic amphiphilic triblock copolymers of ethylene oxide (EO) and propylene oxide (PO) of a general formula EO_n-PO_m-EO_n, known under trade names Pluronics,

Synperonics, or Poloxamers. The in vivo studies have demonstrated that these synthetic amphiphiles are tissue-compatible, nonimmunogenic, and less toxic than low-molecular-mass surfactants.[12] Experiments in vitro showed that some Pluronics, such as P85, can completely inhibit MDR of tumor cells growing in culture.[13,14]

The chemosensitizing activity of Pluronics depends on their chemical structure, as shown by Batrakova et al., who revealed a correlation between the hydrophilic−lipophilic balance (HLB) of Pluronics and their efficacy in MDR reversal.[13] This issue was also studied in more detail in our previous work, in which we described the relationship between the structure of a copolymer and its ability to affect properties of model lipid membranes (liposomes).[15] Using a broad range of amphiphiles with different chemical structure and composition, we had shown that the ability to accelerate flip-flop of lipids and permeation of antitumor drug doxorubicin (DOX) into liposomes was determined by the van der Waals volume of their hydrophobic block.[15] More than 30 structurally related copolymers with diblock and triblock architectures containing different hydrophobic blocks and poly(ethylene glycol) (PEG) as the common hydrophilic unit have been analyzed regarding cytotoxicity and their influence on the P-gp efflux pump.[16] Meanwhile, less is known about the role of hydrophilic blocks in polymer−cell interaction. All surfactants and polymeric chemosensitizers proposed thus far have one common

structural feature: their hydrophilic block consists of a linear PEG.[10,13,14,17] However, it is unknown if precisely this chemical structure and architecture of the hydrophilic block is a prerequisite for chemosensitizing activity and other biological effects of amphiphilic block copolymers.

To clarify these issues, we tested a series of novel block copolymers of alkylene oxide and polyglycerol (PPO-NG copolymers) containing a hyperbranched polyglycerol segment as a hydrophilic block[18] on cells in culture. Their biological effects were compared with those of Pluronic L61, bearing the linear PEG hydrophilic blocks, and verapamil, a known P-gp inhibitor.[19] To verify, whether cytotoxicity and chemosensitiz-ing properties of PPO-NG copolymers depend on the nature of the cells and the expression level of P-gp, the copolymers were examined on drug-sensitive and MDR cell lines differing in their origin (epithelial-like MCF7/R cells, erythroleukemic K562/R, and K562/i-S9 cells), the way of resistance acquisition (selection or infection) and resistance level.

■ EXPERIMENTAL SECTION

Materials. Jeffamine M-2005 (PPO-NH$_2$) was obtained from Huntsman. Glycidol was distilled prior to polymerization. 1,1,1,-Tris(hydroxymethyl)propane (TMP) and vincristine sulfate were purchased from Fluka. DOX was purchased from Lense-Pharm (Russia). Pluronic L61 was obtained from Serva (Germany) and used without further purification. Verapamil hydrochloride, 3-(4,5-dimethyl-2-thiazolyl)-2,5-diphenyltetrazolium bromide (MTT), Dulbecco's phosphate-buffered saline (PBSD) and monoclonal anti-P-glycopro-tein clone F4Mouse Ascites Fluid, product no. P 7965, antibodies of mouse IgG1 isotype were purchased from Sigma-Aldrich. Cell culture media and trypsin-free versene solution were obtained from PanEco (Russia). Human leukemia cell line K562, human breast carcinoma cell line MCF7, and their drug-resistant sublines, K562/i-S9 and MCF7/R, were kindly provided by Prof. A. A. Shtil (Blokhin Cancer Research Centre, Moscow, Russia). The resistant K562/R cells were a gift of Prof. A. N. Saprin (Institute of Chemical Physics, Moscow, Russia).

Methods. *PPO-NG Copolymers.* PPO-NG copolymers were synthesized according to the literature.[20,21] All polymers were characterized by ^{1}H NMR spectroscopy (300 MHz, D$_2$O or MeOD) and size exclusion chromatography (SEC, PEG standards). A good agreement between the theoretical and experimental molecular weights could be observed. Polydispersity indices (M_w/M_n) were rather low and ranged between 1.2 and 1.4. Yields were between 70 and 95% depending on the molecular weights of the respective block copolymer.

Cell Cultures. Five human cell lines have been used in this study. Two of them were drug-sensitive and different in their origin: human leukemia cell line K562 established from a patient with chronic myelogeneous leukemia in blast transformation[22] and epithelial-like adhesive human breast adenocarcinoma cells MCF7 isolated from the pleural effusion of a 69-year-old Caucasian woman with metastatic mammary.[23] Three resistant sublines were derived from these two parental cell lines. One of them, the K562/i-S9 cell line, was produced by infection of K562 cells with a recombinant retrovirus carrying human MDR1 cDNA followed by subcloning (without cytotoxic selection).[24] Two others, K562/R[25] and MCF7/R, had been obtained after long-time culturing of K562 and MCF7 cells with increasing amounts of either vincristine or DOX, respectively.

K562, K562/i-S9, and K562/R cells grew in suspension in RPMI 1640 medium, with 10% of heat-inactivated fetal bovine serum (Gibco), 2 mM glutamine, and 50 mg/L gentamycin. The adhesive epithelial-like MCF7 and MCF7/R cells were maintained in Dulbecco's modified Eagle's medium (DMEM) containing 10% of fetal bovine serum, 4 mM glutamine, 100 μg/mL streptomycin, and 100 units/mL penicillin. The cells were grown in the incubator (NAPCO, USA) at 37 °C and 95% humidity in the atmosphere of 95% air and 5% CO$_2$. All cell lines were routinely examined for mycoplasma and other DNA-containing organisms using 4',6-diamidino-2-phenyl-indole dihydrochloride (Invitrogen), according to manufacturer's instructions. Only uncontaminated cell cultures were used in the experiments. To maintain the resistance of K562/R and MCF7/R cells, we added 10 nM vincristine or 4 to 5 μg/mL DOX, respectively, to their culture medium once a month. The cells were used for experiments after at least three passages in the drug-free medium.

Cytotoxicity Test. The adhesive MCF7 and MCF7/R cells were detached with EDTA, seeded into 96-well flat-bottomed plates (Costar, Cambridge, MA) at a density of 3000−4000 cells/well, and kept overnight in the incubator to allow cell adhesion. K562, K562/i-S9, and K562/R cells growing in suspension were plated directly prior to the experiment. DOX stock solution in distilled water was prepared just before use, and its concentration was checked by absorbance at 490 nm ($\varepsilon = 10\,500$ M^{-1} cm^{-1}).[26] The copolymer stock solutions in distilled water were prepared under refrigeration (4 °C) and sterilized by filtration at 4 °C through a 0.2 μm pore size filter (Durapor, USA). The testing solutions containing a polymer, or DOX, or their mixtures were appropriately diluted in serum-free culture medium. The cells were treated with test samples, 0.2 mL/well, for 1 h in the CO$_2$ incubator. Controls were exposed to the serum-free medium without additives. All experimental points were run in triplicate. After incubation, the test solutions were replaced with the medium containing 10% serum, and the cells were maintained for an additional 3 days under standard conditions. To replace the media of cells growing in suspension, the plates were centrifuged using Sigma σ-15 culture centrifuge (Bioblock Scientific). Cell survival was evaluated with MTT assay.[27] In brief, 1 mg/mL MTT solution in DMEM or RPMI was added directly to the culture medium, 50 μL/well, and the reaction developed within 3 to 4 h at 37 °C in the CO$_2$-incubator. Then, the medium was aspirated, violet crystals of water-insoluble formazan were dissolved in 100 μL of dimethyl sulfoxide, and the absorbance at 550 nm was measured with microplate reader Multiscan (Titertek, USA). The percentage of surviving cells relative to the controls was plotted versus the concentrations of the tested compound and fitted with Logistic function using Origin 8.5 Software.

Tritium-Labeled Copolymers and Their Binding with MCF7/R Cells. The polymers were labeled with tritium, as previously described,[28] and purified from the exchangeable tritium by several ethanol dissolution−vacuum evaporation cycles. The material was further subjected to chromatography in ethanol on Sephadex LH-20 column (Amersham, USA), 1 × 18 cm. Specific radioactivity of tritium-labeled polymers varied from 19 to 49 Ci/mmol corresponding to average tritium content from 0.7 to 1.7 atoms per molecule. Tritium-labeled polymer was mixed with the corresponding unlabeled polymer, and their mixture was appropriately diluted with serum-free DMEM. Specific radioactivities of the mixtures were for 0.068, 0.57, and 0.126 Ci/mmol for Pluronic L61, PPO-NG2, and PPO-NG30 copolymers, respectively. About 0.4 millions of MCF7/R cells were seeded per well in 12-well plates (Greiner). The next day, they were incubated with appropriate amounts of tritium-labeled copolymers in 1 mL of serum-free DMEM supplemented with 20 mM HEPES buffer, pH 7.3, for 1 h at 37 °C in the CO$_2$ incubator. Then, the cell monolayers were carefully washed with PBSD (1 mL × 5) and lysed in 250 μL of 1 N NaOH (overnight). About 100 μL of the lysates was used for estimation of protein content according to Lowry method. These values were used for evaluation of the amount of cells in each sample using a calibration curve constructed in the same experiment. The amount of bound polymers was evaluated by measuring the radioactivity of the lysates with a Delta scintillation counter and was normalized per million of cells.

Western Blot Analysis of P-gp. MCF7 and MCF7/R cells were detached from a plastic culture flask with trypsin-free versene to avoid digestion of cell surface proteins. Thereafter, all cell cultures (K562, K562/i-S9, K562/R, MCF7, and MCF7/R) were treated in the same manner. 2−8 million cells per sample were washed twice with PBSD at 0 + 4 °C to remove serum proteins. A homogeneous cell suspension was made with a loosely fitted Dounce homogenizer, and 10 μL aliquots were picked out from each sample for protein determination in cell pellets by Lowry method. The rest of the cells were sedimented

Biomacromolecules   `Article`

Table 1. Molecular Characteristics of the Studied Block PPO-Based Copolymers

polymer	composition	M_n (g mol^{-1})	mass fraction of hydrophilic block (%)	CMC (μM)	MTC (μM)
Pluronic L61	EO$_2$PO$_{30}$EO$_2$	2000	9	11 ± 1	90 ± 10
		Polyglycerol-Based Block Copolymers			
PPO-NG2	PO$_{29}$EO$_6$-NG$_2$	2267	14	8 ± 1	10 ± 1
PPO-NG30	PO$_{29}$EO$_6$-NG$_{30}$	3600	46	45 ± 15	100 ± 20
PPO-NG76	PO$_{29}$EO$_6$-NG$_{76}$	7760	75	1000[18]	2800 ± 300
PPO-(NG2)$_2$	G$_2$N-PO$_{29}$EO$_6$-NG$_2$	2378	18	40 ± 10	13 ± 5
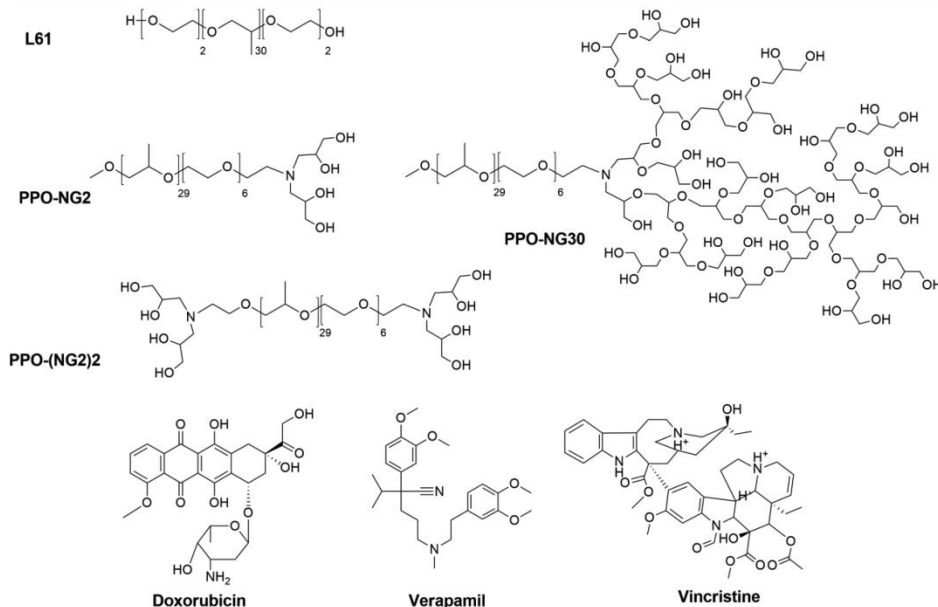
Figure 1. Chemical structures of Pluronic L61, polyglycerol-based block copolymers PPO-NG2, PPO-(NG2)$_2$, PPO-NG30, doxorubicin, verapamil, and vincristine.

and lysed by twice repeated freeze−thawing procedure in 10 mM Tris-HCl buffer, pH 7.4, containing 10 mM NaCl, 10 mM CaCl$_2$, 6 mM MgCl$_2$, 0.1% Triton X-100, 20 μg/mL DNAase, aprotinin, and leupeptin (10 μg/mL each) and 2 mM PMSF. The lysates were incubated with an equal volume of 2 × Laemmli loading buffer[29] for 30 min at 37 °C. Cellular proteins were resolved by SDS-electrophoresis in 7% polyacrylamide gel and electroblotted (4 h, 200 mA) onto a nitrocellulose membrane with 0.2 μm pore size using semidry technique (Multiphore II, LKB, Sweden). The membrane was incubated overnight in the blocking solution containing 100 mM Tris-HCl buffer, pH 8, 3% casein, 2% BSA, 0.25% gelatin, 0.05% Tween-20, and 0.9% NaCl and probed with primary mouse monoclonal anti-P-gp antibodies diluted 1:2000 with PBSD (1.5 h, 37 °C), followed by incubation with horseradish-peroxidase-labeled secondary antimouse IgG antibodies diluted 1:300 with PBSD containing 1 mg/mL of BSA (30 min, 37 °C). After each step, the membrane was washed with PBSD containing 0.05% Tween-20. Protein bands were visualized with peroxidase substrate, 0.15 mg/mL 3,3′,5,5′-tetramethylbenzidine (Sigma, USA), and their molecular weights were estimated using commercial standard markers with molecular weights of 94.6, 66.2, 45, 31, 21.5, and 14.4 kDa (low-molecular-weight markers, Helicon, Russia).

Critical Micelle Concentration. Critical micelle concentration (CMC) values of the polymers were estimated from the increase in the intensity of fluorescence of 1,6-diphenyl-1,3,5-hexatriene (DPH) (Reanal) resulting from its solubilization in the hydrophobic cores of micelles.[30] The experiments were performed as previously described.[31] In brief, a solution of DPH in acetone (10 mM) was diluted 1000-fold with PBSD, pH 7.3, and intensely stirred for ∼2 h until complete evaporation of the acetone. Equal volumes of thus prepared 10 μM DPH and the testifying solutions containing the polymer at different concentration in PBSD were mixed and incubated for 45−60 min at 37 °C. The fluorescence was measured with a Hitachi 650_10S spectrofluorometer (Japan) in a thermostated cuvette at 37 °C (λ_{ex} =366 nm and λ_{em} =433 nm). The CMC values were determined by the intercept of the straight line through the fluorescence at low polymer concentration with the straight line through the values of rapidly increasing fluorescence.

■ **RESULTS AND DISCUSSION**

Structure of Polyglycerol-Based Copolymers and Their Micellization. Amphiphilic polyglycerol-based block copolymers were synthesized by ring-opening polymerization
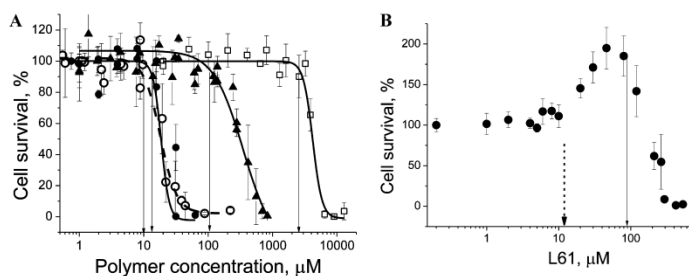
Figure 2. Cytotoxicity of block copolymers toward MCF7/R cells. Percentage of surviving cells determined by MTT-assay was plotted as a function of polymer concentration. MTC values are indicated by arrows. Average values obtained in two to three experiments are shown. (A) Cytotoxicity of PPO-NG2 (O, dashed line), PPO-(NG2)$_2$ (●), PPO-NG30 (▲), and PPO-NG76 (□). (B) Cell survival after treatment with Pluronic L61. The dotted arrow indicates CMC value of L61.

of glycidol, initiated by an end-functional linear random copolymer macroinitiator, composed of 29 repeat units of PO and 6 repeat units of EO.[20,21] The copolymers composition and molecular weights (M_n) (Table 1) were defined on the basis of NMR spectra.[15,21]

Using the random copolymer with one amino group, PO$_{29}$EO$_6$NH$_2$ (Jeffamine M-2005), resulted in the formation of an end-functionalized block copolymer containing two glycerol residues (PPO-NG2) (Figure 1). Its molecular weight and CMC value are comparable to those of Pluronic L61 (Table 1).

Under alkaline conditions, PPO-NG2 can be used as a macroinitiator in the slow monomer addition reaction of glycidol, resulting in diblock copolymers with a hyperbranched hydrophilic block. Two such diblock copolymers containing either 30 (PPO-NG30) (Figure 1) or 76 (PPO-NG76) glycerol repeat units (depending on the amount of glycidol) were synthesized via this "hypergrafting" process.[32,33]

To clarify the significance of block architecture of PPO-NG copolymers, we synthesized a triblock PPO-(NG2)$_2$ copolymer in the same manner as PPO-NG2. A random copolymer H$_2$NPO$_{29}$EO$_6$NH$_2$ with two terminal amino groups was used as the central hydrophobic block to form a triblock copolymer containing two glycerol moieties at each side of the polyalkylene oxide chain (PPO-(NG2)$_2$) (Figure 1), while its hydrophobic block was the same as that for the diblock PPO-NG copolymers.

In summary, all PPO-NG copolymers contained the same hydrophobic block PO$_{29}$EO$_6$, while their hydrophilic blocks composed of glycidol residues significantly varied in the extent of branching, thus giving rise to a set of di- and triblock copolymers with systematically varied molecular architecture.

CMC values of diblock copolymers increased from 8 μM (PPO-NG2) to 45 μM (PPO-NG30) and further to 1000 μM for PPO-NG76 (Table 1), in line with the amount of glycerol repeat units and therefore the hydrophilicity. According to this tendency, the CMC value of triblock copolymer PPO-(NG2)$_2$ containing only four glycerol repeat units was expected to be ∼15 μM. However, micellization of PPO-(NG2)$_2$ occurred at significantly higher concentration. Its CMC value equal to 40 ± 10 μM is nearly the same as that of the more hydrophilic PPO-NG30 (45 ± 15 μM) (Table 1). Probably, repulsive interactions between two ionizable amino groups in PPO-

(NG2)$_2$ molecule can impede micellization of the copolymer, thus increasing the CMC value.

Cytotoxicity. A key objective of the present work was to study whether PPO-NG copolymers were able to enhance DOX toxicity toward MDR cells. In such experiments, the polymers should be used at nontoxic concentrations to avoid their contribution to overall cytotoxicity. Therefore, instead of the commonly used cytotoxicity index IC50, that is, the polymer concentration corresponding to 50% inhibition of cell growth, we estimated maximum tolerable concentrations (MTCs) of the polymers that ensured survival of 90−100% cells.

The results presented in Figure 2A clearly show that cytotoxicity of PPO-NG copolymers strongly depends on their structure. Their MTC values varied within two orders of magnitude from 10 ± 1 μM (PPO-NG2) to 2800 ± 300 μM (PPO-NG76). Cell tolerance to PPO-NG copolymers increased in accordance with their hydrophilicity. Thus, PPO-NG2 and PPO-(NG2)$_2$ polymers that contained only two and four glycerol residues displayed MTC values around 10 and 13 μM, respectively. The increasingly hydrophilic PPO-NG30 was not toxic up to 100 μM. A further increase in the degree of polymerization of the hyperbranched polyglycerol block rendered the copolymer PPO-NG76 nontoxic up to 2800 μM (Figure 2A). Thus, the structure of PPO-NG copolymers strongly influenced their cytotoxicity. Previously, we have shown that the toxic concentration range of Pluronics increased in accordance with their hydrophilicity.[31] Here we report that PPO-NG copolymers exhibit the same trend.

It is noteworthy that MTCs of all diblock PPO-NG copolymers were higher than their CMC values (Table 1). This means that these polymers acquired cytotoxicity only in micellar form. In contrast, the MTC values of the triblock copolymer PPO-(NG2)$_2$ (13 ± 5 μM) were lower than its CMC (40 ± 15 μM). Thus, this polymer exhibits cytotoxicity in the disaggregated form. We ascribe this to two ionizable amino groups in the PPO-(NG2)$_2$ molecule that facilitate binding of the positively charged macromolecules to the negatively charged outer cell membrane and thus enhance the PPO-(NG2)$_2$ copolymer effect. This explanation agrees with the previously published observation that tertiary amino groups in Tetronics increase their cytotoxicity toward Caco-2 cells.[34]

Cytotoxicity of PPO-NG copolymers was compared with that of Pluronic L61 (Figure 1), a well-known chemosensitizer.
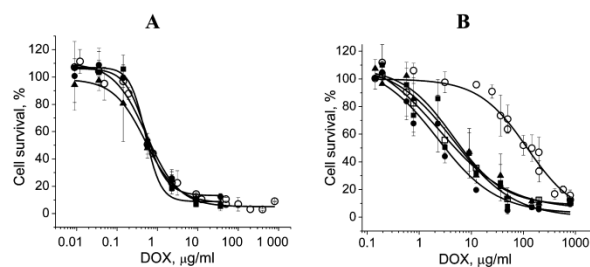
Figure 3. Influence of block copolymers on doxorubicin toxicity toward drug-sensitive MCF7 (A) and drug-resistant MCF7/R cells (B). The cells were incubated for 1 h with DOX in the absence of polymers (○) or in the presence of 6.6 μM of PPO-NG2 (●), 15 μM of PPO-(NG2)$_2$ (■), 83 μM of PPO-NG30 (▲), and 22 μM of Pluronic L61 (□) in the serum-free culture medium.
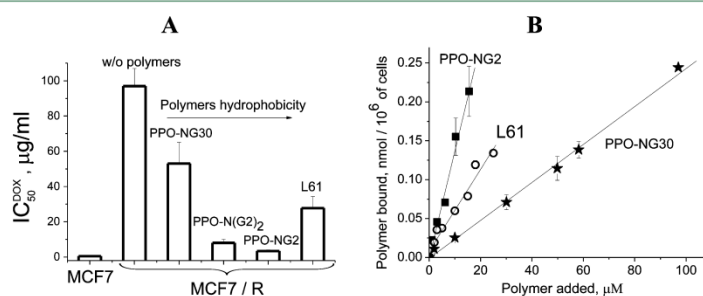
Figure 4. Interaction of PPO-NG copolymers and Pluronic L61 with MCF7/R cells. (A) Decrease in IC$_{50}^{DOX}$ values caused by PPO-NG copolymers and Pluronic L61 added at the same concentration (6.6 μM). The efficacy of the polymers may be evaluated from comparison with the IC$_{50}^{DOX}$ value of the drug-sensitive MCF7 cells shown by the column on the left. (B) Binding of PPO-NG2 (■), L61 (○), and PPO-NG30 (★) to MCF7/R cells as assessed by use of tritium-labeled polymers.

Upon addition at concentrations below its CMC, this polymer did not affect cell viability as compared with controls. However, in the range between CMC and MTC, Pluronic L61 induced pronounced and reproducible stimulation of cell growth (Figure 2B). This observation is in good agreement with the previously noticed capability of other Pluronics (P85 and F127) to increase cell survival at subtoxic concentrations.[35] In contrast, all studied PPO-NG copolymers produced a smooth horizontal segment at all concentration up to MTC (Figure 2A). Hence, PPO-NG copolymers did not increase cell viability. The incapability of PPO-NG copolymers to stimulate growth of cancer cells is an important property, which makes them promising candidates for application as novel MDR reversal agents.

Taking into account the fact that mass fractions of hydrophilic blocks in PPO-NG2, PPO-NG30, and PPO-NG76 copolymers (Table 1) are close to those in Pluronics L61, P85, and F127, respectively, the difference between PPO-NG and PPO−PEG copolymers in their biological effects on cell viability cannot be explained merely by the degree of their hydrophilicity. Rather, it reflects the difference in chemical structure, architecture, and number of end groups of the hydrophilic blocks. As far as (in contrast with Pluronics) PG copolymers not supporting cell survival, our data strongly indicate that the chemical structure of hydrophilic block

determines to a large extent the protective properties of copolymers.

Chemosensitization. The ability of PPO-NG copolymers to reverse MDR was determined by cell treatment with mixtures containing a constant amount of a polymer and DOX sequentially diluted with serum-free medium. All copolymers were tested at nontoxic concentrations, which were equal or lower than their MTC values. Nonresistant MCF7 cells treated with different PPO-NG copolymers produced overlapping DOX cytotoxicity curves that matched the control obtained in the absence of polymers (Figure 3A). Cell sensitivity was characterized by the DOX concentration that caused 50% inhibition of cell growth (IC$_{50}^{DOX}$). IC$_{50}^{DOX}$ values of nonresistant MCF7 cells determined in the presence of polymers and in their absence varied within a narrow range of 0.5 to 0.6 μg/mL of DOX. This translates to no change of the drug toxicity toward the drug-sensitive cells.

In contrast, the same polymers significantly increased DOX toxicity toward drug-resistant MCF7/R cells and shifted the cytotoxicity curves to lower DOX concentrations (Figure 3B). In the absence of polymers, the IC$_{50}^{DOX}$ value was equal to 97 ± 30 μg/mL of DOX. The addition of 6.6 μM of PPO-NG2, 15 μM of PPO-(NG2)$_2$, or 83 μM of PPO-NG30 decreased IC$_{50}^{DOX}$ values to 3.3 ± 0.7, 4.7 ± 0.9, and 6.4 ± 1.5 μg/mL, respectively. Thus, the most effective PPO-NG2 copolymer increased the drug cytotoxicity 30-fold. The effect of block

copolymers was compared with that of verapamil, MDR inhibitor (Figure 1), that directly binds to P-gp.[19] The addition of 20 μM verapamil decreased the IC_{50}^{DOX} value to 6.1 ± 1.8 μg/mL. Hence, all tested PPO-NG copolymers inhibited MDR to the same extent as this specific MDR inhibitor used in clinics.

To evaluate the significance of the polymer architecture for MDR suppression, we compared the effects of PPO-NG copolymers and Pluronic L61. The cytotoxicity curves of DOX formulated with 22 μM Pluronic L61 or PPO-NG copolymers overlapped (Figure 3B). IC_{50}^{DOX} value in the presence of Pluronic L61 was equal to 5.5 ± 1.3 μg/mL that was within the range of IC_{50}^{DOX} values observed with PPO-NG copolymer formulations.

Thus, despite the differences in the overall architecture and the chemical structures of Pluronic L61 and PPO-NG copolymers (Figure 1), both types of polymers induced overlapping curves of DOX cytotoxicity (Figure 3B) and decreased IC_{50}^{DOX} values to the same level. These results prove that the ability to overcome MDR is a peculiar feature not only for surfactants with hydrophilic PEG block but also for hyperbranched polyglycerol-based copolymers as well.

Relationship between MDR Inhibition by the Polymers and Their Binding to Cells. All copolymers reduced the resistance of MCF7/R cells to the same level (Figure 3B) if each of them was tested at the most effective concentration. However, these concentrations for hydrophobic and hydrophilic PPO-NG polymers are significantly different. 83 μM of PPO-NG30 was necessary to obtain the effect produced by 6.6 μM of PPO-NG2, suggesting that hydrophilic copolymers inhibited P-gp less effectively.

To disclose the relationship between the structure of a copolymer and its ability to reverse MDR, we compared the effects of the copolymers at an equal molar concentration (Figure 4A). All tested block copolymers decreased IC_{50}^{DOX} values as compared with untreated cells (the column "without polymers"). The chosen molar concentration of all copolymers, 6.6 μM, was less than their CMC values (Table 1). Thus, MDR inhibition by PG copolymers was mediated by the unimers (i.e., single molecular chains of block copolymers). In this respect, PG copolymers are similar to Pluronics.[13] Comparatively hydrophobic PPO-NG2 and PPO-(NG2)$_2$ copolymers decreased IC_{50}^{DOX} to lower values than hydrophilic PPO-NG30 (Figure 4A), while PPO-NG76 had no effect at all (data not shown). The efficacy of the polymers increased in the series PPO-NG76 ≪ PPO-NG30 < PPO-(NG2)$_2$ < PPO-NG2 concurrently with the increase in the copolymer hydrophobicity, estimated previously as partition coefficients of these copolymers in biphasic hexane/water mixture (Log $P_{hexane/water}$).[15] However, Pluronic L61 does not follow this rule. Being more hydrophobic than PPO-NG2 (Log $P_{hexane/water}$ of Pluronic L61 and PPO-NG2 are equal to −0.24 and −0.51, respectively[15]), Pluronic L61 decreased IC_{50}^{DOX} value less effectively (Figure 4A). Taking into account that PPO-NG2 and Pluronic L61 contain nearly identical hydrophobic blocks, this result emphasizes the role of the hydrophilic block architecture in the interaction of an amphiphile with the cell membrane. The polyglycerol-based branched hydrophilic block of PPO-NG2 appeared to be more advantageous than the two linear PEG blocks of Pluronic L61.

PPO-(NG2)$_2$ inhibited MDR more effectively than Pluronic L61 (Figure 4A), although these polymers have a similar architecture, both being triblock copolymers with two hydrophilic residues at each side of the polyalkylene oxide chain. The only difference consists of the chemical structure of their hydrophilic part: that of PPO-(NG2)$_2$ is presented by two di(2,3-dihydroxypropyl)amino groups, while Pluronic L61 contains two linear diethylene oxide fragments. Most probably, higher efficacy of PPO-(NG2)$_2$ results from Coulomb interactions of two positively charged amino groups in its molecule with the anionic centers in cell membranes.[36]

It is reasonable to suggest that efficacy of a copolymer depends on its ability to bind to cells, and enlargement of the hydrophilic block diminishes the polymer adsorption. To verify this point, we examined binding of polymers with MCF7/R cells. For this purpose, we introduced tritium into CH bonds of PPO-NG2, PPO-NG30, and Pluronic L61 in amounts of approximately one atom per macromolecule to ensure a minimal influence of labeling on the properties of the polymer. All copolymers were tested within the same range of concentrations as in the experiments on MDR reversal. The cells' radioactivity normalized per million of cells was used as a measure of polymer binding. We observed that the amount of bound polymer was directly proportional to its concentration in the medium and did not reach a saturation level (Figure 4B). If the polymers had a higher affinity toward a specific receptor, the binding isotherm should not be linear but is expected to bend at the concentration corresponding to receptors saturation. Linearity of the binding isotherms indicates unspecific interaction between polymers and cells.

The slopes of the curves shown in Figure 4B were equal to 14.2 ± 0.76, 5.7 ± 0.27, and 2.4 ± 0.07 pmol/μM × 10^6 cells for PPO-NG2, Pluronic L61, and PPO-NG30, respectively, indicating different binding capacity of the copolymers. The increase in the amount of hydrophilic residues decreased the polymer adsorption. At any concentration of added polymers, the amount of bound PPO-NG2 was six to seven times higher than that of PPO-NG30. The observed agreement of the polymer chemosensitizing effect (Figure 4A) and its binding to cell membranes (Figure 4B) indicates that the efficacy in MDR reversal is determined by binding efficacy and membrane-disturbing activity of the unimers.

Two independent approaches to the study of polymer–cell interactions led to a similar estimate of their efficacy. The chemosensitizing activity of the polymers increased in the row PPO-NG30 < L61 < PPO-(NG2)$_2$ < PPO-NG2 (Figure 4A). This tendency was supported by their relative binding capacity (Figure 4B). Moreover, these data are in a full agreement with the copolymers' ability to accelerate lipid flip-flop and DOX permeation through lipid membranes in liposomes.[15] In summary, these observations support the high potency of the novel amphiphiles as chemosensitizers.

Multidrug Resistance of K562/i-S9 and K562/R Cells. Biological effects of PPO-NG copolymers previously described for MCF7 and MCF7/R cells were verified on cell cultures of different origin: leukemic drug-sensitive K562 cell line and its two sublines derived either by infection of K562 cells with a recombinant retrovirus carrying human MDR1 cDNA[24] (K562/i-S9 cells) or by selection with increasing amounts of vincristine (K562/R cells).[23]

To ascertain multidrug resistance of K562/i-S9 and K562/R cells, we used two drugs: DOX and vincristine sulfate, for which the structure (Figure 1) and the mechanism of action are significantly different. The former inhibits cell proliferation via intercalation in DNA, while vincristine binds to tubulin dimers and inhibits mitotic spindle formation, thus affecting cell division.[37]
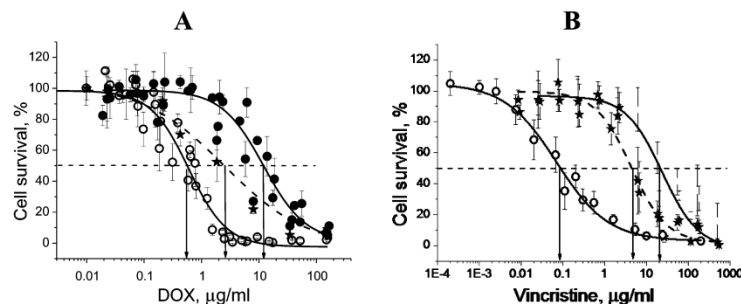
Figure 5. Resistance of the parental K562 (○), K562/i-S9 (★), and K562/R (●) cells to doxorubicin (A) and vincristine (B). Concentrations of the drugs that decreased cell survival to 50% are indicated with arrows.
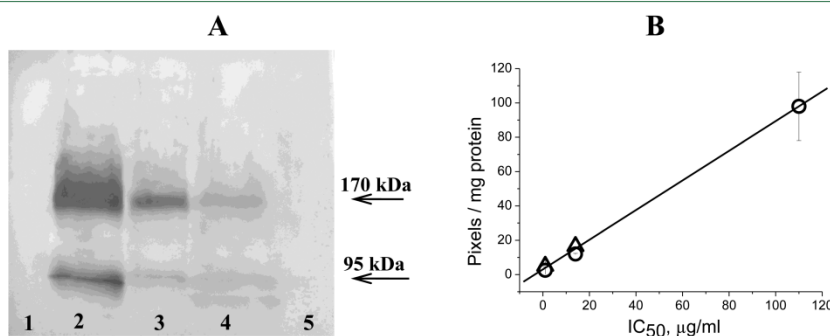
Figure 6. Analysis of P-gp level in different cell lines. (A) Western blot of the sensitive MCF7 (1) and K562 (5) cells and the resistant cells MCF7/R (2), K562/R (3), and K562/i-S9 (4). The lanes were loaded with 25 μL samples containing 24 μg (1), 18 μg (2), 74 μg (3), 870 μg (4), and 30 μg (5) of total cellular protein. The position of P-gp, 170 and 95 kDa, is shown by the arrows on the right. (B) Correlation between P-gp relative content (indicated in the text) and cell resistance to vincristine (△) and doxorubicin (○) expressed as IC_{50}^{vincr} and IC_{50}^{DOX}.

The parental K562 cells displayed different sensitivity toward these drugs. 50% inhibition of their growth could be achieved at 0.08 μg/mL of vincristine, a concentration one order of magnitude less than IC_{50}^{DOX} equal to 0.5 to 0.6 μg/mL (Figure 5, ○). This means that vincristine is more toxic than DOX for drug-sensitive cells in culture. This conclusion is in line with medical observations of higher toxicity of vincristine as compared with DOX.[38]

Insertion of mdr1-gene in the genome of K562 cells increased the IC_{50}^{DOX} value of K562/i-S9 cells up to 2 to 3 μg/mL (Figure 5A, ★). K562/R cells, which had been selected by long-time cultivation in the vincristine containing medium, displayed higher resistance to DOX. Their IC_{50}^{DOX} value increased up to 12 ± 1.4 μg/mL (Figure 5A, ●).

Testing these cells with vincristine (Figure 5B) showed that the survival of K562/i-S9 (asterisks) and K562/R (closed circles) cells decreased to 50% at vincristine concentrations (IC_{50}^{vincr}) equal to 4 to 5 μg/mL and 20−22 μg/mL, respectively. These concentrations are one to two orders of magnitude higher than the vincristine concentration, 0.08 μg/mL, sufficient for 50% growth inhibition of the drug-sensitive K562 cells (○). These results evidenced that K562/i-S9 and K562/R cell lines displayed resistance to vincristine.

Thus, our results clearly show that K562/i-S9 and K562/R cells are resistant to two drugs, that is, DOX and vincristine, used in clinics. Taking into account the different structure of these antibiotics (Figure 1) K562/i-S9 and K562/R cells could be considered as multidrug resistant.

Western Blot Analysis of P-gp Expression in Different Cell Lines. Multidrug resistance of tumor cells often results from overexpression of P-gp, an integral membrane protein with M_w ≈ 170 kDa. However, MDR could also be caused by other biochemical mechanisms.[1] With this in mind, we have examined all of our cell lines for the presence of P-gp by Western blot technique, using monoclonal anti-P-gp antibodies, which recognize an epitope located in the amino terminal half of P-gp, at the third extracellular loop of the glycoprotein molecule. These antibodies are specific toward P-gp and do not react with MRP3 according to the supplier data.

Two major protein bands of 170 and 95 kDa were detected in MDR cells: MCF7/R, K562/R, and K562/i-S9 (Figure 6A, lanes 2−4). Obviously, 170 kDa band corresponds to intact P-gp molecules, while 95 kDa is most likely the product of P-gp degradation in-half due to cleavage in the protease-sensitive site.[39]

A

B
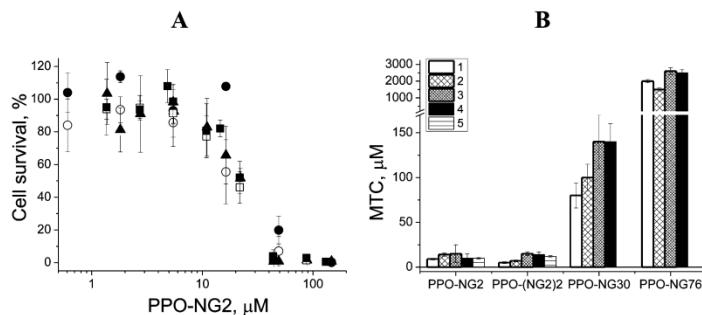
Figure 7. Comparison of cytotoxicity of PPO-NG copolymers toward different cell lines. (A) Toxicity of PPO-NG2 toward K562 (○), K562/i-S9 (▲), K562/R (●), MCF7 (□), and MCF7/R (■) cells. (B) Maximal tolerable concentrations of PPO-NG2, PPO-(NG2)₂, PPO-NG30, and PPO-NG76 copolymers for K562 (1), K562/i-S9 (2), K562/R (3), MCF7/R (4), and MCF7 (5) cells. The experiments were carried out as described in the legend to Figure 2

A

B
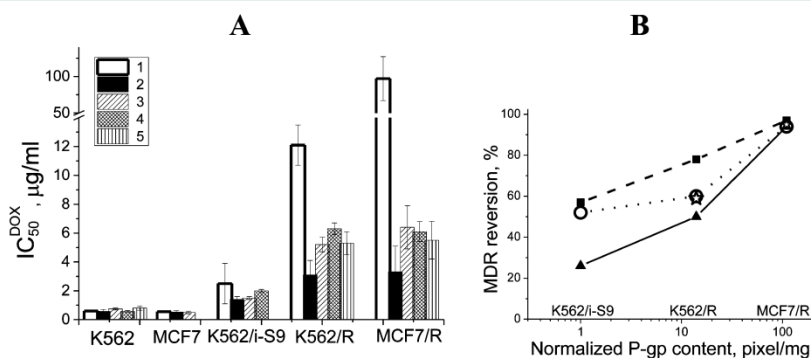
Figure 8. Dependence of chemosensitizers activity on P-gp expression. (A) Sensitivity of different cell lines to DOX, expressed as IC_{50}^{DOX} values, in the absence of additives (1) and in the presence of 11 μM of PPO-NG2 (2), 97 μM of PPO-NG30 (3), 20 μM of verapamil (4), and 17 μM of Pluronic L61 (5). (B) Extent of MDR reversion (R) by PPO-NG2 (■), PPO-NG30 (○), Pluronic L61 (☆), and verapamil (▲) as a function of the P-gp content estimated from Western blot results (Figure 6).

No discernible protein bands were seen in the lanes loaded with lysates of the parental drug-sensitive K562 and MCF7 cells (Figure 6A, lanes 1 and 5), even when up to 800 μg of total protein per lane was applied. This result demonstrates the lack of appreciable amounts of P-gp in K562 and MCF7 cells.

The intensity of P-gp bands in MDR cell lines differed widely (Figure 6A, lanes 2–4). Thus, 18 μg of total protein of MCF7/R cells produced overloaded P-gp bands (lane 2), while 870 μg of protein was required to visualize P-gp in K562/i-S9 cells (lane 4). Therefore, to detect P-gp in all MDR cell lines, different amounts of cellular protein were used for analysis. (See the legend to Figure 6.) To correct for loading differences, the intensity of protein bands evaluated with ImageJ program (version 1.34s) was normalized per mg protein applied onto lane. The resulting values (pixels/mg) reflect the relative content of P-gp in the cells. Referring to K562/i-S9, K562/R, and MCF7/R cells, these values were in the ratio 1:14:110, which correlated with the resistance of these cells to DOX and vincristine expressed as IC_{50}^{DOX} and IC_{50}^{vincr} values (Figure 6B). This relationship suggests P-gp system as the main factor

determining resistance of K562/i-S9, K562/R, and MCF7/R cells, although involvement of other MDR mechanisms cannot be excluded.

Comparison of PPO-NG Copolymers Toxicity toward Different Cells. Cytotoxicity of PPO-NG copolymers was determined toward all five cell lines used in this study, that is, K562, K562/i-S9, K562/R, MCF7, and MCF7/R. Cytotoxicity of each PPO-NG polymer appeared to be similar for resistant and nonresistant cell lines. Results obtained with PPO-NG2 illustrate the type of evidence supporting this observation. 80–100% of cells of any line survived after treatment with PPO-NG2 concentrations of 6–15 μM. The polymer acquired cytotoxicity at higher concentrations and displayed it toward nonresistant and resistant cell lines in the same concentration range (Figure 7A).

Similar results were obtained with other PPO-NG copolymers: PPO-(NG2)₂, PPO-NG30, and PPO-NG76. MTC values of each polymer toward drug-sensitive and MDR leukemic and breast carcinoma cell lines were nearly the same within accuracy of the method (Figure 7B), indicating that polymer cytotoxicity

does not depend on the origin of the cells and their resistance level. Similar toxicity of the polymer to different cells irrespective of P-gp presence renders direct interaction of the polymer with P-gp improbable. This conclusion supports our aforementioned supposition relying on binding curves of tritium-labeled polymers with MCF7/R cells (Figure 4B).

MDR Reversal in Different Cell Lines. The influence of PPO-NG copolymers on DOX cytotoxicity was studied also on K562, K562/i-S9, and K562/R cell lines. The cells were treated with subtoxic concentrations of PPO-NG2 (11 μM), PPO-NG30 (97 μM), and the reference chemosensitizers, Pluronic L61 (17 μM) and verapamil (20 μM) formulated with various DOX concentrations. Treatment of the drug-sensitive K562 and MCF7 cells with PPO-NG copolymers did not reveal reliable changes in IC_{50}^{DOX} values (Figure 8A). Thus, the PPO-NG copolymers did not change DOX toxicity for cells lacking P-gp.

In contrast, IC_{50}^{DOX} values for K562/i-S9, K562/R, and MCF7/R cells decreased after incubation with PPO-NG copolymers (Figure 8A). The effect of chemosensitizers toward K562/i-S9 and K562/R cells increased in the same order PPO-NG2 > Pluronic L61 ≥ PPO-NG30 > verapamil as in the case of MCF7/R cells. So, MDR reversal induced by PPO-NG copolymers has been observed with all resistant sublines tested, independent of their origin.

Nevertheless, the extent of MDR reversal caused by PPO-NG copolymers depended on the initial resistance level of the cells. Thus, 6.6 μM PPO-NG2 decreased 30-fold the IC_{50}^{DOX} value of the most resistant MCF7/R cells but only 2-fold that of the least resistant K562/i-S9 cells (from 2.5 to 1.4 μg/mL). To reveal the relationship between the initial cell resistance and the polymers efficacy more obviously, we evaluated the portion of resistant cells that acquired sensitivity (R) under treatment with chemosensitizers. R values were calculated according to the following equation:

$$R = \frac{IC_{50}^{DOX}(res) - IC_{50}^{DOX}(res + additive)}{IC_{50}^{DOX}(res) - IC_{50}^{DOX}(sens)} \times 100\% \quad (1)$$

where IC_{50}^{DOX}(sens) is the IC_{50}^{DOX} value displayed by the parental cell line (K562 or MCF7), IC_{50}^{DOX} (res) is the IC_{50}^{DOX} value of the respective resistant cell line, and IC_{50}^{DOX} (res + additive) is the IC_{50}^{DOX} value of the resistant cells treated with a chemosensitizer.

It was observed that PPO-NG2, PPO-NG30, and Pluronic L61, reversed MDR of the least resistant K562/i-S9 cells by 52−57% (Figure 8B). The extent of MDR reversion of more resistant K562/R cells appeared to be higher (59−78%). The highest chemosensitizing activity of the copolymers was observed in the case of the most resistant MCF7/R cells (94−97%) (Figure 8B). Hence, more resistant cells are more sensitive to the polymers. These results are consistent with the previously published observations on other MDR cells.[40] The dependence of the extent of MDR reversion on P-gp content was displayed most noticeable by verapamil (Figure 8B, ▲). It exhibited only marginal effect on the resistance of K562/i-S9 cells ($R = 26\%$) and induced more pronounced MDR reversal in K562/R and MCF7/R cells (R amounted up to 50 and 94% respectively). What are the possible reasons for such regularity?

Western blot analysis of the studied cell lines showed that the initial resistance level correlates with the P-gp content (Figure 6B). Hence, the efficacy of a chemosensitizer depends on the content of P-glycoprotein in the cells. The dependence was

qualitatively similar for all tested chemosensitizers, although their mechanisms of action were quite different. Verapamil inhibits P-gp activity via direct and specific interaction, while PPO-NG copolymers hardly bind specifically to P-gp, as previously discussed (Figures 4B and 7B). Therefore, it seems improbable that the dependence of R values on P-gp content is determined by the nature or mechanism of action of chemosensitizers. Rather, peculiarities of P-gp itself are responsible for this effect.

We propose that the dependence shown in Figure 8B is determined by the arrangement of P-gp molecules in plasma membranes of MDR cells. Increase in P-gp content induces cooperativity in its response to chemosensitizers, resulting in coordinated inhibition of efflux system. It may be the reason, why P-gp is inhibited more effectively in highly resistant cell lines than in the lines with low expression level of P-gp. Our hypothesis on the functional cooperativity of P-gp agrees with the previously published data, indicating that P-gp self-associates in cell membrane.[41−43]

■ CONCLUSIONS

The present paper aimed at understanding the role of the hydrophilic block in amphiphilic poly(propylene oxide)-based linear−hyperbranched block copolymers in their interaction with living cells. To this end, biological effects of novel amphiphilic copolymers containing hyperbranched polyglycerol as a hydrophilic block were compared with those of Pluronic L61 with the linear PEG hydrophilic blocks.

Most properties of PPO-NG copolymers were similar to those of Pluronic L61. Thus, intrinsic cytotoxicity of the novel copolymers increased in accordance with their hydrophobicity, just as it has been previously shown for Pluronics.[31] Both types of copolymers displayed cytotoxicity only in the micellar form. PPO-NG copolymers were found to suppress MDR in cancer cells to the same extent as Pluronic L61, indicating that the linear PEG can be substituted by a hyperbranched polyglycerol block without loss of the chemosensitizing activity. The efficacy of the polymers in MDR reversal correlated with their affinity toward cell membranes, as assessed by use of tritium-labeled copolymers. The extent of MDR reversion by both types of the copolymers depended on the initial resistance level of MDR cells. The increase in the expression level of P-gp rendered cells more sensitive to the copolymers and verapamil.

The only striking difference between the novel copolymers and Pluronic L61 was revealed in experiments on the influence of the copolymers on viability of tumor cells in the absence of drugs. It was found that, in stark contrast with Pluronics P85, F127,[35] and L61, PPO-NG copolymers do not support the survival of cancer cells. This finding indicates that only the PEG hydrophilic block of Pluronics is responsible for their cell protective effects. Its substitution by hyperbranched polyglycerol completely abolishes this effect, which is clearly undesired in cancer therapy.

■ AUTHOR INFORMATION

Corresponding Author
*E-mail: grozdova@genebee.msu.ru. Tel: +7-916 018 7870. Fax: +7-495 939 01 74.

Author Contributions
The manuscript was written through contributions of all authors. All authors have given approval to the final version of the manuscript.

Notes

The authors declare no competing financial interest.

REFERENCES

(1) Vadlapatla, R. K.; Vadlapudi, A. D.; Pal, D.; Mitra, A. K. *Curr. Pharm. Des.* **2013**, *19*, 7126−7140.

(2) Borst, P.; Elferink, R. O. *Annu. Rev. Biochem.* **2002**, *71*, 537−592.

(3) Gottesman, M. M.; Fojo, T.; Bates, S. E. *Nat. Rev. Cancer* **2002**, *2*, 48−58.

(4) Eckford, P. D. W.; Sharom, F. J. *Chem. Rev.* **2009**, *109*, 2989−3011.

(5) Germann, U. A.; Pastan, I.; Gottesman, M. M. *Semin. Cell Biol.* **1993**, *4*, 63−76.

(6) Markman, J. L.; Rekechenetskiy, A.; Holler, E.; Ljubimova, J. Y. *Adv. Drug Delivery Rev.* **2013**, *65*, 1866−1879.

(7) Yu, H.; Xu, Z.; Chen, X.; Xu, L.; Yin, Q.; Zhang, Z.; Li, Y. *Macromol. Biosci.* **2014**, *14*, 100−109.

(8) Yin, Q.; Shen, J.; Zhang, Z.; Yu, H.; Chen, L.; Gu, W.; Li, Y. *Biomacromolecules* **2013**, *14*, 2242−2252.

(9) Sosnik, A. *Adv. Drug Delivery Rev.* **2013**, *65*, 1828−1851.

(10) Woodcock, D. M.; Linsenmeyer, M. E.; Chojnowski, G.; Kriegler, A. B.; Nink, V.; Webster, L. K.; Sawyer, W. H. *Br. J. Cancer* **1992**, *66*, 62−68.

(11) Coon, J. S.; Knudson, W.; Clodfelter, K.; Lu, B.; Weinstein, R. S. *Cancer Tes.* **1991**, *51*, 897−902.

(12) Moghimi, S. M.; Hunter, A. C. *Trends Biotechnol.* **2000**, *18*, 412−420.

(13) Batrakova, E. V.; Lee, S.; Li, S.; Venne, A.; Alakhov, V.; Kabanov, A. *Pharm. Res.* **1999**, *16*, 1373−1379.

(14) Alakhova, D. Y.; Zhao, Y.; Li, S.; Kabanov, A. V. *PLoS One* **2013**, *8*, e72238.

(15) Demina, T.; Grozdova, I.; Krylova, O.; Zhirnov, A.; Istratov, V.; Frey, H.; Kautz, H.; Melik-Nubarov, N. *Biochemistry* **2005**, *44*, 4042−4054.

(16) Cambon, A.; Brea, J.; Loza, M. I.; Alvarez-Lorenzo, C.; Concheiro, A.; Barbosa, S.; Taboada, P.; Mosquera, V. *Mol. Pharmacol.* **2013**, *10*, 3232−3241.

(17) Zhong, Y.; Wang, C.; Cheng, L.; Meng, F.; Zhong, Z.; Liu, Z. *Biomacromolecules* **2013**, *14*, 2411−2419.

(18) Hofmann, A. M.; Wurm, F.; Hühn, E.; Nawroth, T.; Langguth, P.; Frey, H. *Biomacromolecules* **2010**, *11*, 568−574.

(19) Meier, M.; Blatter, X. L.; Seelig, A.; Seelig, J. *Biophys. J.* **2006**, *91*, 2943−2955.

(20) Sunder, A.; Hanselmann, R.; Frey, H.; Mülhaupt, R. *Macromolecules* **1999**, *32*, 4240−4248.

(21) Istratov, V.; Kautz, H.; Kim, Y.-K.; Schubert, R.; Frey, H. *Tetrahedron* **2003**, *59*, 4017−4024.

(22) Lozzio, B. B.; Lozzio, C. B. *Int. J. Cancer* **1977**, *19*, 136.

(23) Soule, H. D.; Vazquez, J.; Long, A.; Albert, S.; Brennan, M. *J. Natl. Cancer Inst.* **1973**, *51*, 1409−1416.

(24) Choi, K.; Frommel, T. O.; Stern, R. K.; Perez, C. F.; Kriegler, M.; Tsuruo, T.; Roninson, I. B. *Proc. Natl. Acad. Sci. U.S.A.* **1991**, *88*, 7386−7390.

(25) Kalinina, E.; Novichkova, M.; Scherbak, N. P.; Solomka, V.; Saprin, A. N. *Adv. Exp. Med. Biol.* **2001**, *500*, 241−244.

(26) Harrigan, P. R.; Wong, K. F.; Redelmeier, T. E.; Wheeler, J. J.; Cullis, P. R. *Biochim. Biophys. Acta* **1993**, *1149*, 329−338.

(27) Mosmann, T. *J. Immunol. Methods* **1983**, *65*, 55−63.

(28) Melik-Nubarov, N. S.; Pomaz, O. O.; Dorodnych, T.Yu.; Badun, G. A.; Ksenofontov, A. L.; Schemchukova, O. B.; Arzhakov, S. A. *FEBS Lett.* **1999**, *446*, 194−198.

(29) Laemmli, U. K. *Nature* **1970**, *227*, 680−685.

(30) Chattopadhyay, A.; London, E. *Anal. Biochem.* **1984**, *139*, 408−412.

(31) Budkina, O. A.; Demina, T. V.; Dorodnykh, T. Y.; Melik-Nubarov, N. S.; Grozdova, I. D. *Polymer Sci. (Rus.) Ser. A* **2012**, *54*, 707−717.

(32) Schüll, C.; Rabbel, H.; Schmid, F.; Frey, H. *Macromolecules* **2013**, *46*, 5823−5830.

(33) Wurm, F.; Frey, H. *Prog. Polym. Sci.* **2011**, *36*, 1−52.

(34) Alvarez-Lorenzo, C.; Rey-Rico, A.; Brea, J.; Loza, M. I.; Concheiro, A.; Sosnik, A. *Nanomedicine* **2010**, *5*, 1371−1383.

(35) Exner, A. A.; Krupka, T. M.; Scherrer, K.; Teets, J. M. *J. Controlled Release* **2005**, *106*, 188−197.

(36) Tkachenko, E.; Rhodes, J. M.; Simons, M. *Circ. Res.* **2005**, *96*, 488−500.

(37) Jordan, A.; Hadfield, J. A.; Lawrence, N. J.; McGown, A. T. *Med. Res. Rev.* **1998**, *18*, 259−296.

(38) McIllmurray, M. B.; Bibby, R. J.; Taylor, B. E.; Ormerod, L. P.; Edge, J. R.; Wolstenholme, R. J.; Willey, R. F.; O'Reilly, J. F.; Horsfield, N.; Johnson, C. E. *Thorax* **1989**, *44*, 215−219.

(39) Hrycyna, C. A.; Airan, L. E.; Germann, U. A.; Ambudkar, S. V.; Pastan, I.; Gottesman, M. M. *Biochemistry* **1998**, *37*, 13660−13673.

(40) Kabanov, A. V.; Batrakova, E. V.; Alakhov, V.Yu. *J. Controlled Release* **2003**, *91*, 75−83.

(41) Boscoboinik, D.; Debanne, M. T.; Stafford, A. R.; Jung, C. Y.; Gupta, R. S.; Epand, R. M. *Biochim. Biophys. Acta* **1990**, *1027*, 225−228.

(42) Poruchynsky, M. S.; Ling, V. *Biochemistry* **1994**, *33*, 4163−4174.

(43) Naito, M.; Tsuruo, T. *Biochem. Biophys. Res. Commun.* **1992**, *185*, 284−290.

A.6 Hydroxyfunctional Oxetane-Inimers with Varied Polarity for the Synthesis of Hyperbranched Polyether Polyols via Cationic ROP

Eva-Maria Christ[1,2], Sophie S. Müller[1,2], Elena Berger-Nicoletti[1] and Holger Frey[1,*]

[1]Institute of Organic Chemistry, Johannes Gutenberg-University Mainz, Duesbergweg 10-14, D-55128 Mainz, Germany

[2]Graduate School Materials Science in Mainz (MAINZ), Staudingerweg 9, D-55128 Mainz, Germany

Note: the following pages contain the revised manuscript of this article , which differ in minor details from the final version.

ABSTRACT

Synthesis and characterization of novel hydroxyl-functionalized oxetane-inimers with varied alkyl chain length - 3-hydroxymethyl-3-methoxymethyloxetane (HMMMO), 3-hydroxymethyl-3-propoxymethyloxetane (HMPMO) and 3-hexoxymethyl-3-hydroxymethyloxetane (HMHMO) - is reported. Cationic ring-opening polymerization of these latent, cyclic AB_2-monomers leads to hyperbranched polyether polyols with degrees of branching (DB) between 34% and 69%, confirmed by *inverse gated* (IG) ^{13}C NMR spectroscopy. The hyperbranching polymerization yielded apparent molecular weights (M_n) ranging from 500 to 2500 g mol^{-1} (size exclusion chromatography). Remarkably, by copolymerization of 1,1,1-tris(4-hydroxyphenyl)ethane as a "focal" unit, polymerization under slow monomer addition conditions lead to higher apparent molecular weights up to 11,220 g mol^{-1}. The end groups of the hyperbranched polymers were studied via matrix-assisted laser desorption/ ionization time of flight mass (MALDI-TOF) and NMR spectrometry. By varying the alkyl chain length, tailoring of the solubility and glass transition temperatures of the materials is possible. Potential applications range from macro-initiators with defined polarity to tailoring of surface properties of antifouling materials.

KEYWORDS: Hyperbranched polyether polyols; cationic ring-opening polymerization; polyhydroxyoxetanes; multibranching polymerization; slow monomer addition

INTRODUCTION

Oxetanes are four-membered, strained ring systems. In comparison to the three-membered oxirane analogs, they are more basic (pKA (oxetane)=-2.02, pKA (oxirane)=-3.7) and exhibit lower ring strain (oxetane: 106 kJ mol^{-1}, oxirane: 116 kJ mol^{-1}).[1, 2] This leads to a more facile polymerization following a cationic mechanism than via an anionic one. However, anionic ring opening polymerization (AROP) of oxetanes with the aid of activating agents has been reported.[3]

Hyperbranched (hb) polyoxetanes, which are commonly obtained by the cationic ring-opening polymerization (CROP) of oxetanes with a pendent hydroxyl group (latent AB$_2$ monomers), have attracted increasing attention in recent years.[4–8] In contrast to their linear homologues, hyperbranched polymers show lower viscosity, improved solubility and almost no entanglements because of the compact structure and multivalency.[9] The unique structure of hyperbranched polymers renders them excellent building blocks for supramolecular self-assembly.[10, 11, 12] Despite the polydispersity and the usually poor control of the structure in comparison to the perfectly branched dendrimers, hyperbranched polymers are used in a variety of applications, ranging from biomedical purposes to nanotechnology.[12–17] The obvious advantage over perfectly branched dendrimers is their facile and fast synthesis in large quantities.[19–21] An established hyperbranched polyether is *hb*polyglycerol (*hb*PG), due to its excellent biocompatibility, chemical stability and inertness under biological conditions.[22–27]

In contrast to *hb*PG, *hb*polyoxetanes possess exclusively primary hydroxyl groups, in contrast to the presence of both primary and less reactive secondary hydroxyl groups in *hb*PG. This could be an advantage for applications such as hyperbranched ionic liquids.[5] Furthermore, hyperbranched polyoxetanes are less hydrophilic than *hb*PGs and dissolve in various organic solvents. Despite their hydrophobicity, polyoxetanes have bactericidal properties[28], which could enlarge the number of possible applications from surface modifications to biomedical applications.

Previously described hyperbranched oxetane inimers are generally functionalized with hydroxymethyl groups at the 3-position. Vandenberg et al. described the polymerization of 3,3-bis(hydroxymethyl)oxetane (BHMO), which represents an AB$_3$ monomer, to result in an almost insoluble product.[29] By derivatizing one of the two hydroxyl groups by an alkyl chain, the resulting polymer becomes soluble in a few organic solvents like pyridine and cresol, as mentioned in a patent by Schnell long ago.[30] Penczek and coworkers investigated the synthesis and the polymerization mechanism of poly-3-ethyl-3-(hydroxymethyl)oxetane (PEHO) and achieved molecular weights of 2000-5000 g mol^{-1} and polydispersity indices (PDI = M_w/M_n) as low as 1.5.[31–34] Competition between the active monomer (AM) mechanism and the active chain end (ACE) mechanism was reported. The authors concluded that only the AM mechanism leads to branching units. Due to the existence of both mechanisms, the degree of branching (DB) is limited and lower than for *hb*PG obtained from the controlled anionic polymerization of glycidol (around 67%).[9, 24, 35] However, by following a slow monomer addition (SMA) protocol, the degree of branching should increase also for the case of oxetane polymerization, because of the favored AM mechanism in this case.[36] Additionally, Yan et al. demonstrated that the degree of branching depends on the catalyst - monomer ratio.[37] Liu et al. reported molecular weights of PEHO up to 9400 g mol^{-1} and Xia et al. PDIs of poly(3-methyl-3-hydroxymethyl)oxetane around 1.2 via cationic ring-opening polymerization.[6, 38] The degree of branching varied around 50%[39, 40] and seemed to be dependent on the reaction temperature in a lower temperature range (-50 °C to 30 °C).[41] Schulte and coworkers reported that during polymerizations to linear products self-initiation of oxetanes can lead to cyclic byproducts, which impedes a controlled cationic ring-opening polymerization.[42] Also, Bednarek and coworkers suggested termination of the hyperbranched polymerization of EHO by cyclization via an intramolecular chain transfer reaction.[32] The presence of cyclic products, as detected in matrix-assisted laser

desorption/ionization time of flight mass spectrometry (MALDI-ToF MS) analysis was mentioned as a possible reason for the limited molecular weights.

The objective of our current work is to establish a systematically varied series of new oxetane inimers by monoalkylation of 3,3-bishydroxymethyl oxetane (BHMO). Three novel oxetane-inimers, 3-hydroxymethyl-3-methoxymethyloxetane (HMMMO), 3-hydroxymethyl-3-propoxy¬methyloxetane (HMPMO) and 3-hexoxymethyl-3-hydroxymethyloxetane (HMHMO) were synthesized and polymerized, as shown in Scheme 1. Comprehensive characterization of all polymers via MALDI-ToF MS, NMR spectroscopy and size exclusion chromatography (SEC) has been carried out. Three monoalkyl derivatives of BHMO with alkyl chains of varying lengths were prepared to investigate the structure/solubility properties relationships of the resulting polymers.
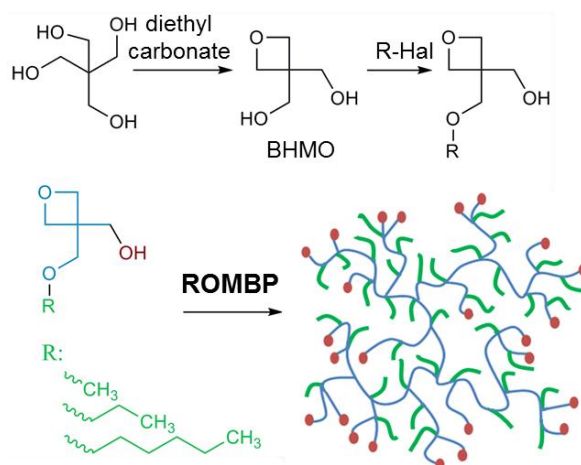
Scheme 1: Reaction scheme for the synthesis of 3,3-bis(hydroxymethyl)oxetane to functional oxetane inimers with varied alkyl chain length and the following ring-opening multibranching polymerization (ROMBP) to hyperbranched polyether polyols.

EXPERIMENTAL

Materials
All reagents were purchased from Acros Organics or Sigma Aldrich and were used as received, unless otherwise stated. Anhydrous THF and toluene were stored over a sodium/potassium mixture and freshly distilled prior to use. Boron trifluoride etherate was purified by distillation. Deuterated chloroform-d_1, DMSO-d_6 and pyridine-d_5 were purchased from Deutero GmbH.

Instrumentation
^{1}H NMR (300 MHz and 400 MHz) and ^{13}C NMR spectra (75 MHz and 100.6 MHz) were recorded on a Bruker AC300, Bruker AC400, Avance III HD 300 (300 MHz, 5 mm BBFO-head with z-gradient and ATM, B-ACS 60 sample changer) with Open-Access-Automation, Avance II 400 (400 MHz, 5 mm BBFO-head with z-gradient and ATM, SampleXPress 60 sample changer) with Open-Access-Automation or Avance III HD 400 (400 MHz, 5 mm BBFO-SmartProbe with z-gradient and ATM, SampleXPress 60 sample changer), respectively, and were referenced internally to residual proton signals of the deuterated solvents. ^{19}F NMR spectra were recorded on a Bruker 400 MHz FT NMR spectrometer.
For size exclusion chromatography (SEC) measurements in tetrahydrofuran (THF) a PU 1580 pump, an auto sampler AS1555, a UV-detector UV 1575 (detection at 254 nm) and an RI-detector RI 1530 from JASCO were used. Columns (MZ-Gel SDplus 102 Å and MZ-Gel SDplus 106 Å) were obtained from MZ-Analysentechnik. Calibration was carried out with polystyrene

standards purchased from Polymer Standard Services (PSS). MALDI-ToF MS measurements were performed using a Shimadzu Axima CFR MALDI-TOF mass spectrometer, using dithranol (1,8,9-trishydroxyanthracene) or CHCA (α-Cyano-4-hydroxycinnamic acid) as a matrix. The samples were prepared from pyridine and ionized by adding lithium chloride or potassium trifluoro acetate. Mass spectra were obtained on a QTof Ultima 3 (Waters, Milford, Massachusetts) apparatus employing ESI. Column chromatography was performed on silica gel (particle size 63-200 µm, Merck, Darmstadt, Germany). DSC measurements were carried out using a PerkinElmer DSC7 with a PerkinElmer thermal analysis controller TAC7/DX in the temperature range of -100-150 °C, using heating and cooling rates of 40 °C min^{-1} (first cycle) and 10 °C min^{-1} (second cycle), respectively. The melting points of indium (T_m=156.6 °C) and Millipore water (T_m=0 °C) were used for calibration.

Synthesis of 3,3-bis(hydroxymethyl)oxetane (BHMO)[29]

Pentaerythritol (200 g, 1.47 mol), diethylcarbonate (220 mL, 1.64 mol) and potassium hydroxide (0.3 g, 7.5 mmol) in ethanol (25 mL) were refluxed under argon atmosphere for 19 h. After removal of ethanol by distillation and cooling to room temperature, potassium hydroxide (0.23 g) in ethanol (20 mL) was added. Under reduced pressure (0.019 mbar) the crude product was obtained by distillation (yield: 57%).^{1}H NMR (300 MHz, DMSO-d_6): δ (ppm) = 4.54 (s, 4H, -CH_2OH), 4.27 (s, 4H, -CH_2O-), 4.75 (t, 2H, J = 15 Hz, -CH$_2$OH).

Synthesis of 3-hydroxymethyl-3-methoxy-methyloxetane (HMMMO)

BHMO (4 g, 34 mmol) was dissolved in 20 mL DMSO under argon atmosphere. At 0 °C sodium hydroxide (813.6 mg, 34 mmol) was added. The mixture was stirred at room temperature for 4 h. Methyl iodide (6.4 mL, 102 mmol) was added slowly with a syringe under argon atmosphere, and the mixture was stirred for 3 d at 35 °C. After cooling to room temperature, DMSO was evaporated under reduced pressure, the product was dissolved in diethyl ether and washed with water several times. Diethyl ether was evaporated and the product was purified by distillation (yield: 41%). ^{1}H NMR (300 MHz, CDCl$_3$): δ (ppm)= 4.43 (d, 2H, J = 7.3 Hz -CH_2O-), 4.40 (d, 2H, J = 7.3 Hz -CH_2O-), 3.84 (d, 2H, J = 7.4Hz, -CH_2O-), 3.67 (s, 2H, -CH_2O-) 3.35 (s, 3H, CH_3O-), 2.7 (t, 1H, J = 10.4 Hz, -OH). ^{13}C NMR (75 MHz, CDCl$_3$): δ (ppm) = 76.42 (-CCH$_2$-O-CH$_2$-), 76.37 (-CH$_2$OH), 66.10 (-O-CH$_2$-), 59.65 (-CH$_3$), 40.85 (CH$_2$-C-CH$_2$), ESI MS: 154.99 g mol^{-1} with sodium as cation (calc. isotopic mass=155.07 g mol^{-1}).

Synthesis of 3-hydroxymethyl-3-propoxy-methyloxetane (HMPMO)

HMPMO was prepared in a similar procedure as HMMMO. Instead of iodomethane, 1-propyl bromide was added (15.5 mL, 170 mmol). After cooling to room temperature, DMSO was evaporated under reduced pressure and the product was dissolved in ethyl acetate and washed with water several times. Ethyl acetate was evaporated and the product was precipitated by distillation (yield: 42%). ^{1}H NMR (300 MHz, CDCl$_3$): δ (ppm)= 4.44 (d, 2H, J = 6.2 Hz, -CH_2O-), 4.39 (d, 2H, J = 6.2 Hz, -CH_2O-), 3.87 (d, 2H, J = 5.1 Hz, -CH_2O-), 3.72 (s, 2H, -CH_2O-) 3.38 (t, 3H, J = 7.4 Hz, CH$_3$O-), 2.80 (s, 1H, -OH), 1.63-1.42 (m, 2H, CH_2-), 0.87 (t, 3H, J = 7.4 Hz, CH_3-). ^{13}C NMR (75 MHz, CDCl$_3$): δ (ppm) = 76.56 (-CCH$_2$-O-CH$_2$-), 74.83 (-CH$_2$OH), 73.46 (-CCH$_2$-O-), 66.58 (-O-CH$_2$-), 40.70 (CH$_2$-C-CH$_2$), 22.71 (-CH$_2$-), 10.40 (-CH$_3$), ESI MS: 183.1 g mol^{-1}, cationized with sodium (calc. isotopic mass=183.1 g mol^{-1}).

Synthesis of 3-hexoxymethyl-3-hydroxy-methyloxetane (HMHMO)

HMHMO was prepared in analogy to HMMMO and HMPMO. As an alkylation agent 25 mL of freshly distilled bromohexane (170 mmol) were added. After cooling to room temperature, DMSO was evaporated under reduced pressure and the product was dissolved in ethyl acetate and washed with water at least three times. Ethyl acetate was evaporated and the product was destillated (yield: 51%). ^{1}H NMR (300 MHz, CDCl$_3$): δ (ppm)= 4.46 (d, 2H, J = 6.2 Hz, -CH_2O-), 4.39

(d, 2H, *J* = 6.2 Hz, -C*H*$_2$O-), 3.90 (s, 2H, -CH$_2$O-), 3.74 (s, 2H, -C*H*$_2$O-), 3.43 (t, 2H, *J* = 6.6 Hz, CH$_2$O-), 2.64 (s, 1H, -O*H*), 1.68-1.44 (m, 2H, C*H*$_2$-), 1.37-1.16 (m, 6H, -C*H*$_2$-) 0.9 (t, 3H, *J* = 6.8 Hz, C*H*$_3$-). ^{13}C NMR (75 MHz, CDCl$_3$): δ (ppm) = 76.62 (-CCH$_2$-O-CH$_2$-), 75.31 (-CH$_2$OH), 72.02 (-CCH$_2$-O-), 67.01 (-O-CH$_2$-), 31.57 (CH$_2$-C-CH$_2$), 29.45 (-CH$_2$-), 29.40 (-CH$_2$-), 25.67 (-CH$_2$-), 22.44 (-CH$_2$-), 13.97 (-CH$_3$), ESI MS: 225.14 g mol^{-1} with sodium as cation (calc. isotopic mass=225.15 g mol^{-1}).

General procedure for the synthesis of hyperbranched polyoxetanes
Distilled boron trifluoride etherate (0.06 mL, 0.47 mmol) was added to dichloromethane via a syringe at room temperature under argon atmosphere. Freshly distilled monomer (HMMMO: 0.5 mL, 4.7 mmol, 132.08 g/mol, HMPMO: 0.5 mL, 3.4 mmol, 160.11 g/mol, HMHMO: 0.5 mL, 2.7 mmol, 202.16 g/mol) was dissolved in 11.5 mL freshly distilled dichloromethane and added slowly via syringe over 8 h. After 12 h, the polymerization was quenched with pyridine. The product was dissolved in 0.5 mL pyridine and precipitated three times in diethyl ether. The polymer was dried under reduced pressure at 70 °C for 2 d (yield: 64.2% PHMMMO, 75.0% PHMPMO, 66.0% PHMHMO).

^{1}H NMR (PHMMMO, 400 MHz, pyridine-*d*$_5$): δ (ppm) = 4.7-4.4 (m, -C*H*$_2$O-), 4.15-4.05 (m, -O*H*), 4.1-3.8 (m, -C*H*$_2$O-), 3.3-3.1 (m, C*H*$_3$O-). ^{13}C NMR (100.6 MHz, pyridine-*d*$_5$): δ (ppm) = 76.2-74.2 (polyether backbone), 65.2-62.8 (-CH$_2$-OH), 58.7-59.2 (-CH$_3$), 45.3 (CH$_2$-C-CH$_2$).

^{1}H NMR (PHMPMO, 400 MHz, pyridine-*d*$_5$): δ (ppm)= 7.0 (m, O*H*), 4.4-3.9 (m, -C*H*$_2$O-), 3.9-3.6 (m, -C*H*$_2$O-), 3.6-3.4 (m, C*H*$_2$O-), 3.4-3.3 (m, C*H*$_2$O-), 1.8-0.6 (m, CH$_3$CH$_2$-). ^{13}C NMR (PHMPMO, 100.6 MHz, pyridine-*d*$_5$): δ (ppm) = 74.2-69.5.2 (polyether backbone), 65.0-67.2 (-CH$_2$-OH), 64.2 (-CH$_2$-), 46.0-47.2 (CH$_2$-C-CH$_2$), 23.6 (-CH$_2$-), 10.3 (-CH$_3$).

^{1}H NMR (PHMHMO, 400 MHz, pyridine-*d*$_5$): δ (ppm)= 6.3 (m, -O*H*), 4.4-3.9 (m, -CH$_2$O-), 3.9-3.6 (m, -C*H*$_2$O-), 3.6-3.4 (m, C*H*$_2$O-), 3.4-3.3 (m, C*H*$_2$O-), 1.8-0.6 (m, CH$_3$CH$_2$-). ^{13}C NMR (100.6 MHz, pyridine-*d*$_5$): δ (ppm) = 74.2-69.5.2 (polyether backbone), 65.0-67.2 (-CH$_2$-OH), 61.1 (-CH$_2$-), 46.0-47.2 (CH$_2$-C-CH$_2$), 32.4-23.5 (-CH$_3$).

General procedure for the synthesis of hyperbranched oxetanes with core molecules
Distilled boron trifluoride etherate (0.06 mL, 0.47 mmol, 141.93 g mol^{-1}) was added to a solution of dichloromethane and 1,1,1-tris(4-hydroxyphenyl)ethane (306.36 g mol^{-1}) via a syringe at room temperature under argon atmosphere. Freshly distilled monomer (HMMMO: 0.5 mL, 4.7 mmol, 132.08 g mol^{-1}, HMPMO: 0.5 mL, 3.4 mmol, 160.11 g mol^{-1}, HMHMO: 0.5 mL, 2.7 mmol, 202.16 g mol^{-1}) was dissolved in 11.5 mL freshly distilled dichloromethane and added slowly via syringe over 8 h. After 12 hours the polymerization was quenched with pyridine. Subsequently, the product was dissolved in 0.5 mL pyridine and precipitated three times in diethyl ether. The polymer was dried under reduced pressure at 70 °C for 2 d (yield: 65.0% PHMMMO, 84.2% PHMPMO, 84.0% PHMHMO). ^{1}H NMR of PHMHMO, polymerized with 1,1,1-tris(4-hydroxyphenyl)ethane (the corresponding values of PHMMMO and PHMPMO are given in the Supporting Information) (400 MHz, pyridine-*d*$_5$): δ (ppm) = 7.41-6.87 (m, arom. H), 6.01 (m, -OH), 4.25-3.28 (m, polyether backbone), 2.22 (s, -CH$_3$), 1.8-0.6 (m, CH$_3$CH$_2$-). ^{13}C NMR (100 MHz, pyridine-*d*$_5$): δ (ppm) = 156.58 (=C-, arom.), 141.24 (=C-, arom.), 129.98 (=CH-, arom.), 115.08 (=CH-, arom.),71.33-62.66 (polyether backbone), 58.69 (-CH$_3$), 46.09 (-C-), 31.52(-CH$_2$-), 29.83 (-CH$_2$-), 25.89 (-CH$_2$-), 22.60 (-CH$_2$-), 13.97 (-CH$_3$).

Functionalization with trifluoroacetic an-hydride (TFAA)
100 mg of polymer (PHMMMO, PHMPMO or PHMHMO) were dissolved in 5 mL of trifluoroacetic anhydride under argon atmosphere and refluxed for 8 h. The solution was cooled to room temperature and trifluoroacetic anhydride was evaporated under reduced pressure. The product was dried under reduced pressure at 50 °C for 8 h (yield: 89%). ^{1}H NMR of functionalized PHMMMO (400 MHz pyridine-*d*$_5$): δ (ppm)= 4.79-4.44 (m, -CH$_2$O-CO-), 3.81-3.07 (m, polyether backbone, m, -CH$_3$). ^{13}C NMR of functionalized PHMMMO (100.6 MHz, pyridine-*d*$_5$): δ (ppm) =

164.23-160.55 (-C=O), 121.30-112.73 (CF$_3$), 75.14-65.99 polyether backbone, CH$_2$-CO-), 59.69 (-CH$_3$), 47.94-42.43 (-C-).
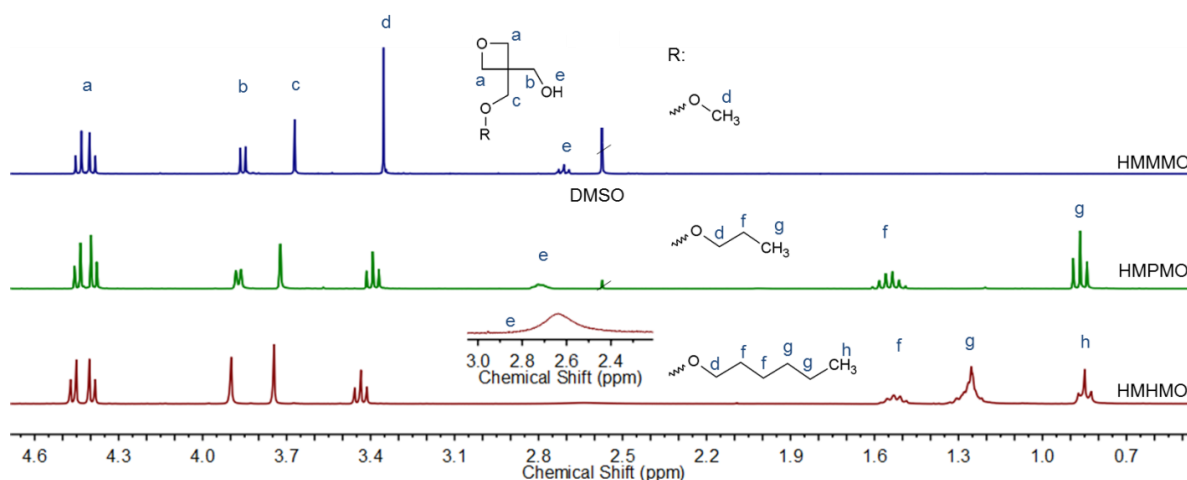
Figure 1: ^{1}H NMR spectra (300 MHz, CDCl$_3$) of HMMMO, HMPMO and HMHMO with methyl, n-propyl and n-hexyl substituent, respectively.

RESULTS AND DISCUSSION

As illustrated in Scheme 1, the novel oxetane-inimers were synthesized in two steps. In the first reaction, 3,3-bis(hydroxymethyl)oxetane (BHMO) was prepared, starting from pentaerythritol and diethyl carbonate.[29] In the second step, one of the two hydroxyl groups of BHMO was functionalized by alkylation using either methyl iodide, 1-propyl bromide or 1-hexyl bromide.

Since alkylation of the second hydroxyl group of BHMO also occurred as an inavoidable side reaction, yields of the desired monoalkylated BHMO-derivative did not exceed 51%. After extraction in diethyl ether or ethyl acetate and distillation the products possessed a purity of 98%, confirmed by gas chromatography. Electro spray ionization mass spectroscopy (ESI MS) showed molecular weights of HMMMO, HMPMO and HMHMO and demonstrated the absence of side products. Characterization by IR spectroscopy shows a signal at 920-930 cm^{-1} which can be assigned to the oxetane ring and a broad signal at 3200-3500 cm^{-1} for the hydroxyl groups. In Figure 1 the ^{1}H NMR spectra of the new oxetane inimers HMMMO, HMPMO and HMHMO are presented, which show the characteristic doublets of the protons of the oxetane rings and the signals of the protons of the hydroxyl groups.

Polymerization and functionalization

HMMMO, HMPMO and HMHMO were polymerized by cationic ring-opening polymerization with boron trifluoride etherate as the cationic catalyst, following the synthetic procedure published by Bednarek and coworkers for poly(3-ethyl-3-hydroxymethyl oxetane) (PEHO).[31, 43] The corresponding hyperbranched polymers PHMMMO, PHMPMO and PHMHMO were characterized by SEC, MALDI-ToF MS as well as ^{1}H NMR and ^{13}C NMR spectroscopy.
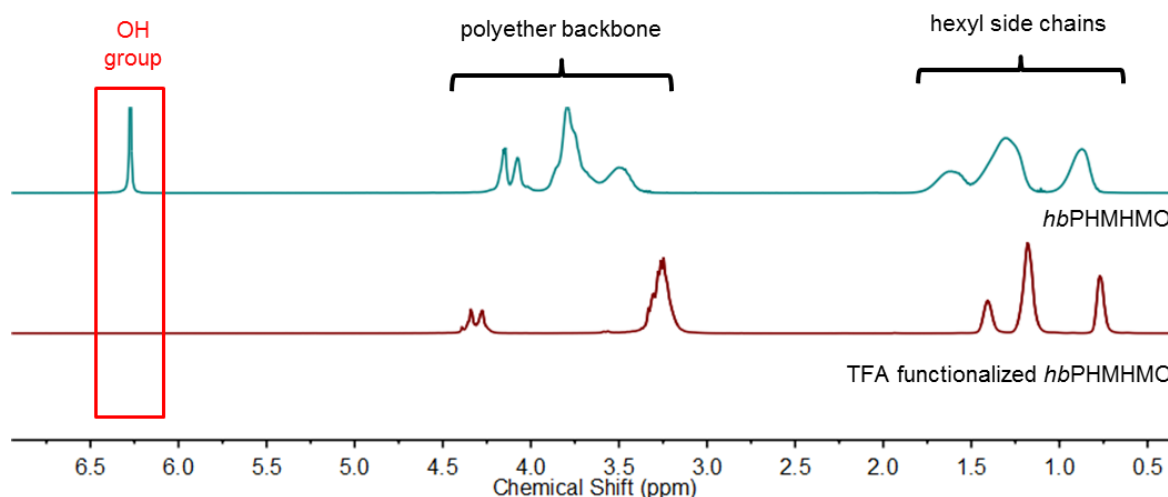
Figure 2: ^{1}H NMR (400 MHz) spectra of PHMHMO (sample No. 9) before (top) and after functionalization (bottom) with TFAA, measured in pyridine-d_5.

Table 1: Characterization data of *hb*PHMMMO, *hb*PHMPMO and *hb*PHMHMO.

No.	polymer	M_n[a]	PDI[a]	DB[b]
1	PHMMMO	500	1.16	58.4
2	PHMMMO	600	2.50	61.4
3	PHMMMO	600	1.68	62.1
4	PHMMMO	1200	1.20	54.2
5	PHMPMO	900	1.45	52.1
6	PHMPMO	2000	2.22	43.0
7	PHMPMO	2500	1.83	46.0
8	PHMHMO	1000	2.91	47.0
9	PHMHMO	1100	1.33	54.0
10	PHMHMO	1400	1.29	60.3

a: apparent molecular weights, determined by SEC after functionalization with TFAA (THF, PS-standard) in g mol^{-1}, RI detector. b: determined from IG ^{13}C NMR spectra after functionalization with TFAA, in %.

To dissolve PHMMMO, PHMPMO and PHMHMO in organic solvents like THF for SEC characterization, the hydroxyl groups were acylated with TFAA. The resulting molecular weights and PDIs obtained by SEC as well as the degrees of branching (vide infra) are listed in Table 1. Compared to the PHMPMO and PHMHMO samples, PHMMMO possesses the lowest molecular weight. The different molecular weights obtained by SEC support the conclusion that the cationic ring opening polymerization is not controllable in the sense that targeted molecular weights could be reached.

Molecular weights obtained by SEC suggest that in several reactions merely oligomers were obtained (e.g. sample 1-3, 5). However, from the solid appearance of the products, the decreasing solubility in organic solvents and water, the broad signals obtained by NMR spectroscopy and particularly the results obtained by MALDI ToF MS as well as by DSC, there is evidence that the apparent molecular weights by SEC are underestimated.

Figure 2 presents the ^{1}H NMR spectra of PHMHMO and acetylated PHMHMO (sample No. 9). Prior to derivatization a signal at 6.51 ppm is detectable, which is due to the protons of the hydroxyl groups. After functionalization with TFAA the signal disappears completely. From these

results, successful functionalization of the hydroxyl groups of PHMHMO is evident. Additionally, complete functionalization is supported by the disappearance of the signals of the hydroxyl groups (3200-3000 cm⁻¹) in the IR spectrum.
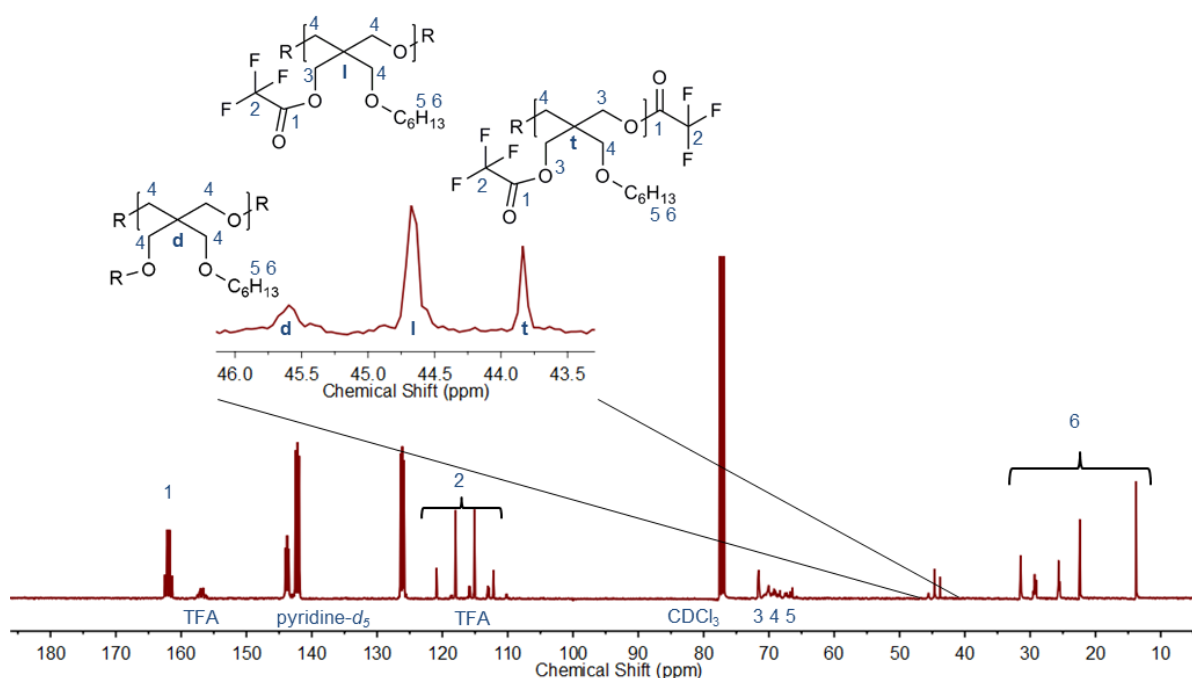
Figure 3: IG ^{13}C NMR (100.6 MHz) of PHMHMO (sample No. 9), functionalized with TFAA, measured in CDCl₃. Pyridine-d_5 was used as solvent for the reaction and is therefore visible as a pyridinium salt in the spectrum, R: oxetane-unit.

The degree of branching (DB) was first defined by Fréchet and coworkers who introduced the following equation:[44]

$$DB = \frac{D+T}{D+T+L} \qquad (1)$$

A systematic consideration led to the generally valid equation (2), which is also used in this work:[9, 45]

$$DB = \frac{2D}{(2D+L)} \qquad (2)$$

The values for D and L were obtained from inverse gated (IG) ^{13}C NMR spectra by integrating the quaternary carbon signals of the functionalized polyoxetanes. This procedure was already used for PEHO, as reported by Magnusson et al.[46] The separated signals belong to the dendritic (D), linear (L) and terminal (T) units of the polymer. Figure 3 shows an exemplary IG ^{13}C NMR spectrum (PHMHMO, sample No. 9, after acylation) with the mentioned signals highlighted (see enlargement). The resulting degrees of branching vary between 43 and 62%, as shown in Table 1. PHMPMO shows the lowest degrees of branching (around 44%). The average DB of all listed polymers is 52.9%, consistent with results of related polymers like *hb*PEHO in literature (around 50%, vide supra).[39, 40]

Characterization by MALDI-ToF MS

Based on the absolute mass/charge ratios of the distinct macromolecular species of a poly-disperse polymer sample provided by MALDI-ToF MS, this tool permits end group analysis and was employed to characterize the molecular weights of the polyoxetanes synthesized.

Furthermore, intramolecular chain transfer reactions, which result in cyclic products, can be detected via MALDI-ToF MS. Figure 4 shows a MALDI-ToF mass spectrum of PHMHMO (sample No. 8) after purification by precipitation.

a.) $(C_{11}H_{22}O_3)_7 \cdot Li^+ = 1423.32$ g mol^{-1}, calc. isotopic mass $= 1422.11$ g mol^{-1}
b.) $(C_{11}H_{22}O_3)_7 \cdot K^+ H_2O = 1473.73$ g mol^{-1}, calc. isotopic mass $= .1472.07$ g mol^{-1}
c.) $(C_{11}H_{22}O_3)_7 \cdot Li^+ BF_3 H_2O = 1508.80$ g mol^{-1}, calc. isotopic mass $= 1508.94$ g mol^{-1}
d.) $(C_{11}H_{22}O_3)_7 \cdot Li^+ BF_3 OEt_2 = 1562.69$ g mol^{-1}, calc. isotopic mass $= 1564.04$ g mol^{-1}
e.) $(C_{11}H_{22}O_3)_7 \cdot K^+ BF_3 OEt_2 = 1595.31$ g mol^{-1}, calc. isotopic mass $= 1595.99$ g mol^{-1}
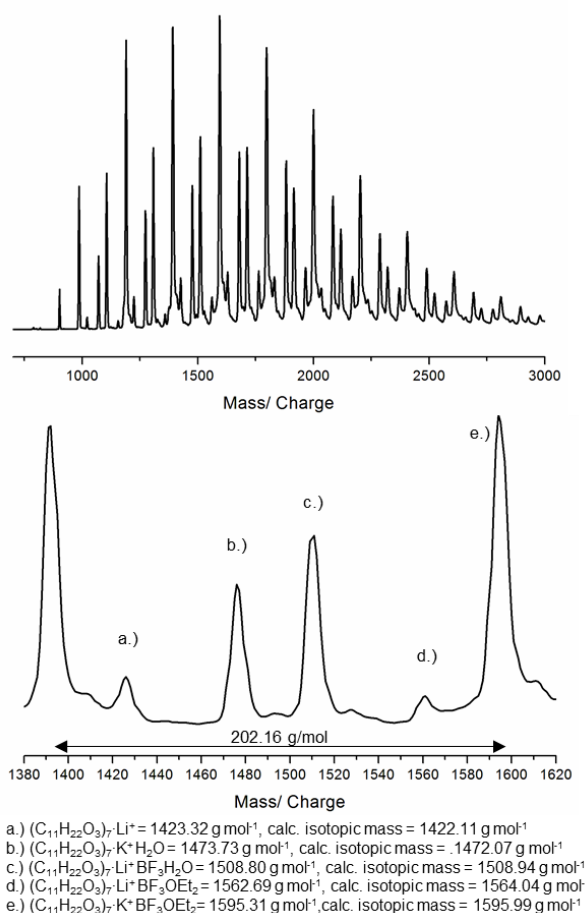
Figure 4: MALDI-ToF MS of sample 3, CHCA matrix, cationized with potassium.

The inset presents five different series of signals, which occur in the interval of the molecular weight of the monomer HMHMO (202.16 g mol^{-1}). The signals with the highest intensity stem from PHMHMO, initiated with boron trifluoride etherate, cationized with potassium. In the inset the hexamer and heptamer are shown. Two signals of medium intensity can be assigned to heptamers of PHMHMO, initiated with water and boron trifluoride and water, cationized with lithium and potassium. The polymerization with boron trifluoride etherate as initiator is known to start with water, although initiator and monomers were freshly distilled under argon atmosphere.[47] The remaining distribution with lowest intensity belongs to the heptamer of PHMHMO and the heptamer of PHMHMO initiated with boron trifluoride. Both were cationized with lithium. The heptamer of PHMHMO, initiated without boron trifluoride or water, could either exist in a cyclized form or including an oxetane unit. Scheme 2 shows the mechanism of the propagation of the polymerization with boron trifluoride etherate and the assembly of boron trifluoride in the polymer. Protons can result by intermolecular transfer steps (Scheme 2.2), which are capable of initiating further chains, whereas the other modes can be explained by polymer molecules without initiator as starting molecules. In summary, polymerizations with boron trifluoride etherate are expected to be either initiated by boron trifluoride or by a proton formed by reaction with a co-initiator like water (see Scheme 2.3). Propagation of the polymerization with boron trifluoride etherate is additionally supported by ^{19}F NMR (see Supporting Information). PHMHMO was measured using pyridine-d_5 as a solvent. PHMHMO shows one signal at 149.06 ppm, boron trifluoride etherate shows two signals at 148.84 ppm

and 149.60 ppm. The chemical shift of the signals implies that residual initiator is removed during purification of the polymer and that boron trifluoride etherate is incorporated in the polymer. One of the two signals of the measurement of boron trifluoride etherate in pyridine can be explained by complexation of the boron atom with the oxygen atom of diethyl ether and the second signal by complexation of the boron atom to the nitrogen of the pyridine solvent. It is well-known that MALDI-ToF MS commonly underestimates molecular weights due to discrimination of the higher molecular weight fractions, the so called "mass discrimination effect".[48] In the present case, MALDI-ToF MS leads to higher molecular weight for sample 8 (see Table 1) than SEC (M_n= 1000 g mol^{-1}, PDI= 2.91), since the hyperbranched structure of the polymer strongly differs from the linear polystyrene standard. We attribute this to the hyperbranched structure of the polymer, which results in a lower hydrodynamic volume than for the linear polystyrene standard used in SEC.

Scheme 2: Mechanism of the initiation processes, including boron trifluoride etherate, oxetane-inimer and water.
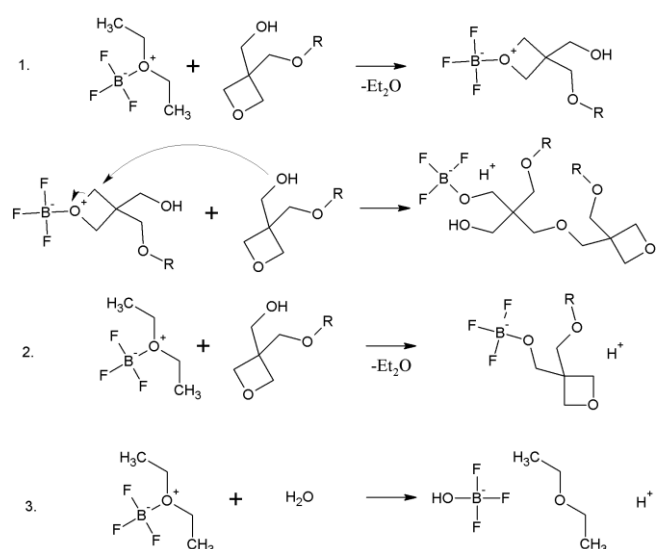
Cationic ring-opening polymerization initiated by THPE

Polymerizations under SMA (slow monomer addition)[49] conditions with a core-molecule (Table 2) were conducted to investigate the correlation between the active monomer and the active chain end mechanism. SMA conditions were chosen, because in this case self-initiated polymerization should be suppressed. The probability of the reaction between an oxetane monomer and a propagating main chain increases in comparison to reaction with another monomer.[6, 50] Nevertheless, the degree of branching should increase by inserting a focal unit for the following reason: In the first step, a hydroxyl group of the focal unit attacks an oxetane-inimer, which leads to opening the oxetane ring-system, whereas without a focal unit, propagation commences with the attack of an oxetane hydroxyl group at an additional oxetane-inimer. The remaining oxetane rings in the main chain lead to an ACE-mechanism, which finally results in a lower degree of branching.[31] 1,1,1-tris(4-hydroxyphenyl)ethane (THPE) was chosen as a focal unit. In addition, this moiety renders the resulting polyethers detectable by the UV detector of the SEC setup. In addition, it allows for the determination of the number-averaged molecular weight from the ^{1}H NMR spectra due to the low field resonances of its aromatic protons. However a crucial requirement for this method is complete incorporation of the core molecule in all polymer chains formed. Table 2 lists the molecular weights and PDIs of a series of PHMMMOs, PHMPMOs and PHMHMOs with THPE incorporated as a focal unit. In comparison to

the results of the polymerizations in absence of THPE (Table 1), the average molecular weights and the average DB increased consiedrably, confirming the effect of the slow monomer addition.

In polymerizations initiated with THPE, the AM mechanism predominates, as explained above. The average molecular weights measured by SEC deviate from the targeted molecular weights, being somewhat lower, which is again most likely a consequence of the linear polystyrene standards. Furthermore, molecular weights obtained from ^{1}H NMR differ from the molecular weights measured by SEC. ^{1}H NMR spectroscopy is more precise than IG ^{13}C NMR spectroscopy, because protons show shorter relaxation times than carbon atoms and higher sensitivity. Therefore, an interpretation of the molecular weights from ^{13}C NMR does not lead to reliable values. Generally, a low deviation of the integration of the initiator signals results in enormous differences in the resulting molecular weights. NMR spectroscopy may overestimate the molecular weights because of self-initiated NMR spectroscopy may overestimate the molecular weights because of self-initiated polymerization of the oxetanes as a side reaction.
Altogether, the values are closer to the targeted molecular weight, with the exception of sample 14. However, the molecular weight is not controllable under the conditions of the cationic ring-opening polymerization.

Table 2: Characterization data of *hb*PHMMMO, *hb*PHMPMO and *hb*PHMHMO, polymerized with THPE.

No.	Polymer	M_n^a	M_n^b	M_n^c	M_n^d	PDI^c	PDI^d	DB^c
11	THPE-PHMMMO	4040	2300	1600	2000	1.84	1.85	33.8
12	THPE-PHMMMO	2950	800	2400	2000	2.13	1.2	65
13	THPE-PHMPMO	3030	5000	4200		1.68		69
14	THPE-PHMPMO	9000	10200	7000		1.66		53.5
15	THPE-PHMPMO	5900	3000	8100	8000	1.4	1.24	48.5
16	THPE-PHMPMO	2070	37700	11200	9900	1.44	1.34	53.2
17	THPE-PHMHMO	6000	1200	1100	1100	1.68	1.2	67.3
18	THPE-PHMHMO	1900	4400	1400	1300	1.13	1.23	61.8
19	THPE-PHMHMO	2900	2400	1700	1000	1.34	1.61	61.7
20	THPE-PHMHMO	10000	23200	2100		1.33		46.2
21	THPE-PHMHMO	4200	4500	2900	5000	1.42	1.2	64
22	THPE-PHMHMO	5000	1600	5000	4900	1.26	1.21	56

a: targeted molecular weight in g mol-1. b: determined by ^{1}H NMR in g mol-1. c: determined by SEC (THF, PS-Std.) in g mol-1, RI detector. d: determined by SEC (THF, PS-Std.) in g mol-1, UV detector.
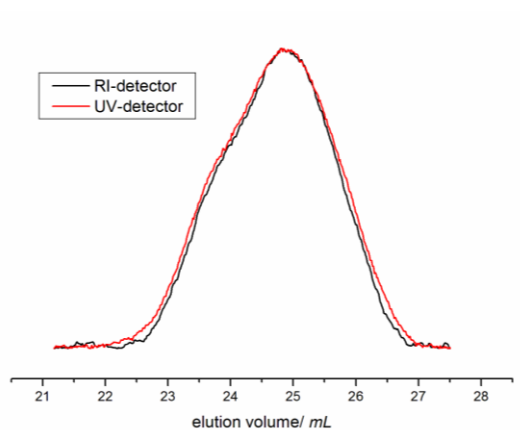
Figure 5: SEC-diagram of THPE-PHMHMO (sample No. 22) in THF, polymerized with THPE, demonstrating incorporation of the aromatic core unit in all polymer chains of the distribution.

Figure 5 shows an SEC diagram of PHMHMO (sample No. 22), recorded by both detectors RI and UV. Further SEC results are shown in the Supporting Information (fig. S15-S20). SEC diagrams of the samples THPE-PHMPMO (sample No. 13), THPE-PHMPMO (sample No. 14) and THPE-PHMHMO (sample No. 20) do not show a signal of the UV-detector in SEC analysis. However, polymerizations without the core molecule can be excluded, because no lower molecular weight fractions were detected by SEC, assigned to THPE. Additionally, NMR spectroscopy shows a shift of the aromatic signals in comparison to the signals of THPE.

For further characterization, a ^{1}H DOSY (Diffusion Ordered Spectroscopy) NMR spectrum of THPE-PHMHMO (sample No. 20), was measured (Figure S21, Supporting Information). The objective of the measurement is to guarantee incorporation of the focal unit in the polymer. The ^{1}H DOSY NMR spectrum reveals two distinct diffusion coefficients, which range from 6.78-6 to 1.67-6 cm^2 s^{-1} for the polymeric species and from 1.88-5 to 1.21-5 cm^2 s^{-1} for the lower molecular weight compounds, such as pyridine-d_5 and DMSO. The aromatic signals that stem from the focal unit exhibit a diffusion coefficient of 6.78-6 to 1.96-6 cm^2 s^{-1} and are located within the range of the polymer backbone. A higher magnification of the aromatic signals in the upper left corner reveals two doublets. For the DOSY transform, standard values by ´Mestrelab Research´ were used. The results support the theory that the polymerization is initiated by the focal units under SMA conditions.[6, 50]

Table 4: Solubility of *hb*PHMMMO (sample No. 4), *hb*PHMPMO (sample No. 5) and *hb*PHMHMO (samples No. 9) in various organic solvents and water (+: good solubility, -: no solubility).

polymer	water/ ethanol/ methanol	DMF	DMSO	triethylamine	pyridine	acetonitrile	n-hexane	THF
*hb*PHMMMO	-	-	-	-	+	-	-	-
*hb*PHMPMO	-	-	+	+	+	-	-	-
*hb*PHMHMO	-	+	+	+	+	-	-	-

Properties of *hb*PHMMMO, *hb*PHMPMO and *hb*PHMHMO

To investigate the thermal properties of the polyethers differential scanning calorimetry (DSC) measurements were carried out.

Table 3 lists the glass transition temperatures (T$_g$) of *hb*PHMMMO, *hb*PHMPMO and *hb*PHMHMO. The T$_g$s vary with molecular weight, polydispersity and degree of branching and range from -59 to -24 °C. The direct comparison of the T$_g$s of the polymers with different alkyl chain length (samples 4, 5 and 9 with similar molecular weights, polydispersities and degrees of

branching (see Table 3) permits to evaluate the influence of the alkyl chain length. The polyether with the shortest alkyl chain length (*hb*PHMMMO) exhibits the highest T_g (-30 °C), and the polymer with the longest alkyl chain length (*hb*PHMMMO) the lowest T_g (-51 °C), as expected. In comparison to PEHO, the T_gs of *hb*PHMMMO, *hb*PHMPMO and *hb*PHMHMO are considerably lower (T_g (PEHO): 54 °C[48]). Also PHMO exhibits higher glass transition temperatures (T_g (PMHO): 15 °C)[51]. To the best of our knowledge, the T_gs listed in Table 3 represents the lowest values for hyperbranched polyoxetanes reported to date. We attribute this to the flexibilizing effect of the alkyl end groups.

Table 3: Glass transition temperatures of *hb*PHMMMO, *hb*PHMPMO and hbPHMHMO with molecular weights, polydispersities and DB.

No.	polymer	M_n^a	PDI^a	DB^b	T_g^c
2	PHMMMO	600	2.50	61.4	-51
3	PHMMMO	600	1.68	62.1	-49
4	PHMMMO	1200	1.20	54.2	-30
5	PHMPMO	900	1.45	52.1	-39
6	PHMPMO	2000	2.22	43	-30
7	PHMPMO	2500	1.83	46.0	-24
8	PHMHMO	1000	2.91	47	-59
9	PHMHMO	1100	1.33	54	-51
10	PHMHMO	1400	1.29	60.3	-49

a: determined by SEC after functionalization with TFAA (THF, PS-Std.) in g mol^{-1}, RI detector. b: determined from IG ^{13}C NMR spectra after functionalization with TFAA, in %, c: determined by DSC in °C, heating rate: 10 °C from -70 to 50 °C, second heating phase.

Besides DSC measurements, the solubility of all polymers in different solvents has been investigated. Even though hyperbranched polyoxetanes exhibit higher solubility than their linear homologues[13], they are soluble in a few solvents only, such as cresol[30] or, depending on the degree of branching, in DMSO.[52] Table 4 lists the results of a comprehensive study of the solubility of *hb*PHMMMO, *hb*PHMPMO and *hb*PHMHMO in different solvents. To this end, sample 4, 5 and 9 were chosen, because of their similar molecular weights, polydispersities and degrees of branching.

The hydrophobic polyoxetanes show good solubility in pyridine. With growing alkyl chain length solubility increases, rendering *hb*PHMHMO (sample No. 9) soluble in DMF. Clearly, variation of the alkyl chain length permits tailoring of the solubility.

Conclusion

In summary, we present a straightforward two-step synthesis for three novel, hydroxyfunctional oxetanes and their cationic ring-opening polymerization to hyperbranched polyethers. The resulting polymers h*b*PHMMMO, *hb*PHMPMO and *hb*PHMHMO exhibit degrees of branching between 43 and 62% (M_n=500-2500 g mol^{-1} via SEC). As a key result, with the use of THPE as a focal unit under slow monomer addition polymerization conditions, enhanced degrees of branching (DB) up to 69% and elevated molecular weights (up to 11200 g mol^{-1} via SEC) have been achieved. This supports the hypothesis that the AM mechanism is preferred under these conditions. However, cationic ring-opening polymerizations (CROP) of oxetanes to hyperbranched structures are not controllable in the sense that the targeted molecular weights can be obtained.

Nevertheless, the novel hyperbranched polyoxetanes are interesting materials with respect to surface functionalization or biomedical application. Further exploration will be focused on kinetic in situ studies of the ROMBP of the novel oxetane-inimers to hyperbranched structures and their application as functional, yet hydrophobic surface coatings.

REFERENCES AND NOTES

1. J. A. Burkhard; G. Wuitschik; M. Rogers-Evans; K. Müller; E. M. Carreira, *Angewandte Chemie* **2010**, 122 (48), 9236.
2. H. K. Eigenmann, D. M. Golden, S. W. Benson, *The Journal of Physical Chemistry*, **1973** (77), 1687.
3. T. J. Smith, L. J. Matthias, *Polymer*, **2002** (43), 7275.
4. Y. Zhou; D. Yan, *Adv. Mater.* **2010**, 22 (41), 4567.
5. F. Schüler; B. Kerscher; F. Beckert; R. Thomann; R. Mülhaupt, *Angew. Chem. Int. Ed.* **2013**, 52 (1), 455.
6. Y. Liu; J. Chunyang; J. Haibao; B. Jiang; X. Zhu; Y. Zhou; Z. Lu; D. Yan, *J. Am. Chem. Soc.* **2013**, 135 (12), 4765.
7. A.-K. Appel, R. Thomann, R. Mülhaupt, *Macromol. Rapid Commun.* **2013**, 34 (15), 1249.
8. B. Kerscher, A.-K. Appel, R. Thomann, R. Mülhaupt, *Macromolecules* **2013**, 46 (11), 4395.
9. M. Schömer, C. Schüll, H. Frey, *J. Polym. Sci. A Polym. Chem.* **2013**, 51 (5), 995.
10. Q. Zhu; J. Wu; C. Tu; Y. Shi; L. He; R. Wang; X. Zhu; D. Yan, *J. Phys. Chem. B* **2009**, 113 (17), 5777.
11. Y. H. Kim, O. W. Webster, *J. Am. Chem. Soc.* **1990**, 112 (11), 4592.
12. Y. Zhou, D. Yan, *Chem. Commun.* **2009**, 1172-1188.
13. C. Gao, D. Yan, *Prog. Polym. Sci.* **2004** (29), 183.
14. C. Siegers, M. Biesalski, R. Haag, *Chem. Eur. J.* **2004**, 10 (11), 2831.
15. B. I. Voit, A. Lederer, *Chem. Rev.* **2009**, 109 (11), 5924.
16. R. Haag, *Angew. Chem. Int. Ed.* **2004**, 43 (3), 278.
17. V. Labhasetwar, D. L. Leslie-Pelecky, *Biomedical Applications of Nanotechnology* **2007**, 105-129.
18. R. Vestberg; R. Westlund; A. Eriksson; C. Lopes; M. Carlsson; B. Eliasson; E. Glimsdal; M. Lindgren; E. Malmström, *Macromolecules* **2006**, 39 (6), 2238.
19. C. J. Hawker, J. M. J. Fréchet, *J. Am. Chem. Soc. 1990*, 112 (21), 7638.
20. E. Buhleier, W. Wehner, F. Vögtle, *Synthesis,* **1978** (02), 155.
21. G. R. Newkome, Z. Yao, G. R. Baker, V. K. Gupta, *J. Org. Chem.* **1985**, 50 (11), 2003.
22. M. Calderón, M. A. Quadir, S. K. Sharma, R. Haag, *Adv. Mater.* **2010**, 22 (2), 190.
23. A. Dworak, W. Walach, B. Trzebicka, *Macromol. Chem. Phys.* **1995**, 196 (6), 1963.
24. A. Sunder, R. Hanselmann, H. Frey, R. Mülhaupt, *Macromolecules* **1999**, 32 (13), 42, 40.
25. D. Wilms, F. Wurm, J. Nieberle, P. Böhm, U. Kemmer-Jonas, H. Frey, *Macromolecules* **2009** (42), 3230.
26. D. Wilms, S.-E. Stiriba, H. Frey, *Acc. Chem. Res.* **2010**, 43 (1), 129.
27. C. Schüll, L. Nuhn, C. Mangold, E. Christ, R. Zentel, H. Frey, *Macromolecules* **2012**, 45 (15), 5901.
28. K. J. Wynne et al., US 20130183262, **2012**.
29. E. J. Vandenberg, J. C. Mullis, R. S. Juvet, *Journal of Polymer Science Part A: Polymer Chemistry,* **1989** (27), 3083.

30. H. Schnell et al., 2917468, **1956**.
31. M. Bednarek et al., *Macromol. Rapid Commun.* **1999** (20), 369.
32. M. Bednarek, P. Kubisa, S. Penczek, *Macromolecules* **2001**, 34 (15), 5112.
33. Y. Chen, M. Bednarek, P. Kubisa, S. Penczek, *J. Polym. Sci. A Polym. Chem.* **2002**, 40 (12), 1991.
34. T. Biedroń, M. Bednarek, P. Kubisa, *Macromol. Rapid Commun*. **2004**, 25 (8), 878.
35. D. Wilms, J. Klos, H. Frey, *Macromol. Chem. Phys.* **2008**, 209 (4), 343.
36. A. Möck, A. Burgath, R. Hanselmann, H. Frey, *Macromolecules* **2001**, 34 (22), 7692.
37. D. Yan et al., *Macromol. Rapid Commun.* **2000**, 21, 557–56.
38. Y. Xia et al., *Macromol. Chem. Phys.* **2011**, 212 (10), 1056.
39. B. Kerscher, A.-K. Appel, R. Thomann, R. Mülhaupt, *Macromolecules* **2013**, 46 (11), 4395.
40. Y. Xu; C. Gao; H. Kong; D. Yan; P. Luo; W. Li; Y. Maiet, *Macromolecules* **2004**, 37 (17), 6264.
41. Y. Mai, Y. Zhou, D. Yan, H. Lu, *Macromolecules* **2003**, 36 (25), 9667.
42. B. Schulte, C. A. Dannenberg, H. Keul, M. Möller, *J. Polym. Sci. A Polym. Chem.* **2013**, 51 (5), 1243.
43. M. Bednarek, *Polym. Int.* **2003**, 52 (10), 1595.
44. C. J. Hawker, R. Lee, J. M. J. Fréchet*, J. Am. Chem. Soc.* **1991**, 113, 4583–4588.
45. D. Hölter, A. Burgath, H. Frey, *Acta Polymerica*, **1997** (48), 30.
46. H. Magnusson, E. Malmström, A. Hult, *Macromolecules* **2001**, 34 (17), 5786.
47. K. Matyjaszewski, *Cationic polymerizations: Mechanisms, synthesis and applications*, **1996**.
48. H. Magnusson, E. Malmström, A. Hult, Macromol. Rapid Commun. **1999** (20), 453.
49. R. Hanselmann, D. Hölter, H. Frey, *Macromolecules* **1998**, 31 (12), 3790.
50. M. Rahm, R. Westlund, C. Eldsäter, E. Malmström, *J. Polym. Sci. A Polym. Chem.* **2009**, 47 (22), 6191.
51. A. Möck, *Dissertation*, Universität Freiburg/Brsg., **2001**.
52. H. Magnusson, E. Malmström, A. Hult, M. Johansson, Polymer **2002** (43), 301.

A.7 List of Publications

Journal Articles

2012

1. "Synthesis of oxetane-functional aliphatic polyesters via enzymatic polycondensation",
S. S. Müller, H. Frey, *Macromol. Chem. Phys*, **2012**, 213, 1783-1790.

2013

2. "Polyether-based lipids synthesized with an epoxide construction kit: Multivalent architectures for functional liposomes"
S. S. Müller, C. Dingels, A. M. Hofmann, H. Frey, **2013**, ACS Symposium Series 1135, p. 11-25. *("Tailored Polymer Architectures for Pharmaceutical and Biomedical Application.*

3. "Universal concept for the implementation of a single cleavable unit at tunable position in functional poly(ethylene glycol)s"
C. Dingels, S. S. Müller, T. Steinbach, C. Tonhauser, H. Frey, *Biomacromolecules,* **2013**, 14 (2), 448–459.

4. "Block copolymers in giant unilamellar vesicles with proteins or with phospholipids" R. Schöps, E. Amado, S. S. Müller, H. Frey, J. Kressler, *Faraday Discuss.*, **2013**, 166, 303-315.

2014

5. "Beyond Poly(ethylene glycol): Linear Polyglycerol as a Multifunctional Polyether for Biomedical and Pharmaceutical Applications"
A. Thomas, S. S. Müller, H. Frey. **2014**, *Biomacromolecules, 15,* 1935-1954.

6. "A Challenging Comonomer Pair: Copolymerization of Ethylene Oxide and Glycidyl Methyl Ether to Thermoresponsive Polyethers"
S. S. Müller, C. Moers, H. Frey, **2014**, *Macromolecules*, accepted.

7. "Click Modification of Multifunctional Liposomes with Hyperbranched Polyether Chains"
T. Fritz, M. Hirsch, F. C. Richter, S. S. Müller, A. M. Hofmann, U. Massing, H. Frey, and M. Helm. *Biomacromolecules* **2014**, *15*, 2440-2448.

8. "Cytotoxicity and Chemosensitizing Activity of Amphiphilic Poly(glycerol)–Poly(alkylene oxide) Block Copolymers"
T. V. Demina, O. A. Budkina, G. A. Badun, N. S. Melik-Nubarov, H. Frey, S. S. Müller, J. Nieberle, I. D. Grozdova, *Biomacromolecules* **2014**, *15*, 2672-2681.

9. "Unusual Triskelion Patterns and Dye-Labeled GUVs:
   Consequences of the Interaction of Cholesterol Containing Linear-Hyperbranched
   Block Copolymers with Phospholipids"
   P. Scholtysek, S. S. Müller, R. Schöps, H. Frey, A. Blume, and J. Kressler, *Langmuir*
   2014, in revision.

10. "Hydroxyfunctional Oxetane-Inimers with Varied Polarity for the Synthesis of
    Hyperbranched Polyether Polyols via Cationic ROP"
    E.-M. Christ, S. S. Müller, E. Berger-Nicoletti,, H. Frey, *J. Polym. Sci. Polym. Chem.*
    2014, in revision.

11. "Evaluation of Multifunctional Liposomes in Human Blood Serum by Light
    Scattering"
    K. Mohr, S. S. Müller, L. K. Müller, K. Rusitzka, S. Gietzen, H. Frey, and M.
    Schmidt, **2014**, submitted to Langmuir.

12. "Characterization of Polyether-Lipids in Stealth Liposomes by ^{18}F-TEG-N$_3$ click
    Radiolabeling and Positron Emission Tomography"
    A. Reibel, S. S. Müller, S. Pektor, N. Bausbacher, M. Miederer, H. Frey, F. Rösch,
    2014, to be submitted.

13. "Allyl-Functionalized Cholesterol-Lipids: From Thiol-ene Coupling to Liposomes"
    S. S. Müller, A. Reddy, and Holger Frey, **2014**, to be submitted.

14. "Tackling the Biodegradability of Hyperbranched Polyether-Lipids with In-Chain
    pH-Sensitive Linkages "
    S. S. Müller, T. Fritz, F. Prochnow, M. Gimnich, M. Helm, and Holger Frey, **2014**,
    to be submitted.

15. "Nanovesicles as drug delivery vehicles: Liposomes and Polymersomes"
    S. S. Müller and Frederik Wurm, **2014**, submitted to *Encyclopedia of Polymeric
    Nanomaterials*, edited by Shiro Kobayashi and Klaus Müllen.

Conference Contributions

"Synthesis of oxetane-functional aliphatic polyesters via enzymatic polycondensation"
S. S. Müller, H. Frey
243rd ACS Spring Meeting March **2012**, San Diego, CA, USA

"Mesogen initiated linear polyglycerols"
S. S. Müller, H. Frey
24th International Liquid Crystal Conference ILCC August **2012**, Mainz, Germany

"Polyether-based lipids: Multivalent architectures for functional liposomes"
S. S. Müller, H. Frey
15th International Conference "Polymeric Materials" September **2012**, Halle (Saale), Germany

"From Inert to Labile: Well-Defined Functional pH-sensitive Poly(ethylene glycol)s"
C. Dingels, S. S. Müller, T. Steinbach, C. Tonhauser, H. Frey
Smart Polymers, **2012**, Mainz, Germany

"Implementation of pH-sensitive acetal units in cholesteryl-polyethers"
S. S. Müller, C. Dingels, H. Frey
IUPAC International Conference on Advanced Polymers via Macromolecular Engineering APME, August **2013**, Durham, UK

"Multifunctional polyether-based lipids via oxyanionic-polymerization: A versatile platform for functional amphiphiles"
S. S. Müller, H. Frey
IUPAC International Symposium on Ionic Polymerization September **2013**, Awaji Island, Japan